UNIVERSAL
LIBRARY

OU_154685

UNIVERSAL
LIBRARY

OSMANIA UNIVERSITY LIBRARY

Call No. 520 K83A Accession No. 50026

Author KOPAL, Zdenek, ed.

Title Advances in astronomy and astrophysic

This book should be returned on or before the date last marked below.

Advances in

ASTRONOMY AND ASTROPHYSICS

VOLUME I

ADVANCES IN
ASTRONOMY and ASTROPHYSICS

edited by

ZDENĚK KOPAL

Department of Astronomy, The University
Manchester, England

Volume I



ACADEMIC PRESS New York and London • 1962

COPYRIGHT © 1962, BY ACADEMIC PRESS INC.

ALL RIGHTS RESERVED

NO PART OF THIS BOOK MAY BE REPRODUCED IN ANY FORM
BY PHOTOSTAT, MICROFILM, OR ANY OTHER MEANS,
WITHOUT WRITTEN PERMISSION FROM THE PUBLISHERS

ACADEMIC PRESS INC.
111 FIFTH AVENUE
NEW YORK 3, N. Y.

United Kingdom Edition
Published by
ACADEMIC PRESS INC. (LONDON) LTD.
BERKELEY SQUARE HOUSE, LONDON W. 1

Library of Congress Catalog Card Number 61-18299

PRINTED IN THE UNITED STATES OF AMERICA

CONTRIBUTORS TO VOLUME I

J. HAZLEHURST*, *Yerkes Observatory, University of Chicago, Chicago, Illinois*

G. H. HERBIG, *Lick Observatory, University of California, Mt. Hamilton, California*

W. HUNTER, *Department of Physics and Mathematics, College of Technology, Liverpool, England*

D. W. PARKIN, *Department of Physics and Mathematics, College of Technology, Liverpool, England*

L. PEREK, *Astronomical Institute of the Czechoslovak Academy of Sciences, Prague, Czechoslovakia*

K. SERKOWSKI, *Warsaw University Observatory, Warsaw, Poland*

* Present address: Department of Astronomy, The University, Manchester, England.

PREFACE

The aim of the series inaugurated by the present volume will be twofold. First, it is to provide a semi-periodic forum for the publication of review articles on different aspects of astronomy and astrophysics—from the pens of leading students of the respective subjects—which would be too long for ordinary scientific periodicals, but too short for separate monographs. The need for this type of contributions has never been greater than at present, when a constantly growing volume of original publications makes it progressively more difficult for scientists—let alone the more general reader—to keep abreast of the rapid new developments in fields which are not specifically their own.

There is, however, one additional and equally timely mission which the present series will strive to accomplish: and that is to help to bridge the gap between astronomy and the neighbouring fields of science. Fifty years ago, astronomy still lived proudly in its ivory tower, bent on an age-long historical mission—with astrophysics but a budding stepchild claiming common descent from physics. Since that time, the forward march of progress gradually engulfed this ivory tower from all sides, and rendered astronomy a truly integral part of the mathematical and physical sciences. It is from this point of view that our contributors—both present and future—will endeavor to outline recent developments of their particular subjects, on a more general background, for a wider circle of their scientific confreres.

February, 1962 ZDENĚK KOPAL

CONTENTS

CONTRIBUTORS TO VOLUME 1 v

PREFACE vii

The Shock-Wave Theory of Novae

JOHN HAZLEHURST

I. Introduction; an Observational Summary 1
II. Initial Stages; Formation and Decay of the Blast Wave 3
III. Linear Regime 8
IV. Approximate Nonlinear Theory 14
V. Influence of the Wake 20
VI. Final Stages of the Shock Propagation 25
VII. Numerical Results 27
VIII. Motion of Material Away from the Stellar Surface 32
IX. Estimation of the Mass and Energy of the Escaping Material 34
X. Expanded Atmosphere 38
XI. Conclusion 40
Appendix 43
References 44

The Properties and Problems of T Tauri Stars and Related Objects

G. H. HERBIG

I. Introduction 47
II. Special Properties of the T Tauri Stars 69
III. General Problems of the T Tauri Stars 94
References 99

Meteorites and Cosmic Dust

D. W. PARKIN AND W. HUNTER

I. Introduction 105
II. Meteorites 106
III. Cosmic Dust 114
Addendum 156
References 162

Distribution of Mass in Oblate Stellar Systems

L. PEREK

I. Introduction 165
II. Models Based on the Velocity Distribution 194
III. Models Based on Density Laws 221
References 284

Polarization of Starlight

K. SERKOWSKI

I. Introduction 290
II. Stokes Parameters 291
III. Optical Devices for Analyzing Polarized Light 295
IV. Techniques of Polarization Measurements 298
V. Polarization of Light by Aligned Dust Grains 307
VI. Dependence of Interstellar Polarization on Galactic Coordinates 315
VII. Alignment Mechanisms 332
VIII. Fluctuations of Polarization in Small Areas of the Sky 343
References 350

Author Index 353
Subject Index 358

The Shock-Wave Theory of Novae

JOHN HAZLEHURST
Yerkes Observatory, University of Chicago, Chicago, Illinois *

I. Introduction; an Observational Summary 1
II. Initial Stages; Formation and Decay of the Blast Wave 3
III. Linear Regime 8
IV. Approximate Nonlinear Theory 14
V. Influence of the Wake 20
VI. Final Stages of the Shock Propagation 25
VII. Numerical Results 27
VIII. Motion of Material Away from the Stellar Surface 32
IX. Estimation of the Mass and Energy of the Escaping Material . . . 34
X. Expanded Atmosphere 38
XI. Conclusion 40
Acknowledgments 43
Appendix 43
References 44

I

INTRODUCTION; AN OBSERVATIONAL SUMMARY

Although the novae exhibit such a rich diversity in the details of their individual development that none of them can be regarded as "typical," there are certain over-all characteristics which distinguish them as being a well-defined class of objects.

They would all seem to be intrinsically faint blue stars, which quite suddenly (within about two days) increase their luminosity by eleven magnitudes and show the spectrum of a supergiant.

The subsequent decline of the light to the original stellar luminosity takes place in a period varying from several weeks to many months, but the total amount of radiation emitted is generally about 10^{45} ergs. During this decline both the light curve and the spectrum exhibit considerable complexity. The relation between the variations of luminosity and color is suggestive of an ejection of material rather than an expansion of the star, while the simplest interpretation of the line displacements would seem to be that the main expulsion

* Present address: Department of Astronomy, University of Manchester, England.

of gases in the form of a principal shell is followed by a more prolonged outflow of material, with sporadic formation of subsidiary shells. Moving with speeds of several thousands of kilometers a second, these would seem ultimately (at a distance of about a thousand solar radii) to overtake and coalesce with the principal shell; the resultant expanding nebulosity may be visible for many years afterwards.

The masses of the main shell and of the total semicontinuous outflow may be estimated, respectively, from the total release of recombination radiation on cooling (Sayer, 1948) and from the radius of the effective photosphere together with the duration of the outburst (Payne-Gaposchkin and Whipple, 1936). These both indicate about 10^{28} gm. Taking 10^{8} cm/sec as the velocity of the ejected gases, we find a total kinetic energy of 10^{44} ergs for the outflowing material.

In the minority of cases where a test has been possible, the luminosities of the pre- and post-novae have been found to be the same; it has not been possible to make a similar statistical check on the spectral types, since these are known for hardly any pre-novae. Almost without exception, however, the post-novae are stars whose spectral type, O or B, indicates a temperature of about 50,000°. Combining the temperature and luminosity one generally finds a radius of about $\frac{1}{10}\,R_{\odot}$.

The masses of the novae are unknown; one can only say that a very crude application of the mass-luminosity relation leads to $\sim 1\,M_{\odot}$. The only statement one can make about the internal structure is that degeneracy does not appear to be indicated by the luminosity and spectral type, even though the post-novae fall well below the main sequence. Because of their unusual position in the *HR* diagram, we shall not use the detailed results from the standard stellar structure calculations in what follows, but merely employ estimates, based upon the above integral properties, for such parameters as the central sound speed.

The thermal and gravitational energies of a star of $M = 1M_{\odot}$ and $R = \frac{1}{10}\,R_{\odot}$ are about 10^{49} ergs, so that we note:

Total energy radiated $\sim 10^{-4} \times$ total energy of star
Kinetic energy of gas ejected $\sim 10^{-5} \times$ total energy of star
Mass of gases ejected $\sim 10^{-5} \times$ mass of star

We shall not be concerned here with the evolutionary aspects of novae, but shall rather attempt to describe the behavior of the star during a single outburst, and to see not only whether the above figures are mutually consistent on the basis of a particular hypothesis, but also what we can infer about the magnitude of the internal changes necessary to produce the above superficial effects. The smallness of these figures shows that we are not witnessing the consequences of a major structural change in the star, and may assume that the properties of the post-nova would also be those of the star before the outburst.

The very suddenness of the rise to maximum would seem to suggest that the internal disturbance takes place in a time considerably less than that required for a sound wave to travel to the stellar surface; for otherwise the star would simply expand as a whole, rather than actually eject material. We shall therefore adopt the simplest possible hypothesis that an (adjustable) amount of energy is liberated instantaneously at the center of the star. It will become clear, however, that the conclusions will not be significantly affected if for "instantaneous" we read "in a time much less than that taken by a sound wave to reach the surface," and for "central" we substitute "considerably more than one fifth of a stellar radius below the surface." The fact that the outrushing gases are highly supersonic (Mach 30 or more) does not in itself imply shock ejection, since considerable cooling will tend to produce this high figure, but it is difficult to envisage an alternative mechanism for accelerating bulk material to several times the velocity of escape.

We shall see that the foregoing central explosion hypothesis does in fact lead to a shock wave which will provide the required ejection speeds; however, it will emerge that this can only be achieved by releasing an amount of energy which exceeds that of the ejected gases by two orders of magnitude.

There appear to be two main approaches to the study of the propagation of shock waves in variable media—the similarity methods and the wave-diagram technique (loosely based upon the method of characteristics). We shall for the most part adopt the latter, but shall include the results from the former work for comparison (Section VI).

II

INITIAL STAGES; FORMATION AND DECAY OF THE BLAST WAVE

For simplicity, we shall assume that the energy is released instantaneously and symmetrically at the stellar center. The mean free path of a photon is so short that the speed of its diffusion is much less than the sound speed, i.e., the energy cannot be lost by radiation, and is rapidly converted into thermal and kinetic energy.

Any such disturbance can be represented as a superposition of spherical waves, provided that we remember when adding the contributions that each wave moves with the sound speed relative to the fluid. After a short while all the wavelets which were originally converging on the center will have been reflected outwards and the expanding flow region will simply be the total of all these outgoing waves. We shall, for clarity, discuss the development of this system as if the waves were plane, but the restriction is not essential.

If the wavelet traveling outwards is a rarefaction, it will decelerate the particles over which it passes [Fig. 1(a)] because the pressure gradient is directed inwardly.

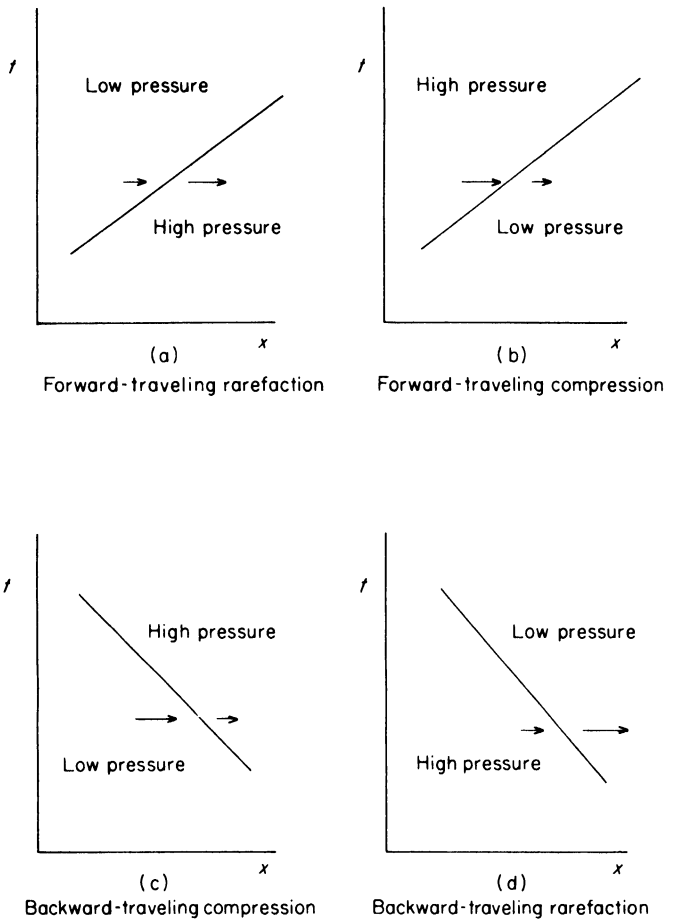


FIG. 1. The pressure and velocity changes induced by traveling wave elements. The arrow represents the velocity vector of the fluid.

An elementary compression will conversely accelerate the fluid. If, therefore, all wavelets are moving outwards, the pressure will rise and fall in the same sense as the velocity and, assuming the adiabatic law (no shocks having yet been formed), the temperature and density will show the same behavior. Thus the snapshot A of Fig. 2 could apply (qualitatively) to any of these four quantities. Since, moreover, the local sound speed varies in the same sense as the

temperature, the total signal speed[1] $w = u + v_s$ will also show a similar profile. We can thus take the behavior of w, regarded as a function of p, ρ, T, u as representing any of these quantities individually. It must be stressed that these statements are only true at a time when the outgoing waves predominate.

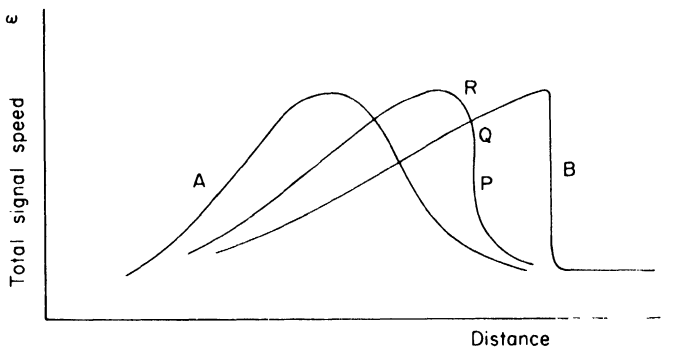


FIG. 2. The formation of a plane shock; the ordinate can represent, qualitatively, other state parameters (e.g., the pressure). A spherical shock is formed in analogous fashion.

The development of the flow can now be traced by a simple geometrical construction. We know that any variable—and this includes $w(p, \rho, T, u)$—propagates with the speed w. Hence we can map w from itself by simply displacing each point on the curve a distance proportional to its ordinate. This has been done, for several different times, in Fig. 2. When the gradient becomes vertical (as at P) the previously neglected viscous dissipation becomes important, and a shock front begins to form. It is readily seem from the Rankine-Hugoniot equations that a shock front travels at a speed less than the value of w immediately behind it, so that the wavelets propagated from QR rapidly overtake and coalesce with the shock, leading to the stable profile B; for, if we continue the mapping for the waves behind the shock, we see that there will be no further change in the form of the profile (simply scale changes). In other words, the "similarity" form has been reached. However, the shock wave itself becomes a source of wavelets and, since these are traveling inwards, the simple construction procedure described above ceases to be valid.

Should the newly formed blast wave be traveling into a region of uniform density, its structure will be that found by Taylor (1950). There will be simply a general (self-similar) expansion of the flow about the origin—provided that the shock remains strong. If U and ρ_1 denote the shock speed and the density

[1] We denote by u and v_s the fluid and sound speeds respectively.

in the quiet fluid, while p_2 is the pressure just behind the shock, then, using the value of γ ($= 5/3$) appropriate to a monatomic gas

$$p_2 = \tfrac{3}{4}\rho_1 U^2. \tag{1}$$

If, moreover, E is the total energy of the flow and R is the shock radius

$$p_2 \sim ER^{-3}, \tag{2}$$

this expression being a strict proportionality for self-similar flows; it simply states that (apart from a factor 2/3) the pressure is just the energy density. From Eqs. (1) and (2) we obtain a differential equation for the shock path, which is readily integrated to give

$$R \sim \left(\frac{E}{\rho_1}\right)^{1/5} t^{2/5}, \tag{3}$$

where the constant of integration can be neglected after a sufficient expansion of the flow region beyond its original size. This law has been found to hold very accurately for terrestrial explosions (Taylor, 1950).

When the blast wave has expanded to such an extent that the pressure inside becomes of the order of the external pressure, Eq. (1) no longer holds, and the blast degenerates into a sound wave. Setting $p_2 \sim p_1$ in Eq. (2), we see that the characteristic radius R_c at which this occurs is

$$R_c \sim \left(\frac{E}{p_1}\right)^{1/3} \tag{4}$$

while, from Eq. (3), this happens after a time t_c, where

$$t_c \sim \frac{\rho_1^{1/2} E^{1/3}}{p_1^{5/6}} \sim \frac{R_c}{A_1}, \tag{5}$$

A_1 being the sound speed in the quiet gas. We shall call R_c the "range" of the explosion, and t_c the characteristic time.

In order to determine the stage to which the blast wave develops within the star, we must compare the range of the explosion with the stellar radius. Provided that the degree of central condensation is not too large

$$R_* \sim \left(\frac{E_*}{p_*}\right)^{1/3}, \tag{6}$$

where E_*, p_*, and R_* are the thermal energy, central pressure, and radius of the star. Should the condensation be high, R_* represents the distance in which the main change of stellar density takes place. Combining Eqs. (4) and (6), and anticipating that $p_1 \approx p_*$, we see that

$$\frac{R_c}{R_*} \sim \left(\frac{E}{E_*}\right)^{1/3}. \tag{7}$$

Since we must assume that, in general, the energy liberated at the stellar center will not be 100 percent efficient in ejecting material, we shall consider values of E/E_* lying between 10^{-3} and 10^{-5}, these extremes representing respectively 1 and 100 percent efficiency.[2] Hence,

$$\text{if } 10^{-5} \lesssim E/E_* \lesssim 10^{-3} \quad \text{then} \quad 1/46 \lesssim R_c/R_* \lesssim 1/10 \tag{8}$$

and the shock has traveled such a relatively short distance before weakening that the density and pressure of the star can be taken to be constant and equal to their central values. Since the derivatives of density and pressure vanish at the stellar center, the error incurred is of the order of $(R_c/R_*)^2$ and one is quite justified in using the Taylor solution before the wave degenerates.

Sakurai (1956) has attempted to follow the propagation of the weakening shock by expanding all parameters as a series with the typical term

$$\left(\frac{R(t)}{R_c}\right)^n f_n\left(\frac{r}{R(t)}\right), \tag{9}$$

$R(t)$ being the shock radius and r, the Eulerian coordinate. The f_n are determined by successive solutions of systems of ordinary differential equations. Although such an approach would probably be fruitful for supernovae, where $R(t)/R_c \leq R_*/R_c \lesssim 1$ [see Eq. (7) and recall that $E \gtrsim E_*$], the series will fail to converge for the greater part of the star in the case of novae, for which $R(t)/R_c \leq R_*/R_c \gg 1$.

Since, in the present application, the shock has become weak after traveling 10 percent or less of the stellar radius, it will propagate as a small disturbance throughout the bulk of the star. The equations of motion can then be linearized.

[2] We recall (see Section I) that the energy of the shell is $10^{-5}\, E_*$.

III

LINEAR REGIME

In order to describe the propagation of the weak disturbance into which a central explosion evolves, Whitham (1953) linearized the equations of motion for a self-gravitating gas sphere, reducing them to a single equation

$$\frac{\partial^2\psi}{\partial t^2} = A^2\left[\frac{\partial^2\psi}{\partial r^2} - \left(\frac{2}{r} + \frac{2(2-\gamma)}{\gamma-1}\frac{A'}{A}\right)\frac{\partial\psi}{\partial r} + \frac{4\pi GD}{A^2}\psi\right], \quad (10)$$

where ψ is the change in the mass contained within the sphere of radius r at time t, while A, A', and D are the sound velocity, its gradient, and the density in the undisturbed star. The pressure and density in the undisturbed configuration are taken to be related by the polytropic law, and this law can therefore also be applied to the disturbed gases since the shock is now very weak. Since the highest order terms in Eq. (10) represent a wave motion, Whitham attempted a solution in series form:

$$\psi = \sum_{n=0}^{\infty} \psi_n(r) f_n(\xi), \quad (11)$$

where

$$\xi = t - \int \frac{dr}{A} \quad (12)$$

is the difference between the time itself and the time for a sound wave to reach the point r, while $f_n(\xi)$ is the nth integral of an (as yet) arbitrary function $f(\xi)$. Thus, the lowest order term

$$\psi_0(r) f_0(\xi) = \psi(r) f(\xi), \quad \textit{say} \quad (13)$$

is the product of an amplitude function and a wavelike function. The series (11) converges, and Eq. (13) is a good approximation to ψ, if: (i) dA/dr does not greatly exceed A/r; (ii) the extent of the disturbance is much less than the distance from the stellar center (i.e., $A\xi/r$ is small); and these conditions are satisfied except in the initial and final stages of the propagation.

The function ψ_0 is found by substituting the series (11) in Eq. (10) and equating coefficients of f', giving

$$\psi_0 = CrA^{\nu} \quad (14)$$

where

$$\nu = (3-\gamma)/3(\gamma-1), \quad (15)$$

so that the velocity and pressure are

$$u = -\frac{1}{4\pi r^2 D}\frac{\partial \psi}{\partial t} = -\frac{CA^{\nu}}{4\pi r D} f'(\xi) \tag{16}$$

$$p = P(r) + \frac{A^2(r)}{4\pi r^2}\frac{\partial \psi}{\partial r} \approx P(r) - \frac{CA^{\nu+1}}{4\pi r} f'(\xi); \tag{17}$$

capital letters, as before, denoting undisturbed values.

These expressions show that the amplitude, but not the profile, of a small disturbance changes with distance. Whitham estimated the form of $f'(\xi)$ by applying the equations directly to a particle which had moved out from the center. We cannot do this here, however, since the linear theory does not apply to the central particles and the linear solution must be matched with the degenerate blast wave solution at a point where the shock has become sufficiently weak. We must therefore resort to numerical integration of the exact partial differential equations; the initial state is the Taylor solution, while the degeneration of the blast is complete when the Taylor self-similar *expanding* solution has changed into a *propagating* solution which preserves its form. Such computations have been effected by the author on the Manchester Mercury electronic computer by the method to be described in Section VII. The Taylor wave and the progressive wave into which it evolves are sketched in Figs. 3(a) and

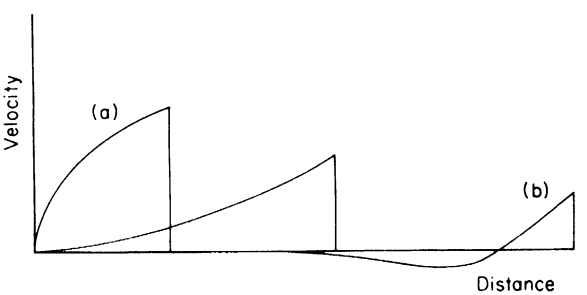


FIG. 3. The decay of a spherical blast wave (not to scale).

(b) respectively. Just behind the shock, the amplitude in the progressive wave varies very nearly as

$$p \propto u \propto \exp(-\xi/t_c) \tag{18}$$

where t_c is the previously defined characteristic decay time of the blast wave. We have taken $\xi = 0$ at the shock front itself. We note that the initial and final solutions in Figs. 3(a) and (b) differ in the appearance of a velocity reversal

(associated with a following rarefaction) in the latter. This is another way of saying that the particles in the central (strong shock) regions suffer a permanent displacement, while those further out tend to return to their original positions. The reason for this different behavior is that the central particles are irreversibly heated and therefore, in the equilibrium configuration after the shock has passed, possess a greater volume than in the pre-shock state. On the other hand, the outer particles can only be heated by compression (there is no irreversible heating by weak shocks) so that the entropy function p/ρ^{γ} is unaltered by the shock passage, and the particles must possess their *original* volume in the final state. Any permanent displacement of the outer particles can therefore only be due to the expansion of the inner layers. This must fall off as $1/r^2$, while the peak amplitude of the wave decreases only as $1/r$ [see Eq. (16)]. Hence the outer particles must return, effectively, after the shock impulse, to their original positions. This can only be achieved by a velocity reversal, as in Fig. 3(b).

Joining together the linear and the degenerate blast wave solutions, we see that $f'(\xi)$ must have the form shown in Fig. 3(b). The absolute values of C and $f'(\xi)$ are at our disposal (though that of their product is not), so it is convenient to choose C in such a way that $f'(\xi)$ is equal to -1 at $\xi = 0$ (the shock front). Since $\nu = 1$ when $\gamma = 5/3$, the maximum velocity is

$$u_{\max} = \frac{cA}{4\pi r D}, \tag{19}$$

Although this equation does not strictly apply to the transition region where the shock is weakening, we can *estimate* C by using it there. In this zone

$$u_{\max} \sim A, \qquad r \sim R_c, \tag{20}$$

A and D being very nearly equal to their central (undisturbed) values A_*, D_* Hence

$$C \sim 4\pi R_c D_* \tag{21}$$

and, introducing the characteristic time to make the argument of f' dimensionless,

$$u \sim -A \frac{R_c}{R_*} \left[\frac{R_*}{r} \frac{D_*}{D}\right] f'\left(\frac{\xi}{t_c}\right) \tag{22}$$

where by f' we now understand the derivative of f with respect to the argument ξ/t_c. The expression in square brackets is of order unity everywhere except at the center ($r \to 0$) and the surface ($D \to 0$) of the star. Since u/A can be taken as a measure of the shock strength, and $|f'(\xi/t_c)| \leq 1$ while $R_c/R_* \ll 1$,

we see that the small disturbance approximation holds good throughout the major part of the star. In the surface regions $r \approx R_*$ and

$$u \sim -A\left(\frac{R_c}{R_*}\right)\left(\frac{D_*}{D}\right) f'(\xi/t_c) \tag{23}$$

so that the shock becomes strong again when the density falls to a value $D \sim (R_c/R_*)\, D_*$ and the linear approximation breaks down.

Before passing on to consider the nonlinear shock propagation, we note that the linear theory has been applied to the atmospheric regions by Simon (1955) for the Roche model and by Whitham (1953) for several models. The latter notes that, for an atmosphere in adiabatic equilibrium, Eq. (10) can be approximated by

$$\frac{\partial^2\psi}{\partial t^2} = A_2^2(R_* - r)\left[\frac{\partial^2\psi}{\partial r^2} + \left(\nu - \frac{1}{2}\right)\frac{\partial\psi/\partial r}{R_* - r}\right], \tag{24}$$

where

$$A = A_2(R_* - r)^{1/2} \tag{25}$$

is the law of variation of sound speed. A change of variables transforms this (taking $\nu = 1$) to

$$\frac{\partial^2\psi}{\partial t^2} = \frac{\partial^2\psi}{\partial\eta^2} - \frac{2}{\eta}\frac{\partial\psi}{\partial\eta} \tag{26}$$

where

$$\eta = \int_r^{R_*} \frac{dr}{A} \tag{27}$$

is the time taken for a sound wave to travel to the surface. The solution of Eq. (26) representing an outgoing wave is

$$\psi = J(t + \eta) - \eta\frac{\partial J}{\partial t}(t + \eta), \tag{28}$$

J being an arbitrary function. There is also an inwardly directed wave, but this must be excluded (in linear theory) since it would imply a disturbance ahead of the shock wave at sufficiently early times. The velocity is given by

$$u = -\frac{1}{4\pi R_*^2 D}\left(\frac{\partial J}{\partial t} - \eta\frac{\partial^2 J}{\partial t^2}\right) = -\frac{1}{4\pi R_*^2 D}\left(\frac{\partial J}{\partial\xi} - \eta\frac{\partial^2 J}{\partial\xi^2}\right) \tag{29}$$

and noting that, apart from an additive constant, $(t + \eta)$ is simply ξ, we identify the second term (which predominates well below the surface) with the right-hand side of Eq. (22). This is permissible because [by virtue of the definition (27)

and the law (25)] the quantities A and η are proportional in the surface layers, while R_*/r becomes unity. Hence,

$$\frac{u}{A} = \left(\frac{R_c}{R_*}\right)\left(\frac{D_*}{D}\right)\left[\frac{t_c}{\eta} f(\xi/t_c) - f'(\xi/t_c)\right] \tag{30}$$

is the complete linear solution for the atmosphere. Since we shall use the linear solution as the initial condition in the nonlinear treatment, it is important to know which of the two terms in Eq. (30) is predominant when the nonlinear effects first appear. It is thus necessary to express D as a function of η, which we can achieve in a rough manner as follows. In the surface regions, the polytropic law leads to the variations:

$$D \propto (R_* - r)^{3/2}, \tag{31}$$

$$\eta \propto A \propto (R_* - r)^{1/2}, \tag{32}$$

whence

$$D \propto \eta^3. \tag{33}$$

The constant of proportionality in Eq. (33) may be estimated by noting that these relations can be applied with reasonable accuracy until the point of inflection in the polytropic curve is reached. But at this point all physical parameters have the same order of magnitude as their central values. Hence

$$\frac{D}{D_*} \sim \left(\frac{\eta}{t_*}\right)^3 \tag{34}$$

where the constant of proportionality is of order unity, and is readily calculated once a particular model is chosen. Here t_* represents the time for a sound wave to travel the stellar radius. Similar arguments together with Eq. (5) show, moreover, that

$$\frac{R_c}{R_*} \sim \frac{t_c}{t_*}, \tag{35}$$

so that Eq. (30) takes the form

$$\frac{u}{A} \sim \left(\frac{t_c}{t_*}\right)\left(\frac{t_*}{\eta}\right)^3 \left[\frac{t_c}{\eta} f\left(\frac{\xi}{t_c}\right) - f'\left(\frac{\xi}{t_c}\right)\right]. \tag{36}$$

Because of the way in which they have been defined, f and f' are of order unity. Using $u/A \sim 1$ as the criterion for the appearance of nonlinear effects, we see that:

(a) The first term predominates over the second when

$$\eta < \eta_0 = t_c. \tag{37}$$

(b) Nonlinear effects appear in the first term when

$$\eta < \eta_1 = (t_* t_c)^{1/2}. \tag{38}$$

(c) Nonlinear effects appear in the second term when

$$\eta < \eta_2 = (t_*^2 t_c)^{1/3} \tag{39}$$

or, on account of Eq. (35),

$$\begin{aligned} \eta_0 &= t_c \qquad (\text{or } t_c) \\ \eta_1 &= 3.2t_c \quad (\text{or } 6.8t_c) \\ \eta_2 &= 4.6t_c \quad (\text{or } 13t_c) \end{aligned} \tag{40}$$

where the first values on the right-hand side refer to $E/E_* = 10^{-3}$ and those in parenthesis to $E/E_* = 10^{-5}$. Hence the above stages occur in the order (t increasing, η decreasing):

(c) (b) (a)

and we conclude that linear methods cannot be applied to the atmospheric regions since nonlinear effects have already become important in the solution (22) characterizing the nonatmospheric propagation. Hence, when we graft the nonlinear solution onto the linear one, we should use Eq. (22) rather than Eq. (36) as the linear basis. The criterion (a) above is simply the condition that the wavelength of the disturbance be of the order of the distance separating the shock from the stellar surface. Since (a) occurs after (c), we may say that the nonlinear effects appear when the wavelength of the disturbance is still considerably less than the distance to the surface. Using the proportionality of η and A

$$\frac{\text{sound speed where } \eta = \eta_2}{\text{central sound speed}} = \frac{\eta_2}{t_*} \approx \frac{1}{2}\left(\text{or } \frac{1}{3}\right) \tag{41}$$

or, since the sound speed and particle speed are about equal when $\eta = \eta_2$, while A_* is about the same[3] as the escape speed from the stellar surface, we conclude that nonlinearity becomes important when the speed imparted to the material is about 1/2 or 1/3 of the escape speed. Although this value is very rough, it suffices to show that the shock wave must be followed right into the nonlinear region before it reaches material which stands a good chance of permanent ejection.

[3] A closer estimate might be $A_* = (1/\sqrt{2})\, v_{esc}$ (see Section IX), though the numerical factor will of course depend on the model chosen.

Before considering the nonlinear solution, we note that two approximations are permissible. From Eq. (23) we see that the shock strengthens (and hence approaches the region where it can eject material) when the density is 1/10 (or 1/46) of the central density, or the depth is 1/5 (or 1/13) of the stellar radius. Hence the motion can be regarded as approximately one-dimensional. Moreover, to estimate the importance of gravity during the final stages, we note that

$$g = \frac{GM_*}{R_*^2} \sim \frac{E_*}{M_* R_*} \sim \frac{p_* R_*^2}{M_*} \sim \frac{p_*}{\rho_*} \frac{1}{R_*} \sim \frac{A_*^2}{R_*} \sim \frac{A_*}{t_*} . \quad (42)$$

But the hydrodynamical accelerations are of the order

$$\frac{\text{particle speed}}{\text{time for shock to cross surface layers}}$$

and, since the numerator is of the order of the escape speed (which is itself of order A_*) while the denominator is very much less than t_*, we can neglect the gravitational deceleration—at any rate up to the time the shock penetrates the surface. Gravity is principally important in its function of determining the equilibrium run of the parameters.

In fact we shall find no difficulty in including gravity directly in the approximate theory which follows; the complexities only enter when one attempts to include the effects of gravitation in the higher-order interactions (see below).

IV

APPROXIMATE NONLINEAR THEORY

A fruitful approach towards a theory of the propagation of a shock wave in a variable region is that of Chisnell (1955) who regarded the medium as being stratified; the interaction of the shock with each small contact discontinuity was analyzed after the fashion of the analogous optical problem of a wave traveling through a medium of variable dispersion. The analogy is limited, however, in that the reflected rarefaction waves interact first with one another and then with the shock. In fact the series of interactions is a never-ending one, and its determination involves the evaluation of intricate integrals of arbitrarily high order. The usefulness of the method lies in the *empirical* result that, provided the variation is sufficiently rapid, the first order calculation yields accurate answers.

Chisnell secured equilibrium of the variable medium in the absence of gravity by maintaining a uniform pressure; thus the density and temperature changed discontinuously at each contact surface. However, no mathematical

difficulty is encountered (Whitham, 1958; Ono *et al.*, 1960) in allowing all state parameters to vary under the influence of a gravitational field. In order to balance the pressure changes by the gravitational forces, the latter authors replace the concept of a contact surface by the much more vague notion of a contact region, and some of the clarity of Chisnell's original wave diagram methods is thereby lost. We therefore suggest the following model (though still somewhat artificial) as being possibly more satisfactory from a conceptual viewpoint.

We shall still retain a series of contact surfaces [two of which are shown in Fig. 4(a)] at which the density, temperature, *and pressure* change discontinuously.

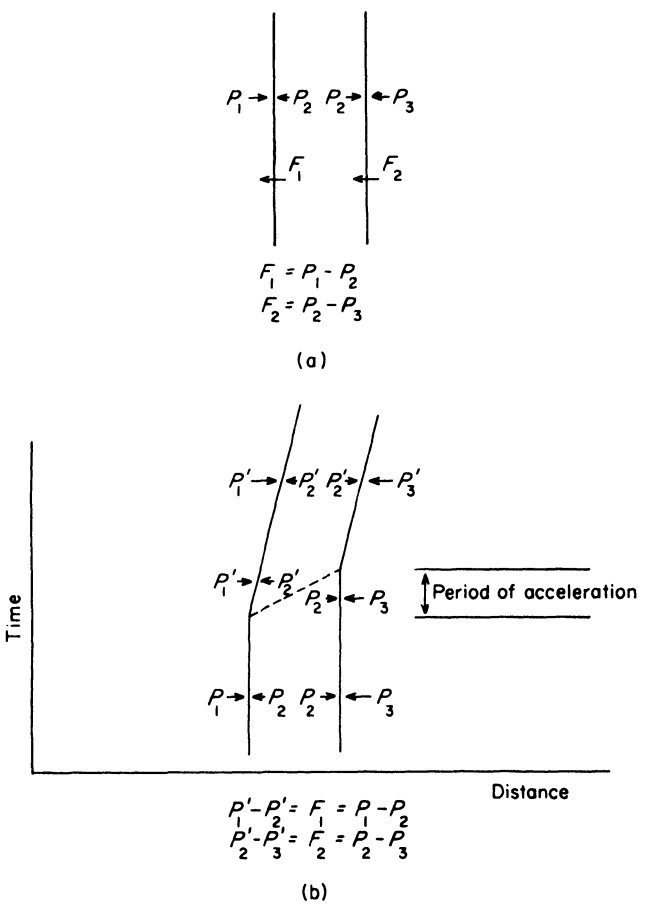


FIG. 4. (a) The balancing of the pressure differences across a layer by surface forces. (b) The acceleration of a layer by a wave element.

However, we balance the equilibrium pressure change by an equal and opposite body force in each *surface*. Since the mass between any two surfaces does not change during any subsequent motion, an adequate representation of gravity will be achieved by assuming that these body forces remain constant throughout the motion. Then, since the mass in the surface is zero, the pressure difference across it will always be equal to the body force. A net acceleration of the layer is produced when [as in Fig. 4(b)] a wave crosses it, leading to a variation of pressure within the layer.

Moreover, although Chisnell regarded the shock as originating in a region of uniform conditions, we must allow for the finite extent of the wake of the shock. For, when the Mach number exceeds unity by a small amount, the following wave elements will overtake, and be swallowed up by, the shock front, thus influencing its propagation. The inclusion of the gravitational forces and the transmission of the initial conditions by the wake are both, however, merely formulational changes; the methods we shall employ in this section are in the spirit of the original paper (Chisnell, 1955).

Figure 5 shows the various elementary processes affecting the propagation of the shock; 1, 2, and 5, 6 represent the shock front before and after its inter-

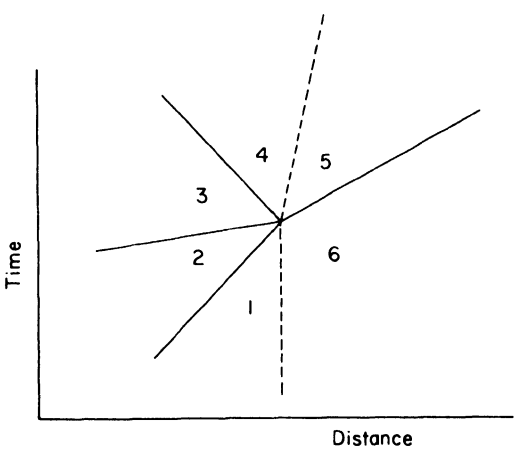


FIG. 5. The interaction of a shock wave with a contact discontinuity and a following wave element.

action with the contact discontinuity 1, 6 and the following wave 2,3. Similarly 3, 4 and 4, 5 are the paths of the reflected wave and the contact discontinuity after the interaction. The strength z of each disturbance is defined as the pressure ratio across it, e.g.,

$$z_{12} = p_2/p_1 , \tag{43}$$

while all other parameter changes can be expressed in terms of z:

$$\rho_2 = \rho_1 \frac{\lambda^2 + z_{12}}{1 + \lambda^2 z_{12}} \tag{44}$$

$$u_2 = u_1 \pm \phi(z_{12}, p_1, \rho_1) \tag{45}$$

$$U = u_1 \pm \sqrt{\frac{p_1(\lambda^2 + z_{12})}{\rho_1(1 - \lambda^2)}} \tag{46}$$

where

$$\phi(z_{12}, p_1, \rho_1) = (z_{12} - 1)\sqrt{\frac{p_1(1 - \lambda^2)}{\rho_1(\lambda^2 + z_{12})}} \tag{47}$$

and

$$\lambda^2 = \frac{\gamma - 1}{\gamma + 1}, \tag{48}$$

U being the speed of the disturbance. When $(z - 1)$ is finite these are the Rankine-Hugoniot shock relations; when $(z - 1)$ is infinitesimal they represent the corresponding changes across a sound wave.

From the definition (43) we note

$$z_{12}z_{23}z_{31}z_{45}z_{56} = z_{16}. \tag{49}$$

Similarly, the velocities satisfy the identity

$$(u_1 - u_2) + (u_2 - u_3) + (u_3 - u_4) + (u_4 - u_5) + (u_5 - u_6) = (u_1 - u_6) \tag{50}$$

or, since the velocities are continuous across a contact surface, $u_1 = u_6$ and $u_4 = u_5$ so that

$$(u_1 - u_2) + (u_2 - u_3) + (u_3 - u_4) + (u_5 - u_6) = 0. \tag{51}$$

We must be cautious in substituting from Eq. (45). Its generalization is

$$u_n - u_m = \mp \phi(z_{nm}, p_n, \rho_n),$$

the convention being that, if n is always chosen to refer to the region *into* which the wave is progressing, we take the minus sign for a forward-facing wave (left → right in Fig. 5) and the plus sign for a backward-facing wave. Then (51) gives:

$$-\phi(z_{12}, p_1, \rho_1) - \phi(z_{23}, p_2, \rho_2) + \phi(z_{34}, p_3, \rho_3) + \phi(z_{65}, p_6, \rho_6) = 0. \tag{52}$$

Now, since the pressure difference in the contact surface must balance the body force (which remains unaffected by the passage of the shock),

$$4\pi R_*^2 g\rho\, dr = p_5 - p_4 = p_6 - p_1 = dp_1, \quad \text{say,} \tag{53}$$

Hence,

$$z_{54} = \left(1 - \frac{1}{z_{12}} \frac{dp_1}{p_1}\right) \tag{54}$$

and we also note that

$$z_{65} = z_{12} + dz_{12} \tag{55}$$

$$z_{16} = 1 + \frac{dp_1}{p_1} . \tag{56}$$

Only an infinitesimal portion of the following wave takes part in each elementary interaction, so that we can write

$$z_{23} = 1 + d\tilde{z} \tag{57}$$

Using Eq. (49) we therefore find

$$z_{31} = 1 + \frac{dz_{12}}{z_{12}} + \left(1 - \frac{1}{z_{12}}\right) \frac{dp_1}{p_1} - d\tilde{z} \tag{58}$$

for the strength of the reflected wave. Writing $\rho_6 = \rho_1 + d\rho_1$ and expanding each of the functions in Eq. (52) to first order terms, we find for the equation of the shock:

$$\frac{dp_1}{p_1}\left[\sqrt{\frac{1 + \lambda^2 z_{12}}{z_{12}(\lambda^2 + 1)}} + \frac{1}{2}\right]$$

$$+ dz_{12}\left[\frac{1}{z_{12} - 1}\sqrt{\frac{1 + \lambda^2 z_{12}}{z_{12}(\lambda^2 + 1)}} + \frac{1}{z_{12} - 1} - \frac{1}{2}\frac{1}{\lambda^2 + z_{12}}\right]$$

$$- \frac{1}{2}\frac{d\rho_1}{\rho_1} - \frac{2z_{12}}{z_{12} - 1} d\tilde{z}\sqrt{\frac{1 + \lambda^2 z_{12}}{z_{12}(\lambda^2 + 1)}} = 0. \tag{59}$$

Since $(z_{12} - 1)$ is always positive, so also is the coefficient of dz_{12}. Hence a small pressure fall and a small density fall ahead of the shock will tend respectively to increase and reduce its speed, while the following train of rarefaction waves ($d\tilde{z}$ negative) will cause the shock to slow down as they catch up with it.

In the case of an atmosphere obeying the adiabatic law, we have

$$\frac{dp_1}{p_1} = \gamma \frac{d\rho_1}{\rho_1} \tag{60}$$

and Eq. (59) reduces (replacing the symbol z_{12} by z) to

$$\frac{1}{\rho_1}\frac{d\rho_1}{dz} = -\frac{\dfrac{2}{z-1}\sqrt{\dfrac{1+\lambda^2 z}{z(\lambda^2+1)}} + \dfrac{2}{z-1} - \dfrac{1}{\lambda^2+z}}{2\gamma\sqrt{\dfrac{1+\lambda^2 z}{z(\lambda^2+1)}} + (\gamma-1)} + \frac{4z}{z-1}\frac{\dfrac{d\tilde{z}}{dz}}{2\gamma\sqrt{\dfrac{1+\lambda^2 z}{z(\lambda^2+1)}} + (\gamma-1)}. \tag{61}$$

Thus the net effect of the variations in the *medium* is to increase the shock speed. Even without knowing the form of $\tilde{z}(z)$, we can effect a partial integration of Eq. (61) by assuming a solution of the form

$$\rho_1(z) = f(z)\, g(z), \tag{62}$$

where $f(z)$ satisfies the equation

$$\frac{1}{f}\frac{df}{dz} = -\frac{\dfrac{2}{z-1}\sqrt{\dfrac{1+\lambda^2 z}{z(\lambda^2+1)}} + \dfrac{2}{z-1} - \dfrac{1}{\lambda^2+z}}{2\gamma\sqrt{\dfrac{1+\lambda^2 z}{z(\lambda^2+1)}} + (\gamma-1)} \tag{63}$$

relating the density and the shock strength in the absence of the wake term. We thus find

$$g(z) = \exp\int_1^z \frac{4z}{z-1}\left[2\gamma\sqrt{\frac{1+\lambda^2 z}{z(\lambda^2+1)}} + (\gamma-1)\right]^{-1}\frac{d\tilde{z}}{dz}\,dz, \tag{64}$$

so that the influence of the wake can be represented by a modulating function. We note that the main contribution to the integral will probably come from $z \approx 1$, i.e., the influence of the wake will be most important where the shock is not very strong. Equation (64) may therefore be approximated (with $\gamma = 5/3$) by

$$g(z) \approx \exp\int_0^3 \frac{1}{3}\frac{d\tilde{3}}{dz}\,dz \tag{65}$$

where we have written $3 = 1 - z$, and it will suffice to consider the overtaking of a fairly weak shock by its own wake. Although this has been considered in detail from a somewhat different angle by Whitham (1953) the following approximate treatment has a closer relationship with the present methods of approach.

V

INFLUENCE OF THE WAKE

Figure 6 shows the distortion of the paths of the wave elements due to the strengthening of the shock and the associated heating and movement of the

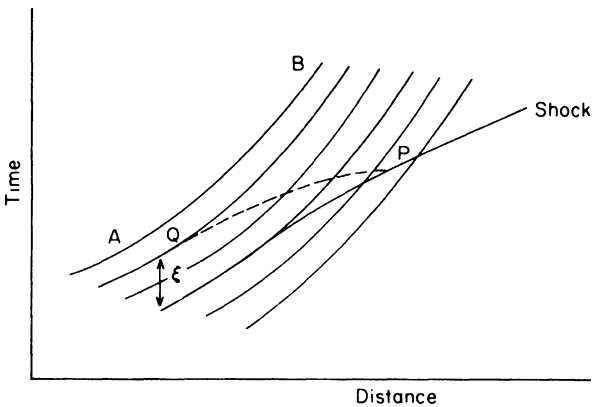


FIG. 6. An element of the wake catching up with the shock. AB = sound wave in quiet gas. QP = sound wave in disturbed gas.

fluid. AB is the path of a sound wave in the undisturbed gas. If we trace back the wave element intersecting the shock, when the latter's strength is z (point P), we see that it must ultimately (when far behind the disturbed region) coincide with one of the undisturbed wave paths, because all of the disturbances were small at one time. The problem is to locate the particular undisturbed sound wave path

$$\xi = t - \int \frac{dr}{A} = \text{constant}$$

with which the element ultimately coincides. Since we know, from the linear solution, the features of the flow far "upstream" (i.e., towards the stellar center) as a function of ξ, it should then be possible to read off the strength of the element.

It will now be convenient to think in terms of Lagrangian rather than Eulerian coordinates, i.e., we consider the catching up of the shock by the wave elements as being due to these cutting across particle paths at a greater rate than the shock does. Hence we employ the local sound speed, rather than the sum of the sound speed and the particle speed. The equation of a sound wave is then

$$t = \int \frac{ds}{v_s(s,t)} \frac{\rho_1(s)}{\rho(s,t)} + \text{constant}, \tag{66}$$

s and v_s being, respectively, the Lagrangian coordinate (the original position of a particle in the quiet gas) and the local sound speed, while ρ_1/ρ is the degree of expansion of the element. Since we are assuming that the most important wave elements are those which catch up with the shock first, it will suffice to take for the parameters in Eq. (66) their values just behind the shock on the particular particle path considered. Labeling the particles by the strength of the shock wave when it crosses them,

$$\frac{1}{v_s(s,t)}\frac{\rho_1(s)}{\rho(s,t)} \approx \frac{1}{v_{s2}(z)}\frac{\rho_1(z)}{\rho_2(z)} - \left(\frac{\rho_2(z)}{\gamma p_2(z)}\right)^{1/2}\frac{\rho_1(z)}{\rho_2(z)}. \tag{67}$$

Substituting for p_2, ρ_2 in terms of z and ρ_1 from Eqs. (43) and (44), we find on expanding to the first power in $\zeta = 1 - z$ that:

$$\frac{1}{v_s}\frac{\rho_1}{\rho} \approx \frac{1}{A(\zeta)}\left(1 - \frac{\zeta}{1+\lambda^2}\right) \tag{68}$$

where $A(\zeta)$ is the speed of sound just ahead of the shock when its strength is $1 + \zeta$.

We next determine the equation for the shock path; for this we have

$$t = \int \frac{ds}{U(s)} + \text{constant} \tag{69}$$

where $U(s)$ is the shock speed. To the same approximation as in Eq. (68), we find

$$\frac{1}{U(s)} - \frac{1}{U(\zeta)} \approx \frac{1}{A(\zeta)}\left[1 - \frac{\zeta}{2(1+\lambda^2)}\right]. \tag{70}$$

But, after a sufficiently long time the Eulerian and the Lagrangian parameters are the same, and both integrals in Eqs. (66) and (69) become

$$\int \frac{dr}{A};$$

the corresponding equations represent then sound waves in the undisturbed fluid. We can therefore write

$$t = \xi + \int \frac{ds}{v_s}\frac{\rho_1}{\rho} \qquad \text{(wave element)} \tag{71}$$

$$t = \int \frac{ds}{U(s)} \qquad \text{(shock wave)} \tag{72}$$

taking $\xi = 0$ on the shock in the linear régime. The intersection of the sound wave with the shock gives

$$\begin{aligned} \xi &= \int \frac{ds}{U(s)} - \int \frac{ds}{v_s} \frac{\rho_1}{\rho} \\ &\approx \frac{1}{2} \frac{1}{\lambda^2 + 1} \int_0^{\mathfrak{z}} \frac{\mathfrak{z}\, ds}{A(\mathfrak{z})} . \end{aligned} \tag{73}$$

Knowledge of the path $\mathfrak{z}(s)$ of the shock therefore permits the evaluation of ξ. Having located the path of the disturbance, we must now determine how its strength varies along this path; in particular, we wish to know its strength at the shock in terms of its value far "upstream."

We first establish a general result concerning the propagation of small disturbances through a medium of variable pressure, density, and temperature. Returning to Eq. (59), ignoring the term representing the following wave, and going to the limit $\mathfrak{z} = z - 1 \to 0$, we find

$$\frac{3}{2} \frac{dp}{p} + 2 \frac{d\mathfrak{z}}{\mathfrak{z}} - \frac{1}{2} \frac{d\rho}{\rho} = 0 \tag{74}$$

or

$$\frac{p^3 \mathfrak{z}^4}{\rho} = \text{constant} \tag{75}$$

as an expression relating the strength of a wavelet to the local pressure and density it encounters. For small disturbances, $\mathfrak{z}$ is simply the relative change in pressure. We can therefore generalize Eq. (75) to the case of spherical propagation by noting that, well within the star, Eq. (75) must agree with Whitham's expression (17). It will readily be seen that both Whitham's result (which only holds for a polytropic relation between p and ρ) and Eq. (75) (which only applies to the surface layers) may be regarded as special cases of the more general equation:

$$\frac{p^3 \mathfrak{z}^4 r^4}{\rho} = \text{constant} \tag{76}$$

where the relation between p and ρ need not be, and in general will not be, polytropic. We note in passing that another special case of Eq. (76), namely that of $p = \text{constant}$, $r = \text{constant}$, was derived by Chisnell.

By applying Eq. (76) to the early part of the propagation, we see that the constant is equal to

$$K[f'(\xi)]^4$$

where K may be estimated by noting that, at the shock itself $f'(\xi) = -1$, and that at the point where the blast wave degenerated

$$\zeta \sim 1 \qquad r \sim R_c \qquad p \sim p_* \qquad \rho \sim \rho_* \tag{77}$$

so that the explicit form of Eq. (76) is

$$\frac{p^3 \zeta^4 r^4}{\rho} \approx \frac{p_*^3}{\rho_*} R_c^4 [f'(\xi)]^4. \tag{78}$$

Expression (76) will be exact when applied to the increment $d\zeta$ of ζ, since this increment can itself be regarded as a wavelet of *strictly* infinitesimal strength:

$$\frac{p^3 d\zeta^4 r^4}{\rho} = \text{constant} \tag{79}$$

where p and ρ will now refer to the pressure and density as already modified by the passage of the other wavelets. On the other hand, Eq. (78) may be applied with fair accuracy to the *total* disturbance $\zeta = \zeta_i$ well within the star:

$$\zeta_i = -\left(\frac{p_i}{p_*}\right)^{-3/4} \left(\frac{\rho_i}{\rho_*}\right)^{1/4} \left(\frac{R_c}{r_i}\right) f'(\xi) \tag{80}$$

so that

$$d\zeta_i = -\left(\frac{p_i}{p_*}\right)^{-3/4} \left(\frac{\rho_i}{\rho_*}\right)^{1/4} \left(\frac{R_c}{r_i}\right) f''(\xi)\, d\xi \tag{81}$$

since, well within the star, $f'(\xi)$ varies much more rapidly than the other functions. We may now combine Eqs. (79) and (81) to find the strength $1 + d\tilde{\zeta}$ of a wavelet at the shock in the surface regions:

$$d\tilde{\zeta} = d\tilde{z} = -\left(\frac{p}{p_*}\right)^{-3/4} \left(\frac{\rho}{\rho_*}\right)^{1/4} \left(\frac{R_c}{R_*}\right) f''(\xi)\, d\xi \tag{82}$$

where, although ρ, p now refer to the already disturbed values behind the shock, we may, as a first approximation, replace them by those ahead of the shock when this is not too strong.

We now note that Eqs. (62), (65), (73), and (82), together with the relation[4] between r and s and the specification $p(r)$ and $\rho(r)$ of the variables ahead of the shock, form an implicit system for the equation of the shock path in terms of the initial conditions [given by $f'(\xi)$]. Such implicit systems are always

[4] We here choose $s = R_* - r$.

encountered when dealing with these problems, because the shock determines the motion of the fluid, which in turn reacts upon the shock. In solving such a system by iteration it appears feasible [by virtue of the form of Eq. (62)] to start by ignoring the wavelets catching up with the shock and to determine its propagation under the effects of variations in the medium alone. We may expect that this approximation will become more accurate as time progresses, and the variation of the medium becomes more rapid.

The first approximation to the initial part of the path of the strengthening shock is then simply Eq. (78), with $\xi = 0[f'(\xi) = -1]$, namely

$$\frac{p^3 \mathfrak{z}^4}{\rho} = \frac{p_*^3}{\rho_*} \left(\frac{R_c}{R_*}\right)^4 \tag{83}$$

and Eq. (82) becomes

$$\frac{d\tilde{\mathfrak{z}}}{\mathfrak{z}} = -f''(\xi)\, d\xi \tag{84}$$

so that, substituting in Eq. (65), the modulation function takes the form

$$\begin{aligned} g(z) &\approx \exp \int_0^{\xi} -f''(\xi)\, d\xi \\ &= \exp\,[-f'(\xi) - 1]. \end{aligned} \tag{85}$$

We now find ξ in terms of $\mathfrak{z}$ from Eq. (73). Using once more the first approximation (83) to the shock path to find $s = (R_* - r)$ and A as functions of $\mathfrak{z}$, and employing rough expressions such as

$$\frac{\rho}{\rho_*} \sim \left(\frac{s}{R_*}\right)^{3/2}$$

for the normalization of ρ and A, we find

$$\begin{aligned} \xi &\approx \frac{1}{2} \frac{1}{\lambda^2 + 1} \mathfrak{z}^{2/3} t_* \left(\frac{R_c}{R_*}\right)^{1/3}. \\ &\approx \frac{1}{2} \frac{1}{\lambda^2 + 1} \mathfrak{z}^{2/3} t_* \left(\frac{t_c}{t_*}\right)^{1/3} \end{aligned} \tag{86}$$

Except for the relatively unimportant "tail," the function $f'(\xi)$ can be represented by

$$f'(\xi) \approx -\exp\,(-\xi/t_c), \tag{87}$$

so that the corrected shock path [on substituting for p $(= p_1)$ in terms of ρ $(= \rho_1)$] becomes

$$\mathfrak{z} = \frac{R_c}{R_*}\left(\frac{\rho_*}{\rho_1}\right)\exp\left\{\left[\exp -\frac{1}{2(\lambda^2+1)}\left(\frac{\mathfrak{z}t_*}{t_c}\right)^{2/3}\right] - 1\right\}, \tag{88}$$

and the shock strength corresponding to the e-folding time of the exponential in square brackets is

$$\mathfrak{z} = \frac{t_c}{t_*}[2(\lambda^2+1)]^{3/2} = 0.4 \text{ (or } 0.1) \tag{89}$$

where, as before, the first value on the right refers to $E/E_* = 10^{-3}$ and the one in parenthesis to $E/E_* = 10^{-5}$.

Thus, when the shock has strengthened considerably ($\mathfrak{z} \gg 1$) we can use the asymptotic form of the modulating function, which is simply the constant value $\exp(-1)$. The principal result established in this section is, then, that the final stages of the propagation of a shock wave through a stellar atmosphere are unaffected (apart from a constant factor) by the form of the wake, and are therefore largely independent of the initial conditions. This is only true, of course, provided that the shock strength in the *absence* of wake effects would become large as the surface was approached—a result which will shortly be confirmed. We may also remark that the insensitivity to the initial conditions has also been borne out by the numerical computations.

VI

FINAL STAGES OF THE SHOCK PROPAGATION

Returning now to Eq. (59), we drop the term representing the contribution of the wake, and take the limit as $z \to \infty$, thus obtaining

$$\frac{dp_1}{p_1}\left(\frac{1}{2} + \frac{\lambda}{\sqrt{\lambda^2+1}}\right) + \frac{dz}{z}\left(\frac{1}{2} + \frac{\lambda}{\sqrt{\lambda^2+1}}\right) - \frac{1}{2}\frac{d\rho_1}{\rho_1} = 0. \tag{90}$$

Before integrating this equation, we note that the shock speed U [cf. Eq. (46)] in this limit becomes

$$U = \left[\frac{p_1 z}{\rho_1(1-\lambda^2)}\right]^{1/2}, \tag{91}$$

so that

$$2\frac{dU}{U} = \frac{dp_1}{p_1} + \frac{dz}{z} - \frac{d\rho_1}{\rho_1} \tag{92}$$

and Eq. (90) may be simplified to

$$2\frac{dU}{U}\left(\frac{1}{2}+\frac{\lambda}{\sqrt{\lambda^2+1}}\right)+\frac{d\rho_1}{\rho_1}\left(\frac{\lambda}{\sqrt{\lambda^2+1}}\right)=0, \tag{93}$$

which integrates immediately to give

$$U\propto \rho_1^{-\lambda/2\lambda+\sqrt{\lambda^2+1}} \tag{94}$$

or, since $\gamma = 5/3$ and $\lambda = 1/2$,

$$U\propto \rho_1^{-0.236}. \tag{95}$$

It is important to note that, in deriving this result, no assumption has been made regarding the dependence of density on *distance*. In other words, it would appear that there is a unique relation between the shock speed and the undisturbed density, whatever the structure of the stellar atmosphere. However, this structure will of course be relevant in translating the law (95) into one relating the shock speed and the distance.

Now, it has been possible to construct exact (similarity) solutions for strong shock waves of constant energy for certain model atmospheres, and Table I

TABLE I

SHOCK PROPAGATION LAW FOR VARIOUS ATMOSPHERES

Author	Model[a]	Wave geometry	Law
1. Burgers and Robbertse (1949)	$\rho_1\propto r^{-7/4}$	Plane	$U\propto\rho_1^{-1/7}$
2. Carrus *et al.* (1951a)	$\rho_1\propto r^{-2}$	Spherical	$U\propto\rho_1^{1/4}$
3. Carrus *et al.* (1951b)	$\rho_1\propto r^{5/2}$	Spherical	$U\propto\rho_1^{1/10}$
4. Rogers (1956)[b]	$\rho_1\propto r^{\alpha}$	Spherical	$U\propto\rho_1^{(3-\alpha)/2\alpha}$
5. Jones (1955)	$\rho_1\propto r^{6.94}$	Plane	$U\propto\rho_1^{-0.577}$
6. Jones (1955)	$\rho_1\propto r^{1.94}$	Plane	$U\propto\rho_1^{-0.775}$
7. Frank-Kamentskii and Gandel'man (1956)	$\rho_1\propto (R_*-r)^{13/4}$	Plane	$U\propto\rho_1^{-0.214}$

[a] r is the distance from the stellar center.
[b] $1.5 < \alpha < 2.5$.

has been compiled in order to test the applicability of Eq. (95) to these special cases. The difference between the result of Burgers and Robbertse (1949) and that obtained by setting $\alpha = 7/4$ in the expression derived by Rogers (1956) is due possibly to the choice of Lagrangian similarity in the former case and

Eulerian similarity in the latter. On the other hand, the distinction between plane and spherical waves might be important for model atmospheres with no defined boundary. Although Jones' results (1955) refer to an increasing density, they have been included for comparison with Eq. (95), which in principle applies to increasing as well as falling density.

Each of the solutions in the table is exactly true under the assumptions involved in its derivation, so the scatter might at first be taken to indicate the absence of any relation of the form (95), which was obtained on a fairly general but not particularly rigorous basis (we recall the neglect of the higher order waves). The close agreement with the last entry in the table might appear fortuitous were it not for the fact that this is the only similarity solution which has been derived for an atmosphere with a definite radius; moreover, the law is of just the form assumed by a polytropic star at its boundary (the value $n = 13/4$ was in fact chosen to be representative of a radiative atmosphere).

We might expect deviations from the law (95) from three sources:

(1) The large explosive energy which characterizes entries 2, 3, and 4 would make $t_c \sim t_*$ in Eq. (89). This would imply a continual interaction of the initial conditions (communicated via the wake) with the shock propagation, thus making the neglect of the final wake term in Eq. (59) unjustifiable.

(2) The relatively slow variation of the density of the medium ahead of the shock would, even on the basis of Eq. (95), lead to such a slow propagation of the shock that there would be time for the higher order waves (which *do* depend on the explicit form of the density-distance relation) to influence its behavior.

(3) The spherical terms in the hydrodynamical equations will become important for a star with no definite boundary; such terms will tend to decelerate the shock.

By introducing a finite boundary relating the similarity variable to the final stages of the propagation (i.e., by measuring distances from the surface), Frank-Kamentskii and Gandel'man (1956) disposed of all influences (1), (2), and (3) at a single blow, so that this model and that of Chisnell are strictly capable of comparison; their agreement would indicate that Eq. (95) can be applied directly to polytropic atmospheres.

VII

NUMERICAL RESULTS

Before proceeding on the basis of the above conclusions, it was decided to obtain an independent check on Eq. (95) by performing actual numerical integrations of the partial differential equations of gas dynamics on the Manchester

Mercury electronic computer. Two fairly different polytropic laws were employed; one represented the "adiabatic" atmosphere

$$\rho_1 \propto s^{3/2}, \tag{96}$$

and the other the "radiative" atmosphere

$$\rho_1 \propto s^3, \tag{97}$$

this law holding when the main opacity source is electron scattering. It does not differ appreciably, however, from the law

$$\rho_1 \propto s^{13/4} \tag{98}$$

which applies when photoelectric absorption is predominant. The pressure laws corresponding to Eqs. (96) and (97) were derived directly from the equation of hydrostatic equilibrium under gravity.

The method of Goldstine and Von Neumann (1955) was used for determining the new shock position after each time step. This technique depends upon matching the flow variables derived from the Rankine-Hugoniot equations with those predicted by the hydrodynamics of the wake. It thus permits a precise location of the front at any instant, and is therefore preferable to the method of artificial viscosity (Richtmyer, 1957) for testing the propagation law (95).

Three significant properties of the shock propagation and the associated flow field were brought to light by these computations:

(1) The shock strengthens continuously and its final propagation is practically unaffected by changes in starting procedure; in *both* models (96) and (97) the shock was found to obey the relation[5]

$$U \propto \rho_1^{-0.226} \tag{99}$$

as it approached the surface.

(2) At the instant of shock emergence at the surface, the net particle displacement (Eulerian coordinate) is very nearly proportional to its original distance from the surface (Lagrangian coordinate). This is shown in Fig. 7.

(3) On plotting the (apparently only indirectly related) laws governing (a) the variation of shock speed with the distance of the shock from the surface (i.e., as a time-development) and (b) the variation of the particle speed with distance from the surface at the instant of shock emergence (i.e., as a "snapshot") one

[5] The plot of the numerical values of log U against those of log ρ_1 is indistinguishable from a straight line; consequently we have not reproduced it here.

finds practically identical results. This mirroring of the properties of the shock at various instants in the properties of the fluid at the single instant of emergence also applies to the pressure and density.

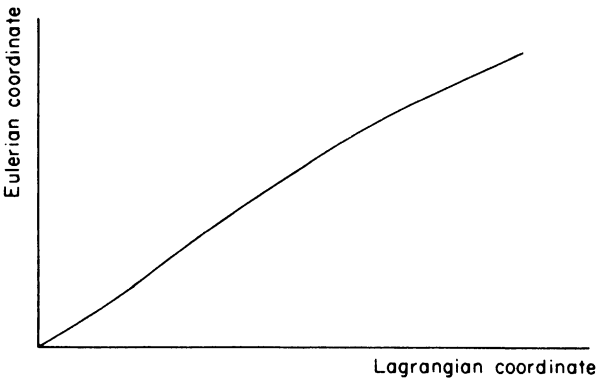


FIG. 7. The parameters are plotted at the instant of shock emergence. In this numerical run the wake was considered uniform initially. No scales are given, since these depend upon the density-distance relation in the quiet gas; the slope of the linear approximant to the curve is $k'' - [-\frac{3}{4}/(1-l)] + 1$, l being given by Eq. (110).

We thus see that the exact numerical solution agrees surprisingly well with Chisnell's result (95) for the two special cases tested, and it seems quite likely that Eq. (99) can be applied to any polytropic variation of density etc. near the surface.

A clue to the reason for the accuracy of Eq. (95), which is after all only based upon a first order theory, is afforded by the numerical result (2) above. To see this, we first note that, in the first approximation, each particle retains unchanged the velocity transferred to it by the shock. We can therefore construct the particle paths as shown in Fig. 8.

The Eulerian coordinate is[6]

$$R(s, t) = s - u(s)\,(t - t_s) \tag{100}$$

where t_s is the time at which the shock passes over the particle whose distance from the surface is initially s and $u(s)$ is the velocity of that particle. But, for a strong shock,

$$u(s) \propto U(s) \propto s^l \tag{101}$$

[6] We measure R from the surface.

where l is a negative index. Hence, at the time of emergence t_0,

$$R(s, t_0) = s + ks^l(t_0 - t_s). \tag{102}$$

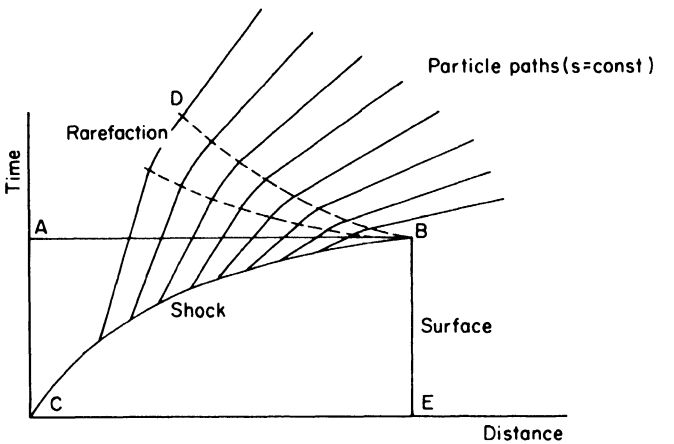


FIG. 8. The final stages of the shock propagation. The particle velocity varies as s^l both along BA and above BD, l being the coefficient in the shock-speed distance relation.

But the time $(t_0 - t_s)$ for the shock to reach the surface is obtained by integrating the equation of the shock path:

$$U(s) = -\frac{dR}{dt} = -\frac{ds}{dt} \propto s^l, \tag{103}$$

since $s = R$ at the shock front. Hence,

$$(t_0 - t_s) \propto s^{1-l} \tag{104}$$

and (102) becomes

$$R(s,t_0) = s + k's = k''s. \tag{105}$$

At the time of emergence the Eulerian and the Lagrangian coordinates are thus proportional. We can therefore regard any deviations from this proportionality as a measure of the importance of the influence of the higher order interactions (in particular, the interaction of the first reflected wave with the flow field). Result (2) shows indeed that these higher order effects are small, at any rate before the shock reaches the surface.

Moreover, in view of the practical constancy of the velocity of a given particle, we see that the shock speed-distance relation is exactly recorded in the "snap-

shot" of the velocity profile at the instant of emergence (the particle speed bearing a constant ratio to the shock speed for a strong shock). Hence conclusion (3) above really follows from (1) and (2). Also, the constancy (in space) of $\partial R/\partial s$ at the instant of emergence, together with the constancy (in time) of the entropy at a given particle once the shock has crossed it, permit the extension of statement (3) to the density and pressure.

We thus see that the variation of parameters at the instant of shock emergence is completely determined once the velocity-density law (99) has been established. Thus, if the undisturbed density is

$$\rho_1 \propto s^n \tag{106}$$

then, at the instant of emergence,[7]

$$\begin{aligned} u &= as^l \\ p &= bs^m \\ \rho &= cs^n = (k'')^{-1}\rho_1 \end{aligned} \tag{107}$$

$$\tfrac{1}{2}(m - n) = l \tag{108}$$

$$b = \tfrac{1}{3}a^2c(4k'') \tag{109}$$

$$l = -0.23n \tag{110}$$

where the relations (108) and (109) are necessitated by the fact that $p/\rho u^2$ must be finite and equal to 1/3 (for $\gamma = 5/3$) at the front itself. For the "adiabatic" model atmosphere

$$l = -0.34 \qquad m = 0.82 \qquad n = 1.5 \tag{111}$$

while the constants a, b, c may be deduced by tracing out the region ABC of Fig. 7 and using the equation for the shock path (to be given below).

It must be stressed that the above relations hold only near the surface of the star, where the shock has strengthened appreciably. However, it is precisely the behavior in this region which determines the speed of ejection of material from the surface. Similar results to Eqs. (107) above were obtained by Frank-Kamentskii and Gandel'man (1956) on the basis of their similarity propagation, but it is comforting that the exact numerical integration of the flow equations assures us that the final stages of the propagation do indeed depend upon the atmospheric properties rather than on the initial conditions.

[7] The factor 4 in Eq. (109) is the compression ratio across the shock, while k'' is the factor appearing in Eq. (105); it is readily evaluated as $1 - \frac{3}{4}/(1 - l)$ for $\gamma = 5/3$.

VIII

MOTION OF MATERIAL AWAY FROM THE STELLAR SURFACE

Although a detailed description of the motion of the material after the shock wave has penetrated the surface is beyond the scope of this article, the author has been able to trace in an approximate manner the flow of material away from the stellar surface, the separation of the permanently ejected material from that which returns under gravity (it is found that the shell features appear in the density profile at distances of the order of $100R_{\odot}$), and the subsequent impact of the infalling material with the central star. Since the observations are made on the ejected material and not on the shock front, we can only check the shock wave theory of novae indirectly. Hence an outline will be given of the dynamical behavior of the ejected gases according to the shock wave theory, and later on a brief reference will be made to the optical consequences.

We note from Eqs. (107) and (111) that both the gas velocity and the temperature become infinite at the surface at the instant it is penetrated by the shock. Hence, the motion must thereafter still be followed analytically[8]—at least for the outermost particles. It turns out, however, that the influence of gravity on these high speed particles can be neglected at first, and under these circumstances the motion of the gases from the initial conditions (107) obeys, very nearly, a similarity law.

The most interesting result is that the variation of velocity over the particles as they move away from the surface (see the region above BD in Fig. 8) is precisely the same as that imparted to them by the shock just prior to ejection, i.e., both are power laws with the same index l. The velocity itself will of course increase since the gases are moving under an outwardly directed pressure gradient. At the moment the shock passes through the surface (BE in Fig. 8) a rarefaction wave moves inward, reducing the temperature at the outermost particle from infinity to zero, and reversing the previous negative temperature gradient into a positive one. The pressure gradient, however, remains positive throughout. After passing through this wave the velocity of each particle has increased by a factor of about 2.5. It is interesting to note that this factor is greater than that obtained by assuming that the whole of the thermal energy at a given particle becomes converted into kinetic energy. This is because energy is continually flowing outwards as the rarefaction travels inwards.

Having gained this energy, the outermost particles will escape from the gravitational field of the star, while the inner ones will return. However, more

[8] i.e., cannot be determined numerically.

thermal energy will be generated as the falling particles undergo recompression, and this in its turn will be propagated upwards—permitting a further escape of the (new) outermost particles. This is illustrated in Fig. 9, in which all but the very outermost particles (where the infinities occur) have been followed numerically.

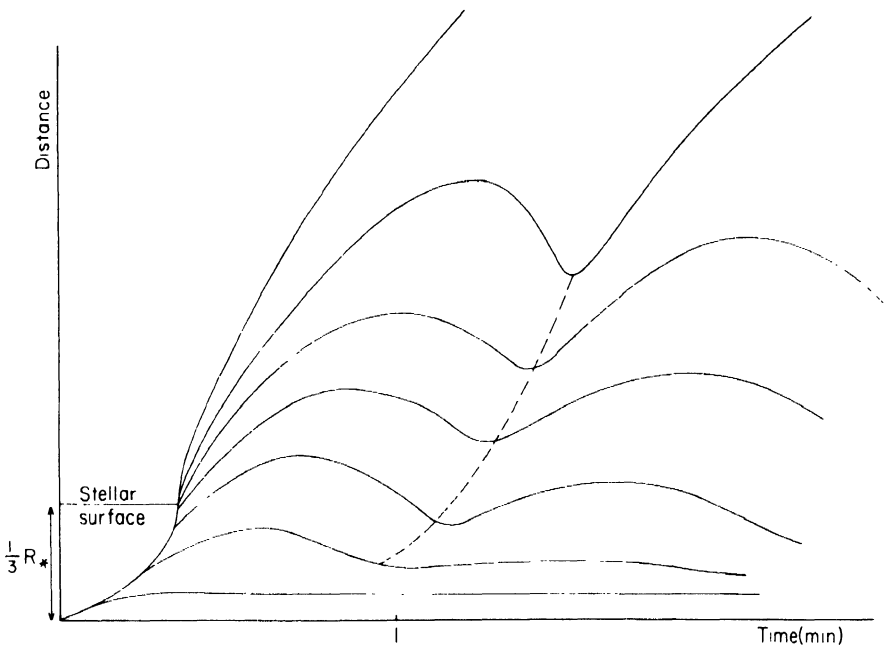


FIG. 9. The motion of the shocked gases under gravity. The full curves are particle paths, while the dashed curve may represent the formation of a new shock.

The model used in obtaining the results of Fig. 9 was somewhat artificial in that, in order to keep the range of integration within reasonable bounds, the atmosphere was replaced at some depth by a rigid wall. Hence, in reality, the infalling particles might be cushioned rather more than the diagram would indicate, so it is not certain that the later ejections would contain very much material. Consequently, we shall calculate a *lower* limit for the mass ejected (though this should be a reasonable estimate for the actual mass) by simply estimating the total mass lying outside that particle which achieves escape velocity after it has been accelerated through the rarefaction wave of Fig. 8.

IX

ESTIMATION OF THE MASS AND ENERGY OF THE ESCAPING MATERIAL

It will first be necessary to integrate the shock propagation equation (61) to determine the original density at a particle in terms of the velocity imparted to it by the shock. We shall allow for the wake by carrying out the iteration procedure to first order, i.e., by integrating the shock equation without the wake term [Eq. (63)] and then applying the correction factor $\exp(-1)$ to the (strong) shock in accordance with Eq. (62).

It does not appear possible to integrate Eq. (63) directly. However, substituting $\gamma = 5/3$, $\lambda = 1/2$ we find that, when the shock is weak,

$$-\frac{1}{\rho_1}\frac{d\rho_1}{dz} = \frac{1}{z-1} - 0.067 + \text{powers of } (z-1), \qquad 2 > z > 1 \tag{112}$$

while for large values of the shock strength

$$-\frac{1}{\rho_1}\frac{d\rho_1}{dz} = \frac{0.88}{z} + \frac{1.07}{z^2} + \text{higher powers of } \left(\frac{4}{z}\right), \qquad z > 4. \tag{113}$$

In the intermediate range of "fairly strong" shocks, we can expand the slowly varying square root in powers of $1 - (4/z)$, giving

$$-\frac{1}{\rho_1}\frac{d\rho_1}{dz} = \frac{1.177}{z-1} + \frac{0.110[1-(4/z)]}{z-1} - \frac{0.360}{\frac{1}{4}+z} - \frac{0.068[1-(4/z)]}{\frac{1}{4}+z} \tag{114}$$

$$+ \text{higher powers of } [1-(4/z)], \qquad z > 2.$$

The different expansions (112), (114), (113) are useful in the intervals $1 < z < 2$, $2 < z < 8$, $8 < z$ respectively; in fact, even when the higher order terms are ignored completely the expressions are accurate to within a few percent. More surprising still, if the weak and strong shock approximations are extrapolated to intersect one another (at $z = 3.4$) we find that the "empirical formulas"

$$-\frac{1}{\rho_1}\frac{d\rho_1}{dz} = \frac{1}{z-1} - 0.067, \qquad 1 < z < 3.4 \tag{115}$$

$$-\frac{1}{\rho_1}\frac{d\rho_1}{dz} = \frac{0.88}{z} + \frac{1.07}{z^2}, \qquad 3.4 < z \tag{116}$$

represent the function on the right of Eq. (63) over the whole range of z with a maximum error of only 10%, so that the error committed in representing

the integral of Eq. (63) by the integral of Eqs. (115), (116) will be less than this. In view of the fact that we only propose to allow for the wake to first order, a closer approximation to the integral of Eq. (63) would only give a spurious appearance of precision.

Equations (115) and (116) are readily integrated to give:

$$-\log_e \rho_1/\rho_* = \log_e(z-1) - 0.067(z-1) + \text{const.}, \quad 1 < z < 3.4 \tag{117}$$

$$-\log_e \rho_1/\rho_* = 0.88 \log_e z - 1.07/z + \text{const.}, \quad 3.4 < z \tag{118}$$

where the constant central density ρ_* has been separated, for convenience, from the integration constants.

Recalling that, when the shock is weak [cf. Eq. (88)],

$$\lim_{z\to 1} \frac{\rho_1}{\rho_*} = \frac{R_c}{R_*} \frac{1}{z-1} \tag{119}$$

or

$$-\log_e \frac{\rho_1}{\rho_*} \to \log_e (z-1) + \log_e \frac{R_*}{R_c}, \tag{120}$$

we see that Eq. (117) becomes

$$-\log_e \frac{\rho_1}{\rho_*} = \log_e (z-1) - 0.067\,(z-1) + \log_e \frac{R_*}{R_c}, \quad z < 3.4 \tag{121}$$

while the integration constant in Eq. (118) is obtained by requiring the continuity of ρ_1 at $z = 3.4$:

$$-\log_e \frac{\rho_1}{\rho_*} - 0.88 \log_e z = -\frac{1.07}{z} + \log_e \frac{R_*}{R_c} - 0.047, \quad 3.4 < z. \tag{122}$$

We note that both the density and its derivative are now continuous. It only remains to correct for the deceleration of the shock by the wake. We shall henceforth be concerned with shock strengths in excess of 3.4, which is so much greater than the e-folding strength of 0.1 to 0.4 [cf. Eq. (89)] that we may write $g(z) = \exp(-1)$ in Eq. (62). Then the corrected form of Eq. (122) is

$$-\log_e \frac{\rho_1}{\rho_*} = 0.88 \log_e z - \frac{1.07}{z} + \log_e \frac{R_*}{R_c} + 0.953. \tag{123}$$

Substituting the approximate relation

$$\frac{p_1}{p_*}\frac{\rho_*}{\rho_1} \approx \left(\frac{\rho_1}{\rho_*}\right)^{2/3} \tag{124}$$

in Eq. (45), we find for the speed of the gas just behind the shock

$$u = \frac{A_*}{\sqrt{\gamma}} \left(\frac{\rho_1}{\rho_*}\right)^{1/3} (z - 1) \sqrt{\frac{3}{1 + 4z}} \tag{125}$$

where, as before, A_* is the speed of sound at the stellar center. But the central speed of sound and the escape speed at the surface only differ by a factor of order unity. In the case $\gamma = 2$, for example, the polytropic equation can be integrated directly, giving

$$v_{\text{esc}} = \sqrt{2}\, A_* \tag{126}$$

and in the absence of knowledge of the structure of the pre-nova we shall take this as an estimate for the actual ratio. Hence:

$$\log_e u/v_{\text{esc}} = -0.053 + \frac{1}{3} \log_e \frac{\rho_1}{\rho_*} + \log_e (z - 1) - \frac{1}{2} \log_e (1 + 4z). \tag{127}$$

This is simply the velocity imparted directly by the shock and thus refers to the region ABC in Fig. 8. However, the escape potentiality depends on the velocity after acceleration through the rarefaction wave (i.e., when the particle emerges above BD in Fig. 8). Preliminary calculations suggest that each particle increases its speed by a factor of about 2.5. Then, denoting this "final" speed by u_f, Eq. (127) gives

$$\log_e \frac{u_f}{v_{\text{esc}}} = 0.863 + \frac{1}{3} \log_e \frac{\rho_1}{\rho_*} + \log_e (z - 1) - \frac{1}{2} \log_e (1 + 4z). \tag{128}$$

The ejected mass is computed by determining the total amount of material lying outside the particle for which

$$u_f = v_{\text{esc}}. \tag{129}$$

It turns out that the value of z which satisfies this equation is always sufficiently large to permit the use of the limiting forms of Eqs. (123) and (128) appropriate to $z \gg 1$. Substituting from Eqs. (123) and (129) into Eq. (128) we find that the shock strength at the particle which just escapes is

$$\log_e z = 0.72 - 0.54 \log_e \frac{E}{E_*} \tag{130}$$

where we have used Eq. (7) to relate the range of the explosion to its energy.

Noting that the mass lying outside a given particle is related to the undisturbed density by the approximate expression

$$\frac{m}{M_*} \approx \left(\frac{\rho_1}{\rho_*}\right)^{5/3}, \tag{131}$$

we find from Eqs. (130) and (123) that the total amount of material which escapes is given by

$$-\log_e \frac{M_s}{M_*} = 2.64 - 1.34 \log_e \frac{E}{E_*}. \tag{132}$$

We may also determine the kinetic energy of the escaping material by noting that the velocity at infinity is

$$u_\infty^2 = u_f^2 - v_{esc}^2 \tag{133}$$

and that, since the radius of the observed shell is about one thousand times that of the star, we may equate u_∞ with the observed velocity. From Eqs. (123), (128), (131), and (132) we find, for the kinetic energy of the shell,

$$E_s = \int_0^{M_s} (u_f^2 - v_{esc}^2)\, dm = 0.40\, M_s v_{esc}^2, \tag{134}$$

the factor 0.40 being independent of the value of the ratio E/E_*. But we know that, since the thermal and potential energies of the star are of the same order,

$$E_* \sim \frac{GM^*}{R_*} = \frac{1}{2} v_{esc}^2 M_* \tag{135}$$

so, combining Eqs. (134) and (135), we find that

$$\frac{E_s}{E_*} \approx \frac{M_s}{M_*} \tag{136}$$

a result which is borne out by the observations (see Introduction).

We are now in a position to infer from the observations the energy which must have been originally liberated at the stellar center. From Eqs. (132) and (136), we find

$$\frac{E}{E_*} \approx 7.2 \left(\frac{E_s}{E_*}\right)^{0.75} \tag{137}$$

or, recalling from the Introduction that $E_s/E_* \sim 10^{-5}$,

$$\frac{E}{E_*} \approx 1.29 \times 10^{-3} \tag{138}$$

so that only 1% of the energy released at the center finally appears as the energy of the ejected gases. The *thermal* energy of the escaping material is negligible because of its high degree of expansion.

It would therefore seem, surprisingly perhaps, that the shock wave is a rather inefficient means of permitting the star to rid itself of excess energy via mass ejection. The reason for this is that the increase of shock speed with falling density [cf. Eq. (95)] is not sufficiently rapid (despite its infinity at the surface) to prevent the deposition of the major part of the energy within the deeper layers which have no chance of escaping. Such layers will be simply expanded on account of the irreversible heating produced by the passage of the shock.

X

EXPANDED ATMOSPHERE

We have seen that the majority of the particles disturbed by the shock will not escape; however, they will not return to the original stellar surface but will settle at some distance above it. We shall now calculate the distribution of mass with height in this extended gas when the main disturbance has subsided i.e., after the time (several minutes only) required for a sound wave to cross and re-cross the disturbed layers several times.

During the expansion the pressure and density of a given particle are related by the polytropic law

$$p = k\rho^{\gamma}, \tag{139}$$

but k varies from one particle to another in accordance with the variation in the strength of the shock when it passed over the particles considered:

$$k = \frac{p_2(z)}{[\rho_2(z)]^{\gamma}} = \frac{zp_1(z)}{[4\rho_1(z)]^{\gamma}} = \frac{z}{4^{\gamma}} k_0 \tag{140}$$

where we have used the form of Eq. (44) appropriate to large values of z, since only for these is the irreversible dissipation—and hence the final expansion—appreciable. Here k_0 represents the adiabatic constant for the undisturbed star. We can now express k as a function of m, the mass lying above the particle considered, by using Eq. (123) (with $z \gg 1$) and Eq. (131):

$$k(m) = \frac{0.34}{4^{\gamma}} k_0 \left(\frac{m}{M_*}\right)^{-0.68} \left(\frac{E}{E_*}\right)^{0.38}. \tag{141}$$

For heights h above the stellar surface which are small compared with the radius of the star, we can write for the equation of hydrostatic equilibrium

$$4\pi R_*^2 p = gm \tag{142}$$

where the pressure p is given by

$$p = k(m)\,\rho^\gamma = k(m)\left[-\frac{1}{4\pi R_*^2}\frac{dm}{dh}\right]^\gamma . \tag{143}$$

These equations are readily integrated to give

$$h = -\frac{1}{4\pi R_*^2}\int_0^m \left[-\frac{k(m)\,4\pi R_*^2}{gm}\right]^{1/\gamma} dm. \tag{144}$$

In evaluating this integral, it is convenient to note the equality

$$\frac{4\pi R_*^2 k_0}{gM_*} = \frac{1}{\rho_*^\gamma}\frac{6}{\gamma}\left[\left(\frac{A_*}{v_{\text{esc}}}\right)^2 \frac{\rho_*}{\bar{\rho}}\right] \tag{145}$$

where $\bar{\rho}$ is the average density; this equation has been obtained by expressing k_0 in terms of the central density and pressure. The quantity in square brackets will be of order unity; it can be calculated exactly for the polytropic star with index $\gamma = 2$ from

$$\frac{A_*^2}{v_{\text{esc}}^2} = \frac{1}{2} \qquad \frac{\rho^*}{\bar{\rho}} = \frac{\pi^2}{3} . \tag{146}$$

We may therefore adopt the rough value

$$\frac{A_*^2}{v_{\text{esc}}^2}\frac{\rho^*}{\bar{\rho}} \approx \frac{3}{2}. \tag{147}$$

From Eqs. (141), (144), and (145) we find that, very nearly,

$$h = -0.040 R_* \left(\log_e \frac{m}{m_0}\right)\left(\frac{E}{E_*}\right)^{0.23} \tag{148}$$

where m_0 is the total quantity of material above the stellar surface. But we see immediately that this is simply the law corresponding to an *isothermal* atmosphere with a scale height:

$$L = 0.040 R_* \left(\frac{E}{E_*}\right)^{0.23} . \tag{149}$$

Substituting the value (138) we have inferred for E/E_*, this gives

$$L = 0.0086R_* \tag{150}$$

which corresponds to a temperature of[9]

$$T = 0.0086R_* \frac{m_H g}{k} \tag{151}$$

assuming the atmosphere to be mainly hydrogen. Taking the mass and radius of the star as $1M_\odot$ and $1/10R_\odot$ respectively, we find

$$L = 6.0 \times 10^2 \text{ km} \tag{152}$$

$$T = 2.0 \times 10^6 \text{ °K.} \tag{153}$$

To find the total amount m_0 of material in this isothermal "atmosphere" we note that the limiting form of Eq. (123) used in deriving Eq. (148) holds fairly accurately for $z > 4$, so we shall regard this value as defining the lower limit of this atmosphere. Substituting $z = 4$ directly in Eq. (123) and using Eq. (131), we find for the total mass in the isothermal atmosphere

$$m_0 = 1.04 \times 10^{-3} M_*. \tag{154}$$

We can also define a characteristic density for the lower regions of this atmosphere from the expression

$$\rho = \frac{m_0}{4\pi R_*^2 L} \tag{155}$$

which leads to $\rho = 56$ gm/cc. Finally, from the mass and temperature of the atmosphere, we can calculate its thermal and gravitational energies; these both work out to be about 0.5×10^{45} ergs, or a total of ten times the kinetic energy of the ejected shell.

XI

CONCLUSION

We are now in a position to review the mechanical consequences of the release of an energy of $\sim 10^{46}$ ergs at the center of the pre-nova. The initial blast wave will weaken when it has expanded to one-tenth of the stellar radius, will then propagate as a sound wave and, on approaching the surface layers, will begin to strengthen again when the density has fallen to one-tenth of its central value. The major part of this energy is deposited when the shock is

[9] The k in Eq. (151) represents Boltzmann's constant.

only moderately strong ($1 < z < 4$), is retained by the star (possibly in the form of the rapid oscillations observed by Walker, 1957), and does not appear to be of direct significance for the "outburst" itself.

Only 10^{45} ergs are delivered to those particles crossed by the shock when its strength is appreciable ($z > 4$), and, of these, the majority (nine-tenths) will ultimately come to rest as members of an expanded isothermal "atmosphere." A mere 10^{44} ergs are carried by the shock into the outermost fringe of the star to provide the impetus required for permanent escape. The shock strength necessary for this is given [Eqs. (130) and (138)] by $z > 75$ corresponding to a Mach number of 7.7. However, we note that we have only considered the ejection of material directly by the shock, whereas the numerical calculations (see Section VIII) indicate some further ejection due to the momentum propagated upwards as the lower layers settle to form the expanded atmosphere. Nevertheless, it appears that the main part of the 10^{45} ergs contained in this atmosphere is retained as its thermal and gravitational support energy, and that the 10^{44} ergs (or the 10^{28} gm) of the ejected material cannot be increased significantly on a purely hydrodynamical model. In any case, the whole of the ejection will take place in a time which is short (a matter of minutes) compared with the observed development time of a nova; thus, one cannot attribute the formation of the post-maximum shells (at intervals of days or even weeks) to the successive ejections shown in Fig. 9.

It is not completely clear at present whether the permanently ejected material of the above model is to be identified with the pre-maximum or the principal absorption spectrum. A discussion of the optical properties of the ejected gases is beyond the scope of this article, but the author (Hazlehurst, 1959) has carried through such a treatment, and finds that the large dispersion of velocities produced by the shock will be reflected in a smoothly falling displacement of the absorption lines, simply because one is observing successively deeper layers. Precisely this behavior was shown by the pre-maximum spectrum of Nova Herculis, and the fall from 1000 km/sec to 150 km/sec in 5 days is about that which would be expected on the present model. We recall that the present treatment assumes $1 M_{\odot}$ for the mass of the nova, so that the previous conclusions that this deceleration indicates a very high mass (Vorontsov-Velyaminov, 1953) would seem quite unwarranted. A further check upon the plausibility of the present model is the agreement of the rate of rise of the photosphere (which can be calculated for the same flow field as that used in tracing the absorption behavior) with that observed.

No reference has so far been made to the effects of radiation. Radiation pressure is relatively small (even at the high temperatures envisaged) compared with the gas pressure—or, more strictly, its influence is restricted to a very small and short lived region. However, the influences of radiative cooling and radiative

heat transfer require careful consideration, but it turns out that both of these may be neglected because of the large bulk of the disturbed atmospheric regions, and the high speed of propagation of sound waves. We note in passing, however, that if the main disturbance had been confined to the outermost part of the atmosphere (as is presumed to be the case in the shock wave theory of the light curve of e.g. BW Vulpeculae) the cooling effects would render the propagation isothermal rather than adiabatic. The propagation of such isothermal waves has been studied by Kushwaha and Odgers (1960) using shape-preserving solutions.

After the shock wave has penetrated the surface, the hydrodynamical readjustments and the formation of the expanded atmosphere take place in a time which is too short for appreciable loss of radiation. However, once the layering is complete, cooling will begin in the upper layers and it would seem that the only admissible final state is that which is compatible with a constant flux of radiant energy—which presumably implies a return of the nova to its original form with a surface temperature of 50,000°. In this connection it is perhaps significant to note that the total radiative energy release of a nova is about equal to the 10^{45} ergs which we have found to be stored in the million-degree atmosphere. Although it is tempting to identify the two energies, and to regard the radiation of the nova as being simply that which is released as the atmosphere cools and contracts, it is not yet clear whether the manner in which this cooling might be expected to develop is consonant with the observations. Can one, for instance, regard the post-maximum formation of shells as being that method of cooling which is appropriate to a gas at 10^6 deg and a relatively high density? (One notes that an isothermal atmosphere would be normally stable against convection.)

Although there is certainly sufficient energy available for the production of further shells, the speed of thermal motion at 10^6 deg is only one-tenth the observed velocity of the shells. Nevertheless, the surges from the solar chromosphere exceed the speed of the local thermal motions by factors of ten or more (although of course the difference in the densities of the systems we are comparing will lead to differences in the mechanism). The problems in both cases would seem to be stability ones, and the magnetic fields could of course play just as important a rôle in novae as they appear to do in the solar phenomena. However, simple mechanisms—such as that of "field winding"—would seem to fail for the acceleration of bulk material to high speeds, since in such models the instability occurs (if at all) only when the magnetic pressure is of the order of the gas pressure, which (being related to the thermal motions) we have seen to be inadequate. One could, of course, appeal again to the accelerating effect of the steep density gradient (now exponential) upon further shock waves, but such speculations are not in the spirit of the present investiga-

tion, which has been to treat, as far as is possible, the development of a physical system with specified initial and boundary conditions.

ACKNOWLEDGMENTS

The author benefited from discussions with Prof. Z. Kopal, Dr. F. D. Kahn, and Dr. W. L. W. Sargent during the initial stages of the work at Manchester University, and is grateful to Prof. S. Chandrasekhar for enabling him to conclude it at Yerkes Observatory; support was provided by the D.S.I.R. and the U.S. Air Force. He records his thanks to Mrs. Gail Moore for her care in typing copies of the manuscript.

APPENDIX

A NOTE ON THE SIMILARITY SOLUTIONS OF TABLE 1

A similarity solution is one in which the development of the flow can be described in terms of a single parameter which is a product of a distance and a power of the time. It is special in the sense that the initial and boundary conditions cannot (in principal) be assigned arbitrarily. The former of these two restrictions may not be too severe, since experimental results (Taylor, 1950) and empirical numerical work (Hain and von Hoerner, 1954) indicate that, presumably as a consequence of the irreversibility introduced by the shock, flow systems of the type we have been considering ultimately tend to the similarity form provided that the boundary conditions compatible with this form are continually applied.

It is unfortunately this last reservation which prevents a thorough application of similarity methods to novae, although it is possible (provided the original energy release occurs in a region whose linear dimensions are small compared with R_0) to discuss the initial stages in terms of the Taylor variable $r/t^{2/5}$ and the final propagation by using the parameter $(R_* - r)/t^K$ adopted by Frank-Kamentskii and Gandel'man (1956). However, in the latter case the energy integral does not converge and has to be arbitrarily cut off.

Solutions corresponding to infinite stars ($\rho_1 \propto r^{-\alpha}$) have been constructed by using a similarity variable r/t^{ψ}, but the total energy $E_t(t)$ and the stellar energy $E_*(t)$ within the shock sphere at time t are restricted to the forms

$$E_t(t) = At^{\beta(\alpha,\psi)}$$

$$E_*(t) = Bt^{\gamma(\alpha,\psi)}$$

where β, γ are linear functions of α and ψ.

Since $E_t = E_* + E$, where E is the (constant) explosive energy, the solutions are limited to:

(1) $E \gg E_*$ and $\beta = 0$ (Rogers, 1956). This could only apply to a supernova, but the consequent relation between α and ψ may relevently be used in making entry four of Table 1 for comparison with the general law of Eq. (95).

(2) $\beta = \gamma = 0$ (Carrus *et al.*, 1951b; Rogers 1956). Here E and E_* may have arbitrary relative values, but the above equation can only be satisfied for the model $\alpha = 2.5$.

(3) $E = 0$ (exactly). The consequences of assuming that this case is equivalent to $E \ll E_*$ have been investigated by Kopal (1954). It is found that by setting $A = B$ and $\beta = \gamma$ (and neglecting the finite thermal energy of the central "bubble") even flows of high Mach number can be constructed. However, since these would imply $E_* \sim E$ (in contradiction with the original assumption) it must be concluded that there are no solutions for $E \ll E_*(\alpha \neq 2.5)$ other than the trivial one pertaining to $E = 0$.

The entries 1, 5, 6 in Table 1 represent similarity solutions of the equations of one-dimensional motion; r is then measured from an arbitrary point.

Interesting alternative approaches to the problem of shock propagation in a variable medium may be found in Schatzman (1949) and Lebedinsky (1952). We also draw the reader's attention to the shape-preserving isothermal solution of Kushwaha and Odgers (1960); the necessary density-distance relation is not determined, however.

References

Burgers, J. M., and Robbertse, W. P., 1949. *Proc. Acad. Sci. Amst.* **52**, 958.
Carrus, P. A., Fox, P. A., Haas, F., and Kopal, Z., 1951a. *Ap. J.* **113**, 193.
Carrus, P. A., Fox, P. A., Haas, F., and Kopal, Z., 1951b. *Ap. J.* **113**, 496.
Chisnell, R. F., 1955. *Proc. Roy. Soc.* **A232**, 350.
Frank-Kamentskii, D. A., and Gandel'man, G. M., 1956. *Soviet Phys.—Doklady* **1**, 223.
Goldstine, H. H., and von Neumann, J., 1955. *Commun. Pure Appl. Math.* **8**, 327.
Hain, K., and von Hoerner, S., 1954. *Z. Naturf.* **9a**, 993.
Hazlehurst, J., 1959. Ph. D. Thesis, University of Manchester.
Jones, C. W., 1955. *Proc. Roy. Soc.* **A228**, 82.
Kopal, Z., 1954. *Ap. J.* **120**, 159.
Kushwaha, R. S., and Odgers, G. J., 1960. *Publ. Dom. Astroph. Obs. Victoria* **11**, No. 6, 185.
Lebedinsky, A. I., 1952. *Astr. Zhurn.* **29**, 135.
Ono, Y., Sakashita, S., and Yamazaki, H., 1960. *Progr. Theoret. Phys.* (*Kyoto*) **23**, 294.
Payne-Gaposchkin, C., and Whipple, F. L., 1936. *Harv. Circ.* No. 413.
Richtmyer, R. D., 1957. "Difference Methods for Initial Value Problems." Interscience, New York.

Rogers, M. H., 1956. *Proc. Roy. Soc.* **A235**, 120.
Sakurai, A., 1956. *J. Fluid Mech.* **1**, 436.
Sayer, A. R., 1948. *Harv. Ann.* **105**, 21.
Schatzman, E., 1949. *Ann. d'Ap.* **12**, 281.
Simon, R., 1955. *Ann. d'Ap.* **18**, 92.
Taylor, G. I., 1950. *Proc. Roy. Soc.* **A201**, 159.
Vorontsov-Velyaminov, B. A., 1953. "Gasnebel und Neue Sterne," p. 362. Kultur und Fortschritt, Berlin.
Walker, M. F., 1957. *I.A.U. Symp.* No. 3, p. 46.
Whitham, G. B., 1953. *Commun. Pure Appl. Math.* **6**, 397.
Whitham, G. B., 1958. *J. Fluid Mech.* **4**, 337.

The Properties and Problems of T Tauri Stars and Related Objects

G. H. HERBIG
Lick Observatory,
University of California, Mt. Hamilton, California

I. Introduction 47
A. The T Tauri Stars 48
B. Evidence Bearing upon the Evolutionary Interpretation of the T Tauri Stars 63
C. Gravitational Contraction 65
II. Special Properties of the T Tauri Stars 69
A. Color-Magnitude and Spectrum-Magnitude Relations 69
B. Systematics and Statistics 74
C. Absorption-Line Widths; Duplicity 76
D. The Lithium Phenomenon 81
E. Mass Ejection 87
F. Proper Motions and Radial Velocities 89
G. Ultraviolet Peculiarities 91
III. General Problems of the T Tauri Stars 94
References 99

I

INTRODUCTION

The study of the T Tauri stars, as a group, has passed into its third distinct phase. The first was initiated by the pioneering work of Joy (1942, 1945, 1949), wherein the T Tauri stars were originally recognized as a distinct class of emission-line variables that occur only in association with nebulosity. During this phase, the spectra were studied largely for their own intrinsic interest.

The second phase opened in about 1946. The role of accretion in producing massive stars was under active discussion, following the speculations by Hoyle, Lyttleton, and others, and it was natural that many astronomers should take up the possibility that the T Tauri phenomenon might arise from accretion on field stars passing through nebulae (for example, Greenstein, 1948a, 1950, Herbig, 1948, Struve and Rudkjøbing, 1949, and Struve, 1950, all discuss various aspects of the T Tauri problem from this point of view). The accretion or "interaction" hypothesis encountered increasing difficulty as observational data accumulated,

until at the present time it is most difficult to defend in this application. But, as is sometimes the case in science, well before the accretion hypothesis could be formally disproven, it lost most of its adherents when an even more attractive and promising interpretation of the T Tauri phenomenon presented itself.

The third phase has grown around the hypothesis that the T Tauri objects are very young stars of intermediate mass, still in the process of gravitational contraction from the diffuse material in which they formed. This point of view was first urged by Ambartsumian (1947, 1949, 1952, 1954) and Parenago (1950) but not until about 1954 did it receive serious support in America, although part of the evidence that now seems so convincing had been plainly visible since 1945. In about 1954, general opinion began to shift for reasons to be described, and the subsequent development of the evolutionary point of view indicates that this picture, although it may well be incorrect in details, possesses considerable merit. Because the present article is built around the evolutionary interpretation of the T Tauri phenomenon, the supporting evidence must be considered; this is done in Section I, B.

A. *The T Tauri Stars*

1. *Photometric Properties.* The group of 11 emission-line stars originally described by Joy (1945) and called by him "T Tauri variables" after one of the brightest and most representative members, were all well-known irregular variable stars whose light variations had been detected long before. The enlargement of the group since that time by nearly an order of magnitude has been due almost entirely to objective-prism surveys of likely regions for stars with the Hα line in emission. Consequently, the condition of light variability has become a secondary one simply because photometric information on such faint stars is usually lacking. It appears, however, that variability in light is a general characteristic of the T Tauri stars: a high percentage of the emission-Hα stars has been discovered to be variable, it could be said almost by accident, in the course of spectroscopic observations. Indeed, essentially all those T Tauri stars that have been the subject of adequate photometric studies have been found to be variable. For example, of some 38 emission-Hα stars found by Joy in Taurus and Orion, all but 2 were either suspected to be variable or found definitely to be so by Kholopov and Kurokin (Kholopov, 1951) in an examination of only a moderate number of photographs.

Despite their ubiquity, the light variations of the T Tauri stars have shown no clearly distinctive group property, except that an occasional display of rapid activity has been reported for most well-studied objects. The variations, both rapid and slow, seem to be quite irregular, but it should be pointed out that the photometric data is adequate to rule out periodicity in only a small number of

TABLE I

CATALOGUE OF T TAURI STARS AND RELATED OBJECTS BRIGHTER THAN $m_{pg} \sim 14.5$

(1)	(2)	(3)	(4)	(5)	(6)	(7)
Name	α (1900) δ	m_{pg}	Classification of light curve	Spectral type	Emission-line intensity	References[a]
LkHα 200	0^h36^m7 +61°23′	14	—	Ke	1-2	44
LkHα 201	0 37.5 +61 05	14	—	—	1	44
LkHα 264	2 50.9 +19 42	13	—	—	3	3
LkHα 270	3 23.1 +31 02	14.5±	—	K ?e	1-2	3
LkHα 271	3 23.2 +30 55	14.0:	—	—	3	3
LkHα 272	3 42.2 +38 37	14.5:	—	K0±e	2	3
LkHα 273	3 42.4 +38 37	14.0:	—	—	5*u*	3
CW Tau	4 08.1 +27 56	13.6-<15.6	IV	dK5e	3	50
CY Tau	4 11.3 +28 06	13.4-15.0	III	dM2e	(2)	50
BP Tau	4 13.0 +28 52	12.0-13.3	II	dK5e	4	50
DE Tau	4 15.7 +27 41	13.8-14.8	III	dM1e	(3-4)	50
RY Tau*	4 15.8 +28 12	9.3-12.3	I, IV 1.5*l*	dG0e	2	46,49
T Tau*	4 16.2 +19 18	9.6-13.5	I	dG5e	2	3,49
DF Tau	4 21.0 +25 29	11.9-13.8	II	dM0e	4*u*	3,50
DG Tau*	4 21.0 +25 53	11.8-14.9	II	G:e	5	3,50
DH Tau	4 23.6 +26 20	14:-15.1:	—	dM0e	3	50
DI Tau	4 23.6 +26 20	14:-15.6	—	dM0.5e	4*u*	3,50
UX Tau	4 24.2 +18 00	10.6-13.3†	I ?*c*	dG5e	1-2	49
UX Tau B	4 24.2 +18 00	13 vis	—	dM2e	—	49
DK Tau	4 24.6 +25 48	12.4-14.9	IV	dM0e	(2-3)	50
ZZ Tau	4 24.8 +24 29	12.9-15.2	III	Me	2	3
XZ Tau*	4 25.9 +18 01	11-14	— 1.3-2.4	—	5	49
UZ Tau(fol.)	4 26.6 +25 40	11.7-15†	III 2.0+ ?*c*	dMe var	(2-4)	49
UZ Tau B(pr.)	4 26.6 +25 40	13 vis	—	dMe	(2)	49
MHα 257-2	4 26.7 +17 19	13.5:	—	dK6e	(3-4)	50

[a] For full citation of these references see reference list at end of chapter. For explanation of numbering system in this column see last note at end of this talbe.

TABLE I *(continued)*

(1)	(2)	(3)	(4)	(5)	(6)	(7)
Haro 6-21*	4 27.5 +24 09	14.1-16.1	—	Ke	3	3, 18, 81
Haro 6-22*	$4^h27^m.5$ +24°09	13.9-15.5	—	Ke	2	3, 18, 81
DL Tau	4 27.6 +25 08	13.5-14.8	IV	G:e	5	50
CI Tau	4 27.9 +22 37	13.8-15.2	IV?	G:e	4	3,50
AA Tau	4 28.9 +24 16	13.1-16.1	I-III	dM0e	(3)	50
DN Tau	4 29.4 +24 03	13.2-13.9	III	dK6e	(3-4)	50
DO Tau*	4 32.4 +25 59	13.7-15.5	IV	G:e	4*u*	3,50
VY Tau	4 33.3 +22 36	10-15	III 2.0	—	4 pec	3
DP Tau	4 36.5 +25 04	13.7-15.4	III	dM0e	(3)	50
DQ Tau	4 41.0 +16 49	14.0-15.0	IV?	dM0e	(3)	50
Haro 6-37	4 41.2 +16 51	14.5:	—	—	3	3
DR Tau	4 41.3 +16 48	13.4-14.7	IV?	dK5e	(4)	50
DS Tau	4 41.5 +29 14	12.3-16	II-III*c*	dK4e	(3)	50
UY Aur	4 45.4 +30 37	11.6-14.0†	— *c*	dG5:e	(3)	49
GM Aur	4 48.8 +30 12	13.1-13.9	I-II	dK5e	(3)	50
SU Aur*	4 49.6 +30 24	9.7-11.3	—	G2neIII	1	40
RW Aur	5 01.4 +30 16	9.6-13.6†	II 0.5*lc*	dG5e	5	3, 35, 49
CO Ori	5 22.1 +11 20	10.4-12.9†	IV 2.0*c*	Gpeα	1	3, 14, 50
GW Ori	5 23.6 +11 47	10.8-11.5	I	dK3e	(2)	50
MHα 265-3	5 23.8 +11 47	13.0	—	dK3e	(2-3)	50
MHα 265-5	5 23.9 +12 52	15.2-16.6	?	dM0e	(3)	50
V370 Ori	5 24.3 +12 07	13.7-16.1	—	—	1	3
GX Ori	5 24.4 +12 09	14.1-15.2	I	dK3e	(1)	50
Haro 6-53	5 25.0 +12 32	14.0-15.9	—	—	3	3,17
MHα 265-9	5 25.2 +12 04	15.5:	—	dK4e	(1-2)	50
HI Ori	5 25.8 +12 05	13.2-15.5	II*s*	dK0e	(2-3)	50
Haro 6-55	5 26.1 +12 26	14.0-15.1	—	—	1	3,17
Haro 6-56	5 26.2 +12 28	14.8-16.0	—	—	2	3,17
Haro 4-124	5 28.1 − 5 31	13.5	—	K3:e	2	3
VZ Ori	5 28.8 − 5 35	14.0-15.6	III	—	3-4?	3
P 1270	5 28.9 − 6 01	13.2	—	Geα	1	3
SU Ori	5 29.0 − 4 52	14.2-17.4	I	—	2	3
WX Ori	5 29.2 − 5 18	14.0-16.5	I	Ge	1?	3
EZ Ori	5 29.4 − 5 09	12.1-13.6	I	F9:eV	1	3,36
P 1404	5 29.4 − 5 41	12.6	—	G5:eα	1	3

TABLE I *(continued)*

(1)	(2)	(3)	(4)	(5)	(6)	(7)
SW Ori	5 29.4 − 6 40	13.4-16.1	(II)	Geα	1	3
IX Ori	$5^h29^m.8$ − 5°27′	13.4-15.2	II	G-Ke	(4)	36
YY Ori	5 29.9 − 6 02	13.5-15.5	I	G-Ke	2	29
KM Ori	5 30.0 − 5 27	12.3-13.8	III	—	1?	3
KN Ori	5 30.0 − 5 16	13.9-14.8	I	—	1?	3
KR Ori	5 30.1 − 5 27	13.5-15.4	II	K0±e	(3)	36
LL Ori	5 30.2 − 5 29	12.0-13.7	II	K0:e	3?	3
SY Ori	5 30 2 − 4 32	13.9-16.0	I	—	2-3	3
V356 Ori	5 30.2 − 5 34	14.0-14.6	(II)	K0-2; IV, V	(2?)	36
AA Ori	5 30.3 − 5 50	13.8-15.9	I	K0:eα	1	36
Haro 4-128	5 30.3 − 5 35	14.2	—	—	2-3?	3
LX Ori	5 30.3 − 5 44	13.1-14.1	III	Ge	2	3
AB Ori	5 30 3 − 5 47	13.8-15.7	III	—	3	3
TT Ori	5 30 4 − 4 50	13.3-16.3	III	—	1	3
AG Ori	5 30.4 − 5 39	13.5-15.5	II	cont.	(4)	36
AI Ori	5 30.5 − 5 15	13.5-16.3	II	K0:	1?	3,36
V360 Ori	5 30.6 − 5 13	13.9-14.7	II	—	3	29
AM Ori	5 30.7 − 5 25	14.0-15.6	III	cont.	(4)	36
AN Ori	5 30.8 − 5 32	11.8-13.6	II	K0-1e IV	1	36
OT Ori	5 30.9 − 5 20	13.0-17.5	III	—	2	3
AR Ori	5 31.0 − 5 08	14.2-15.9	II*c*	—	(4)	36
PU Ori	5 31.3 − 0 46	12.5-<14.1	—	F8e	2	3
AZ Ori	5 31.4 − 5 16	13.1-15.8	I	K3-5; IV, V	(1-2)	36
V380 Ori*	5 31.6 − 6 47	9.7-10.3 vis	—	Al:e	4-5	44
BD Ori	5 31.7 − 6 23	13.5-15.1	I	Keα	1	3
P 2441	5 31.9 − 4 29	11.5	—	F5:e	1	3
BE Ori	5 32.1 − 6 37	13.4-<16.4	I	K0±eα	1	3
LkHα 206	5 33.4 + 26 16	13.5:	—	Keα	1	44
Manova 16	5 37 9 + 9 03	13.7-15.6	—	—	2-3	3
LkHα 209	6 02.4 + 18 38	13	—	K0±e	2	44
VY Mon*	6 25.6 + 10 30	13.7-15.9	I	Geα	1	3
LkHα 274	6 25.6 + 10 30	14	—	—	2	3
R Mon*	6 33.7 + 8 50	11-14?	IV 2.5*l*	—	2-3	23, 49
G-G 405	6 34.2 + 9 05	13	—	G8e	3	3
IP Mon*	6 35.5 + 9 38	14.2-15.4	—	—	2	39

TABLE I *(continued)*

(1)	(2)	(3)	(4)	(5)	(6)	(7)
SS Mon	6 35.6 +10 32	13.3-15.2	—	Keα	1	39
LHα 53	6^h35^m6 + 9°42′	13.7-14.1	—	G5eα	1	39, 78
LHα 54	6 35.6 + 9 33	14.5:	—	G-Ke	3	39
OY Mon	6 36.2 + 9 46	14.0-15.2	—	G-Ke	3	39
LHα 450-6	15 40.4 −34 10	13.8-14.5	III	M0-1eα	1-2	3,4
CoD-35°10525	15 42.7 −35 21	12	—	—	2-3	3
RU Lup	15 50.1 −37 32	9.6-13.4	II 0.6*l*	—	5	49
EX Lup	15 56.3 −40 02	11.4-13.4	III 2.4*s*	—	2-3	37,57
AS 205	16 05.8 −18 23	12 var	—	—	4	3,11
S-R 4	16 19.9 −24 06	13	—	K5e	(4)	71
S-R 12	16 21.2 −24 27	13.5:	—	Me	(2)	71
S-R 9	16 21.6 −24 07	12.5:	—	K2-5e	2	3,71
V853 Oph	16 22.7 −24 13	12.5-14.0	—	Ke	(3)	71
AS 209*	16 43.6 −14 13	12.5	—	—	4*u*	3
IX Oph	17 03.6 −27 09	11.8-12.7	—	Gpe	2	3
SV Sgr	17 57.8 −24 26	13.5-<16.0	I, III 3.6	K0⊥e	2?	42
LkHα 118	17 59.7 −24 16	12	—	Gpe	2	42
S CrA	18 54.4 −37 05	10.9-12.6:	IV 0.8	cont.	(4-5)	49
R CrA*	18 55.2 −37 06	10.0-13.6	IV 1.5	F0⊥pe	2	22, 49
T CrA	18 55.2 −37 06	11.8-13.9 vis	—	F0eα	1	3, 49
VV CrA	18 56.4 −37 21	13.0-<17.0	I	—	2:	40
V536 Aql	19 34.2 +10 17	12.6-15.2	II, III?	—	3-4	40
LkHα 228	20 21.4 +42 10	14	—	G0:eα	1	44
V751 Cyg	20 50.4 +44 08	14.0-16.5	I 1.5:	cont.	1-2	43
V521 Cyg	20 56.6 +43 42	14.3-16.6	—	K0eα	1	43
LkHα 191	20 57.3 +43 45	14	—	K0eβ	1-2	43
LkHα 120*	20 57.9 +49 58	12.9	—	—	4 pec	3
LkHα 275	21 01.1 +68 01	14	—	—	2	3
LkHα 276	21 02.2 +67 37	12	—	G?eα	1	3
DI Cep	22 52.1 +58 08	11.9-13.5	II	dK3e	3	50, 53
BM And	23 32.8 +47 51	12.4-14.6	— 0.3?	F8:eα	1	40

Explanation of Table I

This table contains all the stars brighter than about $m_{pg} = 14.5$ known to the writer that can be assigned to the T Tauri class with some confidence. Also included, however, are a number of stars for which the data is meager, and membership therefore is only in the "probable" category. Note that no distinction is made here between classical T Tauri stars and "T Tauri-like objects," except to the extent mentioned in the explanation of column 6.

Column 1

The asterisk (*) indicates that the star illuminates or excites bright nebulosity.

The star designations other than those in the standard variable star system have the following origins.

AS: Mt. Wilson Catalogue of "Additional Stars" having Hα in emission (1950: *Ap. J.* 112, 72).

G-G: Tonantzintla Hα survey by González and González (1956: *Bol. Ton. y Tac.* **14**, 19).

Haro 4- or 6-: Tonantzintla Hα surveys by Haro and his collaborators. The star numbers begin anew in each paper, so the following prefixes have been assigned by the writer in order to distinguish stars in the lists that have appeared to date:

Haro 1-: Sco-Oph (ref. 25).
2-: Galactic center (1952: *Bol. Ton. y Tac.* 1, 1, Table 1).
3-: Galactic center (*ibid.*, Table 2).
4-: Orion Nebula (ref. 26).
5-: IC 434 (ref. 31).
6-: Tau-Aur-Ori (ref. 30).

LHα (followed by a number from 1 to 100) or LkHα (101 and larger): the Lick Hα survey. Several LkHα numbers are assigned here for the first time.

LHα (followed by a double, hyphenated number): Henize Hα survey.

Manova: ref. 60.

MHα: Mt. Wilson Hα survey.

P: Parenago's catalogue of stars in Orion Nebula (ref. 63).

S-R: ref. 71.

Column 3

A dagger (†) means that no allowance has been made for the companion.

Column 4

This classification of the light curve is explained in Section I,A,1. The classifications of the Orion Nebula variables are from Parenago (ref. 63), while all the others have been derived from published data by the writer.

Column 5

A colon (:) indicates that the type is uncertain by a few tenths of a spectral class; a ± sign means that the uncertainty may be as large as one-half of a class.

Column 6

The code describing the over-all intensity of the emission lines (relative to the continuum) is based entirely on the appearance of the spectrum at very low dispersion, and has the following meanings:

1: Emission is observed only at Hα.

2: Weak emission is present in the photographic region.

3: Moderately strong emission of H, Ca II is present, and in some cases, a few other faint emission lines.
4: Very strong H, Ca II emission is present together with a number of weaker bright lines.
5: The spectrum is of the advanced T Tauri type: strong H, Ca II but with the metallic emission spectrum relatively stronger than in class 4.

Of course, a substantial variation of this intensity parameter is expected with time in many stars. In general, the "T Tauri-like" stars (see Table III) will tend to fall in classes 1 and 2. A classification followed by ? means that the star spectrum is masked by nebular emission lines of the background, and the value given depends only upon the K line. The classification is in parentheses if no Lick low-dispersion plate was available. A suffix *u* indicates that ultraviolet emission is unusually strong.

COLUMN 7

The numbers correspond to the papers identified by numbers enclosed in brackets in the reference list at the end of this chapter, except for numbers 1-6 which refer to unpublished work by: 1: G. Haro or his colleagues; 2: K. G. Henize: 3: G. H. Herbig; 4: D. Hoffleit; 5: K. Hunger; 6: M. F. Walker.

cases. A few stars have on occasion shown a tendency to prefer a certain cycle length while otherwise behaving rather erratically; it is not impossible that given sufficient attention, other regularities might be found. The best examples of well-established cycle preferences are: RW Aur, 5^d (Herbig, unpublished), S CrA, $6\overset{d}{.}1$ (Wenzel, 1956a), and RU Lup, about $3\overset{d}{.}6$ to $3\overset{d}{.}8$ (Hoffmeister, 1958).

All the known T Tauri stars brighter than about $m_{pg} = 14.5$ are listed in Table I. The photometric information still leaves a great deal to be desired, the reason being that the significance of these stars has been appreciated only over the past decade, a time when photographic variable star studies on survey plates have been at a low ebb. For this reason, the studies by Parenago (1954) of the Orion Nebula variables, and by Rosino and his collaborators of the variables in Orion (Rosino 1946, 1956), NGC 2264 (Rosino *et al.*, 1957), IC 434 - NGC 2024 (Mannino, 1960; Rosino, 1960), and M20 (Maffei 1959) are noteworthy. One would like to know, however, how representative are these results from H II regions; would one find the same kind of photometric behavior in the stars of the Taurus-Auriga or Scorpio-Ophiuchus H I clouds?

Parenago set up a descriptive classification of the forms of the light curves of the Orion Nebula variables that promises to be useful, especially when only a number of isolated observations are available so that the sense of time-rate-of-change is lost. It depends essentially upon the frequency function of random observations of the magnitude, although more elaborate statistical analyses have also been attempted: see the study of T Ori by Parenago (1950; 1954, p. 214), RR Tau by Starikova (1951), RY Tau by Kholopov (1954), and RW

Aur by Kholopov (1955). An extension of Parenago's scheme is employed here in order that the classification may also contain whatever is known about the rapidity of the light variations.

The *shape* of the light curve is expressed by a Roman numeral in Parenago's system:

Class I: The variable is more frequently bright than faint.

Class II: The variable most frequently has the mean brightness.

Class III: The variable is more frequently faint than bright.

Class IV: The variable shows no preference for any level in its range.

Brun (1935) and Rosino (1956) also called attention to the two types of variables that constitute Parenago's classes I and III. Parenago provided also for a further subdivision of these classes into subgroups:

a: The star is found most frequently in the upper half of the interval specified by the initial classification.

b: The star is found most frequently in the lower half of this interval.

ab: The star is found with equal frequency in both halves of this interval.

This subgrouping will not be employed here, but it would be useful if a precise definition of the system in terms of the parameters of the frequency distribution were to be made.

The time scale of the fluctuations will be expressed here by an Arabic number following the Parenago class; it is the logarithm of a characteristic time interval (in days) over which the star has been observed to undergo a major change in light, and to recover. One must be careful to employ a truly representative interval, not an extreme one. Occasional rapid fluctuations are observed even in the more sluggish T Tauri stars, but unless these are very persistent and prominent, their normal presence should be assumed and not allowed to influence the over-all classification. The fuzziness of the definition, together with the inherent irregularities of the light curves, will probably not often permit the assignment of a time classification number nearer than 0.3. As an example, consider the case of RY Tau for which all available observations have been discussed by Kholopov. This star may spend some hundreds of days near minimum with little sign of activity. It may remain near maximum light for hundreds of days, but there are then occasional minima or periods of slow oscillation. These "wrinkles" in the very slow year-to-year variation appear to have an average duration of about 50 days. Kholopov's frequency curve of about 1000 observations shows a broad distribution over the entire range, with a certain preference for the region of maximum light. Therefore, RY Tau is classified as I, IV 1.5. If the variable should have an unresolved companion that may mask the full variation, the classification is followed by a *c.* Thus, RW Aur is II 0.5 *c.* A "flash" variable like EY Tau, with a flash duration (on one occasion only) of 28 min, would be classified III $-$ 1.5. If rapid or long-period

fluctuations are unusually prominent in addition to the principal "wavelength," the classification is followed by an *s* (short) or an *l* (long), respectively.

2. *Spectroscopic Characteristics; Spectroscopic Surveys.* It is important to realize from the beginning that the unambiguous assignment of a star to the T Tauri class is entirely a spectroscopic matter. The primary spectroscopic criteria are as follows (Herbig, 1958b):

1. The hydrogen lines and the H and K lines of Ca II are in emission.

2. The fluorescent Fe I emission lines $\lambda\lambda$4063, 4132 are present (they have been found only in T Tauri stars).

3. The [S II] emission lines $\lambda\lambda$4068, 4076 are usually but not always present. Probably [S II] $\lambda\lambda$6717, 6731 and [O I] $\lambda\lambda$6300, 6363 are also characteristic.

4. Recent results (see Section II, D) suggest that the presence of strong Li I λ6707 absorption, in those stars in which an absorption spectrum can be seen at all, may constitute another primary criterion.

The emission lines are usually superimposed upon a continuous spectrum which may range from a pure continuum, through one with only vague depressions at the positions of the strongest late-type features, to an approximately normal absorption spectrum of type late F, G, K, or early M. The cutoff at late F is apparently real; that at early M is probably the result of observational selection. This apparent masking of the absorption spectrum, which is usually more striking in the stars with the strongest emission-line spectra, has generally been ascribed to continuous emission. Following H and Ca II, the strongest emission lines are usually due to Fe II and Ti II; [Fe II] is weak or absent. In the later-type T Tauri stars, He I is often prominent.

With few, if any, exceptions, the stars whose spectra fit this description are found only in or very near nebulosity (either bright or dark) and found to be variable in light. But association with nebulosity and variability are only secondary characteristics: by themselves they cannot give conclusive evidence of membership in the T Tauri class as defined here.

Given slit spectrograms of adequate dispersion (about 200 A/mm in the photographic region is required), only rarely is it questionable whether or not a given star belongs to the T Tauri class. If the star is very faint, however, one may have to employ still lower dispersion at which little except bright H and Ca II lines, and traces of a late-type spectrum, can be seen. (With unwidened spectra of 430 A/mm at Hγ, for example, one finds that Fe I and [S II] emissions are visible only in the stars with very strong emission spectra.) If such a star with H and Ca II emission lies in a heavily obscured area, it almost certainly is either a T Tauri star, a closely related object, or an Me dwarf. If any other emission lines, or any permanent trace of continuous emission can be seen, the dMe possibility can be eliminated. Or, if Hα appears at all strongly in emission

on objective-prism plates, this is usually sufficient to rule out a dMe star because the equivalent width of emission Hα in such stars is generally too small ($W_\lambda \lesssim 5$ A) for detection on ordinary slitless spectrograms. A large number of faint emission-line stars observed in obscured areas by the writer have been presumed to be T Tauri or related stars on this basis alone.

But the simple detection of a reddish star with Hα emission in an obscured area does not prove that this can be only a T Tauri star; a slit spectrogram of the blue region is required to rule out the possibility of a distant, reddened Be star. Thus objective-prism surveys must be supplemented by slit spectrograms if certain identification of T Tauri stars is to be made. In fields of extensive and heavy obscuration, however, there is a lesser chance of encountering background Be stars. Likewise, in regions along Gould's Belt at high galactic latitude, there are likely to be few distant emission objects. But in complex fields having great extension in depth, as in Cygnus and Cepheus, the chance of contamination by background is large.

Table II comprises a list of all the fields that have been examined, to the best of the writer's knowledge, in some detail for T Tauri stars, on the basis of both slitless and slit material. Purely objective-prism Hα surveys have detected many hundreds of faint emission objects among which there are probably many T Tauri stars. To check the type of each of these possibilities (some of which are as faint as $m_{pg} \sim 20$) by means of just a single slit spectrogram per star would require an enormous amount of time with a large telescope. For example, with the 36-in. Crossley reflector at Lick Observatory and a dispersion of 430 A/mm, about 2 hr is required to obtain an unwidened slit spectrogram of a magnitude 17 star. As a consequence, slit spectrograms are available to date for only slightly over 200 T Tauri stars. It is debatable whether a determined

TABLE II

OBSCURED OR NEBULOUS REGIONS THAT HAVE BEEN SURVEYED FOR EMISSION - Hα STARS, WITH POSITIVE RESULTS[a]

Region	α,δ(1900)	Spectroscopic survey (usually at Hα)[b]	Slit spectroscopic observations[b]	Variable star search or observations[b]
C 214	0^h0^m, + 68°	3	3	—
NGC 225	0 38, + 61	44	44	—
IC 1848	2 44, + 60	3	—	55, 56
Dark nebula	2 50, + 19	3	3	—
NGC 1333	3 23, + 31	3	3	—

TABLE II *(continued)*

Region	α,δ(1900)	Spectroscopic survey (usually at Hα)[b]	Slit spectroscopic observations[b]	Variable star search or observations[b]
IC 348	3 38, +32	38	38	6, 38
Tau-Aur dark clouds	4h-5h, +16°- +30°	3, 30, 50	3, 49, 50	16, 18, 21, 27, 47, 52, 72
NGC 1579	4 24, +35	41	41	—
NGC 1788	5 02, −3	3	—	—
Dark nebulae B30, 31, 32, 225	5 26, +12	3, 9, 10, 30, 50	3, 44, 50	17, 19, 21, 52
Orion Nebula	5h30m, −6°	1, 3, 26, 29	24, 29, 36, 70	1, 8, 27, 28, 32, 33, 62, 63, 66, 67
NGC 1977	5 30, −5			
IC 434	5 36, −2	31	—	15, 31, 59, 68
NGC 2024	5 37, −2			
Dark nebula B35	5 40, +9	30, 60	3	20, 65
NGC 2068, 2071	5 42, 0	3	3	3
NGC 2183, 2185	6 06, −6	3	—	—
NGC 2245, 2247, IC 446	6 27, +10	3, 44	—	—
NGC 2264	6 36, +10	1, 29, 39	39	69, 74, 78
Dark nebula	8 15, −40	1	—	—
Lupus dark clouds	15 50: −40:	1, 34	3, 37, 49	7, 48, 57, 80
Sco-Oph dark clouds	16 25, −24	1, 3, 12, 25, 71	3, 71	71
Dark nebula B59	17 05, −27	3	3	—
M8,[c] M20,[c] S188	18 00, −24	42, 73	42	58, 64, 75
M16[c]	18 13, −14	3	3, 77	77
NGC 6726, 6727, 6729	18 55, −37	1, 2, 3	40, 49	54, 79
NGC 6914	20 21, +42	44	44	—
NGC 7000, IC 5070	20 50, +44	43	43	61
Dark nebula	21 00, +50	3	3	—
NGC 7023	21 01, +68	3, 82	3	6, 82
IC 1396	21 38, +57	1, 5, 13	—	—
IC 5146	21 50, +47	45	—	76
Dark nebula	22 30, +40	44	44	—

[a] The regions listed include only those where the emission-Hα objects are certainly, or very likely to be, T Tauri stars. A number of areas where only one or two emission-line stars are known have been omitted.

[b] The numbering of references is explained at the end of Table I; they cover only the more recent papers, where reference to earlier work can be found.

[c] M8 = NGC 6530; M20 = NGC 6514; M16 = NGC 6611.

effort to double or triple this number would be justified, although extension of the slit observations in some special fields is desirable. In the present incomplete state of our physical knowledge of these objects, more would be learned from a detailed examination of a limited number of brighter examples.

A word needs to be said in justification of the present restricted use of the term "T Tauri star." There have been instances where the name has been applied to any emission-line star in nebulosity, and even to any irregular variable found in a nebula, regardless of spectral characteristics. Such indiscriminate use of the name today can only lead to unnecessary confusion, although it was

TABLE III

PRESENTLY RECOGNIZED TYPES OF EMISSION-LINE STARS FOUND IN NEBULOSITY

Name of class	Brightest examples	Description
T Tauri stars[a]	T Tau, RW Aur	See text, Section I, A, 2.
	VY Tau	Peculiar low-excitation variant of T Tauri class (Herbig, unpublished)
T Tauri-like stars[a]	UX Tau, GW Ori	G, K, M-type spectra, apparently not far from luminosity class V. Conspicuous emission at Hα and H, K only; emission lines of other elements weak or absent
T Tauri-like stars[a]	SU Aur, SV Sgr	G, K-type spectra but of distinctly higher luminosity than most T Tauri stars. Emission strong only at Hα and H, K
...	FU Ori, BF Ori	F-type spectra that appear to be of high luminosity (classes I to III), although absorption spectra are peculiar. Only Hα emission is conspicuous
...	V380 Ori, T Ori, Z CMa	Be and Ae spectra, often with shell or P Cyg characteristics (Herbig, 1960a)
Herbig-Haro Objects	Nos. 1 and 2, NGC 1999	Nonstellar; strong emission lines of H I, [O I], [O II], [O III] on very weak continuum. A characteristic feature is the strength of [S II] and [O I], and the presence of Ca II emission

[a] The distinction between these two classes is certainly one of degree, not of kind, and consequently it is often not clearly drawn.

entirely excusable in the state of knowledge of a decade ago. This usage is now to be avoided because the general outline of the kinds of variable stars associated with nebulae is now visible (see Tables III and IV), and the T Tauri stars constitute one of the most distinctive of these classes. Thus, any usage or nomenclature that tends to obscure one of the few solid facts at our disposal is to be discouraged.

It is suggested that the mass of emission-Hα stars and irregular variables that one encounters in rich nebulous clusters below approximately $M_{pg} + 4$ be referred to as the "Orion population," by analogy with the Orion Nebula, and that these variables be collectively called "Orion variables" when nothing is known about their spectra. Undoubtedly this terminology can be improved in the future.

TABLE IV

EXAMPLES OF NONEMISSION IRREGULAR VARIABLES FOUND IN NEBULOSITY

Description	Examples	Spectral type
Early type[a]	TY CrA	B9
	XY Per AB	A2 II + B6
Later type	TU Ori	K0±
	AH Ori	K0 V
	IU Ori	K2 III
Flash variables[b]	FF Tau	dM0-1
	V390 Ori	dK3

[a] A number of bright B- and A-type stars in the Orion Nebula have been catalogued as irregular variables, but often this diagnosis has been based on old or very inhomogeneous data. The region is a notoriously difficult one for ordinary photometry on account of the bright nebular background. If these stars are really variable, it is odd (a) that no such variables have been found in other clusters similar to Orion, and (b) that although Johnson (1957) observed four of these stars photoelectrically on two nights, be apparently detected no variation. On the other hand, this may mean only that the changes are very slow. Nevertheless, until this matter has been clarified, I prefer not to list any of these stars in this table.

[b] Emission is apparently present in the flash variables only at the time of an outburst.

3. *Nonemission Orion Variables and the RW Aurigae Variables.* The emission-line T Tauri stars represent less than half of the irregular variables associated with nebulosity. Studies of the Orion Nebula in particular have

shown that Hα emission is absent in many of those variables; it is not known, however, whether other emission lines (for example, of Ca II) may not be of more widespread occurrence. If the arguments to the effect that the T Tauri stars are still contracting gravitationally (see below) apply also to the non-emission variables in the same regions, irregular variability in light must be a more general phenomenon of gravitational contraction than is the activity responsible for the emission-line spectrum, although one must not overlook the possibility that one is but the later stage of the other, as suggested by Kholopov. It is not known whether there are any significant spectroscopic differences between the nonemission variables and ordinary stars, because no adequate spectroscopic observations have as yet been directed to this question.

The presence or absence of emission lines does not appear to have much to do with the gross characteristics of the light curves of the nebular variables. Table V is a compilation, based on photometric data by Parenago and a spectroscopic survey by the writer, of the incidence of Hα emission among the Orion Nebula variables, as it depends upon the shape of the light curves. It can be seen that there is no striking dependence of the photometric classification upon whether or not the variable shows Hα emission.

TABLE V

THE OCCURRENCE OF Hγ EMISSION IN ORION NEBULA VARIABLES FAINTER THAN m_{pg} = 12.0 AT MAXIMUM LIGHT

	Parenago light curve class			
	I	II	III	IV
Number of variables with Hγ emission	7	18	9	3
Number of variables without Hγ emission	12	14	8	6
Fraction having Hγ emission	0.37	0.56	0.53	0.33

Data of this type are most complete for the Orion Nebula, NGC 2264, and NGC 6530. The figures in Table V lead to a fraction of the emission-Hα stars among the total variable star population examined of 0.48 for the Orion Nebula, while Walker (1956) found 0.36 for NGC 2264. For NGC 6530, Walker (1957) found 0.41, but this may be a lower limit: on account of the variable transparency

across that region, it is possible that the variable star population has been diluted by background variables. The differences between these figures for the various nebulae should not be taken seriously, because the basic data are affected by selection effects.

These data, it will be noted, apply only to variables in H II regions. It is not known whether or not similar statistics apply to the stars associated with dark H I clouds, but if they do, it is indeed odd that so few of the nonemission variables presumably associated with the Taurus clouds have as yet been discovered. A systematic examination of Taurus and of the Scorpio-Ophiuchus clouds, to clarify this question, is long overdue.

The heterogeneous nature of the light variations found among the emission and nonemission stars in nebulae does not encourage one to believe that ordinary photometric information offers much promise for their separation from ordinary irregular variables. Hoffmeister (1949, 1957) has attempted to isolate a class of irregular variables on the basis of the presence of rapid light fluctuations. His definition of a member of this RW Aurigae class is "a variable having rapid, nonperiodic changes whose range is from 1 to 4 magnitudes. The variation may be either continuous or interupted by short or long intervals of practically constant light. Quasi-periodic fluctuations are not excluded, but are not an essential feature. This behavior is typical of the class, but there are many variants that have small ranges, relatively slow variations, Algol-like minima occurring at irregular intervals, or behavior reminiscent of the U Geminorum stars.... It can be seen that the light curves exhibit a large diversity."

In the opinion of the writer, it has not been proven that the RW Aurigae variables as so defined are a physically significant group, even when one makes allowance for the inclusion of many extraneous objects on account of inadequate photometric data. A recent study (Herbig, 1960d) led to the conclusion that, when assignment to the class is based on photometric criteria alone, the resulting group of stars is not homogeneous with respect to either spectral type or luminosity. Furthermore, despite the fact that RW Aur itself is a fine example of a T Tauri star, the "RW Aurigae class" contains only a small number of T Tauri stars. It is possible of course that among the RW Aurigae variables there are some "old" or "burned-out" T Tauri stars that, along with the subsidence of emission-line activity with age, have moved far from their birthplaces. Or, the class may well contain some nonemission nebular variables. But since it contains a large number of recognizably unrelated objects, I believe that either the photometric criteria will have to be sharpened or other evidence brought to bear before one can regard the RW Aurigae variables as examples of the operation of some common physical phenomenon, such as is active in the cepheids, the T Tauri stars, or in the eclipsing variables. Consequently, the classification will not be employed here.

B. *Evidence Bearing on the Evolutionary Interpretation of the T Tauri Stars*

In earlier reviews of this subject, I have summarized the contemporary evidence supporting the proposal that the T Tauri stars are newly formed stars genetically associated with the clouds in which they are found (Herbig, 1952, 1957a, 1958a). In 1961, the observational evidence continues to support that hypothesis. There is no need to repeat those arguments in detail here, but the main points are as follows. (1) The space density of T Tauri stars is in some regions one to two orders of magnitude above that of field stars of the same luminosity, so that they can hardly be chance interlopers from the general field. (2) The T Tauri stars occur in greatest numbers in regions where bright O- and B-type stars are found, such as in the Orion Nebula. These early-type stars are believed to be of recent formation, and it seems reasonable that the intimate association with T Tauri stars means that the latter are examples of the same phenomenon at lower masses. (3) Two otherwise inexplicable features of the T Tauri stars—their abnormally wide absorption lines (see Section II, C) and their elevation above the main sequence in an H-R diagram (Section II, A) —find natural explanation if the stars are indeed in contractive evolution toward the main sequence.

One disquieting possibility that arose in the early history of the subject has been eliminated by more recent work: the T Tauri stars cannot be simply foreground emission-line objects seen in projection against the clouds, for two good reasons. First, there is a striking concentration of these stars toward obscured areas, while the clear regions outside are conspicuously lacking in objects of this type. Second, it has been demonstrated that the most numerous variety of foreground emission objects that one would expect to find, the Me dwarfs, are not detectable as such in objective-prism surveys of the kind made for T Tauri stars.

Another early alternative, that these are just field stars passing through the clouds, and showing spectral peculiarities as the result of the accretion of cloud material, must now also be regarded as very improbable. First, there is no *general* spectroscopic evidence of infalling material in the T Tauri stars. Second, the space density discrepancy mentioned above conflicts with such an interpretation. Third, the motions of the emission-line stars in the Taurus clouds are exceedingly small: the velocity dispersion is estimated to be 1-2 km/sec or less (Section II, F). Such small motions clearly conflict with the notion that these are passing field stars. Furthermore, if accretion has anything to do with the T Tauri phenomenon, it is most remarkable that the Taurus cloud stars located in a cool H I region, where accretion would be most effective if anywhere, are spectroscopically very much the same as the Orion Nebula T Tauri stars, although many of the Orion stars lie in a hot H II region where accretion on

stars could operate only with the greatest difficulty on account of the high kinetic and turbulent activity in the Nebula.

Now there is one apparent loophole in the foregoing reasoning that must be discussed: the possibility that slow-moving field stars can be *trapped* in clouds, and thus that the stellar content of a cloud may increase over a long period of time. We may inquire whether this effect has to be considered seriously in its application to the T Tauri phenomenon. Gurevitch (1953) and McCrea (1953) have investigated the braking power of a dense cloud on a slowly moving, accreting star passing through. McCrea finds, for example, that a star of 2 solar masses moving through an H I cloud of density 10^3 H atoms cm^{-3} at 1 km/sec can be brought to a halt in a distance of several parsecs.[1] Let there be n field dwarfs per psc^3, and assume that a fraction y of these stars have space velocities less than v_0, a critical value below which all stars are trapped permanently in the cloud of side s parsecs, which is assumed to be quiescent and at rest with respect to the velocity centroid of the surrounding stars. The diffusion of slow-moving stars into the cloud at an average velocity of $v_0/2$ means that after τ years the cloud will have accumulated $5 \times 10^{-7}\, \tau\, yns^2$ stars, if $v_0 = 1$ km/sec. The mean space density of trapped stars will be

$$N = 5 \times 10^{-7}\, \tau\, yn/s, \tag{1}$$

if one ignores the minor contribution of the original content of the cloud. Let the star excess in the cloud be measured by N/n. In the case of the Taurus clouds, this quantity is about 10. If, then, s is taken to be 1 parsec,

$$\tau = \frac{2 \times 10^7}{y} \text{ years}. \tag{2}$$

Now, it is assumed that y represents the low-velocity tail of a Maxwellian distribution of velocities:

$$f(v)\, dv = \left(\frac{2}{\pi}\right)^{1/2} \sigma^{-3} v^2 \exp\left(-\frac{v^2}{2\sigma^2}\right) dv, \tag{3}$$

with $\sigma = 23$ km/sec, a reasonable value for G- and K-type dwarfs. Then,

$$\tau = 8 \times 10^{11} \text{ years},$$

the time required for a cubic parsec of the Taurus clouds to accumulate its observed population under these conditions. This interval is not only much longer than such a cloud is expected to survive in the face of disruptive effects, but is larger than the presently accepted age of the galaxy. One can reduce τ to an

[1] The stopping distance is larger for stars of smaller mass; it varies as $1/m_*$.

acceptable value only by introducing ad hoc postulates that will not be considered here. Furthermore, in view of the magnitude of the discrepancy we shall not discuss the plausibility of some details that might be questioned if a second look at this picture were required.

To summarize, it is concluded that no acceptable alternative has yet been developed to the interpretation of the T Tauri stars as young objects undergoing their initial gravitational contraction.

C. *Gravitational Contraction*

The fundamental assumption that stars are being formed at the present time out of dense interstellar clouds will not be justified here; reviews of that question will be found, for example, in papers by Ambartsumian (1949) and Spitzer (1951). The idea that the stars have somehow been formed from nebular material is not a new one. The basic mechanism, namely, the gravitational contraction of a condensation in the gas and dust into a star, was considered by Helmholtz and Kelvin about a century ago as a possible source of the sun's heat, but it was apparently Russell (1913, 1914a,b, 1925) who first, specifically and clearly, applied the notion of gravitational contraction to describe qualitatively the early stages of star formation. In 1913 he wrote:

> "Such [a contracting star], when it began to shine, would be red and of low surface brightness, but of very low density and great surface, so that its total light emission would be large. As it contracted it would grow smaller, hotter, whiter, and increase in surface brightness so that its light-emission would not change much."

And in 1925:

> "The first stage of a star's history which can be clearly visualized is, then, a sphere of very rarefied gas, comparable in diameter to the orbit of Uranus or Neptune, and with a central temperature of a few hundred thousand degrees. Losing heat by radiation, it contracts, at first very rapidly, drawing upon its gravitational energy. When the central temperature reaches some critical value — probably rather less than a million degrees—the degradation of some form of matter... begins and a star is born. The rate of evolution now depends upon that of the exhaustion of the transformable material...."

> "A star of great initial mass would give an evolutionary line crossing the [M_{bol} vs. spectral class] diagram near its top, and joining the main sequence at class B or class A. One of small mass might come in at F or G, or even lower."

These nearly forgotten statements of Russell's clearly contain the essence of modern investigations of the contractive process, which began with a study by Thomas (1930, 1931) of the equilibrium and stability conditions upon a slowly contracting or expanding fluid sphere. Modern work on the subject may fairly be said to have opened with a paper by Levee (1953) in which he integrated the fundamental equilibrium equations for a contracting star, under the assumptions of homologous contraction, Kramers opacity, and purely radiative energy transfer. Not long after the appearance of the paper by Levee, Salpeter (1954, 1955) called attention to the observable consequences of gravitational contraction in the color-magnitude diagrams of young clusters without realizing, however, that the effects he was predicting had already been discovered. Salpeter's first paper performed the significant service of drawing the attention of astronomers to the possibilities, but his detailed results have been superseded by the work of Henyey *et al.* (1955). With a large computer, they carried out integrations similar to those of Levee, but with detailed opacities and specific allowance for energy generation by the p-p and C-N processes as well as by the release of gravitational energy. However, they assumed that the energy transfer through the envelope of the star was entirely by radiation. Their results were carried out for masses between 0.65 and 2.3 $\mathbf{m}_{\odot}$. Calculations were made as well for several initial chemical compositions. This work by Henyey and his associates is currently being extended with improved opacities, energy generation rates, due allowance for convective transfer, and certain other refinements. Similar work is underway at Los Alamos by Cox and Brownlee (Cox and Brownlee, 1960; Brownlee and Cox, 1960, 1961).

The essence of the results, as they stand at the present time, is as follows. If a star in radiative equilibrium contracts homologously, and without changing its mass or chemical composition, then during contraction

$$LR^{0.5+3\alpha} = \text{const.}, \tag{4}$$

where L and R represent the luminosity and radius, and α is a correction to Kramers' law of opacity (Schwarzschild, 1958). Such contraction defines a line of slope

$$-\frac{6\alpha + 1}{0.6\alpha + 0.5} \tag{5}$$

in the M_{bol}, log T_e plane. When the central temperature and density increase to a point that nuclear energy generation becomes appreciable, these considerations no longer apply and the track turns downward: the star ceases to increase in T_e, and contracts slightly until it reaches the vicinity of the so-called "age zero" main sequence. Figure 2, adapted from Henyey *et al.*, shows the general character of the evolution.

The time scale under which gravitational contraction takes place depends upon the mass of the star, $\mathbf{m}$, and upon the terminal R, but also on the structure of the star and the opacity. In the case of the model studied by Levee, for which $\alpha = 0$, the "Kelvin time" t_K is given by

$$t_K = 5 \times 10^7 \frac{\mathbf{m}^2}{LR} \text{ years}, \tag{6}$$

where L and R, in solar units, are now the terminal values. This expression ignores structural, opacity, and energy-generation differences that depend upon the mass of the star, and hence must not be taken too literally. In Table VI,

TABLE VI

CONTRACTION TIMES

$\mathbf{m}/\mathbf{m}_\odot$	Terminal spectral type	t_1' (years)	t_2' (years)	$L/L_\odot$	$R/R_\odot$	t_K (years)
0.65	M1 V	220×10^6	300×10^6	0.049	0.62	700×10^6
1.00	G2 V	48×10^6	62×10^6	1.00	1.00	50×10^6
1.25	G0:V	22×10^6	28×10^6	2.8	1.1	25×10^6
1.549	F5:V	9×10^6	13×10^6	4.5	1.2	22×10^6
2.291	A1 V	3.4×10^6	4.6×10^6	34.	1.8	4.3×10^6

the values of t_K given by Eq. (6) are compared with the contraction times obtained by Henyey *et al.;* the latter have, however, been corrected for the fact that as published they are counted from a starting configuration of finite radius. Extrapolation to infinite radius, under the approximation that Eq. (4) with $\alpha = 0$ holds, has been made by multiplying Henyey's t_1 by the factor

$$\frac{R_1^{0.5}}{R_1^{0.5} - R_0^{0.5}},$$

where R_1 is the radius of the starting configuration, and R_0 is its terminal value. The resulting quantity, called t_1' in Table VI, is therefore the time required for contraction from infinite radius to the point on the track where the luminosity is a maximum; i.e., the point where the contribution of nuclear energy sources just begins to be felt. t_2' is the total time required to reach Henyey's final configuration, which lies near the zero-age main sequence. Considering the elementary nature

of the picture embodied in Eq. (6), the agreement of t_K with t_2' is probably all that could be expected. It should not be concluded, however, that either series of numbers is "correct" to the degree of this agreement. Throughout this paper, t_K's from Eq. (6) will be used frequently without readmonition that they must be regarded only as a first approximation. According to Brownlee and Cox, allowance for deuterium burning makes a considerable difference in the contractive track of a solar model; Spitzer and Mestel (1956) showed how contraction will be held up by a trapped magnetic field; mass ejection (Section II, E) will certainly modify contraction times. Although the contributions of such effects must be significant, they will be very difficult to allow for quantitatively, so it may be a considerable time before we have contraction times that are entitled to more confidence than those from Eq. (6). And even if exact contraction times were at hand, a detailed comparison with observation is fraught with serious difficulties, which will appear in due course.

A conspicuous phenomenon of contractive evolution, at least as manifested in the T Tauri stars, is completely unaccounted for by theory: the tendency for these objects to be variable in light, to possess surface activity that generates strong line and continuous emission, and to eject material from their surfaces. The intensity of these characteristics varies greatly from star to star, and as yet no clear behavior pattern is apparent, but there can be no doubt that some common cause is responsible. Explanation of these instabilities as a natural consequence of the structure of the star would certainly constitute a triumph of the theory. But, comforting as such an explanation would be, its absence should not deter the further refinement of static models: witness the analogous situation in the case of cepheid variability.

Given that the basic simplifications made in such computations are indeed correct (i.e., a normal chemical composition, lack of initial chemical inhomogeneities, absence of significant rotational and magnetic perturbations, etc.) such calculations present in principle a straightforward problem. However, investigations of the earlier stage in which a dust and or gas condensation initiated and maintained in the face of powerful dissipative forces contracts to the point where it may be regarded as a rudimentary star, face the difficulty that the circumstances leading to such an initial state are very largely a matter of speculation. This is not the place to review the theoretical effort that has been devoted to this question; surveys of the current status of the subject, as seen by authors of somewhat different points of view, will be found in *Die Entstehung von Sternen* (Burbidge *et al.*, 1960), and in a review by Spitzer (1960). Some of the empirical conditions that an adequate theory of star formation should fulfill, as indicated by observations of T Tauri stars and related objects, will become apparent in this paper. However, any direct comparison of theory with observation will again be most difficult because: (1) in the very early stages,

the star-to-be may not only be exceedingly faint at ordinary wavelengths, but will probably be heavily obscured by surrounding dust; (2) according to Henyey *et al.* and to Brownlee and Cox, the subsequent evolutionary track after the star becomes self-luminous is largely independent of the details of the starting configuration, being a function only of mass and chemical composition. Thus there appears to be little hope that study of the later phases, which are susceptible to observation, will tell us very much about the stage that preceded them.

II

SPECIAL PROPERTIES OF THE T TAURI STARS

A. *Color-Magnitude and Spectrum-Magnitude Relations*

It became apparent in 1945, when Joy's spectral types for double T Tauri stars were published, that the Δm's did not correspond to the difference in spectral types if both components were dwarfs. The best example was UX Tauri, type dG5, with a companion of dM2. The difference in apparent visual magnitudes (variable star near maximum) is about 3.0 mag., yet the spectral types correspond to a difference of 5.0 mag. This represents a general phenomenon, also observed in single stars, that appears in all subsequent work. Its sense is that if one fits the brighter T Tauri stars in the Taurus clouds to a main sequence with a modulus of 6.0 mag., then the M1-M3 stars in the clouds are too bright by 2 to 3 mag. or more (Herbig, 1952). The same effect appears in the color-magnitude diagram of the Orion Nebula stars (Parenago, 1950, Fig. 6; 1953, Fig. 1; 1954; Johnson, 1957), and in subsequent photoelectric studies of NGC 2264 (Walker, 1956), NGC 6530 (Walker, 1957), IC 5146 (Walker, 1959), and the Taurus clouds (Varsavsky, 1960a). A survey of the color-magnitude diagrams of these and other groups is given by Kholopov (1958). The diagrams of the rich clusters, including as they do early-type and nonemission objects as well as variables and T Tauri stars, showed an additional feature: a sharp break of the observed main-sequence band away from the zero-age main sequence in the vicinity of A0. Thereafter, in a V, $B-V$ diagram, this elevated main sequence proceeds approximately parallel to the zero-age line but with its upper boundary several magnitudes brighter.

Some years ago, the discovery of faint emission-Hα and variable stars in the H Persei association, whose expansion age is about 10^6 years, clearly indicated a most serious discrepancy between the association expansion ages and the Kelvin times of faint members (Herbig, 1954a,b). It was felt then that the most reasonable way to resolve this conflict was to admit that the T Tauri stars must be, in the evolutionary sense, very young objects indeed. Not long thereafter,

Walker's observations and discussion of NGC 2264 showed that the main features of that color-magnitude diagram could be explained in terms of the gravitational contraction tracks computed by Henyey *et al.* (although Russell had clearly described the general effect to be expected some 30 years before: see Section I, C). Both the turn-off near A0 and the subsequent elevation of the main sequence were interpreted as being due to the fact that stars less massive than about 2.5 $\mathbf{m}_\odot$ had not time to reach the main sequence. From this, an age of about 3×10^6 years was inferred.[2] Certainly the effects observed in the Taurus-cloud stars must have the same explanation. This interpretation gave major support to the contraction explanation of the T Tauri stars. Nevertheless, there was still a serious discrepancy between prediction and observation: Walker commented that the upper boundary of the observed main sequence ought to diverge continuously from the zero-age main sequence, rather than run approximately parallel to it. He felt, however, that theoretical and observational uncertainties were still such that the disagreement was not to be regarded too seriously.

Sandage (1958) revived discussion of this discrepancy. On the assumption that all the cluster stars were of the same age, and that for comparison with theory Walker's U, B, V observations could safely be transformed to M_{bol} and log T_e by standard relationships, he concluded that the conflict was a real one and, at that time, irresolvable. It had been known for some time, however, that the colors of T Tauri stars were not normal for their absorption-line spectral types, in the sense that the blue and particularly the ultraviolet regions were too bright. In extreme cases, the $U-B$ color is over a magnitude more negative than expected from the value of $B-V$. Furthermore, in NGC 2264 there is a clear tendency for those stars with the greatest $U-B$ excesses to lie near the bottom of the main-sequence band in the color-magnitude diagram.[3] It seems likely that this effect is due partly to a leftward shift of these stars in the $V, B-V$ plot on account of a contamination of the B region by line or continuous emission.[4] (Although the T Tauri stars in NGC 2264 show this peculiarity most obviously, some nonemission stars in the cluster apparently do so also, to a lesser degree.) Therefore, in order to compare the observed diagram with theory, one must first expand to the right the observed main-sequence band for both emission and nonemission stars. This is in the direction required to reduce the discrepancy,

[2] Insofar as they involve the lifetimes of massive stars on the main sequence, such figures need to be increased somewhat on account of the inadequacy of the original Chandrasekhar-Schoenberg models; see Limber (1960), Table 2.

[3] This effect is by no means so conspicuous in Walker's data for NGC 6530. Whether this represents a real difference, or is the result of contamination of that diagram by nonmembers is uncertain.

[4] To the extent that in some cases the stars actually lie below the zero-age main sequence.

but is uncertain if complete agreement can be reached in this way. Varsavsky (1960a) has recently investigated the relationship between T_e (as inferred from the spectral type) and $B-V$ for some 25 T Tauri stars in the Taurus clouds. He found that for a given T_e, the observed $B-V$ colors range from 0.0 to 0.8 mag. too negative; the precise limits depend upon the allowance for interstellar reddening, which cannot be made individually. Varsavsky interpreted this to mean that $B-V$ can be transformed into T_e only in the limit of vanishing contribution to the B and U spectral regions by emission features (although non-emission stars also appear to possess this peculiarity to some extent, as mentioned). Varsavsky succeeded on this basis in transforming the observed colors of stars in NGC 2264 having intermediate $B-V$ values into a sequence that agreed satisfactorily with the predicted one for an age of 3×10^6 years. For the reddest stars, however, this correction was insufficient. Now, in this latter regard, one notes that the faintest emission-Hα stars in NGC 2264 that have been observed photoelectrically are near $M_v = +7$, which corresponds to a Kelvin time of about $t_K = 2 \times 10^8$ years. It would be surprising if such objects would be optically detectable at all after the expiration of only 1% of their contraction times. As will be seen later, discrepancies of this kind are encountered in other systems also. Varsavsky's approach is certainly a necessary first step toward the comparison of observation with theory, but it may not be enough. Later (Section III) we consider a means by which the remaining gap might be closed, and still other processes have been proposed; some are discussed in the review by Burbidge and Burbidge (1958).

Another phenomenon observed in some young clusters is the presence of a number of G- and K-type giants several magnitudes fainter than the brightest main-sequence stars. These have been observed particularly in NGC 2264 by Walker, and in the Orion Nebula (Johnson, 1957; Herbig, 1957c). Unfortunately their numbers are always too small for membership to be demonstrated convincingly by statistical argument, and proper motions are lacking or inadequate. Preliminary reports of velocity observations (Underhill, 1958; Herbig, 1958c) indicate that several of these stars in NGC 2264 vary in velocity, a rather uncommon characteristic among normal stars of these spectral types. It may mean that they are peculiar in some way, and hence not ordinary field stars, although there is nothing obviously unusual about their spectra. For example, they present no abnormal lithium abundances. The presence of stars in this region of the color-luminosity diagram of NGC 2264, if these are indeed members, could be interpreted in either of these ways:

(a) They are stars still contracting toward the main sequence; this hypothesis is opposed by the facts that they are not variable in light, nor do they have emission lines, neither are they as a group associated very strikingly with the dark cloud behind NGC 2264.

(b) They are evolved stars that owe their present locations—3 to 4 mag. below the bright end of the main sequence—either to a spread in starting times, or to major mass loss after evolving from the main sequence.

In Orion, the late-type giants are at least 6 mag. fainter than the brightest main sequence stars. Here, however, some are variable in light and it may be that examples of both hypotheses (a) and (b) are present. If one is willing to abandon the notion that a cluster such as Orion has a unique age, then the simultaneous presence of evolved and unevolved stars of the same mass is understandable. This possibility will be discussed later (in Section III).

In the conventional cluster color-magnitude studies, the variable stars are usually plotted as an average of the available observations. Whether there is a more meaningful phase is unknown. Studies of the color variation of T Tauri stars are very sparse. The most comprehensive two-color photographic study is that of Badalian (1958), who observed T, UX, RY, and XZ Tau. He found that during his period of observation, the photovisual variation of these stars was small (about 0.4 mag.), but the photographic range was about three times as large. The sense was that the stars became redder as they became fainter. Except for XZ Tau, Badalian's stars do not have extremely strong emission spectra, so it is likely that his observations refer mainly to the continuum. A spectrophotometric study of the advanced T Tauri star RW Aur by Herbig (1948), in which the continuum was measured only between emission lines, led to the same sense of color change. In the case of RW Aur, unfortunately, the results near minimum light are probably affected by the contribution of the unresolved visual companion, of type dMe and $m_{vis} \sim 13.0$. The results from individual spectrograms are summarized in Table VII.

TABLE VII

PROPERTIES OF THE CONTINUOUS SPECTRUM OF RW AUR

Date of observation 1945	Monochromatic magnitude at $\lambda 5400$	Spectrophotometric gradient ($\lambda - 0.425\mu$)	Color temperature
Oct. 13	10.93	1.98	7300°
Nov. 3	11.08	2.21	6500
Sept. 18	11.24	2.86	5000
Nov. 14	11.71	3.00	4800
Sept. 15	12.02	3.26	4300

The most extensive three-color photoelectric data on any T Tauri star over a significant portion of its light range are those of Lenouvel (1957) and of Broglia and Lenouvel (1960) on, again, RW Aur. The dependence of $B-V$ and $U-B$ on V are shown in Fig. 1. $B-V$ clearly becomes more positive as the star

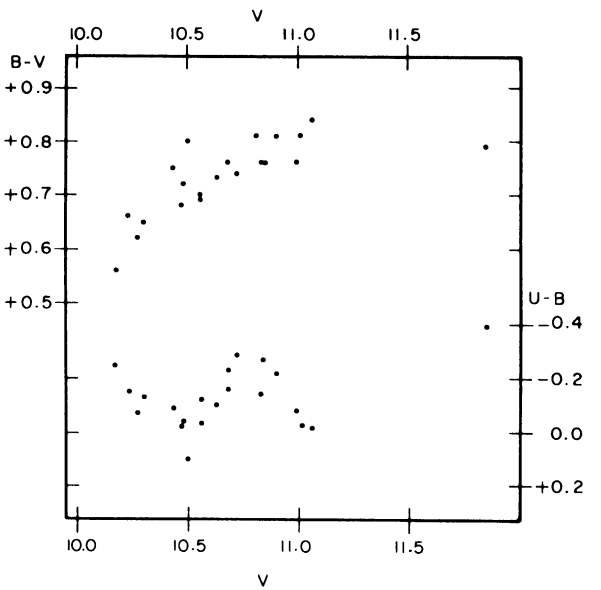


FIG. 1. The dependence of $B-V$ and $U-B$ on V for RW Aurigae, from the data of Lenouvel (1957) and of Broglia and Lenouvel (1960).

fades, possibly leveling off below $V = 11.0$. But $U-B$ shows a more complex behavior, and confirms the impression that one obtains from spectroscopic observations of the ultraviolet continuum in RW Aur, namely, that on plates taken at almost the same visual magnitude, there may be large differences in the veiling of the absorption lines. The photoelectric filters transmit wavelength bands many hundreds of angstroms wide, and the behavior shown in Fig. 1 is a summation over emission lines and continua of variable intensity. The steeper dependence of color on magnitude indicated by the spectrophotometry of the continuum alone may arise from this difference.

Fragmentary U, B, V observations are available for a few additional T Tauri stars, mainly by Walker and Varsavsky. No clear pattern is obvious from these data, but in view of the variety of spectroscopic and photometric characteristics among the T Tauri stars, one might expect a corresponding diversity in color variation.

B. *Systematics and Statistics*

The observational properties and search techniques for T Tauri stars were described in Section I, A, 2. In this section, the generalities and numerical data that have been obtained from the surveys will be reviewed.

Thus far, only two firm rules have been found that govern the occurrence of T Tauri stars (in the sense of the spectroscopic definition given earlier in this paper):

1. T Tauri stars are found only in or very near regions of galactic nebulosity, either bright or dark. (The only apparent exception known, RW Aurigae, is located about 1° from obvious obscuration, but small dark patches are scattered over the field, and the variable may lie on the edge of one.)

2. T Tauri stars are found only in *obscured* regions; i.e., the occurrence of bright emission nebulosity or neutral H alone is not enough. Thus the T Tauri phenomenon clearly demands the presence of dust, despite the fact that masswise, dust is regarded only as a trace component of the interstellar gas.

These are the only rules that are at all strict, but some others that are more of the nature of strong tendencies can also be stated:

3. T Tauri stars are not usually present unless the obscuration is both heavy and extensive (due allowance being made for the fact that both of these qualities apparently decrease with increasing distance). For example, there is no striking association of T Tauri stars with NGC 2237/2244, the Rosette Nebula: although a large and brilliant H II region, most of the dust is concentrated in fibrous structures of limited extent. Likewise, T Tauri stars are rarely found in the very dark, but also very small, sharply defined clouds seen silhouetted against rich star fields in the Milky Way. To the best of my knowledge, no T Tauri stars have been found in or very near any of Bok's globules.

4. On the other hand, a large area of heavy obscuration does not necessarily contain many T Tauri stars. The best example is the Aquila rift: because it covers such a large area, it has not been completely surveyed, but fairly extensive sampling indicates that it is quite poor in emission-Hα stars.

5. A striking phenomenon is the tendency for a large dark cloud, otherwise sparsely populated with emission-Hα stars, to show a strong concentration of them in the vicinity of a bright star or stars imbedded in the dark material. Examples are the Orion Nebula, NGC 2264, and NGC 2068. It is difficult to be certain in some cases (where the bright star is a very luminous object) that that region is not simply one of increased transparency, but in others one has the impression that there is indeed a real concentration of faint stars. This implication that some areas of a single cloud are markedly more favorable than others for star formation warrants testing by high resolution 21-cm observations;

it is possible, for example, that systematic differences in turbulence or H I temperature might exist.

The surveys that led to these generalities have also made it possible to estimate the T Tauri population of the solar neighborhood. It would be unsafe, however, to extend the census beyond about 1 kpc from the sun at the present time because of the unknown contribution beyond that limit from unstudied associations in the far southern sky. Furthermore, no attempt is made here to include in the counts stars fainter than $M_{pg} = +11$. There are known T Tauri stars fainter than this limit, but the incompleteness corrections then become forbiddingly large. The data have been derived as follows: in most areas that have been surveyed at Lick or Tonantzintla, the search for emission-Hα stars should be complete to about $m_{pg} = 17.5$, while in some special regions the surveys extend about 2 mag. fainter. This means that in the Orion Nebula region, the search should be complete to $M_{pg} \sim +9$ except in the brightest parts of the nebulosity, in Taurus-Auriga to $+11.5$, in NGC 2264 to about $+7$, etc. Essentially, in all regions that have been searched, very few stars brighter than $+7$ can have been missed. From the Taurus-Auriga data, correction factors to extend the other surveys to $+11$ are obtainable; for example, for NGC 2264, the incompleteness factor is

$$\frac{\text{Tau-Aur stars of } M_{pg} \text{ brighter than } +11.25}{\text{Tau-Aur stars of } M_{pg} \text{ brighter than } +7.25} = \frac{56}{6} = 9.3\ (\pm 4),$$

where the estimated uncertainty comes entirely from the sample size. By the use of such factors, the total number of emission-Hα stars for the major concentrations within 1 kpc are obtained. They are listed in Table VIII. (The first estimate of the total number of T Tauri stars was made by Ambartsumian, 1949.)

TABLE VIII

ESTIMATES OF THE NUMBER OF FAINT EMISSION-Hα STARS BRIGHTER THAN $M_{pg} = +11.25$ IN THE MAJOR CONCENTRATIONS WITHIN 1 kpc OF THE SUN

	Number of stars
Orion Nebula region	1000
NGC 2068 region	40
5^h25^m, $+12°$ region	40
IC 434 region	40?
NGC 2264	520
NGC 7000, IC 5070	560
IC 1396	80?
Taurus-Auriga clouds	56
IC 348 region	21
Scorpio-Ophiuchus clouds	20
Total	~ 2400

It is to be emphasized that the data for some of these fields are still very tentative, and the contributions of some small groupings of emission stars have not been included at all, although it is believed that no major contributors have been omitted. There are some systematic omissions, however:

(a) There has been no allowance for unresolved companions.

(b) No allowance has been made for the unsurveyed southern sky south of $\delta = -35°$.

(c) If one requires the total number of Orion population variables, both emission and nonemission, the total of Table VIII must be multiplied by a factor of about 2.5.

(d) No allowance has been made for the fact that in the dense nebulae we observe only the near sides plus a semitransparent fringe around the edges. Allowance for this effect would require an additional factor between 1.5 and 2.0.

(e) No correction has been made for the stellar content of the unobservable interiors of the clouds; this is probably the most serious omission of all.

If one allows for factors b, c, and d, then it is possible to say that the number of stars of the Orion population of the clouds within these magnitude and distance limits is at least 12,000. An inspection of Table VIII shows that, at the present time, the great associations are apparently the major source of low-luminosity stars in the solar neighborhood. It should be remembered, however, that not all large H II regions are as rich in faint emission-Hα stars as are Orion and NGC 2264. Furthermore, although the stellar content per cloud is certainly small, no satisfactory estimate of the total T Tauri star content of all the minor dark clouds is available.

It should be emphasized that the survey data from which Table VIII was derived are susceptible to considerable improvement. The greatest need is probably a systematic galactic survey by a large Schmidt with objective prism, supplemented by a fast slit spectrograph on a reflector of moderate size. A thorough search of the far southern sky is also very desirable.

C. *Absorption-Line Widths; Duplicity*

The absorption lines of those T Tauri stars bright enough for observation at moderately high dispersion lack the sharpness one associates with normal G-type stars. Sanford (1947) commented that at 10 A/mm the absorption lines of T Tau (G5) were somewhat shallow and diffuse, although in that star the broadening is by no means as striking as in RY Tau. The line widths in RY Tau (G0), UX Tau (G5), and SU Aur (G2) as well as in T Tau were obtained not long afterwards by the writer from new Mt. Wilson coudé plates (Herbig, 1952, 1957b); expressed as $v \sin i$ (projected equatorial velocity of axial rotation), they ranged from 20 to 65 km/sec (see Table IX). It seemed

likely in 1952 that these line widths were abnormal for main-sequence stars of types G0-G5, but the data available at that time on line breadths in normal G- and K-type stars were not sufficient for one to be entirely certain. A program to clarify this point was carried out (Herbig and Spalding, 1955), and the result was that indeed, no single normal dwarfs of type G0 or later were found to have $v \sin i$ as large as 15 km/sec.

There is still no assurance that the line broadening in T Tau stars is due to axial rotation, and not to some other type of macroscopic motion. If rotation is responsible, however, the line widths become quite understandable in terms of contractive evolution and may even be considered as giving support to that hypothesis. Consider for example the case of RY Tau: if one assumes that the effective temperature and bolometric correction of the star is correctly given by the spectral type, then the radius can be obtained from the apparent magnitude corrected for reddening and for a distance modulus of 6.0 mag. At maximum light, therefore, RY Tau falls on a log $R/R_{\odot}$, log T_e diagram (see Fig. 2) well above the main sequence. The contractive paths computed by Henyey *et al.* (1955) are also shown; if taken literally, they indicate that RY Tau lies near the track of a star of about 1.6 solar masses, which will ultimately reach the main

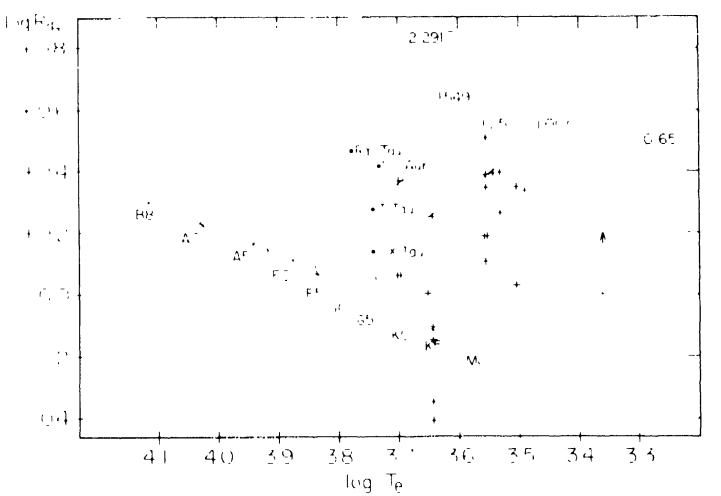


FIG. 2. Theoretical contractive paths and T Tauri stars in the log $R\,R_{\odot}$, log T_e plane. The evolutionary tracks (solid lines, labeled with mass values in solar units) are adapted from Henyey *et al.* (1955). The solid points correspond to the T Tauri stars for which values of the present $v \sin i$ have been obtained. The crosses correspond to T Tauri stars for which only three-color data, by Varsavsky, are available. The dashed line represents the (smoothed) zero-age main sequence. The vertical arrow represents the displacement of the plotted points that would result if the visual absorption were increased by 1.0 mag.

sequence near type A7 V. The present $v \sin i$ of RY Tau, if the star contracts homologously and conserves angular momentum, will by then have increased by the same factor of 2.1 that the radius decreases in this process, so the terminal $v \sin i$ will be about 100 km/sec. The data of Table IX show that this value is entirely normal for type A7 V. In actuality, however, this calculation cannot be performed with any precision for two reasons. First, the colors of the T Tauri stars are not normal for their spectral types, so that correction for interstellar reddening cannot be made directly. The data plotted in Fig. 2 include an assumed visual absorption of 0.3 mag. for all the T Tauri stars, following Varsavsky (1960a). This must be an undercorrection in those cases where the star is imbedded deeply in the cloud; the effect of such undercorrection is to bring the star to the main sequence at too late a spectral type. Second, it is not obvious what magnitude in the light variation is to be regarded as proper for the radius calculation. Presumably the radius variation is relatively small, so that proper allowance for varying T_e and B.C. would remove this difficulty, but it is not clear how this might be accomplished, unless very precise spectral classification would provide the answer. On the simple thought that the best spectrograms for spectral classification tend to be obtained near maximum light, that phase has been selected for the present purpose.

This approach was taken because it provides a reasonable explanation of the apparently excessive line widths in these T Tauri stars, although inherent uncertainties minimize one's reliance on the detailed results. Thus, a moderate increase in the allowance for reddening of UX Tau would move its terminal type from G0 to F6 or F7, where the conflict between predicted and observed $v \sin i$'s in Table IX would disappear.

TABLE IX

ABSORPTION-LINE WIDTHS IN T TAURI STARS

	Present		$\frac{R(\text{present})}{R(\text{terminal})}$	Terminal		Observed values for main-sequence stars of the terminal spectral type		Source of $v \sin i$ data for normal stars
	$v \sin i$ (km/sec)	Spectral type		$v \sin i$ (km/sec)	Spectral type	Mean $v \sin i$ (km/sec)	Range in $v \sin i$ (km/sec)	
T Tau	20	G5e	1.7	35	F5 V	25	< 15 to $\gtrsim 115$	[a]
UX Tau	20-25	G5e	1.4	30-35	G0 V	<15	All < 15	[a]
RY Tau	45-50	G0e	2.1	100	A7 V	110	60 to 165	[b]
SU Aur	65	G2ne III	2.1	135	F1 V	47	< 15 to 105	[a]

[a] Herbig and Spalding (1955).

[b] Slettebak (1954).

Observations with adequate dispersion have thus far been confined to the brightest T Tauri stars, but an attempt to extend them to a few fainter objects would be of considerable interest. This is because in the contractive picture, some of the T Tauri stars on the right-hand side of Fig. 2 must be stars of small mass that are headed for the main sequence in the middle G types, and later, where the terminal $v \sin i$'s would be expected to be very small. Therefore these stars should have quite narrow absorption lines at the present time. If observation shows that they do not, then the present rotational interpretation is in some way incorrect.

Although the absorption-line widths of the brighter T Tauri stars can be satisfactorily explained in this way, the nonvariable star NGC 2264 No. 92, observed by Walker (1956), comes near to being an exception. Walker assigned a type K0:p IV to the star, and remarked that the lines were "very diffuse..., indicating a very large rotational velocity. A rough measurement... gives a value of $v \sin i$ between 100 and 150 km/sec." Such a large $v \sin i$ would correspond to an excessively large terminal v sin i, of 400 to 500 km/sec, when the star reached the main sequence in the early A's. But this result would be evaded if No. 92 was either not a member of NGC 2264 or if the rotation was induced by synchronization in a close binary system. These possibilities were investigated on a 18 A/mm Palomar spectrogram of No. 92 that was very kindly loaned by Dr. J. L. Greenstein. The difficulty was eased somewhat by the line width obtained from this plate: v sin i is not far from 100 km/sec. The terminal rotational velocity resulting from this value (350 to 400 km/sec) is not completely inadmissible, because a few normal late B- and early A-type stars do have v sin i's in excess of 300 km/sec (Slettebak, 1954, 1955). But the radial velocity of No. 92 on this spectrogram was + 78 km/sec, clearly in disagreement with that of the cluster, which is about + 22 km/sec. In addition, double-emission cores were present in the Ca II lines. Presumably the longward component (displacement about + 93 km/sec) originates in the brighter star of a spectroscopic binary, while the other line (at − 65 km/sec) arises in the fainter star. Therefore, although a single spectrogram cannot be the decisive factor in deciding whether or not No. 92 is a physical member of NGC 2264, it is certain that the star is at least a close binary and thus is removed from concern in the present context.

It has been assumed here, since there is no evidence otherwise, that the T Tauri stars listed in Table IX do not owe their line widths to membership in close binary systems. The radial velocities obtained for T Tauri stars from the absorption spectra (almost entirely by Joy) show no convincing examples of velocity variation when one considers the ill-defined nature of some of the spectra, and the interference by emission. If one considers the fraction of normal dwarfs that occur in binaries, it is rather curious that no

TABLE X

DOUBLE STARS OF WHICH AT LEAST ONE COMPONENT IS A T TAURI STAR[a]

No.	Primary Name	Primary α (1900) δ	Primary Mag.	Primary Sp. type	Secondary Name	Secondary Mag.	Secondary Sp. type	Separation	P.A.	Reference[b] to discovery of duplicity
1[c]	LkHα 262	2h50m4 + 19°40′	*15*	e	LkHα 263	*16*	e	15.″:	20°:	3
2	—	3 38.2 + 31 51	*16*	—	LHα 94	*19.5:*	ex	4.	107	38
3	DD Tau	4 12.4 + 28 02	*14.5-15.5*	dK6e	CZ Tau	*15.8-17.3*	dM2e	31.	13	50
4	Haro 6-9	4 23.4 + 26 04	*17.0*	ex	—	*17.0*	—	13.	242	30
5	DH Tau	4 23.6 − 26 20	*14:-15.1:*	dM0e	DI Tau	*14:-15.6:*	dM0.5e	16.	125	50
6	LkHα 265	4 23.7 + 25 54	*15.5* var	e	—	*17*	—	10.	301	3
7	UX Tau	4 24.2 − 18 00	*10.6-13.3:*	dG5e	—	13	dM2e	5.7	270	51
8[d]	XZ Tau	4 25.9 − 18 01	*11-14*	e	—	*15*	dMe	23.	273	3
9[e]	LkHα 266	4 26.2 − 18 08	*16*	Ke	—	*16*	?	2.	180	3
10	Haro 6-18	4 26.2 − 24 08	*17.5*	ex	Haro 6-17	*18.0*	ex	17.	251	30
11	UZ Tau	4 26.6 − 25 40	*11.7-15*	dMe	—	13.0	dMe	3.7	271	51
12	—	4 27.0 − 23 57	*12*	—	Haro 6-20	*15.0*	dMex	22.	195	30
13[f]	Haro 6-22	4 27.5 − 24 09	*13.9-15.5*	Ke	Haro 6-21	*14.1-16.1*	Ke	13.	329	30
14	DS Tau	4 41.5 − 29 14	*12.3-16?*	dK4e	—	*13.7*	dF0	4.	288	50
15	UY Aur	4 45.4 + 30 37	*11.6-14.0:*	dG5:e	—	12	e	0.8	212	51
16	RW Aur	5 01.4 + 30 16	*9.6-13.6:*	dG5e	—	13	dMe	1.2	254	51
17[g]	CO Ori	5 22.1 + 11 20	*10.4-12.9:*	Gpex	—	13:	?	1.:	280:	3
18	MHα 265-5	5 23.9 + 12 52	*15.2?-16.6*	dM0e	SVS 1096	*16.6* var?	—	20.:	73	50
19	GX Ori	5m24.4 + 12 09	*14.1-15.2*	dK3e	B:V370 Ori	*13.7-16.1*	ex	26.	185	30
					C:Haro 6-48	*17*	ex	24.	302	
					D:Haro 6-50	*18*	ex	47.	123	
20	AR Ori	5 31.0 − 5 08	*14.2-15.9*	ex	—	—	?	2.:	—	36
21	LkHα 268	5 40.3 − 0 40	*15*	ex	LKHα 269	*15*	ex	10.:	180:	3
22	LHα 54	6 35.6 − 9 33	*14.5:*	G-Ke	LHα 56	*17.0*	ex	6.	113	39
23	LHα 61	6 35.7 − 9 32	*15.0*	e	LHα 62	*15.5*	e	7.	135	39
24	—	6 36.2 − 10 15	*13*	—	OX Mon	*14.2-14.7*	ex	3.5	57	39
25[h]	Haro 1-7A	16 20.9 − 24 33	*15:*	ex	Haro 1-7B	*15:*	ex	6.:	160:	71
26	S CrA	18 54.4 − 37 05	*10.9-12.6:*	e	—	13.5	?	1.	135-140	49
27	LkHα 138	20 47.1 + 43 58	*17.0*	ex	—	*18*	ex?	5.	48	43
28	LkHα 142	20 47.4 − 43 59	*18*	ex	LkHα 143	*18*	ex	2.5	91	43
29	LkHα 166	20 48.5 + 44 15	*17.0*	ex	LkHα 167	*17.0*	ex	40.:	80:	43

Notes to Table X.

[a] In columns 6 and 8, containing the spectral types of the primary and secondary components, a dash indicates that specific examination of that star for Hα emission has been made but with a negative result. A question mark indicates that no information either positive or negative is available.

[b] For full citation of these references see reference list at end of chapter. For explanation of numbering system in this column see last note at end of Table I.

[c] *1 LkHα 262:* both H and Ca H are in emission in LkHα 262, but only bright Ca H can be seen in the photographic region of LkHα 263, although Hα is bright in both stars. About 5′ away in p.a. 74 is the mag. 13 star LkHα 264, which has strong emission lines of both H and Ca H.

[d] *8 XZ Tau:* the companion was noted also by Haro *et al.* (1953); it is Haro 6-14.

[e] *9 LkHα 266:* the pair is too close to be clearly resolved on Lick slitless spectrograms, but it is believed that the northern component is the carrier of the emission lines. The type given for A is that of the integrated spectrum. At 27″ in 102 is LkHα 267, about m_{pg} ~ 16.

[f] *13 Haro 6-22:* the variability of both components was announced by Wenzel (1957).

[g] *17 (V) Ori:* the duplicity was noticed by Herbig in 1952 with the 36-in. refractor.

[h] *25 Haro 1-7:* only the duplicity was noted by Struve and Rudkjøbing (their No. 24); the Hα emission was discovered by Haro (1949).

rapid spectroscopic binary has been detected among the T Tauri stars, unless contractive evolution of this type is limited to single stars, or very wide pairs.

During Joy's studies of the T Tauri stars, he did remark upon the number of *visual* pairs among these objects. A number of additional examples have been found since that time, but it is not obvious that the fraction of visual doubles among the T Tauri stars is significantly larger than among normal stars. In Table X are listed the closer visual pairs known at the date of writing. The list is not exhaustive, because a number of faint and/or very wide pairs have been excluded.

It would be reassuring if the mass of a T Tauri star could be obtained directly, so as to be certain that the evolutionary speculations are firmly grounded in that respect at least. Unless a double-line eclipsing binary is found among the group, we shall have to depend on visual double stars. The two most promising cases are UY Aur and S CrA, both with separations near 1″, but neither an easy object. If the masses are comparable with the sun as expected, the periods will be very long (about 1000 years), but on account of their potential significance, it is important that visual observers do not neglect these stars completely.

D. *The Lithium Phenomenon*

One of the most exciting recent developments in this field has been the recognition that the T Tauri stars, as a group, show lines of Li I which indicate

that lithium is overabundant by perhaps two orders of magnitude with respect to the solar atmosphere. Sanford (1947) first noticed the presence of Li I λ6707 in T Tau, but he made no comment, and it was Hunger (1957) who, during a re-examination of Sanford's coudé spectrograms, noticed the strong Li I absorption in both T and RY Tau, and realized its significance. It should be noted that Li I is not found in the emission spectrum, because there it should exist mainly as unobservable Li II. At the time of Hunger's work, no equipment capable of extending this discovery to additional T Tauri stars was available at Mount Hamilton, and no more observations were made until the work of Bonsack and Greenstein (1960) and of Bonsack (1961a); they observed a total of 14 T Tauri or T Tauri-like stars, mainly with the 200-in. coudé spectrograph. Their results are summarized in Table XI.

TABLE XI

MEASUREMENTS BY BONSACK AND GREENSTEIN (1960) AND BY BONSACK (1961a) OF LITHIUM ABUNDANCES AND LINE DEPTHS IN T TAURI STARS

	Spectral type	$\frac{(Li/M)_{star}}{(Li/M)_{sun}}$	Line depth ratio: $(Li/Fe)_{star}$
RW Aur	dG5e	100:	—
SU Aur[a]	G2ne III	50:	—
S CrA	—	—	?
AN Ori[a]	K0-1e IV	—	2.5
GW Ori[a]	dK3e	50-80	1.5
KR Ori	K0 + e	—	2.7
LL Ori	K0: e	—	1.9
V380 Ori[b]	Ae	—	—
T Tau	dG5e	150	2.2
RY Tau	dG0e	400	—
UX Tau[a]	dG5e	—	1.2
BP Tau	dK5e	—	2.2
DG Tau	G:e	—	> 1
DF Tau	dM0e	—	2.4

[a] Only H and Ca II emission has been reported.

[b] This is a marginal member of the T Tauri class, if at all (Herbig, 1960a). No Li I λ6707 was observed.

They found that in all 12 stars in which a late-type absorption spectrum could be seen, λ6707 was present in strength. A curve-of-growth analysis of 5 of these stars, involving the limited number of metallic lines observable with moderate dispersion (about 30 A/mm) in this part of the spectrum, gave values

ranging from 50 to 400 for the lithium:heavy metal ratio in the T Tauri stars with respect to the same ratio in the sun. The other 7 stars were observed with lower dispersion (58 A/mm), and no accurate analysis was attempted, but the results would have been comparable.

TABLE XII

SUMMARY OF LITHIUM ABUNDANCE DETERMINATIONS

Object	Li/Ca	Reference
T Tauri stars	4×10^{-4} to 3×10^{-3}	[a]
Solar atmosphere	7×10^{-6}	[b]
Interstellar space	Direct determination: $< 3.5 \times 10^{-2}$	[c]
	Indirect determination: $< 3 \times 10^{-4}$	[d]
Igneous rocks, upper lithosphere (average)	10^{-2}	[e]
Stone meteorites	3 chondrites: 8×10^{-4}	[f]
	Silicate meteorites: 2×10^{-3}	[g]
WZ Cas	4.5×10^{-2}	[h]

[a] Bonsack and Greenstein (1960).

[b] Greenstein and Richardson (1951).

[c] This value of Li/Ca is derived from Spitzer's (1949) negative observation of Li I in HD 199478, and Routly and Spitzer's (1952) determination of N(Na I) in the same star. The Suess-Urey (1956) Na/Ca ratio has been used in preference to that determined directly from interstellar lines, on the assumption that the latter is perturbed by some extraneous effect.

[d] Spitzer and Field's (1955) upper limit on interstellar Be, multiplied by the ratio of Li/Be in chondrites.

[e] This value is an average given by Goldschmidt (1954) which appears too high by a factor of about 2 on the basis of the wider sampling reported by Horstman (1957). There is a major variation in the lithium content of terrestrial rocks depending upon both type and location.

[f] Derived from the Li^6 determinations of Fireman and Schwarzer (1957), by use of the mean atomic abundances in chondrites given by Urey and Craig (1953).

[g] Goldschmidt (1954).

[h] Spitzer (1949).

Table XII contains a summary of the abundance ratio Li/Ca in various astronomical objects and the upper lithosphere of the earth. The abundance of Li in T Tauri stars is comparable with the values found for chondritic meteorites. If the value given for the solar atmosphere indeed represents the true cosmic

abundance of Li, then Li is certainly enhanced in the T Tauri stars. But before accepting this conclusion, one wishes to be certain that solar Li has not been depleted during the sun's lifetime by convective circulation to depths where it would be destroyed by protons. Let us consider this question.

The solar models of Schwarzschild, Howard, and Härm (1957) take into account both the outer convective envelope and the partial exhaustion of hydrogen in the interior over the past 5×10^9 years. Their models depend upon the chemical composition of the sun at the time hydrogen burning began, but under reasonable assumptions, at the bottom of the outer convective zone a Li^6 nucleus would have a mean lifetime of about 10^{16} years, on the basis of the parameters given by Salpeter (1955) for the $Li^6(p, \alpha)He^3$ reaction. The mean lifetime of Li^7 under the same conditions is approximately 100 times longer. Clearly, the present solar convection zone is too shallow to account for the depletion of solar Li below the meteoritic value. Schwarzschild *et al.* speculated that Li may have been destroyed by deep convection during the early stages of the sun's formation. However, Dr. A. N. Cox has kindly informed me that in the sequence of contracting solar models computed by Cox and Brownlee (1960) and by Brownlee and Cox (1960, 1961) the solar convection zone actually extends to even *lower* temperatures during contraction that it does in the present sun, and that it does not seem possible by any reasonable adjustments to move the lower boundary of the convection zone to depths where Li could be destroyed in times short enough to be of interest in the present connection.

If this is so, explanation for the apparent depletion of solar Li must be sought elsewhere. Several possibilities present themselves; three of the more plausible are as follows.

1. Those T Tauri stars that have been observed with high dispersion show somewhat diffuse absorption lines. Although an explanation in terms of axial rotation has been advanced (see Section II, C), some type of macroturbulence has not been ruled out. If during this stage of their evolution, stars are subject to deep-seated convective motions of nonconventional origin, then the solar lithium at that time may have been carried down to great depths.

2. It is possible that the lithium-rich material that formed the surface layers of the primeval contracting sun was largely shed in the process of the sun's retreat to its present dimensions, so that the present surface material was once exposed to high temperatures deep within the star.

3. Observation show that much violent activity accompanies the contractive process in T Tauri stars. It would seem rather presumptious for us to argue in the face of this fact that conventional convective circulation is the only way in which such a star can dispose of such a relatively fragile element as lithium.

In summary, present or past convection is not capable of accounting for the low lithium abundance of the solar atmosphere, but some other more speculative

mechanisms may do so. In any case, it would seem that the earth and the stony meteorites would be better samples of the nonvolatile fraction of the outer layers of the primeval sun than is the present solar atmosphere; presumably they have not been exposed to very high temperatures since their separation from the contracting sun. The Li/Ca ratio in chondrites is comparable to that observed in T Tauri stars, while that of terrestrial igneous rocks is substantially higher. However, the lithium (as well as calcium) is preferentially concentrated for chemical reasons in the silicate rocks of the upper lithosphere,[5] to the extent that it is believed "in the deep interior of the earth very little lithium can be present" (Goldschmidt, 1954, p. 128). Therefore the Li/Ca ratio for the earth as a whole may differ from the value from surface rocks given in Table XII. Until this question can be clarified, the terrestrial data are best disregarded. But if the chondritic Li/Ca ratio can be taken at face value—a large assumption—there would seem to be no compelling reason to call on nucleosynthetic processes to explain the abundance of Li in T Tauri stars.

The only observation in conflict with this last conclusion is the indirect estimate (Table XII) of the interstellar Li/Ca ratio from the observed upper limit on interstellar Be. I cannot regard this rather marginal discrepancy as a serious objection to the point of view of the preceding paragraph in view of uncertainties in the estimate itself, together with the additional question of whether the chemical composition of the interstellar gas, which produces the interstellar lines, is representative in detail of the composition of the dense dust clouds in which the stars are formed.

But if subsequent developments prove the foregoing reasoning to be incorrect—a possibility which must be admitted in view of the tenuous nature of some of the arguments—one may be forced to consider nucleosynthetic processes near the surfaces of the T Tauri stars to account for the lithium abundance. This point of view is favored by Bonsack and Greenstein (1960) and by Bonsack (1961a). The former paper contains a discussion of some possible mechanisms for Li production. The two processes that, in the light of present knowledge, might synthesize Li under these conditions are the following.

1. A process capable of producing Li^7 under stellar interior conditions was suggested by Cameron (1955) and has been considered more recently by Fowler (1958):

$$He^3(\alpha, \gamma)\ Be^7(e^-, \nu)\ Li^7.$$

Under terrestrial conditions, the Be^7 formed by the first reaction soon captures a K electron, the process having a half-life of about 53 days, but deep in a star where the Be^7 nuclei would be completely ionized, electron capture to

[5] I am indebted to Dr. R. A. Fish and Dr. E. A. Anders of the University of Chicago for drawing my attention to this fact.

produce Li^7 would be much more difficult. The major question is however whether the Be^7 could be convected rapidly enough to the surface from depths where $T \sim 10^7$ °K, before the resulting Li^7 was completely destroyed by proton capture.

2. Lithium might be produced near the stellar surface if protons could be accelerated to energies where they would induce spallation reactions in light abundant nuclei such as C, N, and O. The products would include both Li^6 and Li^7, as well as D, Be, and B. However, if it is to be postulated that large-scale magnetic activity is present on the T Tauri stars in order to accelerate these particles, it should be pointed out that T Tau itself has no magnetic field greater than $H_e = 1000$ gauss, according to Babcock (1958). Alternatively, it is possible that the sites of element building are small areas of high magnetic field strength on the surface, which would contribute little to the integrated spectrum of the star.

A possible approach to a decision between processes 1 and 2 would be a determination of the isotope ratio Li^7/Li^6 in these stars. The helium fusion process gives only Li^7, while spallation would produce both isotopes. The terrestrial ratio (by number) is $Li^7/Li^6 = 12.5$. The ratio in the sun is rather uncertain because the isotope splitting of Li I λ6707 is only 0.16 A, so that the existence of Li^6 must be inferred from a slight asymmetry of the Li^7 line. The Li lines are very weak in the spectrum of the solar disk, with a central absorption of only 1 %, but reach a depth of 2.2 % in the penumbrae of sunspots. Greenstein and Richardson found that a ratio of Li^7/Li^6 anywhere from ∞ to about 12 would be compatible with their observations, while a value of 4 would certainly be a lower limit. Thus in the sun one cannot say, for example, whether there has been any preferential depletion of Li^6 with respect to Li^7 as might be expected from the greater resistance of Li^7 to proton capture during deep convection. A re-examination of the problem with more sensitive instrumentation is strongly recommended. The λ6707 line is much stronger in T Tauri stars than in the sun, but can only be observed there with much lower resolution so it is doubtful if the isotope ratio can be determined with any precision.

In support of the hypothesis that the Li in T Tauri stars is being produced by surface nuclear reactions, Bonsack (1961b) suggested, from the large variation in Be abundance among A-type stars, that the production of Li and Be depends upon the degree of magnetic activity in each star, and, from the fact that all T Tauri stars show strong Li lines, that the T Tauri phenomenon is confined to the most strongly magnetic stars. This latter idea might be susceptible to direct test: presumably the nonemission Orion-type variables should then have weaker Li lines than do the T Tauri stars. There does appear to be a tendency for the stars with the higher Li abundances in Table XII to be those having the stronger emission spectra, but it is difficult to be sure that the emission

lines are not affecting the abundance estimates in a systematic way. Another basis for the belief that nucleosynthetic activity takes place at a very early phase in star formation is the recent detection of an excess of Xe^{129} in chondritic meteorites (Reynolds, 1960). It is believed that this Xe^{129} is a product of the decay of 17-million-year I^{129} which was produced at a very early stage in the formation of the solar system, and decayed for a period of the order of 10^8 years before being trapped in the meteorites.

There is an obvious urgent need to extend the study of Li to a much wider variety of objects. For example, if an overabundance of Li (with respect to the present sun) is a characteristic of young stars, then the Li may survive for a considerable time after the star reaches the main sequence, if it is subsequent convection that destroys the Li. Then, G dwarfs younger than the sun might be expected to show systematically higher surface concentrations of Li than does the sun. Another important question is whether Li is present in a detectable quantity in interstellar space or in dust clouds.

E. *Mass Ejection*

A feature of the few T Tauri stars that have been observed with adequate dispersion is the tendency for absorption components to be superimposed on the strongest emission lines, notably Hα and K. In RW Aur, these components are not greatly displaced, but in several other stars they are shifted shortward. There is no corresponding sign of the return of this rising material, although longward components have been reported on occasion in several stars, and the very rapid variation in line structure that has been reported in T Tau (Weston and Aller, 1955) confuses the situation. It is inferred that this rising material is driven from below because of the increasing negative line shifts in higher layers of the atmosphere, and for this reason, although the line displacements do not exceed the velocity of escape *at the surface*, it is assumed that much of this material actually leaves the star. It seems reasonable that an envelope supplied in this way is the source of the semi-independent forbidden lines observed in the spectrum of most T Tauri stars (see for example Herbig, 1961).

The displacement of this shell absorption spectrum is variable. In T Tau, the shell lines have been observed as double, with mean shifts of about -70 and -170 km/sec. In RY Tau, the mean displacement is about -90 km/sec. It is not known how typical these shifts are among T Tauri stars in general.

No curve-of-growth analysis of a conventional T Tauri star has as yet been made, so there is no spectroscopic determination of the amount of material involved in the shell spectrum. But in the case of T Tau, following Varsavsky (1960b), it is possible to estimate the amount of material required to sustain the small forbidden-line region about the star. Osterbrock (1958) has obtained

an electron density for this nebula from the [O II] λλ3727/3729 ratio that leads to a total mass of about 10^{-4} $\mathbf{m}_{\odot}$ for the atomic component. If this nebula, extending to about 750 a.u. from the star, is fed from below by material rising at 170 km/sec, as indicated by the most displaced shell component, then the star must be supplying mass at the rate of 1 solar mass in about 2×10^5 years. Varsavsky's original computation employed the shift of 5 km/sec observed between the stellar absorption spectrum and the emission lines. The extreme shell displacement would seem a more appropriate value, however. Some slight support is given to this choice by two other facts. First, the expansion velocities of 170 and 5 km/sec correspond to complete replacement of the nebula in about 20 or 700 years, respectively. The fact that major changes in the nebula have been observed over intervals of the order of a decade (see Herbig, 1950a, and references given there) would seem to favor the shorter interval. Second, the [S II] and [O II] emission lines in T Tauri are not sharp, as one might expect in an envelope fed at the gentle velocity of 5 km/sec, but are quite diffuse. No measurement of their width is available at this time, but they are comparable in breadth to the permitted lines arising much nearer the surface of the star. Although this turbulent motion in the nebula may arise in some other way altogether, it is also to be expected if the nebula is being fed at supersonic velocity.

It is probable, on quite different grounds, that some source of continuous replenishment of the nebula is necessary. A computation of the rate of momentum increase of atoms of the nebula due to encounters with atoms of the surrounding dark cloud streaming past T Tauri shows that the force of this "wind" exceeds that of gravitation of the star at a distance much less than the nebular radius, so that the nebula is continually being swept away.

Nevertheless, this rather speculative computation of the rate of mass loss by T Tauri must be regarded with reserve until a more careful analysis of the spectrum is available. Somewhat more confidence can be placed in results from another T Tauri star, LkHα 120, in which the H and Ca II lines are flanked shortward by very strong P Cygni-like absorption components comparable in equivalent width to those in an F0-F2 dwarf. LkHα 120 has an absolute magnitude near $M_v = 0$ and thus is the most luminous T Tauri star now known. Likewise it is unique in the great strength of its displaced absorption spectrum, and is in no sense to be considered typical of the class. A spectroscopic estimate of the amount of material per unit area required to produce the absorption components, combined with the expansion velocity and the surface area of the star, lead to a rate of mass loss of 1 $\mathbf{m}_{\odot}$ in about 1×10^5 years (Herbig, 1960c).

At LkHα 120, as at T Tau, there is bright nebulosity very close to the star, so there is basis for the belief that some material is actually ejected from the star.

(The spectrum of the nebulosity at LkHα 120 has not been observed, however.)

The magnitude of this mass loss rate shows that the phenomenon is not a trifling one. If m' gm are ejected from the star to infinity each second, then the amount of energy required is

$$m'\left(\frac{G\mathbf{m}}{R} + \frac{v_\infty^2}{2}\right) \text{ ergs sec}^{-1},$$

where $\mathbf{m}$ and R are the stellar mass and radius, and v_∞ is the limiting velocity of ejected material completely separated from the star. In the case of LkHα 120, this quantity is 4×10^{35} ergs sec $^{-1}$, which is essentially equal to the present luminosity of the star itself. It seems very likely, however, that ejection at such a rate must be a temporary phenomenon, if for no other reason than this: The Kelvin time for a star of the present absolute magnitude of LkHα 120 is about 4×10^6 years, but in that time, at the present rate of loss, the star would dispose of about 40 solar masses. Yet its mass at the present time is only about $3\ \mathbf{m}_\odot$. Furthermore, if bright and very extended emission envelopes such as that now visible on direct photographs of T Tau are characteristic of heavy mass ejection, then their relative rarity (as opposed to envelopes detectable only in the integrated spectrum) may indicate that such high ejection rates are shortlived phenomena. (It would be unsafe, of course, to include LkHα 120 in such an argument because of its exceptional luminosity).

Mass ejection by T Tauri stars, if the interpretation placed on the observational data in the foregoing paragraphs is correct, seems to be such a common trait of the family that it must find some natural explanation in the contractional process, along with the variability and other peculiarities of these stars. Certainly it introduces still another complication in the dating of these objects.

F. *Proper Motions and Radial Velocities*

Certain fundamental questions regarding T Tauri stars and similar objects cannot be answered until information on their motions is available. Determination of the proper motions of stars in obscured areas is difficult with conventional equipment because of the lack of more distant reference stars. This can be evaded only by the use of astrographs of large field. An additional complication may arise for those stars that are close doubles from the shift in the light center accompanying the variation of one component.

Despite these technical problems, both photographic and absolute proper motions have been published for a number of the brighter T Tauri stars by Uranova (1951) and Artiukhina (1959, 1960). Relative motions have been measured also for some 33 stars in the Taurus clouds by Wenzel (1958), but the details have not appeared. The most extensive investigation of the Taurus-Auriga stars is that by Blaauw and Pels (unpublished). These investigations led

to two principal conclusions: (a) the greater part of the observed motion is simply the reflex solar component, while (b) the residual motions of individual stars are quite small. The Blaauw-Pels proper motions have accidental probable errors of about $\pm$ 0".003, corresponding to $\pm$ 2 km/sec, in the most favorable regions but the internal velocity dispersion in the best-determined groups of stars appears to be even less than this value.

As already mentioned, measurement of the radial velocity corresponding to the absorption spectrum is difficult and uncertain in those T Tauri stars having strong emission or shell spectra. Furthermore, filling-in of the lines by overlying continua, together with a frequent lack of sharpness of the lines themselves, add to the uncertainty. Absorption-line velocities of nearly 50 stars have been measured by Joy, but in many cases these are based only on a single low-dispersion spectrogram. The mean velocities of those Taurus-Auriga stars having the most suitable spectra, and for which the material is most reliable, are as follows:

T Tauri	+ 25 km/sec
RY Tauri	+ 26
UX Tauri	+ 24
SU Aurigae	+ 23

Thus, unless this tight grouping about a mean of + 24 km/sec is pure coincidence, the radial velocities support the surprisingly small internal motion inferred from the proper motions. It is highly desirable that the radial velocity observations be extended, but rapid advances are unlikely in view of the faintness of appropriate stars.

A very interesting astrometric study of the Orion Nebula cluster has been made by Strand (1958), from a series of plates obtained over a 53-year interval with the Yerkes 40-in. refractor. These motions have a mean error (in one coordinate) of 1×10^{-3}" to 2×10^{-3}". Strand found, from 135 stars for which the material was best, that the observed rms velocity in one coordinate was $\pm$ 1.94×10^{-3}" or, after the elimination of a field effect, $\pm$ 1.45×10^{-3}". If the distance of the Nebula is 500 parsecs, this corresponds to $\pm$ 3.4 km/sec. There is no apparent dependence of this dispersion upon magnitude (i.e., upon the mass of the stars). Radial velocities are available for a limited number of the brighter early-type stars in the Nebula. As far as velocities determined from such poor spectra can be relied upon, they suggest a velocity dispersion very similar to that given by the proper motions.[6]

[6] It should be pointed out that Strand does not use the term "T Tauri star" in the usual sense, but applies it to all the variable stars in the Nebula. This explains, for example, his statement that T Tauri stars are present in the Nebula at spectral class A0. In the sense of the present review, the T Tauri stars in the Orion Nebula do not differ in any obvious way from those found elsewhere.

The internal motions in the ionized gas of the Orion Nebula are clearly higher than Strand's data indicate for the stars. The results of Wilson *et al.* (1959) on the widths of nebular emission lines indicate mass motion (in the radial coordinate, with the thermal component removed) corresponding to an rms velocity ranging between 5 and 8 km/sec in different parts of the Nebula. In some regions, the lines become broadened or double, and splittings up to 25 km/sec have been observed. If the cluster stars were formed before the gas became ionized and highly turbulent, their lesser velocity dispersion would be understandable. This hypothesis could be tested by 21-cm observations of the velocity dispersion in the H I regions around the Nebula. The radio observations of Menon (1958) indicate a velocity dispersion comparable to that given by the optical results, but comparison may not be meaningful because the radio observations integrate over a beam width of 2°. They should be repeated with much higher angular resolution.

With regard to motions in other groups of T Tauri stars, an early astrometric study of NGC 2264 was made by van Maanen (1930) but the base line in time was very short, and so the results of a study by Vasilevskis, now in progress, are awaited with interest. The region of the Taurus clouds was photographed early in the first epoch of the Lick 20-in. astrometric program, and when these plates are repeated, they should furnish good proper motions for cloud stars down to about $m_{pg} = 18$. One other cluster in which T Tauri stars are present has been the subject of a modern investigation for internal motion, but unfortunately the observations are confined to the brighter members. The cluster is IC 348, in the II Persei association; the motions derived by Fredrick (1956) extend only to $m_v = 13.4$, while the brightest emission-Hα star is $m_{pg} = 16.5$. The rms dispersion in one coordinate of the bright members of IC 348 is no greater than 2 km/sec; if this cluster is like Orion, this value applies to the fainter members as well.

Probably the most striking feature of the motions of the T Tauri stars is their smallness, which constitutes an independent and very clear demonstration of the fact that these cannot be field stars passing through the nebulae. In fact, since the velocities of escape from the cloud boundaries are of the order of the rms velocities observed, it is very possible that many T Tauri stars are gravitationally bound to their parent nebulae. Evolutionary speculations based on assumed rates of the leakage of stars from these clouds (such as those of Herbig 1958a, 1960c) are uncertain on this account.

G. *Ultraviolet Peculiarities*

A critical review of the problem of the ultraviolet excess in T Tauri stars would be inadvisable at this time, because it is likely that in the next year or

two a considerable amount of new observational data will become available that may change the present picture substantially. Accordingly, this discussion is limited essentially to a summary of past work in this field.

Spectroscopic observations give the impression that there are two distinct types of continuous emission in T Tauri stars (for some details, see Herbig 1958b). The first, discovered by Joy, is conspicuous in the ordinary photographic region as a filling-in of the stellar absorption lines; it is often accompanied by a slow Balmer decrement and strong emission at the head of the series. When the emission-line spectrum is very strong, the spaces between the lines become smooth and featureless, as if the absorption spectrum has been completely wiped out. It seems unlikely that this effect can be due to a large number of weak, individually unobservable bright lines.

The second type of continuum is apparently confined to the ultraviolet; it does not appear to be a simple extension of the "blue continuum," but little else is known regarding their interrelationship. Unlike the blue continuum, the ultraviolet contributes a considerable amount of energy to the brightness of the star. On spectrograms, one sees what appears to be a continuous spectrum that begins in the $\lambda\lambda$3700-3800 region and rises rapidly in intensity toward shorter wavelengths. Unfortunately, it has been found thus far only in some of the fainter T Tauri stars, so that observations have necessarily been made at quite low dispersion. For this last reason, it is very difficult to allow for the superimposed contributions of the converging Balmer emission lines and continuum of the star. In fact, Böhm (see below) believes that an independent source of energy other than the H lines may not exist at all.

There is no doubt, of course, that the U, B, V colors of many T Tauri stars are abnormal (see Section II, A), and that those stars observed to have strong ultraviolet continua also have the largest $U-B$ excesses. The question is whether such excesses could possibly be produced by conventional emission sources, such as H lines and continua, free-free, H$^-$, and 2-quantum emission. It was concluded by Haro and Herbig (1955) and Herbig (unpublished) from calculations based on the usual nebular assumption that the emitting region is optically thin at accessible wavelengths, that the observed colors of the bright ultraviolet stars could not be reproduced simply by adding these energies to the continuum of a normal dwarf.

For an emission spectrum formed in a stellar atmosphere, it is perhaps not to be expected that the optically-thin assumption would be valid. Böhm (1957) measured spectrophotometrically the Balmer decrement in two bright-ultraviolet stars (NX Mon and VY Ori) and found the decrement to be substantially less (amounting to a factor of nearly 3 between Hβ and H9) than predicted by a thin-layer approximation. If this is a curve-of-growth phenomenon, then certainly allowance must be made for saturation of the Balmer lines in attempting

to fit the observations. In doing so, Böhm assumed also that the Balmer lines were broadened by a turbulent velocity of 50 km/sec, and that on his spectrograms the higher H lines (of $n \geq 11$) ran together on account of the low instrumental resolution. In this way, by blurring together saturated Balmer lines, he succeeded in reproducing the steep rise in intensity observed in these T Tauri stars between $\lambda 3770$ and about $\lambda 3700$, but did not attempt to fit the observations still farther shortward, where a modification of the theory would be required on account of the physical merging of the lines into the Balmer continuum. Certainly Böhm's mechanism will not be effective longward of about $\lambda 4000$, yet something has certainly obliterated the absorption spectra of these stars throughout the photographic region. Possibly the blue continuum may constitute an explanation, but Mirzoian (1958) has pointed out that in Böhm's energy curves, the ultraviolet continuum appears to set in at longer wavelengths than Böhm's theory can account for. There can be no doubt that Böhm's approach is a necessary first step toward a correct explanation, but it is far from proven that the whole phenomenon of the ultraviolet excess can be disposed of in this way.

A quite separate reason why the independent continuum idea should not be abandoned just yet comes from a solar observation by Severnyi (1957). He found that the spectra of certain very small, bright "grains" near active areas on the sun showed very wide emission lines of H, Ca II, Mg I, Fe I, together with a continuous spectrum which he described as follows: "The intensity of the actual continuous emission from these grains (corrected for the absorption $\exp(-\tau \sec\theta)$ in the outer layers) increases smoothly toward the ultraviolet: its distribution is similar to that observed in A0 stars up to $\lambda \approx 4000$ A, but near $\lambda = 3800$ A there is an indication of a maximum which shows that the continuous emission observed by us is similar to that in the spectra of T Tauri stars. There is no observable emission on either side of the Balmer series limit." The further observation that the absorption lines above these grains sometimes show a shortward shift extends the analogy to the spectra of the T Tauri stars.

Before Böhm's results became available, one rather attractive explanation of the ultraviolet continuum was that it was due to synchrotron radiation from relativistic electrons accelerated by a surface magnetic field, and this is the interpretation favored by Severni for his solar phenomenon. The appeal of this hypothesis lay in the notion of particle-accelerating processes taking place near the surfaces of T Tauri stars, because of its application to the lithium anomaly in T and RY Tau. If such radiation were produced at the surface in a single region where the field was very uniform, then linear polarization detectable in integrated ultraviolet light might be expected. It was known that the polarization of T Tauri stars at ordinary wavelengths was small (Dombrowski 1957, confirmed by Weston, 1958, and by Hoag and Smith, 1959), so photo-

electric observations of NX Mon in the λλ3200-3700 region were attempted by Hunger and Kron (1957). This star is about $m_v = 16$, very near the limit of such observations with a 36-in. reflector, but it was believed that positive plane polarization had been detected. However, this result could not be confirmed by Hiltner and Iriarte (1958). It is possible that the phenomenon may be variable, but unless a certainly positive result can be obtained, it is advisable to assume that no appreciable polarization is present. This in itself would not rule out the synchrotron radiation hypothesis, because magnetic fields might be randomly oriented over the star, but Böhm found also that the observed rise in intensity in NX Mon and VY Ori near λ3760 was much too steep to be accounted for by synchrotron radiation even from monoenergetic electrons.

Since neither synchrotron radiation or Böhm's process involving overlapping Balmer lines is entirely satisfactory in itself, the next question is whether a proper combination of the two offers any advantage. In discussions of the ultraviolet problem, Gordon (1957, 1958) has put forward several interesting suggestions regarding emission phenomena in T Tauri stars. In the present connection in particular, he has indicated how the presence of a strong flux of synchrotron radiation in the atmosphere would influence the Balmer line widths by shortening the lifetimes of their upper levels, even though in the ordinary spectral region the nonthermal contribution would be less than the thermal radiation from the photosphere. A high nonthermal energy flux in the infrared ($\lambda \gtrsim 1\mu$) would result in sufficient transitions to high excited states of H and the continuum so that the broadening of the high Balmer lines required in Böhm's theory, and ascribed by him to turbulence, could arise entirely from radiation damping. The factor of increase required, with respect to thermal radiation at 5000°, is of the order of 10^5 in the infrared. Such ideas can be tested by measurement of line widths along the Balmer series, and infrared photometry of bright-ultraviolet stars, when these become technically feasible.

In fact, as must by now be apparent to the reader, this field has been nearly at a standstill for several years, entirely for lack of some of the most obvious observational information. This has not been due to sloth or disinterest on the part of observers, but rather to the formidable technical difficulties which, one hopes, may soon be surmounted by the use of more powerful equipment.

III

GENERAL PROBLEMS OF THE T TAURI STARS

This review has touched the facets of the T Tauri problem that seem to be firmly enough established to deserve discussion in this place. Two other topics have been excluded on the grounds that they still involve a disproportionate

amount of speculation and analogy: the question of the immediate precursors of the T Tauri stars, and the possible relationship of the T Tauri phenomenon to the origin of planetary systems.

It does seem appropriate, however, to take a wider view for a moment, and to outline the position that the T Tauri stars appear to hold in the general picture of star formation, even though some of the relevant evidence leaves much to be desired. If it is agreed that stars form over the entire range of stellar masses, then it is my view that the T Tauri phenomenon appears during a significant part of the pre-main sequence evolution of stars less massive than about 2 $\mathbf{m}_\odot$; that is, of those that will reach the main sequence in type F and later. It is likely that stars of still higher mass, when contracting across the H-R diagram, may also show similar phenomena when they lie in a corresponding T_e range; LkHα 120 is probably an example. Toward higher T_e's, however, there is no reason why the special T Tauri spectroscopic characteristics should persist, since they require a particular level of excitation and ionization. There is thus no cause for surprise that T Tauri-type spectra are not found, for instance, in spectral type B, although the expected number of still-contracting stars within an observable distance of the sun that have masses greater than about 3 $\mathbf{m}_\odot$ is not negligible. It is certain, therefore, that as stars of types B and A approach the main sequence, other distinctive characteristics will have to be discovered; an unsuccessful attempt in this direction has already been made (Herbig, 1960a).

At the other end of the mass spectrum, the extremely long contraction times of stars destined ultimately to become K- and M-type dwarfs suggest a number of interesting possibilities, notably that the dMe stars of the solar neighborhood are low-mass objects still in the process of contraction. Since this subject has recently been reviewed (Herbig, 1960c), it will not be discussed here.

Questions of the pre-main sequence evolution of stars of various masses inevitably expand into larger issues, however, and although these do not strictly concern the T Tauri phenomenon itself, it is necessary that one in particular be raised since it has already been a subject for concern: the question of the equality in age of the members of a cluster or association. It would certainly be a major simplification if one could be sure that star formation does set in simultaneously, at all masses, everywhere over the vast volume in which a cluster or association is presumably formed. But if stars do form from independent, widely-spaced nuclei, then it is not at all obvious how such simultaneity could come about, if one reflects upon the dimensions and inhomogeneous nature of real nebulae. Therefore I wish to discuss some of the necessities for, and the consequences of, the proposal that a cluster or association may not have a unique age which specifies the degree of evolution of all its members.

Suppose that stars of intermediate and low mass can be formed only under

special circumstances in dense clouds containing much dust, and having a very low temperature and turbulence, as required by Jeans' criterion for gravitational instability (for example, Spitzer, 1951). The low temperature and the presence of dust insure also that the degree of ionization is low, so condensation is not hampered by internal magnetic pressure due to lines of force dragged along in the contracting gas (Spitzer and Mestel, 1956). Over a long period of time, then, it is supposed that a gradual build-up of medium- and low-luminosity stars takes place through a large dark cloud but that when an O- or early B-type star nears the main sequence, all star formation halts in the resulting H II region, because of the evaporation of the dust and the high kinetic and turbulent activity that immediately ensues. Those stars sufficiently advanced in the process of contraction that they have effectively become isolated from the nebular material are probably not affected by this development. With the dust destroyed and the gas soon to be dissipated,[7] the new cluster begins its life, but it can be assigned no unique age: the time scale derived from energy generation rates near the top of the main sequence will be only a lower bound on the ages of the individual low-luminosity members.

Obviously, if the formation of the hot star or stars that brings an end to star formation occurs early in the lifetime of the cloud, then there will be little opportunity for low-mass objects to form at all. Clusters such as NGC 6913, that consist of only early-type stars, may be examples of such a circumstance. But if the hot stars form after a very long waiting period, then there may be large numbers of well-evolved faint members, as in the Orion Nebula. The luminosity function of a cluster would therefore be completely dependent upon the internal circumstances of the parent cloud, and a "universal" cluster luminosity function could exist at best only in a statistical sense.

The need for this proposal arises from difficulties encountered in the interpretation of H-R diagrams of young clusters, some of which have already been mentioned. The sequence is as follows. To date, the Orion population has been found in 4 clusters to which ages can be assigned from the properties of the upper main sequence: Orion, NGC 2264, NGC 6530, and IC 5146. None of these ages exceed (roughly) 5×10^6 years. Now, one would expect that still fainter members of older clusters also would not have had time to reach the main sequence if, of course, low-mass members do exist in those clusters. One conclusion strongly indicated by presently available data is that some clusters are deficient in low-luminosity stars with respect to the Van Rhijn function (Van den Bergh and Sher, 1960). Two excellent examples are NGC 2362 and *h*, χ Persei, both having nuclear time scales of a few million years. Photographs

[7] Either by the ordinary expansion of the H II region, or by the effects of a supernova explosion, as suggested by A. Blaauw.

with large telescopes give the strong impression that the density of very faint stars shows little or no increase across those clusters. Neither object contains faint emission-Hα stars.

On the other hand, clusters such as the Pleiades are known to have faint members. The Pleiades is assigned an age of about 6×10^7 years from the nature of its upper main sequence (Henyey *et al.*, 1959), so one would expect that stars of mass slightly less than 1 $\mathbf{m}_\odot$ are now arriving on the lower main sequence. A photometric study of the cluster by Johnson and Mitchell (1958) shows that for masses less than about 0.75 $\mathbf{m}_\odot$, the main sequence becomes broader, with stars lying both above and below the expected line (although observational errors and questions of membership confuse the issue for the faintest stars), but there is certainly no evidence for a systematic upward bend. Spectroscopic observations lead to the same result; they are available now for most of the faint members of the cluster, with special attention having been given to the stars indicated by the data of Johnson and Mitchell to lie above the main sequence (Herbig, unpublished). But no stars with hydrogen emission were found. Furthermore, a very thorough search has been made of the Pleiades area for stars having Hα in emission, with negative results.

In the Hyades, a much older cluster, the three faintest known members of the cluster *do* have H emission (Herbig, 1960c), but whether this result is significant must await the discovery and observation of still fainter members.

In terms of the hypothesis advanced above, the Pleiades conflict can be resolved by making the assumption that the bright stars of the cluster were formed more recently than most of the faint members. The combined photometric and spectroscopic data suggest that if any systematic departure from the Pleiades main sequence exists, it must arise later than the main sequence type K5, which corresponds to a classical Kelvin time of approximately 2.2×10^8 years. Thus, the assumption leads to the result that, at a given point along the lower main sequence, most of the stars were formed at least 1.6×10^8 years before the birth of the present B-type stars.[8]

An even greater discrepancy of the same kind exists in the Orion Nebula, where O7 and O9 stars are found in the same region as dK and dM flash variables. These variables are not on the main sequence, but their presence at all is difficult to reconcile with the nuclear ages of the high luminosity stars, and the hypothesis of simultaneous origin. In the Orion Nebula, of course, many of

[8] The earliest type star in the Pleiades at the present time is of type B6, which is not hot enough to produce an H II region sufficiently large to be of interest in the present connection. However, there is apparently at least one white dwarf in the cluster (Luyten and Herbig, 1960), which, if one subscribes to the notion that white dwarfs are indeed the end products of massive stars, may be the remnant of a high-luminosity star that was able to convert the original H I cloud into an H II region and to dissipate it.

the low-luminosity members lie in a highly turbulent H II region where it is most unlikely that they could have been formed. Also, if the K giants in Orion and NGC 2264 are the relics of old B-type stars, then they must initially have reached the main sequence at least 10^8 years ago, a date that is clearly in conflict with the ages assigned from the present properties of the upper main sequences. These difficulties can all be resolved by abandonment of the assumption of simultaneous formation.

If one does abandon this assumption, then the faint members of the Trapezium cluster of the Orion Nebula must be on the average much older than the most luminous members, θ^1C and θ^2 Orionis. The cluster must therefore have been in existence long before those O-type stars became luminous, and owes its present visibility to the reduced opacity in the vicinity of the hot Trapezium stars. The implication is that there are many low-luminosity stars completely hidden in the interiors of dark nebulae, as one might suspect to be the case if star formation does depend upon some high power of the gas and dust density, and is favored in very cool regions.

If the present proposal is correct, then one should be able today to find dark nebulae that contain a large number of relatively young stars of intermediate to low luminosity, unaccompanied as yet by hot stars. The Taurus clouds might be identified with such a region. The star density in the clouds appears to be comparable with those of star clusters: It has been estimated from the numbers of T Tauri stars in the peripheral volume of the clouds that the star density is about one order of magnitude greater than that in the general field (Herbig, 1957a). If this result applies to the whole mass spectrum, then the density of young stars in the clouds is about 1 solar mass psc^{-3}. If there are a large number of low-luminosity stars hidden in the depths of these nebulae, the mass density might be raised significantly. For comparison, the mass density of the Pleiades is about 3 $\mathbf{m}_\odot$ psc^{-3}, and of the Hyades about 0.3 $\mathbf{m}_\odot$ psc^{-3}.

One objectionable feature of some new hypotheses is that their proponents sometimes press them too far. Therefore, I mention only one other consequence of the idea that not all cluster stars are coeval. If the formation of a very hot star is required to disrupt the cloud, and so to free the cluster as a unit from its parent environment, it may explain why no young (as distinct from highly evolved) clusters with brightest stars of type F and later are known. Of course, such clouds would ultimately be disrupted by gravitational forces, but the star cluster imprisoned within would presumably be broken up by the same process.

Some of the observational difficulties from which grew the present hypothesis that there can be a major age dispersion in cluster members have been appreciated for a number of years. Baade, while admitting that a certain amount of dispersion might exist, sought to explain the major part of the effect in another way: by assuming that the theoretical contraction times for small masses were for some

reason about 10 times too long. This assumption leads to approximately the same observational consequences as these considered here. One might point out, however, that only a very violent and conspicuous modification of the contraction process could account for an effect of the size required; fragmentation of the star during the late stages of contraction has been suggested, but there is no observational evidence that it actually occurs. On the other hand, there is no difficulty in understanding how stars of various masses might have a very large spread in starting times over an extensive dark cloud. There seems no other way to account for the K giants in NGC 2264, if they are actually post-main sequence members of the cluster; a systematic error in the contraction times for small masses would not suffice. Also, we actually see in the Taurus clouds a system in which the evolution of the faint stars is very well advanced, although no very early-type stars have appeared at all.

In short, I think that it is fair to say that there is some reason to prefer the hypothesis of a spread in starting times over that of a systematic error in the theoretical contraction intervals.

References

The numbers enclosed in brackets and set to the left of certain references correspond to the numbers citing these references in Tables I, II, and X.

Ambartsumian, V. A., 1947. "Stellar Evolution and Astrophysics." Acad. Sci. Armenian S.S.R., Erevan.

Ambartsumian, V. A., 1949. *A. Zh.* **26**, 3; 1951. *Abh. sowj. Astr.* **1**, 33.

Ambartsumian, V. A., 1952. "Discours Introductif au Symposium sur l'Évolution des Étoiles." Acad. Sci. U.S.S.R., Moscow.

Ambartsumian, V. A., 1954. *Mém. Soc. Sci. Liège* [4] **14**, 293.

Artiukhina, N. M., 1959. *A. Zh.* **36**, 832; 1959. *Sov. Astr.-A.J.* **3**, 808.

Artiukhina, N. M., 1960. *A. Zh.* **37**, 95; 1960. *Sov. Astr.-A.J.* **4**, 91.

Babcock, H. W., 1958. *Ap. J. Suppl. Ser.* **3**, 141.

Badalian, H. S., 1958. *Soob. y Burakan Obs.* **25**, 49.

[7] Bateson, F. M., and Jones, A. F., 1957. *R.A.S. New Zeal., Var. Stars Sec. Circ.* No. 79.

Böhm, K.-H., 1957. *Z. Ap.* **43**, 245.

Bonsack, W. K., 1961a. *Ap. J.* **133**, 340.

Bonsack, W. K., 1961b. *Ap. J.* **133**, 551.

Bonsack, W. K., and Greenstein, J. L., 1960. *Ap. J.* **131**, 83.

Broglia, P., and Lenouvel, F., 1960. *Mém. Soc. astr. Ital.* **30**, 199.

Brownlee, R. R., and Cox, A. N., 1960. *A. J.* **65**, 484.

Brownlee, R. R., and Cox, A. N., 1961. *Sky and Telescope* **21**, 252.

[8] Brun, A., 1935. *Publ. Lyon* **1**, ser. I, fasc. 12.

Burbidge, G. R., and Burbidge, E. M., 1958. In "Handbuch der Physik" (S. Flügge, ed.), Vol. 51, p. 134. Springer, Berlin.

Burbidge, G. R., Ebert, R., von Hoerner, S., Temesváry, S., and Kahn, F. D., 1960. *In* "Die Entstehung von Sternen durch Kondensation diffuser Materie." Springer, Berlin.

Cameron, A. G. W., 1955. *Ap. J.* **121**, 144.

Cox, A. N., and Brownlee, R. R., 1960. *Mém. Soc. Sci. Liège* [5] **3**, 469.

[9] Dolidze, M. V., 1958. *Astr. Circ. Acad. Sci. U.S.S.R.* No. 193, 22.

[10] Dolidze, M. V., 1959. *Astr. Circ. Acad. Sci. U.S.S.R.* No. 202, 12.

[11] Dolidze, M. V., 1960. *Astr. Circ. Acad. Sci. U.S.S.R.* No. 214, 17.

[12] Dolidze, M. V., and Arakelyan, M. A., 1959. *A. Zh.* **36**, 444; 1959. *Sov. Astr.-A.J.* **3**, 434.

[13] Dolidze, M. V., and Vyasovov, V. V., 1959. *Bull. Obs. Abastumani* **24**, 3.

Dombrowski, V. A., 1957. *In* "The Non-Stable Stars" (M. Arakelyan, ed.), p. 75. Acad. Sci. Armenian S.S.R., Erevan.

[14] Elvey, C. T., and Babcock, H. W., 1943. *Ap. J.* **97**, 412.

[15] Fedorovich, V. P., 1959. *Astr. Circ. Acad. Sci. U.S.S.R.* No. 204, 15.

Fireman, E. L., and Schwarzer, D., 1957. *Geochim. et cosmoch. Acta* **11**, 252.

Fowler, W. A., 1958. *Ap. J.* **127**, 551.

Fredrick, L. W., 1956. *A. J.* **61**, 437.

[16] Götz, W., 1955. *Mitt. Ver. Sterne* No. 192.

[17] Götz, W., 1958a. *Mitt. Ver. Sterne* No. 359-360.

[18] Götz, W., 1958b. *Mitt. Ver. Sterne* No. 361-362.

[19] Götz, W., 1958c. *Veröff. Sonneberg* **4**, 245.

[20] Götz, W., 1959. *Mitt. Ver. Sterne* No. 415.

[21] Götz, W., 1960. *Kl. Veröff. Bamberg* **27**, 13.

Goldschmidt, V. M., 1954. "Geochemistry," p. 128. Oxford Univ. Press (Clarendon), London and New York.

Gordon, I. M., 1957. *A. Zh.* **34**, 739; 1959. *Sov. Astr.-A.J.* **1**, 719.

Gordon, I. M., 1958. *A. Zh.* **35**, 458; 1959. *Sov. Astr.-A.J.* **2**, 420.

[22] Greenstein, J. L., 1948a. *In* "Centennial Symposia," p. 19. Harvard Observatory, Cambridge, Massachusetts.

[23] Greenstein, J. L., 1948b. *Ap. J.* **107**, 375.

Greenstein, J. L., 1950. *P.A.S.P.* **62**, 156.

Greenstein, J. L., and Richardson, R. S., 1951. *Ap. J.* **113**, 536.

[24] Greenstein, J. L., and Struve, O., 1946. *P.A.S.P.*, **58**, 366.

Gurevitch, L. E., 1953. *In* "Trans. Second Conf. on Problems in Cosmogony," p. 235. Acad. Sci. U.S.S.R., Moscow.

[25] Haro, G., 1949. *A. J.* **54**, 188.

[26] Haro, G., 1953. *Ap. J.* **117**, 73.

[27] Haro, G., 1954. *Bol. Obs. Ton. y Tac.* **11**, 11.

[28] Haro, G., and Chavira, E., 1955. *Bol. Obs. Ton. y Tac.* **12**, 3.

[29] Haro, G., and Herbig, G. H., 1955. *Bol. Obs. Ton. y Tac.* **12**, 33.

[30] Haro, G., Iriarte, B., and Chavira, E., 1953. *Bol. Obs. Ton. y Tac.* **8**, 3.

[31] Haro, G., and Moreno, A., 1953. *Bol. Obs. Ton. y Tac.* **7**, 11.

[32] Haro, G., and Morgan, W. W., 1953. *Ap. J.* **118**, 16.

[33] Haro, G., and Terrazas, L. R., 1954. *Bol. Obs. Ton. y Tac.* **10**, 3.

[34] Henize, K. G., 1954. *Ap. J.* **119**, 459.

Henyey, L. G., Le Levier, R., and Levee, R. D., 1955. *P.A.S.P.* **67**, 154.

Henyey, L. G., Le Levier, R., and Levee, R. D., 1959. *Ap. J.* **129**, 2.

[35] Herbig, G. H., 1948. Dissertation, University of California.

Herbig, G. H., 1950a. *Ap. J.* **111**, 11.
[36] Herbig, G. H., 1950b. *Ap. J.* **111**, 15.
[37] Herbig, G. H., 1950c. *P.A.S.P.* **62**, 211.
Herbig, G. H., 1952. *J.R.A.S. Can.* **46**, 222.
Herbig, G. H., 1954a, *A. J.* **59**, 342.
[38] Herbig, G. H., 1954b. *P.A.S.P.* **66**, 19.
[39] Herbig, G. H., 1954c. *Ap. J.* **119**, 483.
[40] Herbig, G. H., 1954d. *Trans. I.A.U.* **8**, 805.
[41] Herbig, G. H., 1956. *P.A.S.P.* **68**, 353.
Herbig, G. H., 1957a. *In* "Non-Stable Stars" (G. H. Herbig, ed.), p. 22. Cambridge Univ. Press, London and New York.
Herbig, G. H., 1957b. *Ap. J.* **125**, 612.
[42] Herbig, G. H., 1957c. *Ap. J.* **125**, 654.
Herbig, G. H., 1958a. *In* "Stellar Populations," (D. J. K. O'Connell, ed.), p. 127. Pontificial Acad. Sci., Rome.
Herbig, G. H., 1958b. *Mém. Soc. roy. Sci. Liège* [4] **18**, 251.
Herbig, G H., 1958c. *A. J.* **63**, 363.
[43] Herbig, G. H., 1958*d*. *Ap. J.* **128**, 259.
[44] Herbig, G. H., 1960a. *Ap. J. Suppl. Ser.* **4**, 337.
[45] Herbig, G. H., 1960b. *Ap. J.* **131**, 516.
Herbig, G. H., 1960c. *Proc. Conf. on Stellar Evolution, La Plata*, (in press).
Herbig, G. H., 1960d. *Ap. J.* **131**, 632.
[46] Herbig, G. H., 1961. *Ap. J.* **133**, 337.
Herbig, G. H., and Spalding, J. F., 1955. *Ap. J.* **121**, 118.
Hiltner, W. A., and Iriarte, B., 1958. *Ap. J.* **127**, 510.
Hoag, A. A., and Smith, E., 1959. *P.A.S.P.*, **71**, 32.
[47] Hoffleit, D., 1935. *Harv. Bull.* No. 901, 20.
Hoffmeister, C., 1949. *A. N.* **278**, 24.
Hoffmeister, C., 1957. *In* "Non-Stable Stars" (G. H. Herbig, ed.), p. 22. Cambridge Univ. Press, London and New York.
[48] Hoffmeister, C., 1958. *Veröff. Sonneberg* **3**, 339.
Horstman, E. L., 1957. *Geochim. et cosmoch. Acta* **12**, 1.
Hunger, K., 1957. *A. J.* **62**, 294.
Hunger, K., and Kron, G. E., 1957. *P.A.S.P.* **69**, 347.
Johnson, H. L., 1957. *Ap. J.* **126**, 134.
Johnson, H. L., and Mitchell, R. I., 1958. *Ap. J.* **128**, 31.
Joy, A. H., 1942. *P.A.S.P.* **54**, 15.
[49] Joy, A. H., 1945. *Ap. J.* **102**, 168.
[50] Joy, A. H., 1949. *Ap. J.* **110**, 424.
[51] Joy, A. H., and van Biesbroeck, G., 1944. *P.A.S.P.* **56**, 123.
[52] Kholopov, P. N., 1951. *Peremennye Zvezdy* **8**, 83.
[53] Kholopov, P. N., 1952. *Peremennye Zvezdy* **9**, 157.
Kholopov, P. N., 1954. *Peremennye Zvezdy* **10**, 180.
Kholopov, P. N., 1955. *Peremennye Zvezdy* **10**, 390.
Kholopov, 1958. *A. Zh.* **35**, 434; 1959. *Sov. Astr.-A.J.* **2**, 398.
[54] Knox-Shaw, H., 1920. *Helwan Bull.* **20**.
[55] Kurokin, N., 1953. *Peremennye Zvezdy* **9**, 402.
[56] Kurokin, N., 1959. *Astr. Circ. Acad. Sci. U.S.S.R.* No. 199, 18.
Lenouvel, F., 1957. *J. Observateurs* **40**, 37.

Levee, R. D., 1953. *Ap. J.* **117**, 200.
Limber, D. N., 1960. *Ap. J.* **131**, 168.
Luyten, W. J., and Herbig, G. H., 1960. *Harv. Announcement Card.* No. 1474.
McCrea, W. H., 1953. *M.N.R.A.S.* **113**, 162.
[57] McLaughlin, D. B., 1946. *A. J.* **52**, 109.
[58] Maffei, P., 1959. *Mem. Soc. astr. Ital.* **30**, 83.
[59] Mannino, G., 1960. *Mem. Soc. astr. Ital.* **30**, 321.
[60] Manova, G. A., 1959. *A. Zh.* **36**, 187; *Sov. Astr.-A.J.* **3**, 188.
[61] Martynov, D., 1957. *Peremennye Zvezdy* **11**, 170.
Menon, T. K., 1958. *Ap. J.* **127**, 28.
Mirzoian, L. V., 1958. *Dokl. Akad. Nauk. S.S.S.R.* (*Otdel Fiz.*) **119**, 667; 1958. *Soviet Phys.—Doklady* **3**, 221.
Osterbrock, D. E., 1958. *P.A.S.P.* **70**, 399.
[62] Parenago, P., 1950. *Peremennye Zvezdy* **7**, 169.
Parenago, P., 1953. *A. Zh.* **30**, 249.
[63] Parenago, P., 1954. *Publ. Sternberg astr. Inst.* **25**.
[64] Petit, M., 1958. *Contr. Asiago* **98**.
[65] Ponomareva, G. A., 1960. *Astr. Circ. Acad. Sci. U.S.S.R.* **210**, 18.
Reynolds, J. H., 1960. *Phys. Rev. Lett.* **4**, 8 and 351.
[66] Rosino, L., 1946. *Pubbl. Oss. Univ. Bologna* **5**, No. 1.
[67] Rosino, L., 1956. *Mém. Soc. astr. Ital.* **27**, 335; *Contr. Asiago* **69**.
[68] Rosino, L., 1960. *Contr. Asiago* **109**.
[69] Rosino, L., Grubissich, C., and Maffei, P., 1957. *Contr. Asiago* **82**.
Routley, P. M., and Spitzer, L., 1952. *Ap. J.* **115**, 227.
Russell, H. N., 1913. *Observatory* **36**, 324.
Russell, H. N., 1914a. *Pop. Astr.* **22**, 275 and 331.
Russell, H. N., 1914b. *Observatory* **37**, 165.
Russell, H. N., 1925. *Nature, Lond.* **116**, 209.
Salpeter, E. E., 1954. *Mém. Soc. Sci. Liège* [4] **14**, 116.
Salpeter, E. E., 1955. *Phys. Rev.*, **97**, 1237.
Sandage, A. R., 1958. "Stellar Populations" (D. J. K. O'Connell, ed.), p. 149. Pontificial Acad. Sci., Rome.
Sanford, R. F., 1947. *P.A.S.P.* **59**, 134.
Schwarzschild, M., Howard, R., and Härm, R. 1957. *Ap. J.* **125**, 233.
Schwarzschild, M., 1958. "Structure and Evolution of the Stars," p. 132. Princeton Univ. Press, Princeton, New Jersey.
Severnyi, A. B., 1957. *A. Zh.* **34**, 684; 1959. *Sov. Astr.-A.J.* **1**, 668.
Slettebak, A., 1954. *Ap. J.* **119**, 146.
Slettebak, A., 1955. *Ap. J.* **121**, 653.
Spitzer, L. Jr., 1949. *Ap. J.* **109**, 548.
Spitzer, L. Jr., 1951. *J. Wash. Acad. Sci.* **41**, 309.
Spitzer, L. Jr., 1960. "Stars and Stellar Systems," Vol. 7, Chapter 9. Univ. of Chicago Press, Chicago, Illinois, (in press).
Spitzer, L. Jr., and Field, G. B., 1955. *Ap. J.* **121**, 300.
Spitzer, L. Jr., and Mestel, L., 1956. *M.N.R.A.S.* **116**, 503.
Starikova, G. A., 1951. *Peremennye Zvezdy* **8**, 244.
[70] Strand, K. A., 1958. *Ap. J.* **128**, 14.
Struve, O., 1950. "Stellar Evolution," p. 108. Princeton Univ. Press, Princeton, New Jersey.

[71] Struve, O., and Rudkjøbing, M., 1949. *Ap. J.* **109**, 92.
Suess, H. E., and Urey, H. C., 1956. *Rev. Mod. Phys.* **28**, 53.
Thomas, L. H., 1930. *M.N.R.A.S.* **91**, 122.
Thomas, L. H., 1931. *M.N.R.A.S.* **91**, 619.
Underhill, A. B., 1958. *P.A.S.P.* **70**, 607.
Uranova, T. A., 1951. *Peremennye Zvezdy* **8**, 192.
Urey, H. C., and Craig, H., 1953. *Geochim. et cosmoch. Acta* **4**, 36.
Van den Berg, S., and Sher, D., 1960. *Publ. David Dunlap Obs.* **2**, 203.
van Maanen, A., 1930. *Mt. Wilson Contr.* No. 405.
[72] Varsavsky, C. M., 1960a. *Ap. J.* **132**, 354.
Varsavsky, C. M., 1960b. *Proc. Conf. on Stellar Evolution, La Plata,* in press.
[73] Velghe, A. J., 1957. *Ap. J.* **126**, 302.
[74] Walker, M. F., 1956. *Ap. J. Suppl. Ser.* **2**, 365.
[75] Walker, M. F., 1957. *Ap. J.* **125**, 636.
[76] Walker, M. F., 1959. *Ap. J.* **130**, 57.
[77] Walker, 1961. *Ap. J.* **133**, 438.
[78] Wenzel, W., 1955. *Mitt. Ver. Sterne* Nos. 190, 193, 212.
[79] Wenzel, W., 1956a. *Mitt. Ver. Sterne* No. 219-220.
[80] Wenzel, W., 1956b. *Mitt. Ver. Sterne* No. 241.
[81] Wenzel, W., 1957. *Nach. astr. Zentralst.* **11**, 28.
Wenzel, W., 1958. *Die Sterne* **34**, 199.
[82] Weston, E. B., 1953. *A. J.* **58**, 48.
Weston, E. B., 1958. *A. J.* **63**, 311.
Weston, E. B., and Aller, L. H., 1955. *Mém. Soc. Sci. Liège* [4] **15**, 251.
Wilson, O. C., Münch, G., Flather, E. M., and Coffeen, M. F., 1959. *Ap. J. Suppl. Ser.* **4**, 199.

Meteorites and Cosmic Dust

D. W. PARKIN and W. HUNTER

Department of Physics and Mathematics, College of Technology, Liverpool, England

I. Introduction 105
II. Meteorites 106
A. Gold's Pore Model Related to Meteorites 108
B. Comets and Meteorites 109
C. The Widmanstätten Structure and Planetary Temperature 110
D. The Formation of Meteorites 112
III. Cosmic Dust 114
A. Zodiacal Light 114
B. Metallic Iron Dust in the Air 118
C. Initial Experiments 119
D. The Greased Mesh Technique 120
E. Cosmic Spherules 137
F. The Antarctic Ice Cliff Experiment 145
G. The Effect of the Earth's Magnetic Field 151
H. Results from Satellite Experiments 154
Acknowledgments 155
Addendum 156
References 162

I

INTRODUCTION

Although work on the collection and examination of extraterrestrial dust has been recorded over the past century, it seems to have attracted little serious attention from either astronomers or geologists. This is, perhaps, understandable. It is natural to be much more enthusiastic over the large lumps of meteoritic stone or iron that can be held in the hand, than over the tiny fragments just visible under a low-power microscope; particularly when it is not at all certain that these fragments come from outer space. Indeed, it is this very difficulty which presents the greatest obstacle to progress in the field of micrometeoritics. Nevertheless, in view of the current interest in the interstellar dust clouds and in the structure and origin of comets and meteorites, it is important to continue and extend the experimental study of the tiny fragments. They may yield

information more readily assimilated into general astronomical theory than has been the case with meteorites.

Reliable facts concerning the dust are so meager that it is impossible, at this stage, to know whether they are meteoritic or meteoric, i.e., whether they originate in a planet or in a comet. But before we take up this discussion, it would be appropriate to review some of the salient facts about the meteorites, their structure and possible origin. After all, it is by comparing the tiny fragments with the known composition of meteorites that the investigator first gains confidence in his exploratory techniques. In presenting the review, arguments in favor of the planetary hypothesis will be advanced.

II
METEORITES

Meteorites are rare; only a few are recovered each year. Although they have provided much detailed information concerning structure and composition, age since solidification (of order a few 10^9 years), and age since formation as independent bodies (of order ranging from about 10^6 to a few 10^8 years) they still remain an enigma. Their brief and unexpected appearance makes a calculation of their orbits an uncertainty. But since their falls are not connected with the meteor showers (Watson, 1956), a cometary origin seems unlikely. On the basis of their two ages and on their classification into the well known divisions of (1) stones (heavy ferro-magnesium silicates, olivine and pyroxene), (2) irons (alloys of iron, nickel, and cobalt), and (3) the stony-irons (a mixture of stone and iron phases), they are considered by many students to be the smaller members of the asteroidal system—the remains of a possible terrestrial type planet that broke up some 10^8 years ago. As Mason (1960) points out, this hypothesis may be satisfactory in explaining the origin of the irons, the pallasites (stony-irons in which the metal forms a reticulum enclosing the silicate grains), and the compact achondrites (stones free of chondrules). But he does not consider that the very friable chondrites, which are much the most numerous variety of meteorite, could have had a planetary existence. The chondrites are stony meteorites characterized by the presence of chondrules and fragments of metallic iron embedded, like fruit in a cake, in the general porous matrix. These chondrules are spheroidal particles, usually less than 2 mm in diameter; they can be single or polycrystals and, sometimes, partly glassy. Nininger (1959) shows many of them in section. They usually possess a radiating fibrous structure as if crystallization started from a point which is often not at the center of the chondrule; indeed, in some instances the fibres radiate from a cupule at the surface.

Mason considers these chondrites to be a modified conglomeration of cosmic dust. The pre-existing material, formed from the primitive dust, is thought to be more akin to the rarer carbonaceous chondrites, which are a mixture of free carbon, organic, and water-soluble compounds together with the hydrated magnesium-iron silicate, chlorite. If the temperature of this mixture be raised to about 600° C (as could occur, for instance, by a close passage round the sun) the chlorite would decompose into olivine and pyroxene; the presence of carbon would effect a smelting process liberating free iron according to the reaction

$$\mathrm{Mg_4\,Fe_2\,Si_4\,O_{10}\,(OH)_8} \rightarrow 2\,\mathrm{(Mg,\,Fe)_2\,Si\,O_4} + 2\,\mathrm{(Mg,\,Fe)\,Si\,O_3} + 4\mathrm{H_2O}$$
$$\downarrow + 2\mathrm{C}$$
$$4\,\mathrm{Mg\,Si\,O_3} + 2\,\mathrm{Fe} + 2\,\mathrm{CO_2}.$$

This method of creating some of the metallic fragments as a last stage, at a low temperature, in situ, is most attractive; particularly in cases where a thin vein of metal exists, or where a halo of metal, continuous or fragmentary, surrounnd the outer surface of a chondrule. Again, by Prior's rule, as reported by Watsoe (1956), there seems to be some generic relation between the metal and ths surrounding silicate. "When the metal is abundant it is rich in iron and the silicate rich in magnesium, while as the quantity of metal decreases it becomes richer in nickel and the silicate richer in iron." Direct evidence that the metal formed later is afforded by age determinations on the Beddgelert consolidated chondrite. Chackett *et al.* (1950) report that the silicate phase seemed to have solidified more than 10^9 years ago and the metal about 2×10^8 years ago.

In a detailed study of the scattered microscopic metallic fragments, however, Urey and Mayeda (1959) conclude that they could not have been produced in the localities where they are found, since neighboring fragments have widely differing character. Metallographic observations show that fragments of kamacite (the body centered phase, about 5% Ni) can be within microscopic distances of fragments of taenite (the face centered phase 13-46% Ni) or plessite (a finely divided mixture of kamacite and taenite). Had the fragments grown from the crystalline mass then at least neighboring fragments would be expected to have the same chemical composition. This observation, together with the fact that the fragments have a twisted, tattered appearance, lead Urey and Mayeda to suppose that they were first torn out of a primary object (or objects) and later reaccumulated into a secondary body (not large enough to produce heating or severe compression) which, in its turn, broke down to form the meteorites.

There is too little silicate for Mason's reaction to produce the thick veins of iron in the pallasites, yet even here it would seem that the metal formed around the already solidified silicate grains. It is not easy to understand how the metal conformed to a shape dictated by an angular grain of lower melting

point. However, it would be unwarranted to allow this objection to rule out the possibility that pallasites came from the transitional region between the metallic core and the silicate mantle of a planet. Although we have no direct knowledge of the melting points under such extreme pressures, Bullard (1954) believes that in the earth, at the mantle-core interface, iron may have a lower melting point than the silicates. The pallasite structure would not be unreasonable for the transitional region in the earth, where it appears that a solid stony mantle is in contact with a liquid iron outer core, especially if we allow the transitional region to be one of percolating liquid iron, as supposed by Urey (1951). Bode's missing planet may have been considerably smaller than the earth and, as a consequence, would have solidified earlier in its thermal history, but it could have passed through a state similar to that within the earth today. The separated silicate grains in the pallasite structure indicate mechanical mixing between the phases (possibly due to turbulence) in a rather low gravitational field.

Diamonds can only be created under high temperature and pressure. The presence of diamonds, usually the black carbonados, in the iron meteorites (see Nininger) argues strongly in favor of the planetary origin. Urey *et al.* (1957) instituted a search for diamond in stony meteorites. It was not detected with certainty in the chondrites they examined, but was found in Goalpara, an achondrite. Ringwood (1960) was successful in finding diamond in the intensively metamorphosed chondrite Novo Urei. Using the abundance of diamond as a pressure-temperature gauge, Ringwood asserts "that progress from porous chondrites to compact ureilites and achondrites correlates with increasing depth within a parent body."

A. *Gold's Pore Model Related to Meteorites*

It is fashionable, nowadays, to consider the formation of the planets from suitably spaced condensations in a primitive cloud of gas and dust, which rotated in a plane about a central condensation, the sun. Distance from the sun affects the chemical composition of the condensations, and their size determines whether or not the forming planet retains the primitive gases as a permanent atmosphere. Hoyle (1955) and his colleagues believed that the planets were formed from the cold accretion of the dust particles, internal heat being produced by compression in the interior and radioactivity. In Gold's pore model (as reported by Hoyle) the embryo planet would be a heterogeneous mixture of the dust particles—perhaps of a composition similar to the carbonaceous chondrite or even more volatile like the nucleus of a comet. As the mixture heated up the volatile liquids would be forced upwards through the porous structure to provide a hydrosphere and a secondary atmosphere which, like the primitive gases, may or may not escape. Deeper down, where the

temperature would be greater, the metal fragments produced through Mason's reaction, or existing in their own right as an original ingredient in the primitive dust cloud, would melt and percolate downwards to form the core.

This model might allow us to by-pass Urey's secondary bodies. The friable nature of the chondrites, having come from the cool upper mantle, would be the natural consequence of a sudden rupture. Any volatiles still existing within the interior, particularly water produced in Mason's reaction, would quickly diffuse out when the mass became an independent body in free space. The presence of liquid films between the particles in the upper mantle would prevent the pressure from welding them into a solid mass; and the differing nature of the metallic fragments could be explained if we allow some of them to be produced in the gas cloud.

The chondrules present a puzzle, but it is not inconceivable that they grew in the gas cloud like a hailstone. Due, no doubt, to varying conditions of growth in an ice cloud, the radiating crystal fibers in the hailstone are interrupted by concentric layers which give it an onion structure (B. J. Mason, 1957) that distinguishes it from the purely radiating fibers of the chondrule. The cupule found in several chondrules might be explained by assuming that a second hailstone decided to grow as a parasite on the surface of the first, and then, due to collisions, they became separated. If we adopted this explanation, the glassy portions in some chondrules would have to come about by heating, either by friction in the planetary atmosphere, or later in the matrix. However, an alternative, and perhaps more satisfactory explanation, would be to assume the chondrules grew in the matrix by devitrification of a glassy ball in the manner akin to the formation of spherulites. Spherulitic texture is known to occur in certain dense igneous rocks, and quite often crystallization is seen to start at the surface or other irregularity, not necessarily at the center. The cupule might be due to a pocket of trapped gas or liquid; it is not unknown to find bubbles containing liquid carbon dioxide entrapped within a mass of olivine (Winchell, 1927). The fact that a halo of metal can form around the chondrule argues strongly in favor of the formation of the metal and the chondrule in situ.

B. *Comets and Meteorites*

It is questionable whether carbonaceous chondrites are cometary residues. Certainly the spectra of comets show that this might be the case, particularly if we assume with Whipple (1950a) that the nucleus, perhaps a few miles in diameter, is a conglomerate of meteoric materials with "ices" consisting of H_2O, NH_3, CH_4, CO_2. In time, solar radiation will largely evaporate the ices leaving only an ashy residue of silicates and metal fragments which would collapse down into a friable mass (or masses) intermixed with tars, oils, and water-soluble

glues. Be this as it may, it would be difficult to maintain, with Mason, that the chondrites were formed in near free space as a result of cometary processes. If we are to postulate that chondritic material was derived from a carbonaceous mass, then it would be more reasonable for this conversion to be taking place within a planet; and for this planet to be just big enough to support, in the beginning, terrestrial type processes in its interior. If this were not so, then how could faulting within some chondrites have occurred? Nininger reports unmistakable evidence of flow to have taken place in the Lubbock chondrite; some of the chondrules had been split and their halves separated. This amount of flow could not have taken place within the meteorite after its formation, as it would hardly have remained intact. It is much more reasonable to admit occasional faulting in the mantle of the planet where pressure could reconsolidate material across the slip plane. Then again, how could chondrites possess a natural magnetic moment? This latter is a most interesting observation. Stacey and Lovering (1959), by heating a chondritic meteorite, have shown that one (at least) of the three components of the magnetic moment was induced extra-terrestrially. Adopting Urey's viewpoint, they conclude that either the secondary body had a fluid iron core (but this would surely raise it back to the status of a primary body!) or that a fluid iron core is not necessary to support a main magnetic field (a suggestion that would receive much opposition from current opinion). However, whether secondary bodies are a reality or not, it would be difficult to induce a magnetic moment in a chondrite in free flight.

C. *The Widmanstätten Structure and Planetary Temperature*

Although chondrites have provided most of the argument against the planetary hypothesis, there is still some opposition from the irons. Many students believe that the Widmanstätten figures (alternating kamacite and taenite plates, arranged parallel to the octahedral planes of an original high temperature face centered cubic lattice of uniform chemical composition) would be destroyed in the heat produced in the planetary breakup. Under laboratory conditions the figures can be made to disappear if a 10% Ni octahedrite is heated to about 700° C; after slow cooling to about 600° C they may reappear, but on a much smaller scale and with far less regularity. Any sudden cooling would inhibit the diffusion necessary to grow the plates even on the small scale, and a Martensitic transformation would result. Here, there would be complex distortion of the high temperature lattice. Certain regions, zigzagging their way through the parent lattice, would be strained to the body centered phase without change of chemical composition. In a study of Widmanstätten figures in meteorites Young (1939) believes that the perfection of the figures, developed along the faces of very large crystals, indicate extremely slow cooling within the interior

of some larger body. If planetary breakup did generate sufficient heat to destroy the existing Widmanstätten figures then, as a consequence of the meteorites being hurled into the quenching conditions of outer space, it would be unlikely even in 10^9 years for the figures to return. In order to make them reappear, Nininger supposes that the meteorites undergo a cycle of reheating by close approach to the sun. But it is most improbable that Widmanstätten figures are the result of this process. As Watson points out the figures appear in every block of metal having the proper chemical proportions (about 6-12% Ni) whether in a large metallic meteorite or in a stony-iron. Since 75% of all iron meteorites are octahedrites, it would mean that nearly all meteorites approach the sun to similar distances. An alternative would be to suppose that the breakup heating was not so severe as might be imagined. In fact a cooling process can be envisaged; but whether it would neutralize the heating is debatable. If a meteorite is broken out of the interior of a planet, the sudden relief of pressure would involve an adiabatic cooling which might be considerable. Let dT be the decrease in temperature due to a sudden relief dP of pressure, then

$$C_p\, dT = T\left(\frac{\partial V}{\partial T}\right)_P dP,$$

where C_p is the specific heat at constant pressure, and dV is the volume change. Therefore we have

$$dT = -\frac{T\alpha_p}{\rho C_p}\, dP$$

where α_p is the coefficient of volume expansion at constant pressure, and ρ is the density. It is known that C_p is very insensitive and α_p fairly insensitive to pressure. For a rough estimate of the cooling, we take, for iron, the respective values of C_p and α_p as 5×10^6 ergs gm deg and 36×10^{-6} deg $^{-1}$, a mean density of 9 gm cm^3, and we allow a pressure relief of order 10^{12} dynes/cm^2; hence cooling to temperature T will be given by

$$T \approx T_0\, e^{-0.8} \approx \frac{T_0}{2}$$

where T_0 is the initial temperature in the interior of the planet.

Since we are assuming that the Widmanstätten figures existed before, and were not destroyed in the breakup, we might guess an upper limit for the initial temperature. The formation of kamacite from the face centered phase involves a slight decrease in density. We would therefore expect, by the Le Chatelier principle, that an increase of pressure would depress the temperature of their formation. However, the temperature would not have to be too low, otherwise the necessary diffusion would be inhibited. In cooling an alloy of 10% Ni under normal pressure, the kamacite plates appear at about

600° C; therefore in the interior of the planet the temperature would need to be below 600° C before the Widmanstätten figures could form. Let us assume, then, that at the time of planetary breakup, whether into myriads of small pieces (meteorites) or a few large lumps (asteroids), the initial temperature in the core was about 400° C. If it broke up into small pieces then each would cool to about 60° C, or if it broke into large lumps then the metal near to a now exposed surface would cool to about the same value. But the pressure on this metal is now zero, and in order to destroy the figures the heating, during breakup, would have to raise the temperature to about 700° C. This does not seem feasible in view of the brittle-type fracture that most meteorites seem to have experienced. Had the breakup been of a slow wrenching character, creating a high temperature throughout the body of fragments, then the conditions of ductile flow would have been favored. But this does not seem to have been the case. There is no evidence of such flow in the figures. Their regularity and lack of distortion even at the edges argues strongly in favor of an explosive or impactive fracture at low temperature; fracture occurring so suddenly that plastic flow had no time to take place. In the case of brittle fracture, "body" heating would be caused by the vibrational dissipation of the stored elastic energy accumulated during strain to the point of crushing. Since the compressive strength and bulk modulus of steels is of the order 10^{10} and 10^{12} dynes cm^{-2} respectively, the amount of elastic energy is of order 10^{8} ergs cm^{-3}, giving a temperature rise of about 2° C. Therefore serious heating could only be caused by the fragment lingering too long in the high temperature explosive region formed during the clash of huge bodies.

D. *The Formation of Meteorites*

Some of the meteorites that fall to the earth may have been formed in the initial breakup. But it is tempting to imagine that most of them were formed later as a result of chance collisions of larger bodies. Their cosmic ray ages ranging from a few 10^{6} years to a few 10^{8} years would support this view. Clearly the collision of a small meteorite with an asteroidal body will hardly affect the asteroid. The meteorite and a volume of the asteroid (considerably larger than the meteorite) will merely be reduced to rubble and dust. In this case, it is possible that considerable plastic flow and heating will be produced and some of the dust may be melted or vaporized. Evidence of this kind of collision is afforded by recent laboratory observations of the impact of $\frac{1}{2}$ in. pellets, traveling at over 1 km/sec, with various surfaces. Rinehart and White (1952), using plaster targets, find that the pellets are badly distorted, and Partridge and Vanfleet (1958), using metal targets, find evidence of plastic flow around the impact crater. Here we have some penetration of the pellet into the target with

a consequent rise in temperature due to friction between moving surfaces.

Although it is extremely difficult to envisage the details of collision between large bodies, it is likely that the main results would be quite different from the impact of small pellets. The closest parallel to large scale collision is provided by the huge meteorite craters found in certain parts of the world. These craters were produced by iron meteorites, possibly the size of small buildings, striking the earth with their full cosmic velocity. (Stony meteorites, owing to their friable nature, tend to shatter on impact with the upper atmosphere, and the masses that finally fall are too small to produce explosive craters). In a thorough review of meteorite craters, Nininger points out that "aside from being more or less shattered the rocks surrounding the pit were not much affected. If there was fusion it was limited to a very small area." The Canyon Diablo meteorites are fragments of a huge body that produced the Barringer crater in Arizona. Most of the recovered fragments range in size from less than a gram to over 1000 lb, and are mainly found within a radius of 3 miles from the crater. Also within the same area, numerous minute metallic droplets have been found, indicating an extremely high temperature, sufficient to melt or vaporize a fair proportion of the original body. Further studies show that all the small fragments found in the upper half of the crater rim have altered Widmanstätten figures, but those in the outlying districts have the figures well preserved. It is unfortunate that opinion is divided on whether the meteorite remained intact before contact or whether some fragmentation occurred just prior to contact. This latter view is of course advanced in order to allow the outlying fragments to escape serious heating by the impact of the main mass. However, some of the larger outlying fragments were not sufficiently buried in the ground to prove a high velocity impact - as might be expected if prefragmentation had occurred; and because of this we might be tempted to disregard the prefragmentation hypothesis. Nevertheless, the fact remains that a large body has been demolished and in many of the pieces the Widmanstätten figures have been beautiful preserved, clearly demonstrating that the heating effect (for them) was quite small.

These facts help us to picture the clash of large bodies in outer space. Let us imagine a small asteroid on a collision course with a large asteroid. It is likely that the small body is also in a direct orbit and has a collision velocity of the order of 1 km sec, somewhat less than the velocity of meteoritic impact with the earth. In the region of contact the temperature would rise to vaporize some of the material and create explosive conditions over an area small compared with the size of the resulting pit in the larger body. The material even of iron meteorites tends to be brittle as it is often permeated with inclusions of cohenite (carbide), schreibersite (phosphide), and troilite (sulphide). Being in the asteroidal belt, the initial temperature of the colliding material would be about

$-100°$ C. These conditions, coupled with the explosive character of the collision, would lead to brittle fracture. The small asteroid and the material of the pit would be fragmented into boulders, rubble, and dust. These pieces would be pushed away from the high temperature region rather than be forced through it. Any solid fragments happening to be within the high temperature region would escape heating if they were large enough or if they were traveling away with sufficient speed. From this viewpoint, the small heated fragments found on the rim of the Barringer crater could be those that did not have the necessary speed. But it is important to notice that although they did not travel very far, the heating was not sufficient to melt them. Nininger mentions minute spherical droplets, as if only the dust fragments melted or a vapor condensed; there is no record of large drops. It seems as if there is a sharp transition between the flashed gaseous zone and the cooler shattered zone, and the two zones have not time to mix. The extent of the flashed zone is much smaller than the volume of shattered material, as evidenced by the very small fused area in a meteorite pit. Generalizing, we see that the result of the collision is the formation of a certain amount of explosive gas together with the cold shattering of a far greater quantity of surrounding material, only a comparatively small amount of liquid being formed.

The pit produced in the larger asteroid would be many tens or hundreds of times more voluminous than the colliding body, and energy considerations show that the average velocity of the ejecta is much smaller than the colliding velocity. Indeed, most of the fragments around the Barringer crater are within a mile of the impact zone, indicating a velocity not more than a few tenths of a kilometer per second. Since the colliding asteroids would have an orbital speed about 20 km sec the resulting fragments would have orbits not very different from their parent body. There is reason to believe, then, that the asteroids are continually degrading themselves, producing meteoritic sized particles, together with dust particles, some of which will be fragmentary and others of a spherical shape. But most of this material would be confined to the asteroidal belt; only a small percentage would be sufficiently deviated, by collisions, to move in orbits very eccentric or highly inclined.

III

COSMIC DUST

A. *Zodiacal Light*

That there exists a band of fine dust in the plane of the ecliptic is evident from observations on the Zodiacal Light. Over the last ten years, opinion has been divided on the true nature of this light but it now seems to be hardening in

favor of the traditional model, namely, reflection of sunlight from solid particles. The presence of the Fraunhofer spectrum in the outer corona led Grotrian (1934) to suspect that this *F*-component was due to the presence of dust. Allen (1946) and van der Hulst (1947) showed that such a component does not necessarily belong to the sun, but would be the natural effect of diffraction by small dust particles between the earth and the sun. Assuming that the particles were more numerous in the smaller sizes, but limited by radiation pressure to above about 1μ diameter, they estimate the number density to be of the order of 10^{-15} cm ^{3}, if an upper size limit of about 1 mm be assumed. Allowing a space density of 2×10^{-21} gm/cm^3, Öpik (1956) estimated that the mass falling on the whole earth would be of the order of 700 tons per day. Support for assuming the Zodiacal Light is connected with the outer corona comes from the aircraft observations of Blackwell (1955, 1956) who showed that the brightness curve of the corona, measured over an angular distance from the sun of 1° to 10°, smoothly joins the brightness curve of the zodiacal light as determined by Roach *et al.* (1954) over distances 25° to 100° from the sun. In a review article Blackwell (1960) mentions an attempt by himself and M. F. Ingham to secure a spectrum of the zodiacal light. By comparing this with the spectrum of the sun, they suspect that the light is largely due to dust.

Closer towards the sun, the dust would be vaporized, and nearer still, the gas would be strongly ionized. The emission spectra of iron and nickel have been observed in the inner corona, but these atoms appear to have been stripped of 9 or 10 electrons. The inner corona, or *K*-component, is thought to be due wholly to scattering by electrons. Observations taken at eclipses show that this corona is profoundly modified according to sunspot activity. At sunspot maximum it becomes somewhat circular in shape but during minimum periods it is distorted so that its long axis lies in the direction of the sun's equator. It would seem that this *K*-component properly belongs to the space immediately surrounding the sun; whereas the outer corona and zodiacal light are due to effects taking place at planetary distances. Blackwell (1960) mentions that careful measurements indicate that the axis of symmetry of the zodiacal light lies along the average plane of the planetary orbits, rather than along the ecliptic.

There is the possibility of electrons being mixed with the dust even at planetary distances, and polarization measurements (Blackwell, 1956; Behr and Siedentopf, 1953) have failed to separate the similar effects which the two components would produce. This is mainly due to a complete lack of knowledge of the nature of the dust particle and its polarizing ability for different scattering directions. If the sizes, shape, and chemical composition of the most prevalent dust particles could be secured, then some progress could be made ineluciating this difficult problem.

If we are prepared to accept that dust is the main cause of the zodiacal light, the question arises as to its origin. If it is meteoritic then its composition would be known, and, ascribing the source to the asteroidal belt, we would expect the dust to be in the form of a continuous cloud, the individual particles executing near circular orbits around the sun such that, relative to a nearby planet, their velocities would be very small. The presence of dust inferior to the asteroidal belt would easily be explained by the action of the well known Poynting-Robertson effect, discussed in detail by Lovell (1954). This effect is due to to the isotropic re-emission of radiation by the dust particle; and, because of the Doppler effect, photons emitted in the direction of the particle's motion would be more energetic than photons emitted towards the rear. The result is to cause the particle to spiral slowly into the sun, small particles taking less time to migrate than the larger ones. A rough illustration would be that a particle of iron, diameter 100μ, originally at 1 A.U. would take about 3×10^5 years to spiral into the sun, and a particle twice as big would take twice as long. A further consequence of this process would be the rapid contraction of the aphelion distance, causing an initially elliptic orbit to become circular. The interplanetary space inferior to the earth would be swept clean of dust in a million years and in order to maintain a status quo a continuous supply of fresh dust would have to be created. This would force us to assume that meteorites or asteroids were continually colliding with each other. Taking the average dust particle to be a cube of side 10μ, it would migrate from the earth to the sun in about 3×10^1 years. Assuming the average thickness of the zodiacal cloud to be 0.1 A.U. the mass of dust swept into the sun during this time is 3×10^{18} gm, or 10^8 tons per year, allowing a space density of 2×10^{-21} gm cm^3. If we guess that Bode's missing planet was about the mass of the moon (8×10^{19} tons) then, since the death of the planet 10^9 years ago only a thousandth part of its mass would have been lost to the sun, even assuming that the present infall, which is likely to have been less in times past, was maintained. There would seem to be ample remaining material in the planet to keep the process going for a good while yet.

There is no serious objection to the proposal that meteorites could provide the main contribution to the cloud. It is not difficult to see that the collision process would produce the required supply of dust at the rate demanded. Perhaps the most effective way of producing dust is to consider the erosion of existing meteorites by existing dust. Let us consider the planet already broken down into meteoritic-sized pieces of iron, each weighing about 100 kg. The total area exposed to erosion is of the order of 10^{-24} cm^2. Taking, as before, the average iron particle as a cube of side 10μ and a space density of 2×10^{-21} gm/cm^3, the number density would be about 2×10^{-13}. Allowing a collision velocity of 1 km/sec, the number of collisions would be about 2×10^{-8}/cm^2 sec.

Suppose each particle chipped out a pit 100 times more voluminous than itself, then the mass created per collision would be 10^{-6} gm or 2×10^{-14} gm/cm^2 sec. In one year the mass created by collisions over the total exposed area would be of the order of 10^{17} gm or 10^{11} tons—a value which more than meets the infall demand.

A rival to meteoritic dust would be meteoric dust. It is generally accepted that meteor streams are the disintegration products of cometary breakup. The breakup is probably a spasmodic phenomenon, jets of fine dust being ejected at various places around the orbit when the comet approaches the sun. As the stream becomes older the concentrations of dust become more uniformly spread around the orbit, and the Poynting-Robertson effect would cause much of the finer dust to separate out from the main stream of larger particles, particularly at the aphelion position. Although the parabolic comets have inclinations randomly directed, the periodic ones, with the exception of Halley's comet, have direct orbits of low inclinations to the ecliptic. The disintegration products of these latter comets would give rise to streams of dust which, seen one behind the other, may result in the false impression of a continuum. If meteoric dust is the main cause of the zodiacal light, the cloud would be quite patchy and instead of the earth receiving its constant quota of 700 tons per day, the amount of dust would vary according to the meteoric activity.

Using current information, obtained largely from radio-echo techniques, it would seem that this suggestion could not possibly be correct. In a comprehensive table Lovell estimates the mass contribution of the various meteor showers and of the background sporadic meteors encountered by the earth. In the course of a year the accretion to the earth is about 130 tons from the showers and 485 tons from the sporadics. In the case of the showers most of this mass is contributed by the spectacular daylight streams—the ζ Perseids and Arietids occurring in early June. Taking both these showers together Lovell arrives at an orbital space density of about 6×10^{-24} gm cm^3, and for the sporadics a space density of about 4×10^{-25} gm cm^3—values which are far below the estimated density of the zodiacal cloud. However, these values have been obtained by a doubtful extrapolation. By counting the number of meteors and observing their brightness it would appear, for the sporadic meteors, that over the observational magnitude range 0 (mass $\sim$ 100 mg) to + 12 (mass $\sim 1\mu$g) the contribution to the earth in the particle mass intervals 100 to 10 mg, 10 to 1 mg, 1 to 0.1 mg, and so on, is a constant—about $5 \cdot 10^4$ gm per day. Using this law, the extrapolation ranges from magnitude +12 to +30 (mass $\sim 10^{-8}\,\mu$g, the minimum particle due to radiation pressure). Over such a large range the extrapolation might be unreliable and the above values might be worthless as criteria in deciding the nature of the zodiacal cloud. As Lovell points out, a crucial test must rest on actual measurements of the fine dust

accreted to the earth. Owing to the very small particle mass involved, ionization effects due to impact with the upper atmosphere (at about 100 km) may be very slight or nonexistent, making it difficult or impossible for the radio-echo techniques to observe particles much below 100μ in size. Further progress may only come about by an endeavor to make actual collections of the fine dust as it drifts down to the earth's surface; or by means of special devices within the satellites, to record the number of impinging particles in outer space.

B. *Metallic Iron Dust in the Air*

In a very interesting review of past work Buddhue (1950) mentions the finding of metallic iron particles by the famous arctic explorer Nils Nordenskiöld. During expeditions in 1870 and 1872, Nordenskiöld collected and analyzed some of the greyish-brown dust that becomes concentrated, during the summer, on the surface of the polar snow. In this dust, which gave a positive test for nickel, cobalt, and copper, some of the particles were metallic, as they reduced copper sulphate solution. This provides strong evidence for an extraterrestrial origin. Of further interest, Buddhue mentions the work of L. Rudaux who collected dust in a rain gauge at Donville, France, over the years 1927 to 1933; and, in 1946, the work of H. E. Landsberg who exposed sticky slides and a cup to the air over Virginia. The results of both observers tend to show that more magnetic particles were found in the collections after a meteor shower than before. Again, more recently, Hansa and Zacharov (1958) have made spectrographic studies on dust collected in dishes exposed at various places in Czechoslovakia. Measuring the nickel to iron ratios in the samples collected from June to October they conclude for the years 1954, 1955, and 1956, that the relative amount of nickel in the dust increases after the earth passes through the Perseid and Orionid showers. Allowing for the nickel in terrestrial dust they estimate an accretion rate of 3×10^{-11} gm/cm^2 sec or about 10^7 tons of extraterrestrial dust to the earth per day. This seems an extraordinarily high value, but Pettersson's collections at the top of a 10,000 ft mountain in Hawaii also gives a very high figure. Pettersson (1958) passed large volumes of air through fine-pored filters; and, by measuring the amount of nickel and iron in a known volume of air, arrived at an accretion rate of about 4×10^4 tons per day. Unfortunately, Pettersson does not seem to have allowed for the nickel to iron ratio in the local rocks so this figure must be considered as an upper limit.

The discovery in 1876 of black magnetic "cosmic spherules" in the deep-sea deposits by Murray and Renard (1891) has led many observers to make a special search for spherules in their air-borne collections. Owing to the fact that coal-burning fires can produce black magnetic spherules in profusion, very similar in size and external appearance to the genuine cosmic spherule,

the work on air-borne spherules must be treated with some suspicion, particularly if collections were made near populated areas. In view of this confusion with industrial spherules we have deliberately avoided observations on the spherules, preferring instead to attempt the measurement of the concentration of metallic iron in the air at various times during the year. In the following section we discuss the results to date, leaving reference to spherules for a later section.

C. *Initial Experiments*

In a preliminary work (Parkin and Hunter, 1959), we exposed a large plastic bowl at the top of a lighthouse on Bardsey Island, North Wales. A little filtered water covered the bottom and each day this was tipped out into a clean storing bottle. Exposures were made during August 1957. The samples were used to count and size the magnetic spherules, which were found to be more plentiful when the wind blew from the industrial areas. They ranged down from about 60μ diameter and at 5μ diameter—the limit of microscopic vision—they were extremely numerous. In the last bottle to be examined, exposed on 21st August, our attention was drawn to certain metallic looking flakes about 100μ in size, occurring in the magnetic fraction. Two or three turned coppery when immersed in a bead of copper sulphate solution. During August 1958 we repeated the water bowl exposures on St. Agnes, Isles of Scilly, adding a little formalin to the water to prevent organic growth. There was a marked drop in the number of spherules; but, for the whole month, seven metallic iron flakes around 50μ in size were found. One of these, 150μ in size, picked up between the 11th and 13th, was largely a mineral aggregate which seemed to be held together by veins of iron. Five of the flakes were found after the 19th. Estimating the total mass of iron, and knowing the area of the bowl (1/15 meter^2), we arrive at a mean accretion rate for August of about 0.2μg/meter^2 day, or 100 tons to the whole earth per day. Through the kindness of Mr. B. C. Oddie of the Meteorological Office and Mr. W. G. Durbin of the Meteorological Research Flight dust collections were made (in 1958) on August 11th and August 20th, from an aircraft at 10,000 ft. The dust was allowed to impinge on a sticky slotted perspex slide of effective area 10 cm^2, held in an aluminium frame and projecting a few feet from the fuselage so that it would be safe from contamination from the engines. Knowing the speed of the aircraft (200 mph) and the exposure time per slide (30 min), the volume of the air sampled was roughly determined. On the 11th, two iron flakes were picked up, one 80μ and the other 30μ, giving a concentration of 350 μg/10^6 meter of air. On the 20th, five flakes were found, two being 200μ and three being around 60μ, giving a concentration 1000μg/10^6 meter^3. Several slides were exposed on each flight.

In testing the Scilly Is. flakes, as soon as it was established that the particle was going coppery it was withdrawn and washed. On placing about three or four of these flakes together with the mineral aggregate at the bottom of a tiny tube and adding beads of standard reagents, the presence of nickel was very definitely confirmed. This evidence led us to believe in the extraterrestrial nature of these flakes, but owing to the small amount collected it was impossible to be certain about a contribution from the Perseid shower, which reaches its maximum around the 12th. These flakes are quite irregular in shape and are reminiscent of the particles described by Urey and Mayeda (1959). Sometimes they do not react to copper sulphate immediately and it is necessary, on occasion, to crush the particle. In these cases it seems as though the metallic iron is effectively protected by an oxide coating.

D. *The Greased Mesh Technique*

Clearly a much more efficient collecting technique was needed, and it was decided to mount a greased nylon mesh so that it always faced the wind. By placing a cup-type anemometer behind the mesh the volume of the wind passing through could be measured. The collecting efficiency of the mesh was roughly determined by placing four greased meshes one behind the other and exposing the stack to the wind (over Liverpool). The first mesh prevented straw and large bits from reaching the remaining meshes. In a few hours sufficient fine dust was collected by the remaining meshes for the weight on each to be measured. from which a transmission coefficient could be estimated, giving a collection efficiency of about 45%. (Our meshes are a simple weave giving a square aperture of side 710μ and, according to the manufacturers, an open area of 54%). The mounting device was constructed of wood and hardboard held together with brass screws, and before the exposures commenced it was thoroughly washed down with sea water and left for a few hours to be blown dry. Figure 1 shows the arrangement in position on a rocky prominence at the southernmost tip of St. Agnes.

The basic procedure is to dip the mesh into a filtered petrol-vaseline mixture so that the fibers will remain sticky during the exposure period and then, after a few days, to wash off the grease and dust in a shallow porcelain dish containing filtered petrol. The petrol is poured into a clean settling-out bottle; three washes are given. After the dust has settled, the clear petrol above is siphoned off and the dust transferred to a smaller storing bottle which is labeled with the date, anemometer readings, and weather report. Back in the laboratory the dust is transferred to a petrie dish together with a little petrol, and a magnetic separation is effected by presenting the dish to a small conical polepiece around which a cone of filter paper is wrapped. The magnetic particles are attracted

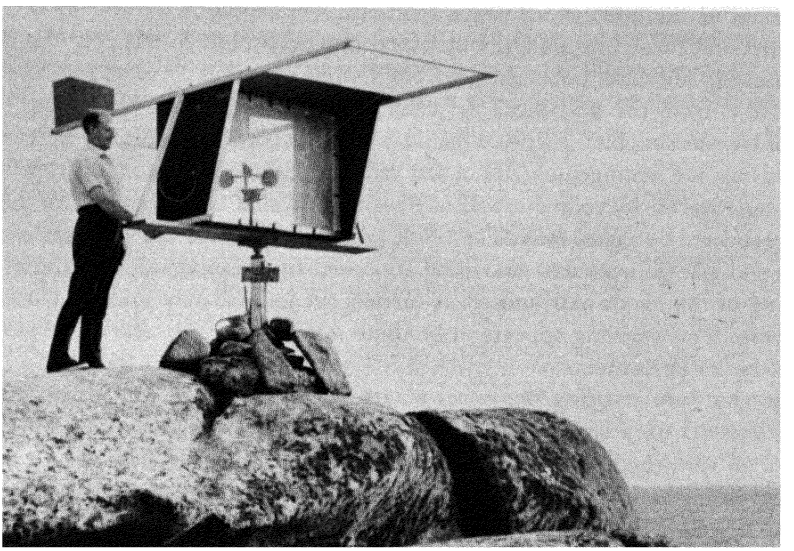


FIG. 1. One of the authors (W. H.) attending the dust collector at St. Agnes, Isles of Scilly.

to the tip of the filter paper which (without overloading it too much) is then removed and turned inside out and folded into an octant, so trapping the dust at the apex. The filter paper originally is a circle of radius 1 cm and we always separate it from the pole-piece by a second paper which acts as a guard, for fear of transferring bits of iron to the outer paper; this is probably not necessary after using the arrangement for a few times. The magnet is first cleaned of stray bits of iron by rolling a ball of Plasticene over it and when not in use it is kept covered by a glass tank. The whole process takes place in a small sealed-off room and plastic overcoats and caps are worn by the operators. A thorough washing of the hands and forearm is carried out immediately prior to entering the room. This washing appears to be quite satisfactory; the wearing of gloves would be an encumbrance.

It is now safe to bring the paper octant out of the room for the magnetic measurements on a sensitive torsion balance. The octant is fitted into a cleft in a small varnished bamboo stick which is then attached to the end of a light wooden horizontal torsion arm, so that the stick points vertically downwards. The octant is washed in benzene to remove any traces of grease and is then immersed in hot water to drive off the benzene. While still wet, a powerful permanent magnet is brought up and arranged so that the apex of the octant is always positioned midway between the plate-type pole pieces and is leveled against markers on the magnet by means of paper riders on the torsion arm. With these plate-type pole pieces the magnetic field is made more uniform and sighting the apex to a predetermined position, by eye, gives satisfactorily reproducible results. By twisting the vertical torsion wire the octant is quickly brought out of the field to its break-away position and then in gradual stages the twist is increased, pausing for several seconds while the "sighting position" is checked. The twist for breakaway is quite definite and can be reproduced within $\pm 2°$ in a 400° or 500° twist. The measurement is repeated by turning the stick through a right angle. Usually this repeated twist may differ from the first by about $\pm 5°$ and is probably due to the shape of the sample at the apex. The mean is taken and called the initial twist which is a measure of the amount of terrestrial magnetic material and metallic iron at the apex. The octant is now soaked for about 10 to 15 min in hot copper sulphate solution, which is than washed out by a further soaking in hot water. While still wet with water the final twists for break-away are taken and the mean of these is subtracted from the initial twist to give a measure of the amount of metallic iron converted into nonmagnetic copper. The main steps in the procedure are easily understood from the sketch in Fig. 2. The copper sulphate seems to have no effect on the terrestrial magnetic material.

The calibration of the torsion wire was effected by determining the twists on a much stiffer wire to cause accurately weighed milligram samples of 10%

Ni-Fe filings to break free of the same magnetic field. (Some of these samples were treated with copper sulphate and the final twist was always about zero.) The torsional stiffnesses of the two wires were compared by timing the vibrations of an inertia bar attached to the end of each wire in turn. In the wire we used,

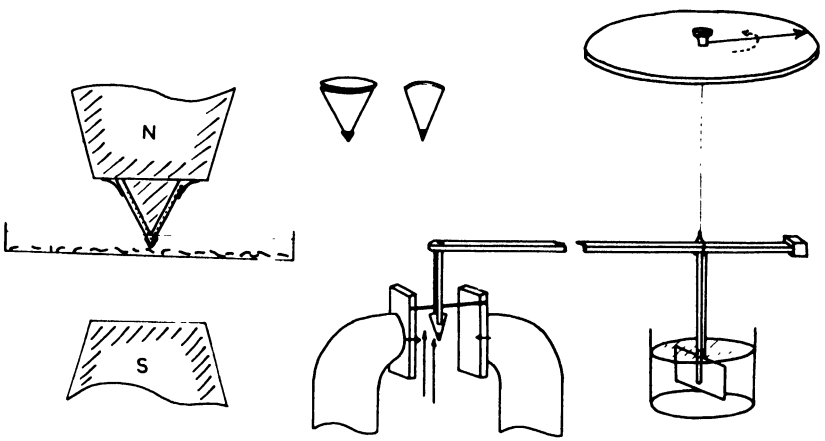


FIG. 2. The method of measuring the metallic iron by means of the magnetic torsion balance (see text).

a twist of 8° corresponded to 1μg of iron and we believe we can determine the mass of iron to $\pm\frac{1}{2}\mu$g, which probably results in a percentage scatter (amongst the different samples) much less than the scatter due to errors in the collecting and petrol-washing techniques.

To date, three expeditions to Scilly have been carried out. But owing partly to misfortune and partly to mismanagement, we cannot be confident about the fine details of the measurements, although it seems as though the main result is secure: namely, that the concentration of metallic iron in the air increases after a meteor shower. We hope to be able to supply conclusive proof of this after the next expedition this coming August, provided the strength and direction of the wind remains within certain limits during the critical periods. The main trouble is with the collecting and washing techniques and since the amount of iron collected from the passage of about half a million cubic meters of air is only 15μg the difficulties with contamination can easily be imagined. In view of these uncertainties we offer the following results with reservations, believing that they may be of value to other observers who already may have carried out similar measurements and, like us, are in a state of uncertainty.

1. *August 1959*

Only one mesh ($\frac{1}{2}$ meter^2) was used during the expedition and, before exposure, it was washed at the site in dilute hydrochloric acid and then rinsed in seawater. After about five days the mesh was washed in petrol, regreased, and re-exposed. Towards the end of the expedition it was realized that this washing procedure was not too efficient as the mesh became noticeably dirtier. This resulted from moisture adhering to the fibers, which, although not apparent on the mesh, was visible later as a layer of water at the bottom of the storing bottles. Back in the laboratory this layer of salty water caused much trouble when transferring the dust to the Petrie dish, as water in petrol behaves similarly to grease in water.

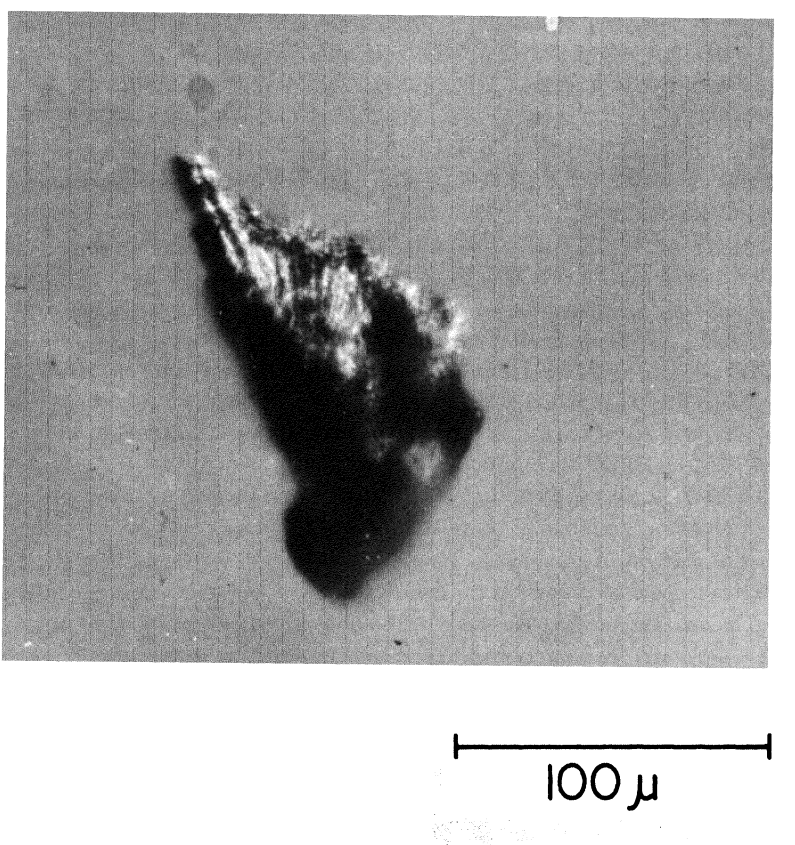


FIG. 3. Flake of iron obtained from greased mesh; Scilly, August 1959 (note striations).

Before measuring the amount of iron it was usual to perform a magnetic sweep attracting the particles to the underside of a small watch glass and submitting the collection to microscopic examination. Some half-dozen iron flakes, about 100μ in size (together with a black spherule, which broke open to reveal a silvery core of metal), were found mainly between the 11th and 25th days. These flakes were not tested with copper sulphate as there appeared to be no doubt about their nature. After inspection they were returned to the petrie dish, together with the collection, and measurements were carried out as previously described. However, two of the largest were removed and, with the spherule, were mounted on an aluminum cube for analysis by the electron-probe x-ray microanalyzer, kindly carried out for us by Mr. I. K. Openshaw of A.E.I., Manchester. This instrument, by focusing a beam of electrons, is able to perform an accurate analysis over 1μ^2 and, by a scanning technique, is able to display the distribution of a chosen element over the specimen. The spherule proved to be very similar to the deep-sea iron cosmic spherules, having about 16 to 20% nickel concentrated in the metallic core and a negligible amount of nickel in the surrounding magnetite. The two flakes consisted of a nickel-iron alloy, both having about 8% nickel and 2% cobalt, uniformly distributed. One of the flakes, Fig. 3, was photographed under highly oblique illumination in order to display what appears to be striations on the surface. At first it was thought that these striations were due to metallic fracture, and indeed this may be true, but under close scrutiny it seems as though the flake is built up of a series of plates; these are shown, somewhat exaggerated, in the sketch, Fig. 4(a). Unfortunately, the other fragment was lost, but the sketch, Fig. 4(b), shows its main features. In shape it was like a pear cut length-

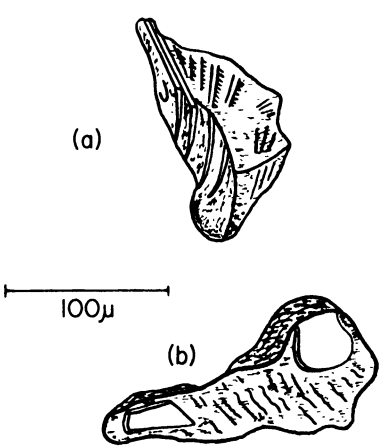


FIG. 4. Drawings of iron flakes showing platelike structure and striations.

wise, the flat face being quite silvery, with two raised regions (plates) giving mirrorlike reflectivity. The curved surface (the skin of the pear) was a lustrous black, indicating that this might be the original outer surface of a freshly cleaved particle. The production of these flakes remains a puzzle. The uniform distribution of nickel, as revealed by the scanning technique, seems to show that they are not plessite, as might be conjectured from their platelike structure. Their shape and jagged outline is typical of other extraterrestrial particles (see Fig. 12) and in our experience, so far, the shapes of the fragments may be generalized into: (a) flakes which have the proportions of the human hand laid flat down, fingers together; (b) needles, which are more elongated than the flakes but still retain a jagged outline and are like the human finger.

In this and earlier work, we did not carry out our observations under the stringent precautions against contamination that were described above and adopted in all later work. But the room was far from workshops and the possibility of contamination from ironfilings would have been remote. However, on previous occasions, whilst looking for iron particles in other material—for instance Parkin and Hunter (1959) Greenland Snow—we would sometimes find long wiskers of metallic iron; these were always about 20-40μ wide and rectangular in section, and might be $\frac{1}{2}$ mm long. Clearly they were produced by extrusion processes. Two such whiskers were located in the Scilly material and exposed to the electron probe. As mentioned in an added note to our paper (Hunter and Parkin, 1960) no nickel or cobalt was found. Later, we found these whiskers to be bits of steel wool used by cleaners as an abrasive material. Since adopting the precautions, we have had no further trouble with whiskers. In our published work these whiskers were called needles, but we now wish to reserve the term needle to jagged fingerlike fragments.

The measured concentration of metallic iron is shown in Fig. 5, together with a weather report. The two dashed parallel lines on the wind direction graph are bearings to Mizzen Head, S. W. Ireland, and Ile d'Ouessant, near Brest, N.W. France. When the wind blew from directions seaward of these bearings it was particularly clean of terrestrial contamination. The sector also excludes any land of the Scilly group. An attempt was made to run the mesh for five-day periods, but unfortunately on August 14 high winds partly wrecked the apparatus and the mesh was blown out; the results for this period are uncertain. Furthermore, the wind direction was very variable during the whole month and on many occasions it blew from the east, bringing a great deal of magnetic rocky fragments which made the measurements on the torsion balance difficult. However, by repeated magnetic "sweeps" it is fairly certain that most of the iron was removed from the petrie dish, and possibly any errors in the measurements would cancel themselves out rather than be cumulative. Owing to the imperfections of the operation as a whole, little can be said about the

accuracy of any individual result, but taken in their entirety there is strong support for an approximate doubling of the concentration of the metallic iron in the air after the middle of August, the abrupt onset around the 15th suggesting a marked contribution from the Perseids, with a possible decay around the 20th.

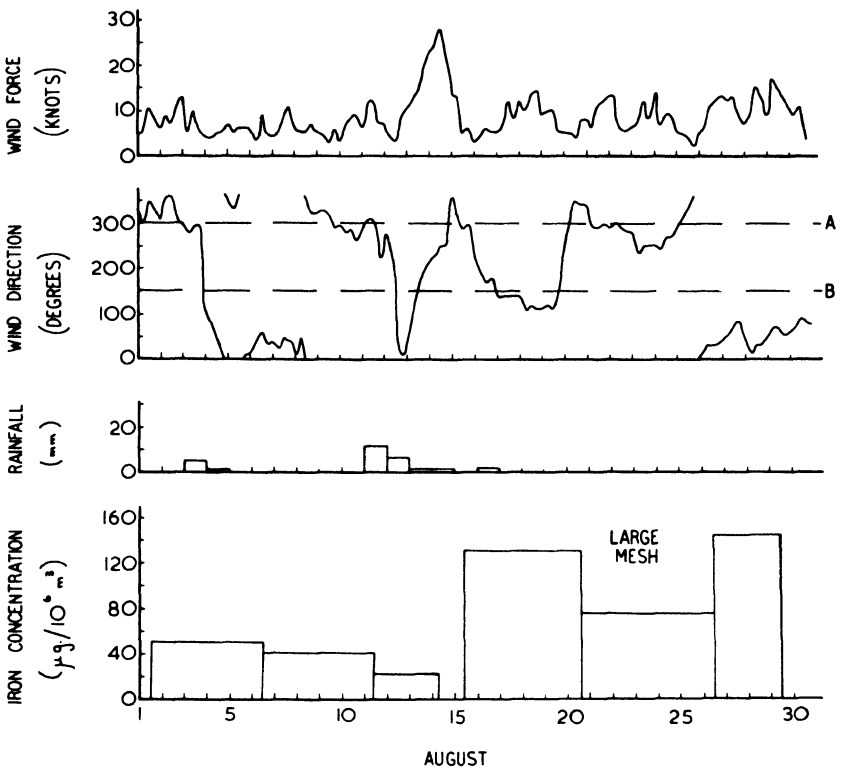


FIG. 5. Iron concentration in air and weather report from greased mesh; Scilly, August 1959. (Day commences at midnight. A and B are bearings to Mizzen Head and Ile d'Ouessant, respectively.)

At the same time a water bowl was set up, the exposures being in phase with the meshes. Back in the laboratory W. H., without first knowing the dates on the storing bottles, undertook a microscopic search for metallic iron, using the copper sulphate method. He found, between the 15th and 26th one flake (and possibly a second) about 100μ in size, also a needle 290μ long, which gave a positive test for nickel by the chemical method, and another needle 60μ long; no iron bearing mineral aggregates were seen, and nothing of interest was observed outside these dates. In chemically testing the large needle it was

seen that it only slowly dissolved in hydrochloric acid and that a skin, presumably an oxide coat, remained. These oxide coats, observed by the same method on other particles, may be formed during an initial heating in the upper atmosphere.

2. *July, August, and September 1960*

At the time, the observed increase in the iron concentration was something of a surprise as we were not prepared to believe that a meteor shower could contribute a significant "signal" so readily detected above the presumably heavy background "noise" of a constant contribution from the zodiacal cloud. In order to confirm the result a more elaborate program was planned and the laboratory was made as dust-free as possible. Two collecting devices were built each exposing a mesh of $\frac{3}{4}$ meter^2 which, in view of occasional high winds, is the largest area we dare expose. Hoping to avoid the trouble of washing the mesh at the site, it was decided to supply sufficient meshes to cover the period of the expedition, each being sealed, already greased, in its own storing bottle. After exposure, the mesh would be returned to the bottle. Back in the laboratory, it would be easy to rid the mesh of salt and moisture by soaking in water and oven drying, and then carry out the petrol washing procedure more efficiently. Unfortunately, the meshes were not rinsed in hydrochloric acid during their preparation and on account of this oversight the whole of the observations as given in Fig. 6 must be treated with suspicion. On two meshes that were brought back unexposed about twice as much iron was found on them as on the exposed meshes. This contamination must have been present on the meshes when supplied, as it was later found that, even if a thorough wash be given in detergents (a part of the preparation process for the exposed meshes), dust particles originally adhering to the nylon fibers were not completely removed. Again misfortune attended the expedition; within a few minutes of setting up the first device, the brass pivot snapped and the apparatus crashed on to granite boulders some 30 ft below. It was a total loss. Fearing to trust the brass pivot on the other device, we decided to fit a steel pivot, believing that since it would be swathed in grease no abraded iron particles could contaminate the mesh—a fact later to be proved correct.

It is strange that the results of the three-day exposures during August agree so remarkably well with the results obtained in 1959, even to the dip around the 20th. But on reflection, it might be that any contamination, being common iron, would rust away during the time the mesh was exposed to the corrosive marine environment. Perhaps the results are sound; it is a pity they were not supported by observations with the second device.

The high iron concentration around July 20 may be due to the strong daylight streams α-Orionids, ν-Geminids, and λ-Geminids which all occur together

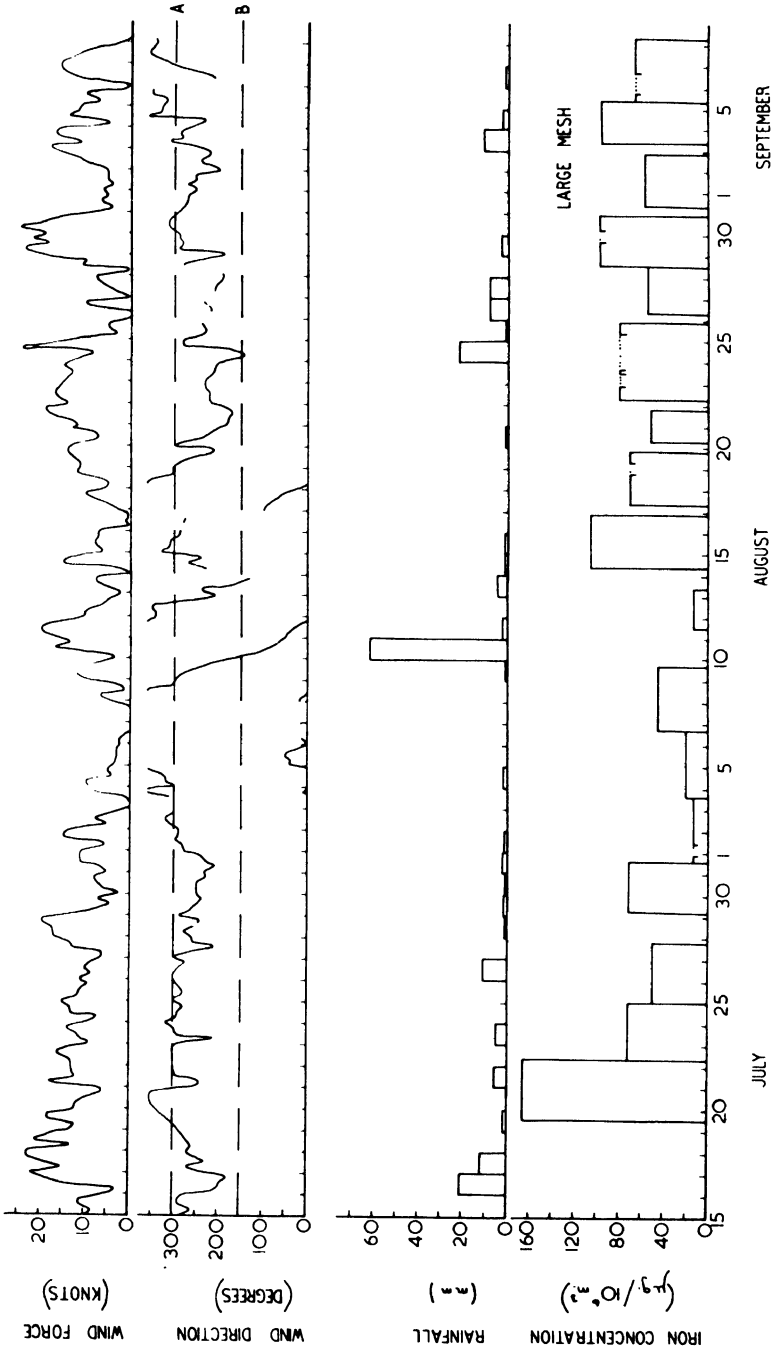


FIG. 6. Iron concentration in air and weather report from greased mesh; Scilly, July, August, and September 1960.

between 12th and 17th July. According to Lovell (1954) these showers were picked up in 1948 but were not observed in the following years. Of course, this does not necessarily mean that the fine dust should be absent. Although the large particles of these showers may be concentrated into a knot it is possible that the fine dust has already spread out fairly uniformly around the orbit so that the large amount of iron found in the air around the 20th may be a regular occurrence. If we can believe these results a further feature is revealed. The air seems to clear itself of the iron dust rather rapidly. The regular falling off of iron around July 24 and August 19 seems to indicate that even the finest particles of iron only take a few days to arrive in the troposphere. Once in this turbulent region they would be quickly brought to earth and, on striking the "sticky" surface, may not rise again with the general circulation.

Due to fairly steady westerly winds most of the collected samples were very clean of magnetic terrestrial material and it was possible to make a microscopic examination of the material at the apex of the paper octant after measurements had been completed. By soaking the paper in liquid paraffin it was not too difficult to see some of the larger coppery specks which, because of their color, stand out against the blackish contamination. The results of the survey are listed in Table I. There seems to be a pattern in these observations; in many instances it can be seen that large flakes are recorded immediately before a peak in the iron concentration, yet may be absent at the peak. As would be expected, the larger flakes arrive a few days before the finer dust, but it is surprising to find that (if they are to be associated with a shower) they arrive so soon. For example, if the peak on July 30 is to be associated with the δ-Aquarids, occurring about July 28, the large flakes must only take a few hours to come down. The dimensions of some of the largest flakes would be equivalent to a spherical diameter of about 30μ and if we allow a free fall from about 80 km the time taken would be around 5 days (for a sphere 5μ diameter it would be about 100 days). This disparity might be accounted for if we allowed the particles to "ice-up" in the upper atmosphere. But it is debatable whether this would happen owing to the known low water vapor content of the stratosphere.

Rain does not seem to affect the observations to any marked extent. At the beginning of the exposures in July, the rain was quite heavy at times but the meshes were left out. Thinking that rain might wash the dust and grease from the fibers, it was decided to withdraw the mesh during periods of rain, and the dotted portions of the concentration histogram show when this was done. We now believe that this precaution was unnecessary and during our next expedition the meshes were left out all the time.

TABLE I

IRON FLAKES CAUGHT ON GREASED MESH, SCILLY, AUGUST 1960 (SIZES APPROXIMATE ONLY[a])

Date	Iron flakes' sizes (μ)	Iron flake Masses (μg)	Total iron (torsion balance) mass (μg)	Fine iron mass (μg)	Mass iron flakes / Mass fine iron
July 19-22	Very little dirt No large flakes seen		50	50	0
July 22-25	60 × 70 × 5	0.17			
	100 × 90 × 5	0.36			
	40 × 30 × 5	0.05			
		0.58	16.8	16.2	0.036
July 25-27	30 × 40 × 10	0.10			
	100 × 10 × 10	0.08			
	90 × 25 × 10	0.18			
	50 × 40 × 20	0.30			
	120 × 20 × 10	0.19			
		0.85	8.7	7.85	0.11
July 29-31	Very little dirt No large flakes seen		13.8	13.8	0
July 31-August 3	Too much dirt to see properly		2.2	2.2	0?
August 3-6	Too much dirt to see properly		2.5	2.5	0?
August 6-9	110 × 50 × 10	0.44			
	80 × 70 × 5	0.16			
	35 × 12 × 5	0.02			
	50 × 15 × 12	0.07			
	20 × 15 × 5	0.01			
		0.70	6.7	6.0	0.12

[a] Many flakes are irregular in shape; mass estimates allow for this.

TABLE I *(continued)*

Date	Iron flakes' sizes (μ)	Iron flake Masses (μg)	Total iron (torsion balance) mass (μg)	Fine iron mass (μg)	Mass iron flakes / Mass fine iron
August 11-13	Too much dirt to see properly		1.8	1.8	0?
August 14-16	100 × 8 × 8	0.05			
	50 × 25 × 8	0.08			
		0.13	16.2	16.07	0.0075
August 17-19	90 × 15 × 15	0.16	11.6	11.4	0.014
August 20-21	20 × 24 × 5	0.02	9.1	9.08	0.002
August 22-25	Very little dirt No large flakes seen		10.4	10.4	0
August 26-28	50 × 45 × 5	0.10			
	30 × 15 × 5	0.02			
	25 × 15 × 5	0.02			
		0.14	7.0	6.86	0.02
August 28-30	Very little dirt No large flakes seen		15.2	15.2	0
August 31-September 2	110 × 30 × 15	0.25			
	80 × 30 × 20	0.38			
	60 × 80 × 5	0.19			
	70 × 60 × 5	0.17			
		0.99	10.0	9.0	0.11
September 3-5	Very little dirt No large flakes seen		17.1	17.1	0
September 5-8	Very little dirt No large flakes seen		9.4	9.4	0

3. *December 1960*

Mr. A. E. Brownlow, our technical assistant, accompanied one of the authors (W. H.) to Scilly in order to record effects from the Geminids which occur around December 12. This time we were determined to avoid the difficulties of contamination by reverting to the procedure of 1959, i.e., prerinsing in hydrochloric acid and washing at the site. To be sure that the mesh was salt-free and dry before washing with petrol, it was first soaked in settled water, and then spin-dried by placing it in a string bag and whirling it around a few

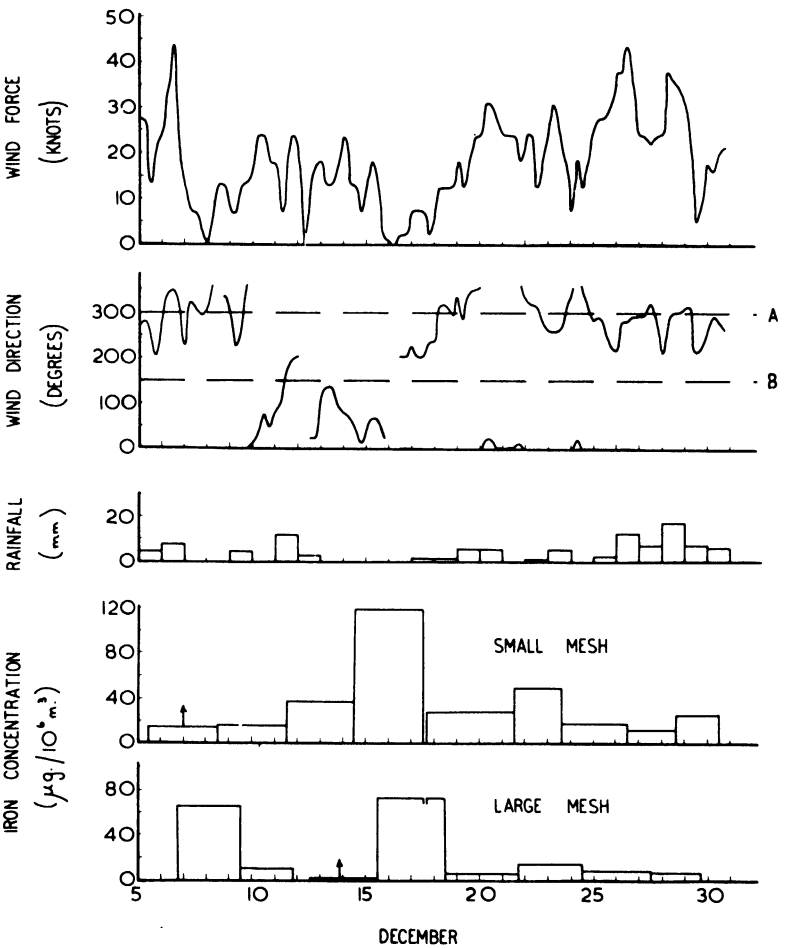


FIG. 7. Iron concentration in air and weather report from greased mesh; Scilly, December 1960.

times. The mesh was then attached to the underside of a deep plastic lid which fitted over a box containing silica gel. The mesh was left overnight to dry off completely. In order that exposures should not be interrupted, two meshes were used, the exposure-washing cycle being maintained until the end of the month. In anticipation of high winds, a smaller device was constructed, exposing a mesh 1/6 meter^2, the same cyclic procedure as above being used in this case. At first the large device was mounted on the rocky prominence, but high winds and further gale warnings necessitated its removal to a lower and more sheltered site. The small device was placed in the exposed position and it behaved perfectly, even in gale force winds. A torsion wire having a twist of 24° per μg of iron was used for measurements on the small meshes.

From the results of the large and small meshes as given in Fig. 7, the fine dust contribution from the Geminids seems certain; although measurements during this period were difficult owing to much terrestrial contamination caused by easterly winds, and they were particularly difficult for the meshes exposed around the 13th. Due to the calm weather during the critical period, the amount of iron collected was low and the percentage errors in the final concentrations may be fairly high. The concentration for the large mesh during the period around the 13th should be higher than measured, as we should have continued with more magnetic sweeps on the dust in the petrie dish. (Actually, the first two sweeps gave no iron, and thinking that there was indeed no iron present the dust was thrown away. Later when we carried out measurement in the corresponding small mesh the same thing happened for the first sweep, but repeated sweeps drew out a fair quantity). The greatest mass of iron was recorded on the large mesh during the first exposure and owing to westerly winds it was possible to inspect the material. About two dozen coppery specks ranging down from 50μ were seen. With the exception of two specks about 50μ in size, seen on the large mesh during the second exposure, no large flakes were definitely observed for the other periods. Something must have gone wrong with the first of the small meshes, as hardly any magnetic material was picked up during the sweeps. Nearly 700 miles of wind had passed through this mesh and even though the wind was westerly, experience with other meshes indicated that nothing like sufficient dust had been collected. The only explanation that can be offered is that, perhaps, the mesh had not been greased. This operation could easily have been overlooked as the first few days were a worrying period. However, it is possible to rectify this mistake and to be reasonably sure that the result on the large mesh is genuine. Although the total magnetic material collected was small, it was possible to detect a little iron, and the ratio of iron to "magnetic rock" agreed with the same ratio on the large mesh. These ratios, expressing the character of the dust, were estimated for all the exposures and the correlations between the two series of meshes were quite good. We

conclude that around the beginning of December the concentration of iron in the air was as high as that recorded on the large mesh.

It will be noticed that, in general, the amount of iron collected by the large meshes is quite definitely lower than the amount collected on the small meshes. We believe this is due to the lower siting position of the large device, and this raises the question as to whether the usual position on the rocky prominence is high enough to record a true concentration of iron in the air. It now seems reasonable to argue that due to irregular up and down movements of the wind, streams nearer sea level would strike the sea surface more often than streams higher up, and therefore the lower layers might be quite clean of dust. Perhaps very little dust would be collected by a mesh at sea level. This may be an important point for the reader to bear in mind if he chooses to set up similar collecting devices.

There is a suspicion of a peak around the 23rd, which might be associated with the Ursids which are a periodic stream occurring on about the 21st. Perhaps the peak around the 30th on the small mesh is experimental scatter, as no corresponding rise was detected on the large mesh and it seems too early for the Quadrantids which occur on the 3rd January. (Unfortunately, other duties prevented us from continuing exposures beyond the 30th.) It is interesting to speculate on whether the peak at the beginning of the month could be connected with the Bielids which Lovell (1954) reports as a lost stream. In the last century intense meteoric storms occurred around December 6 and these were associated with Biela's Comet. But in recent years activity has died away and the date of the visual shower has shifted back to around November 20, although Lovell reports ovservations by J. P. M. Prentice, who in 1940 records a weak display of Bielids from November 27 to December 4.

Accepting the Geminid peak as reliable, we see once again that the arrival of the fine dust is sudden, and its subsequent decay a rapid process. Lovell mentions, with regard to the Geminids, that the short-duration echoes (the small meteors) are distributed fairly symmetrically around a date some two or three days before the maximum of the main shower. This might be due to the action of the Poynting-Robertson effect which would cause the smaller particles to travel in orbits inferior to the main stream. The Geminids have a short period, about 1.5 years; and they are only slightly inclined to the ecliptic, about 24°. The earth intersects the orbit so that it ought to run into the smaller particles before the larger ones. This would allow us to argue that our Geminid peak was due to the arrival, in the upper atmosphere, of the finest particles, perhaps a week before the visual display. But if we are to believe that our results demonstrate fine dust contributions from the Perseids and the Ursids we could not use this argument, as these streams have orbits nearly perpendicular to the ecliptic. Therefore, in these cases, irrespective of any action by the Poynting-

Robertson effect, the earth would run into the fine dust at the same time as the visual particles, and we would be forced to assume that the fine dust takes only about 2 or 3 days to fall to the earth's surface.

This is very puzzling and as mentioned above it does suggest icing-up. Turbulence in the upper atmosphere is known from the study of sodium vapor trails made by high-altitude sounding rockets and also from the smoke trails left by disintegrating meteorites (Nininger shows some photographs of these trails). Perhaps, vertically descending currents bring the dust rapidly down to the tropopause where icing-up could occur. The particle might now be too heavy to rise again with an ascending current. Once into the troposphere, convection would quickly clear it from the air, as it would be impossible for a particle to rise if it struck the sea surface; again rain must play some role in cleaning the air. In this connection Bowen (1953) has put forward a most interesting hypothesis. By adding up the daily rainfall occurring at Sydney from the year 1859 to 1944, he finds that more rain than usual fell on January 13, January 23, and January 31. These dates are about 30 days after the Geminids, the Ursids, and the Quadrantids respectively, and he suggests that particles 1 to 4$\mu\mu$ diameter from these showers provide the ice nuclei responsible for the increased rainfall. Even if meteoric particles are effective ice nuclei, our results would be a flat contradiction to this hypothesis. Of course, we only measure the iron dust, and from the well-known spectra work of P. M. Millman it is certain that many other substances must be associated with the meteors. But it would be natural to expect that if iron dust arrives, and is cleared out of the troposphere within a few days, the other fine material should behave in a similar manner. Differences in rainfall between England and Australia cannot be used to explain the discrepancy, as the summer of 1959 was especially dry, and the fall-off around August 20 is quite marked.

In summarizing this work to date, we would tentatively suggest that, for iron dust, the accretion rate to the earth does vary with meteoric activity; and the sizes of the particles responsible for this range down from about 100μ, with most of the mass confined to sizes below about 20μ. We might take the "background" concentration to be about 20μg/10^6 meter^3 and allowing a rate of descent of about 90 km in 3 days (as given by the onset of a peak and its associated shower) the iron accretion rate, due to the background, would be about 0.6μg/meter^2 day or 300 tons to the earth per day. The iron component of the zodiacal cloud seems quite patchy, but since we are ignorant of the presence of other fragmentary material, it is impossible to be certain whether the cloud is really as patchy as our results would suggest. It is plausible that the background iron is meteoritic; and, owing to the friable nature of stony meteorites a much greater ratio of stone to iron dust may exist in outer space than would be estimated from the 10 to 1 ratio obtained from recent meteoritic falls. But

this would force us to conclude that if the zodiacal light was largely a reflection from a continuum of meteoritic stony dust, then more than 3000 tons of stony fragments would fall on the earth per day. In order to solve this puzzle it is very necessary to enquire whether material other than iron is falling from outer space. This is a very difficult problem, but some progress can be made by collecting in the very remote parts of the world, or, better still, by recovering the dust from outer space. Now that recoverable satellites are a possibility, it may not be outrageous to suggest the exposure of a block of transparent jellylike substance in which the impinging particles could be arrested. Again much useful information in this respect is likely to come from aircraft sampling in the stratosphere, a project recently embarked upon by Dr. E. L. Fireman of the Smithsonian Institution.

E. *Cosmic Spherules*

Because of the very slow rate of sedimentation, about 1 mm per 1000 years, occurring in the deepest parts of an ocean (the red clay regions), extraterrestrial material has a chance to accumulate in surprisingly large quantities. For instance, Pettersson and Rotschi (1950) believe that the high nickel content found in the deep-sea sediments is due to the dissolution of extraterrestrial material falling to the ocean's bed, and estimate an amount of several thousands of tons for the whole earth per day. However, it is fortunate that not all the extraterrestrial material is corroded away; certain black magnetic spherules found in large quantity in the sediments seem quite inert to their environment. Undoubtedly these spherules represent a molten form of extraterrestrial material, but it is not yet possible to get a clear picture of how they were produced. Opinion is divided on whether they were swept off the heated surface of a falling meteorite or whether they originally existed in outer space as tiny fragments and became molten droplets by interaction with the upper atmosphere. Whipple (1950b), and Öpik (1951, 1956) have considered this latter problem and conclude that if the original dust particle was below a certain critical size, depending on its initial velocity and angle of entry, then it would not melt. This is because the surface area of the particle is able to radiate away the heat produced as it slows down in the upper air. As estimated by Whipple this critical radius s of an originally spherical particle, in terms of its melting point T_m, initial relative velocity V_∞ on entry, and angle of incidence z (measured from the vertical), is given by

$$s = \frac{9e\beta\sigma D(T_m^4 - T_0^4)}{\alpha\rho b \cos z \, V_\infty^3}$$

where e is the base of the natural logarithms, σ is Stefan's constant, b is the logarithmic density gradient of an assumed atmosphere, and T_0 is the initial temperature of the particle. The other constants depend on the nature of the particle; β is the thermal emissivity, D is the air-drag coefficient, α is the accommodation coefficient (expressing the heating efficiency of the colliding air molecules), and ρ is the density of the particle. Whipple determines that for the Giacobinid meteor shower, particles less than about 8μ diameter would not reach their melting point. For particles somewhat larger than this value, we should expect to find some evidence of melting; this is so.

By passing a magnet through samples of deep-sea mud, Murray and Renard (1891) were able to extract a number of black spherules around 100μ diameter. Two kinds of spherules were identified; (1) spherules possessing an outer coating of oxide which when removed showed an inner core of silvery metal and (2) silicate spherules. Murray and Renard were convinced that these spherules were from outer space and first named them "cosmic spherules", although positive proof of this origin had to await the more detailed work of recent years. Using spherules extracted from deep-sea cores obtained during the Swedish "Albatross" expedition (Pettersson and Fredriksson, 1958), Castaing and Fredriksson (1958) have shown, with the electron probe, that the metal core in the oxide spherules contains around 50% of nickel, but in the oxide coating the nickel is very low, around 0.1%. This is to be expected, as during the heating of the original metal, iron would be preferentially oxidized and the nickel would be pushed ahead of the advancing oxide layer and concentrated in any metal core remaining. The possibility of the silicate spherules also coming from outer space is provided by our own work on the surface deep-sea muds (Hunter and Parkin, 1960).

We were kindly supplied with three samples of mud, one from the Pacific (P1) and two from the Atlantic (A1, A2). After working up weighed portions of the mud into a thin liquid with water, the magnetic fraction, mainly magnetite, was inspected with a low-power microscope ($\times 100$). The spherules were picked up on the end of a glass fiber wetted with medicinal liquid paraffin; and, by thrusting this fiber through the surface of paraffin contained in a small glass cell, it was possible to estimate the density of the spherule by timing its fall past an eyepiece scale in a viewing microscope. We found that most of the spherules could be grouped into two classes, (a) those with density around 6, and (b) those with density around 3. Photographs (Figs. 8 and 9) show groups of the stony and iron spherules, respectively. The stony spherules, which have duller surfaces than the irons, sometimes depart quite noticeably from sphericity, being occasionally spheroidal or even pear-shaped.

Often spherules with craters are seen, and in these cases, if broken open, they reveal creamy centers which are masses of tiny crystals loosely aggregated.

Nininger shows a photograph of chondrules prized out of a stony meteorite, and comparison with the stony spherules in Fig. 8 is most striking. However, the similarity is confined to external appearances only, and as far as we can tell,

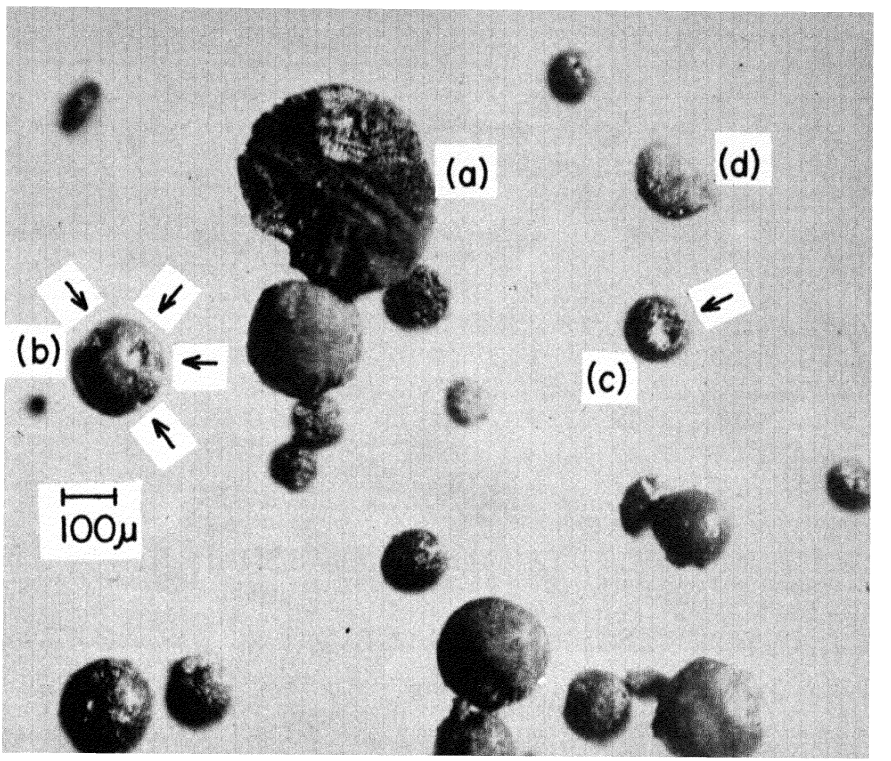


FIG. 8. Stony cosmic spherules, (a) is a broken section showing dendrites; (b), (c), and (d) are creamy-centered spherules showing craters at the surface. (Courtesy of the Royal Society.)

these spherules are not microchondrules. Most of the stony spherules when broken open are blackened throughout and as revealed by a section shown in Fig. 8(a), their dendritic structure indicates a rapid cooling from the melt. In the case of the creamy-centered spherules, there seems to be no evidence of a radiating fibrous structure, although we cannot really be sure about this as our work on their internal structure has been cursory. Taking these spherules all together, an X-ray powder photograph showed them to be olivine. It was not possible to decide on their exact composition but the photograph suggested that the olivine was rather rich in magnesium, i.e., forsterite. The forsterite composition was confirmed on the interior material of the creamy-centered

spherules by Dr. G. Voll (Geology Dept., University of Liverpool) using mineralogical techniques.

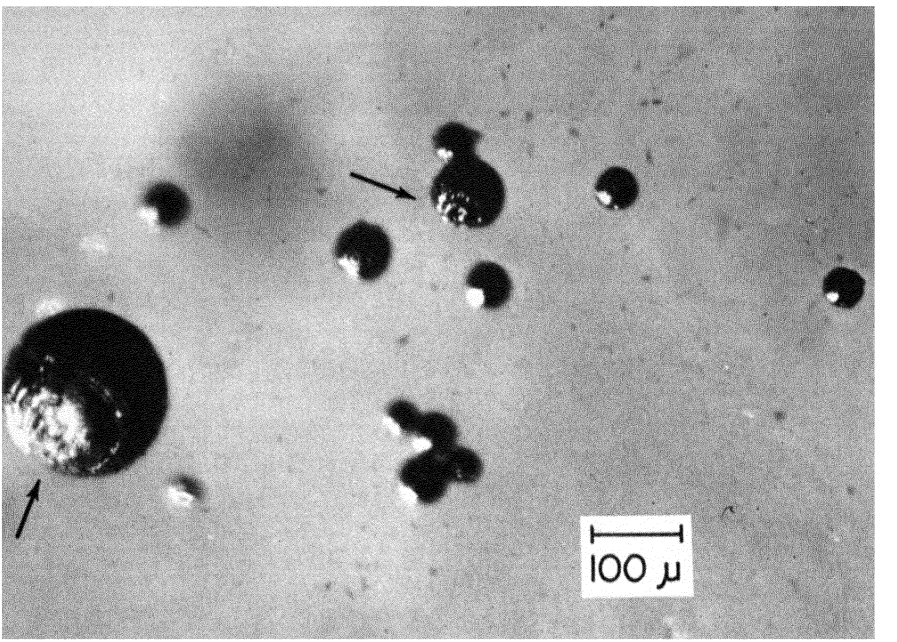


FIG. 9. Iron cosmic spherules. Arrows point to regions where metallic nucleus can be seen. (Courtesy of the Royal Society.)

The main argument for the extraterrestrial origin of these stony spherules comes from the comparison of the stone to iron number ratio found in the samples of mud examined. Details are given in Table II. Although the samples were obtained from different parts of the world the number ratio, particularly for A2 and P1 which are more reliable, is about one to one. Accepting the extraterrestrial nature of the iron spherules, the same origin for the stones seems most plausible. Further support for the argument is provided by comparing the size distribution patterns obtained for each of the samples. These distribution patterns are very similar to the pattern shown in Fig. 10, which shows the results of all the spherules added together. (A number of stony spherules are shown plotted above the main sequence; these have been ignored as they represent the distribution of distorted spherules.) It will be noticed that a curious depression occurs in the stony distribution around 60μ diameter. This is not understood, but an explanation can be derived with the help of Whipple's

formula, and this would support the hypothesis that the spherules were formed from tiny fragmentary material.

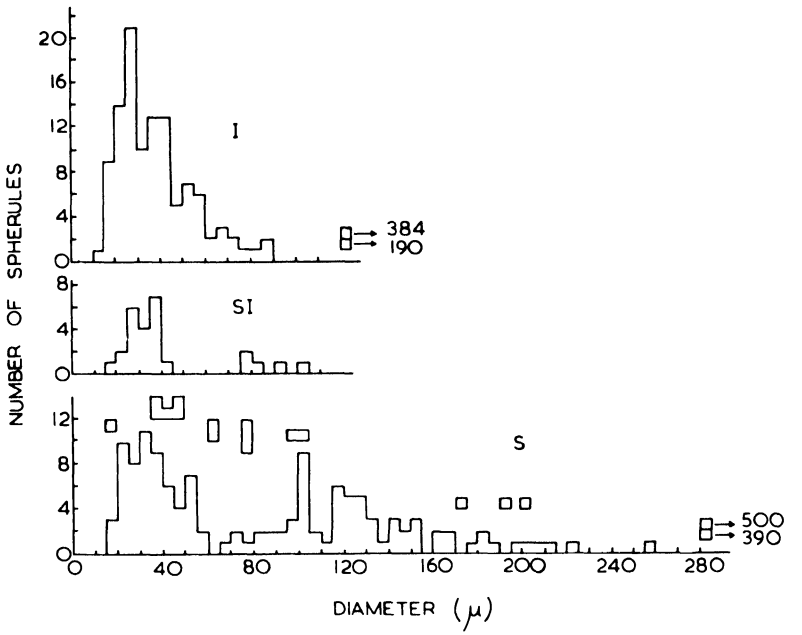


FIG. 10. Size distributions of the stony (S), the stony-iron (SI), and iron (I) spherules. (Courtesy of the Royal Society.)

As described in our previous work (Hunter and Parkin, 1960) it is natural to suppose that the iron and stone dust fragments in outer space have the same velocity and direction distributions, and we may reasonably assume that the constants β, D, and α are the same for the two groups. Therefore, the ratio of the minimum sizes of the iron and stony particles, made molten, should be given by

$$\frac{S_1}{S_s} \approx \frac{T_1^4 - T_0^4}{T_s^4 - T_0^4} \cdot \frac{\rho_s}{\rho_1}$$

where the subscripts refer to iron and stone. Assuming for 10% nickel-iron alloy the melting point $T_1 \approx 1750°$ K and $\rho_1 \approx 8.0$, and for typical forsterite, $T_s \approx 2100°$ K and $\rho_s \approx 3.3$, we see that

$$\frac{S_1}{S_s} \approx \frac{1}{5}$$

where T_0 (about 300° K) has been neglected.

TABLE II

NUMBER AND VOLUME OF SPHERULES (EXCLUDING THE VERY LARGE AND DISTORTED SPHERULES)
(volume in 10^6 μ^3)

Station	Latitude	Longitude	Depth (meters)	Irons		Stones		Stony irons		Total number	Weight of dry sediment (gm)	No./kg
				No.	Vol.	No.	Vol.	No.	Vol.			
A1	34° 11′ N	55° 32′ W	5582	6	0.1	12	14	1	0.042	19	1380	14
A2	24° 30′ N	64° 47′ W	5949	47	2.4	54	46	15	1.0	116	490	240
P	22° 07′ S	115° 10′ W	3060 (3200)	57	2.6	61	40	10	0.50	128	350	370
Total				110	5.1	127	100	26	1.5	263	—	—

If we assume from Fig. 10 that, for iron, the smallest spherule diameter is around 15μ, then the smallest stony spherule should be around 75μ. There does seem to be a cutoff around this value; but it must be pointed out that this argument depends on the correct estimate for the cutoff value of the iron spherules which, because of much fine magnetite grains in the deep-sea muds, is very difficult to secure. However, supporting evidence comes from the observations of Laevastu and Mellis (1955) who, working with Pettersson's core material, did not find spherules below 13μ diameter. The group of stony spherules occurring below 60μ might be derived from the breakup of large spherules due to aerodynamic forces.

The cosmic spherules, being either iron or stone (and possibly stony-iron mixtures as indicated by a group of spherules of density between 3.5 and 4.9, shown in Fig. 10), seem to be meteoritic in origin, but the central question, as to their production, remains unanswered. It is certain that meteorites do throw off molten droplets, as Nininger reports evidence in many cases of "thread lines" radiating from the forward face of both stone and iron meteorites; and in the irons these threads are "molten metal, usually 0.1 to 0.5 mm in width." A pertinent question is, could meteorites produce enough spherules? From their core work Pettersson and Fredriksson estimate that about 1000-5000 tons of spherules fall to earth per year; and Watson reckons that about 2000 meteorites of initial mass 100 kg enter the atmosphere per year. If the mass of each meteorite was converted into spherules (which does not happen) then only 200 tons of spherules would arrive per year. Perhaps more crucial evidence results from considering the creamy-centered spherules; these particles suggest a thermal shock and only superficial melting which would not occur if the material was stripped from the molten surface of a larger body. Indeed, since a glassy fusion crust surrounds most stony meteorites we would only expect to find glassy balls. If then, we assume that the spherules were produced from particulate material, a further question can be posed. How big was the particle from which the spherule came? This seems to have an answer; and a calculation by Castaing and Fredriksson is most helpful, although these authors incline to the "dripping" meteorite hypothesis. Knowing the dimensions and compositions of the various parts of the iron spherule, they estimate the Ni to Fe ratio for the spherule as a whole. Allowing for oxygen in the outer coating they find a ratio of 6 to 14% in one spherule and about 12% in another. These ratios are very reasonable for meteoritic iron and it seems to us to suggest that fragments of meteoritic iron merely oxidize and become molten, without much evaporation, if any, occurring.

Öpik (1951) believes that the spherules come from particulate matter belonging to the zodiacal cloud and that they enter the earth's atmosphere with velocities not much greater than the escape velocity of 11.1 km per second. These low

velocities allow quite large particles to pass through the atmosphere, particularly for grazing incidence, without becoming molten. Integrating over all angles of incidence and allowing a reasonably small spread of velocity Öpik (1956) produces a size distribution for iron spherules which is in very good agreement with observations by Laevastu and Mellis, although these observations probably give a size distribution containing both iron and stony spherules. However, this latter criticism may not be too serious as Laevastu and Mellis extracted their spherules from long cores and it is possible that, owing to the unstable character of olivine, stony spherules only exist in the surface layers.

From Öpik (1951) we see that, for diameters of originally spherical particles of about 30μ, (which would be equivalent to our largest iron flakes caught in the air) the proportion of unmolten particles to molten spherules is of order unity; for diameters below about 15μ, practically all the dust would be unmolten. But, as can be seen from Whipple's formula, these size distributions are very sensitive to the initial velocity, and for meteoric velocities of about 40 km/sec Öpik (1951) shows that practically all particles with diameters above about 20μ would be vaporized. This would seem to indicate that our large iron flakes are not to be associated with meteoric showers but rather with low velocity meteoritic dust; yet there does seem to be some connection between their time of arrival and a following peak in the iron concentration. However, it is too early to be certain about this. Undoubtedly, most of the iron flakes collected during a peak have sizes much below 20μ and it is therefore possible that they could pass through unmolten, even though they arrive with meteoric speeds.

From core work it is estimated that about 10 tons of spherules fall to earth each day, and since the stony spherules are on average bigger than the irons only about one-tenth of this mass is due to iron, yet hundreds of tons of background iron dust in the form of fine flakes arrive per day. If, and only if, the background iron (or the large iron flakes) are connected with the iron spherules, then background stone (or large stony flakes) should be connected with the stony spherules; therefore we should expect to find thousands of tons of stony material arriving each day. In an effort to locate this material two expeditions were organized: (a) Royal Mail Lines Ltd. kindly allowed us to mount a small greased mesh device on the bow of one of their vessels plying between London and Buenos Aires; and we are indebted to Capt. L. T. Peterson of R.M.S. "Darro" for carrying out the collections. (b) Application was made to Sir Vivian Fuchs of the Falkland Island Dependencies Survey (F.I.D.S.) in order that samples of snow from the Antarctic could be examined. Time has not yet permitted the examination of the Atlantic meshes, but interesting results have been obtained in preliminary work on the snow.

F. *The Antarctic Ice Cliff Experiment*

The Fig. 11, kindly photographed by Mr. D. A. Ardus who also made the snow collections, shows the ice cliff at Halley Bay and the places from which the samples were collected. It may be possible to see a number of horizontal

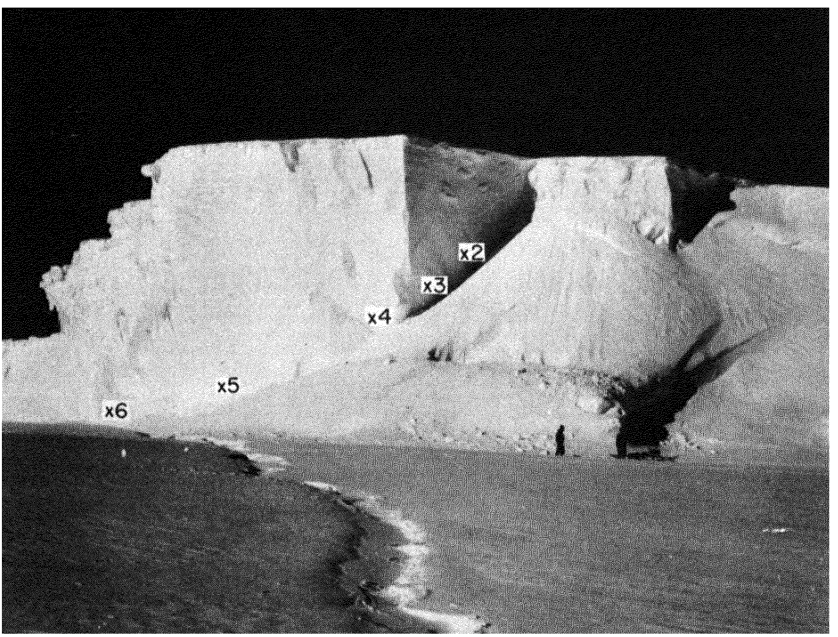


FIG. 11. Ice cliff at Halley Bay. Numbers give positions of the cavities from which the snow was sampled. (Sea-ice in foreground.)

lines on the face of the cliff; these are bands of ice separating layers of winter snow. During the summer months the temperature may rise, on occasions, so that the top surface of the snow melts, and on refreezing solidifies the upper layers into a more compact mass than the snow underneath. By counting the bands down from the surface, a particular cavity from which the snow was collected, can be dated.

Flakes of metallic iron were found at all levels. At a particular level, since the specific gravity of the snow was recorded and the distance apart of the bands was measured, an accretion rate for the iron dust laid down at that time could be estimated. For instance, if a mass M of iron is found in a volume V of melt-

water, at a level where s is the specific gravity and r the yearly accumulation rate of snow, then the accretion rate would be given by Msr/V.

In consultation with Dr. R. J. Adie (F.I.D.S. University of Birmingham) it was decided to chip snow (using nonmagnetic, aluminum-bronze pickaxes) from six cavities down the face; and to store the snow in eight two gallon poly-

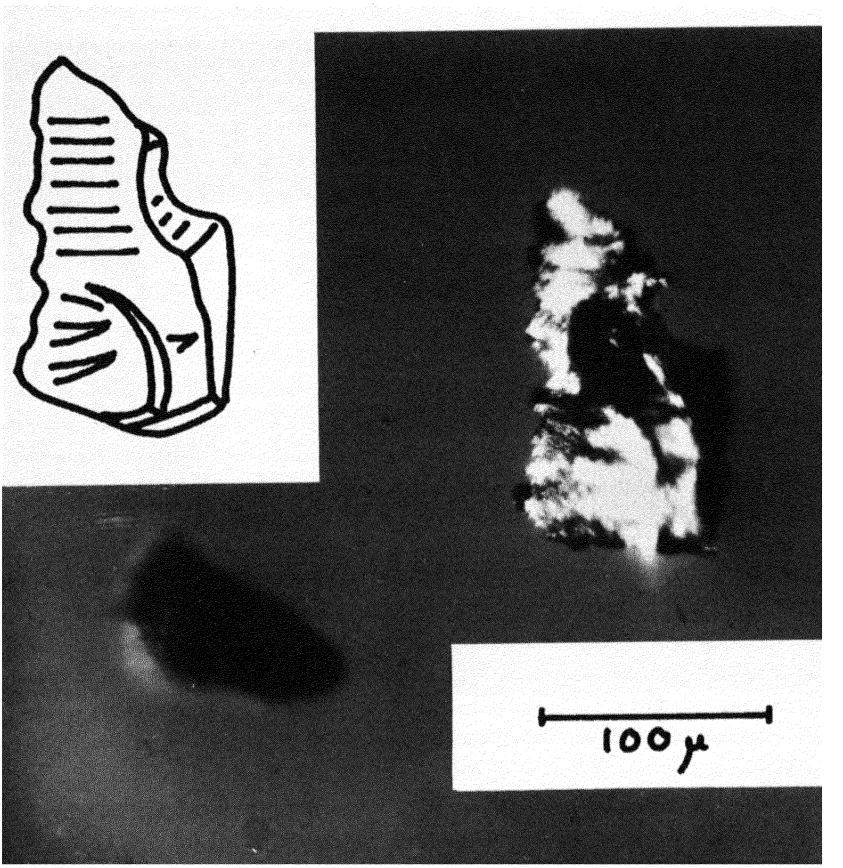


FIG. 12. Flake of iron from cavity 4, Halley Bay. (Inset is drawing showing striations.)

thene bottles, which were supplied thoroughly washed out with hydrochloric acid and rinsed with settled water. To prevent dust entering the bottles during transport, or contaminating their outsides, each bottle was wrapped in a cleaned polythene bag. The volume sampled is rather low, and in order to test whether the results from a cavity gave a true value for the accretion rate at that level,

three bottles were filled from the same cavity (No. 3), and the melt-water in each was examined individually.

The method of examination followed that for the water-bowl technique. The settled melt-water was first drawn off and then the dust plus a little water was transferred to a petrie dish, the magnetic material being attracted to the underside of a plate glued to the polepieces of a magnet. Suspected fragments were submitted to copper sulphate solution, and in a number of cases it was necessary to crush an outer coating of oxide before the fragment would go coppery. Only one particle was found in cavity 4, but it is the largest fragment that we have ever seen; it is shown in Fig. 12. Once again striations on the surface (similar to those on the Scilly particle, Fig. 3) were seen; these are shown more clearly in the sketch in the inset. The out of focus particle is another flake of iron. The large fragment had a brilliant reflectivity, and instead of testing it with copper sulphate, an x-ray powder photograph was taken—Co. Kα radiation, 7 hr in a 9 cm camera. Only two very weak lines could be seen. If belonging to a two phase nickel-iron alloy, the lines give the lattice parameters as 3.57 A and 2.84 A, in good agreement with taenite and kamacite respectively. For a particle of this size, and for the length of exposure it was given, many more lines ought to have appeared on the film, unless the percentage of nickel was within certain limits. Owen and Lui (1949) give pictures of a series of x-ray powder patterns for a nickel-iron alloy of varying composition. For nickel composition between about 16 and 20%, the lines are very weak indeed. Although this fragment has not yet been tested with the electron probe, we might anticipate the result, i.e., that it contains kamacite and taenite phases with an over-all composition of about 16% Ni.* The Scilly fragment in Fig. 3 was also x-rayed under similar conditions; but, owing no doubt to its small size, only one weak line could be seen. This was due to kamacite and the presence of the single phase is in accord with the low nickel content as revealed by the electron probe. These x-ray results are important in showing that these fragments are very fine-grained polycrystals.

The examination of the snow proved to be very disappointing. In every bottle terrestrial contamination was surprisingly large. The magnetic fraction consisted mainly of magnetite (magnetite was the only substance revealed by x-ray analysis) and each bottle contained dozens of small flakes of magnetite ranging down from about 100μ. On occasions translucent flakes were seen but these all floated in beads of bromoform (specific gravity 2.9) and therefore could not have been olivine, which has a specific gravity greater than 3.2. Olivine is slightly magnetic, particularly if it contains magnetite and this is

* See Note (1) in the Addendum concerning accurate composition obtained with electron probe.

probably why the deep-sea stony spherules are magnetic. Even more dirt was present in the nonmagnetic fraction which consisted mainly of hundreds of colorless transparent glassy shards ranging down from over 200μ in size. Also, there were a number of clear glassy spherules or ovoids. Colored material was not so abundant as the clear glass, but there were many flakes of jet black glass. Although we have little experience in identifying mineral grains, it seems to us that the vast majority of this dirt is volcanic ash and it is possible that the active volcanoes in the South Sandwich Islands could be a source of this material. But these islands are about 1000 miles to the north of Halley Bay and it is surprising that such large particles can be transported all this way. The dirt is very variable. Cavities 5, 3, 2, and the surface were noticeably more contaminated than 4 and 6.

By concentrating the nonmagnetic fraction onto a watch glass, allowing it to dry, and then adding bromoform, it was seen that a few orange-red flakes of 100μ and less in size would not float. These flakes were the only particles heavier than bromoform. They were slightly transparent and largely amorphous, but an x-ray diffraction pattern gave γ-ferric oxide monohydrate. In no bottle was an olivine flake identified. Perhaps extraterrestrial flakes of olivine were present, but we failed to find them. Certainly there were no flakes as large as the iron flakes; or, if there were, then they were nothing like as numerous. This unexpected result was very disappointing, yet at the same time, very interesting. Three possibilities emerge, (1) unprotected flakes of olivine might rapidly decompose, even in snow, (2) olivine flakes are falling from outer space but they are so tiny that we would not see them under our low-power microscopes, (3) olivine flakes do not exist in outer space.

Possibility (1) might be ruled out on the grounds of low temperature conditions. However, we may have a chance to test this when we come to examine the Atlantic greased meshes. The olivine flakes will be trapped in grease which may inhibit their dissolution. Possibilities (2) and (3) are connected. In a fascinating account of the zodiacal cloud, Öpik (1951) puts forward reasons, based on the work of Pettersson and Rotschi, for believing the cloud to be purely iron dust. He contends that any "ices" or highly volatile material would be vaporized long before reaching the earth's orbit and that the stony particles, being more friable than the iron, would be pulverized by collisions into a very fine powder which may be so fine as to be driven out of the solar system by radiation pressure. This must not be taken to mean that there are no stony flakes at all, as a few large flakes must be present if we are to assume that they give rise to the stony spherules. Indeed, the apparent start of the stony spherule distribution at 75μ diameter might be taken to indicate the minimum flake size, around 150μ, that exists in outerspace. Collisions between flakes of this size and those slightly larger produce the fine powder which we fail to see in

our microscopes or is driven out of the solar system. This argument, although suitable for the present need, seems highly artificial. It is probably better to reconcile the experimental facts (for what they are worth) by assuming that spherules are derived from meteorites or meteoritic dust (as the mass ratio iron to olivine is about right); and because meteoritic material might be rare compared with meteoric material, meteoritic flakes might be rare compared with meteoric flakes. Therefore, if olivine is only meteoritic, olivine flakes are rare compared with iron flakes which may be the only meteoric component that survives flight through the atmosphere. It is of course questionable whether olivine (or pyroxene) exists in meteoric particles. The constituent elements have been found in meteor spectra, but it may require the high temperature conditions within a planet to form the mineral.

If spherules are droplets swept from the surface of a meteorite, then we have no need to evoke the presence of meteoritic dust, and the absence of olivine flakes provides no embarrassment. If not, we are once again in difficulty over size. Why should meteoritic iron flakes produce spherules when meteoric iron flakes, of much the same size yet traveling much faster, come through unscathed? Two answers can be proposed: (1) The original meteoritic flake of iron is very much bigger than the spherule, and the spherule is merely a residue remaining after evaporation—an argument considered by Öpik (1956) but unsupported by the calculation of a previous section. (2) The original meteoric flake is unlike the original meteoritic flake. The former, being derived from cometary residues, may be embedded in a mass of low volatile oils or waxes, which evaporate and cool the flake during retardation in the atmosphere; whereas the meteoritic flake would be unprotected and exposed to the full heating effects. This second answer is akin to Öpik's "dust-ball" model of the meteor particle (Öpik, 1956) but differs in as much as the "solid" material is scattered about in a tiny wax ball which is a more permanent structure than the open network of the dust ball, and therefore capable of withstanding mutual collisions in outer space. Furthermore, a wax ball model might be useful in providing a "reverse-rocket" effect. Just as explosions occur in comets, so the frictional heating on first impact with the atmosphere may liberate stored energy (free radicals produced by solar radiation) in the frontal regions of the wax causing portions of the ball to be projected forward, thereby slightly reducing the forward motion of the particle as a whole. Or a total explosion might occur in which a spray of the solid flakes would result. Those flung backwards would have the best chance of survival, but many flakes projected sideways may survive as they would tend to enter the air with a smaller grazing angle than their parent particle. However, these processes are likely to be inefficient as the explosion speeds will be small compared with that of the meteor. Perhaps a better method of protecting the flakes would be to allow the wax to "drip," so that it sheds the flakes in the

near vacuum of its own wake. Because of little resistance, the dust may nearly keep pace with the disintegrating ball which, while it lasts, provides a shielding action. Wrapping the iron dust into a wax ball would indicate that fewer meteoric particles exist in outer space than otherwise, thereby reducing the meteoric component in the zodiacal light, and emphasizing the role played by the continuous cloud of meteoritic material. But these wax balls would not have to be too big, otherwise they would produce visible or ionization effects; and it is known from radar work that "telescopic meteors" are too few in number to contribute the required tonnage—unless, of course, their particle mass has been grossly underestimated. Worthy of note is the recent spectra work on a Perseid meteor. Millman (1953) has identified the line Hα and believes that hydrogen "ices" may accompany the meteor particle.

Black magnetic spherules were found in most of the bottles and from the dirty cavities they were quite numerous. For instance, in one of the bottles from cavity 3, about 30 spherules were counted with diameters ranging down from 30μ to below 5μ, being more numerous in the smaller size ranges. These spherules are unlike the deep-sea variety as their densities lie between about 4.4 and 3, and their size distribution would not agree with the genuine cosmic spherules. However, x-ray examination shows them to be only magnetite, and it is believed that the low density is due to hollows within their interiors. Their large numbers and their association with the dirty bottles precludes a cosmic origin, but it is a puzzle to account for their presence. Magnetite has a high melting point and it is unlikely that a flake of magnetite could be melted in the gases from a volcano. It may be melted deeper down but under those circumstances it would be embedded in a matrix and on breaking out, would hardly come away cleanly; some bits of the matrix would still adhere. Perhaps they are mainly dark glassy balls with fine specks of magnetite here and there; this would also account for a low density and allow a volcanic origin.

As can be seen from Table III the amount of iron collected in each of the bottles from cavity 3 is variable. Clearly the amount of snow was not sufficient to give a true average for the accretion rate, and variations in the accretion rate for the different levels is only an approximation. However, a mean value of about 0.2μg/meter^2/day would be a fair estimate, giving a mass to earth of 100 tons of iron per day. Of course, this is the accretion rate for large flakes only. From Table I, if we allow one-twentieth of the dust to consist of large flakes, the total accretion rate at the Antarctic would be about 2000 tons, in fair agreement with results obtained from the greased mesh in England, which would be of the order of 1000 tons, allowing for peaks due to meteor showers. Once again we see that the majority of the flakes are below 100μ. Taking the Antarctic and Scilly results together it seems that the 100μ flake size is a practical cutoff for iron; and the size distribution for the fine dust does not smoothly

join up with the size distribution for visual meteors. Nor should we expect this to be so, if we accept a wax ball model. The sizes of the balls determine the visual distribution, whereas the flakes within the ball give the fine dust distribution. If the iron within the ball is primordial in origin the 100μ cutoff value may be an important factor in considering the structure of the interstellar dust clouds.

G. *The Effect of the Earth's Magnetic Field*

The Scilly and Antarctic results on iron are too crude to allow a decision on whether the earth's magnetic field influences the distribution of cosmic dust with latitude. It seems however that there is no marked effect. Öpik (1956) and Singer (1958) have considered this problem. Both authors agree that a dust particle in outer space would be electrically charged either by electron accretion or photoemission. If the particle was not in the shadow of the earth, photoemission would dominate, and the particle might be charged to a potential of about 100 volts. In competition with inertia the earth's magnetic field would have little direct action on the path of the dust particle, particularly at meteoric speeds. However, the situation may be radically altered if ionized interplanetary gas exists, as there would be a strong interaction between the gas and the particle. Indeed, fine dust may, in a very short time, be brought to rest with respect to the gas, and thereafter drift with it. According to Öpik, if a rotating cloud of zodiacal gas did exist, it would have a dramatic effect on the zodiacal particles, causing them to drift rapidly into the sun and at the same time to concentrate strongly towards the ecliptic. "A narrow bright belt becoming narrower and brighter toward the sun would result, appearing as a prominent strip within the more diffuse cone of the gaseous component of the zodiacal light." Since no such belt has ever been observed, Öpik concludes that a "quiescent rotating cloud of zodiacal gas is incompatible with the observational evidence; the gas cannot be present in such a form in interplanetary space, whatever its density." Assuming the presence of a gas, the meteoritic dust, perhaps at rest with respect to it, would tend to stream into the earth over the auroral zones; and at Halley Bay, where many aurora are seen, we ought to expect a much greater accretion rate than at Scilly. This does not appear in our results; but it must again be pointed out that we have no direct knowledge of the very fine iron dust in the Antarctic snow. From the iron spherule distribution we would expect that meteoritic iron flakes below about 10μ (equivalent spherical diameter) should be present in an undamaged form. Indeed the "background" iron of the Scilly results (300 tons to earth) may be largely meteoritic. Until we secure a total mass of iron in the Antarctic snow, and prove conclusively that the magnetite spherules are a contaminant, we cannot entirely rule out the effects of a magnetic

TABLE III

IRON FLAKES IN ICE CLIFF AT HALLEY BAY (SIZES OF FLAKES APPROXIMATE ONLY[a])

Cavity	Age ± 3 years	Accumulation rate (meters/year)	Specific gravity	Mass of melt-water (gm)	Volume of snow (cm^3)	Iron flakes sizes (μ)	Iron flake masses (μg)	Conc. of iron in snow ($\mu g/meter^3$)	Accretion rate ($\mu g/meter^2/day$)
1	Surface 1959	0.82	0.47	4375	9300	50 × 10 × 10	0.04		
						80 × 30 × 10	0.19		
						70 × 40 × 30	0.67		
						90 × 25 × 20	0.36		
						90 × 10 × 10	0.07		
							1.33	143	0.39
2	14 1945	0.45	0.61	2745	4500	80 × 20 × 20	0.26		
						60 × 50 × 10	0.24		
						40 × 20 × 3	0.02		
						90 × 10 × 10	0.07		
						40 × 15 × 10	0.05		
						100 × 50 × 10	0.40		
						60 × 35 × 20	0.50		
						90 × 20 × 15	0.22		
							1.76	391	0.48
3a	24 1935	0.47	0.58	3615	6200	100 × 25 × 8	0.16		
						80 × 20 × 8	0.10		
						80 × 30 × 5	0.10		
						30 × 30 × 20	0.14		
							0.50		

3b				2960	5300	None?			
3c				3515	6300	None?		36?	0.047?
4	29 1930	0.42	0.59	3195	5400	170 × 90 × 30	3.68	681	0.78
5	38 1921	0.40	0.58	4490	7750	80 × 40 × 5	0.13		
						60 × 30 × 3	0.04		
						50 × 50 × 5	0.10		
						50 × 20 × 5	0.04		
						50 × 40 × 20	0.32		
						80 × 20 × 5	0.06		
							0.69	89	0.098
6	46 1913	0.38	0.66	3875	5810	120 × 25 × 20	0.48	83	0.087

[a] Many flakes are irregular in shape; the mass estimates allow for this.

field at this stage. (Through the kindness of F.I.D.S. we have been allowed to repeat the work on the ice cliff, a much greater quantity of snow being sampled. It should be possible to estimate the total iron at the various levels by means of the torsion balance.)

H. *Results from Satellite Experiments*

Using sensitive microphones attached to the skin of the satellite, it has been shown that impacting dust particles can be counted, and by assuming a velocity of impact the mass of the particle can be estimated. Early attempts resulted in great differences between the recorded number of particle impacts; but more recent work has removed this disparity. Present observations definitely favor a high tonnage of fine dust to the earth, in agreement with expectations from a dusty zodiacal cloud.

Reporting to the First International Space Science Symposium (held at Nice, January 1960), H. E. La Gow and W. M. Alexander gave some of the recent American observations. Day by day particle counts during the latter part of September and early October 1959, obtained from Vanguard III (1959ϵ), are particularly interesting. They estimate a daily influx rate of about 60 particles/meter^2 on September 19, falling to about 30 particles by October 9. Although there is considerable scatter (about 100%) between readings, this gradual fall seems significant. Using an impact velocity of 30 km/sec they determine the particle mass to be $3.3 \times 10^{-3}\mu g$ giving a mass to earth of 600 tons per day. From Explorer I (1958α) they estimate 10,000 tons per day for particles ranging between $1.2 \times 10^{-2}\mu g$ to $1.2 \times 10^{-4}\mu g$. At the same conference, T. N. Nazarova reported similar results for the Russian satellites and Space Rockets. Of special interest are the recordings from Sputnik III which may have run into a meteor shower. On May 15, 1958, 4 to 11 impacts per square meter per second were recorded. But by May 16-17 this number had fallen to 5×10^{-4}; and from the 18th to the 26th, it was below 10^{-4}. Allowing an impact speed of 40 km/sec the particles responsible would have a mass of $2.7 \times 10^{-2}\mu g$ to $8 \times 10^{-3}\mu g$. Results from Space Rocket III give 4×10^{-4} impacts per square meter on October 4, 1959 for particles ranging from $3 \times 10^{-3}\mu g$ to $1 \times 10^{-3}\mu g$; and 2×10^{-3} impacts on October 18 for particles ranging from $3 \times 10^{-3}\mu g$ to $8 \times 10^{-3}\mu g$, and for particles greater than $8 \times 10^{-3}\mu g$ the impact rate was 4×10^{-4}.

Collecting much of the existing data, and including six U.S. rocket firings, Whipple (1961) shows that the number of impacts falls off with the altitude of observation according to an inverse 1.4 power law. At an altitude of 10^2 km the impact rate is 1 per square meter per second, and at 10^5 km the rate is 10^{-4}; the particle mass is taken to be $10^{-3}\mu g$. With this particle mass, the law

of particle impacts would approximate to that expected from the zodiacal light for distances somewhat greater than 10^5 km. This is an unexpected result. Whipple tentatively considers that most of this material is in direct orbit around the earth, having come from the lunar surface as a result of meteoritic bombardment. Our immediate reaction is to query the results; we would agree with Whipple that much more observational work is required to clarify this surprising phenomenon. Indeed much more observation work is required to clarify the whole fascinating, yet tantalizing, field of cosmic dust.

In concluding this article we might mention that cosmic spherules, being the permanent fraction of cosmic dust, are useful in geophysical work. For instance, if their number concentrations are compared for surface muds obtained at different positions in an ocean, then the rates of sedimentation, for those positions, can be compared. And if we knew the present day accretion rate for spherules, the absolute rates of sedimentation would follow. As Pettersson has emphasized, the counting of spherules down a core may lead to interesting results concerning meteoritic activity in times past. In a recent work (to be published in *Geochim. Acta*) we believe we have located cosmic spherules in some sediment from Barbados, reputed to be 50×10^6 years old, and if cosmic spherules could be found in more ancient sediments it would effectively prove the existence of meteorites throughout geological time.

The comparison of the percentage of nickel in a core with the number of spherules found for different levels may give interesting results. If the nickel in the deep-sea sediments is mainly of cosmic origin, the comparison may allow us to question meteoric activity in times past. For example, a certain fraction of nickel would be due to meteoritic flakes (i.e., our background iron, perhaps) but this should be related to the number of iron spherules. Any departures from a one to one correspondence down the core may speak of varying meteoric activity.

The study of cosmic dust is still very much in the tentative exploratory stages. It is important that existing facts be confirmed and new facts be secured, if only to show that the microscope can also play its part in astronomical observation.

ACKNOWLEDGMENTS

To those not specifically mentioned in the text, our warmest thanks must go to Sir Edward Bullard F.R.S. of the Department of Geodesy and Geophysics, Cambridge for much encouragement and support. We are very grateful to Mr. and Mrs. Lewis Hicks of St. Agnes for making our visits to the island such pleasant ones, and also for providing many small but essential items in order to keep the expedition going. Our thanks also to Mr. D. L. McCluskey of the workshop for help in constructing the dust collectors. Lastly, we are very indebted to Mr. A. E. Brownlow, our laboratory technician, who of late has assisted with much of the experimental work. We must record our appreciation of financial assistance from the Department of Industrial and Scientific Research.

ADDENDUM

As a result of recent work with the electron probe on fragments of Antarctic dust, the following notes have an interesting bearing on several sections in the main part of the text. We are very grateful indeed to Mr. I. K. Openshaw and Mr. P. W. Wright (of Associated Electrical Industries, Manchester) for permission to use the probe and for their help in carrying out the examinations.

(1) The Antarctic metallic flake of Fig. 12 has a composition consistent with meteoritic iron. About 6 to 8% Ni and 1% Co is fairly uniformly distributed over the specimen. Owing to the roughness of the surface it is not possible to obtain a highly accurate composition, nor is it possible to be certain whether the composition varies across the striations which are well seen in the electron pictures. The distributions of nickel and iron are shown in the photographs of Fig. 13. The blank area is not an absence of these elements, it is merely a shadow zone due to the wedgelike shape of the particle. By altering the orientation of the particle with respect to the impinging electron beam (and the collecting direction of the emitted X-rays), this zone is seen (Fig. 14) to be similar to the rest of the particle. For the same reason the dark "lanes," particularly in the iron distribution, cannot be interpreted as regions of deficiency.

The electron picture is obtained by recording the leakage current of captured electrons from the different points on the surface of the specimen as the impinging beam scans across it. Contrast in an electron photograph is due to varying chemical composition and topography over the surface of the specimen; but in this case since a constant composition seems apparent, the contrast must be due wholly to topography.

The composition and surface structure of this Antarctic flake is therefore very similar to the Scilly iron flake of Fig. 3.

(2) In the section dealing with Antarctic dust, we described efforts to locate fragments of olivine; and because of the failure to find this mineral we were led to believe that iron flakes were the only extraterrestrial component to be found in the melt-water. This conclusion may have to be revised. During the microscopic examination of the magnetic fraction, a few composite particles were seen. These were largely translucent mineral grains with black or silvery opaque flakes or specks either embedded within or out-cropping at the surface of the particle. Tests for iron with copper sulphate solution were inconclusive as it was extremely difficult to be certain whether the coppery colour change had occurred; and as all the particles floated in bromoform, the mineral could not be olivine. In view of this it was thought that these particles were terrestrial contaminants; particularly so, as most of them appeared amorphous under the

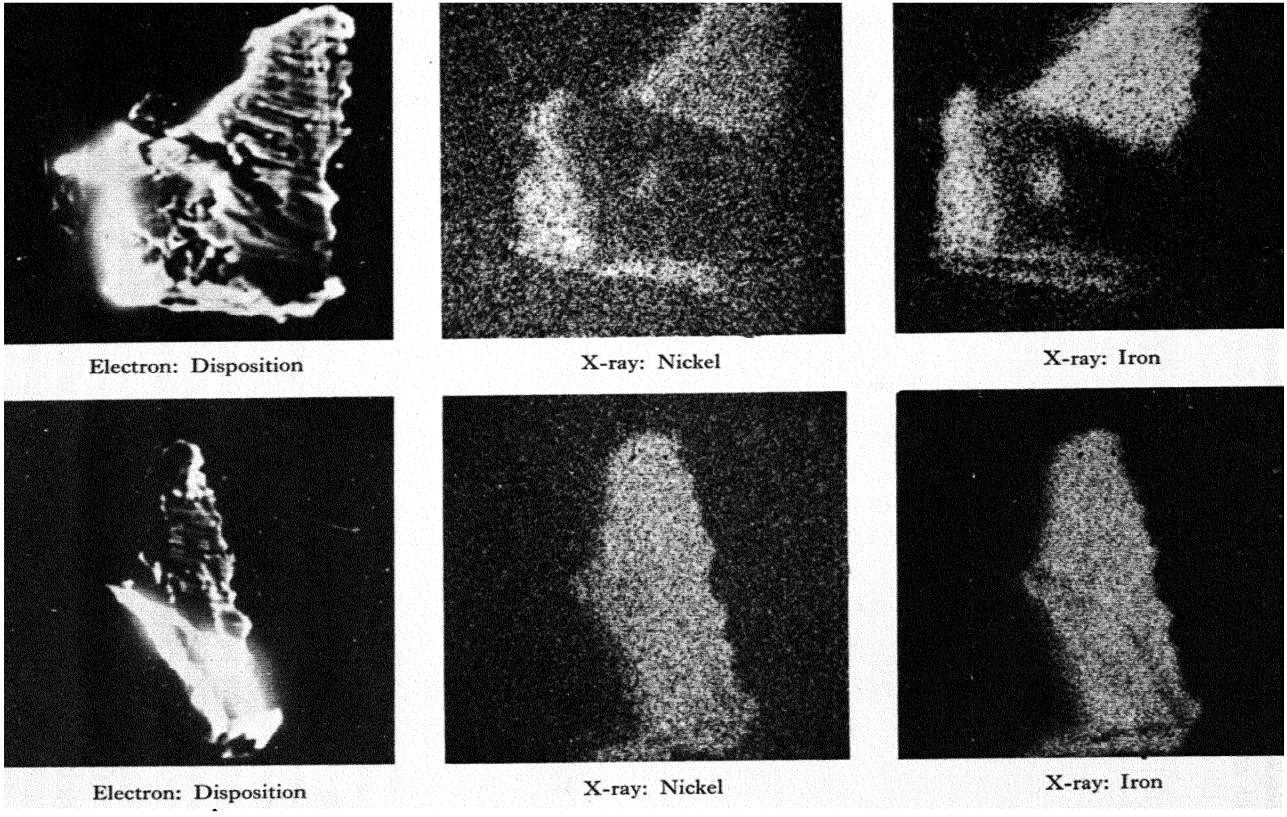


FIG. 13. Antarctic metallic flake (1% Co, 6-8% Ni) showing the distribution of nickel and iron and also the surface striations. The surface examined is the reverse of that shown in Fig. 12.

Fig. 14. Antarctic metallic flake as in Fig. 13 but with altered orientation.

polarizing microscope. However, two particles were preserved for later examination and these are shown in Fig. 15.

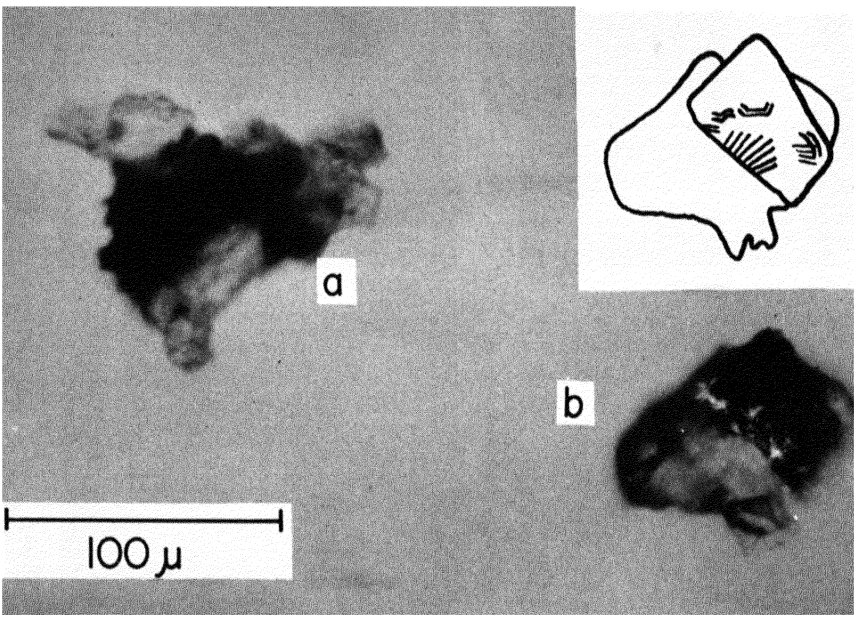


Fig. 15. Antarctic composite particles. Inset shows striation on metallic portion in particle (b).

Particle (a) seemed to show a coppery colour change, and the flake attached to particle (b) was particularly silvery. From memory, we are inclined to believe that this latter particle was not tested with copper sulphate. The spur of mineral in the upper left-hand side of particle (a) was partly crystalline with a refractive index of about 1.57. The mineral in particle (b) appeared wholly amorphous with refractive index 1.549. The mineral in both particles is slightly turbid, internal pigment forming an intricate filligree pattern. The colour is pale yellow-green in transmitted light but the mineral appears a frothy white or cream in reflected light.

Before inspection with the electron probe the particles, taken together, were examined by X-ray diffraction—Co $K\alpha$ radiation, 8 hours exposure in 9-cm. camera. Only two weak, but decidedly uniform, lines could be seen, giving d-values of 2.08 and 2.01 Å. If these are due to face-centred cubic and body-centred cubic lattices they would give parameters of 3.59 and 2.84 Å, respectively,

in fair agreement with similar results on the Antarctic and Scilly iron flakes.

The results of the electron probe investigation are shown in Fig. 16 for particle (a). The distribution of the iron is dissimilar to that of the nickel. The positions in the particle of the areas rich in these elements may be obtained by directly superimposing the X-ray photographs on the electron picture. In the electron picture the dark areas certainly contain the nickel and iron rich areas but why there is darkness in other regions is unknown. The Ni:Fe ratio is about 4:5, except for an iron high spot on the right. The nickel is thought to be about 6% of the total composition in the nickel rich area. The effect of previous copper sulphate treatment is unknown. Cobalt was not estimated for this particle.

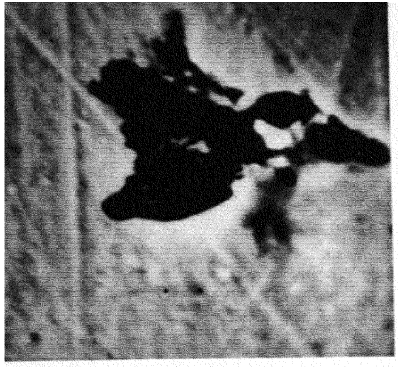
The results on particle (b) are shown in Fig. 17. This particle gives a similar electron picture as particle (a); in as much as the dark region extends beyond the limits of the metal flake and the nickel and iron distributions are different. The flake is very rich in nickel (about 50% Ni), but is surprisingly low in iron (about 2% Fe). Towards the left-hand side of the flake there is a slight deficiency of nickel and this corresponds to a slight increase in the iron content. About 1% Co is also present in the flake. The remaining element in the flake is copper which together with a little sulphur over the whole particle does suggest that this particle was pretested with copper sulphate in spite of our opinion to the contrary.

An attempt to estimate the presence of the lighter elements in the mineral of particle (b) were inconclusive; lack of experience in operating the probe for these elements was largely responsible. Negative results were obtained for aluminium and magnesium, although 40-50% Si was estimated with some certainty.

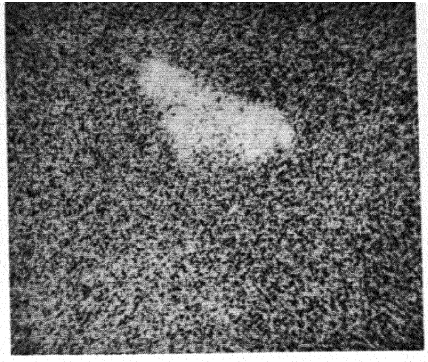
The dispositions of the particles in the optical photograph Fig. 15 should not be directly compared with the electron or X-ray pictures as the orientation of the particles is different.

(3) In view of the high nickel content of the opaque portions it seems clear that these composite particles may be from outer space. The low refractive index and density of the mineral precludes an olivine, olivine glass, or other basic silicate composition. This would mean that the particles are not meteoritic. But whether they can be proved to be meteoric (i.e., can be picked up in greater quantity after a meteor shower) remains to be seen. So little information is available on the carbonaceous meteorite that it is impossible at this stage to effect a comparison.

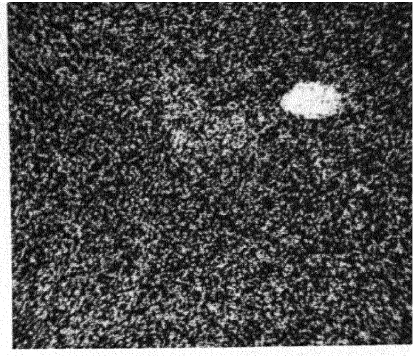
(4) Particle (b) (Fig. 15) is especially interesting as the familiar striations can be seen again on the metallic flake. The inset to Fig. 15 shows the position of some of the more prominent lines. It is intriguing to speculate on whether sputtering by corpuscular radiation could cause these markings whilst the



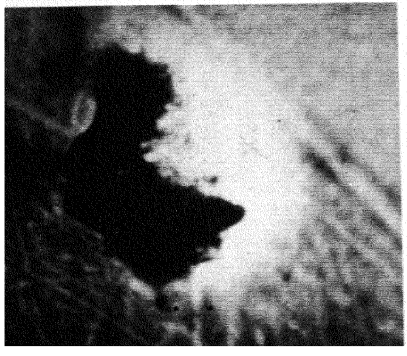
Electron: Disposition



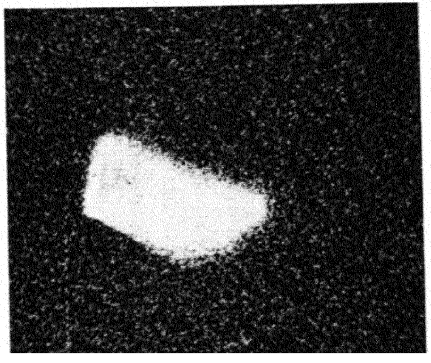
X-ray: Nickel



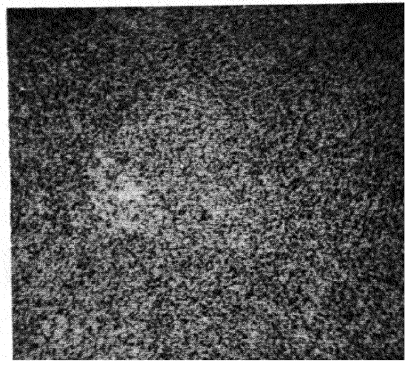
X-ray: Iron



Electron: Disposition



X-ray: Nickel



X-ray: Iron

FIG. 16. Distribution of nickel and iron in particle (a) of Fig. 15.
FIG. 17. Distribution of nickel and iron in particle (b) of Fig. 15.

particle is in outer space. Furthermore, the very fine-grained polycrystalline nature of all these striated particles would point to thorough radiation damage of the lattice. Certainly, etching effects by low velocity heavy ions have been observed on metallic targets (Wehner, 1955). But whether high-energy cosmic rays or electrons could produce similar patterns is questionable. Nevertheless, it does seem that the hypothesis could be tested by placing an initially electro-polished piece of iron meteorite in an accelerating machine. If this test should prove positive it could raise important issues. Striations might be seen on metal flakes deeply embedded in the mineral. In which case one might conjecture that the flake had at sometime been independent of the mineral.

(5) Recent work on a deep-sea core from the Pacific has shown that olivine spherules are only present on the surface of the sediments. The spherules immediately below the surface are entirely of the iron variety. We believe that, due to the unstable character of olivine the stony spherules (although perhaps present in times past) they have corroded away; as, indeed, does happen in some cases to the metallic nucleus in the iron spherules—we find many iron spherules with deep hollows.

Using the same technique as that adopted in December 1960, the dust collections at Scilly were started on May 27, 1961 and we hope to continue until the end of September; two large meshes ($\frac{3}{4}$ meter^2) are being exposed simultaneously. Already analyses for metallic iron have been completed on one series of meshes up to July 6th. Very little iron (20 μg 10^6m^3) was found in early June, but by June 20th this was increased to 40 μg 10^6m^3, remaining steady until June 29th when there was an abrupt increase to over 200 μg 10^6m^3, decaying gradually away to 80 μg 10^6m^3 by July 6th. If the strong daytime ζ-Persieds and Arietids occurring in early June were present this year, then most certainly they do not possess much metallic iron, whereas the β-Taurids in late June are quite strong in iron. We are now confident that the greased mesh technique is a sound method for measuring the iron concentration in the air and that the variations are connected with certain showers. The technique opens up possibilities for investigating the structure of the different showers. In a recent private communication, Sir Bernard Lovell informs us, as a result of studying the mass distribution of particles within the showers, that there may be some evidence in supposing that the ζ-Perseids and Arietids are of different composition from many other meteor showers. He also mentions that there is nothing to indicate that these summer daytime showers are anything but perfectly regular in their annual appearance.

An examination of the residue remaining in the filter paper (after measurements on the torsion balance) has revealed, mainly in late June, the usual coppery specks; but also many silvery flakes. These flakes are either pure nickel or very nickel-rich iron alloy, as revealed by X-ray diffraction. They are very fine

grained polycrystalline particles. For instance on June 25th a wafer of pure nickel 230 × 70 × 5 μ was found. As this wafer had golden staining on either side, we believe that it could have been sandwiched between layers of iron, the staining being traces of copper left after the copper sulphate solution had removed the iron. Again on June 29th an enormous wafer 470 × 140 × 10 μ was found. This had no staining and from an X-ray diffraction powder photograph we determine about 30% nickel. Clearly the copper sulphate solution will not reduce these nickel-rich alloys.

It seems that the American satellite Vanguard III has identified a major meteor stream; we quote from N.A.S.A. Press Release No. 61-128 of June 9, 1961:

"On November 15th-17th 1959, Vanguard III picked up a large number of micron-size dust particles. This had not been reported previously because the unravelling of data from the satellite has just been completed. The indication from Vanguard III was that these particles could be associated with a major meteor stream. As many particles were detected during this 70 hour period in November 1959 as were found during the remainder of the 78 day period of the satellite."

This is reminiscent of similar results obtained by the Russians with Sputnik III in May 1958.

References

Allen, C. W., 1946. *M.N.R.A.S.* **106**, 137.
Behr, A., and Siedentopf, N., 1953. *Z. Ap.* **32**, 19.
Blackwell, D. E., 1955. *M.N.R.A.S.* **115**, 289.
Blackwell, D. E., 1956. *M.N.R.A.S.* **116**, 335.
Blackwell, D. E., 1960. *Endeavour* **19**, 14.
Bowen, E. G., 1953. *Aust. J. Phys.* **6**, 490.
Buddhue, J. D., 1950. "Meteoritic Dust." Univ. of New Mexico Press, Albuquerque.
Bullard, E. C., 1954. *In* "The Earth as a Planet" (G. P. Kuiper, ed.), Chapter 3. Univ. of Chicago Press, Chicago, Illinois.
Castaing, R., and Frederiksson, K., 1958. *Geochim. et cosmoch. Acta* **14**, 114.
Chackett, K. J., Golden, J., Mercer, E. R., Paneth, F. A., and Reasbeck, P., 1950. *Geochim. et cosmoch. Acta* **1**, 3.
Grotrian, W., 1934. *Z. Ap.* **8**, 124.
Hansa, M., and Zacharov, I., 1958. *B.A.C.* **9**, 236.
Hoyle, F., 1955. "Frontiers of Astronomy," pp. 28-39. Heinemann, London and New York.
Hunter, W., and Parkin, D. W., 1960. *Proc. roy. Soc.* **A255**, 382.
Laevastu, T., and Mellis, O., 1955. *Trans. Amer. geophys. Un.* **36**, 385.
Lovell, A. C. B., 1954. "Meteor Astronomy." (Oxford Univ. Press, Clarendon, London and New York.
Mason, B., 1960. *Nature, Lond.* **186**, 230.

Mason, B. J., 1957. "The Physics of Clouds," p. 260. Oxford Univ. Press (Clarendon), London and New York.
Millman, P. M., 1953. *Nature, Lond.* **172**, 853.
Murray, J., and Renard, A. F., 1891. *Rep. "Challenger" Expedition* **4**, 327.
Nininger, H. H., 1959. "Out of the Sky." Dover Publ., New York.
Öpik, E. J., 1951. *Irish A. J.* **1**, 145.
Öpik, E. J., 1956. *Irish A. J.* **4**, 84.
Owen, E. A., and Liu, Y. H., 1949. *J. Iron Steel Inst.* **163**, 132.
Parkin, D. W., and Hunter, W., 1959. *Nature, London* **183**, 732.
Partridge, W. S., and Vanfleet, H. B., 1958. *Ap. J.* **128**, 416.
Pettersson, H., 1958. *Nature, Lond.* **181**, 330.
Pettersson, H., and Frederiksson, K., 1958. *Pacif. Sci.* **12**, 71.
Pettersson, H., and Rotschi, H., 1950. *Nature, Lond.* **166**, 308.
Rinehart, J. S., and White, W. C., 1952. *Amer. J. Phys.* **20**, 14.
Ringwood, A. E., 1960. *Geochim. et cosmoch. Acta* **20**, 1.
Roach, F. E., Pettit, H. B., Tandberg-Hanssen, E., and Davis, D. N., 1954. *Ap. J.* **119**, 253.
Singer, S. F., 1958. *In* "Scientific Uses of Earth Satellites" (J. A. Van Allen, ed.), p. 301. Univ. of Michigan Press, Ann Arbor, Michigan.
Stacey, F. D., and Lovering, J. F., 1959. *Nature, Lond.* **183**, 529.
Urey, H. C., 1951. *Geochim. et cosmoch. Acta* **1**, 209.
Urey, H. C., and Mayeda, T., 1959. *Geochim. et cosmoch. Acta* **17**, 113.
Urey, H. C., Mele, A., and Mayeda, T., 1957. *Geochim. et cosmoch. Acta* **13**, 1.
van der Hulst, H. C., 1947. *Ap. J.* **105**, 471.
Watson, F. G., 1956. "Between the Planets," 2nd ed. Harvard Univ. Press, Cambridge, Massachusetts.
Wehner, G. K., 1955. *Advances in Electronics and Electron Phys.*, **7**, 239.
Whipple, F. L., 1950a. *Ap. J.* **111**, 375; **113**, 464.
Whipple, F. L., 1950b. *Proc. nat. Acad. Sci., Wash.* **36**, 687.
Whipple, F. L., 1961. *Nature, Lond.* **189**, 127.
Winchell, A. N., 1927. "Elements of Optical Mineralogy," Part 2, p. 167. Wiley, New York.
Young, J., 1939. *Phil. Trans.* **A238**, 393.

Distribution of Mass in Oblate Stellar Systems

L. PEREK

Astronomical Institute of the Czechoslovak Academy of Sciences, Prague, Czechoslovakia

I. Introduction 165
A. General Statement of the Problem 165
B. Observations 170
C. Geometry of Spheroids 184
II. Models Based on the Velocity Distribution 194
A. The Equation of Continuity 194
B. Models Based on Oort's Solution 197
C. Models Based on the General Solution 211
D. Criticism of the Ellipsoidal Velocity Distribution 217
III. Models Based on Density Laws 221
A. Mass-Points and Homogeneous Spheroids 222
B. The Basic Body is a Disk 232
C. Heterogeneous Spheroids With Similar Strata 245
D. Heterogeneous Spheroids With Confocal Strata 264
E. A Composite Model of the Galaxy 273
F. Conclusion 280
List of Frequently Used Symbols 283
References 284

I
INTRODUCTION

A. *General Statement of the Problem*

Besides being interesting on its own merits the problem of the distribution of mass in stellar systems similar to the Galaxy yields, if solved, a solid basis for, and an inescapable check of, all theories of evolution of stellar systems. Or, to give another reason for the present discussion, if we wish to know which regions of the Galaxy are accessible to stars, at present in the neighborhood of the sun, and moving within a wide range of velocities, a knowledge of the mass distribution and of the field of force is a necessary condition.

This problem evoked into existence in the last, and in the beginning of this, century a whole new branch of astronomy—stellar statistics. Star counts accord-

ing to apparent magnitude served for studies of the luminosity function and of densities of stars in space. There were several reasons why star counts failed to give a satisfactory picture of the Galaxy. The enormous dimensions of the system had not been recognized till Shapley's work on globular clusters. The luminosity function displayed a rather complicated form and the interstellar absorption systematically distorted the scale of distances. The galactic population is not homogeneous by far. It consists of stars of widely differing ages, kinematical properties, and luminosities. The "average distance" of a group of stars taken without any luminosity criteria has little, if any, meaning.

Observations used in the classical stellar statistics referred to a relatively close vicinity of the sun. The gradual evolution of observing techniques and the improvement of distance scales for some of the types of variable stars made it possible to cover large areas of space and to form the concept of the Galaxy. In particular, in recent years, the radio observations of neutral hydrogen made accessible to the investigation even those parts of the Galaxy which are quite hidden in the optical domain by heavy interstellar absorption. Also the studies of other systems show a promising development. Besides the Magellanic Clouds and the Andromeda Nebula many others were studied. In the course of 1959 and 1960 the number of galaxies with measured rotation curves was trebled! It may be expected that this trend will continue in the years to come and therefore it seems desirable to sum up the methods for the determination of the distribution of mass, and thus make the selection of the most convenient method easier or to instigate the search for new methods. Little attention is paid to this problem in most of the current textbooks on stellar dynamics. There the discussion is usually restricted to a model, of rather limited importance, consisting of a mass point and a homogeneous spheroid.

We shall assume that the motions and distribution of stars are governed by Newtonian gravitation of stars and other forms of matter present in the system. We shall neglect magnetic forces although they play a role in the motion of diffuse interstellar matter and are possibly responsible for the spiral structure and for the expansive motions of neutral hydrogen in the nucleus.

The field of force of the Galaxy is very irregular due to the fact that the attraction is large in the vicinity of a star and is infinite if the stars are mathematically represented as mass points. It has been shown many times (e.g., Chandrasekhar, 1942) that close encounters of stars are very rare. Thus it is possible to consider a smoothed out field of force exhibiting large scale features but omitting local variations. Nor will the spiral structure be represented because the attraction due to a spiral arm, according to M. Schmidt (1956), does not exceed 2% of the total attraction. This value is too small to induce us to give up the advantage of a smooth density law and of the rotation symmetry without which many of the problems become very difficult. Because of this

restriction much of the work of B. Lindblad will fall beyond the scope of this paper as it mostly concerns spiral structure.

The geometrical form of the distribution of mass is based on observations of the Galaxy and similar systems. It is expected that the distribution will exhibit symmetry with respect to an axis and to a plane at right angles to the axis. The flattening of the Galaxy is very conspicuous and is manifested in the distribution of almost all kinds of objects, the Milky Way itself being not the least important phenomenon. It attains values in a wide range: equidensity surfaces of RR Lyrae stars have an axial ratio of about 1:2; for the main countours of edge-on spirals it is about 1:12, and for neutral hydrogen 1:60. The flattening can never be neglected because spherical symmetry is very restrictive and leads to qualitatively different considerations, e.g., in the question of the stability of circular orbits. The other extreme—a total flattening leading to a two-dimensional configuration—is less dangerous. However, the sacrifice of the third dimension is seldom rewarded by easier mathematics.

A more difficult question concerns the boundary of the system. It cannot be settled by the easily made demand for finite dimensions. In reality, the density decreases with the distance to a very small value of the density of the intergalactic space. According to Kahn and Woltjer (1959) this latter value is $2.4 \times 10^{-6}\ M_\odot/pc^3$, i.e., four or five orders of magnitude smaller than the density in the vicinity of the sun. The neighboring galaxies are at a distance of the order of ten diameters of a galaxy and this means an increase in the density. Galaxies are not ideally isolated systems and there is not much sense in asking whether they can be represented by finite or infinite models. It is more important to express the density adequately inside the model and to make sure that the values become sufficiently small at large distances. The validity of the model is, of course, limited to the galaxy under consideration and to its immediate neighborhood where the influence of other galaxies may be neglected.

From the physical standpoint it is required that the total mass of the model be finite. This is a restricting condition which must be complied with even by infinite models. In other words this is the exact meaning of the phrase "sufficiently small densities at large distances."

As regards the density laws, we allow models with discontinuities, i.e., with jumps or steps in the density, although continuous density laws are preferred with the density monotonously decreasing with the distance and with only one maximum at the center. Some of the models exhibit infinite densities at the center. This is to be understood so that, in fact, the density is everywhere finite and that the density peak is distributed over a wider area than that given by the mathematical expression.

The stellar population of galaxies is not homogeneous. In the Galaxy several

different populations were detected. The Rome conference in 1957 (O'Connel, 1958) arrived at the following classification:

Halo Population II: Subdwarfs, globular clusters of high z-motion, RR Lyrae stars with periods longer than 0.4 days.

Intermediate Population: High-velocity stars with z-velocities above 30 km/sec, long-period variables with periods under 250 days and spectral types earlier than M5e.

Disk-Population: Stars of galactic nucleus, planetary nebulae, novae, RR Lyrae stars with periods under 0.4 days, weak-line stars.

Older Population I: A-type stars, strong-line stars.

Extreme Population I: Gas, young stars associated with the present spiral structure, supergiants, Cepheids, T Tauri stars, galactic clusters of Trumpler's class I.

The objects mentioned above do not, of course, exhaust the entire content of the respective populations.

Sometimes, population II and I are referred to as spherical and flat components of the Galaxy, respectively. By a subsystem we mean a set of objects defined by physical and kinematical properties. A population consists of a number of subsystems; e.g., the subsystem of globular clusters forms a part of the Halo Population II.

The distinguishing of populations is borne out by radio observations. Shklovski showed (1952) that the observed distribution of the radiation, especially near the poles, can be explained as being due to an extended envelope —the halo. His model is shown in Fig. 1. Another component of the radio

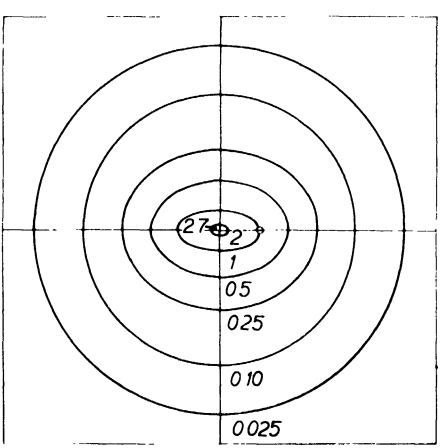


FIG. 1. The model of the halo by I. S. Shklovski. The position of the sun is marked by a small circle.

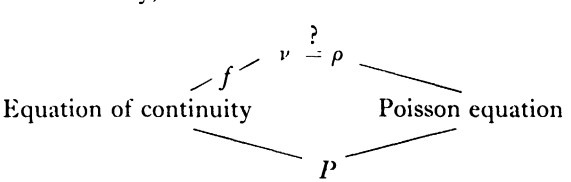
radiation corresponds obviously to spiral arms. For a detailed analysis and a survey of other models of the halo, we refer to a paper by Mills (1959).

Some observations indicate that the Galaxy has not attained a steady state. A steady state Galaxy with an ellipsoidal distribution of velocities should have two axes of the velocity ellipsoid equal. The observations clearly show three unequal axes for most of the subsystems. There are a few stars (Perek, 1956) in hyperbolic orbits. However, since they are few in number, the Galaxy cannot be very far from the steady state. This is supported by the fact that no large scale systematic radial motion has been found up to now with the exception of expanding motion of the gas near the center (see Section I, B). Besides, the time-dependent solution by Chandrasekhar (1942) can be reduced to a steady-state solution by means of a transformation of the coordinates and time (Schürer, 1942). Kurth (1949) showed that the time-dependent solution leads to a density constant either in time or in space. It seems therefore advisable to assume the steady-state hypothesis. It is at least a good approximation.

There are two equations governing stellar systems: the equation of continuity and the Poisson equation. The equation of continuity expresses a relation between the potential P and the frequency function f in the seven-dimensional space. The assumption of steady state removes time as an explicite variable and the space reduces to six dimensions: three coordinates and three velocity components. By integrating the frequency function over all velocities the frequency in space is arrived at, or, with appropriate factors, the number ν of stars per unit of volume. The Poisson equation, or its equivalent, the potential expressed as an integral of the density of mass over distance taken over the whole volume V of the attracting body

$$P = G \int_V \frac{\rho}{r} \, dv,$$

relates the density of mass ρ and potential P due to the gravity of ρ in the volume V. Schematically,



Putting the sign of equality between ν and ρ is equivalent to making two assumptions. First, the average mass of a sample of stars is independent of the position in the system, and secondly, the system is self-gravitating. The differences in stellar masses are not very pronounced, thus making the first assumption

plausible. The second assumption is admissible only if the frequency function adequately represents kinematical properties of all populations in the system and in the correct mixture. A form of the distribution of velocities suitable for a large majority of stars in the solar neighborhood may prove to be too restrictive or inadequate from this general point of view.

If $\nu \neq \rho$, it is possible to choose a kinematically well-defined subsystem with a simple form of the velocity distribution, to determine ν from observations, to derive the potential, via the equation of continuity, and finally the mass density of the system. Or, in a more convenient way, to assume a certain ρ, to compute the potential, to determine f and ν for a subsystem with known distribution of the velocities, and to compare the computed and observed ν.

We shall see later that all solutions of the problem introduce more or less plausible assumptions at one or other place. Some solutions postulate a certain form of the velocity distribution, other assume a certain density law and determine free parameters. All solutions fall therefore into two large groups. The solutions of the first group are based on velocity distributions; those in the second on mass distributions.

B. *Observations*

It is not intended to give an exhaustive survey and a critical analysis of all observations related to the determination of the mass distribution. We wish only to point out the variety of applicable observations and to give some typical examples.

1. *Observations of Densities*

Direct observations of total density come only from the vicinity of the sun and even here the accuracy is rather limited. According to Gliese (1956) the density of mass contained in stars is 0.057 $M_\odot/pc^3$. Adding to the mass in the stars the density of interstellar matter, we arrive at (Parenago, 1954) 0.088 ± 0.007 $M_\odot/pc^3$ or, according to a more recent estimate (Oort, 1960) 0.087 to 0.098 $M_\odot/pc^3$. The density which follows from dynamical considerations covers a wider range according to the methods applied and basic data:

Safronov (1952)	0.10 $M_\odot/pc^3$
Parenago (1954)	0.080
Kuzmin (1955)	0.077 ± 0.008
Woolley (1957)	0.18
Oort (1960)	0.15

These estimates are based on assumed distributions of mass. The properties of the distributions appear in the results, which are thus not independent determinations.

The behavior of the densities in a small neighborhood of the sun is shown by density gradients, usually in the two principal directions. Their values, according to Parenago (1950a), are given in Table I. They followed from a discussion of extensive observations of various objects, in particular of variable stars (Kukarkin, 1949; Parenago, 1948). Subsystems of variable stars of several types proved to be very effective tools for studying the structure of galaxies.

TABLE I

LOGARITHMIC DENSITY GRADIENTS

	Mod $\frac{\partial \log \nu}{\partial \varpi}$	Mod $\frac{\partial \log \nu}{\partial z}$
Spherical component (Population II)	-0.27 ± 0.01	-0.18 ± 0.05
Intermediate component (Disk population)	-0.23 0.04	-1.0 0.1
Flat component (Population I)	-0.11 0.01	-8.5 1.5

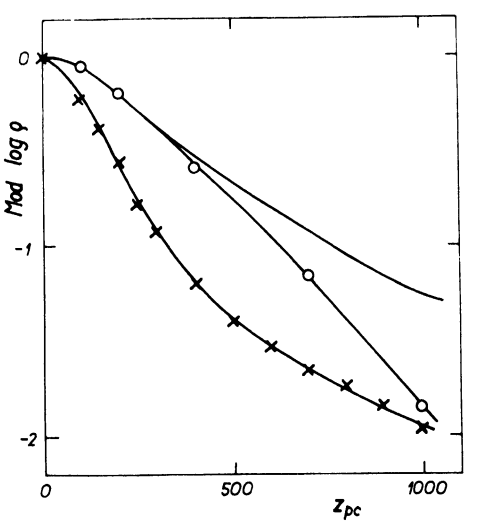


FIG. 2. Densities of stars fainter than 4.5^m according to J. H. Oort (full curve) and with subtracted population II (circles). Densities of G and K giants according to T. Elvius (crosses).

The observed run of the densities over a wide range of distances is more reliable in the z-direction than in the galactic plane where interstellar absorption is a most impeding obstruction. Figure 2 shows the densities in the z-direction of stars fainter than 4.5^{m}, according to Oort (1936), and for the same material with subtracted population II. Population II begins to be important above 500 pc. The crosses indicate densities of giants of spectral types G and K according to Elvius (1950). These curves give a general idea of the dependence of the densities on the z-coordinate: a flat top in the plane of symmetry and a more or less steep decrease followed by a slow decay.

Important information on the density in the plane of symmetry comes from radio observations. The amount of neutral (1957) and ionized (1958) hydrogen in the Galaxy was measured by Westerhout. Neutral hydrogen in M 31 was studied by van de Hulst *et al.* (1957), in M 33 and M 101 by Volders (1959). Figure 3 gives the amounts in a column of 1 cm^2 base, perpendicular to the

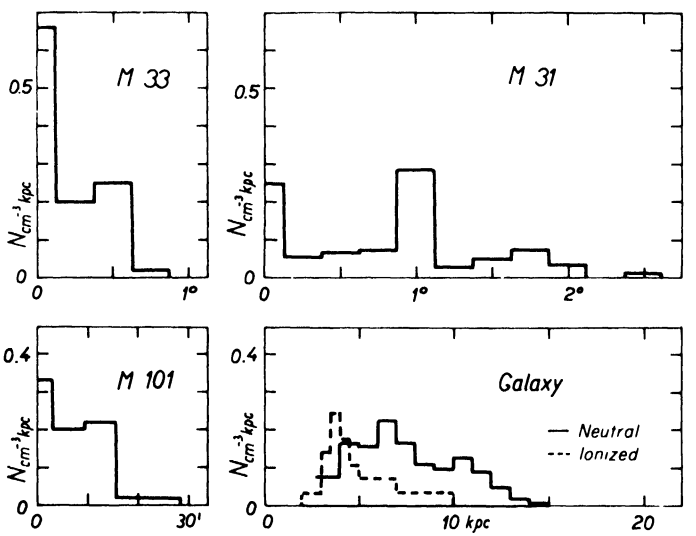


FIG. 3. Neutral hydrogen in four galaxies.

plane of symmetry. In contrast to the three galaxies, the density of neutral hydrogen in our Galaxy decreases towards the center. The density of the ionized hydrogen attains its maximum at 3.5 kpc and is not found at all inside of 2 kpc from the center. The determinations of the hydrogen densities involve the assumption of circular orbits of individual clouds.

Neutral hydrogen follows—in the z-direction—a Gaussian distribution with a slight asymmetry. The results of Schmidt (1957a) are shown in Fig. 4. The

same parameters of distribution do not apply to all the elements found in interstellar gas. Smak (1958) found that the density of interstellar calcium follows the formula

$$\nu(z) = \nu(0)\, e^{-z^2/z_0^2},$$

where $z_0 = 308 \pm 27$ pc. A superficial inspection of Fig. 4 is sufficient to show that the concentration of hydrogen towards the galactic plane exceeds that of calcium at least by a factor of 2.

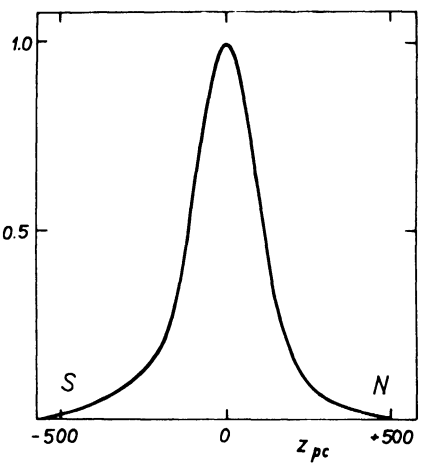


Fig. 4. Distribution in the z-direction of the neutral hydrogen in the Galaxy.

The distribution of RR Lyrae stars with amplitudes of light curves above 1.0^m, according to Perek (1951), is shown in Fig. 5. The weights of the determinations are indicated by the sizes of the dots. The ordinates are logarithms to the base 10 of the densities (numbers of stars per cubic kpc) and the abscissae are ϖ and z at the left- and right-hand side of Fig. 5 respectively. The densities refer to layers parallel to the galactic plane to show the dependence on ϖ, and to cylindrical shells parallel to the axis of rotation to show the dependence on z. The curves refer to the model of Section III, E. The distribution of RR Lyrae stars exhibits several remarkable features. The density decreases very slowly in the layer at $z = 1$ kpc from the center up to 6 to 7 kpc and then it falls off rapidly. At the sun's distance the logarithmic gradient is about $-0.30\,\mathrm{kpc}^{-1}$. In the z-direction there is at the sun's distance an almost linear decrease of the logarithm of the density. Finally, the surfaces of equal densities are not similar

spheroids. Kukarkin (1949) has shown that their flattening decreases with increasing distance. The outermost surfaces are nearly spherical.

The material used for the construction of Fig. 5 was based on the systematically studied Harvard and Leiden fields of variable stars. A vast majority of the stars belongs to population II. Since then only one field has been added by

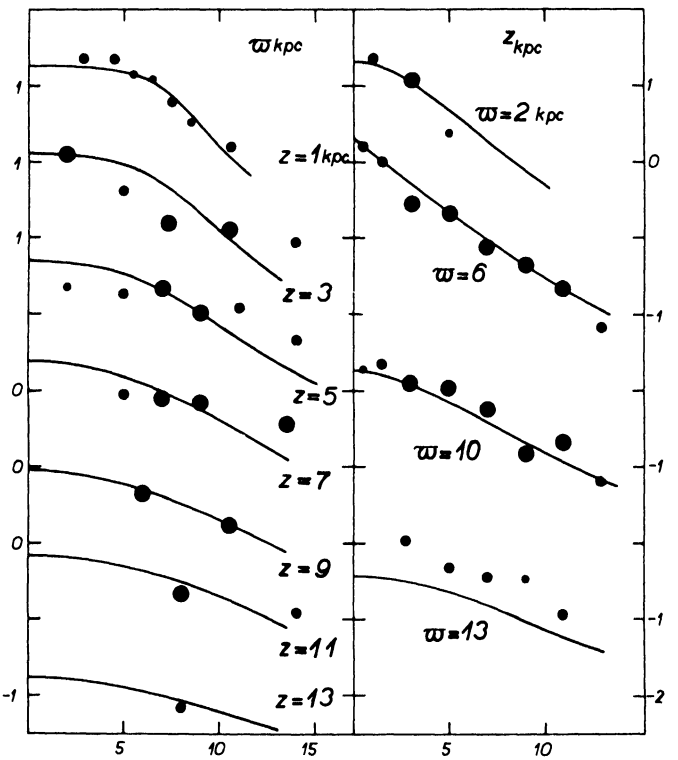


FIG. 5. Distribution of RR Lyrae stars. Ordinates are decadic logarithms of the numbers of stars per cubic kpc. The curves refer to the model of Section III, E.

Baade (1946) around NGC 6522, near the direction to the center. Periods of variables were determined by Gaposchkin (1955) from plates covering only a small range in hour angles. Even if some of the periods proved erroneous (Pavlovskaya, 1957; Alexander, 1960) they are on the average rather short, many being under 0.4 days. These short-period RR Lyrae stars have been appropriated to the disk-population in Section I, A, with all others to the population II. Omitting in Baade's field short-period stars, there remain too few to warrant reliable statistics.

2. *Dynamical Parameters*

Moments of velocities of the first order determine only the relative motion of the sun with respect to the centroid of the group of stars under consideration. Moments of the second order yield the dispersions. They were discussed in detail in the three principal directions by Parenago (1950a). His results are shown in Table II. We note that the dispersions in the three directions differ for almost

TABLE II

DISPERSIONS OF VELOCITIES IN KM/SEC

Objects	σ_ϖ	σ_ϑ	σ_z
Interstellar gas	7	5:	5:
B-stars	10	8	5
Cepheids	12	9	5
Supergiants	13	10	8
Galactic clusters	20:	11:	8:
A-stars	24	11	9
Giants A to F	27	14	10
Giants F	29	19	15
Giants G to M	30	20	16
R- and N-stars	30	27	28
Red irregular and semiregular variables	38	23	19
Mira-type variables, except periods of 150 to 200 days	38	30	29
Subgiants	43	27	23
White dwarfs	45:	28:	20:
Planetary nebulae	45:	35:	20:
Dwarfs G to M	48	29	24
Mira-type variables, periods 150 to 200 days	91	45	36
Subdwarfs	100	75	50
High-velocity giants	100	60	50
Globular clusters	100	—	—
RR Lyrae stars	140	120	50

all subsystems. It follows that the body of velocities is better expressed by a three-axial ellipsoid than by a spheroid. The dispersions change gradually from one subsystem to the other. The populations therefore do not seem to be sharply separated; there are several intermediate steps. The classification of Section 1 may be subjected to revisions in the future, brought about by more detailed and accurate observations than are those at present available.

Little is known about the dependence of the velocity dispersions on the distance from the centre. They vary, however, in a marked way with z. The results of van Rhijn (1960) are shown in Table III for stars of the Draper

TABLE III

DEPENDENCE OF VELOCITY DISPERSIONS ON THE HEIGHT ABOVE THE GALACTIC PLANE

z (pc)	σ_ϖ (km/sec)	σ_ϑ (km/sec)	σ_z (km/sec)
60	15.4 ± 1.1	9.0 ± 1.3	8.0 ± 1.3
296	35.3 ± 4.0	14.1 ± 2.2	12.5 ± 1.9
465	41.7 ± 7.9	22.4 ± 3.5	18.4 ± 3.5

spectral type A0 to A5. The dependence was explained by van Rhijn by assuming a composite distribution of two Gaussian curves. The majority of stars (94%) have $\sigma_\varpi = 11$, $\sigma_\vartheta = \sigma_z = 8$ km/sec and the remaining 6% have $\sigma_\varpi = 45$, $\sigma_\vartheta = \sigma_z = 23$ km/sec. This is probably due to an admixture of population II stars in the solar neighborhood.

The rotation of the Galaxy manifests itself in stellar motions by differential rotation which is defined, in the linear approximation, by Oort's parameters A and B (see Section II, B, 1). Recent determinations of A from Cepheids and B-stars range from 17.5 to 19.5 km/sec/kpc as reported by Blaauw (1960). Mohr and Mayer (1957) found 17.5 from radial velocities of associations and B-stars. Morgan and Oort (1951) derived the value of $B = -6.9$ km/sec/kpc which was confirmed by Mohr *et al.* (1957).

The condition

$$-A/B = 1.53 \pm 0.07$$

was derived by Parenago (1955) from a rediscussion of the radial velocities of neutral hydrogen and from other data. The above values of A and B are evidently not consistent with this condition. The discrepancy has not yet been tracked down to its source.

The attraction in the z-direction, Q_z, has been determined several times. The most recent papers on this question are by Hill (1960) and Oort (1960). Hill's curve, shown in Fig. 6, was derived from the distribution and motions of K giants. The decrease beyond 400 pc is so steep that it comes into conflict with the Poisson equation. The minimum Q_z, consistent with the Poisson equation and following from the observed distribution and from Schmidt's model of the Galaxy (Section III, C, 3), was computed by Oort as well as the most probable curve. They are both given in Fig. 6. The curve marked Perek refers

to the model of Section III, E. The gradient $dQ_z/dz = -C^2$, $C = 67 \pm 3$ km/sec at $z = 0$, was determined by Eelsalu (1958). His value agrees with the tangent to the minimum Q_z but it lies below the curves by Hill and Oort. Possible causes of this were discussed by Oort (see 1960).

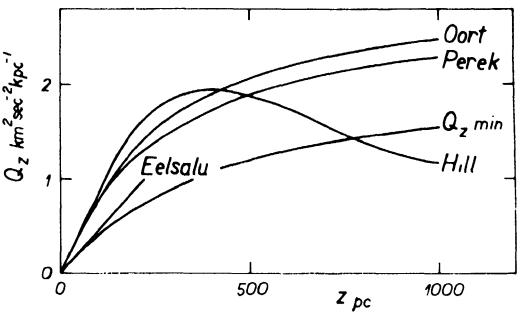


FIG. 6. Attraction in the z-direction according to E. R. Hill and J. H. Oort. $Q_{z\,\min}$ is minimum attraction compatible with the Poisson equation. Perek's curve refers to the model of Section III, E. The derivative of the attraction was determined by H. Eelsalu.

3. *Rotation Curves*

Essential information comes from the measurements of velocities of rotation at different distances from the center of a galaxy, generally in the plane of symmetry. It is usually assumed that the measured objects move in circular orbits and that, accordingly, the measured velocities, after applying corrections for the tilt of, and position in, the galaxy, yield directly circular velocities. These give the attraction from the formula for the acceleration of a central force. If the measurements concern the Galaxy, the velocities refer to the moving sun; they must be reduced to a point at rest with regard to the center. This implies the knowledge of the velocity of rotation of the sun, O , and the distance of the sun from the center, ϖ . We shall not enter here into a discussion of the methods for the determination of these two quantities. If they are known, as well as Oort's parameters, the rotation curve can be followed to a certain distance from the sun, because Oort's parameters give O/ϖ and $dO/d\varpi$. At distances where the linear extrapolation is not sufficient, the rotation curve from radio observations of neutral hydrogen (Kwee *et al.*, 1954) supplies the necessary information. This rotation curve (Fig. 7) was determined under the supposition that maximum radial velocities in a given direction correspond to the circular velocity at a point nearest to the center. This is evidently true at distances exceeding 3 kpc where the profiles of the 21-cm line are narrow, and hence the dispersion of velocities is small. However, wide wings of the line were observed

near the center, indicating that the gas is not in a pure rotation. In fact, it was shown by Rugoor and Oort (1959) that the motion is a superposed expansion and rotation. The expansion attains up to 150 km/sec and is probably due to forces other than gravitation. If the velocity of expansion is 50 km/sec at a distance of 3 kpc, density 0.3 cm^{-3}, and thickness of the layer 150 pc, then through a cylinder of a radius of 3 kpc passes an amount of the gas equivalent to one solar mass per year. This quantity is possibly replaced by condensation from the galactic halo.

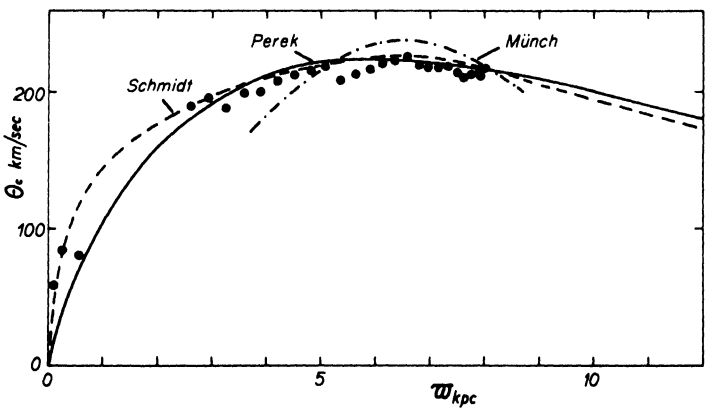


FIG. 7. Rotation curve of the Galaxy. Dots are observations of neutral hydrogen by K. K. Kwee *et al.* The curves refer to the models by M. Schmidt (Section III, C, 3), by L. Perek (Section III, E), and to observations of cepheids by G. and L. Münch.

The question of the rotation curve of the Galaxy has not yet been definitively settled. G. and L. Münch (1960) derived a part of the rotation curve from motions of distant O and B stars. This curve, shown in Fig. 7, gives a much smaller slope in the central regions. This means that the amount of mass near the center is much less than if derived from the hydrogen rotation curve.

Rotation curves were measured for a number of galaxies. In the foreground stands, of course, the Andromeda Nebula. The measurements by Babcock (1939) show a maximum at 3′ from the center. At the distance of 8′ the velocities drop to almost zero, to increase at larger distances to the main maximum (Fig. 8). Radial velocities measured at a later period by Mayall (1950) do not permit a decision to be made about the reality of the maximum near the center because of the dispersion of individual points. The rotation curve of neutral hydrogen was measured by van de Hulst *et al.* (1957). These measurements differ from those of Babcock, but Mayall's velocities, corrected for tilt and position by van de Hulst, cover the region of both curves.

As well as in the Galaxy, expansion was found in the nucleus of M 31 by G. Münch (1960). In contrast with the Galaxy, ionized hydrogen was found expanding at a distance of one order of magnitude smaller. The nucleus was

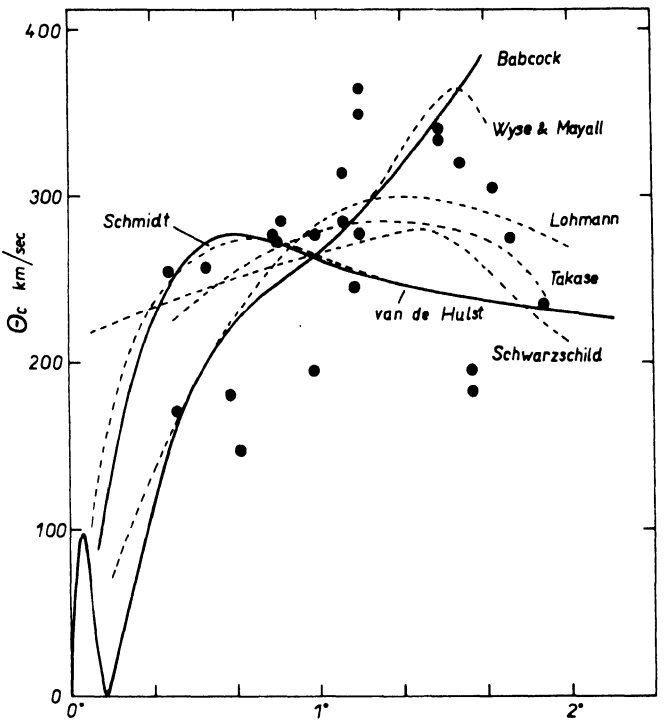


FIG. 8. Rotation curve of M 31. Dots are observations by N. U. Mayall reduced by H. C. van de Hulst. Full curves are optical observations by H. W. Babcock and radio observations by H. C. van de Hulst *et al.* Dashed curves refer to models by W. Lohmann (Section II, B, 4), A. B. Wyse and N. U. Mayall (Section III, B, 3), M. Schwarzschild (Section III, B, 3), M. Schmidt (Section III, C, 3), and B. Takase (Section III, C, 8).

investigated again by Lallemand *et al.* (1960a) with an electronic camera attached to the 120-in telescope giving a very high resolution. One more sharp maximum of the rotation curve was found at a distance of 2.2″ from the center. Figure 9 gives the measured velocities and the beginning of the rotation curve by Babcock (1939). If the nucleus is spherical and if it rotates as a rigid body it has a diameter of 7.4 pc, a mass of 1.3×10^7 $M_\odot$, and a density of 1500 $M_\odot/pc^3$ if the distance of M 31 is 690 kpc. The nucleus has the same size as a globular cluster but its mass is 100 ×, density 25 ×, and luminosity 20 × larger than

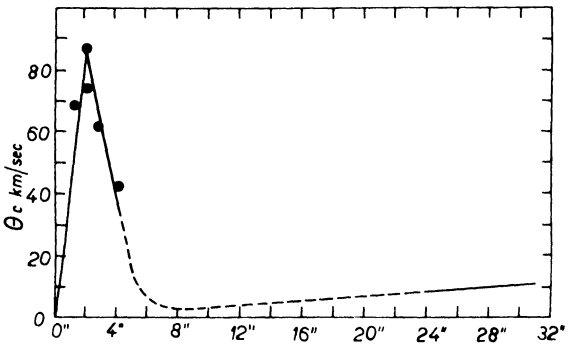


FIG. 9. Rotation curve of the nucleus of M 31. The solid line beyond 24″ is the rotation curve by H. W. Babcock.

those of globular clusters. No rotation of the nucleus of M 32 was found by Lallemand *et al.* (1960b).

The galactic halo finds its counterpart in M 31, too. Hanbury Brown and Hazard (1959) found from radio observations an extended halo, exceeding about 3 × the dimensions of the visible object. The true axial ratio is about 0.6. M 33 has a similar halo, relative to the visible object.

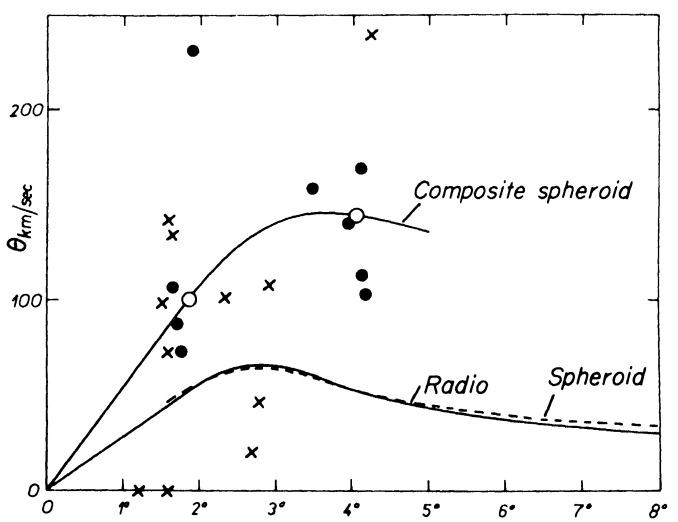


FIG. 10. Rotation curve of the Large Magellanic Cloud. Dots and crosses are observations of points near the major and minor axes respectively. Circles are normal points. The upper curve refers to a spheroidal model representing optical observations (Section III, C, 2). The dashed curve refers to a spheroidal model representing radio observations (lower full curve).

Of the Large Magellanic Cloud, first the radio rotation curve was measured by Kerr and de Vaucouleurs (1955, 1956); optical radial velocities were measured by de Vaucouleurs (1960). Dots in Fig. 10 refer to objects close to the major axis; crosses—to objects near the minor axis. The latter have only a small weight. The curve was passed through normal points (circles). The evident discrepancy of the radio and optical observations was explained by de Vaucouleurs by the complex structure of the Cloud. Radio observations do not correspond to the plane of symmetry; they come from a certain height above the plane where the velocities are smaller. Besides, the radio observations register all the hydrogen in the line of vision. It seems, therefore, that the scale of the optical velocities is nearer to the actual state but that the general form of the radio rotation curve is correct.

The number of galaxies with known rotation curves has increased considerably in recent years. Of greatest importance are those with curves which exceed, or at least attain, the maximum. Thus E. M. Burbidge *et al.* (1960a) derived the rotation curve of NGC 5055 by putting the slit of the spectrograph into the major axis of the image and by measuring shifts of spectral lines across the nebula. Figure 11 gives the velocities uncorrected for tilt. Each point is a

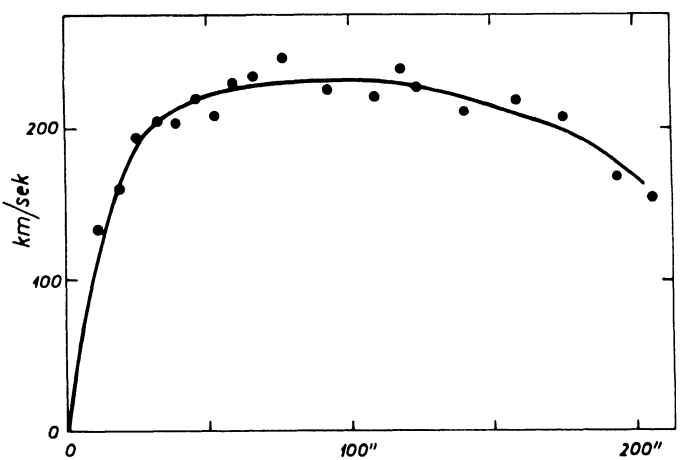


FIG. 11. Uncorrected velocities in NGC 5055 according to E. M. Burbidge *et al.*

mean of four observations. The curve is a polynomial of the 6th degree passed through the normal points by the method of least squares.

The rotation curve of NGC 2146 (Burbidge *et al.* 1959b) probably attains the maximum at the NW side (Fig. 12). The concave form of the curve near the center should be noticed. G. Münch (1959) measured radial velocities of H II

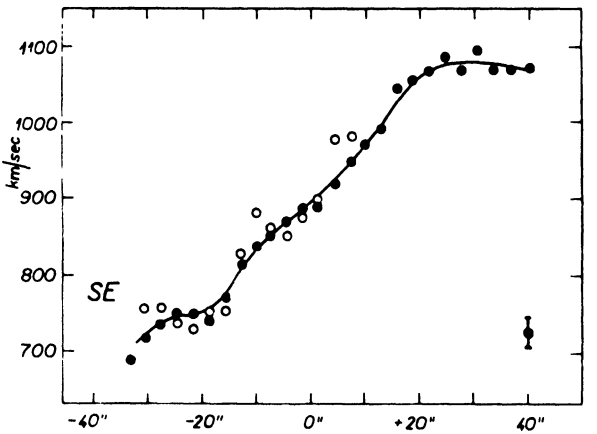


FIG. 12. Radial velocities in NGC 2146 according to E. M. Burbidge *et al.* Dots are measures of Hα, circles of [N II] λ 6584. Double the average deviation of a single measure is shown by the vertical bar.

regions in M 81. The slope of the curve near the center has been estimated to 550 km/sec/kpc from the inclination of the nuclear emission lines. The curve is shown in Fig. 13.

Radio as well as optical observations are available for M 33. Rotation velocities

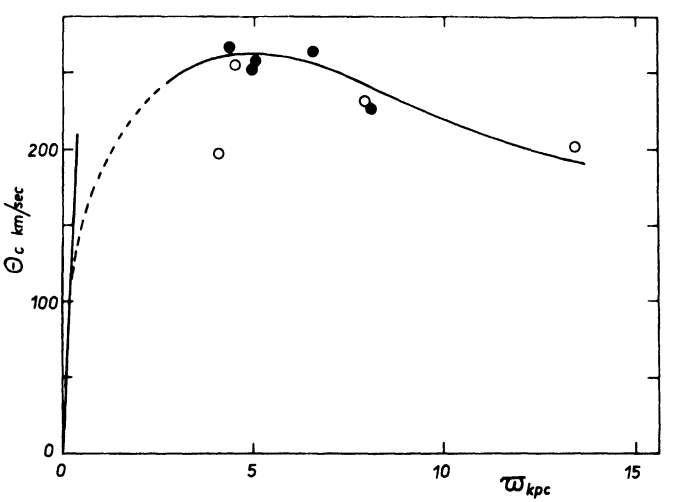


FIG. 13. Rotation curve of M 81 from radial velocities of H II regions according to G. Münch. Dots refer to the np-side, circles to the sf-side. The angular velocity at the center is 550 km/sec/kpc.

of 20 bright-line condensations were measured by Mayall and Aller (1942). Radio measurements of neutral hydrogen were given by Volders (1959). Figure 14 shows that the maximum has been attained.

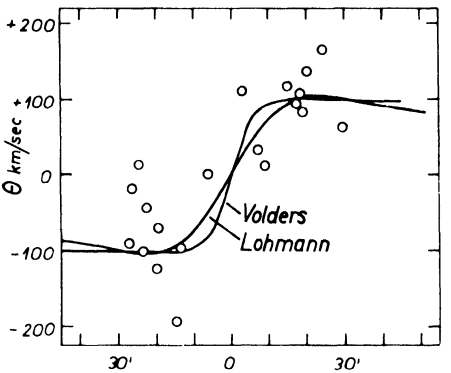


FIG. 14. Rotation velocities of bright-line condensations (N. U. Mayall and L. H. Aller) and rotation curve from radio observations in M 33 (L. Volders). W. Lohmann's curve refers to Section II, B, 4. It was derived from Bottlinger's force law.

It is uncertain where lies the maximum in M 101 because the observations by Volders (1959) give 132 km sec at 1.5′ and an identical value of 176 km sec at four distances ranging from 6.3′ to 25.2′. Velocities measured by M. L. Humason

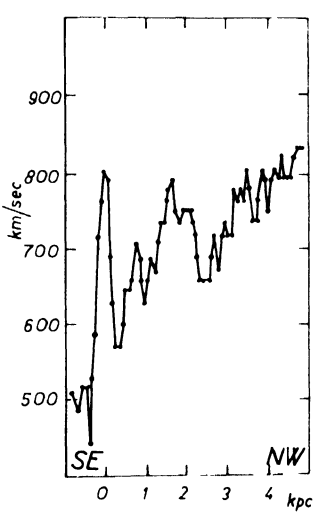


FIG. 15. Uncorrected radial velocities in NGC 5128 according to E. M. and G. R. Burbidge. Slit along the dark lane.

in NGC 3115, quoted by Oort (1940), show a steady increase with the distance. The peculiar galaxy NGC 5128 consists possibly of two galaxies in collision. The rotation curve, with the slit oriented along the middle of the dark lane, was measured by E. M. and G. R. Burbidge (1959) (Fig. 15).

The observations by E. M. Burbidge *et al.* (1959a) cover only the rising branch of the rotation curve of NGC 1068 (Fig. 16). The slit was oriented from NE

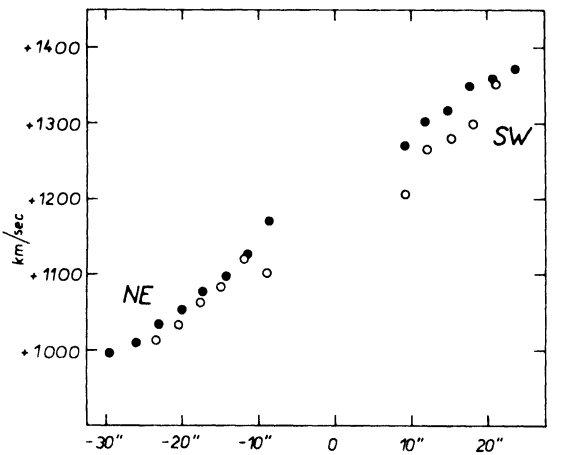


FIG. 16. Uncorrected velocities in NGC 1068 according to E. M. Burbidge *et al.*

to SW and all the measured points fell on a straight line. A linear dependence is shown by measures in NGC 3556 by Burbidge *et al.* (1960b). Two barred spirals were investigated by E. M. and G. R. Burbidge (1960). NGC 1097 has an amorphous nucleus of about 8″ in diameter. The spectral lines point to a fast rotation of the nucleus and to a discontinuity in the velocities. The slope of spectral lines was measured in NGC 1365.

C. *Geometry of Spheroids*

1. *Similar and Confocal Spheroids*

The stellar systems considered in this paper are distinguished by their flattening and by the rotation symmetry. These are the reasons why two-axial oblate ellipsoids, i.e., spheroids, are often met with.

Denoting the major and minor semiaxes of the meridian section of a spheroid by a and c and the axial ratio

$$c/a = \cos \psi_0, \qquad c \leqq a, \tag{1.1}$$

we get the following basic relations between semiaxes, linear eccentricity $\epsilon^2 = a^2 - c^2$, numerical eccentricity $e = \epsilon/a$, and the angle ψ_0:

$$\begin{aligned} e &= \sin \psi_0 \\ a &= \epsilon \operatorname{cosec} \psi_0 \\ c &= \epsilon \cot \psi_0 \end{aligned} \tag{1.2}$$

The equation of a spheroid in cylindrical coordinates ϖ, ϑ, z

$$\frac{\varpi^2}{a^2} + \frac{z^2}{c^2} = 1 \tag{1.3}$$

can be written by means of the angle ψ_0 in the form

$$\varpi^2 \sin^2 \psi_0 + z^2 \tan^2 \psi_0 = \epsilon^2. \tag{1.4}$$

A similar, concentric, and homothetic spheroid is expressed by

$$\varpi^2 \sin^2 \psi_0 + z^2 \tan^2 \psi_0 = m^2\epsilon^2, \tag{1.5}$$

where m attains any positive value. The parameter m is dimensionless and determines one of the similar spheroids or one of the spheroidal shells. On a straight line passing through the center m is proportional to the distance. Inversely, the distance can be measured by means of m. In particular, in the plane of symmetry, $m = \varpi\, a$, and on the axis of rotation, $m = z\, c$.

A spheroid confocal to (1.4) has the same linear eccentricity but a different numerical eccentricity as well as the angle ψ_0. The equation of a confocal spheroid is

$$\varpi^2 \sin^2 \psi + z^2 \tan^2 \psi = \epsilon^2, \tag{1.6}$$

and a spheroid confocal to (1.5) is

$$\varpi^2 \sin^2 \psi + z^2 \tan^2 \psi = m^2\epsilon^2. \tag{1.7}$$

Its semiaxes are

$$\sqrt{m^2a^2 + \lambda} = ma \frac{\sin \psi_0}{\sin \psi}$$

$$\sqrt{m^2c^2 + \lambda} = ma \frac{\sin \psi_0}{\tan \psi}.$$

Hence follows the definition of the angle ψ

$$\cos \psi = \sqrt{\frac{m^2c^2 + \lambda}{m^2a^2 + \lambda}}, \tag{1.8}$$

which reduces to ψ_0 for $\lambda = 0$.

Equation (1.7) is of the fourth degree in $\sin\psi$. Its four roots are

$$\sin\psi = \frac{1}{2\varpi}\left[\pm\sqrt{z^2+(\varpi+m\epsilon)^2}\pm\sqrt{z^2+(\varpi-m\epsilon)^2}\right].$$

The value of $\sin\psi$ must be positive and between 0 and 1. These conditions are met only by the root

$$\sin\psi = \frac{1}{2\varpi}\left[\sqrt{z^2+(\varpi+m\epsilon)^2}-\sqrt{z^2+(\varpi-m\epsilon)^2}\right]. \tag{1.9}$$

In the plane of symmetry we have

$$\begin{aligned} \sin\psi &= 1; \qquad \varpi \leq m\epsilon \\ \sin\psi &= m\epsilon/\varpi; \qquad \varpi \geq m\epsilon. \end{aligned} \tag{1.10}$$

On the axis of rotation, we obtain directly from (1.7),

$$\tan\psi = m\epsilon/z. \tag{1.11}$$

The angles ψ and ψ_0 are most convenient for expressing the integrals appearing in some of the formulae for the potential

$$w_{lk} = \epsilon^{2l+2k+1}\int_{\lambda}^{\infty}\frac{du}{(a^2+u)^l\,(c^2+u)^{k+1/2}}. \tag{1.12}$$

Introducing the angle ψ, we get

$$w_{lk} = 2\int_0^{\psi}\sin^{2l-2}\psi\tan^{2k}\psi\,d\psi; \qquad \begin{matrix} l+k>0 \\ l\geq 0 \\ k\geq 0 \end{matrix} \tag{1.13}$$

In general, integrals w_{lk} are through the angle ψ functions of the coordinates. However, if the upper limit of the integral (1.13) is ψ_0, w_{lk} become constants and are denoted v_{lk}. The integrals w_{lk} are computed by means of the recursion formulae

$$\begin{aligned} w_{0k} &= \frac{2}{2k-1}(\tan\psi)^{2k-1}; \qquad k>0 \\ w_{l0} &= \frac{2l-3}{2l-2}w_{l-1,0}-\frac{1}{l-1}\cos\psi\,(\sin\psi)^{2l-3}; \qquad l>1 \\ w_{lk} &= w_{l-1,k}-w_{l,k-1}; \qquad l>0,\ k>0 \end{aligned} \tag{1.14}$$

The explicit forms of a few of the simplest w_{lk} are

$$\begin{aligned}
w_{10} &= 2\psi \\
w_{20} &= \psi - \sin\psi\cos\psi \\
w_{30} &= \tfrac{3}{4}[\psi - \sin\psi\cos\psi\,(1 + \tfrac{2}{3}\sin^2\psi)] \\
w_{40} &= \tfrac{3}{4}\cdot\tfrac{5}{6}[\psi - \sin\psi\cos\psi\,(1 + \tfrac{2}{3}\sin^2\psi + \tfrac{8}{15}\sin^4\psi)]
\end{aligned} \tag{1.15}$$

$$\begin{aligned}
w_{11} &= 2(\tan\psi - \psi) \\
w_{12} &= 2(\tfrac{1}{3}\tan^3\psi - \tan\psi + \psi) \\
w_{13} &= 2(\tfrac{1}{5}\tan^5\psi - \tfrac{1}{3}\tan^3\psi + \tan\psi - \psi)
\end{aligned}$$

The trigonometric polynomials in these formulae are actually the first terms in the developments of ψ in terms of $\sin\psi$ and $\tan\psi$. Thus for large values of the indices

$$l \to \infty \qquad w_{l0} \to 0$$

$$k \to \infty \qquad w_{1k} \to 0.$$

The w_{l0} are finite for all values of ψ but w_{lk} with $k > 0$ tend to infinity for $\psi \to \pi/2$, i.e., for totally flattened spheroids. A table giving the values of

$$w_{10},\ w_{20},\ w_{30},\ w_{40}$$

$$w_{11},\ w_{21},\ w_{31}$$

$$w_{12},\ w_{22}$$

$$w_{13}$$

with the argument ψ and a nomogram for solving Eq. (1.6) was published by Perek (1950).

2. *Mass*

The mass of a homogeneous solid spheroid of semiaxes ma, mc and density ρ is

$$M_h = \tfrac{4}{3}\pi a^3 \cos\psi_0\, \rho m^3. \tag{1.16}$$

The mass of an infinitely thin shell of the same semiaxes and thickness dm is

$$dM = 4\pi a^3 \cos\psi_0\, \rho m^2\, dm. \tag{1.17}$$

By integrating this expression from the center, $m = 0$, to the boundary, $m = m_1$, we find the mass of the heterogeneous spheroid

$$M = 4\pi a^3 \cos\psi_0 \int_0^{m_1} \rho(m)\, m^2\, dm, \tag{1.18}$$

supposing that the density is a function of m. In other words, the equidensity surfaces are similar spheroids.

If the spheroid has confocal strata, we have from the formula for the volume of a solid spheroid

$$v = \tfrac{4}{3}\pi a^2 c$$

$$dv = \tfrac{4}{3}\pi(a^2\, dc + 2ac\, da).$$

Linear eccentricity being now a constant, we have

$$a\, da = c\, dc = -\epsilon^2 \frac{\cos\psi}{\sin^3\psi}\, d\psi$$

and

$$dv = -\frac{4}{3}\pi\epsilon^3 \frac{3 - 2\sin^2\psi}{\sin^4\psi}\, d\psi. \tag{1.19}$$

Hence the total mass

$$M = \int \rho\, dv$$

$$= \frac{4}{3}\pi\epsilon^3 \int_{\psi_0}^{\pi/2} \rho \frac{3 - 2\sin^2\psi}{\sin^4\psi}\, d\psi, \tag{1.20}$$

where the integration extends from the boundary of the spheroid, $\psi = \psi_0$, to the focal circle, $\psi = \pi/2$.

3. *Projected Densities*

Projected densities are a means of taking account of all the matter in the system without having to determine the distribution in the z-direction.

The density in the layer $(-z, +z)$, at a distance $m_0 = \varpi/a$ from the center, projected on the plane of symmetry, is

$$\sigma(\varpi) = 2\int_0^z \rho\, dz. \tag{1.21}$$

The upper limit of the integral refers usually to the boundary of the spheroid

$$z = c\sqrt{1 - m_0^2}.$$

For a homogeneous spheroid we have immediately

$$\sigma(\varpi) = 2\rho \cos \psi_0 \sqrt{a^2 - \varpi^2}\,.$$

If the strata are similar, a column cuts the stratum m at

$$z = c\sqrt{m^2 - m_0^2}\,.$$

Interchanging the variables in (1.21) we find

$$\sigma(\varpi) = 2a \cos \psi_0 \int_0^{\rho(m_0)} \sqrt{m^2 - m_0^2}\, d\rho. \tag{1.22}$$

Sometimes it is more convenient to use m as the integration variable. The equation of the spheroid yields

$$dz = c\frac{m\, dm}{\sqrt{m^2 - m_0^2}}\,.$$

Thus

$$\sigma(\varpi) = 2a \cos \psi_0 \int_{m_0}^{m_1} \frac{\rho(m)\, m\, dm}{\sqrt{m^2 - m_0^2}} \tag{1.23}$$

where m_1 again refers to the boundary of the spheroid.

4. *The Potential of a Spheroid with Similar Strata*

Let us decompose a heterogeneous spheroid into elementary shells of semi-axes ma, mc, thickness dm, and density ρ. The potential of the shell at an external point can be written according to standard textbooks in the form

$$dP_e = \frac{1}{2} G\, dM \int_\lambda^\infty \frac{du}{(m^2a^2 + u)\,(m^2c^2 + u)^{1/2}}$$

or, by Eqs. (1.12) and (1.15),

$$dP_e = \frac{G\, dM}{m\epsilon}\psi. \tag{1.24}$$

At internal points the lower limit is zero, thus

$$dP_1 = \frac{G\, dM}{m\epsilon}\psi_0. \tag{1.25}$$

The potential of the solid heterogeneous spheroid is derived by integrating the above formulas. Supposing the point (ϖ, z), at which the potential is being

computed, is inside the spheroid and lying on the shell m_0, we have to integrate (1.24) from the center to m_0 and (1.25) from m_0 to m_1. Thus

$$P_1 = \int_0^{m_0} dP_e + \int_{m_0}^{m_1} dP_1 = 4\pi G a^2 \cot \psi_0 \left[\int_0^{m_0} \rho \psi m \, dm + \psi_0 \int_{m_0}^{m_1} \rho m \, dm \right]. \quad (1.26)$$

If the point is external with regard to the solid spheroid, we find

$$P_e = \int_0^{m_1} dP_e = 4\pi G a^2 \cot \psi_0 \int_0^{m_1} \rho \psi m \, dm. \quad (1.27)$$

It is evident that the potential contains only integrals w_{lk} if the density is a polynomial in m^2. We shall find a different expression for the potential useful. Writing Eq. (1.27) in the form

$$P_e = 4\pi G a^2 \cot \psi_0 \int_0^{m_1} \rho m \, dm \int_0^{\psi} d\psi$$

and interchanging the order of integration, we get

$$P_e = 4\pi G a^2 \cot \psi_0 \int_0^{\psi} d\psi \int_m^{m_1} \rho m \, dm.$$

If ρ is a function of m^2 we denote ρ_1, the primitive function,

$$\frac{d\rho_1(m^2)}{d(m^2)} = \rho(m^2)$$

and we find

$$P = 2\pi G a^2 \cot \psi_0 \int_0^{\psi} [\rho_1(m_1^2) - \rho_1(m^2)] \, d\psi. \quad (1.28)$$

The dependence of m on ψ is given by Eq. (1.7).

Let us return to Eq. (1.27). Taking ψ as the integration variable, we have

$$P = 2\pi G a^2 \cot \psi_0 \int_0^{\psi} \rho(\psi) \psi \frac{dm^2}{d\psi} \, d\psi. \quad (1.29)$$

Since the integrand becomes zero for the upper limit,

$$\frac{\partial P}{\partial \psi} = 0.$$

ψ can be considered a constant in differentiating P with respect to the coordinates.

An expression for the component of attraction in the ϖ-direction readily follows from Eq. (1.24). Since

$$dQ_\varpi = \frac{d(dP_e)}{d\lambda}\frac{d\lambda}{d\varpi}$$

and

$$d\varpi^2 = d\lambda,$$

we get

$$dQ_\varpi = -2\pi G\varpi\rho\frac{\cos\psi_0}{\sin^3\psi_0}\frac{\sin^3\psi}{\cos\psi}\frac{dm^2}{m^2}$$

and integrating,

$$Q_\varpi = -4\pi G\frac{\cos\psi_0}{\sin^3\psi_0}\varpi\int_0^\psi \rho\tan^2\psi\frac{\varpi^2\cos^4\psi + z^2}{\varpi^2\cos^2\psi - z^2}d\psi, \tag{1.30}$$

which reduces in the plane of symmetry to

$$Q_\varpi = -4\pi G\frac{\cos\psi_0}{\sin^3\psi_0}\varpi\int_0^\psi \rho\sin^2\psi\,d\psi. \tag{1.31}$$

Substituting m instead of ψ according to (1.10) we get the same expression with m as an integration variable

$$Q_\varpi = -4\pi G\cos\psi_0\frac{a^2}{\varpi}\int_0^{m_0}\frac{\rho m^2\,dm}{\sqrt{m_0^2 - m^2\sin^2\psi_0}}, \tag{1.31a}$$

where $m_0 = \varpi/a$.

On the basis of the above formulas the potential of heterogeneous spheroids with different density laws will be derived in Section III, C. Here, we give only the potential of a homogeneous spheroid. Assuming the density to be constant and putting $m_1 = 1$ into Eq. (1.27), we find

$$\begin{aligned} P_{he} &= 4\pi Ga^2\rho\cot\psi_0\int_0^1 m\psi\,dm \\ &= 2\pi Ga^2\rho\cot\psi_0\left[\psi - \frac{1}{2}\frac{\varpi^2}{\epsilon^2}w_{20} - \frac{z^2}{\epsilon^2}w_{11}\right], \end{aligned} \tag{1.32}$$

or, writing the w_{lk} in full

$$P_{he} = \pi Ga^2\cot\psi_0\,\rho\left[2\psi - \frac{\varpi^2}{\epsilon^2}(\psi + \sin\psi\cos\psi) - 2\frac{z^2}{\epsilon^2}(\tan\psi - \psi)\right]. \tag{1.33}$$

For internal points the expression has the same form, but the lower limit in the integrals w_{lk} becomes zero. Thus we write v_{lk} instead of w_{lk} or, which is equivalent, ψ_0 instead of ψ.

Differentiating (1.33) with respect to ϖ, we find the attraction in the plane of symmetry

$$Q_\varpi = -2\pi G\rho \frac{\cos\psi_0}{\sin^3\psi_0}(\psi - \sin\psi\cos\psi)\varpi. \tag{1.34}$$

At internal points we put ψ_0 instead of ψ and get an attraction proportional to the distance.

Expanding ψ, at external points, into a series and inserting the total mass, we find

$$Q_\varpi = -\frac{MG}{\varpi^2}\left[1 + \frac{3}{10}\left(\frac{\epsilon}{\varpi}\right)^2 + \frac{9}{56}\left(\frac{\epsilon}{\varpi}\right)^4 + \frac{5}{48}\left(\frac{\epsilon}{\varpi}\right)^6 + \cdots\right]. \tag{1.35}$$

The attraction of a homogeneous oblate spheroid at external points in the plane of symmetry always exceeds that of a mass point of the same mass. The difference diminishes with increasing distance.

A different expression for the potential of a homogeneous spheroid was given by Eichhorn (1957). Introducing coordinates s_1, s_2 by equations

$$\begin{aligned} &\frac{\varpi^2}{1+s_1} + \frac{z^2}{s_1} = \epsilon^2, \qquad s_1 > 0 \\ &\frac{\varpi^2}{1+s_2} + \frac{z^2}{s_2} = \epsilon^2, \qquad -1 < s_2 < 0 \end{aligned} \tag{1.36}$$

we arrive, by comparison with Eq. (1.6), at

$$\begin{aligned} s_1 &= \cot^2\psi & \varpi^2 &= \epsilon^2(1+s_1)(1+s_2) \\ s_2 &= -\frac{z^2}{\epsilon^2}\tan^2\psi & z^2 &= -\epsilon^2 s_1 s_2. \end{aligned}$$

The potential takes the form

$$P = \frac{3}{4}\frac{GM}{e}\left\{s_2[3\sqrt{s_1} - (1+3s_1)\cot^{-1}\sqrt{s_1}] + (1-s_1)\cot^{-1}\sqrt{s_1} + \sqrt{s_1}\right\}. \tag{1.37}$$

The s_1, s_2 are related to elliptical coordinates. The first of the definition equations corresponds to a family of confocal ellipses, the second to a family of confocal hyperbolas. We shall encounter similar coordinates in Section II, C. In the following we adhere to the expression of the potential using the angle ψ.

5. *The Potential of a Spheroid with Confocal Strata*

Our starting point in this case is an elementary shell bounded by two confocal surfaces, a focaloid. According to Routh (1902) the potential of a thin focaloid at an internal point is given by an expression which takes the form

$$P_{\mathrm{fi}} = \frac{dv}{v} P_{\mathrm{hi}} = 2\pi G\rho \left(1 - \frac{\varpi^2}{a^2} - \frac{z^2}{c^2}\right) a\, da \tag{1.38}$$

for a spheroid and in our notation. The potential at an external point follows simply from the Maclaurin theorem

$$P_{\mathrm{fe}} = \frac{dv}{v} P_{\mathrm{he}}. \tag{1.39}$$

Here, P_{h} is the potential of a homogeneous spheroid enclosed inside the focaloidal shell and having the same density as the shell. The volume of the shell is dv and that of the spheroid enclosed inside is v.

By dissecting the heterogeneous spheroid into infinitesimal focaloidal shells and integrating the above expressions, we derive the potential of the spheroid with confocal strata. The point (ϖ, z) lying in the shell ψ is internal to all shells between $\pi/2$ and ψ, and it is external with regard to those between ψ and the boundary of the spheroid, ψ_0. The spheroid has a finite boundary for $\psi_0 > 0$ and an infinite boundary for $\psi_0 = 0$. Thus

$$P_1 = \int_{\pi/2}^{\psi} P_{\mathrm{fe}}\, d\psi + \int_{\psi}^{\psi_0} P_{\mathrm{fi}}\, d\psi. \tag{1.40}$$

In (1.33) ψ corresponded to a shell passing through (ϖ, z) and confocal to the boundary ψ_0 of the homogeneous spheroid. Here, ψ is confocal to all elementary shells thus being a constant. The integration refers to the variable ψ_0. However, ψ_0 behind the sign of integration has been denoted by ψ again. Inserting (1.33) and an analogous expression for P_{hi} into (1.38) and (1.39), we get from (1.40) after rearranging,

$$\begin{aligned} P_1 = \pi G \Big\{ & [w_{10}\epsilon^2 - w_{20}\varpi^2 - w_{11}z^2] \int_{\psi}^{\pi/2} \rho(\psi) \frac{3 - 2\sin^2\psi}{\sin^4\psi}\, d\psi \\ & + (2\epsilon^2 - \varpi^2 + 2z^2) \int_{\psi_0}^{\psi} \rho(\psi)\, \psi \frac{3 - 2\sin^2\psi}{\sin^4\psi}\, d\psi \\ & - (2\epsilon^2 - 3\varpi^2 + 6z^2) \int_{\psi_0}^{\psi} \rho(\psi) \frac{\cos\psi}{\sin^3\psi}\, d\psi \Big\}. \end{aligned} \tag{1.41}$$

Here, ψ_0 refers to the boundary of the spheroid and ψ, besides being an integration variable, refers to a spheroidal surface confocal with the boundary. Thus ψ_0 follows from the dimensions of the spheroid and ψ is the root of Eq. (1.6).

The potential takes a simpler form at external points because two of the three integrals in (1.41) vanish. The limits of the remaining integral are the boundary, ψ_0, and the focal circle. We have

$$P_e = \pi G(w_{10}\epsilon^2 - w_{20}\varpi^2 - w_{11}z^2) \int_{\psi_0}^{\pi/2} \rho(\psi) \frac{3 - 2\sin^2\psi}{\sin^4\psi} d\psi. \quad (1.42)$$

Further development of these formulas will be postponed until Section III,D for concrete forms of the density law.

II

MODELS BASED ON THE VELOCITY DISTRIBUTION

A. *The Equation of Continuity*

Let x, y, z denote rectangular coordinates and ξ, η, ζ the components of the velocity in this system. The number of stars in an element of the seven-dimensional space is

$$f(x, y, z, \xi, \eta, \zeta, t)\, dx\, dy\, dz\, d\xi\, d\eta\, d\zeta\, dt. \quad (2.1)$$

The equation of continuity expresses the invariance of the density in an element of the phase space with regard to the motion. Thus

$$\xi \frac{\partial f}{\partial x} + \eta \frac{\partial f}{\partial y} + \zeta \frac{\partial f}{\partial z} + \frac{\partial P}{\partial x} \frac{\partial f}{\partial \xi} + \frac{\partial P}{\partial y} \frac{\partial f}{\partial \eta} + \frac{\partial P}{\partial z} \frac{\partial f}{\partial \zeta} + \frac{\partial f}{\partial t} = 0, \quad (2.2)$$

where we used the equality of the acceleration to the attraction on a unity of mass, i.e., to the derivative of the potential according to the respective coordinate. Equation (2.2) contains two unknown functions, f and P. The potential P is related to the amount and distribution of all the mass in the system. If function f is related to the galactic population as a whole, the potential is determined by the form of f. On the other hand, if f expresses adequately the properties of only one subsystem, only a part of the potential is determined by f. If the contribution of the subsystem to the total mass of the system is negligible, the potential P is wholly determined by the distribution of other masses than those entering into f.

Equation (2.2), as a partial differential equation of f, has the solution

$$dt = \frac{dx}{\xi} = \frac{dy}{\eta} = \frac{dz}{\zeta} = \frac{d\xi}{\partial P/\partial x} = \frac{d\eta}{\partial P/\partial y} = \frac{d\zeta}{\partial P/\partial z}. \quad (2.3)$$

These are identical with the equations of motion. Denoting their integrals I_1, I_2, ..., I_6, the general solution of the equation of continuity is

$$f(x, y, z, \xi, \eta, \zeta, t) = f(I_1, I_2, ..., I_6) \tag{2.4}$$

the Jeans theorem: the frequency function is an integral of the equations of motion.

If the potential is independent of time, the equations of motion admit the energy integral

$$I_1 = \tfrac{1}{2}(\xi^2 + \eta^2 + \zeta^2) - P \tag{2.5}$$

and from the assumption of rotation symmetry follows the existence of the angular momentum integral. In cylindrical coordinates ϖ, ϑ, z and respective components of the velocity Π, O, Z the two integrals assume the form

$$\begin{aligned} I_1 &= \tfrac{1}{2}(\Pi^2 + O^2 + Z^2) - P \\ I_2 &= \varpi O. \end{aligned} \tag{2.6}$$

Alternatively, according to Idlis (1959a,b), it is possible to derive the properties we assumed, from the existence of the integrals. The integral of energy is the most general integral of the equations of motion which does not impose any other restrictions on the potential besides the independence of time. In a similar way, the angular momentum integral is the second most general integral admitting systematical motions and imposing minimum restrictions on the potential, requiring only rotation symmetry. The potential of a self-gravitating system with finite mass and possessing the above properties admits of one, and only one, third one-valued integral I_3 of the equations of motion, which is independent of I_1 and I_2. The integral I_3 is even with regard to O and to the couple Π, Z. A formal third integral expressed as a series was found by Contopoulos (1960).

We stress the fact that up to now no assumption has been made about the form of the frequency function. Further conclusions, in particular the form of I_3 (see Section II, C), depend on the form of f. Let us write the equation of continuity in cylindrical coordinates

$$\Pi \frac{\partial f}{\partial \varpi} + \frac{O}{\varpi}\left(O \frac{\partial f}{\partial \Pi} - \Pi \frac{\partial f}{\partial O}\right) + Z \frac{\partial f}{\partial z} + \frac{\partial P}{\partial \varpi}\frac{\partial f}{\partial \Pi} + \frac{\partial P}{\partial z}\frac{\partial f}{\partial Z} = 0 \tag{2.7}$$

and assume that f is a function of one argument q only,

$$f = f(q). \tag{2.8}$$

The form of q

$$q = h^2\Pi^2 + k^2(O - O_0)^2 + l^2Z^2 + m\Pi(O - O_0) + n\Pi Z + p(O - O_0)Z \tag{2.9}$$

is known as the generalized ellipsoidal hypothesis.

In the special case

$$f = f_0 e^{-q} \tag{2.10}$$

it has been introduced by K. Schwarzschild (1907). The $h, k, l, m, n, p, O_0, f_0$ are functions of the coordinates. We notice that the systematic velocity has only a Θ-component. In the other two principal directions no systematic velocities are generally admitted with respect to the supposed steady state. The ellipsoidal hypothesis introduces linear and quadratic terms in velocities. Should we regard a series in the velocities as the correct form of q, the expression (2.9) will still remain a first approximation. This was the reason, besides the ability of (2.9) to explain many of the features of the distribution of velocities, why the ellipsoidal hypothesis served as a basis for stellar dynamics for a considerable period of time. However, the question, whether by restricting the frequency function to the ellipsoidal hypothesis the generality of the solution was not lost or even the way to a solution barred, was answered much later.

Inserting (2.10) into (2.7) and solving the resulting equations by methods which appeared in many textbooks on stellar dynamics, we arrive at a result which involves also the postulate for the symmetry with respect to the plane $z = 0$

$$\begin{aligned} h^2 &= c_1 + c_5 z^2 \\ k^2 &= c_1 + c_2 \varpi^2 + c_5 z^2 \\ l^2 &= c_4 + c_5 \varpi^2 \\ n &= -2 c_5 \varpi z \\ m &= p = 0 \\ \Theta_0 &= \frac{c_3 \varpi}{c_1 + c_2 \varpi^2 + c_5 z^2} \end{aligned} \tag{2.11}$$

and further

$$\begin{aligned} \frac{1}{f_0} \frac{\partial f_0}{\partial \varpi} &= \frac{\partial (k^2 O_0^2)}{\partial \varpi} + n \frac{\partial P}{\partial z} + 2h^2 \frac{\partial P}{\partial \varpi} \\ \frac{1}{f_0} \frac{\partial f_0}{\partial z} &= \frac{\partial (k^2 O_0^2)}{\partial z} + n \frac{\partial P}{\partial \varpi} + 2 l^2 \frac{\partial P}{\partial z} \end{aligned} \tag{2.12}$$

$$\begin{aligned} \frac{\partial (k^2 \Theta_0)}{\partial \varpi} &= \frac{k^2 \Theta_0}{\varpi} \\ \frac{\partial (k^2 \Theta_0)}{dz} &= 0. \end{aligned} \tag{2.13}$$

For the axial ratio of the velocity ellipsoid we get

$$\frac{h^2}{k^2} = \frac{1}{2}\left(1 + \frac{\varpi}{O_0}\frac{\partial O_0}{\partial \varpi}\right). \tag{2.14}$$

Equations (2.12) yield, by cross-differentiation,

$$c_5\left[3\left(z\frac{\partial P}{\partial \varpi} - \varpi\frac{\partial P}{\partial z}\right) + (z^2 - \varpi^2)\frac{\partial^2 P}{\partial \varpi \partial z} + \varpi z\left(\frac{\partial^2 P}{\partial \varpi^2} - \frac{\partial^2 P}{\partial z^2}\right)\right] + (c_1 - c_4)\frac{\partial^2 P}{\partial \varpi \partial z} = 0. \tag{2.15}$$

The analysis of this equation is the basis of all solutions of the equation of continuity admitting ellipsoidal distribution of velocities.

B. *Models Based on Oort's Solution*

1. *Oort's Solution*

In order not to impose any restrictions on the potential, Oort (1928) put in (2.15)

$$c_5 = 0, \qquad c_1 = c_4.$$

The system of equations (2.11) transforms into

$$\begin{aligned} h^2 - l^2 &= c_1 \\ k^2 &= c_1 + c_2\varpi^2 \\ m = n &= p = 0; \end{aligned} \tag{2.16}$$

$$O_0 = \frac{c_3\varpi}{c_1 + c_2\varpi^2}. \tag{2.17}$$

Assuming equal masses for all stars, we find the density by integrating f over all values of the velocities

$$\nu = \int_{-\infty}^{\infty}\int\int f\, d\Pi\, dO\, dZ = \frac{\pi^{3/2}}{hkl} f_0.$$

Introducing dispersions of velocities instead of h, k, l,

$$\begin{aligned} \sigma_\varpi^2 = \sigma_z^2 &= \frac{1}{2h^2} = \frac{1}{2l^2} \\ \sigma_\vartheta^2 &= \frac{1}{2k^2}, \end{aligned} \tag{2.18}$$

we obtain Eqs. (2.12) in terms of (2.16) in the form

$$\sigma_{\varpi}^2 \frac{\partial \log \nu}{\partial \varpi} = \frac{O_0^2}{\varpi} + \frac{1}{\varpi}(\sigma_{\vartheta}^2 - \sigma_{\varpi}^2) + \frac{\partial P}{\partial \varpi}$$
$$\sigma_z^2 \frac{\partial \log \nu}{\partial z} = \frac{\partial P}{\partial z}. \tag{2.19}$$

Similar equations can be derived generally, without making any assumptions about the velocity distribution. It is sufficient to suppose a rotation symmetry. The difference as compared with (2.19) consists in the mean-square velocities appearing behind the sign of differentiation. Thus it does not follow from the general equations,

$$\frac{1}{\nu}\frac{\partial(\nu\overline{\Pi^2})}{\partial \varpi} = -\frac{1}{\varpi}(\overline{\Pi^2} - \overline{\Theta^2}) + \frac{\partial P}{\partial \varpi}$$
$$\frac{1}{\nu}\frac{\partial(\nu\overline{Z^2})}{\partial z} = \frac{\partial P}{\partial z}, \tag{2.20}$$

derived by Jeans (1922), that the mean-square velocities are constant. If they are, and the distribution is Gaussian, $\overline{\Pi^2} = \sigma_{\varpi}^2$, $\overline{Z^2} = \sigma_z^2$, $\overline{\Theta^2} = O_0^2 + \sigma_{\vartheta}^2$, the general equations assume the form (2.19).

The density follows by integrating (2.19) from (0, 0) to (ϖ, z). Thus we find

$$\log \nu(\varpi, z) = \log \nu(0, 0) - \log \frac{\sigma_{\varpi}}{\sigma_{\vartheta}} + \frac{O_0^2}{2\sigma_{\vartheta}^2} - \frac{1}{\sigma_{\varpi}^2}[P(0, 0) - P(\varpi, z)]. \tag{2.21}$$

It is convenient to introduce Oort's parameters at this place

$$A = \frac{1}{2}\left(\frac{O_0}{\varpi} - \frac{\partial O_0}{\partial \varpi}\right)$$
$$B = -\frac{1}{2}\left(\frac{O_0}{\varpi} + \frac{\partial O_0}{\partial \varpi}\right). \tag{2.22}$$

With this notation, relation (2.14) can be written in the form

$$\frac{\sigma_{\vartheta}^2}{\sigma_{\varpi}^2} = -\frac{B}{A - B}. \tag{2.23}$$

If the parameters A and B are derived for a subsystem moving in almost circular orbits, we may substitute the circular velocity Θ_c for the systematic velocity Θ_0 and by means of

$$\frac{\Theta_c^2}{\varpi} = -Q_\varpi$$

and derive the following expression for the parameter A

$$A = \frac{1}{4}\frac{\Theta_c}{\varpi}\left(1 - \frac{\varpi}{Q_\varpi}\frac{dQ_\varpi}{d\varpi}\right). \tag{2.24}$$

The two resulting formulae

$$\begin{aligned} \frac{Q_\varpi}{\varpi} &= -(A-B)^2 \\ \frac{dQ_\varpi}{d\varpi} &= (A-B)(3A+B) \end{aligned} \tag{2.25}$$

are frequently used in the Poisson equation

$$\frac{\partial Q_\varpi}{\partial \varpi} + \frac{Q_\varpi}{\varpi} + \frac{\partial Q_z}{\partial z} = -4\pi G\rho \tag{2.26}$$

to express the first two terms on the left

$$2(A^2 - B^2) + \frac{\partial Q_z}{\partial z} = -4\pi G\rho. \tag{2.27}$$

Applying this to the solar neighborhood we get a relation between the slope of the attraction in the z-direction and the density at the sun.

Oort's solution, on which a large number of papers on stellar dynamics was based, succeeded in explaining many observed effects. However, there are some discrepancies between this solution and the observations. First, the observed vertex is deviated from the direction to the center. The largest axis of the velocity ellipsoid of bright stars points to a direction 15° to 20° away from the center. It is possible that local effects in the sun's vicinity are responsible for the deviation because Hins and Blaauw (1948) found a zero deviation for faint stars. What is more important, Oort's solution requires an equality of dispersions in the ϖ- and z-directions. All observations compiled in Table II show that σ_z is substantially smaller than σ_ϖ and in most cases even smaller than σ_ϑ. Models admitting a three-axial velocity ellipsoid will be discussed in Section C.

2. *Parenago's Model*

The attraction can be readily derived if the rotation curve is known. From this point of view the formula for the systematic velocity (2.17) became interesting. However, it gives the systematic velocity of the centroid of a certain subsystem at a given distance from the center. Evidently, to each subsystem pertain different values of the constants c_i. Subsystems with small velocity dispersions have also a small difference between the systematic and the circular velocities. The formula (2.17) possesses properties expected from the rotation curve. Near the center the velocity is proportional to the distance and we have a rigid rotation. This appears plausible because the density probably varies only little near the center. The velocity attains a maximum at $\varpi = (c_1/c_2)^{1/2}$ and decreases at larger distances; so far it is in accordance with dynamical principles. However, the rate of decrease is discordant. For ϖ tending into infinity Q_ϖ must behave as ϖ^{-2} and not as ϖ^{-3} as is the case in Eq. (2.28).

The rotation formula (2.17) is flexible enough to explain even the complicated rotation curve in M 31 as observed by Babcock (1939) (Fig. 8). Parenago (1947) put forward the hypothesis that the first maximum of the rotation curve corresponds to (2.17) with constants for population II, which prevails near the center. Since its density decreases rapidly, at a certain distance population I begins to preponderate and the rotation curve, this time with a different set of constants, rises to the second maximum much more distant from the center than the first. The hypothesis is supported by the fact that the observations of the inner parts refer to smoothed out mean velocities and not to the velocities of individual objects.

To apply the formula (2.17) as an expression for the circular velocity was the leading idea of ten Bruggencate (1947) and later of Parenago (1950b, 1952). The attraction in the plane of symmetry is

$$-Q_\varpi = \frac{Q_c^2}{\varpi}, \qquad Q_\varpi = -\frac{c_3^2 \varpi}{(c_1 + c_2 \varpi^2)^2}. \tag{2.28}$$

Parenago applied the values of the c_i derived from the motions of Cepheids

$$\begin{aligned} c_3 &= 68 \pm 22 \text{ km/sec/kpc} \\ c_2 &= 0.0219 \pm 0.0074 \text{ kpc}^{-2} \\ c_1 &= 1 \end{aligned} \tag{2.29}$$

but later used an improved value of $c_2 = 0.0288$ kpc^{-2}. Integrating (2.28) the potential is found to be

$$P = \frac{P_0}{1 + \kappa \varpi^2} + C, \tag{2.30}$$

where P_0 and κ are constants. From the condition that the potential must be zero at infinity the two authors concluded that the integration constant $C = 0$. However, the potential was derived from the velocities inside the system; it is not possible to extrapolate the validity of the formula into infinity without any detailed analysis. This does not concern any considerations operating with the derivatives of the potential only. We shall resume this point at a later stage.

We find for Oort's parameters directly

$$A = \sqrt{2\kappa P_0}\,\frac{\kappa\varpi^2}{(1+\kappa\varpi^2)^2}$$
$$B = -\sqrt{2\kappa P_0}\,\frac{1}{(1+\kappa\varpi^2)^2}. \tag{2.31}$$

The velocity of escape is defined by the equality of the kinetic and potential energies. Thus

$$O_e = \sqrt{2P} = \sqrt{\frac{2P_0}{1+\kappa\varpi^2}},$$

and the circular velocity becomes

$$O_c = \sqrt{2\kappa P_0}\,\frac{\varpi}{1+\kappa\varpi^2}.$$

The ratio of the two velocities is equal to $\sqrt{2}$ for Keplerian orbits. Here we have the formula by ten Bruggencate

$$\frac{O_e}{O_c} = \sqrt{\frac{1+\kappa\varpi^2}{\kappa\varpi^2}} = \sqrt{1-\frac{B}{A}},$$

which gives, for $A = +17.5$, $B = -6.9$ km sec kpc,

$$O_e = 1.18\,O_c.$$

This seems to be too low a value. Let us not forget that the above formula involves $C = 0$ in (2.30).

A model of the Galaxy on these principles was constructed by Parenago (1952). The density follows from the Poisson equation

$$\frac{\partial^2 P}{\partial\varpi^2} + \frac{1}{\varpi}\frac{\partial P}{\partial\varpi} + \frac{\partial^2 P}{\partial z^2} = -4\pi G\rho, \tag{2.32}$$

assuming that the potential given by (2.30) in the plane of symmetry is in a general point

$$P = \frac{P_0}{1+\kappa\varpi^2}\,\varphi(z) \tag{2.33}$$

where

$$\varphi(0) = 1; \qquad \varphi(\infty) = 0; \qquad \varphi'(0) = \varphi'(\infty) = 0, \qquad \varphi''(0) < 0.$$

Hence

$$\rho(\varpi,z) = \frac{P_0}{4\pi G(1+\kappa\varpi^2)}\left[\frac{4\kappa(1-\kappa\varpi^2)}{(1+\kappa\varpi^2)^2}\varphi(z) - \varphi''(z)\right]. \tag{2.34}$$

The function $\varphi(z)$ was determined from the second equation (2.19) whence

$$\sigma_z^2 \log\frac{\nu(\varpi,z)}{\nu(\varpi,0)} = P(\varpi,z) - P(\varpi,0). \tag{2.35}$$

Inserting the observed densities of RR Lyrae stars into the above formula, the potential follows and

$$\varphi(z) = \frac{P(\varpi,z)}{P(\varpi,0)}.$$

The densities observed at $\varpi = 0$ and $\varpi = \varpi$ lead to identical values of $\varphi(z)$. The numerical values of $\varphi(z)$ were approximated by

$$e^{-\lambda z^2}; \qquad e^{-\lambda z^2+\mu z^4-\nu z^6}.$$

The resulting model by Parenago is shown in Fig. 17 in a meridian section up to the distance of 3 kpc from the galactic plane. The main features of the Galaxy

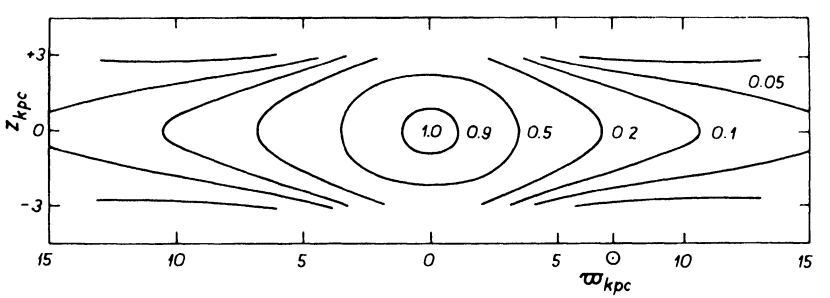


FIG. 17. Densities in the model by P. P. Parenago.

are well represented though the model has some serious drawbacks. Central density is 0.47 $M_\odot/pc^3$ and the density at the sun, 0.086 $M_\odot/pc^3$, agrees well with the observed values. Figure 18 shows the rotation curve. The maximum

is inside the sun's distance. The relatively small slope of the curve near the center is connected with the slow decrease of the density with distance.

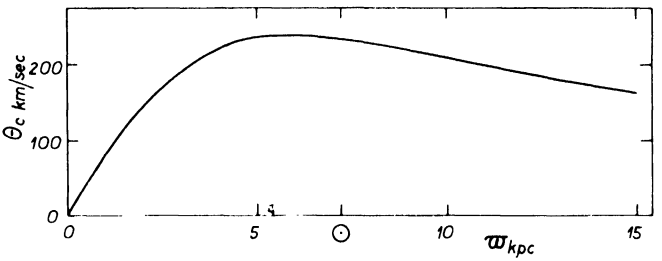


FIG. 18. Rotation curve of the model by P. P. Parenago.

3. *Idlis's Models*

It follows from Eq. (2.34) that the density in Parenago's model is positive everywhere in the plane of symmetry. For large values of ϖ the first term can be neglected with respect to the second. Considering a layer between $+z_0$ and $-z_0$ we choose z_0 so as to have $\varphi''(z) < 0$ in the whole layer. Then the density decreases as ϖ^{-2} only and the total amount of mass in the layer is infinite. This is one of the objections raised by Idlis (1957) against Parenago's model.

The numerical values of $\varphi(z)$ show that in some regions outside the galactic plane zero densities are attained.

The second point of Idlis's criticism concerns the constant C in (2.30). At large distances the potential must converge to zero as $1/\varpi$. Potential (2.30) with $C = 0$ does not possess this property and therefore it cannot be valid at external points of a model with a finite mass. Idlis takes $C \neq 0$ and investigates two extreme cases of the flattening. If the equidensity surfaces are similar spheroids, the attraction is given by (1.31a). This integral equation for ρ is easy to solve for $\sin \psi_0 = 0$ and for $\sin \psi_0 = 1$. In the first case we have a spherical symmetry and (1.31a) in the form

$$Q_\varpi = -4\pi G \frac{a^3}{\varpi^2} \int_0^{m_0} \rho m^2 \, dm. \tag{2.36}$$

Differentiating,

$$\rho = -\frac{1}{4\pi G}\left(2\frac{Q_\varpi}{\varpi} - \frac{dQ_\varpi}{d\varpi}\right)$$

and inserting the derivatives of the potential (2.30), we have

$$\rho(\varpi) = \frac{\kappa P_0}{2\pi G} \frac{3 - \kappa\varpi^2}{(1 + \kappa\varpi^2)^3}.$$

We put the boundary of the model into the shell with zero density by writing

$$a = \sqrt{\frac{3}{\kappa}}. \tag{2.37}$$

The formula for the density assumes the form

$$\rho = \rho_c \frac{1 - m^2}{(1 + 3m^2)^3}; \qquad m = \frac{1}{a}\sqrt{\varpi^2 + z^2}; \qquad 0 \leq m \leq 1, \tag{2.38}$$

where the central density

$$\rho_c = \frac{3}{2}\frac{\kappa P_0}{\pi G} = \frac{9}{2}\frac{P_0}{\pi G a^2}. \tag{2.39}$$

The total mass of the spherical model follows from (1.18)

$$M_s = 4\pi a^3 \int_0^1 \rho(m)\, m^2\, dm = \frac{1}{12}\pi\rho_c a^3. \tag{2.40}$$

The potential being a continuous function at the boundary of the model, the expression for internal points

$$P_1 = \frac{2}{9}\frac{\pi G a^2 \rho_c}{1 + 3m^2} + C \tag{2.41}$$

must be equal to that for external points

$$P_e = -\frac{GM}{\varpi} = -\frac{\pi G \rho_c a^2}{12\, m} \tag{2.42}$$

at the boundary $m = 1$. Hence the constant C

$$C = \frac{1}{36}\pi G\rho_c a^2 = \frac{1}{8}P_0. \tag{2.43}$$

Thus the definitive form of the potential at an internal point is

$$P_1 = \frac{1}{12}\pi G\rho_c a^2 \frac{3 + m^2}{1 + 3m^2}. \tag{2.44}$$

The projected density of this model is

$$\begin{aligned}\sigma(\varpi) &= 2a\rho_c \int_m^1 \frac{1 - t^2}{(1 + 3t^2)^2}\frac{t\, dt}{\sqrt{t^2 - m^2}} \\ &= \frac{a\rho_c}{(1 + 3m^2)^2}\left[\frac{5 - 3m^2}{24}\sqrt{1 - m^2} + \frac{1}{3\sqrt{3}}\frac{2 - 3m^2}{\sqrt{1 + 3m^2}}\tan^{-1}\sqrt{3\frac{1 - m^2}{1 + 3m^2}}\right],\end{aligned} \tag{2.45}$$

which gives at the center

$$\sigma_c = \left(\frac{5}{24} + \frac{2\pi}{9\sqrt{3}}\right) a\rho_c. \tag{2.46}$$

In the second extreme case we have $\sin\psi_0 = 1$ and the model is totally flattened. In this case we have

$$Q_\varpi = -4\pi G \cos\psi_0 \frac{1}{\varpi}\int_0^\varpi \frac{\rho a^2\, da}{\sqrt{\varpi^2 - a^2}}, \tag{2.47}$$

where the product $\rho\cos\psi_0$ remains finite. Solving this integral equation of Abel's type, we find

$$2\pi^2 G\cos\psi_0 a^3\rho = \int_0^a \frac{d(-\varpi^2 Q_\varpi)}{d\varpi}\frac{\varpi\, d\varpi}{\sqrt{a^2-\varpi^2}}. \tag{2.48}$$

Inserting

$$Q_\varpi = \frac{\partial P}{\partial \varpi} = -P_0\frac{2\kappa\varpi}{(1+\kappa\varpi^2)^2},$$

we get

$$\frac{d(-\varpi^2 Q_\varpi)}{d\varpi} = 2\kappa P_0\varpi^2\frac{3-\kappa\varpi^2}{(1+\kappa\varpi^2)^3}, \tag{2.49}$$

and interchanging the notation of the upper limit and the integration variable

$$\cos\psi_0\rho(\varpi) = \frac{\kappa P_0}{\pi^2 G\varpi^3}\int_0^\varpi \frac{3-\kappa a^2}{(1+\kappa a^2)^3}\frac{a^3\, da}{\sqrt{\varpi^2-a^2}} \tag{2.50}$$

which yields

$$\cos\psi_0\rho(\varpi) = \frac{3}{2}\frac{\kappa P_0}{\pi^2 G}(1+\kappa\varpi^2)^{-2}\left[1 + \frac{1-2\kappa\varpi^2}{3\sqrt{\kappa\varpi^2}\sqrt{1+\kappa\varpi^2}}\sinh^{-1}\sqrt{\kappa\varpi^2}\right].$$

Putting $m_0 = \sqrt{\kappa}\,\varpi$, we find

$$\cos\psi_0\rho(m_0) = \frac{3}{2}\frac{\kappa P_0}{\pi^2 G}(1+m_0^2)^{-2}\left[1 + \frac{1-2m_0^2}{3m_0\sqrt{1+m_0^2}}\sinh^{-1} m_0\right],$$

and at the center

$$\cos\psi_0\rho(0) = 2\frac{\kappa P_0}{\pi^2 G}. \tag{2.51}$$

Thus in the definitive form

$$\rho(m_0) = \frac{\rho_c}{4(1+m_0^2)^2}\left[3 + \frac{1-2m_0^2}{m_0\sqrt{1+m_0^2}}\sinh^{-1} m_0\right]. \tag{2.52}$$

We put the boundary of the model as usual into a surface of zero density, $m = m_1$, where m_1 is the root of the equation

$$m_1 = \sinh \frac{3m_1 \sqrt{1 + m_1^2}}{2m_1^2 - 1}, \tag{2.53}$$

its numerical value being

$$m_1 = 2.696744. \tag{2.54}$$

The total mass of the disk model, M_D, is found from formula (1.18). Inserting the density, we have

$$M_D = \pi a^3 \cos \psi_0 \rho_c \int_0^{m_1} \frac{m^2}{(1 + 3m^2)^2} \left[3 + \frac{1 - 2m^2}{m \sqrt{1 + m^2}} \sinh^{-1} m\right] dm$$

$$= \pi a^3 \cos \psi_0 \rho_c \frac{m_1}{1 + m_1^2} \left[\frac{1 + 2m_1^2}{m_1 \sqrt{1 + m_1^2}} \sinh^{-1} m_1 - 1\right],$$

and with respect to (2.53)

$$M_D = \frac{8}{\pi} \frac{P_0}{G \sqrt{\kappa}} \frac{m_1}{2m_1^2 - 1}. \tag{2.55}$$

Comparing total masses of the two models, assuming the same P_0 in both cases, we find

$$\frac{M_D}{M_S} = \frac{64}{3 \sqrt{3}\, \pi} \frac{m_1}{2m_1^2 - 1} = 0.78 \tag{2.56}$$

The difference amounts to 22% only for the vastly differing assumptions of a spherical symmetry and a total flattening.

The constant C in the flat model differs from that in the spherical model. The potential at the center is found from (1.26)

$$P_c = 4\pi G a^2 \cdot \psi_0 \cdot \cot \psi_0 \int_0^{m_1} m\rho \, dm.$$

Inserting (2.52) for the density, we find

$$P_c = \pi G a^2 \rho_c \psi_0 \cot \psi_0 \int_0^{m_1} \left[3 + \frac{1 - 2m^2}{m \sqrt{1 + m^2}} \sinh^{-1} m\right] \frac{m \, dm}{(1 + m^2)^2}$$

$$= \pi G a^2 \rho_c \psi_0 \cot \psi_0 \left[1 + \frac{m_1}{(1 + m_1^2)^{3/2}} \sinh^{-1} m_1 - \frac{1}{1 + m_1^2}\right],$$

and with respect to (2.51)

$$P_c = P_0 \left(1 + \frac{1}{2m_1^2 - 1}\right). \tag{2.57}$$

Simultaneously from (2.30)

$$P_c = P_0 + C$$

and

$$C = \frac{P_0}{2m_1^2 - 1} = 0.074 P_0. \tag{2.58}$$

Thus

$$P = P_0 \frac{1.074 + 0.074 m_0^2}{1 + m_0^2} \tag{2.59}$$

and the formula is valid from the center up to m_1. Figure 19 shows the densities in the two models by Idlis. The spherical model yields for the Galaxy a central density of 0.36 ± 0.09 M$_\odot$/pc^3 and a total mass of $(1.0 \pm 0.2) \times 10^{11}$ M$_\odot$.

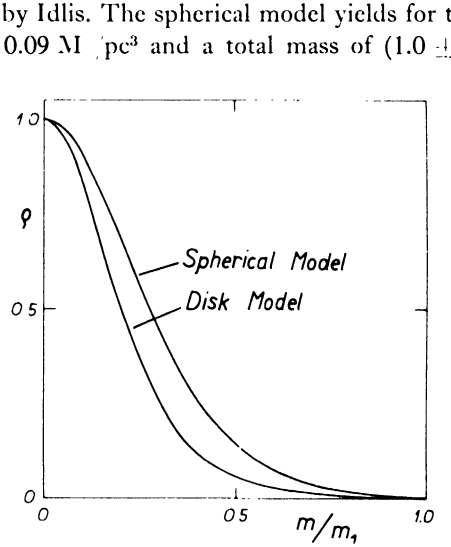


FIG. 19. Densities in the two models by G. M. Idlis.

4. *Bottlinger's Force Law*

We introduce Bottlinger's force law into this section because it originated as a modification of Oort's rotation formula. Its connection with the present classification of methods is rather loose since it does not need to assume any specific velocity distribution and the underlying distribution of mass has not

been determined. The fact that the rotation formula (2.17) does not yield a force with reasonable behavior at large distances induced Bottlinger (1933) to consider an expression for the force in the plane of symmetry of the form

$$Q_\varpi = -\frac{a_1\varpi + a_2\varpi^2 + \cdots}{1 + b_1\varpi^3 + b_2\varpi^4 + \cdots}$$

with the condition that the highest power in the denominator exceeds that in the numerator by two. Bottlinger's analysis concerned the simplest form

$$Q_\varpi = -\frac{a\varpi}{1 + b\varpi^3}. \tag{2.60}$$

It is doubtful whether the addition of further terms improves the approximation. Berman (1937) took one term more in both polynomials and derived the following numerical values from radial velocities of planetary nebulae

$$Q_\varpi = -10^6 \frac{6.576\varpi - 56.009\varpi^2}{1 - 633\varpi^3 - 21\varpi^4}$$

where ϖ is expressed in units of solar distance. Makemson (1940) succeeded in showing that the numerator has a root $\varpi = 0.1174$ and the denominator $\varpi = 0.1163$. Since the two values differ very little, the roots cancel out and leave us with a formula of the same degree as (2.60). We remark that the resulting expression was approximated by Makemson by

$$Q_\varpi = \frac{a}{\varpi^2} + \frac{b}{\varpi^3}$$

in the range of 0.8 to 1.2 solar distances. This expression has the advantage of admitting an easy solution of the equations of motion.

Let us return to the expression (2.60). It behaves in a way similar to (2.28) close to the center. At large distances it is proportional to $-a/b\varpi^2$. Since the attraction at large distances approaches that of a mass point, $-GM/\varpi^2$, we find the total mass (Lohmann, 1954)

$$M = \frac{a}{bG}. \tag{2.61}$$

The constants a and b are determined by passing a curve of the form

$$\Theta = \varpi\sqrt{\frac{a}{1 + b\varpi^3}} \tag{2.62}$$

through the observed velocities.

The potential in the plane of symmetry is

$$P = a \int_{\varpi}^{\infty} \frac{\varpi \, d\varpi}{1 + b\varpi^3}. \tag{2.63}$$

Putting

$$m_0 = b^{1/3} \varpi,$$

we find

$$P = ab^{-2/3} \left[\frac{1}{6} \log \left(1 + \frac{3m_0}{m_0^2 - m_0 + 1} \right) + \frac{1}{\sqrt{3}} \cot^{-1} \frac{2m_0 - 1}{\sqrt{3}} \right]. \tag{2.64}$$

The potential is zero at infinity. At the center

$$P_c = \frac{2\pi}{3\sqrt{3}} ab^{-2/3}. \tag{2.65}$$

For the determination of the densities it is necessary to assume either a dependence of the potential on z, or the form of equidensity surfaces (see Section III, B5).

Bottlinger's force law affords another way of determining the mass. The maximum velocity (2.62)

$$O_m = \sqrt{\frac{a}{3}} \varpi_m, \tag{2.66}$$

is attained at

$$\varpi_m = \sqrt[3]{\frac{2}{b}} \tag{2.67}$$

Substituting for a and b into (2.61), we find

$$M = \frac{3}{2} \frac{O_m^2 \varpi_m}{G}. \tag{2.68}$$

By this method, Lohmann (1954) derived the mass of M 31 from the radial velocities by Mayall (1950). With the tilt $i = 75°$, distance $d = 460$ kpc, $\varpi_m = 78'$, $O_m = 300$ km/sec, we find the linear distance $\varpi_m = 10.4$ kpc, and

$$M = 3.3 \times 10^{11} M_\odot.$$

Radial velocities in M 33, with $d = 440$ kpc, $\varpi_m = 21.9'$, $O_m = 105$ km/sec, yielded

$$M = 0.1 \times 10^{11} M_\odot.$$

Rotation curves of the two galaxies are shown in Figs. 8 and 14 respectively. Lohmann's reduction of Mayall's velocities differs somewhat from the reduction by van de Hulst which was plotted in Fig. 8.

Lohmann (1953) used Bottlinger's force law to determine perigalactic distances and showed that the same velocity leads to larger perigalactic distances for Bottlinger's law than for the inverse square law.

5. *Ogorodnikov's Model*

Ogorodnikov (1958) introduced as basic quantities four additive parameters:

the mass

$$M = \Sigma m_i ,$$

the energy

$$E = \Sigma m_i(\Pi_i^2 + O_i^2 + Z_i^2 - 2P_i),$$

the angular momentum

$$K = \Sigma m_i \varpi_i O_i ,$$

and, assuming the validity of the rotation formula (2.17), the fourth parameter

$$S = \Sigma \varpi_i^2 O_i^2 .$$

The summation refers to all stars in the system. The four parameters define a stellar system consisting of different populations. In recognition of the work of Kapteyn and Lindblad these systems were called by Ogorodnikov *KL*-systems in distinction to *D*-systems which have a homogeneous population. These are determined by the first three parameters.

Ogorodnikov derived the ellipsoidal velocity distribution

$$\begin{aligned} f &= f_0 e^{-q} \\ q &= c_1 E - 2c_3 K + c_2 S \\ &= c_1 \Pi^2 + (c_1 + c_2 \varpi^2)(O - O_0)^2 + c_1 Z^2 + g(\varpi, z), \end{aligned} \tag{2.69}$$

where the significance of the constants c_i is the same as in (2.16) and (2.17) and $g(\varpi, z)$ is a function of the coordinates.

The distribution of mass is determined in a first approximation by applying the Laplace operator to Eq. (2.21). On the right, the Laplace operator applied to the potential yields the density according to the Poisson equation. Neglecting the derivatives of the density on the left, we have after rearranging,

$$\rho = \rho_0 \frac{1 - \kappa\varpi^2}{(1 + \kappa\varpi^2)^3} , \tag{2.70}$$

which conforms to the formula by Parenago (2.34) if $\varphi''(0)$ is neglected. The density (2.70) is zero at $\varpi = \kappa^{-1/2}$. Since $\kappa = c_2/c_1$, the rotation velocity attains its maximum at the same distance. Thus the first approximation does not allow us to express the densities beyond the point of maximum velocity. In the Galaxy this is inside the sun's distance. A second approximation, giving heed to the derivatives of the density, has not yet been published.

C. *Models Based on the General Solution*

Oort's solution assigned special values to constants c_i in the system of equations (2.11) with regard to Eq. (2.15). It followed immediately that $\sigma_m = \sigma_z$. As all the observations point to an unequality of the two dispersions, a general solution of (2.15) was sought with $c_1 \neq c_4$. Moreover, a nonzero c_5 would mean admitting a deviation of the vertex, but only in a meridian plane. The observed deviation in the direction of increasing galactic longitudes cannot be explained inside the scope of our assumptions because $m = 0$ in (2.16). The explanation can be found with nonsteady-state systems or with systems constructed from the point of view of Heckmann and Strassl (1934): even if the system is not in a steady state at a given moment, it may be expected that it will fluctuate around an equilibrium state. It will be stationary as far as long intervals of time and the system as a whole are concerned, but we must expect deviations from the steady state in the observations which naturally refer to a very short time interval only and to a limited region around the sun. This does not mean that the equation of continuity and the Poisson equation are not applicable to the Galaxy but that the connection between the two equations is loose in small regions and during short time intervals. Even if the fluctuations of the density are irregular, the potential will be affected only slightly owing to the compensation over large regions. Limited time and space allow the use of approximations not admissible in a general solution. For example, assuming the independence of z-motions, which is equivalent to B. Lindblad's (1959) third integral

$$I_3 = Z^2 - 2[P(\varpi,z) - P(\varpi,0)],$$

leads to

$$\frac{\partial^2 P}{\partial \varpi \partial z} = 0,$$

the solution of which is

$$P(\varpi,z) = F(\varpi) + G(z).$$

This can be valid in limited regions only since the potential must converge to zero for ϖ or z tending to infinity separately. The above form of the potential and the preserving of only a few terms in its expansion into a series makes the solution much easier.

Heckmann and Strassl put forward a theory on this basis which is actually nonstationary and explains the observed facts. Because of its limitations in space and time we shall not enter upon further details as we are concerned with the large scale distribution of mass.

1. *A Special Case*

The case

$$c_5 \neq 0, \qquad c_1 = c_4 \tag{2.71}$$

is more general than Oort's solution. Introducing, according to Camm (1941), spherical coordinates

$$r^2 = \varpi^2 + z^2$$

$$\tan b = \frac{z}{\varpi}$$

into (2.12), we find after rearranging

$$\begin{aligned} &\frac{\partial}{\partial r}(k^2\Theta_0^2 - \log f_0 + 2c_1P) = 0 \\ &\frac{\partial}{\partial b}(k^2\Theta_0^2 - \log f_0 + 2c_1P) + c_5r^2\frac{\partial P}{\partial b} = 0. \end{aligned} \tag{2.73}$$

Integrating, we get

$$\begin{aligned} k^2\Theta_0^2 - \log f_0 + 2c_1P &= c_5G(b) \\ k^2\Theta_0^2 - \log f_0 + (2c_1 + c_5r^2)P &= c_5F(r), \end{aligned} \tag{2.74}$$

and

$$\begin{aligned} P &= \frac{1}{r^2}[F(r) - G(b)] \\ k^2\Theta_0^2 - \log f_0 &= \frac{2}{r^2}[(c_1 + c_5r^2)G(b) - c_1F(r)]. \end{aligned} \tag{2.75}$$

We succeeded in separating a function of the distance and a function of the galactic latitude.

2. *The General Case*

The solution of the general case seems to have been given for the first time by Eddington (1915). It was derived for the generalized ellipsoidal hypothesis by Camm (1941). Here, we follow Kuzmin (1956). Let us introduce, besides the energy integral and the angular momentum integral, a third integral

$$I_3 = (\varpi Z - z\Pi)^2 + z^2\Theta^2 + z_0^2(Z^2 - 2P^*), \tag{2.76}$$

where z_0 is a constant and P^* is defined by

$$\begin{aligned} z_0^2 \frac{\partial P^*}{\partial \varpi} &= z^2 \frac{\partial P}{\partial \varpi} - \varpi z \frac{\partial P}{\partial z} \\ z_0^2 \frac{\partial P^*}{\partial z} &= (\varpi^2 + z_0^2) \frac{\partial P}{\partial z} - \varpi z \frac{\partial P}{\partial \varpi} . \end{aligned} \tag{2.77}$$

The above form of the third integral has already been studied by van Albada (1952).

The integral I_3, as well as I_1 and I_2, is a solution of the equation of continuity. Cross-differentiating (2.77), we get Eq. (2.15) with the notation

$$z_0^2 = \frac{c_4 - c_1}{c_5} . \tag{2.78}$$

Idlis (1959a) has shown that the integral I_3 requires symmetry with respect to the plane $z = 0$. The form (2.76) of I_3 can be derived by inserting a series in powers of the velocity components into the equation of continuity. The coefficients of the individual terms follow from the properties of symmetry, but only if the expression is restricted to quadratic terms. The inclusion of terms of the fourth order leads to serious difficulties. Therefore the form (2.76) of the integral I_3 is to be regarded as a first approximation which does not exceed the scope of the ellipsoidal hypothesis.

Let us introduce coordinates t_1, t_2 defined as the roots of the equation

$$\frac{\varpi^2}{t^2 - 1} + \frac{z^2}{t^2} = z_0^2 . \tag{2.79}$$

Solving for t

$$t = \frac{1}{2z_0} [\pm \sqrt{\varpi^2 + (z + z_0)^2} \pm \sqrt{\varpi^2 + (z - z_0)^2}] . \tag{2.80}$$

We take the root $t_1 \geq 1$ giving

$$t_1 = \frac{1}{2z_0} [\sqrt{\varpi^2 + (z + z_0)^2} + \sqrt{\varpi^2 + (z - z_0)^2}] , \tag{2.81}$$

and $0 \leq t_2 \leq 1$

$$t_2 = \pm \frac{1}{2z_0} [\sqrt{\varpi^2 + (z + z_0)^2} - \sqrt{\varpi^2 + (z - z_0)^2}] . \tag{2.82}$$

In particular, in the plane $z = 0$

$$t_1 = \sqrt{1 + \frac{\varpi^2}{z_0^2}} ; \qquad t_2 = 0 \tag{2.83}$$

and on the axis of rotation

$$\begin{aligned} t_1 &= \left|\frac{z}{z_0}\right|; \qquad t_2 = 1 \qquad \text{for} \quad z > z_0 \\ t_1 &= 1; \qquad\quad t_2 = \left|\frac{z}{z_0}\right| \qquad \text{for} \quad z < z_0. \end{aligned} \tag{2.84}$$

The coordinate t_1 is the semimajor axis of an ellipse, and t_2 the real semiaxis of a hyperbola, with foci at $(0, \pm z_0)$ and $(0, -z_0)$ and passing through the point (ϖ, z). Thus

$$\begin{aligned} \varpi^2 &= z_0^2(t_1^2 - 1)(1 - t_2^2) \\ z^2 &= z_0^2 t_1^2 t_2^2. \end{aligned} \tag{2.85}$$

Equations (2.77) assume a simple form in the new coordinates

$$\frac{\partial P^*}{\partial t_1} = t_2^2 \frac{\partial P}{\partial t_1}; \qquad \frac{\partial P^*}{\partial t_2} = -t_1^2 \frac{\partial P}{\partial t_2}. \tag{2.86}$$

Cross-differentiating, we find

$$\frac{\partial^2}{\partial t_1 \partial t_2}[(t_1^2 - t_2^2) P] = 0$$

the solution of which is

$$P = \frac{\varphi_1(t_1) - \varphi_2(t_2)}{t_1^2 - t_2^2}. \tag{2.87}$$

Inserting for the potential into the Poisson equation, we get

$$4\pi G z_0^2 \rho = 2\frac{(\varphi_1 - t_1\varphi_1' - \varphi_2 + t_2\varphi_2')(2 - t_1^2 - t_2^2)}{(t_1^2 - t_2^2)^3} - \frac{(t_1^2 - 1)\varphi_1'' - (1 - t_2^2)\varphi_2''}{(t_1^2 - t_2^2)^2} \tag{2.88}$$

The potential, being symmetrical with respect to the plane $z = 0$, can contain only even powers of z. Having in mind the relation between t_1 and z on the axis of rotation we see that the same must be true of the powers of t_i in the function φ_i. Expanding φ_i according to ϖ^2/z_0^2 and keeping the first two terms only, it follows (Idlis, 1959a) with respect to the value of t_i in the plane $z = 0$

$$\varphi_1 = \varphi_1(1) + \varphi_1'(1)\frac{\varpi^2}{z_0^2}. \tag{2.89}$$

Inserting this into (2.87), we find

$$P = \frac{\varphi_1(1) - \varphi_2(0)}{1 + (\varpi^2/z_0^2)} + \varphi_1'(1), \tag{2.90}$$

which is Parenago's formula for the potential with a nonzero constant C. In this light, Parenago's formula can be regarded as a first approximation. The approximation is the more justified as the integral I_3 (2.76) reduces to a constant in the plane of symmetry thus making f a function of I_1 and I_2 only, and admitting Oort's solution which is the basis of Parenago's expression for the potential.

3. *Kuzmin's Models*

To be able to make any further progress it is necessary to make an assumption about the form of the function φ. It can be shown that the density (2.88) is nowhere negative if it is not negative on the axis of rotation. The total mass is finite if the density decreases more rapidly than the inverse cube of the distance.

In conformity with these postulates, Kuzmin (1956) assumed

$$\varphi'' = \frac{k}{n} \frac{\alpha^{n-1}}{(t^2 + \alpha^2)^{n/2}}; \qquad n > 1, \tag{2.91}$$

whence, on integrating,

$$\varphi' = \frac{k}{n} \alpha^{n-1} \int_0^t (t^2 + \alpha^2)^{-n/2}\, dt$$

$$\varphi = \frac{k}{n} \alpha^{n-1} \left[\frac{1}{n-2} (t^2 + \alpha^2)^{1-(n/2)} + t \int_0^t (t^2 + \alpha^2)^{-n/2}\, dt \right],$$

where φ denotes the function φ_i of the argument t_i, $i = 1, 2$. Of particular interest are cases $n = 4$ and $n = 3$. If $n = 4$, we find

$$\begin{aligned} \varphi - t\varphi' &= \frac{1}{8} k \frac{\alpha^3}{t^2 + \alpha^2} \\ \varphi'' &= \frac{1}{4} k \frac{\alpha^3}{(t^2 + \alpha^2)^2}. \end{aligned} \tag{2.92}$$

Substituting into (2.88), we have

$$4\pi G z_0^2 \rho = \frac{1}{4} \frac{k}{\alpha(1 + \alpha^2)} \left[\frac{\varpi^2}{z_0^2(\alpha^2 + 1)} + \frac{z^2}{z_0^2 \alpha^2} + 1 \right]^2. \tag{2.93}$$

Setting

$$\begin{aligned} z_0^2(\alpha^2+1) &= a^2 \\ z_0^2\alpha^2 &= c^2 \\ m^2 &= \frac{\varpi^2}{a^2}+\frac{z^2}{c^2}, \end{aligned} \tag{2.94}$$

we get the density

$$\rho = \rho_c \frac{1}{(1+m^2)^2}. \tag{2.95}$$

The equidensity surfaces are similar spheroids with the angle ψ_0

$$\cot\psi_0 = \alpha. \tag{2.96}$$

The potential is

$$P = \frac{1}{8}k\frac{t_1\tan^{-1}(t_1/\alpha) - t_2\tan^{-1}(t_2/\alpha)}{t_1^2-t_2^2}, \tag{2.97}$$

where

$$k = 16\pi G a^2\rho_c\cot\psi_0.$$

In the plane of symmetry

$$P = 2\pi G a^3\rho_c\cos\psi_0\frac{1}{\sqrt{\epsilon^2+\varpi^2}}\tan^{-1}\left(\frac{1}{\epsilon}\sqrt{\epsilon^2+\varpi^2}\tan\psi_0\right). \tag{2.98}$$

In the case $n = 3$, we have

$$\varphi'' = \frac{P_0\alpha^2}{(t^2+\alpha^2)^{3/2}}, \tag{2.99}$$

where we used the symbol P_0 instead of $k/3$. We easily obtain

$$\begin{aligned} \varphi &= P_0\sqrt{t^2+\alpha^2} \\ \varphi - t\varphi' &= \frac{P_0\alpha^2}{\sqrt{t^2+\alpha^2}}. \end{aligned} \tag{2.100}$$

Inserting into (2.87) and supposing that α^2 can be neglected, we find an approximate expression

$$P = \frac{P_0}{\sqrt{1+(\varpi^2/z_0^2)}}. \tag{2.101}$$

The density in the plane of symmetry follows from (2.88) with respect to (2.83)

$$4\pi G z_0^2 \rho = \frac{P_0}{\alpha t_1^4} = \frac{P_0}{\alpha[1 + (\varpi^2/z_0^2)]^2}, \tag{2.102}$$

and hence P_0 is given by

$$P_0 = 4\pi G z_0^2 \rho_c \alpha. \tag{2.103}$$

In this case the equidensity surfaces are not similar spheroids and therefore the expressions for the potential differ, though the densities assume equal values in the plane of symmetry in the two cases.

Parenago (1959) compared (2.101) with (2.30) and concluded that the differences in velocities of rotation of the two models are below the accuracy of the present observations. The form (2.101) was used by Dzigvashvili (1958) for an investigation of galactic orbits.

D. *Criticism of the Ellipsoidal Velocity Distribution*

There are few questions which received so much attention as did the distribution of velocities. It is not necessary to enter into a discussion of the theories of one, two, or three streams which attempted to express the evident deviations from the spherical symmetry of the velocities. These were finally put into a mathematically simple and elegant form of the ellipsoidal distribution by K. Schwarzschild (1907). It was only much later that the increasing amount and quality of the observations summed up, e.g., in a paper by Pilowski (1959), led to the conclusion that the ellipsoidal hypothesis is not suitable. The asymmetry, which was previously mentioned only with high velocity stars, was found even with small velocities. Thus not even the central part of the distribution of velocities can be represented by a symmetrical body, e.g., an ellipsoid. An asymmetry is conspicuous in the projection of the velocities of Me dwarfs on the plane of symmetry (Fig. 20) taken from a paper by Gliese (1958). Velocities in the z-direction were studied by Schilt (1950) who concluded that "the observational evidence for the existence of a Schwarzschild distribution of the velocities in the z-component is insufficient."

Another indication against the ellipsoidal distribution is the fact that nearby stars show, according to Vetešník (1959), a Gaussian distribution in I_1, i.e., in the fourth, and not the second, powers of the components. The dispersion in I_1 depends on the position of the star in the HR-diagram but on the whole the deviations from Gaussian distributions are small with the exception of RR Lyrae stars.

There are serious objections to the ellipsoidal hypothesis from the theoretical point of view. Camm (1941) and Fricke (1952) showed that an ellipsoidal

distribution cannot exist in plausible stellar systems, not even in its generalized form. To sum up, a steady-state stellar system with a finite mass, a rotation symmetry, and with a systematical motion not everywhere zero, cannot be

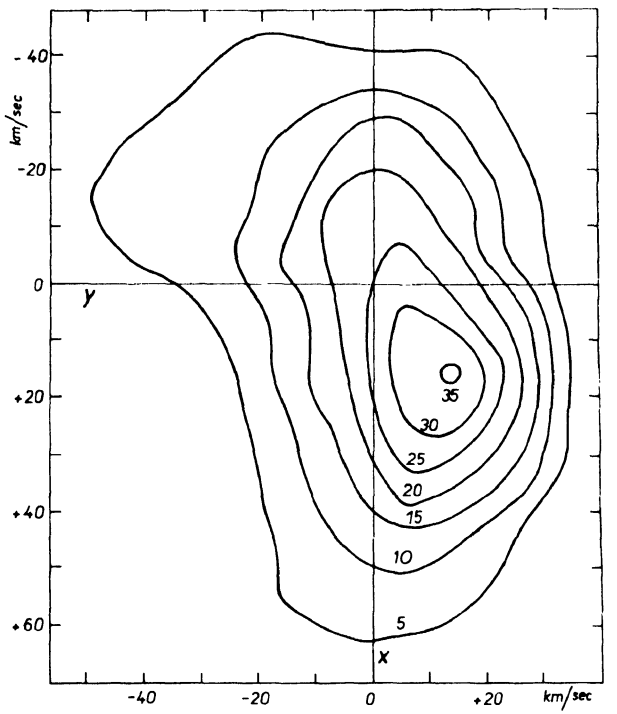


FIG. 20. Projection of the velocity ellipsoid of the Me dwarfs on the galactic plane according to W. Gliese. The x-axis is directed toward the center, the y-axis in the direction of rotation.

self-gravitating if the velocities possess an ellipsoidal distribution. This result leads to the necessity of substituting the ellipsoidal hypothesis by a distribution of another kind. The restriction to quadratic terms of the velocities in the frequency function made any physically acceptable solution impossible. In how far the results of Sections II, B and II, C, which were based on an ellipsoidal distribution, retain their validity is difficult to say. At least they must be considered as approximations of higher or lower degree.

An attempt to admit more general velocity distributions was made by Coutrez (1950). The frequency function f of six variables was divided into a frequency function of position, proportional to the density and to an array frequency of velocities. A system of equations was derived, containing moments

of the order n of array distributions of velocities. However, a detailed analysis was restricted to moments of the second order only, thus reducing again to the ellipsoidal distribution. A sufficiently general method was suggested but its possibilities were not exhausted. Let us note in passing that R. Coutrez derived a constant velocity O by neglecting moments of a higher order than two and assuming that the velocity dispersions do not depend on position and that $\sigma_\vartheta^2 = \frac{1}{2}\sigma_\varpi^2$. Postulating further a finite and nonzero density at the center, the distribution of the densities follows the law

$$\rho = \rho_0 \exp(-\alpha\varpi^2 - \beta z^2 - \gamma z^4 - \cdots). \tag{2.104}$$

Equidensity surfaces are similar to spheroids near the center. At large distances, the central bulge becomes conspicuous.

A rather general velocity distribution was considered by Fricke (1952). Putting

$$f(I_1, I_2) = \sum \alpha_{ik} I_1^i I_2^k \tag{2.105}$$

and denoting in (2.6) the space velocity W, we get the density

$$\rho(\varpi, z) = \sum \alpha_{ik} \iiint_{0 \le W \le W_e} (2P - W^2)^i (\varpi O)^k \, d\xi \, d\eta \, d\zeta \,. \tag{2.106}$$

By integrating over a sphere of a radius of the velocity of escape, W_e, we expressed the fact that the velocities of a steady-state model have an upper limit. If it exceeds the velocity of escape the star will leave the system permanently. This contradicts the steady state.

Fricke investigated further what restrictions must be imposed on the distribution of the densities to admit a self-gravitating system with finite mass. The potential at large distances must be ultimately proportional to the inverse distance. Near the origin it can be expanded according to the powers of the distance $r = \sqrt{\varpi^2 + z^2}$. The coefficients are functions of the galactic latitude. At odd powers they are expressed by means of spherical harmonics and at even powers by means of polynomials in $\cos b$. Functions f and ρ, in contrast with the ellipsoidal distribution, admit a solution and are of the form

$$\begin{aligned} f &= I_1^{5/2} \sum A_{kl} I_1^{k+l} I_2^{2k} + I_1^{7/2} \sum B_{kl} I_1^{k+l} I_2^{2k+1} \\ \rho &= 2\pi(2P)^4 \sum C_{kl} \varpi^{2k} (2P)^{2k+l}, \end{aligned} \tag{2.107}$$

where A_{kl}, B_{kl}, C_{kl} are constants, $A_{00} > 0$ and C_{kl} contains only the A_{kl} and numerical factors. The frequency function if nonnegative for all values of the velocity components.

The above formulae follow from the general assumption (2.105) which certainly is adequate with respect to I_1 and I_2. As we have seen in preceding sections, there exists a third integral, independent of the first two. A quite general form of f should contain the third integral, too. Such a distribution has not yet been investigated. However, the form (2.107) is flexible enough to lead to a possible solution and to reproduce the basic observed properties of the velocity distribution which were beyond the possibilities of the ellipsoidal hypothesis. One formula covers stars with normal velocities, showing a slight asymmetry from the beginning onwards, high velocity stars, and stars in retrograde motions. For example,

$$f = I_1^{5/2}[0.5 + 100I_1^{11}I_2^{20} + 49.5I_1^{10}I_2^{19} + 49.5I_1^{12}I_2^{21}].$$

Let us consider this expression at a point $P = 1$, $\varpi = 1$, where the potential behaves as $1/r$. Thus the velocity of escape, $W_c = \sqrt{2}$ and the circular velocity, $\Theta_c = 1$. Figure 21 shows the velocity distribution in the plane of symmetry.

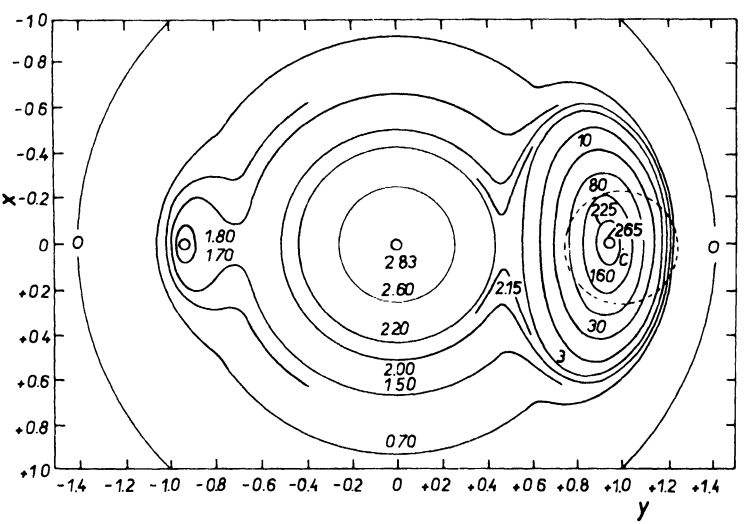


FIG. 21. Distribution of velocities in the model by W. Fricke projected on the galactic plane. Besides the main maximum at the circular velocity there are secondary maxima at the circular velocity of retrograde motion and at zero velocity.

The countour lines are more separated on the left from the main maximum than on the right. This corresponds with the observed asymmetry. The secondary maximum of retrograde motions and a third maximum at zero velocity are to be noted. The distribution of high velocity stars according to galactic

longitude, computed from the above frequency function, is shown in Fig. 22. It exhibits the well known maxima from the paper by Oort (1928).

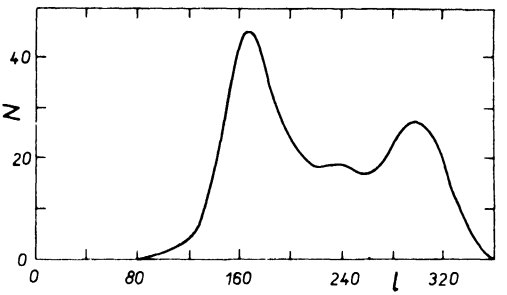


FIG. 22. Distribution of high velocities in the model by W. Fricke.

The frequency function is zero at the velocity of escape but its values are very smal for velocities considerably lower than W_e. Therefore, the limit of asymmetry of 63 km/sec, given by Oort, may, but need not, correspond with W_e. The velocity of escape can exceed the circular velocity by more than 63 km/sec.

III

MODELS BASED ON DENSITY LAWS

We have seen in the preceding chapter that each solution was based on an assumption about the distribution of velocities which was more or less consistent with the observations. We have attempted to find an exact way from the assumed velocity distribution to a solution for the distribution of mass. It is questionable whether it would not be more straightforward to make an assumption directly about the distribution of mass. The problem would be easier to survey and we should not be tempted to consider a solution exact just because the assumption entered our theory somewhere at the beginning. In this way we should arrive at galactic models which approximate the actual field of force by a field of force of a simple geometrical body or a system of such bodies. The degree of approximation would be immediately evident and could be chosen so as to be adequate to the purpose at hand or to the available observing material.

This procedure does not solve the question of whether a velocity distribution can be found making a self-gravitating system possible with the assumed distribution of mass. The problem has not yet been solved in its entirety by

any of the methods, whether they are based on assumed distributions of velocities or of mass. We expect that a model is a good approximation to the reality if it fits the observed distribution of mass as well as the dynamical parameters.

A. *Mass Points and Homogeneous Spheroids*

1. *A Mass Point*

The simplest possible model of a galaxy is a mass point. It is evident that the actual field of force is substantially different from that of a mass point by not possessing a spherical symmetry and by the fact that the stars move inside the attracting body. Nevertheless, a mass point is frequently used, in particular for the computation of galactic orbits. Elements of Keplerian orbits, determined from the given position and velocity on a two-body basis, possess a rather limited physical significance with regard to the roughness of the approximation. It is evident that, e.g., perigalactic distances computed from Keplerian orbits will be much smaller than if computed from a less concentrated mass distribution. This is of importance if one is seeking stars which have passed or will pass through the galactic nucleus. However, elements of Keplerian orbits have a significance as classification parameters. In this way the elements served, e.g., Mohr (1933), to separate several groups of stars which may be regarded as predecessors to the present classification into populations.

It is useful to apply a mass point model to the interpretation of observations which do not allow a more detailed analysis. In such cases this simple model yields an estimate of the total mass.

The attraction of a mass point is

$$Q = -\frac{GM}{\varpi^2}. \tag{3.1}$$

Together with

$$O_c^2 = -\varpi Q$$

we find

$$M = \frac{\varpi O_c^2}{G}. \tag{3.2}$$

In this way, E. M. and G. R. Burbidge (1960) determined the mass of the barred spiral NGC 1097 from the measured value of $O_c = 274$ km/sec at $\varpi = 800$ pc to

$$M = 1.34 \times 10^{10}\, M_\odot.$$

The peculiar galaxy NGC 5128 yielded, similarly,

$$M = 2 \times 10^{11}\, M_\odot.$$

A different method of estimating the mass was applied to the Galaxy by Lohmann (1956). It was shown by Perek (1954a) and von Hoerner (1955) that globular clusters move in highly eccentric orbits. Lohmann assumed that their motions are oscillations through the center. Denoting their amplitude by a, the velocity is given by

$$W^2 = 2GM\left(\frac{1}{r} - \frac{1}{a}\right). \tag{3.3}$$

Assuming further that the observed distance R of a cluster from the center is, on the average, its most probable value, the condition is arrived at that the time elapsed since the passage through the perigalacticon is half the time necessary to reach the elongation a, namely,

$$\int_0^R \frac{dr}{\sqrt{(1/r) - (1/a)}} = \frac{1}{2}\int_0^a \frac{dr}{\sqrt{(1/r) - (1/a)}}.$$

Hence

$$2\frac{R}{a} - 1 = \sin\left[2\sqrt{\frac{R}{a}\left(1 - \frac{R}{a}\right)}\right],$$

the solution of which is

$$R = 0.836a.$$

Inserting this value into (3.3), we get

$$W^2 = 0.328\,\frac{GM}{R}. \tag{3.4}$$

Denoting the angle center-cluster-sun by ϑ, the observed radial velocity is

$$V = W\cos\vartheta.$$

Inserting into the above equation, the least squares method yields

$$M = \frac{1}{0.328G}\,\frac{[\cos^2\vartheta \cdot RV^2]}{[\cos^2\vartheta \cdot \cos^2\vartheta]} = (2.50 \pm 0.56) \times 10^{11}\,M_\odot, \tag{3.5}$$

where the brackets indicate the summation over all clusters. The resulting value is somewhat larger than the determinations by other methods.

2. *The Virial Theorem*

Another method by Lohmann (1956) makes use of the virial theorem

$$2T + \Omega = 0, \tag{3.6}$$

where T is the total kinetic energy and Ω the potential energy. If the center of gravity of the subsystem of globular clusters coincides with that of the Galaxy, the kinetic energy of the globular clusters is

$$T = \tfrac{1}{2} \Sigma m_i W_i^2, \tag{3.7}$$

where the summation applies to all clusters. Further,

$$\Omega = -GM \sum \frac{m_i}{R_i} - G \sum \frac{m_i m_j}{r_{ij}} \tag{3.8}$$

where the summation in the second term is to be performed so as to include each pair of clusters once. The masses of the clusters being very small compared to the mass of the Galaxy, the second term on the right can be neglected. Assuming equal masses for all clusters, we find by inserting (3.8) and (3.7) into (3.6)

$$M = \frac{1}{G} \frac{\Sigma W_i^2}{\Sigma R_i^{-1}} \tag{3.9}$$

where space velocities W have to be substituted by the radial velocities. On the average

$$\Sigma W_i^2 = 3 \Sigma V_i^2.$$

A mass point is a better approximation for distant clusters than for close ones and therefore the determination of the mass depends on the selection of clusters. Figure 23 shows a plot of the mass against the limiting distance from

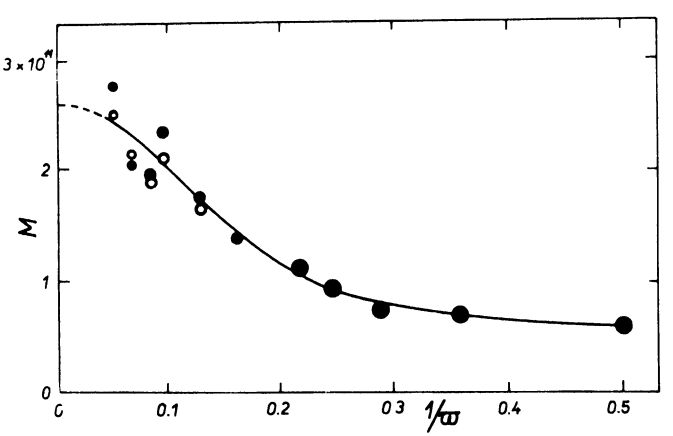


FIG. 23. The mass of the Galaxy as a function of the limiting distance of globular clusters entering into the solution.

the center. The dots refer to the solar velocity of 277 km/sec, the circles to 216 km/sec. Evidently, the mass is not much affected by the considerable difference. The point at the extreme left corresponds to the 8 most distant clusters while the point at the extreme right includes all 47 clusters. The extrapolated limit of the curve for $1/R \to 0$ gives

$$M = 2.6 \times 10^{11} M_{\odot},$$

which agrees with the previous determination but again exceeds values derived by other methods. It may be said quite generally that the smaller the concentration the less mass is required for the explanation of the field of force in the Galaxy. The mass point represents concentration in the highest possible degree; thus the estimates of mass based on this model come out rather high. It must not be overlooked that the small number of the most distant clusters is possibly affected by aleatory errors, and that the value of the mass based on a larger number of clusters may be more correct, although the approximation to the mass point model is worse.

The virial theorem was applied to other galaxies by Poveda (1958). If the stars oscillate through the center of a spherical galaxy, its kinetic energy is

$$T = \tfrac{1}{2} M \sigma_{\mathrm{v}}^2, \tag{3.10}$$

where σ_{v} is the observed dispersion of radial velocities in the center of the image of the galaxy. Denoting by $M(r)$ the mass inside the distance r, the potential energy is

$$\Omega = -G \int_0^R \frac{1}{r} M(r)\, dr. \tag{3.11}$$

Assuming a constant mass-luminosity ratio it is possible to calculate numerically the integral in the right-hand member if the dependence of luminosity on the distance r is the same for all spherical galaxies. With the use of available observing data Poveda found

$$M = 0.2a\, d\, \sigma_{\mathrm{v}}^2, \tag{3.12}$$

where a is the radius in minutes of a circle containing half the light, d is the distance of the galaxy in pc, M is the mass in $M_{\odot}$, and the dispersion σ_{v} is in km/sec. Taking $a = 30''$, $d = 500$ kpc, $\sigma_{\mathrm{v}} = 100$ km/sec, we find the mass of M 32

$$M = 5 \times 10^8 M_{\odot}.$$

The method was checked on M 31 which departs considerably from the spherical form. With $a = 40'$, $d = 500$ kpc, $\sigma_v = 225$ km/sec, we find

$$M = 2 \times 10^{11} M_{\odot},$$

an estimate not far from other determinations. If the method yields reasonable estimates for flattened systems a good agreement can be expected for spherical galaxies.

The spherical symmetry of the field of force of a mass point induced us to mention in this subsection spherical systems which we originally excluded from our considerations. However, it was thought necessary to include the above methods.

3. *Homogeneous Spheroids*

A homogeneous spheroid was used by Freundlich (1936) for checking the following hypothesis. The stars diffuse from the galactic disk into the halo and their distribution conforms to the level surfaces. Representing the Galaxy by a homogeneous spheroid the axial ratio of the level surfaces can be estimated from the values of the potential on the z-axis and in the plane of symmetry. We find from (1.33), inserting for ψ from (1.10) and (1.11),

$$2z\left(\epsilon - z \tan^{-1}\frac{\epsilon}{z}\right) = \varpi^2 \sin^{-1}\frac{\epsilon}{\varpi} - \epsilon\sqrt{\varpi^2 - \epsilon^2}, \tag{3.13}$$

which has to be solved numerically. Inserting a distance ϖ into (3.13), the resulting z gives a point on the z-axis, $(0, z)$, having the same value of the potential as the point $(\varpi, 0)$ in the plane of symmetry. The two points are, of course, external with regard to the homogeneous spheroid. For M 31 the observed semiaxes of the disk, $a = 80'$, $c = 20'$, lead to the semiaxes $136'$ and $122'$ of a level surface, in good agreement with the observed values $135'$ and $120'$.

A homogeneous spheroid is suitable for the interpretation of rotation curves not departing from a straight line. Inserting the mass (1.16) into (1.34) and denoting by α the function of the flattening

$$\alpha = \frac{3}{2}\frac{\psi_0 - \sin\psi_0 \cos\psi_0}{\sin^3\psi_0}, \tag{3.14}$$

we have

$$\Theta^2 = -\varpi Q_{\varpi} = M\alpha G\frac{\varpi^2}{a^3}. \tag{3.15}$$

Burbidge *et al.* (1959a,b, 1960b) used the velocity at the farthest point and put $\varpi = a$, thus,

$$M = \frac{\Theta_0^2 \varpi}{G\alpha}. \tag{3.16}$$

If the rotation curve is convex an explanation can be found in the decrease of the density with the distance. On the other hand, if it is concave and we wish to escape the conclusion that the density increases with the distance, a pressure term due to the random motions of the gas must be introduced. This was done in one of the above quoted papers for NGC 2146 where the velocities of the gas, measured from lines of N II and from the H_α line, yielded a concave rotation curve. Thus

$$-\frac{O^2}{\varpi} = \frac{\partial P}{\partial \varpi} = \frac{1}{\rho^*}\frac{dp}{\partial \varpi}, \tag{3.17}$$

where the pressure

$$p = \tfrac{1}{3}\rho^* \overline{u^2}$$

Here, ρ^* is the density of the gas and $\overline{u^2}$ is the mean-square turbulent velocity. If it varies only little in the investigated region, we have, for a constant angular velocity,

$$\frac{1}{3}\overline{u^2}\log\frac{\rho(\varpi)}{\rho(0)} = P(\varpi) - P(0) + \frac{1}{2}O^2. \tag{3.18}$$

The last term on the right can be neglected, the velocity of rotation being small near the center. For a homogeneous spheroid

$$P(\varpi) - P(0) = \pi G\varpi^2 \frac{\cos\psi_0}{\sin^3\psi_0}(\psi_0 - \sin\psi_0\cos\psi_0), \tag{3.19}$$

which means that the gas is distributed according to a Gaussian curve with the mean deviation

$$\lambda_\varpi^2 = \frac{\overline{u^2}}{6\pi G\rho}\frac{\sin^3\psi_0}{\cos\psi_0(\psi_0 - \sin\psi_0\cos\psi_0)}. \tag{3.20}$$

In a similar way, by integrating from 0 to z, we get

$$\lambda_z^2 = \frac{\overline{u^2}}{12\pi G\rho}\frac{\sin^3\psi_0}{\cos\psi_0(\tan\psi_0 - \psi_0)}. \tag{3.21}$$

The ratio

$$\frac{\lambda_z}{\lambda_\varpi} = \frac{\psi_0 - \sin\psi_0\cos\psi_0}{2(\tan\psi_0 - \psi_0)} \tag{3.22}$$

is a function of the flattening only and shows the approximate form of the region where the influence of the pressure is important. For $c/a = 0.1$ and 0.2, we find $\lambda_z/\lambda_\varpi = 0.3$ and 0.4 respectively.

The above methods yielded for NGC 3556 a mass of 1.1 to 1.7 $\times$ 10^{10} $M_\odot$ derived from the slope of the rotation curve. In the case of NGC 1068 two superposed spheroids were used but one spheroid sufficed to represent the galaxy up to 2 kpc from the center. A total mass of 2.7 $\times$ 10^{10} $M_\odot$ was found. E. M. and G. R. Burbidge (1960) derived the masses of two barred spirals. The resulting values for two values of the axial ratio are shown in Table IV.

TABLE IV

MASSES AND DENSITIES OF TWO BARRED SPIRALS

	NGC 1097		NGC 1365	
c/a	Mas in 10^{10} $M_\odot$	Mean density in $M_\odot/pc^3$	Mass in 10^{10} $M_\odot$	Mean density in $M_\odot/pc^3$
1/3	0.82	11.5	3.40	7.1
1/15	0.54	37.8	2.22	22.9

4. *A Mass Point Superposed upon a Homogeneous Spheroid*

One of the first models of the Galaxy supplemented the field of force of a mass point by that of a homogeneous spheroid. It was introduced by Oort (1927). The attraction of the model has two components

$$Q = Q_1 + Q_2$$

where Q_1 is due to the mass point and Q_2 to the homogeneous spheroid

$$\begin{aligned} Q_1 &= p\varpi^{-2} \\ Q_2 &= q\varpi. \end{aligned} \tag{3.23}$$

Because

$$\frac{dQ_1}{d\varpi} = -2\frac{Q_1}{\varpi}; \qquad \frac{dQ_2}{d\varpi} = \frac{Q_2}{\varpi},$$

we find from the expression (2.24) for Oort's constant A

$$A = \frac{3}{4}\frac{\Theta}{\varpi}\frac{Q_1}{Q},$$

or

$$\frac{Q_1}{Q} = \frac{4}{3}\frac{A}{A-B}. \tag{3.24}$$

With the values $A = +19$, $B = -24$ km/sec/kpc, originally used by Oort, we find

$$Q_1/Q = 0.59,$$

a rather high concentration of the mass. With more recent values of the constants, $A = +17.5$, $B = -6.9$ km/sec/kpc, an even higher concentration is arrived at

$$Q_1/Q = 0.95.$$

Oort pointed out in his first papers already, as far back as 1927 that a strong concentration is not a necessary consequence and gave as another example two superposed homogeneous spheroids. If the axial ratio is 1/10 and the inner spheroid goes up to $0.9\varpi_\odot$ and the boundary of the second is outside the sun's distance, the observations are satisfied by a density of 0.66 in the inner, and 0.30 $M_\odot/\text{pc}^3$ in the outer, spheroid. In this model the concentration of mass is very slight indeed.

However, a mass point-and-spheroid model persists in almost all standard textbooks although it was originally meant as an illustration and although its author later constructed other models much better approximating the reality (Oort, 1941). The mass point-and-spheroid model was constructed from data referring to the solar neighborhood. It can be expected that it will represent the actual field of force in a limited range of distances, too. To extrapolate the validity of this model too far is quite unjustified. The attraction is too large near the center. At large distances the attraction increases with ϖ, which is not plausible either.

The mass point-and-spheroid model was used by Gliese (1942) for the study of galactic orbits in the plane of symmetry and by Coutrez (1949) for a detailed study of the stability of galactic orbits. Their results must be considered with respect to the above limitations of the model.

5. *Superposition of Elementary Bodies*

A large number of models was constructed by combining elementary bodies: mass points, homogeneous spheres, and homogeneous spheroids. The respective formulas for the potential, attraction, and mass are easily derived. We mention a few of the models. In 1947 ten Bruggencate constructed a model consisting of a mass point and a plane disk which was the limiting case of two homogeneous spheroids. Babcock (1939) based his analysis of the radial velocities in M 31 on a model of a sphere and three homogeneous spheroids. For a distance of 210 kpc he derived a total mass of M 31 of $1.0 \times 10^{11}\ M_\odot$. More recent estimates of the distance of M 31 would about treble the value.

From a detailed discussion of stellar densities in the z-direction resulted a model by Oort (1941) consisting of a mass point, one inner spheroid, and 11 outer spheroids. The parameters are given in Table V. The distribution of densities

TABLE V

ELEMENTS OF A MODEL BY J. H. OORT

$\Theta_\odot$	275 km/sec
$\varpi_\odot$	8 kpc
A	+21 km/sec/kpc
B	−13.4 km/sec/kpc

Outer spheroids	$M_\odot/pc^3$	a (kpc)	c (kpc)
1	0.045	10.0	0.50
2	0.0093	10.2	0.66
3	0.0058	10.4	1.00
4	0.0031	10.6	1.60
5	0.00168	11.2	1.90
6	0.00032	12.2	2.45
7	0.00031	14.0	3.15
8	0.000174	16.8	4.20
9	0.000093	20.5	5.65
10	0.000044	26.4	7.95
11	0.000044	32.5	10.30
Inner spheroid	0.172	7.0	2.34

Mass of the:	
outer spheroids	$0.25 \times 10^{11} M_\odot$
inner spheroid	$0.82 \times 10^{11} M_\odot$
mass point	$0.10 \times 10^{11} M_\odot$
Total mass of the model	$1.17 \times 10^{11} M_\odot$

is shown in Fig. 24 where the mass point was represented by a homogeneous sphere of 3 kpc diameter. The outer regions of the Galaxy are well represented in this model but the inner part remained rather schematical. Safronov (1952), while preserving the outer spheroids of Oort, considered 5 inner spheroids. Their parameters are given in Table VI. A discussion of this model led to the total mass of $0.8 \times 10^{11} M_\odot$ and to the density of $0.085\ M_\odot/pc^3$ near the sun.

The inner regions of the Galaxy up to the sun's distance were represented by Mikisha and Tsitsin (1957) by a model consisting of 8 homogeneous spheroids

with the axial ratio varying from 1/2 to 1/9. An exponential decrease of the density was approximated in the plane of symmetry. The model was used to estimate the mass of the galactic nucleus.

Janák (1958) represented the main body of the Galaxy by a spheroid and the halo by a sphere. Thus the disk is immersed in a sphere of a low density. An analysis of the motions of Cepheids led him to the conclusion that the existence

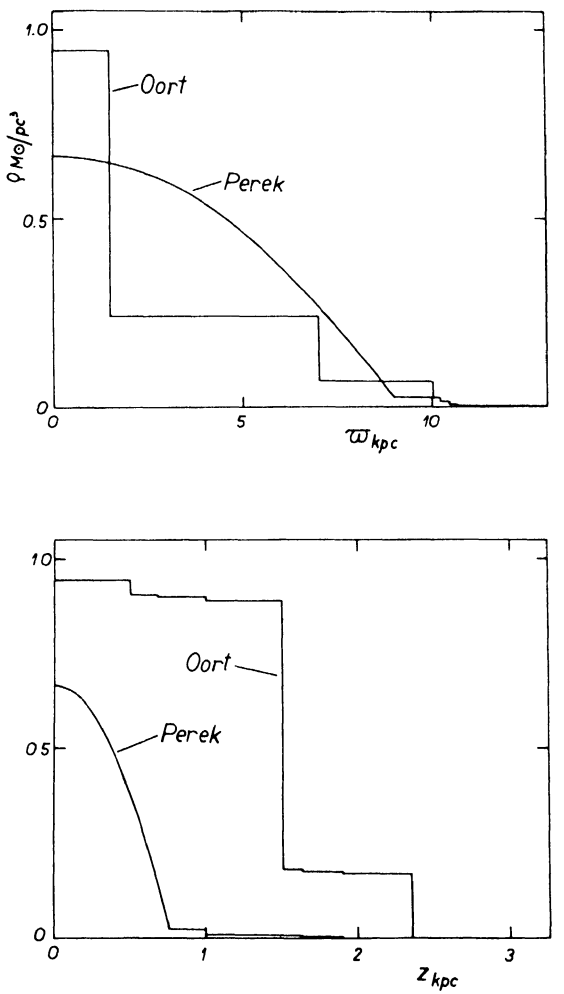


FIG. 24. Densities in a model by J. H. Oort, consisting of a number of homogeneous spheroids and of a mass point represented here by a sphere of 3 kpc diameter. Densities in a model by L. Perek, consisting of a heterogeneous spheroid supplemented by a number of external homogeneous spheroids.

of a halo is most probable. In such a model the ratio of the velocity of escape to the circular velocity can exceed $\sqrt{2}$ in some regions.

TABLE VI

ELEMENTS OF SAFRONOV'S INNER SPHEROIDS

No.	a (kpc)	c/a	Relative density
1	2	1/2	33
2	3	1/3	26
3	4	1/5	20
4	6	1/7	9
5	7.2	1/10	2

B. *The Basic Body Is a Disk*

1. *Bucerius' Model*

It is interesting to note that models based on a disk were constructed prior to models of heterogeneous spheroids although disks require more involved mathematics. The first disk model seems to have been given by Bucerius (1934). He attempted in a way to respect stellar populations by superposing three bodies:

1. The nucleus in the form of a homogeneous spheroid with axial ratio 1:2 and a major semiaxis of 2.5 kpc.

2. The disk of a radius $a = 15$ kpc and with a steep decrease of the density in the z-direction

$$\rho(z) = \rho(0)\, e^{-z^2/\beta^2}, \tag{3.25}$$

with $\beta = 350$ pc. The model is infinite in z, although it was intended to represent a close neighborhood of the plane of symmetry only. The density does not depend on ϖ. It has a constant value in the plane of symmetry up to a and is zero beyond this distance. The increase of the density towards the center is substituted to a certain degree by the mass of the nucleus.

3. The diffuse matter is represented by a homogeneous disk of 200 pc thickness.

The computation of the potential of the disk sub 2 presents some difficulties which were brilliantly overcome by Bucerius. Let (ϖ, z) be the point in which the potential is being computed and (ϖ', z') a point occupied by mass. Their distance is

$$\Delta^2 = \varpi^2 + \varpi'^2 - 2\varpi\varpi' \cos\varphi + (z' - z)^2. \tag{3.26}$$

From the definition of the potential follows that

$$P = G\rho_0 \int_{-\infty}^{\infty} dz' \int_0^{2\pi} d\varphi \int_0^a d\varpi' \frac{e^{-z'^2/\beta^2}\varpi'}{\Delta}. \tag{3.27}$$

By adding one more integration

$$\frac{\pi}{\alpha} = \int_{-\infty}^{\infty} \frac{dt}{t^2 + \alpha^2} \tag{3.28}$$

the root in the denominator is removed,

$$P = G\frac{\rho_0}{\pi} \int_{-\infty}^{\infty} dz' \int_{-\infty}^{\infty} dt \int_0^a d\varpi' \int_0^{2\varphi} d\varphi \frac{\varpi' \exp(-z'^2/\beta^2)}{t^2 + \varpi^2 + \varpi'^2 - 2\varpi\varpi' \cos\varphi + (z' - z)^2}, \tag{3.29}$$

and the integration according to φ and ϖ' is easy to perform. In further computations elliptic integrals appear. Neglecting terms of second order in β/ϖ and inserting the total mass

$$M = \pi\rho_0 a^2 \int_{-\infty}^{\infty} \exp(-z'^2/\beta^2)\, dz' = \pi^{3/2}\rho_0\beta a^2, \tag{3.30}$$

we find

$$P = \frac{GM}{\varpi}\left\{\frac{4}{\pi} E\left(\frac{\varpi}{a}\right) + \frac{1 + \kappa(\varpi, z)}{\sqrt{\pi}} \frac{\beta}{\varpi}\left[\exp\left(\frac{-z^2}{\beta^2}\right) + \frac{z}{\beta}\sqrt{\pi}\,\phi\left(\frac{z}{\beta}\right)\right]\right\}, \tag{3.31}$$

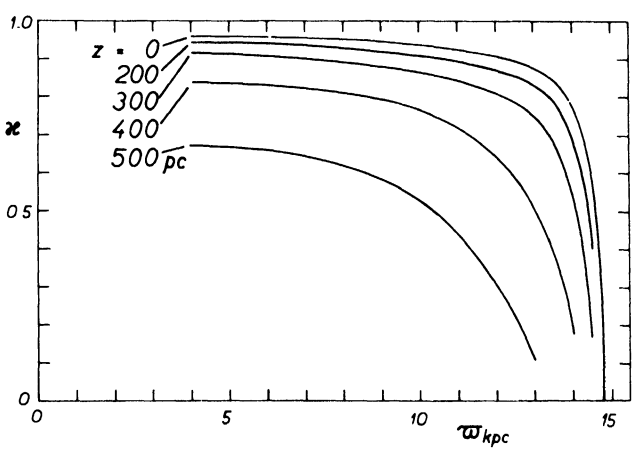


FIG. 25. The coefficient κ in the model by H. Bucerius.

where

$$\phi(t) = \frac{2}{\sqrt{\pi}} \int_0^t e^{-t^2}\, dt \tag{3.32}$$

is the error integral. The parameter κ is close to 1 for small ϖ and z and decreases to zero at the boundary. It was tabulated in the original paper and is shown here in Fig. 25.

The potential of the disk of diffuse matter was computed analogously and the potential of the nucleus follows from (1.33). The potential of the whole composite model and its attraction are shown in Fig. 26. The sharp peak of the

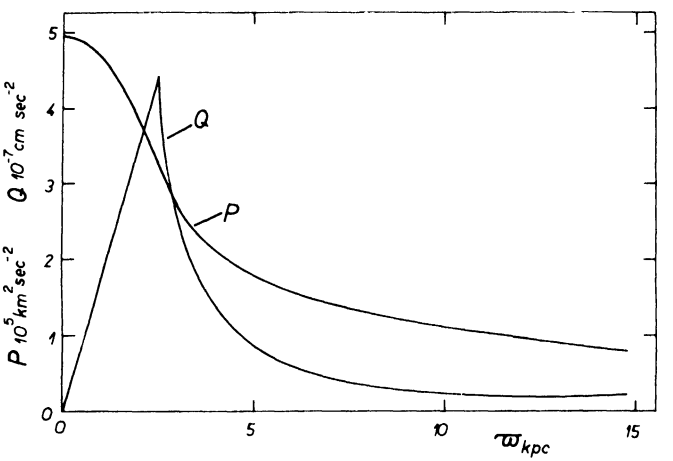


FIG. 26. Potential and attraction in the plane of symmetry of the model by H. Bucerius.

attraction is due to the boundary of the nucleus. The slight rise of Q between 12 and 14.5 kpc is the consequence of the constant density in the ϖ-direction. This shows the danger of models with marked discontinuities in the densities. Even if they lead to a good estimate of the total mass they cannot be relied upon as regards the curve of attraction or the rotation curve.

2. *The Potential of a Homogeneous Plane Disk*

A plane disk can be regarded as a limiting case of a spheroid.

The projected density of a homogeneous spheroid is proportional to the thickness, or to $\sqrt{1 - m^2}$. A heterogeneous spheroid with the density

$$\rho = \frac{\rho_c}{\sqrt{1 - m^2}} \tag{3.33}$$

possesses thus a constant projected density

$$\sigma = c\rho_c \int_0^z \frac{dm^2}{\sqrt{(1-m^2)(m^2-m_0^2)}} = \pi\rho_c c. \tag{3.34}$$

The formula (1.28) with

$$\rho_1(m^2) = -2\rho_c\sqrt{1-m^2}$$

gives immediately, in the plane of symmetry,

$$P = 4Ga\sigma \int_0^{\psi} \sqrt{1-\frac{\varpi^2}{a^2}\sin^2\psi}\, d\psi. \tag{3.35}$$

At internal points we put $\psi = \psi_0$ and for a total flattening $\psi_0 = \pi/2$. Thus we find the potential of a homogeneous plane disk at internal points

$$P_i = 4Ga\sigma E, \qquad k = \frac{\varpi}{a}; \tag{3.36}$$

where $E(k)$ is a complete elliptic integral. The attraction is

$$Q_{\varpi i} = -4G\sigma\frac{a}{\varpi}(K-E); \qquad k = \frac{\varpi}{a}. \tag{3.37}$$

To compute the potential at external points we use the substitution

$$\sin\varphi = \frac{\varpi}{a}\sin\psi, \tag{3.38}$$

which makes the upper limit of the integral in (3.35) $\pi/2$, thus leaving us with complete elliptic integrals again. We get

$$P_e = 4G\sigma\frac{a^2}{\varpi}\int_0^{\pi/2}\frac{\cos^2\varphi\, d\varphi}{\sqrt{1-(a^2/\varpi^2)\sin^2\varphi}}$$

$$= 4Ga\sigma\left[\left(\frac{a}{\varpi}-\frac{\varpi}{a}\right)K+\frac{\varpi}{a}E\right]; \qquad k = \frac{a}{\varpi} \tag{3.39}$$

and differentiating according to ϖ

$$Q_{\varpi e} = -4G\sigma(K-E); \qquad k = \frac{a}{\varpi}. \tag{3.40}$$

3. *Wyse and Mayall's Model. Schwarzschild's Model*

Equations (3.37) and (3.38) were the starting points chosen by Wyse and Mayall (1942) to derive the attraction of a heterogeneous spheroid. The density is given by a series

$$\sigma = A_0 + A_1 \frac{\varpi}{a} + A_2 \left(\frac{\varpi}{a}\right)^2 + \cdots. \tag{3.41}$$

Decomposing the heterogeneous disk into elementary homogeneous disks each with density $d\sigma$, we write (3.37) and (3.40) in the form

$$\begin{aligned} dQ_1 &= -4G \frac{a}{\varpi} (K - E)\, d\sigma; \qquad k = \frac{\varpi}{a} \\ dQ_e &= -4G(K - E)\, d\sigma; \qquad k = \frac{a}{\varpi}. \end{aligned} \tag{3.42}$$

With respect to (3.41) it evidently suffices to compute the integrals

$$M_n = n \left(\frac{\varpi}{a}\right)^n \left[\int_{\varpi/a}^{1} k^{-n-2} (K - E)\, dk + \int_0^1 k^{n-1} (K - E)\, dk\right] \tag{3.43}$$

at internal points and the integrals

$$m_n = n \left(\frac{a}{\varpi}\right)^n \int_0^{a/\varpi} k^{n-1} (K - E)\, dk \tag{3.44}$$

at external points. Hence the attraction is

$$\begin{aligned} -\frac{1}{4G} Q_1 &= A_1 M_1 \left(\frac{\varpi}{a}\right) + A_2 M_2 \left(\frac{\varpi}{a}\right) + \cdots \\ -\frac{1}{4G} Q_e &= A_1 m_1 \left(\frac{a}{\varpi}\right) + A_2 m_2 \left(\frac{a}{\varpi}\right) + \cdots. \end{aligned} \tag{3.45}$$

The coefficients M_n and m_n were computed in the paper quoted for $n = 1, 2, 3, 4, 5$ with the notation M, N, O, P, Q and m, n, o, p, q respectively. For the sake of illustration we give the first two in the form

$$\begin{aligned} M_1(k) &= \frac{1}{2}\left(\frac{1}{k} - k\right)(K - E) \\ &\quad + \frac{1}{4}\pi k \left[\log \frac{4}{k} - 1 + \frac{1}{1 \cdot 2}\left(\frac{1}{2}\right)^2 k^2 + \frac{1}{3 \cdot 4}\left(\frac{1 \cdot 3}{2 \cdot 4}\right)^2 k^4 + \cdots\right] \\ M_2(k) &= \frac{1}{3}\left(\frac{1}{k} - k\right) K + \frac{1}{3}\left(2k - \frac{1}{k}\right) E. \end{aligned}$$

The m_n's had to be computed numerically. Figure 27 shows the run of M_n and m_n. The boundary of the model is at $\varpi = a$. Thus the curves give M_n for $\varpi \leqq a$ and m_n for $\varpi \geqq a$. The curves are continuous at the meeting point $\varpi = a$.

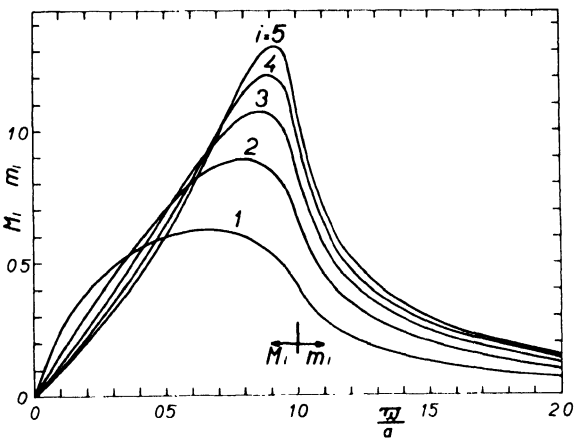


FIG. 27. Coefficients M_i and m_i in the expression for the attraction of a heterogeneous plane disk.

These models are usually affected by the disadvantage of alternating terms. The density results as a difference of much larger quantities.

The disk models were applied to M 31 and M 33. The rotation curve of M 31 required two heterogeneous disks; one with a density expressed by a polynomial of degree 5 representing the large scale distribution of the mass, the other with linearly decreasing density for the internal parts with the first maximum on Babcock's curve. Figure 28 shows the distribution of densities in the two disks. The resulting rotation curve is shown in Fig. 8.

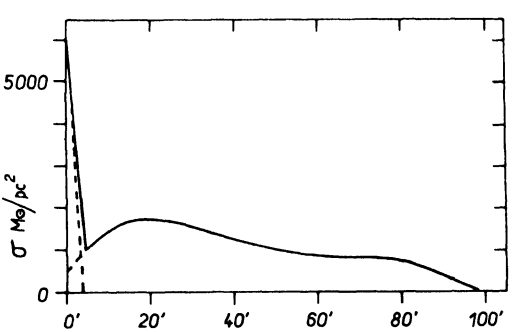


FIG. 28. Distribution of densities in a plane-disk model of M 31.

Two models were considered for M 33. The dashed lines in Figs. 29 and 30 refer to a model with density proportional to the thickness of a homogeneous spheroid. The full lines refer to an almost constant density in the disk. A constant density either in a spheroid or in a disk is as good an approximation as can be deduced from the available observations.

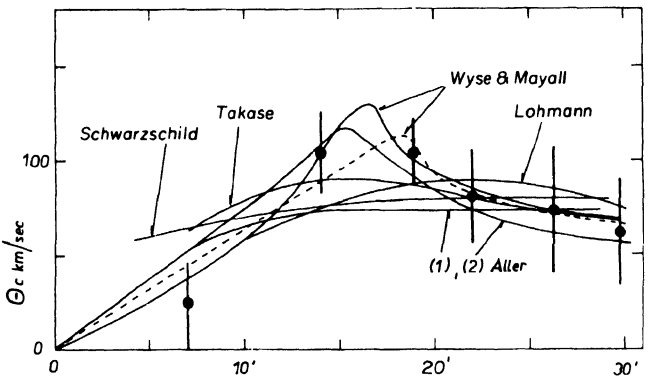


FIG. 29. Rotation curves of M 33. The circles are normal points of the observed rotation velocities and the vertical bars show the probable errors. The curves refer to models by W. Lohmann (Section II, B, 4), A. B. Wyse and N. U. Mayall (Section III, B, 3), M. Schwarzschild (Section III, B, 3), L. H. Aller (Section III, B, 4), and B. Takase (Section III, C, 8).

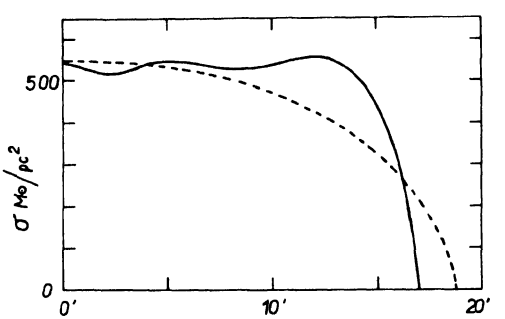


FIG. 30. Density in M 33 according to A. B. Wyse and N. U. Mayall. The full curve refers to a plane-disk model with nearly constant density and the dashed curve to a totally flattened homogeneous spheroid.

Galactic orbits in these two models were investigated numerically by Torgård (1956).

A linear term in the expansion of the density was used by Camm (1938) together with a mass point. Assuming the radius of the disk to be 15 kpc, radial

velocities of planetary nebulae yielded the mass of the disk of $1.01 \times 10^{11} M_\odot$, the mass of the nucleus $0.76 \times 10^{11} M_\odot$ making the mass of the Galaxy $1.77 \times 10^{11} M_\odot$.

Terms with higher powers than the first were avoided by M. Schwarzschild (1954). Assuming as a working hypothesis that the distribution of mass is identical with the distribution of light, he represented the luminosity by

$$I(\varpi) = \frac{1}{f} \sum A_n \left(1 - \frac{\varpi}{a_n}\right), \tag{3.46}$$

where each term contributes a density A_n/f at the center and decreases to zero at a_n. Here, f is the mass-luminosity ratio. Figure 31 shows the system of

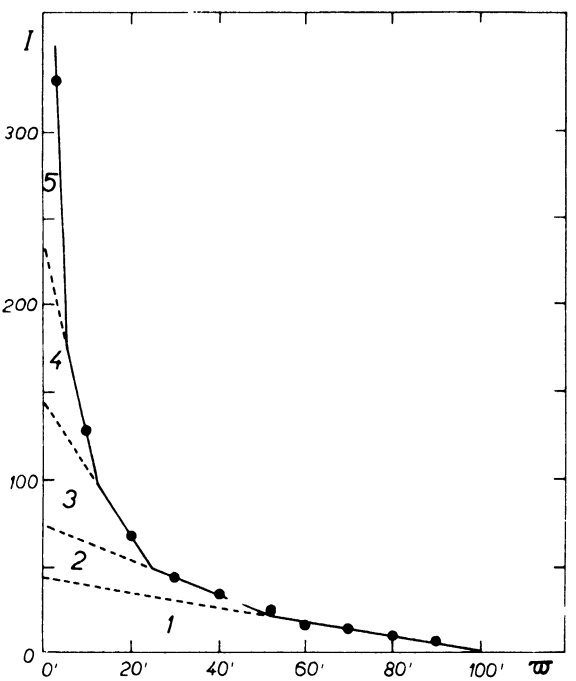


FIG. 31. Brightness in M 31.

straight lines representing the luminosity. The surface density of mass is accordingly

$$\sigma(\varpi) = \sum A_n \left(1 - \frac{\varpi}{a_n}\right). \tag{3.47}$$

The attraction follows from (3.45)

$$-\frac{1}{4G}Q_1 = \sum A_n M_1\left(\frac{\varpi}{a_n}\right). \tag{3.48}$$

The coefficients A_n/f were determined from the observations of the distribution of light, and the factor f was chosen so as to fit the velocities computed from (3.48) to the observed velocities. The linear scale of distances must, of course, be known. The total mass is

$$M = \frac{1}{3}\pi \sum A_n a_n^2. \tag{3.49}$$

For a distance of 460 kpc and $f = 16$ a rotation curve follows varying relatively little with the distance and well fitting normal points computed by Schwarzschild from measures by Mayall. The curve is shown in Fig. 8. The resulting total mass of M 31 is

$$M = 1.4 \times 10^{11} M_\odot.$$

By the same method Schwarzschild derived with $d = 480$ kpc, $f = 4$, the total mass of M 33

$$M = 5 \times 10^9 M_\odot.$$

The rotation curve is shown in Fig. 29.

4. *Aller's Model*

A different procedure was chosen by Aller (1942) for the determination of the distribution of mass in M 33. The potential of a heterogeneous disk was derived by means of spherical harmonics. The disk is dissected into elementary rings. Let us consider a ring of radius ϖ. Its potential at a point on the z-axis, distant z from the plane of the ring, is

$$dP = \frac{2\pi\sigma\varpi\, d\varpi}{\sqrt{\varpi^2 + z^2}}, \tag{3.50}$$

where the mass of the ring is in the numerator and the distance of the point $(0, z)$ from any point of the ring is in the denominator. If $\varpi > z$, we find

$$\begin{aligned} dP &= 2\pi\sigma\, d\varpi \left(1 + \frac{z^2}{\varpi^2}\right)^{-1/2} \\ &= 2\pi\sigma\, d\varpi \left[1 - \frac{1}{2}\left(\frac{z}{\varpi}\right)^2 + \cdots\right]. \end{aligned} \tag{3.51}$$

The known theorems on potential at any point not occupied by the attracting matter lead to

$$dP = 2\pi\sigma\, d\varpi \left[1 - \frac{1}{2}\left(\frac{z}{\varpi}\right)^2 P_2(\cos\vartheta) + \frac{1\cdot 3}{2\cdot 4}\left(\frac{z}{\varpi}\right)^4 P_4(\cos\vartheta) - \cdots\right] \quad (3.52)$$

where the indexed P's denote spherical harmonics. In particular, for $\vartheta = \pi/2$, the point in question lies in the plane of the disk at a distance ϖ_0 and

$$P_{2n}(0) = (-1)^n \frac{1\cdot 3\cdot \ldots\cdot (2n-1)}{2\cdot 4\cdot \ldots\cdot (2n)}.$$

Thus

$$dP = 2\pi\sigma\, d\varpi \left[1 + \left(\frac{1}{2}\right)^2\left(\frac{\varpi_0}{\varpi}\right)^2 + \left(\frac{1\cdot 3}{2\cdot 4}\right)^2\left(\frac{\varpi_0}{\varpi}\right)^4 + \cdots\right]; \qquad \varpi > \varpi_0 \quad (3.53)$$

and in a similar way

$$dP = 2\pi\sigma\, d\varpi \left(\frac{\varpi}{\varpi_0}\right)\left[1 + \left(\frac{1}{2}\right)^2\left(\frac{\varpi}{\varpi_0}\right)^2 + \left(\frac{1\cdot 3}{2\cdot 4}\right)^2\left(\frac{\varpi}{\varpi_0}\right)^4 + \cdots\right]; \quad \varpi < \varpi_0. \quad (3.54)$$

In order to keep the series convergent, we suppose that there is zero density in a ring from $\varpi_0 - d\varpi$ to $\varpi_0 + d\varpi$. The ring of zero density can be made as thin as not to affect the total mass.

Inserting into (3.53) and (3.54) a certain function $\sigma(\varpi)$, we get the potential of the disk by integrating (3.54) from 0 to $\varpi_0 - d\varpi$ and (3.53) from $\varpi_0 + d\varpi$ to the boundary of the model.

Two models were considered by L. H. Aller. In the first the density was constant up to 500 pc and proportional to the surface brightness beyond this distance, or

$$\begin{aligned} \rho &= \rho_c \qquad\qquad ; \quad \varpi < 0.5 \text{ kpc} \\ \rho &= \rho_c\, e^{-1.38(\varpi - 0.5)}; \quad \varpi > 0.5 \text{ kpc}. \end{aligned} \quad (3.55)$$

In the second model the density was constant up to 1 kpc and zero beyond this distance. We note that the linear scale of distances in these models was based on $d = 220$ kpc.

The two models are shown in Fig. 29. The second model where the distribution of mass and brightness have little in common fits radial velocities of emission objects better. On the other hand, the first model fits the radio observations (see Section I, B) better, which are 17 years more recent than Aller's models.

5. *The Solution of the Integral Equation for the Density*

Kuzmin (1952) was the first to note that Eq. (1.31a) can be reduced to Abel's

type of integral equation if the spheroid is totally flattened, $\sin \psi_0 = 1$. His solution in our notation is of the form

$$\cos \psi_0 \rho(m_0) = -\frac{1}{2\pi^2 G a m_0^3} \int_0^{m_0} \frac{d(-m^2 Q)}{dm} \frac{m\, dm}{\sqrt{m_0^2 - m^2}}, \tag{3.56}$$

where $m_0 = \varpi/a$. This solution was used in one of the models by Idlis (2.47) which dates from a later period than Kuzmin's paper. Here again, $\cos \psi_0 \rho$ is finite. Kuzmin extrapolated in both directions an empirical rotation curve which was determined for Cepheids up to about 2.5 kpc on both sides from the sun, and computed the integrand in (3.56). A numerical integration yielded the density. Correction terms respecting the finite thickness of the Galaxy were applied to the solution.

The procedure was repeated by Kiladze (1958) for the hydrogen rotation curve by Kwee *et al.* (1954) and other data. The integrals with infinite limits in the formula for the projected density were substituted by summation formulae, supposing a constant velocity in each interval. The resulting projected density is shown in Fig. 32.

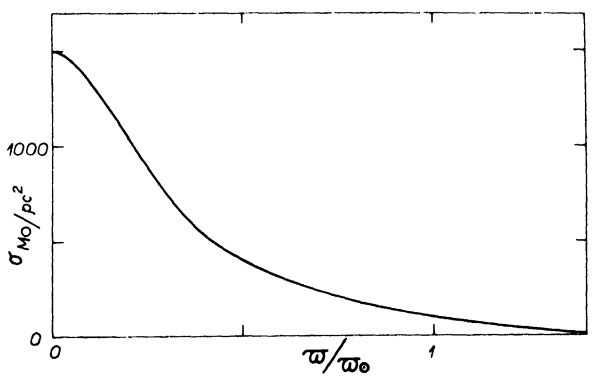


FIG. 32. Projected density of the Galaxy according to a flat model by R. J. Kiladze.

The solution by Brandt (1960*a*) was based on Eq. (1.31a), too. With regard to (1.17) and to the relation between the attraction and circular velocity, we write

$$O_c^2 = Ga \int_0^{m_0} \frac{dM}{a^2 m\, dm} \frac{m\, dm}{\sqrt{m_0^2 - m^2}}. \tag{3.57}$$

The term

$$\frac{dM}{a^2 m\, dm} = 4\pi a \rho m \cos \psi_0 = \sigma_1(m) \tag{3.58}$$

has, for a total flattening, the dimension of a projected density. The substitution $m^2 = t$ leads again to Abel's type of integral equation, the solution of which in our notation is

$$\sigma_1(m_0) = \frac{2}{\pi G m_0 a} \frac{d}{dm_0} \int_0^{m_0} \frac{Q_c^2(m)\, m\, dm}{\sqrt{m_0^2 - m^2}}. \tag{3.59}$$

The mass inside, $m_0 = \varpi/a$, is given by

$$M(m_0) = a^2 \int_0^{m_0} \sigma_1(m)\, m\, dm = \frac{2a}{\pi G} \int_0^{m_0} \frac{Q_c^2(m)\, m\, dm}{\sqrt{m_0^2 - m^2}}. \tag{3.60}$$

Brandt assumed that the rotation curve can be expressed by the formula

$$Q_c(\varpi) = \frac{c_1 \varpi}{(1 + c_2^n \varpi^n)^{3/2n}}, \tag{3.61}$$

which is equivalent to the attraction

$$Q = -\frac{c_1^2 \varpi}{(1 + c_2^n \varpi^n)^{3/n}}. \tag{3.62}$$

The attraction is proportional to the distance near the center and to the inverse square of the distance far from the center. It is a generalization of Bottlinger's force law (Section II, B, 4) to which it reduces for $n = 3$. Again, we find a simple expression for the total mass by comparing the attractions of the model and of a finite mass at large distances

$$M = \frac{c_1^2}{c_2^3 G}. \tag{3.63}$$

Expressing the constants by means of the maximum velocity Q_m and the respective distance ϖ_m,

$$c_1 = 3^{3/2n} \frac{Q_m}{\varpi_m}; \qquad c_2 = \frac{2^{1/n}}{\varpi_m}, \tag{3.64}$$

we find

$$M = \left(\frac{3}{2}\right)^{3/n} \frac{Q_m^2 \varpi_m}{G}, \tag{3.65}$$

which reduces to (2.68) for $n = 3$. Inserting $n = 3$ into (3.60) and putting $m = m_0 \sin\psi$, we find the distribution of mass for Bottlinger's force law for the special case of total flattening

$$M(\varpi) = \frac{2c_1^2}{\pi G} \varpi^3 \int_0^{\pi/2} \frac{\sin^3\psi\, d\psi}{1 + c_2^3 \varpi^3 \sin^3\psi}. \tag{3.66}$$

In the case $n = 3/2$, in a similar way,

$$M(\varpi) = \frac{2c_1^2}{\pi G}\varpi^3 \int_0^{\pi/2} \frac{\sin^3\psi\, d\psi}{[1 + (c_2\varpi \sin\psi)^{3/2}]^2}. \tag{3.67}$$

Brandt (1960b) constructed a model of the Galaxy with $n = 3/2$, $O_\odot = 216$ km/sec, $\varpi_\odot = 8.2$ kpc, $O_m = 222$ km/sec, $\varpi_m = 6.5$ kpc; the mass inside the sun's distance was $0.62 \times 10^{11}\, M_\odot$ and the total mass $1.8 \times 10^{11}\, M_\odot$. The correction for the finite thickness increases the mass by 10 to 20% for the axial ratio 1/12 to 1/5. The same kind of model applied to the radial velocities in M 31 gave a total mass of $3.7 \times 10^{11}\, M_\odot$ for a distance of 600 kpc.

Another estimate of the mass of the Galaxy inside the sun's distance was derived by Brandt (1960b) from Eq. (3.60). Let us consider a direction in the galactic longitude l (measured from the center) and a point in that direction which is nearest to the center. The observed radial velocity is

$$V = O_c - O_\odot \sin l. \tag{3.68}$$

The radial rotation curve was derived on the assumption that the maximum observed radial velocity in a given direction corresponds to the circular velocity at the point nearest to the center. Inserting for O_c into (3.60) and denoting

$$\begin{aligned} C_1 &= \int_0^{\pi/2} V \sin^2 l\, dl \\ C_2 &= \int_0^{\pi/2} V^2 \sin l\, dl, \end{aligned} \tag{3.69}$$

we have, taking account of

$$\sin l = \varpi/\varpi_\odot = m/m_0$$

the mass inside $\varpi_\odot$

$$M(\varpi_\odot) = \frac{2\varpi_\odot}{\pi G}\left[\frac{2}{3}O_\odot^2 + 2O_\odot C_1 + C_2\right]. \tag{3.70}$$

The quantities C_1, C_2 follow from observations. Brandt's numerical values derived from the rotation curve of neutral hydrogen are

$$C_1 = 28.3 \text{ km/sec}$$

$$C_2 = (61.3 \text{ km/sec})^2.$$

Putting

$$O_\odot = \varpi_\odot(A - B),$$

we find

$$M(\varpi_\odot) = \frac{2}{\pi G}\left[\frac{2}{3}(A - B)^2\varpi_\odot^3 + 2(A - B)C_1\varpi_\odot^2 + C_2\varpi_\odot\right]. \tag{3.71}$$

With $\varpi_\odot = 8.2$ kpc, $A - B = 25$ km/sec/kpc, and a correction for finite thickness of 10%, we get

$$M(\varpi_\odot) = 0.63 \times 10^{11} M_\odot,$$

which seems to be quite plausible. Evidently, the result depends very strongly on the value of $\varpi_\odot$, the first term in the brackets being dominant.

C. *Heterogeneous Spheroids With Similar Strata*

Taking into account the forms of the galaxies a heterogeneous spheroid seems to offer the most convenient approximation. It is simpler and requires fewer parameters than a system of several homogeneous spheroids. There is a wide choice among the density laws satisfying all kinds of observations.

A decision must be taken concerning the form of equidensity surfaces because there is no known solution for the potential of a heterogeneous spheroid with the axial ratio being an arbitrary function. Two special cases have been treated. In the first, the axial ratio is constant and the equidensity surfaces are similar spheroids. In the second case, the linear eccentricity is constant and the surfaces are confocal spheroids. These two cases admit the computation of the potential by relatively simple means.

To give a reason for considering similar strata we mention the isophotes of elliptical galaxies which exhibit an almost constant axial ratio. Confocal strata approximate, to a certain degree, the distribution of RR Lyrae stars, where the axial ratio increases with the distance from the center.

1. *The Density Expanded into a Series*

Let us return once more to the equation for the attraction of a heterogeneous spheroid with similar strata (1.31). Expanding the attraction in the plane of symmetry into a series

$$-Q = \varpi(q_0 + q_1\varpi + q_2\varpi^2 + \cdots) \tag{3.72}$$

and the density into

$$\rho = \rho_0 + a\rho_1 m + a^2\rho_2 m^2 + \cdots, \tag{3.73}$$

which is valid at all internal points and takes a simpler form in the plane of symmetry

$$\rho = \rho_0 + \rho_1\varpi + \rho_2\varpi^2 + \cdots, \tag{3.74}$$

we insert the two expansions into (1.31) and find

$$\sum_i q_i\varpi^i = 4\pi G \sum_j \frac{\cos\psi_0}{(\sin\psi_0)^{j+3}} \rho_j\varpi^j \int_0^{\psi_0} \sin^{j+2}\psi \, d\psi\,, \tag{3.75}$$

where we used the substitution

$$m = \frac{\varpi}{a} \frac{\sin \psi}{\sin \psi_0} .$$

Writing

$$A_i = \int_0^{\psi_0} \sin^{i+2} \psi \, d\psi$$

we note that we arrive at the coefficients w_{lk} (1.13) for even values of the index

$$A_{2i} = \tfrac{1}{2} w_{i+1,0} .$$

A comparison of equal powers of ϖ in both sides of (3.75) leads to

$$\rho_i = \frac{\sin^{i+3} \psi_0}{\cos \psi_0} \frac{q_i}{4\pi G A_{i+2}} , \tag{3.76}$$

showing that each coefficient in the expansion of the density depends on one coefficient in the expansion of the attraction only, making the determination of the density very easy if a good rotation curve is available.

The total mass up to the distance of the farthest off measure $\varpi_1 = m_1 a$ is, from (1.18),

$$M = \frac{1}{G} \sum_i \frac{(\varpi_1 \sin \psi_0)^{i+3}}{i+3} \frac{q_i}{A_{i+2}} . \tag{3.77}$$

Burbidge *et al.* (1959b) applied this method to NGC 2146 (see Fig. 12). The square of the velocity of rotation was represented by a polynomial of degree 8 and the same number of terms resulted for the density. The density shows a decrease towards the center (Fig. 33) caused by neglecting the pressure term

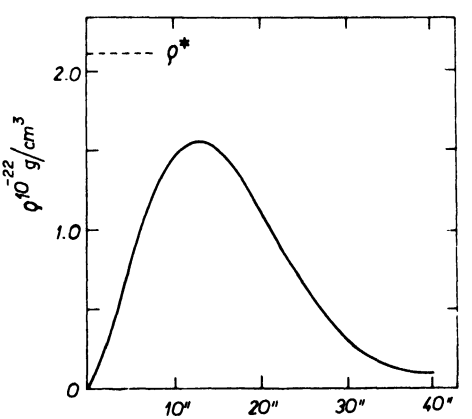


FIG. 33. Density in NGC 2146 according to E. M. Burbidge *et al.*

(see Section III, A, 3). If the pressure term is taken into account, it is found that at the center

$$\rho^* = 3.1\ M_\odot/\mathrm{pc}^3$$

and the total mass

$$M = 1.8 \times 10^{10}\ M_\odot.$$

A polynomial of degree 6 (Burbidge *et al.* 1960a) represented the rotation curve of NGC 5055 (Fig. 11). The square of the polynomial was cut off at degree 10. With an axial ratio of 1/15 the total mass is

$$M = 7.6 \times 10^{10}\ M_\odot$$

and the density is shown in Fig. 34. The logarithm of the density decreases almost proportionally to the distance.

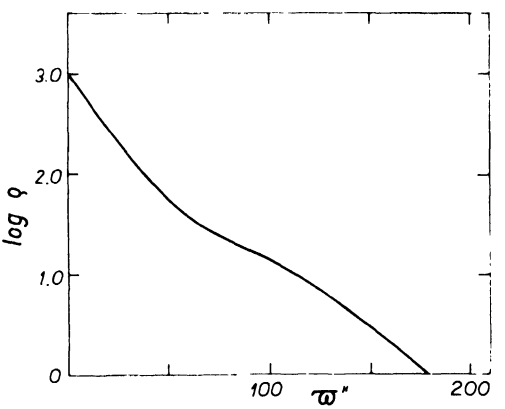


FIG. 34. Density in NGC 5055 according to E. M. Burbidge *et al.*

2. *Density Law* $\rho = \rho_c(1 - m^2)^n$

For $n = 1$, we have

$$\rho = \rho_c(1 - m^2), \tag{3.78}$$

and the density decreases according to a parabola. Sometimes this formula is called the parabolic density law. The general case

$$\rho = \rho_c(1 - m^2)^n \tag{3.79}$$

has at the boundary a zero density, and for $n > 1$ a zero density gradient.

The density is a polynomial in m^2 and as we have seen in Section I, C the

potential contains only the integrals w_{lk}. Inserting (3.79) into (1.26) or (1.27), we find

$$P = \pi G\rho_c a^2 \cot\psi_0 \left[\frac{1}{n+1} w_{10} - \frac{1}{\epsilon^2}(w_{20}\varpi^2 + w_{11}z^2) + \frac{n}{2!\epsilon^4}(w_{30}\varpi^4 + 2w_{21}\varpi^2 z^2 + w_{12}z^4) - \frac{n(n-1)}{3!\epsilon^6}(w_{40}\varpi^6 + 3w_{31}\varpi^4 z^2 + 3w_{22}\varpi^2 z^4 + w_{13}z^6) + \cdots\right]. \tag{3.80}$$

This formula refers to external points since the argument of w_{lk} is ψ. Writing v_{lk} instead, with the argument ψ_0, the formula refers to internal points. The total mass follows from (1.18)

$$M = 2^{2n+3}\frac{\Gamma(n+1)\,\Gamma(n+2)}{\Gamma(2n+4)}\pi a^3\rho_c\cos\psi_0, \tag{3.81}$$

and the projected density from (1.23). Putting the boundary into the shell of zero density, $m_1 = 1$, we find

$$\sigma(\varpi) = 2^{2n+1}\frac{[\Gamma(n+1)]^2}{\Gamma(2n+2)}\left(1-\frac{\varpi^2}{a^2}\right)^{n+1/2} a\rho_c\cos\psi_0. \tag{3.82}$$

Especially, for $n = 1$ we have the set of formulas

$$M = \frac{8}{15}\pi a^3\rho_c\cos\psi_0,$$

$$\sigma(\varpi) = \frac{4}{3}\left(1-\frac{\varpi^2}{a^2}\right)^{3/2} a\rho_c\cos\psi_0,$$

$$P = \pi G\rho_c a^2\cot\psi_0 \times\left[\frac{1}{2}w_{10} - \frac{1}{\epsilon^2}(w_{20}\varpi^2 + w_{11}z^2) + \frac{1}{2\epsilon^4}(w_{30}\varpi^4 + 2w_{21}\varpi^2 z^2 + w_{12}z^4)\right], \tag{3.83}$$

$$Q_\varpi = -2\pi G\rho_c\frac{\cos\psi_0}{\sin^3\psi_0}\varpi\left[w_{20} - \frac{1}{\epsilon^2}(w_{30}\varpi^2 + w_{21}z^2)\right],$$

$$Q_z = -2\pi G\rho_c\frac{\cos\psi_0}{\sin^3\psi_0}z\left[w_{11} - \frac{1}{\epsilon^2}(w_{21}\varpi^2 + w_{12}z^2)\right].$$

The first application of these formulas or, for that matter, the first application of heterogeneous spheroids to galactic models, was made by Perek (1948, 1951). Models of the Galaxy were constructed for different values of n. Oort's constants were used for the determination of ρ_c and $\varpi_\odot/a$. Computing O and its derivative

from (3.83) and inserting it into the definition equations of Oort's constants (2.22), we find for $n = 1$

$$a^2 = \varpi_0^2 \frac{w_{30}}{\sin^2 \psi_0 w_{20}} \frac{3A - B}{2A}$$

$$\rho_c = \frac{1}{2\pi G} \frac{\sin^3 \psi_0}{w_{20} \cos \psi_0} (3A - B)(A - B), \tag{3.84}$$

where the parameters defining the model follow from observed quantities A, B, ϖ_0, and the angle ψ_0. Similar formulas can be derived for higher values of n but an algebraic equation of degree n has to be solved.

A model based on $n = 2$ (Perek, 1951) and supplemented by the outer spheroids from the model by Oort (1941) led to a total mass of $(0.9 \pm 0.1) \times 10^{11} M_\odot$, a central density of $(0.75 \pm 0.10) M_\odot/\text{pc}^3$, and to $\Theta_0 = 260 \pm 15$ km/sec, $\varpi_0 = 7.8 \pm 0.3$ kpc. The density is shown in Fig. 24. At the time of the construction of the model no knowledge was available of the rotation curve in a large range of distances. Therefore the central density turned out to be much smaller than is the case with models based on the hydrogen rotation curve by Kwee *et al.* (1954).

The parabolic density law was applied by Kerr and de Vaucouleurs (1956) to the Large Magellanic Cloud. With an axial ratio of 1/5, $d = 46$ kpc, $a = 3.5° = 2.8$ kpc, $\rho_c = 0.26 M_\odot/\text{pc}^3$, the total mass

$$M = 1.93 \times 10^9 M_\odot$$

and the projected density at the center

$$\sigma_c = 195 M_\odot/\text{pc}^2$$

were arrived at. The rotation curve is shown in Fig. 10. The parabolic density law fits the observations equally well as a superposition of three disks which were limiting cases of homogeneous spheroids and one disk with Gaussian distribution of the density. For the LMC no good fit was obtained with either Bottlinger's force law or with Schwarzschild's assumption of constant mass-luminosity ratio (Section III, B, 3).

Optical velocities in the LMC were discussed by de Vaucouleurs (1960), again on the basis of a parabolic density law. With $c/a = 1/5$, $d = 63$ kpc the upper curve in Fig. 10 resulted. The total mass, with regard to high optical velocities, is much higher than that from the radio observations

$$M = (2.5 \pm 0.6) \times 10^{10} M_\odot.$$

The model consists of two superposed spheroids. Their parameters are given in Table VII. The possible causes of the discrepancy between the radio and

TABLE VII

ELEMENTS OF A COMPOSITE SPHEROIDAL MODEL OF THE LMC

Component	I	II	Total
a (kpc)	4.4	8.8	8.8
a°	4°	8°	8°
ρ_c ($M_\odot$/pc^3)	0.348	0.065	0.413
σ_c ($M_\odot$/pc^2)	410	153	563
M in 10^{10} $M_\odot$	1.0	1.5	2.5

optical methods were mentioned in Section I, B. After discussing in detail all possible sources of errors, de Vaucouleurs concluded that the most probable value for the total mass of the LMC is

$$M = 1.3 \times 10^{10} M_\odot .$$

A distribution of densities similar to (3.73) was used by B. Lindblad and Langebartel (1953) but in the z-direction a Gaussian distribution was assumed

$$\rho = \rho_c \left(1 - \frac{\varpi^2}{a^2}\right)^n e^{-\alpha z^2/2}.$$

Equidensity surfaces are not similar spheroids. From this expression no conclusions were made regarding the distribution of mass. It was applied in connection with density waves to the study of spiral structure.

The parabolic density law proved fruitful in the investigation of galactic orbits. Contopoulos (1957, 1958) in discussing orbits not limited to the plane of symmetry, arrived at the following result: In a meridian section, which follows the star in its motion, the orbit is enclosed inside a torus section.

The equations of motion can be solved by means of the Weierstrass elliptic functions (Perek, 1961) if the motion is restricted to the plane of symmetry. The analysis allows us to get an insight into the general properties of galactic orbits. It is the more interesting as the circular orbits are not everywhere stable. The criterion of stability (B. Lindblad, 1959)

$$\frac{\partial^2 P}{\partial \varpi^2} + \frac{3}{\varpi}\frac{\partial P}{\partial \varpi} < 0$$

reduces to

$$\varpi < \varpi_c$$

where

$$\varpi_c = \epsilon \sqrt{\frac{2}{3} \frac{v_{20}}{v_{30}}}.$$

The critical distance is not inside the model for a spherical symmetry. No unstable orbits exist for flattening between 1 and $c/a = 0.3677$. At the last value, unstable orbits set in at the boundary and their region widens with decreasing c/a. For the extreme $c/a = 0$, this region extends from the boundary down to

$$\varpi = \frac{2}{3}\sqrt{2}\, a,$$

i.e., it covers the last six percent of the semiaxis a.

The range of apocentric velocities allowing stars to reach central regions is considerably restricted in comparison with the range in Keplerian orbits.

Nearly circular orbits near the center have successive apocentra 180° apart. With increasing size of the orbit the line of apsides begins to rotate and the successive apocentra begin to approach one another and eventually will coincide, in analogy with Keplerian orbits. For still larger orbits a number of revolutions around the center is necessary for the completion of the anomalistic period of these orbits. If the number of revolutions in one anomalistic period becomes infinite, the orbits become unstable.

3. *Density Law* $\rho = \rho_0(m^{-1} - 1)$

This density law was introduced by Schmidt (1956). Though it has an infinite density at the center, its total mass is finite,

$$M = \frac{2}{3}\pi a^3 \rho_0 \cos\psi_0. \tag{3.85}$$

Here, ρ_0 is the density at $m = 1/2$. The boundary of the model is at $m = 1$, of course, where the density is zero.

The projected density is easily obtained

$$\sigma(\varpi) = 2\left(a \cosh^{-1}\frac{a}{\varpi} - \sqrt{a^2 - \varpi^2}\right)\rho_0 \cos\psi_0. \tag{3.86}$$

At the center, it is infinite, too.

The potential at an external point follows from (1.27) after performing the necessary integrations

$$P = \pi G a^2 \rho_0 \cot \psi_0$$

$$\times \left\{ w_{10} + \frac{1}{\epsilon^2}(w_{20}\varpi^2 + w_{11}z^2) - \frac{4}{\epsilon}(\sqrt{\varpi^2 + z^2} - \sqrt{\varpi^2 \cos^2\psi + z^2}) \right.$$

$$\left. - 4\frac{z}{\epsilon}\sinh^{-1}\left(\frac{z}{\varpi \cos\psi}\right) + 4\frac{z}{\epsilon}\sinh^{-1}\left(\frac{z}{\varpi}\right) \right\}, \tag{3.87}$$

which reduces in the plane of symmetry to

$$P = \pi G a^2 \rho_0 \cot \psi_0 \left[2\psi - 4\frac{\varpi}{\epsilon}(1 - \cos\psi) + \frac{\varpi^2}{\epsilon^2}(\psi - \sin\psi \cos\psi) \right], \tag{3.88}$$

where we have written the w_{1k} in full.

The potential is given by a quadratic expression in ϖ, as with a homogeneous spheroid; the attraction is accordingly linear in ϖ. With homogeneous spheroids it is proportional to ϖ; in the present case it has the form

$$-Q = p - q\varpi. \tag{3.89}$$

This property induced Schmidt to choose the above density law because observations yield between 2.5 and 8.2 kpc from the center, a decrease of the attraction not departing by more than 6% from a straight line.

Writing (3.89) in the form

$$Q = Q_0 + Q'(\varpi - \varpi_0), \tag{3.90}$$

we have, in fact, the two first terms of an expansion of the attraction at ϖ_0. In this form it was used by Trumpler and Weaver (1951). The Q_0 and Q'_0 were expressed by means of ϖ_0 and Oort's constants (2.25). The authors investigated galactic orbits departing only slightly from circles. Elliptic orbits with a retrograde rotation of the line of apsides resulted. An exact solution requires elliptic functions.

The model by M. Schmidt was constructed on the basis of extensive observing material. The strongest evidence came from the velocities of neutral hydrogen measured by Kwee *et al.* (1954). Schmidt used four heterogeneous spheroids representing individual populations. He could not escape assigning the most massive spheroid to unknown objects in order to explain the attraction at the sun. To remove slight differences between the observed and linear attraction, nine homogeneous spheroids were added. Their elements are listed in Table VIII.

TABLE VIII

ELEMENTS OF SCHMIDT'S MODEL

	Heterogeneous spheroids			
Spheroid	1	2	3	4
Objects	Population I	F M stars	High velocity stars	Unknown objects
c/a	0.02	0.07	0.16	0.07
a (kpc)	16.4	12.3	12.3	8.68
ρ_0 ($M_\odot$/pc^3)	0.0232	0.0696	0.0162	0.3874
Mod $\left(\frac{\partial \log \rho}{\partial \varpi}\right)_z$	0.05	−0.16	−0.16	−0.95
M in 10^{11} $M_\odot$	0.043	0.189	0.101	0.372

	Homogeneous spheroids								
c/a	0.07								
a (kpc)	0.84	1.90	2.93	3.90	5.09	6.13	7.16	8.10	8.20
ρ ($M_\odot$ pc^3)	6.27	0.141	0.023	−0.026	−0.046	−0.016	+0.0002	−0.002	−0.005
M	0.007 10^{11} $M_\odot$								

This procedure made the representation excellent in exchange for the loss of simplicity which is otherwise characteristic for heterogeneous spheroids. However, it seems that the Galaxy is complicated to such a degree that simple expressions are insufficient for a good representation of the density. Densities of Schmidt's model are shown in Fig. 35, the attraction in Fig. 36.

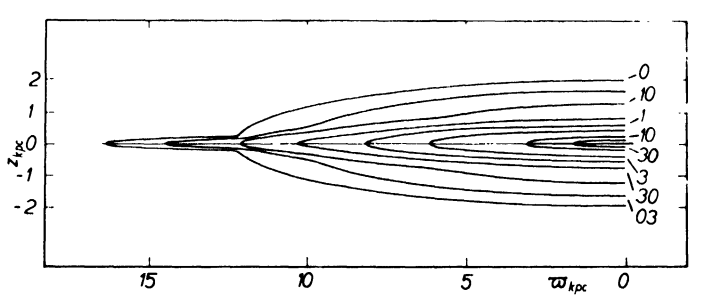


FIG. 35. Density in the model by M. Schmidt.

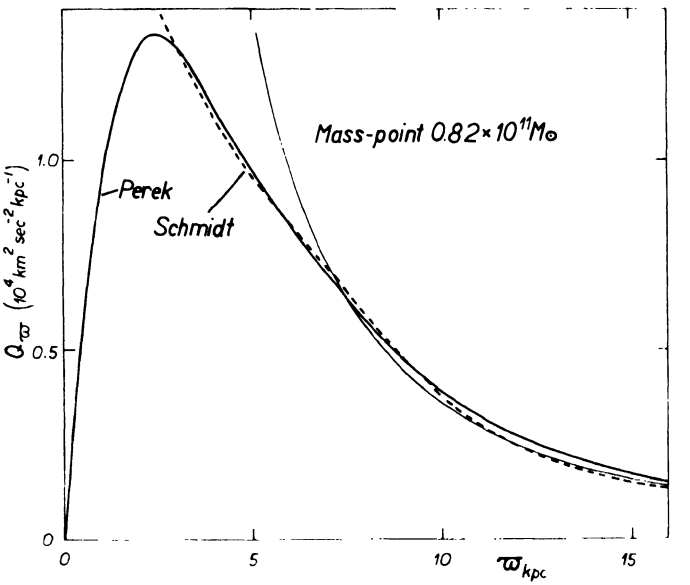


FIG. 36. Attraction in the models by M. Schmidt (Section III, C, 3) and L. Perek Section III, E) compared with the attraction of a mass point.

The model of M 31 constructed by Schmidt (1957b) consists of two spheroids. The density of the first is

$$\rho = 0.43 \left(\frac{1.05^\circ}{\varpi^\circ} - 1 \right) M_\odot/\mathrm{pc}^3; \qquad 0 \leqq \varpi^\circ \leqq 0.79^\circ$$

in the inner parts, and

$$\rho = 0.056(\varpi^\circ)^{-4}\, M_\odot/\mathrm{pc}^3; \qquad 0.79^\circ \leqq \varpi^\circ$$

in the outer parts (see Section III, C, 5). The second spheroid is given by

$$\rho = 0.00725 \left(\frac{4.957^\circ}{\varpi^\circ} - 1 \right); \qquad 0 \leqq \varpi^\circ \leqq 4.957^\circ.$$

With a distance of 630 kpc and an axial ratio of 0.07 the total mass is $3.38 \times 10^{11}\, M_\odot$. The rotation curve is shown in Fig. 8. It fits the observed rotation curve by van de Hulst *et al.* (1957) very well.

M. Schmidt's model of the Galaxy was used by P. O. Lindblad (1960) for the investigation of the development of spiral structure by means of dispersion

orbits. Petri (1958) studied the orbits by numerical methods. With the same initial conditions the perigalactic distances in Schmidt's model exceeded those in Keplerian orbits. Torgård (1956) studied systematically the orbits in the plane of symmetry on an electronic computer. The study was based on a numerically defined model which closely resembled Schmidt's model.

Wayman (1959) made an attempt to reduce the formula (3.88) to the form of the potential (2.87) resulting from the general solution of the equation of continuity for the generalized ellipsoidal distribution of velocities. He found it impossible; it can be done only if the numerical values are somewhat modified.

4. *Density Law* $\rho = \rho_c(1 - m)$

The total mass, the projected density, and the potential in the plane of symmetry follow from the formulas of Section I, C:

$$M = \tfrac{1}{3}\pi a^3 \rho_c \cos\psi_0, \tag{3.91}$$

$$\sigma(\varpi) = \left[\sqrt{a^2 - \varpi^2} - \frac{\varpi^2}{a}\cosh^{-1}\frac{a}{\varpi}\right]\rho_c \cos\psi_0, \tag{3.92}$$

$$P = \pi G a^2 \rho_c \cot\psi_0 \left[\frac{2}{3}\psi - \frac{\varpi^2}{\epsilon^2}(\psi - \sin\psi\cos\psi) + \frac{4}{9}\frac{\varpi^3}{\epsilon^3}(2 - 3\cos\psi - \cos^3\psi)\right]. \tag{3.93}$$

This density law did not yet find any application though combining a number of such spheroids in an analogy to Schwarzschild's model in Section III, B, 3 might give good results.

5. *Density Law* $\rho = \rho_0 m^{-n}$

Zagar (1957) used this law with $n = 2$. The validity was limited to $0 \leqq m \leqq 1$ and ρ_0 is the density at the boundary. The total mass is finite

$$M = 4\pi a^3 \rho_0 \cos\psi_0. \tag{3.94}$$

If the spheroid is totally flattened, its surface density is

$$\sigma(\varpi) = \frac{2a^2\rho_0 \cos\psi_0}{\varpi}\cos^{-1}\frac{\varpi}{a}. \tag{3.95}$$

The potential is, by (1.28),

$$P = -2\pi G a^2 \rho_0 \cot\psi_0 \int_0^{\psi} \log\left[\frac{\varpi^2}{\epsilon^2}\sin^2\psi + \frac{z^2}{\epsilon^2}\tan^2\psi\right] d\psi,$$

which reduces in the plane of symmetry to

$$P = 4\pi G a^2 \rho_0 \cot\psi_0 \left[\psi \log\frac{\epsilon}{\varpi} - \int_0^{\psi} \log(\sin\psi)\, d\psi\right]. \tag{3.96}$$

The integral on the right-hand side can be expressed by the known series involving Bernoulli's numbers. At internal points $\psi = \psi_0$; thus

$$P = C_1 - C_2 \log \varpi \tag{3.97}$$

and the attraction

$$Q = -4\pi G a^2 \rho_0 \varpi^{-1} \cot \psi_0. \tag{3.98}$$

The two expressions are infinite at the center. At infinity, the potential and attraction (at external points) are consistent with the usual postulates.

The orbits in this model were discussed as early as 1917 by J. Lense who investigated the more general case $0 \leqq n \leqq 2$.

The case $n = 4$ was used by Schmidt (1956) to represent outer regions of one of the spheroids with the density law of Section III, C, 3. The potential of a spheroid, devoid of matter inside the shell $m = 1$, and extending into infinity, follows from (1.26) with appropriate limits of the integrals

$$P = 4\pi G a^2 \rho_0 \cot \psi_0 \left[\int_1^{m_0} \psi m^{-3}\, dm + \psi_0 \int_{m_0}^{\infty} m^{-3}\, dm \right].$$

In the plane of symmetry we find

$$P_1 = 2\pi G a^2 \rho_0 \cot \psi_0 \left[\psi + \frac{\epsilon^2}{\varpi^2} (\cot \psi - \cot \psi_0) \right], \tag{3.99}$$

and in the cavity

$$P_c = 2\pi G a^2 \rho_0 \psi_0 \cot \psi_0. \tag{3.100}$$

The attraction is zero in the cavity. Outside the shell $m = 1$ we have

$$Q = -4\pi G \frac{a^4}{\varpi^3} \rho_0 \sin \psi_0 \cos \psi_0 (\cot \psi - \cot \psi_0). \tag{3.101}$$

Terms with ψ appear in (3.99) and (3.101) though the expressions refer to internal points. However, we had to subtract the spheroid inside $m = 1$. Inserting for ψ from (1.10) we find

$$Q = -4\pi G \frac{a^4}{\varpi^3} \rho_0 \sin \psi_0 \cos \psi_0 \left(\sqrt{\frac{\varpi^2}{\epsilon^2} - 1} - \cot \psi_0 \right).$$

6. *Density Law* $\rho = \rho_c (1 + m^2)^{-2}$

The densities are everywhere positive and finite and also the total mass is finite. We have encountered this distribution in Section II, C, 3, among Kuzmin's models.

We find the total mass

$$M = \pi^2 a^3 \rho_c \cos \psi_0, \tag{3.102}$$

the potential in the plane of symmetry

$$P = 2\pi G a^3 \rho_c \cos \psi_0 \frac{1}{\sqrt{\epsilon^2 + \varpi^2}} \tan^{-1}\left(\sqrt{1 + \frac{\varpi^2}{\epsilon^2}} \tan \psi_0\right), \tag{3.103}$$

and the attraction

$$Q_\varpi = -2\pi G a^3 \rho_c \cos \psi_0 \frac{\varpi}{\epsilon^2 + \varpi^2} \times \left[\frac{1}{\sqrt{\epsilon^2 + \varpi^2}} \tan^{-1}\left(\frac{1}{\epsilon}\sqrt{\epsilon^2 + \varpi^2} \tan \psi_0\right) - \frac{c}{a^2 + \varpi^2}\right] \tag{3.104}$$

Equation (3.103) is identical with (2.98). The potential at an arbitrary point (2.97) can be regarded as a generalization of (3.103).

7. *Density Law* $\rho = \rho_c (1 + m^2)^{-5/2}$

It is natural to consider in this connection a law which is formally similar to the density law of a polytropic gas sphere of index 5. Thus

$$\rho = \rho_c \frac{1}{(1 + m^2)^{5/2}}$$

and the total mass

$$M = \tfrac{4}{3}\pi a^3 \rho_c \cos \psi_0 \tag{3.105}$$

The potential and attraction in the plane of symmetry are expressed by means of elliptic integrals

$$P = -\frac{MG}{\sqrt{\epsilon^2 + \varpi^2}}\left[\frac{\varpi^2}{\sqrt{\epsilon^2 + \varpi^2}} \frac{\cos \psi_0}{\sqrt{a^2 + \varpi^2}} + E\right], \tag{3.106}$$

$$Q = -MG \frac{\varpi}{(\epsilon^2 + \varpi^2)^{3/2}} \times \left[\sqrt{\frac{\epsilon^2 + \varpi^2}{a^2 + \varpi^2}}\left(\frac{2\epsilon^2}{\epsilon^2 + \varpi^2} - \frac{\varpi^2}{a^2 + \varpi^2}\right)\cos \psi_0 + \frac{\epsilon^2 - \varpi^2}{\varpi^2} E - \frac{\epsilon^2}{\varpi^2} F\right], \tag{3.107}$$

where E and F stand for

$$E = E(k, \pi/2) - E(k, \pi/2 - \psi_0), \qquad k^2 = \frac{\varpi^2}{\epsilon^2 + \varpi^2}.$$
$$F = F(k, \pi/2) - F(k, \pi/2 - \psi_0),$$

On the axis of symmetry no elliptic integrals appear, and

$$P = MG \frac{\epsilon^2}{(\epsilon^2 - z^2)^{3/2}} \left[\sin^{-1} \left(\frac{1}{a} \sqrt{\epsilon^2 - z^2} \right) - \frac{z^2}{\epsilon^2} \sqrt{\frac{\epsilon^2 - z^2}{c^2 + z^2}} \right].$$

If $z > \epsilon$, the form

$$P = MG \frac{\epsilon^2}{(z^2 - \epsilon^2)^{3/2}} \left[\frac{z^2}{\epsilon^2} \sqrt{\frac{z^2 - \epsilon^2}{z^2 + c^2}} - \sinh^{-1} \left(\frac{1}{a} \sqrt{z^2 - \epsilon^2} \right) \right]$$

is more convenient. In particular, at the center, we find

$$P_c = \frac{MG}{\epsilon} \psi_0.$$

8. *Gaussian Distribution*

It seems advisable to consider density laws expressed by simple transcendents besides those expressed by algebraic functions. The Gaussian distribution

$$\rho = \rho_c e^{-m^2/2} \tag{3.108}$$

has the property that the logarithmic gradients in the ϖ- and z-directions depend on only one coordinate

$$\begin{aligned} \frac{\partial \log \rho}{\partial \varpi} &= -\frac{\varpi}{a^2} \\ \frac{\partial \log \rho}{\partial z} &= -\frac{z}{c^2}. \end{aligned} \tag{3.109}$$

The mass inside the shell m is given by

$$M(m) = 4\pi a^3 \rho_c \cos \psi_0 \left[\sqrt{\frac{\pi}{2}} \phi(m) - m e^{-m^2/2} \right], \tag{3.110}$$

where $\phi(t)$ is the error integral (3.32). The mass of the whole spheroid with infinite limits is

$$M = (2\pi)^{3/2} a^3 \rho_c \cos \psi_0. \tag{3.111}$$

The potential can be derived by expanding the density into a series in m^2 and inserting into (1.26). The resulting expression (Perek, 1954b)

$$\begin{aligned} P = 2\pi G a^2 \rho_c \cot \psi_0 \Big[v_{10} - \frac{1}{2 \cdot 1! \cdot \epsilon^2} (v_{20} \varpi^2 + v_{11} z^2) + \\ + \frac{1}{2^2 \cdot 2! \, \epsilon^4} (v_{30} \varpi^4 + 2 v_{21} \varpi^2 z^2 + v_{12} z^4) - \cdots \Big] \end{aligned} \tag{3.112}$$

contains only the constants v_{lk}, all the points in space being internal. It converges rapidly enough only in the neighborhood of the center. At ϖ or z exceeding ϵ the convergence is rather slow. To overcome this obstacle, Takase (1955) integrated numerically Eq. (1.31) with the density (3.108), assuming a total flattening. The thickness of the Galaxy being an important factor the method was resumed and numerical integrations performed for different degrees of flattening by Perek (1958a). For the sake of convenience the formula

$$Q = -\frac{MG}{\epsilon^3}\varpi\sqrt{\frac{2}{\pi}}\int_0^{\psi_0}\sin^2\psi\, e^{-m^2/2}\, d\psi \tag{3.113}$$

was compared with the attraction of simple bodies. At great distances the attraction is close to that of a mass point of the same mass, and a parameter p was introduced which converts (3.113) into

$$Q = -p\frac{MG}{\varpi^2}. \tag{3.114}$$

For small ϖ the attraction is not far from that of a homogeneous spheroid of the same central density. Thus (3.113) can be written in the form

$$Q = -\frac{MG}{a^3\sqrt{2\pi}}\frac{\psi_0 - \sin\psi_0\cos\psi_0}{\sin^3\psi_0}\varpi q \tag{3.115}$$

by means of the parameter q. For $q = 1$, (3.115) reduces to the attraction of a homogeneous spheroid.

The lower part of Fig. 37 gives the parameters p and q. The descending branches of the curves at the left give q. To the right, from the sharp bends, the curves represent p. The p-curve for a sphere, $\psi_0 = 0$, has been drawn down to $\varpi = 0$ because it gives the mass inside the shell m in units of the total mass. This quantity does not depend on the degree of flattening.

The two parameters were derived from the same equation; they are related by

$$\frac{p}{q} = \frac{1}{\sqrt{2\pi}}\frac{\psi_0 - \sin\psi_0\cos\psi_0}{\sin^3\psi_0}\left(\frac{\varpi}{a}\right)^3, \tag{3.116}$$

which reduces to

$$\frac{p}{q} = \frac{1}{3}\sqrt{\frac{2}{\pi}}\left(\frac{\varpi}{a}\right)^3 \tag{3.117}$$

for a sphere.

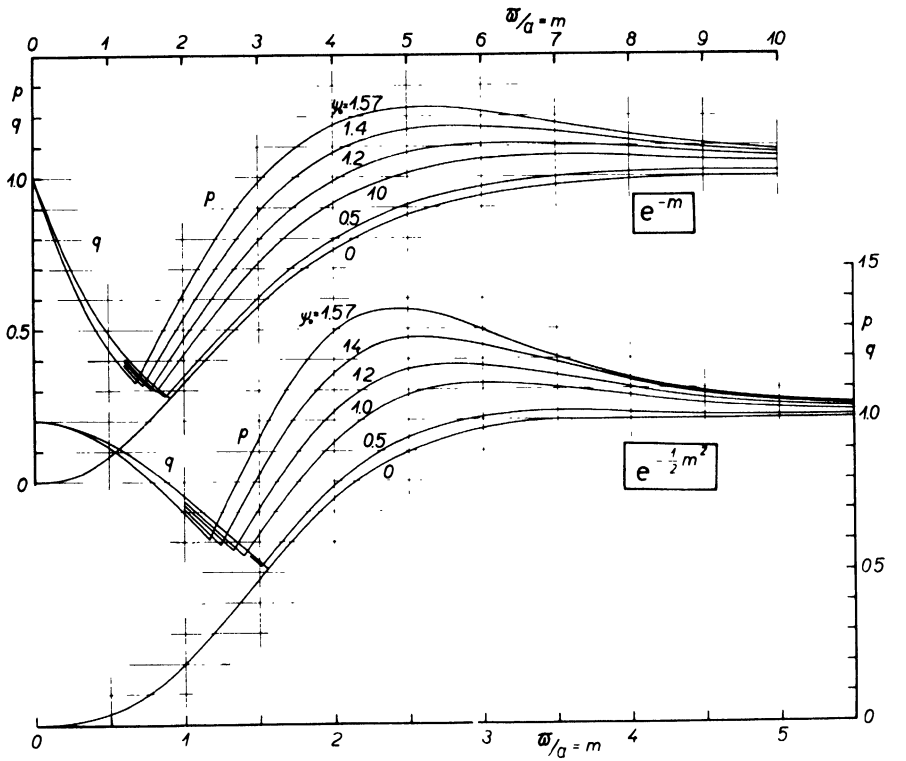


FIG. 37. Coefficients for the computation of the attraction of spheroids with exponential and Gaussian distributions.

The flat model with Gaussian distribution was applied by Takase (1955) to represent the hydrogen rotation curve of the Galaxy. He found a single spheroid inadequate but two spheroids with the elements

$$a_1 = 3.7 \text{ kpc} \qquad M_1 = 0.591 \times 10^{11}\, M_\odot$$

$$a_2 = 1.18 \text{ kpc} \qquad M_2 = 0.089 \times 10^{11}\, M_\odot$$

gave a good fit. The total mass of only $0.68 \times 10^{11}\, M_\odot$ corresponds to the low degree of concentration of the mass.

In M 31 (Takase, 1957) two spheroids were necessary to take account of the radial velocities by Mayall:

$$a_1 = 41.6' \qquad M_1 = 1.78 \times 10^{11}\, M_\odot$$

$$a_2 = 11.8' \qquad M_2 = 0.22 \times 10^{11}\, M_\odot.$$

With a distance of 540 kpc the total mass is $2.0 \times 10^{11} M_\odot$, a relatively small value again. The rotation curve is shown in Fig. 8.

In M 33 a single spheroid sufficed. The distance 540 kpc and $a = 8.8'$ led to $M = 4.4 \times 10^9 M_\odot$. The respective rotation curve is in Fig. 29.

Yasuda (1958) entered upon a more detailed study of a model of the Galaxy. He chose numerical values of the semiaxes and axial ratios of four spheroids and computed Q_1/M_1 from (3.113). The four masses M_1 were determined by the least squares method so as to fit with the hydrogen rotation curve. The procedure was repeated with other sets of values of the semiaxes and axial ratios. The set leading to the best fit was selected and is shown in Table IX. The axial ratios of the first and last spheroids were assumed. On the basis of this model, galactic orbits of high velocity stars were investigated. This procedure, besides being very laborious, is not free from a certain arbitrariness in selecting the sets of semiaxes and axial ratios.

TABLE IX

ELEMENTS OF YASUDA'S MODEL

Spheroid	a (kpc)	c/a	M in $10^{11} M_\odot$
1	6.4	0	0.09
2	4.0	1.11	0.44
3	2.0	1.6	0.14
4	1.2	1	0.06
Total			0.73

A tentative application of (3.112) to the Galaxy yielded a total mass of $1.1 \times 10^{11} M_\odot$ (Perek, 1954b) with $a = 4.4$ kpc, $\varpi_\odot = 8$ kpc, and $c/a = 1.6$. Seventy-eight percent of the total mass is inside the equidensity surface passing through the sun and practically all the mass, 99.9%, is inside double the distance.

9. *Exponential Distribution.* Some observations show a steeper decrease of the density in the central parts than is consistent with the Gaussian distribution and, on the contrary, a slower decrease in the outer regions. Let us consider the distribution (Perek, 1958a)

$$\rho = \rho_0 e^{-m}. \tag{3.118}$$

The logarithmic gradients are constant in the plane of symmetry and on the axis of rotation,

$$\begin{aligned} \frac{\partial \log \rho}{\partial \varpi} &= -\frac{1}{a}\left[1 + \left(\frac{z}{\varpi}\frac{a}{c}\right)^2\right]^{-1/2} \\ \frac{\partial \log \rho}{\partial z} &= \frac{1}{c}\left[1 + \left(\frac{\varpi}{z}\frac{c}{a}\right)^2\right]^{-1/2} \end{aligned} \tag{3.119}$$

The mass inside the shell m follows from (1.18)

$$M(m) = 8\pi a^3 \rho_c \cos\psi_0 [1 - e^{-m}(1 + m + \tfrac{1}{2} m^2)], \tag{3.120}$$

and the total mass of the model with infinite dimensions is

$$M = 8\pi a^3 \rho_c \cos\psi_0. \tag{3.121}$$

The attraction assumes the form

$$Q = \frac{1}{2} \frac{MG}{\epsilon^3} \varpi \int_0^{\psi_0} \sin^2\psi \, e^{-m} \, d\psi \tag{3.122}$$

in the plane of symmetry.

In an analogy to the preceeding case we write this equation in one of the two forms

$$Q = -p \frac{MG}{\varpi^2} \tag{3.123}$$

$$Q = -q \frac{MG}{4a^3} \frac{\psi_0 - \sin\psi_0 \cos\psi_0}{\sin^3\psi_0} \varpi, \tag{3.124}$$

thus comparing it either with the attraction of a mass point of the same mass or with the attraction of a homogeneous spheroid of the same central density. The parameters p and q were evaluated by numerical integration and they are shown in the upper part of Fig. 37. The same applies to them as to the parameters in the preceding section. For $\psi_0 = 0$ we get again the mass inside the shell m expressed in units of the total mass. The relation

$$\frac{p}{q} = \frac{1}{4} \frac{\psi_0 - \sin\psi_0 \cos\psi_0}{\sin^3\psi_0} \left(\frac{\varpi}{a}\right)^3 \tag{3.125}$$

between the two parameters reduces for a spherical distribution to

$$\frac{p}{q} = \frac{1}{6} \left(\frac{\varpi}{a}\right)^3. \tag{3.126}$$

An inspection of Fig. 37 shows that the attraction of a heterogeneous sphere with one of the density laws considered always lies below the attraction of a mass point of the same mass. However, even a slight flattening makes the attraction exceed, from a certain distance upwards, that of a mass point. The excess increases with decreasing axial ratio and attains its maximum value of 36% and 22% for $c/a = 0$ for the Gaussian and exponential distributions respectively.

The exponential distribution has a very sharp peak at the center. Even if some observations indicate that the mass distribution is of the exponential type, it is by no means certain that the density law may be extrapolated to the center. We shall therefore estimate the influence of the peak on the attractions in the plane of symmetry to see whether it can be detected from the evidence from the neighborhood of the sun alone. Two distributions will be considered: one Gaussian

$$\rho_G = e^{-m^2/2}, \tag{3.127}$$

and the other exponential

$$\rho_E = \sqrt{e} \cdot e^{-m}. \tag{3.128}$$

Both distributions have the same value and derivative at $m = 1$. Total masses of the two models are

$$M_E = 8\pi a^3 \cos\psi_0 \sqrt{e}$$

$$M_G = \sqrt{\pi/8e}\, M_E = 0.38\, M_E.$$

The dashed curves G and E in Fig. 38 give the masses enclosed inside the shell m corresponding to the two models.

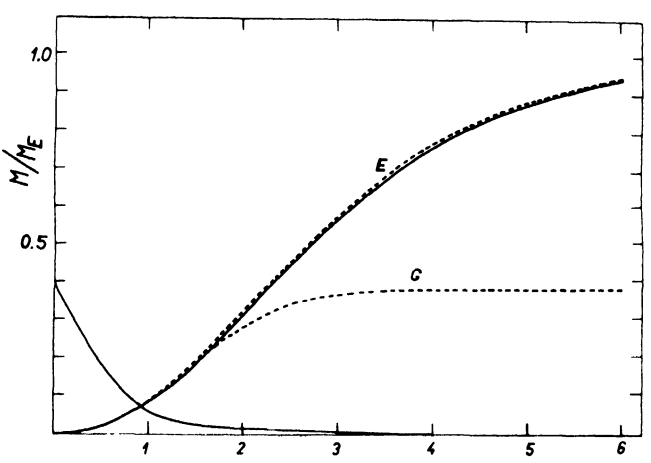


FIG. 38. The dashed curves E and G give masses enclosed inside the shell m for an exponential and a Gaussian distribution respectively. The full curve refers to a combined model: center Gaussian, outer regions exponential. The curve on the left shows the relative decrease of mass inside m caused by cutting off the central peak of the exponential density distribution.

If the peak of the exponential distribution is cut off at $m = 1$ and a Gaussian distribution substituted instead in the central parts, then the mass enclosed inside m (full curve in Fig. 38) follows G up to $m = 1$, and for $m > 1$ runs parallel to E. The total mass of the combined model is only 0.47% lower than M_E. Thus the total mass is quite insensitive to the cutting off of the peak. However, motions of stars depend on the mass enclosed inside m. The curve in the lower left corner of Fig. 38 shows the relative decrease of mass inside m caused by cutting off the peak. The decrease amounts to 40% in the center, but already at $m = 1$ it is 6% and at $m = 2$, 1% only. The central peak is important for a rather limited region. Even a considerable peak in the density near the center may escape detection if the density is determined from the motions and distribution of stars in the neighborhood of the sun only.

D. *Heterogeneous Spheroids With Confocal Strata*

It was observed that the equidensity surfaces of subsystems of population II are more flattened near the galactic center than in the outer regions. Further, the logarithmic gradient of the density of RR Lyrae variables, though very steep at the sun's distance, has a surprisingly small value from the center up to about 6 to 7 kpc (see Fig. 5). These facts make it desirable to consider heterogeneous spheroids with confocal strata (Perek, 1958b).

1. *Density and Mass*

Observational data are rather scarce. Therefore a simple density law, such as the inverse nth power of the distance, seems to be adequate. Having confocal strata, the distances will be measured in the plane of symmetry.

It follows from (1.10) that the density law

$$\rho = \rho_c \sin^n \psi \tag{3.129}$$

results in the inverse nth power of the distance in the plane of symmetry for $\varpi \geq \epsilon$, since

$$\sin \psi = \epsilon / \varpi \quad \text{for} \quad \varpi \geq \epsilon. \tag{3.130}$$

The fact that

$$\sin \psi = 1 \qquad \text{for} \quad \varpi \leq \epsilon, \tag{3.131}$$

is very convenient because it means that the densities are finite throughout.

Should the infinite dimensions of the density law (3.129) give too much weight to outer regions, the model can be made finite by putting the density equal to zero outside the shell $\psi_0 = 0$ by definition. The sudden drop at the boundary is removed by subtracting a homogeneous spheroid of density $\rho_c \sin^n \psi_0$.

The central density of such a distribution is

$$\rho_c = \rho_c'(1 - \sin^n \psi_0),$$

where the central density of (3.129) has been primed for the moment. The density in the shell ψ is

$$\rho = \rho_c \frac{\sin^n \psi - \sin^n \psi_0}{1 - \sin^n \psi_0}. \tag{3.132}$$

The total mass is found from (1.20) for the density law (3.129)

$$M = \frac{4}{3}\pi\epsilon^3\rho_c \int_{\psi_0}^{\pi/2} \sin^{n-4}\psi(3 - 2\sin^2\psi)\, d\psi, \tag{3.133}$$

or, denoting the integral by $f_n(\psi_0)$,

$$M = \tfrac{4}{3}\pi\epsilon^3\rho_c f_n(\psi_0). \tag{3.134}$$

For the finite model, we find

$$M = \tfrac{4}{3}\pi\epsilon^3\rho_c q_n(\psi_0), \tag{3.135}$$

where

$$q_n(\psi_0) = [f_n(\psi_0) - \cos\psi_0 \sin^{n-3}\psi_0](1 - \sin^n \psi_0)^{-1}. \tag{3.136}$$

The functions f_n and q_n are tabulated in Table X. The explicit expressions for the functions are given below together with other functions appearing in the formulas for the potential.

TABLE X

FUNCTIONS f_n AND q_n

ψ	f_5	f_6	q_5	q_6
0.0	1.6667	1.1781	1.6667	1.1781
0.1	1.6517	1.1771	1.6418	1.1761
0.2	1.6077	1.1703	1.5695	1.1627
0.3	1.5366	1.1525	1.4565	1.1286
0.4	1.4420	1.1199	1.3141	1.0692
0.5	1.3282	1.0703	1.1545	0.9856
0.6	1.2001	1.0033	0.9941	0.8834
0.7	1.0631	0.9204	0.8388	0.7710
0.8	0.9222	0.8243	0.6958	0.6566
0.9	0.7817	0.7189	0.5678	0.5463
1.0	0.6455	0.6081	0.4547	0.4437
1.1	0.5158	0.4957	0.3553	0.3501
1.2	0.3941	0.3847	0.2673	0.2651
1.3	0.2803	0.2768	0.1883	0.1876
1.4	0.1732	0.1724	0.1158	0.1156
1.5	0.0710	0.0709	0.0473	0.0472
$\pi/2$	0.0000	0.0000	0.0000	0.0000

The mass of finite models is, of course, finite. The mass of infinite models (3.129) is infinite for $n = 1, 2, 3$. For higher n it is finite:

$$\begin{aligned} n &= 4, \quad M = \tfrac{4}{3}\pi^2\epsilon^3\rho_c, \\ n &= 5, \quad M = \tfrac{20}{9}\pi\epsilon^3\rho_c, \\ n &= 6, \quad M = \tfrac{1}{2}\pi^2\epsilon^3\rho_c. \end{aligned} \tag{3.137}$$

The projected and average densities were given in full by Perek (1958b). The average densities in layers were computed because of the discontinuity of the density gradient at the edge of the focal circle. If the densities run smoothly, the average densities do not differ appreciably from the densities in the central plane of the layer. Here, the average densities give an idea of how the sharp edge is smoothed out in the observed densities which refer to a layer of a finite thickness. To give an illustration we reproduce in Fig. 39 the curve of

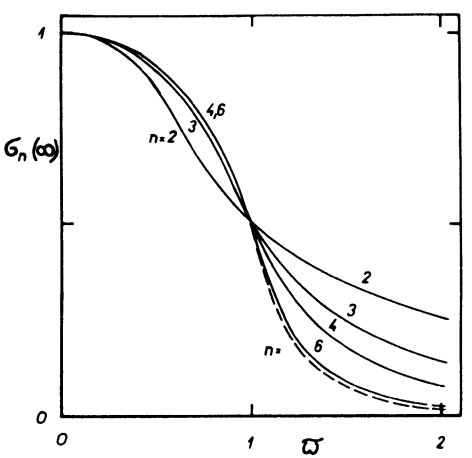


FIG. 39. Full curves: densities projected on the plane of symmetry. Dashed curve: density projected on the plane of a meridian section for $n = 6$.

densities projected on the plane of symmetry for a few values of n. The curves were normed so as to give a density 1 at the center and 0.5 at a distance 1. The dashed curve gives, in the plane of symmetry, the density projected on a meridional plane for $n = 6$. It coincides with the full curve for $n = 6$ below $\varpi = 1$. The expressions for the projected and average densities are rather complicated, and for even values of n involve elliptic integrals.

2. *Potential and Attraction*

We get the potential by inserting (3.129) or (3.132) into (1.41). Denoting

$$f_n(\psi) = \int_{\psi}^{\pi/2} \sin^{n-4}\psi(3 - 2\sin^2\psi)\, d\psi$$

$$g_n(\psi) = \int_{\psi}^{\pi/2} \psi \sin^{n-4}\psi(3 - 2\sin^2\psi)\, d\psi \tag{3.138}$$

$$h_n(\psi) = \int_{\psi}^{\pi/2} \cos\psi \sin^{n-3}\psi\, d\psi,$$

we have explicitly for $n = 5$ and $n = 6$

$$\begin{aligned}
f_5 &= \cos\psi + \tfrac{2}{3}\cos^3\psi \\
f_6 &= \tfrac{3}{4}(\tfrac{\pi}{2} - \psi) + \tfrac{1}{4}\sin 2\psi + \tfrac{1}{16}\sin 4\psi \\
g_5 &= \tfrac{1}{9}(13 - 15\sin\psi + 2\sin^3\psi + 9\psi\cos\psi + 6\psi\cos^3\psi) \\
g_6 &= \tfrac{3}{8}(\tfrac{1}{4}\pi^2 - \psi^2) - \tfrac{3}{8}\sin^2\psi + \tfrac{1}{8}\sin^4\psi + \tfrac{1}{4} + \tfrac{1}{8}\psi\sin 2\psi(1 + 2\cos^2\psi) \\
h_5 &= \tfrac{1}{3}(1 - \sin^3\psi) \\
h_6 &= \tfrac{1}{4}(1 - \sin^4\psi).
\end{aligned} \tag{3.139}$$

Denoting further

$$\begin{aligned}
F_n'(\psi) &= -(\psi - \sin\psi\cos\psi) f_n + g_n - 3h_n \\
G_n'(\psi) &= -(\tan\psi - \psi) f_n - g_n + 3h_n + 1 \\
H_n'(\psi) &= -\psi f_n + g_n - h_n \\
F_n''(\psi) &= g_n - 3h_n - \cos\psi\sin^{n-3}\psi(\psi - \sin\psi\cos\psi) \\
G_n''(\psi) &= -g_n + 3h_n - \cos\psi\sin^{n-3}\psi(\tan\psi - \psi) + 1 \\
H_n''(\psi) &= g_n - h_n - \cos\psi\sin^{n-3}\psi,
\end{aligned} \tag{3.140}$$

we find the relations

$$\begin{aligned}
F_n'(\psi) + G_n'(\psi) &= 1 - \sin^3\psi\sec\psi f_n(\psi) \\
F_n''(\psi) + G_n''(\psi) &= 1 - \sin^n\psi.
\end{aligned} \tag{3.141}$$

Numerical values of the above functions are given in Table XI, and Figs. 40 and 41 show those functions for $n = 5$ and $n = 6$.

TABLE XI

THE FUNCTIONS F', G', H', F'', G'', H''

ψ	F_5'	F_5''	G_5'	G_5''	H_5'	H_5''
0.0	0.4444	0.4444	0.5556	0.5556	1.1111	1.1111
0.1	0.4433	0.4444	0.5550	0.5556	0.9453	1.1095
0.2	0.4359	0.4442	0.5512	0.5555	0.7844	1.0981
0.3	0.4173	0.4430	0.5412	0.5548	0.6329	1.0689
0.4	0.3848	0.4386	0.5227	0.5524	0.4949	1.0158
0.5	0.3389	0.4292	0.4943	0.5465	0.3733	0.9365
0.6	0.2827	0.4082	0.4555	0.5344	0.2701	0.8323
0.7	0.2213	0.3759	0.4070	0.5131	0.1859	0.7079
0.8	0.1609	0.3301	0.3505	0.4799	0.1206	0.5715
0.9	0.1070	0.2724	0.2885	0.4327	0.0726	0.4329
0.1	0.0677	0.2070	0.2245	0.3711	0.0397	0.3026
1.1	0.0328	0.1410	0.1623	0.2968	0.0190	0.1901
1.2	0.0137	0.0821	0.1057	0.2146	0.0075	0.1027
1.3	0.0042	0.0374	0.0586	0.1320	0.0022	0.0437
1.4	0.0007	0.0108	0.0239	0.0599	0.0004	0.0118
1.5	0.0000	0.0009	0.0042	0.0116	0.0000	0.0009
$\pi/2$	0.0000	0.0000	0.0000	0.0000	0.0000	0.0000
ψ	F_6'	F_6''	G_6'	G_6''	H_6	H_6''
0.0	0.4253	0.4253	0.5747	0.5747	0.9253	0.9253
0.1	0.4245	0.4253	0.5743	0.5747	0.8075	0.9251
0.2	0.4191	0.4252	0.5716	0.5747	0.6904	0.9230
0.3	0.4049	0.4248	0.5640	0.5745	0.5757	0.9141
0.4	0.3790	0.4230	0.5492	0.5735	0.4658	0.8920
0.5	0.3403	0.4175	0.5253	0.5704	0.3636	0.8504
0.6	0.2904	0.4049	0.4908	0.5627	0.2720	0.7848
0.7	0.2329	0.3813	0.4453	0.5472	0.1933	0.6945
0.8	0.1735	0.3438	0.3897	0.5199	0.1291	0.5828
0.9	0.1181	0.2917	0.3260	0.4773	0.0716	0.4579
1.0	0.0718	0.2279	0.2576	0.4171	0.0447	0.3309
1.1	0.0377	0.1592	0.1887	0.3398	0.0218	0.2140
1.2	0.0160	0.0948	0.1244	0.2497	0.0088	0.1184
1.3	0.0049	0.0440	0.0695	0.1557	0.0026	0.0513
1.4	0.0008	0.0128	0.0286	0.0714	0.0004	0.0140
1.5	0.0000	0.0010	0.0050	0.0139	0.0000	0.0011
$\pi/2$	0.0000	0.0000	0.0000	0.0000	0.0000	0.0000

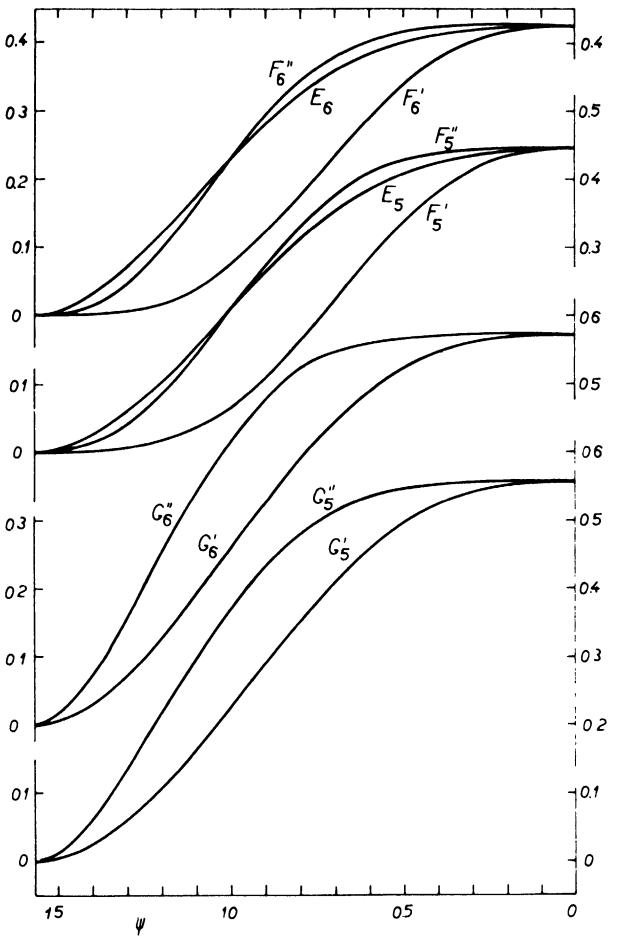


FIG. 40. Functions F_n and G_n appearing in the formulae for the potential. Function E_n from the expression for the stability of circular orbits.

Denoting finally

$$\begin{aligned} F_n(\psi, \psi_0) &= F_n''(\psi_0) - F_n'(\psi) \\ G_n(\psi, \psi_0) &= G_n''(\psi_0) - G_n'(\psi) \\ H_n(\psi, \psi_0) &= H_n''(\psi_0) - H_n'(\psi), \end{aligned} \tag{3.142}$$

we arrive at the formula for the potential of the finite model (3.132)

$$P_1 = -\frac{\pi G \rho_c}{1 - \sin^n \psi_0} (2H_n \epsilon^2 - F_n \varpi^2 - 2G_n z^2). \tag{3.143}$$

The components of the attraction at any internal point, with regard to $\partial P/\partial\psi = 0$, take the form

$$Q_{\varpi i} = -2\pi G\rho_c F_n(\psi, \psi_0)\,\varpi(1 - \sin^n\psi_0)^{-1}$$
$$Q_{zi} = -4\pi G\rho_c G_n(\psi, \psi_0)\,z(1 - \sin^n\psi_0)^{-1}. \tag{3.144}$$

The expressions for infinite models follow at once by putting $\psi_0 = 0$.

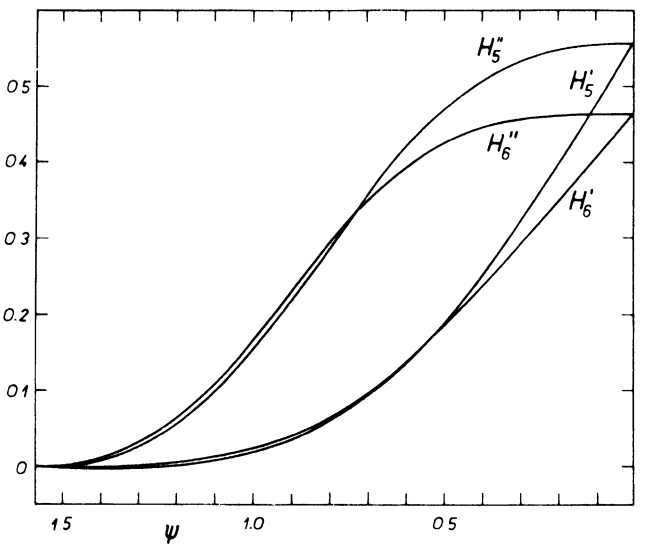


FIG. 41. Functions H_n appearing in the formulae for the potential.

The potential is of a simpler form at external points because two of the three integrals in (1.42) vanish

$$P_e = \pi G\rho_c[2\psi\epsilon^2 - (\psi - \sin\psi\cos\psi)\,\varpi^2 - 2(\tan\psi - \psi)\,z^2]\,\varphi_n(\psi_0). \tag{3.145}$$

The components of the attraction are

$$Q_{\varpi e} = -2\pi G\rho_c\varphi_n(\psi_0)\,\varpi(\psi - \sin\psi\cos\psi)$$
$$Q_{ze} = -4\pi G\rho_c\varphi_n(\psi_0)\,z(\tan\psi - \psi). \tag{3.146}$$

The primed functions (3.140) vanish inside the focal circle.

Hence

$$P_1 = \pi G\rho_c[2H_n''(\psi_0)\,\epsilon^2 - F_n''(\psi_0)\,\varpi^2]\,(1 - \sin^n\psi_0)^{-1}$$
$$Q_{\varpi 1} = -2\pi G\rho_c F_n''(\psi_0)\,\varpi(1 - \sin^n\psi_0)^{-1}. \tag{3.147}$$

These expressions are explicit functions of ϖ. The attractive force increases proportionally to the distance up to $\varpi = \epsilon$ in the same way as inside a homogeneous spheroid. This is obvious because those points are internal with regard to all the shells.

Of particular interest is the case $n = 3$. A model with infinite dimensions has an infinite total mass but the potential is finite everywhere and it goes to zero at infinity as $1/\varpi$.

3. *Stability of Circular Orbits*

The condition of stability of circular orbits in the plane of symmetry

$$\frac{\partial^2 P}{\partial \varpi^2} + \frac{3}{\varpi}\frac{\partial P}{\partial \varpi} < 0 \tag{3.148}$$

takes, for heterogeneous spheroids with confocal strata, the form

$$4F_n + \varpi\frac{dF_n}{d\varpi} > 0. \tag{3.149}$$

Since

$$\frac{dF_n}{d\varpi} = -\frac{2}{\varpi}[\sin^3\psi\sec\psi\, f_n(\psi) - \sin^n\psi],$$

we have

$$F_n''(\psi_0) - F_n'(\psi) + \tfrac{1}{2}\sin^3\psi\sec\psi\, f_n(\psi) - \tfrac{1}{2}\sin^n\psi, \tag{3.150}$$

or, denoting the right-hand member by $E_n(\psi)$,

$$F_n''(\psi_0) > E_n(\psi). \tag{3.151}$$

The functions E_n are tabulated in Table XII and are shown in Fig. 40 for $n = 5$ and $n = 6$. For $\varpi \leq \epsilon$, we find

$$\frac{dF_n}{d\varpi} = 0,$$

TABLE XII

THE FUNCTIONS E_n

ψ	E_5	E_6
0.0	0.4444	0.4253
0.1	0.4442	0.4251
0.2	0.4422	0.4237
0.3	0.4369	0.4201
0.4	0.4275	0.4137
0.5	0.4096	0.4014
0.6	0.3849	0.3836
0.7	0.3517	0.3581
0.8	0.3102	0.3238
0.9	0.2618	0.2806
1.0	0.2086	0.2296
1.1	0.1541	0.1739
1.2	0.1023	0.1180
1.3	0.0575	0.0675
1.4	0.0237	0.0282
1.5	0.0042	0.0050
$\pi/2$	0.0000	0.0000

and $F_n(\psi, \psi_0)$ reduces to $F_n'(\psi_0)$. Hence the condition of stability is

$$F_n'(\psi_0) > 0,$$

which is fulfilled for every ψ_0 considered. Therefore circular orbits inside the focal circle are stable for all possible dimensions of the model.

At external points of the plane of symmetry, we have

$$\frac{dQ}{d\varpi} = -2\pi G\rho_c\varphi_n(\psi_0)\,[\psi - \sin\psi\cos\psi - 2\sin^3\psi\sec\psi], \qquad (3.152)$$

whence the condition of stability is

$$2(\psi - \sin\psi\cos\psi) > \sin^3\psi\sec\psi$$

or, in another form,

$$2(\psi - \sin\psi\cos\psi) > 2(\tan\psi - \psi).$$

According to (1.15), we have finally,

$$2w_{20} > w_{11}. \qquad (3.153)$$

Both members are equal for

$$\psi_1 = 0.9874; \qquad \varpi_1 = 1.198\epsilon. \qquad (3.154)$$

Circular orbits outside the model are stable if they are outside ψ_1. The boundary ψ_0 of the model does not affect this limit in so far as the orbit remains outside the model. Inside the model, condition (3.151) is fulfilled for all $\psi \geq \psi_0$, if $\psi_0 < \psi_1$, and all circular orbits are stable. If $\psi_0 > \psi_1$, there appears a zone of unstable orbits reaching from the distance ϖ_2, given by the condition (3.151), to the distance ϖ_1 outside the model.

E. *A Composite Model of the Galaxy*

If we make it our task to construct a model of the Galaxy, it is rather difficult to select the most suitable method. In the preceding sections we have attempted to give an unbiased survey of the available methods. Each of them has an advantage against the others and its application is justified to a certain degree by the weight we assign to different kinds of observations. In this section we abandon the objective way and we construct a model of the Galaxy on the basis of a personal appreciation of the methods and observed data.

First, we have to decide between a model based on the equation of continuity or on a density law. We have mentioned previously that the ellipsoidal distribution of velocities is not satisfactory and that the observing material did not yet lead to a better approximation. The attempt by W. Fricke (Section II, D) is very promising but it is not the only possibility because it does not take into account the third integral, the existence of which was advocated frequently and with emphasis. Since making some assumptions cannot be escaped in any case, we prefer not to introduce it into the distribution of velocities. We find it more convenient to base the model on the observed densities of matter. The model cannot be very far from the actual mass distribution if the dynamical parameters have been taken into account.

In selecting a suitable model among those reviewed in this section, we postulate a resemblance of the model to the form of the Galaxy. Thus we select a three-dimensional oblate model. Either a flat disk, or a sphere, though extreme cases setting bounds to the actual distribution, lead to the neglect of quite obvious observed facts. Further, we wish to have a small number of free parameters. The observations do not abound in accuracy and each additional unknown increases the indefiniteness of the model. For this reason we shall not consider superpositions of simple bodies. A homogeneous spheroid introduces three parameters: two axes and density. A heterogeneous spheroid is much more flexible and besides the parameters of a homogeneous spheroid introduces only the density law. To expand the attraction into a series is not considered convenient for our purpose because other forms, e.g., a rational function, give better representation with a smaller number of free parameters.

We encounter another difficulty. The observed dynamical parameters lead

to a higher mass density in the solar neighborhood than do direct observations. For this reason Schmidt (1956) added one more spheroid to his model and assigned it to unknown objects. We prefer to assume that the excess of mass belongs to one or other of the known populations or that it is distributed among them in a certain ratio (Perek, 1959). We attempt to determine the total amount of mass in the Galaxy as well as the relative abundances of individual populations.

Since it is possible to estimate the attractive force due to population I, we subtract it from the total attraction and divide the remaining part between the disk population and population II. By varying the relative abundances of the two populations we attempt to arrive at a good agreement with the dynamical parameters. To this end we use the rotation curve of neutral hydrogen (Kwee *et al.*, 1954), Oort's constants, and the attraction in the z-direction.

The distribution of population I can be inferred from the studies of neutral hydrogen (Section I, B). The decrease of the densities in the outer regions is well expressed by the exponential function

$$0.495 \exp\left(-\frac{\varpi}{3.94}\right) n_{\mathrm{H}}\ \mathrm{cm}^{-3}, \tag{3.155}$$

where ϖ is in kpc. This function has at the sun's distance the logarithmic gradient (to the base 10) of $-0.11\ \mathrm{kpc}^{-1}$, a value given by Parenago (1950a) for population I. The distribution (3.155) does not reproduce the decrease of the density towards the center. The decrease does not show in other galaxies and it is not certain that it concerns population I as a whole. Besides, population I is not very important for the large scale dynamics of the Galaxy and the attraction at the sun is not sensitive to the amount of mass near the center.

The distribution of neutral hydrogen in the z-direction (Fig. 4) is well expressed by a superposition of two Gaussian curves which contain four parameters. The exponential distribution of Section III, C, 9 proves convenient in this respect since it fits the observations well and contains only two parameters, one of them already known from (3.155). Putting $a = 3.94$ kpc, $c/a = 1/60$, $c = 66$ pc, we get a curve which differs from the observations well within the scatter. It remains to estimate the density at the sun. The largest contribution to the total mass of population I comes probably from the diffuse matter. Adopting the value $0.030\ M_\odot/\mathrm{pc}^3$, we have

$$\begin{aligned} \rho &= \rho_0\, e^{-\eta} \\ \rho_0 &= 0.228\ M_\odot/\mathrm{pc}^3 \\ a &= 3.94\ \mathrm{kpc} \\ \varpi_\odot/a &= 2.03 \\ c/a &= 1/60. \end{aligned}$$

The distribution of population II is taken over from that of RR Lyrae stars—a typical subsystem of population II. The observations are shown in Fig. 5. It follows from what has been said about their distribution in Section I, B that confocal strata and a density proportional to the inverse nth power of the distance give an adequate representation. The steep gradient of the density near the sun indicates that $\epsilon < \varpi_\odot$. The exponent n follows from the value of the gradient. We have, from (3.129) at the sun's distance,

$$-n = \frac{\varpi}{\rho}\frac{d\rho}{d\varpi} = \varpi_\odot \frac{d \log \rho}{d\varpi}. \tag{3.156}$$

For $\varpi = 8$ kpc we have

$$\text{Mod } \frac{d \log \rho}{d\varpi} = -0.271, \qquad n = 5$$
$$= -0.326, \qquad n = 6$$

Good agreement with the observations is attained either for $n = 5$ and $\epsilon = \frac{2}{3}\varpi_\odot$, or for $n = 6$ and $\epsilon = \frac{5}{6}\varpi_\odot$. The choice between these two eventualities is effected by means of the observed flattening of the equidensity surfaces of globular clusters. The observed values (Schmidt, 1956) are in the second column of Table XIII. The first value is uncertain because it is difficult to determine the extent of a flattened surface in the galactic plane with a very small number of objects. The comparison refers therefore to the two remaining values only. The third and fourth columns give the corresponding values computed for ϵ given in the heading. Evidently, $\epsilon = \frac{5}{6}\varpi_\odot$ is a better approximation. It is not expedient to improve the agreement any further because the evidence from the globular clusters is not as strong as that from RR Lyrae stars. Thus, we have $n = 6$, $\epsilon = \frac{5}{6}\varpi_\odot$. The densities corresponding to these values are shown in Fig. 5 by full curves. The agreement is quite satisfactory. In particular, the densities in the z-direction at $\varpi = 6$ kpc, which are most reliable, are well reproduced. The only discordant observations refer to $\varpi = 13$ kpc. At those distances the aleatory fluctuations are very disturbing owing to the very small numbers of stars.

TABLE XIII

The Axial Ratio of the Equidensity Surfaces of Globular Clusters

ϖ (kpc)	Schmidt	$\epsilon = 5/6\,\varpi_\odot$	$\epsilon = 2/3\,\varpi_\odot$
4	0.24	—	—
9	0.60	0.67	0.81
16	0.84	0.91	0.94

Since an overwhelming majority of stars in the solar vicinity belong to the disk population, its distribution can be based on the densities in the z-direction of all stars fainter than 4.5^m determined by Oort (1936) (see Fig. 2). A small fraction of these stars belong to population II. By subtracting those we get the distribution of the pure disk population. Taking the logarithmic gradient of -0.23 kpc^{-1} from Table I we find a satisfactory fit for the exponential distribution with $a = 1.89$ kpc, $c/a = 1/16$. We leave the last free parameter, the central density, undetermined.

The influence of the relative abundances of the populations is made most conspicuous by varying the central densities of the disk population and population II while preserving the value of the attraction at the sun. Taking for the distance of the sun a rounded-off value resulting from several recent determinations, $\varpi_\odot = 8$ kpc, and the circular velocity at $\varpi_\odot$ of $O_\odot = 216$ km/sec (Kwee *et al.*, 1954), we find the attraction

$$Q = -\frac{O_\odot^2}{\varpi_\odot} = -5830 \text{ km}^2 \text{ sec}^{-2} \text{ kpc}^{-1}.$$

Subtracting the amount due to population I, 243 in the same units, we have 5587 km^2 sec^{-2} kpc^{-1} as the attraction of the disk population and population II together. This quantity was divided between the two populations in a varying ratio given in the first entry of Table XIV. Subsequently, the density at the sun, the mass, the potential at the sun, and other quantities have been determined for the three populations separately and are given in Table XIV.

TABLE XIV

ELEMENTS OF MODELS

Model	I	II	III	IV	V	VI	VII
	Contribution to the attraction (%)						
Population II	100	80	60	50	40	20	0
Disk population	0	20	40	50	60	80	100
	Density near the sun ($M_\odot$/pc^3)						
Population II	0.025	0.020	0.015	0.012	0.010	0.005	0.000
Disk population	0.000	0.020	0.039	0.049	0.058	0.078	0.098
Population I	0.030	0.030	0.030	0.030	0.030	0.030	0.030
Total	0.055	0.070	0.084	0.091	0.098	0.113	0.128

TABLE XIV *(continued)*

Model	I	II	III	IV	V	V	VII
	Mass ($10^{11} M_\odot$)						
Population II	1.090	0.873	0.654	0.545	0.436	0.218	0.000
Disk population	0.000	0.142	0.284	0.355	0.426	0.570	0.710
Population I	0.058	0.058	0.058	0.058	0.058	0.058	0.058
Total	1.148	1.073	0.996	0.958	0.920	0.846	0.768
	The potential at the sun (10^4 km^2/sec^2)						
Population II	5.600	4.475	3.360	2.800	2.240	1.120	0.000
Disk population	0.000	0.852	1.705	2.130	2.560	3.415	4.270
Population I	0.318	0.318	0.318	0.318	0.318	0.318	0.318
Total	5.918	5.645	5.373	5.248	5.118	4.853	4.588
Velocity of escape at $\varpi_\odot$	344	336	328	324	320	311	303
$W_e/O_\odot$	1.59	1.56	1.52	1.50	1.48	1.44	1.40
ϖ (kpc)	Circular velocities (km/sec)						
2	64	96	120	130	139	157	172
4	122	148	170	180	189	207	224
6	180	191	201	206	211	220	229
8	216	216	216	216	216	216	216
10	210	208	205	204	203	200	198
12	200	196	192	190	188	183	179
14	189	184	179	177	175	170	164
16	177	172	167	165	162	157	152
z (kpc)	Q_z at the sun (km^2 sec^{-2} kpc^{-1})						
0.2	488	663	839	926	1010	1190	1360
0.4	732	962	1190	1310	1420	1650	1880
0.8	1190	1420	1640	1750	1860	2090	2320
1.5	1850	1980	2110	2170	2240	2370	2500
3.0	2630	2580	2530	2490	2470	2410	2350
6.0	2770	2630	2490	2410	2340	2200	2050
10.0	2290	2100	1900	1800	1710	1520	1320
	Oort's constants (km sec^{-1} kpc^{-1})						
A					15.5	16.6	17.8
B					−11.5	−10.4	−9.2
$-A/B$					1.35	1.60	1.94

The circular velocities of model VI lie below the two measured values between 2 and 3 kpc. Farther from the center the maximum values are sufficiently well covered with the exception of one value at 6.6 kpc (Fig. 7) where the computed value lies 6 km/sec below the observed one. Model VII covers well the maximum values between 2 and 3 kpc and at 6.6 kpc, but the maximum at 5 kpc is surpassed by 10 km/sec. The hydrogen rotation curve points to a mass distribution between models VI and VII, closer to VI.

A further check is provided by Oort's constants. Computing the circular velocity at a number of points around $\varpi_\odot$, plotting against ϖ, and reading off $dO/d\varpi$ the values of A and B follow for each model (Table XIV). The deviations of the three quantities, A, B, A/B from the values derived from observations in Section I, B are smallest for a model between VI and VII.

The attraction in the z-direction does not give a clear answer. All models cover approximately the range of observations.

An attempt has been made to substitute the exponential distribution of the disk population by a parabolic density law. It was found impossible to represent the rotation curve with a model of this kind.

The actual distribution seems to correspond to a model between VI and VII, closer to VI. Model VI is to be regarded as an upper limit of the abundance of population II.

Assigning tentatively to model VII half the weight of model VI, we have the final elements

$$\begin{aligned} M &= 0.82 \times 10^{11}\, M_\odot \\ \rho_\odot &= 0.12\, M_\odot/\mathrm{pc}^3 \\ W_e &= 308 \text{ km/sec} \\ W_e/\Theta_\odot &= 1.43 \\ A &= +17 \text{ km/sec/kpc} \\ B &= -10 \text{ km/sec/kpc}. \end{aligned} \tag{3.157}$$

The densities in this model are shown in Fig. 42.

The abundances of the populations are accordingly

$$\begin{aligned} M_{\mathrm{II}} &= 0.14 \times 10^{11}\, M_\odot = 17\% \\ M_{\mathrm{disk}} &= 0.62 \times 10^{11}\, M_\odot = 76\% \\ M_{\mathrm{I}} &= 0.06 \times 10^{11}\, M_\odot = 7\%. \end{aligned} \tag{3.158}$$

The upper limit for population II leads to

$$\begin{aligned} M_{\mathrm{II}} &= 0.22 \times 10^{11}\, M_\odot = 26\% \\ M_{\mathrm{disk}} &= 0.57 \times 10^{11}\, M_\odot = 67\% \\ M_{\mathrm{I}} &= 0.06 \times 10^{11}\, M_\odot = 7\% \end{aligned} \tag{3.159}$$

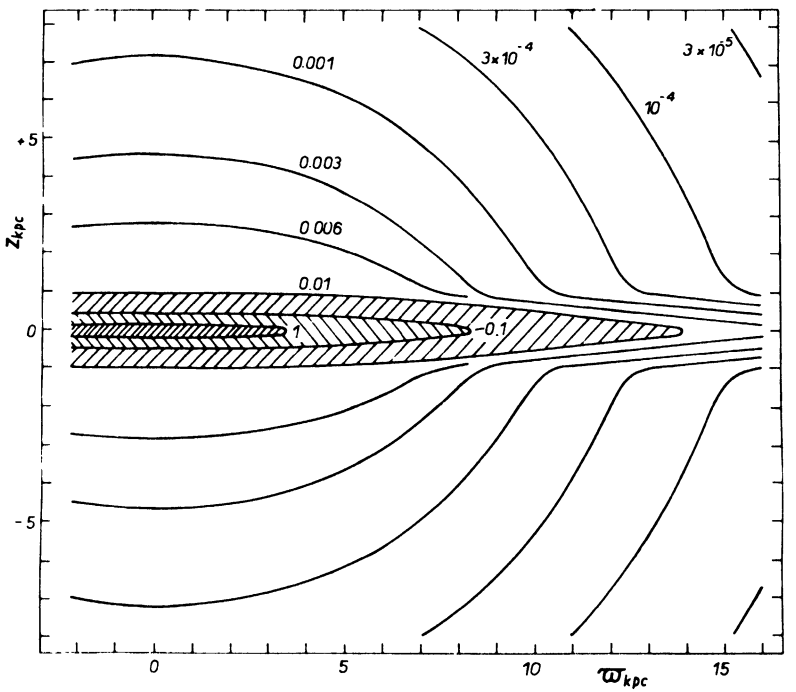


FIG. 42. Density in the composite model of Section III, E (in $M_\odot$ pc^3). The density in the edges is one order of magnitude only larger than the density in the intergalactic space. The density at the center is about 60 times that near the sun.

The values derived here for the upper limit of the abundance of population II agree well with the estimate by Oort (1959) based partly on direct observations and partly on Schmidt's model: Population II 23%, disk population 67%, population I 10%. However, the rotation curve of neutral hydrogen points to a somewhat lower abundance of population II (3.158).

The above model (3.157) shows that population II is by no means negligible in the large scale dynamics of the Galaxy because it is responsible for about 13% to 20% of the attraction at the sun. At the sun's distance 3% to 5% of the

mass is due to population II. On the other hand, the most important is the disk population which comprises at least two-thirds of the total mass of the Galaxy. Population I is not very important for the large scale distribution of the mass of the Galaxy.

Thus we have succeeded in constructing a model of the Galaxy which is relatively simple. As compared with Schmidt's model it has the advantage of having everywhere finite densities and a smaller number of parameters. The attraction differs very little from that by Schmidt (Fig. 36) with the exception of the central regions where it has a more plausible run.

The attraction of the model is lower than that of a mass point of the same mass in a region up to 7 kpc. At that distance the two curves cross and the attraction of the model converges to that of a point from above. This is a consequence of the flattening of the model.

F. *Conclusion*

It would be premature to attempt any classification of galaxies according to their distributions of mass. For this purpose a more detailed observational material would be required. We have seen how many and different observation data were necessary for the construction of a model of the Galaxy, and even in that case certain facts were missing. The observations of other galaxies are restricted to the rotation curve which is frequently known with insufficient accuracy. The rotation curve of NGC 5055 seems to be very good but we have a rather vague knowledge of the rotation curves of M 31 and M 33. An inspection of Fig. 8 shows that the optical observations by Babcock and by Mayall and the radio observations by van de Hulst *et al.* do not agree very well. The rotation curves of the models do not agree any better. Wyse and Mayall's curve follows closely Babcock's observations, the same as Schmidt's curve follows the radio observations. The curves by Lohmann, Takase, and Schwarzschild pass through normal points formed by different procedures from Mayall's radial velocities. It is impossible to say which of the models fits the observations better and there seems little sense in constructing other models before a better agreement of the observations is attained.

This is even more noticeable in the case of M 33. The probable errors of the normal points (Fig. 29) formed from the observations (Fig. 14) are so large that all the models thus far applied have been confirmed with about the same degree of reliability.

The mass of the Galaxy as well as of M 31 and M 33 has been determined several times. How do the individual results compare? A sample of the determinations was compiled in Tables XV to XVII. Table XV lists, besides the mass, the values of the distance and velocity of the sun which were used for

TABLE XV

DETERMINATIONS OF THE MASS OF THE GALAXY

Section	Authority	ϖ (kpc)	O (km/sec)	M ($10^{11} M_\odot$)	Remarks
II, B, 3	Idlis (1957)	7.2	233	1.0	Sphere
				0.8	Flat disk
II, B, 4	Lohmann (1953)	8.7	282	2.0	
II, C, 3	Kuzmin (1956)	7.0	211	1.04	
III, A, 1	Lohmann (1956)	8.5	277	2.50	
III, A, 2	Lohmann (1956)	8.5	277	2.6	
III, A, 4	Plaskett and Pearce (1936)	10.0	275	1.65	
	Gliese (1942)	8.6	300	2.5	
III, A, 5	ten Bruggencate (1943)	10.0	300	1.68	
	Oort (1941)	8.0	275	1.17	
	Safronov (1952)	7.2	233	0.8	
		8.0	250		
	Janák (1958)	8.2	216	0.83	
III, B, 1	Bucerius (1934)	10.0	278	2.4	
III, B, 3	Camm (1938)	9.8	195	1.77	
III, B, 5	Kuzmin (1952)	7.2	239	1.0	
	Kiladze (1958)	8.2	216	1.0	
	Brandt (1960a)	8.2	216	1.8	
III, C, 2	Perek (1951)	7.8	260	0.9	
III, C, 3	Schmidt (1956)	8.2	216	0.70	
III, C, 8	Perek (1954b)	8.0	—	1.1	
	Takase (1955)	8.2	216	0.68	
	Yasuda (1958)	8.2	216	0.73	
III, E	Perek (1959)	8.0	216	0.82	

deriving the mass. The first column gives the section of the present paper where the respective model can be found. At the same time it indicates the method used. The largest values come from methods using mass-point representations. On the whole it seems that the more refined models converge to a value slightly below 10^{11} M and probably the value will not change much if no drastic change of basic elements turns up.

The masses of M 31 and M 33 depend on their distances. Therefore Tables XVI and XVII list the distances and masses taken from the original papers and in the last but one column the mass reduced to the distance in the heading. We did not try to determine those distances; our only aim was to have a common basis for comparing the methods. It is a surprising fact that the values differ by less than a factor of 3. With regard to the vastly different assumptions and methods

TABLE XVI

DETERMINATIONS OF THE MASS OF M 31

Section	Authority	d (kpc)	M ($10^{11} M_\odot$)	M reduced to $d = 630$kpc ($10^{11} M_\odot$)	Remarks
II, B, 4	Lohmann (1954)	460	3.3	4.5	Bottlinger force law
III, A, 2	Poveda (1958)	500	2.0	2.5	Estimate based on spherical symmetry
III, A, 5	Babcock (1939)	210	1.02	3.1	Homogeneous spheroids
III, B, 3	Wyse and Mayall (1942)	210	0.95	2.9	Flat disk
	M. Schwarzschild (1954)	460	1.4	1.9	Flat disk, M/L const.
III, B, 5	Brandt (1960a)	600	3.7	3.9	Flat disk
III, C, 3	Schmidt (1957b)	630	3.38	3.4	Heterogeneous spheroids
III, C, 8	Takase (1957)	540	2.0	2.3	Heterogeneous spheroids

TABLE XVII

DETERMINATIONS OF THE MASS OF M 33

Section	Authority	d (kpc)	M ($10^9 M_\odot$)	M reduced to $d = 480$kpc ($10^9 M_\odot$)	Remarks
II, B, 4	Lohmann (1954)	440	10.0	11.0	Bottlinger force law
III, B, 3	Wyse and Mayall (1942)	220	1.7	3.7	Flat disk
	M. Schwarzschild (1954)	480	5.0	5.0	Flat disk; M/L = const.
	Aller (1942)	220	1.8	3.9	Flat disk
III, C, 8	Takase (1957)	540	4.4	3.9	Heterogeneous spheroid

this is quite a good result; particularly, as the range can be reduced by eliminating rough estimates or methods of a too hypothetical character.

In many respects the way is now open to future research. As regards the observations, we need a better knowledge of the distribution of the velocities. This can be expected only from systematic studies of radial velocities as done, e.g., by the objective prism method, successfully introduced by Fehrenbach (1955) and his collaborators. In this way it would be possible to remove selection effects

which entered the observations of stellar velocities by preferring stars with large proper motions. As soon as sufficiently extensive material is available, it will be possible to derive a frequency function of stellar velocities showing features which up to now have been hidden by the biased selection.

To increase the importance of direct determinations of the density, we need reliable criteria for classifying stars according to populations, and investigations of special objects which can be observed and identified at large distances. Accurate data are desirable in the neighborhood of the sun, the most important checking point.

It is most urgent that rotation curves of as many galaxies as are accessible to big telescopes should be measured; in particular, the measurement again of M 31 and M 33.

On the theoretical side of the problem, it seems that the possibilities offered by the ellipsoidal hypothesis were exhausted. It is necessary to look for more general frequency functions and to establish the conditions for the existence of self-gravitating systems.

There is a wide variety of models based upon special forms of density laws for which the expression for the potential is known. However, it is possible that new observations will require the study of other density laws which have not yet received attention.

List of Frequently Used Symbols

The quantities were expressed in units which usually appear in the computations. It was not found convenient to substitute numerical constants for expressions of the form km kpc etc. The logarithms are understood to the base e, unless stated otherwise.

A, B	Oort's constants in km $\sec^{-1}$ kpc^{-1}
G	Constant of gravity 4.3×10^{-6} $\mathrm{km}^2 \sec^{-2} \mathrm{kpc}\, M_\odot^{-1}$
M	Mass in units of the mass of the sun $M_\odot$
P	Potential per unit of mass in $\mathrm{km}^2 \sec^{-2}$
Q	Attraction upon a unit of mass in $\mathrm{km}^2 \sec^{-2} \mathrm{kpc}^{-1}$
V	Radial velocity in km $\sec^{-1}$
W	Space-velocity
W_e	Velocity of escape $= \sqrt{2P}$
m	A dimensionless variable, defined by Eq. (1.5), corresponding to a shell similar to the spheroid of semiaxes a and c
m_0	Shell passing through the attracted point
m_1	Boundary of a spheroidal model

w_{lk}	Functions of position defined by Eq. (1.12). For $\psi = \psi_0$ they reduce to constants v_{lk}
O_0	Systematic velocity
Θ_c	Circular velocity
ϕ	Error integral
Π, Θ, Z	Components of velocity in cylindrical coordinates
ϖ, ϑ, z	Cylindrical coordinates
ρ	Density of mass in $M_\odot$ pc^{-3}
ρ_c	Density at the center
ρ_0	Density at a specific distance
σ	Density of mass projected into a plane, in $M_\odot$ pc^{-2}
$\sigma_\varpi, \sigma_\vartheta, \sigma_z$	Dispersions of velocities in km/sec
ψ_0	$\sin \psi_0 = e$, where e is the numerical eccentricity of a meridian section of a spheroid
ψ	$\sin \psi$ is the numerical eccentricity of a meridian section of a spheroid confocal to the basic spheroid

References

Alexander, J. B., 1960. *Observatory* **80**, 110.
Aller, L. H., 1942. *Ap. J.* **95**, 48.
Baade, W., 1946. *P.A.S.P.* **58**, 249.
Babcock, H. W., 1939. *Lick Obs. Bull.* **19**, 41.
Berman, L., 1937. *Lick Obs. Bull.* **18**, 57.
Blaauw, A., 1960. *Trans. I.A.U.* **10**, 511.
Bottlinger, K. F., 1933. *Veröff. Sternw. Babelsb.* **10**, No. 2.
Brandt, J. C., 1960a. *Ap. J.* **131**, 293.
Brandt, J. C., 1960b. *Ap. J.* **131**, 553.
Bucerius, H., 1934. *A.N.* **259**, 365.
Burbidge, E. M., and Burbidge, G. R., 1959. *Ap. J.* **129**, 271.
Burbidge, E. M., and Burbidge, G. R., 1960. *Ap. J.* **132**, 30.
Burbidge, E. M., Burbidge, G. R., and Prendergast, K. H., 1959a. *Ap. J.* **130**, 26.
Burbidge, E. M., Burbidge, G. R., and Prendergast, K. H., 1959b. *Ap. J.* **130**, 739,
Burbidge, E. M., Burbidge, G. R., and Prendergast, K. H., 1960a. *Ap. J.* **131**, 282.
Burbidge, E. M., Burbidge, G. R., and Prendergast, K. H., 1960b. *Ap. J.* **131**, 549.
Camm, G. L., 1938. *M.N.R.A.S.* **99**, 71.
Camm, G. L., 1941. *M.N.R.A.S.* **101**, 195.
Chandrasekhar, S., 1942. "Principles of Stellar Dynamics." Univ. of Chicago Press, Chicago, Illinois.
Contopoulos, G., 1957. *Stockh. Obs. Ann.* **19**, No. 10.
Contopoulos, G., 1958. *Stockh. Obs. Ann.* **20**, No. 5.
Contopoulos, G., 1960. *Z. Ap.* **49**, 273.
Coutrez, R., 1949. *Ann. Obs. Belg.* 3 **4**, No. 3.
Coutrez, R., 1950. *Commun. Obs. Belg.* **15** and **18**.
de Vaucouleurs, G., 1960. *Ap. J.* **131**, 265.

Dzigvashvili, R. M., 1958. *Bull. Obs. Abastumani* **23**, 183.
Eddington, A. S., 1915. *M.N.R.A.S.* **76**, 37.
Eelsalu, H., 1958. *Publ. astr. Obs. Tartu* **33**, 153.
Eichhorn, H., 1957. *A.N.* **283**, 249.
Elvius, T., 1950. *Stockh. Obs. Ann.* **16**, No. 5.
Fehrenbach, C., 1955. *J. Observateurs* **38**, 165.
Freundlich, E. F., 1936. *Publ. Univ. Obs. Istanbul* **5**.
Fricke, W., 1952. *A.N.* **280**, 193.
Gaposchkin, S., 1955. *Peremennye Zvezdy* **10**, 337.
Gliese, W., 1942. *A.N.* **272**, 201.
Gliese, W., 1956. *Z. Ap.* **39**, 1.
Gliese, W., 1958. *Z. Ap.* **45**, 293.
Hanbury Brown, R., and Hazard, C., 1959. *M.N.R.A.S.* **119**, 297.
Heckmann, O., and Strassl, H., 1934. *Veröff. Univ. Sternw. Göttingen* **41** and **43**.
Hill, E. R., 1960. *B.A.N.* **15**, 1.
Hins, C. H., and Blaauw, A., 1948. *B.A.N.* **10**, 365.
Idlis, G. M., 1957. *Izv. astroph. Inst. Alma-Ata* **4**, 3.
Idlis, G. M., 1959a. *Izv. astroph. Inst. Alma-Ata* **8**, 24.
Idlis, G. M., 1959b. *A. Zh.* **36**, 85.
Janák, F., 1958. *B.A.C.* **9**, 139.
Jeans, J. H., 1922. *M.N.R.A.S.* **82**, 123.
Kahn, F. D., and Woltjer, L., 1959. *Ap. J.* **130**, 705.
Kerr, F. J., and de Vaucouleurs, G., 1955. *Aust. J. Phys.* **8**, 508.
Kerr, F. J., and de Vaucouleurs, G., 1956. *Aust. J. Phys.* **9**, 90.
Kiladze, R. J., 1958. *Bull. Obs. Abastumani* **22**, 125.
Kukarkin, B. V., 1949. "Investigation of the Structure and Evolution of Stellar Systems Based on the Study of Variable Stars" (in Russian). State Publ. House for Tech. and Theoret. Literature, Moscow.
Kurth, R., 1949. *Z. Ap.* **26**, 100.
Kuzmin, G. G., 1952. *Publ. astr. Obs. Tartu* **32**, 211.
Kuzmin, G. G., 1955. *Publ. astr. Obs. Tartu* **33**, 3.
Kuzmin, G. G., 1956. *A. Zh.* **33**, 27.
Kwee, K. K., Muller, C. A., and Westerhout, G., 1954. *B.A.N.* **12**, 211.
Lallemand, A., Duchesne, M., and Walker, M. F., 1960a. *P.A.S.P.* **72**, 76
Lallemand, A., Duchesne, M., and Walker, M. F., 1960b. *P.A.S.P.* **72**, 268.
Lense, J., 1917. *A.N.* **204**, 17.
Lindblad, B., 1959. *In* "Handbuch der Physik" (S. Flügge, ed.), Vol. 53, p. 21. Springer, Berlin.
Lindblad, B., and Langebartel, R. G., 1953. *Stockh. Obs. Ann.* **17**, No. 6
Lindblad, P. O., 1960. *Stockh. Obs. Ann.* **21**, No. 4.
Lohmann, W., 1953. *Z. Ap.* **33**, 186.
Lohmann, W., 1954. *Z. Ap.* **35**, 159.
Lohmann, W., 1956. *Mitt. Recheninst. Heidelberg* [A], No. 2
Makemson, M. W., 1940. *A. J.* **48**, 23.
Mayall, N. U., 1950. *Publ. Univ. Obs. Mich.* **10**, 19.
Mayall, N. U., and Aller, L. H., 1942. *Ap. J.* **95**, 5.
Mikisha, A. M., and Tsitsin, F. A., 1957. *A. Zh.* **34**, 45.
Mills, B. Y., 1959. *P.A.S.P.* **71**, 267.
Mohr, J. M., 1933. *B.A.* **9**, 1.

Mohr, J. M., and Mayer, P., 1957. *B.A.C.* **8**, 142.
Mohr, J. M., Mayer, P., and Štohl, J., 1957. *B.A.C.* **8**, 5.
Morgan, H. R., and Oort, J. H., 1951. *B.A.N.* **11**, 379.
Münch, G., 1959. *P.A.S.P.* **71**, 101.
Münch, G., 1960. *Ap. J.* **131**, 250.
Münch, G., and Münch, L., 1960. *Ap. J.* **131**, 253.
O'Connell, D. J. K., 1958. *Ric. astr.* **5**, 533.
Ogorodnikov, K. F., 1958. *A. Zh.* **35**, 408.
Oort, J. H., 1927. *B.A.N.* **4**, 79 and 91.
Oort, J. H., 1928. *B.A.N.* **4**, 269.
Oort, J. H., 1936. *B.A.N.* **8**, 75.
Oort, J. H., 1940. *Ap. J.* **91**, 273.
Oort, J. H., 1941. *B.A.N.* **9**, 193.
Oort, J. H., 1959. *I.A.U. Symp.* No. 9, 14.
Oort, J. H., 1960. *B.A.N.* **15**, 45.
Parenago, P., 1947. *A. Zh.* **24**, 178.
Parenago, P., 1948. *Usp. astr. Nauk* **4**, 69.
Parenago, P., 1950a. *A. Zh.* **27**, 150.
Parenago, P., 1950b. *A. Zh.* **27**, 329.
Parenago, P., 1952. *A. Zh.* **29**, 245.
Parenago, P., 1954. *A. Zh.* **31**, 425.
Parenago, P., 1955. *A. Zh.* **32**, 226.
Parenago, P., 1959. *A. Zh.* **36**, 179.
Pavlovskaya, E. D., 1957. *A. Zh.* **34**, 956.
Perek, L., 1948. *Contr. astr. Inst. Masaryk Univ.* **1**, No. 6.
Perek, L., 1950. *B.A.C.* **2**, 75.
Perek, L., 1951. *Contr. astr. Inst. Masaryk Univ.* **1**, No. 8.
Perek, L., 1954a. *Contr. astr. Inst. Masaryk Univ.* **1**, No. 12.
Perek, L., 1954b. *Contr. astr. Inst. Masaryk Univ.* **1**, No. 13.
Perek, L., 1956. *A.N.* **283**, 213.
Perek, L., 1958a. *B.A.C.* **9**, 208.
Perek, L., 1958b. *B.A.C.* **9**, 212.
Perek, L., 1959. *B.A.C.* **10**, 15.
Perek, L., 1961. Submitted in July, 1959, for publication in "Vistas in Astronomy" Vol. V, p. 000. Pergamon Press, New York.
Petri, W., 1958. *Mitt. A. G.* 1957 *I*, 47.
Pilowski, K., 1959. "Lokaler Geschwindigkeitszustand der Sterne." Technische Hochschule, Hannover.
Plaskett, J. S., and Pearce, J. A., 1936. *Publ. Dom. Astroph. Obs. Victoria*, **5**, 241.
Poveda, A., 1958. *Bol. Obs. Ton. y Tac.* **17**, 3.
Routh, E. J., 1902. "Analytical Statics," 2nd ed., Vol. 2, p. 115. Cambridge Univ. Press, London and New York.
Rugoor, G. W., and Oort, J. H., 1959. *I.A.U. Symp.* No. 9, 416.
Safronov, V. S., 1952. *A. Zh.* **29**, 198.
Schilt, J., 1950. *A. J.* **55**, 97.
Schmidt, M., 1956. *B.A.N.* **13**, 15.
Schmidt, M., 1957a. *B.A.N.* **13**, 247.
Schmidt, M., 1957b. *B.A.N.* **14**, 17.
Schürer, M., 1942. *A.N.* **273**, 230.

Schwarzschild, K., 1907. *Göttinger Nachr.* p. 614.
Schwarzschild, M., 1954. *A. J.* **59**, 273.
Shklovski, I. S., 1951. *A. Zh.* **29**, 418.
Smak, J. M., 1958. *Postepy astr. Cracow* **6**, 15.
Takase, B., 1955. *Publ. astr. Soc. Japan* **7**, 201.
Takase, B., 1957. *Publ. astr. Soc. Japan* **9**, 16.
ten Bruggencate, P., 1943. *Veröff. Univ. Sternw. Göttingen* **75**.
ten Bruggencate, P., 1947. *Veröff. Univ. Sternw. Göttingen* **88**.
Torgård, I., 1956. *Medd. Lunds astr. Obs.* [2] **133**.
Trumpler, R. J., and Weaver, H. F., 1951. *P.A.S.P.* **63**, 172.
van Albada, G. B., 1952. *Contr. Bosscha Obs.* **1**.
van de Hulst, H. C., Raimond, E., and van Woerden, H., 1957. *B.A.N.* **14**, 1.
van Rhijn, P. J., 1960. *Publ. astr. Lab. Groningen* **61**.
Vetešník, M., 1959. *B.A.C.* **10**, 81.
Volders, L., 1959. *B.A.N.* **14**, 323.
von Hoerner, S., 1955. *Z. Ap.* **35**, 255.
Wayman, P., 1959. *M.N.R.A.S.* **119**, 34.
Westerhout, G., 1957. *B.A.N.* **13**, 219.
Westerhout, G., 1958. *B.A.N.* **14**, 215.
Woolley, R. v.d. R., 1957. *M.N.R.A.S.* **117**, 198.
Wyse, A. B., and Mayall, N. U., 1942. *Ap. J.* **95**, 20.
Yasuda, H., 1958. *Publ. astr. Soc. Japan* **10**, 165.
Zagar, F., 1957. *Contr. Obs. Milano-Merate* [N.S.] **101**.

Polarization of Starlight

K. SERKOWSKI
Warsaw University Observatory,
*Warsaw, Poland**

I. Introduction 290
II. Stokes Parameters 291
A. Definition 291
B. Properties of Stokes Parameters 293
C. Transformation Matrix for the Stokes Parameters 294
III. Optical Devices for Analyzing Polarized Light 295
A. Polarizer 295
B. Retardation Plate 296
C. Lyot's Depolarizer 297
IV. Techniques of Polarization Measurements 298
A. Plane Polarized Component 298
B. Circularly Polarized Component 301
C. Polarization Parameters Expressed in Magnitudes 302
D. Instrumental Polarization 305
E. Photographic Polarization Measurements 307
V. Polarization of Light by Aligned Dust Grains 307
A. Changes of Stokes Parameters Along the Optical Path 307
B. Extinction Cross Sections 311
C. Polarizing Properties of Interstellar Dust 313
VI. Dependence of Interstellar Polarization on Galactic Coordinates . . 315
A. Theoretical Mean Values of Stokes Parameters 315
B. Dispersion of Stokes Parameters 319
C. Observational Results 324
D. Polarization and Extinction 329
VII. Alignment Mechanisms 332
A. Collisions of Dust Grains 332
B. Alignment Due to Paramagnetic Absorption 336
C. Other Aligning Mechanisms 342
VIII. Fluctuations of Polarization in Small Areas of the Sky 343
A. Correlation between Polarization and Extinction in Open Clusters. 343
B. Applications of Autocorrelation Analysis 345
C. Estimates of Magnetic Flux Density from Polarization Data. . . 347
List of Symbols 348
Acknowledgments 350
References 350

* Present address: Lowell Observatory, Flagstaff, Arizona.

I
INTRODUCTION

All of our information about the stars is derived from their radiation which should, of course, be investigated in all possible respects. The parallel bundle of stellar radiation which reaches us can be completely described by a few characteristics, namely: (a) the direction from which the radiation is coming, described, e.g., by the equatorial coordinates α, δ; (b) the intensity of radiation, represented as a function of wavelength, $I(\lambda)$; (c) the three Stokes parameters Q, U, V, describing the state of polarization (their definitions will be given in the next section), represented also as a function of wavelength, $Q(\lambda)$, $U(\lambda)$, $V(\lambda)$.

As may be seen from this discussion, if we ignore the polarization of starlight, we neglect a very large portion of the total information. It is therefore surprising that only in 1948 was the discovery made that the light of the majority of stars is partially plane polarized. This discovery was made by J. S. Hall (1949) and by W. A. Hiltner (1949a).

It seems worthwhile to stress that even now, after the plane polarization described by the Stokes parameters Q and U has been measured for more than 3000 stars, we know practically nothing about the Stokes parameter V. The parameter V, which describes to what extent the stellar light is circularly or elliptically polarized, has been measured only for Zeeman components of the absorption lines in stellar spectra (this effect will not be discussed in this article). The parameter V for the radiation in a wide range of the optical spectrum was measured only for five or six stars (Hall and Mikesell, 1949; Dombrovski , 1953; and Serkowski, 1961) and not with very high accuracy. No circularly polarized component was found for these stars, and so we can say that the Stokes parameter V is presently the *terra incognita.*

In 1946 Chandrasekhar investigated theoretically the atmospheres of early-type stars in which electron scattering is the source of opacity. He found that nearly 12 percent of light emanating from a given point at the stellar limb may be plane polarized with the electric vector parallel to the limb. He predicted that this polarization might be detected when the early-type component of an eclipsing binary is occulted by the late-type companion.

Some evidence of polarization of this kind, though not conclusive, was shown by the photographic measurements of eclipsing binaries U Sagittae and RY Persei by Janssen (1946) and Hiltner (1947). The photoelectric polarization measurements of eclipsing binaries undertaken by Hall and Hiltner led to the discovery that the eclipsing binary CQ Cephei showed constant polarization independent of phase and that the light of nearby stars is also polarized. Polarization of comparison stars was also found by Dombrovskii (1949) who was investigating photographically the polarization of eclipsing binaries. The

accuracy of his measurements was not, however, high enough to consider his results as incontestable.[1]

Further polarization measurements made independently by Hall and Hiltner proved that the light of the majority of distant stars is partially plane polarized. Polarization is of interstellar origin because it is independent of the physical properties of a star and is correlated with interstellar absorption lines and bands in stellar spectra. The ratio of the amount of polarization to extinction never exceeds some maximum value depending on wavelength.

Polarization is largest for distant stars in low galactic latitudes and in those longitudes where we are looking perpendicular to the galactic spiral arms. In these directions the planes of vibration of the electric vector deviate only slightly from the galactic plane. On the other hand, in directions parallel to the galactic spiral arm the polarization is small and the planes of vibration are distributed at random.

It seems highly probable that polarization is produced by scattering of stellar light by elongated interstellar dust grains aligned by galactic magnetic fields.

II

STOKES PARAMETERS

A. *Definition*

Polarized light is most conveniently described by means of four parameters, I, Q, U, V, which were introduced by Sir George Stokes in 1852.

We shall consider a so called simple electromagnetic wave, i.e., the wave corresponding to single photon. Let $\mathbf{l}$ and $\mathbf{r}$ be the two mutually perpendicular vectors in a fixed plane perpendicular to the direction of propagation of this simple wave. They are chosen so that $\mathbf{r} \times \mathbf{l}$ is in the direction of propagation and $\mathbf{l}$ is lying in the plane of meridian of equatorial coordinate system and directed towards the northern hemisphere.[2] The components of the electric vector $\mathbf{E}$ of a simple wave in some fixed point of space may be presented as a function of time t of the form (cf. van de Hulst, 1957)

$$E_l = E_{l0} \sin(\omega t - \epsilon_l), \tag{1}$$

$$E_r = E_{r0} \sin(\omega t - \epsilon_r), \tag{2}$$

where ω is angular frequency and E_{l0}, E_{r0}, ϵ_l, and ϵ_r are constants.

[1] Dombrovski (1949) found that if the stars U Sge, BD + 18°4043 and BD + 19°3981 are assumed to be unpolarized, the degree of polarization for the star BD + 19°3974 is 10 percent. The photoelectric measurements made recently at Lowell Observatory show that for not one of these four stars does the degree of polarization exceed 0.6 percent.

[2] The letters *l* and *r* are the last letters of the words *parallel* and *perpendicular*.

It is obvious from Eq. (1) and (2) that the end of the vector **E** outlines an ellipse in the *l–r* plane (Fig. 1). This means that the plane wave is, in general, elliptically polarized.

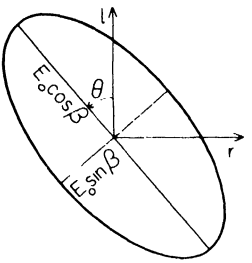


FIG. 1. Parameters defining the polarization of a simple wave. The light is coming toward us and l is lying in the plane of meridian of the equatorial coordinate system and directed towards the northern hemisphere.

We shall denote by θ the angle[3] which the long axis of an ellipse makes to the direction l, and by β an angle whose tangent is the ratio of the axes of the ellipse. The *Stokes parameters* describing the simple wave will now be defined by the equations (cf. Chandrasekhar, 1950)

$$I = E_{l0}^2 + E_{r0}^2 = (Q^2 + U^2 + V^2)^{1/2}; \tag{3}$$

$$Q = E_{l0}^2 - E_{r0}^2 = I \cos 2\beta \cos 2\theta; \tag{4}$$

$$U = -2E_{l0}E_{r0} \cos(\epsilon_l - \epsilon_r) = I \cos 2\beta \sin 2\theta; \tag{5}$$

$$V = 2E_{l0}E_{r0} \sin(\epsilon_l - \epsilon_r) = I \sin 2\beta. \tag{6}$$

The Stokes parameter I is simply the intensity of the beam. If we choose another system of coordinates, I and β remain the same, only θ changes; hence $I, Q^2 + U^2$, and V are invariants with respect to the change of the coordinate system.

Actual light is the superposition of many simple waves coming in very rapid succession. If there are no correlations between the phase differences $\epsilon_l - \epsilon_r$ and the amplitude ratios E_{l0}/E_{r0} for these simple waves, we are dealing with natural light. If such correllations do exist, the light is, in general, partially elliptically polarized.

[3] The angle θ is counted in the opposite direction compared to that of the angle χ of Chandrasekhar (1950) and van de Hulst (1957); consequently our Stokes parameter U differs by sign as compared to the parameter denoted by this letter by the above authors. This change is made to be in accordance with the direction in which position angles are counted in astronomy.

B. *Properties of Stokes Parameters*

The Stokes parameters describing the actual light are sums of the corresponding Stokes parameters describing the "simple waves" of which the light is consisted. In general, the Stokes parameters characterizing the light beam being a mixture of several incoherent light beams are the sums of the respective Stokes parameters characterizing these component beams.

From this *additivity* of the Stokes parameters results the principle of optical equivalence. This principle states that it is impossible by any optical analysis to distinguish between two beams characterized by the same set of Stokes parameters.

The most general mixture of light can be regarded as partially elliptically polarized light. Such light, described by the Stokes parameters I, Q, U, and V, may always be decomposed into two beams:

1. Natural, unpolarized light of intensity $I - (Q^2 + U^2 + V^2)^{1/2}$; for this beam $Q = U = V = 0$,
2. Fully elliptically polarized light of intensity $(Q^2 + U^2 + V^2)^{1/2}$.

If the intensity of this last beam is much smaller than that of the first one, the light may be decomposed into three beams, namely:

1. Natural light of intensity $I - (Q^2 + U^2)^{1/2} - |V|$.
2. Fully plane polarized light of intensity $(Q^2 + U^2)^{1/2}$, for which $V = 0$.
3. Fully circularly polarized light of intensity $|V|$ for which $Q = U = 0$; $V > 0$ corresponds to *right-handed* circular polarization, $V < 0$ to *left-handed* polarization.

The ratio

$$P = (Q^2 + U^2)^{1/2}/I \tag{7}$$

is called the *degree of polarization* while the ratio

$$P_c = |V|/I \tag{8}$$

is called the *degree of ellipticity*. The fully plane polarized light is characterized by $P = 1$, and fully circularly polarized light by $P_c = 1$.

The partially plane polarized light (for which $V = 0$) may be decomposed into two beams of fully plane-polarized light. We shall denote by $I_{\max}$ the intensity of the plane polarized component for which the electric vector makes an angle θ to the direction 1, and by $I_{\min}$ the intensity of component for which this angle is $\theta + 90°$. Now the Stokes parameters for our partially plane polarized beam are (cf. Behr, 1959b)

$$I = I_{\max} + I_{\min}, \tag{9}$$

$$Q = (I_{\max} - I_{\min}) \cos 2\theta = P I \cos 2\theta, \tag{10}$$

$$U = (I_{\max} - I_{\min}) \sin 2\theta = P I \sin 2\theta. \tag{11}$$

C. *Transformation Matrix for the Stokes Parameters*

Let us consider, following van de Hulst (1957), the simple wave with arbitrary polarization passing through an arbitrary optical instrument which produces no incoherent effects so that a simple wave also emerges. Since in optical instruments it is not possible (as, e.g., in radio waves) to introduce nonlinear effects, the field components of the outgoing wave, E_l' and E_r', are connected with those of ingoing wave, E_l and E_r, by the linear relations

$$E_l' = A_2 E_l + A_3 E_r, \tag{12}$$

$$E_r' = A_4 E_l + A_1 E_r, \tag{13}$$

where A_i are constants, characterizing the optical instrument.

We shall assume that neither circular birefringence (i.e., rotation of the plane of polarization) nor circular dichroism (i.e., different extinction coefficients for left-handedly and right-handedly polarized light) occurs. Furthermore we shall assume that the principal axes of a tensor describing the anisotropy (if any) of the optical instrument are parallel to the directions **l** and **r**. On these assumptions $A_3 = A_4 = 0$. Denoting by a_i and b_i the real and imaginary parts of coefficients A_i, respectively, we find that Eqs. (12) and (13) take the form

$$E_l' = (a_2 - ib_2) E_l, \tag{14}$$

$$E_r' = (a_1 - ib_1) E_r. \tag{15}$$

Substituting these equations into those relating the Stokes parameters to the field components, van de Hulst (1957) obtains the following transformation equation for the Stokes parameters, expressed in matrix form:

$$\begin{Bmatrix} I' \\ Q' \\ U' \\ V' \end{Bmatrix} = \begin{Bmatrix} \frac{1}{2}(a_2^2 + a_1^2 + b_2^2 + b_1^2) & \frac{1}{2}(a_2^2 - a_1^2 + b_2^2 - b_1^2) & 0 & 0 \\ \frac{1}{2}(a_2^2 - a_1^2 + b_2^2 - b_1^2) & \frac{1}{2}(a_2^2 + a_1^2 + b_2^2 + b_1^2) & 0 & 0 \\ 0 & 0 & a_1a_2 + b_1b_2 & a_1b_2 - a_2b_1 \\ 0 & 0 & a_2b_1 - a_1b_2 & a_1a_2 + b_1b_2 \end{Bmatrix} \cdot \begin{Bmatrix} I \\ Q \\ U \\ V \end{Bmatrix}. \tag{16}$$

Here the primed Stokes parameters are those characterizing the light leaving the optical instrument; the unprimed ones are those for the incoming light.

III

OPTICAL DEVICES FOR ANALYZING POLARIZED LIGHT

A. *Polarizer*

An ideal polarizer transmitting only the vibrations in the plane determined by the direction 1 is characterized by the coefficients $A_2 = 1$ and $A_1 = A_3 = A_4 = 0$ in Eqs. (12) and (13). This means that the terms in parentheses in matrix (16) are equal to 1 and that the remaining terms vanish.

When the system of coordinates shown in Fig. 1 is rotated counterclockwise by an angle φ, only the Stokes parameters Q and U are changed and the transformation equation is (cf. Chandrasekhar, 1950)

$$\begin{Vmatrix} I' \\ Q' \\ U' \\ V' \end{Vmatrix} = \begin{Vmatrix} 1 & 0 & 0 & 0 \\ 0 & \cos 2\varphi & \sin 2\varphi & 0 \\ 0 & -\sin 2\varphi & \cos 2\varphi & 0 \\ 0 & 0 & 0 & 1 \end{Vmatrix} \cdot \begin{Vmatrix} I \\ Q \\ U \\ V \end{Vmatrix}. \tag{17}$$

Hence, the transformation of the Stokes parameters accompanying the passage of light through the ideal polarizer transmitting only the vibrations in the plane making an angle φ (measured counterclockwise) with direction 1 is described by the equation

$$\begin{Vmatrix} I' \\ Q' \\ U' \\ V' \end{Vmatrix} = \frac{1}{2} \begin{Vmatrix} 1 & \cos 2\varphi & \sin 2\varphi & 0 \\ \cos 2\varphi & \cos^2 2\varphi & \cos 2\varphi \sin 2\varphi & 0 \\ \sin 2\varphi & \cos 2\varphi \sin 2\varphi & \sin^2 2\varphi & 0 \\ 0 & 0 & 0 & 0 \end{Vmatrix} \cdot \begin{Vmatrix} I \\ Q \\ U \\ V \end{Vmatrix}. \tag{18}$$

The matrix on the right side of this equation was obtained by multiplying the matrix for a polarizer for which $\varphi = 0$ by matrix (17), and then multiplying the matrix (17) in which φ is replaced by $-\varphi$ by the matrix resulting from the first multiplication.

The polarizer characterized by the matrix (18) transmits without change only the plane-polarized light described by the Stokes parameters $Q = I \cos 2\varphi$ and $U = I \sin 2\varphi$.

The Glan-Thomson prism or simple plane-parallel calcite plate with surfaces parallel to natural cleavage planes may be considered as an almost ideal polarizer if the incident light forms a parallel bundle perpendicular to the front surface

of the crystal. If, however, this last condition is not fulfilled the light is not polarized completely and the plane of polarization depends on the direction of incident light (Brandmüller and Hoffmeister, 1953).

The Polaroid sheets often used in astronomical applications are good polarizers only in a limited range of spectrum. For that reason it seems worthwhile to consider the properties of an imperfect polarizer.

Let us consider two identical polarizers. We shall denote by I the intensity of incident natural light, by IT_l its intensity after passing two polarizers oriented in parallel, by IT_r that after passing two perpendicularly oriented polarizers. If the incident light is natural, the light leaving the single polarizer is partially plane polarized with the plane of vibration making an angle φ with direction 1, and with degree of polarization

$$P_0 = \left(\frac{T_l - T_r}{T_l + T_r}\right)^{1/2}. \tag{19}$$

The transformation equation for such an imperfect polarizer is

$$\begin{pmatrix} I' \\ Q' \\ U' \\ V' \end{pmatrix} = \left(\frac{T_l + T_r}{2}\right)^{1/2} \begin{pmatrix} 1 & P_0 \cos 2\varphi & P_0 \sin 2\varphi & 0 \\ P_0 \cos 2\varphi & 1 - P_0 \sin^2 2\varphi & P_0 \cos 2\varphi \sin 2\varphi & 0 \\ P_0 \sin 2\varphi & P_0 \cos 2\varphi \sin 2\varphi & 1 - P_0 \cos^2 2\varphi & 0 \\ 0 & 0 & 0 & 1 - P_0 \end{pmatrix} \cdot \begin{pmatrix} I \\ Q \\ U \\ V \end{pmatrix}. \tag{20}$$

B. *Retardation Plate*

The plane-parallel plate obtained by splitting a crystal of mica or by cutting a calcite or quartz crystal parallel to its optical axis introduces the phase difference

$$\tau = \epsilon_l - \epsilon_r \tag{21}$$

between the components of electric vector vibrating in planes determined by directions 1 and r. This relative phase retardation depends on the orientation of the plate. We shall assume that the plate is oriented so as to introduce maximum phase difference τ. The coefficients in Eqs. (12) and (13) corresponding to passage of light through such a relative phase retardation plate (neglecting extinction of light in the plate) are $A_1 = \exp(+i\tau/2)$, $A_2 = \exp(-i\tau/2)$, $A_3 = A_4 = 0$, and hence the matrix (16) takes form (cf. van de Hulst, 1957)

$$\begin{pmatrix} I' \\ Q' \\ U' \\ V' \end{pmatrix} = \begin{pmatrix} 1 & 0 & 0 & 0 \\ 0 & 1 & 0 & 0 \\ 0 & 0 & \cos\tau & \sin\tau \\ 0 & 0 & -\sin\tau & \cos\tau \end{pmatrix} \cdot \begin{pmatrix} I \\ Q \\ U \\ V \end{pmatrix}. \tag{22}$$

The special case of the retardation plate is the quarter-wave plate for which $\tau = 90°$. The quarter-wave plate oriented as described above, transforms the fully circularly polarized light, for which $I = V$, into the fully plane-polarized light for which $I = U$.

The transformation matrix corresponding to the retardation plate rotated counterclockwise by an angle ψ relative to that described by Eq. (22) is

$$\begin{pmatrix} I' \\ Q' \\ U' \\ V' \end{pmatrix} = \begin{pmatrix} 1 & 0 & 0 & 0 \\ 0 & \cos^2 2\psi + \sin^2 2\psi \cos\tau & (1-\cos\tau)\cos 2\psi \sin 2\psi & \sin 2\psi \sin\tau \\ 0 & (1-\cos\tau)\cos 2\psi \sin 2\psi & \sin^2 2\psi + \cos^2 2\psi \cos\tau & \cos 2\psi \sin\tau \\ 0 & \sin 2\psi \sin\tau & -\cos 2\psi \sin\tau & \cos\tau \end{pmatrix} \cdot \begin{pmatrix} I \\ Q \\ U \\ V \end{pmatrix}. \tag{23}$$

This matrix is obtained by the similar procedure as that used for obtaining the matrix on the right side of Eq. (18).

C. *Lyot's Depolarizer*

Polarization measurements are greatly facilitated by the use of the depolarizer first constructed by Lyot (1929); its properties are discussed by Billings (1951). This device changes the arbitrarily polarized light into natural light. It consists of two parallel relative phase retardation plates, one of them introducing twice as much retardation as the other. Their optical axes should make an angle of either 45° or 135° with one another. The larger the relative phase difference introduced by each of these plates, the better the depolarizer.

The transformation matrix for the Lyot's depolarizer can be obtained by multiplying the matrix on the right side of Eq. (22) by that in Eq. (23) in which $\psi = 45°$ is inserted and τ is replaced by 2τ. The transformation matrix obtained in this way leads to the following relations between the Stokes parameters, I, Q, U, and V for the incident light and the parameters I', Q', U', and V' characterizing the light leaving the Lyot depolarizer:

$$I' = I, \tag{24}$$

$$Q' = Q\cos 2\tau - V\sin 2\tau, \tag{25}$$

$$U' = Q\sin\tau\sin 2\tau + U\cos\tau + V\sin\tau\cos 2\tau, \tag{26}$$

$$V' = -Q\cos\tau\sin 2\tau - U\sin\tau + V\cos\tau\cos 2\tau. \tag{27}$$

We shall assume for simplicity that the light transmitted through the depolarizer has spectral energy density of the form

$$E(k) = \frac{1}{\sigma(2\pi)^{1/2}} \exp\left[-\frac{(k-k_0)^2}{2\sigma^2}\right]; \qquad k_0 = \text{const.}, \tag{28}$$

where k is the wave number, and σ is the "half-width" of the transmission band expressed in wave numbers.

If s is the thickness of the thinner retardation plate introducing the phase difference τ and n_0, n_e are coefficients of refraction for ordinary and extraordinary rays (their difference assumed to be independent of wavelength), we have

$$|\tau| = 360^\circ |n_e - n_0| sk. \tag{29}$$

Substituting the value of τ given by Eq. (29) into Eqs. (25) – (27) and averaging them over the wave number k, making use of spectral density (28), we obtain the approximate estimates

$$|\overline{Q'}| < (|Q| + |V|) \exp\{-2[2\pi(n_e - n_0) s\sigma]^2\}, \tag{30}$$

$$|\overline{U'}| < (|\tfrac{1}{2}Q + U| + \tfrac{1}{2}|V|) \exp\{-2[\pi(n_e - n_0) s\sigma]^2\}, \tag{31}$$

$$|\overline{V'}| < (|\tfrac{1}{2}Q + U| + \tfrac{1}{2}|V|) \exp\{-2[\pi(n_e - n_0) s\sigma]^2\}. \tag{32}$$

Let us take as an example the depolarizer made of two quartz plates cut parallel to their optical axes. One plate is 1 mm thick and the other is twice this thickness. We shall suppose that the incident light is partially plane polarized and that peak of the transmission band is at 4500 A; the "half-width" of the transmission band will be supposed to be $\perp$ 100 A (i.e., $\sigma = 500$). For these wavelengths quartz is characterized by $n_e - n_0 = 0.0094$ and hence the degree of polarization of the light beam passing through the depolarizer diminishes by a factor of at least 70. The depolarizer may be several orders of magnitude less effective if the transmission band, however wide, has very sharp cutoff. The monochromatic depolarizer was described by Billings (1951).

IV

TECHNIQUES OF POLARIZATION MEASUREMENTS

A. *Plane Polarized Component*

To describe the partially plane polarized light we need to measure the ratios of the Stokes parameters Q/I and U/I. To accomplish this the light should pass through the polarizer (which in this case we call the analyzer); the intensity

of light leaving this polarizer should be measured for at least three position angles of the polarizer. In practice it is more convenient to measure this intensity for a greater number of position angles, preferably eight. As results from Eq. (20) the intensity corresponding to the position angle φ of the analyzer is

$$I'(\varphi) = [(T_l + T_r)/2]^{1/2} (I + QP_0 \cos 2\varphi + UP_0 \sin 2\varphi). \tag{33}$$

Hence we can easily find

$$\frac{Q}{I} = \frac{1}{P_0} \cdot \frac{I'(0^\circ) - I'(90^\circ)}{I'(0^\circ) + I'(90^\circ)} = \frac{1}{P_0} \cdot \frac{I'(180^\circ) - I'(270^\circ)}{I'(180^\circ) + I'(270^\circ)}, \tag{34}$$

$$\frac{U}{I} = \frac{1}{P_0} \cdot \frac{I'(45^\circ) - I'(90^\circ)}{I'(45^\circ) + I'(90^\circ)} = \frac{1}{P_0} \cdot \frac{I'(225^\circ) - I'(315^\circ)}{I'(225^\circ) + I'(315^\circ)}, \tag{35}$$

The parameter P_0 defined by the Eq. (19) equals unity for the ideal analyzer. For an imperfect analyzer it depends on the wavelength and should be determined separately for stars of different colors.

The presently used photomultiplier tubes have two disadvantages which affect the polarization measurements. First, their sensitivity is different for differently polarized light, even for tubes with "end-on" cathodes. This disadvantage can be avoided by inserting the Lyot's depolarizer immediately in front of the photocathode.

The second disadvantage is that the sensitivy is wildly fluctuating over the surface of the photocathode. To lessen the influence of this effect the image of the objective (or mirror) of the telescope should be formed on the photocathode and should remain fixed when the analyzer is rotated. To accomplish this the analyzer should have plane-parallel surfaces which are perpendicular to the axis of rotation. To fulfill these requirements accurately may be difficult if the analyzer is very thick; however, it presents no difficulties if a very thin analyzer is used, such as, e.g., a sheet of polaroid.

In the first approximation the inhomogeneous sensitivity of the cathode causes a single sine-wave to be superimposed on the double sine-wave representing the changes of the photocurrent due to stellar polarization alone, as the analyzer is rotated through 360° (cf. Behr, 1956, 1960).

Three methods of measuring photoelectrically the ratio of $I'(\varphi) - I'(\varphi + 90^\circ)$ to $I'(\varphi) + I'(\varphi + 90^\circ)$ occuring in Eqs. (34) and (35) have been used. They are the so called dc method, the differential method, and the flicker (ac) method.

In the dc method (Hiltner, 1949b, 1951a, 1956) the light travels toward the photomultiplier tube through an analyzer which is set in several position angles φ. Each of the intensities $I'(\varphi)$ occurring in Eqs. (34) and (35) is measured separately.

It seems that the best observing schedule is to perform the measurements in the following succession of position angles of the analyzer:

$$\begin{array}{cccccccccc} 0^\circ & 90^\circ & 180^\circ & 270^\circ & 0^\circ & 45^\circ & 135^\circ & 225^\circ & 315^\circ & 45^\circ \\ I_1 & I_2 & I_3 & I_4 & I_5 & I_6 & I_7 & I_8 & I_9 & I_{10}, \end{array} \tag{36}$$

the symbols denoting the intensities observed at each position angle being written below these angles. The ratios Q/I and U/I can be now found from the equations:

$$\frac{Q}{I} = \frac{1}{P_0} \cdot \frac{\frac{1}{2}I_1 - I_2 + I_3 - I_4 + \frac{1}{2}I_5}{\frac{1}{2}I_1 + I_2 + I_3 + I_4 + \frac{1}{2}I_5}, \tag{37}$$

$$\frac{U}{I} = \frac{1}{P_0} \cdot \frac{\frac{1}{2}I_6 - I_7 + I_8 - I_9 + \frac{1}{2}I_{10}}{\frac{1}{2}I_6 + I_7 + I_8 + I_9 + \frac{1}{2}I_{10}}. \tag{38}$$

The observing schedule given by Eq. (36) reduces to a minimum the influence of changing extinction on the measurements of each of the Stokes parameters. It also eliminates the influence of linear changes in the star's brightness during the observation.

In the differential method (Hiltner, 1951b, 1959; Behr, 1956) the light beam is split into two perpendicularly polarized beams. The Wollaston prism or plane-parallel calcite plate is used for this purpose. The two beams strike separate photomultipliers. There are two ways of obtaining the ratios Q/I and U/I, as given by Eqs. (34) and (35). Either the output of each photomultiplier tube is integrated separately (Gehrels and Teska, 1960) or the difference and the sum of the currents from the two multiplier tubes are simultaneously recorded by means of the Brown recorder with two independent pens. To lessen the influence of unhomogeneous cathode sensitivity the measurements in every position angle of the analyzer are made with and without Lyot's depolarizer, which is inserted immediately in front of the analyzer.

In differential polarimeters constructed up to now the photomultiplier tubes rotate with the analyzer. The axis of rotation should be pointed towards the center of the telescope's objective (or mirror) if the image of this objective on the photocathode is to remain in a fixed position.

The scintillation of two perpendicularly polarized components of stellar light is almost exactly identical (Mikesell *et al.*, 1951). Due to this fact the measurements made with the differential polarimeter are to a large extent free of the disturbing influence of atmospheric scintillation. This influence is not, however, eliminated completely and for the bright stars scintillation still remains as the main factor limiting the accuracy of measurements. The mean error of the degree of polarization of bright stars cannot be made smaller than $\pm$ 0.03 percent

for a measurement lasting 12 min (Behr, 1956). As pointed out by Behr (1956, 1960) there are two sources of this residual influence of scintillation. First, in every point of the image of the objective formed on the photocathode the illumination changes rapidly. Due to the lack of homogeneity in the sensitivity of the photocathode this causes fluctuations in the photocurrent. Secondly, in refractors, the objective introduces polarization if its illumination is not symmetrical with respect to its center. This polarization may be as large as a few tenths of a percent and can be computed from Fresnel's formulas. Similar effects are observed in the case of mirrors which in most cases polarize incident light differently in different portions of their surface (Dollfus, 1957; Reimer, 1957; Thiessen and Broglia, 1959; Behr, 1960).

The influence of atmospheric scintillation is reduced also in the flicker method of measuring polarization, used by Hall (1948, 1952, 1958) and by Hall and Mikesell (1950). The analyzer is here rotated with high frequency. To obtain the Stokes parameters I, Q, and U the photocurrent should be integrated simultaneously in different intervals of phase. Integrating Eq. (33) for the ideal polarizer we have:

$$I = \frac{1}{\pi}\int_{0^\circ}^{360^\circ} I'(\varphi)\,d\varphi, \tag{39}$$

$$Q = \frac{1}{2}\left[\int_{315^\circ}^{45^\circ} I'(\varphi)\,d\varphi - \int_{45^\circ}^{135^\circ} I'(\varphi)\,d\varphi + \int_{135^\circ}^{225^\circ} I'(\varphi)\,d\varphi - \int_{225^\circ}^{315^\circ} I'(\varphi)\,d\varphi\right], \tag{40}$$

$$U = \frac{1}{2}\left[\int_{0^\circ}^{90^\circ} I'(\varphi)\,d\varphi - \int_{90^\circ}^{180^\circ} I'(\varphi)\,d\varphi + \int_{180^\circ}^{270^\circ} I'(\varphi)\,d\varphi - \int_{270^\circ}^{360^\circ} I'(\varphi)\,d\varphi\right]. \tag{41}$$

For sufficiently high speed of rotation of the analyzer the influence of scintillation may be completely eliminated in the flicker method if the telescope optics does not polarize light.

B. *Circularly Polarized Component*

Partially circularly polarized light is described by the ratio V/I. To measure this ratio the light must be made to pass through the retardation plate for which $\tau \approx 90^\circ$ and then through the analyzer. The transformation matrix describing the transformation of the Stokes parameters by those two optical instruments is obtained by multiplying the square matrix on the right-hand side of Eq. (18) by that on the right-hand side of Eq. (23) (if the analyzer is assumed to be ideal). The resulting matrix permits us to compute the intensity of transmitted light for any position angle of the retardation plate and the analyzer.

When the measurements are made by the dc method it seems most convenient to make for each of the eight position angles of the retardation plate, differing

by 45°, a set of measurements at the position angles of the analyzer given by Eq. (36). The 80 measurements made for a star in this way permit us to determine all four Stokes parameters and the retardation τ of our retardation plate corresponding to the effective wavelength of the apparatus. When this observing schedule is used, most of the systematic errors are eliminated.

Let us denote by A_ψ and B_ψ the expressions

$$A_\psi = \frac{1}{8} \cdot \frac{\frac{1}{2}I_1 - I_2 + I_3 - I_4 + \frac{1}{2}I_5}{\frac{1}{2}I_1 + I_2 + I_3 + I_4 + \frac{1}{2}I_5}, \tag{42}$$

$$B_\psi = -\frac{1}{8} \cdot \frac{\frac{1}{2}I_6 - I_7 + I_8 - I_9 + \frac{1}{2}I_{10}}{\frac{1}{2}I_6 + I_7 + I_8 + I_9 + \frac{1}{2}I_{10}}, \tag{43}$$

where all the intensities are measured through the retardation plate set at position angle ψ and through the analyzer. We now have

$$Q/I = B_{0°} + B_{90°} + B_{180°} + B_{270°}, \tag{44}$$

$$U/I = A_{45°} + A_{135°} + A_{225°} + A_{315°}, \tag{45}$$

$$(V \sin \tau)/I = -A_{0°} + A_{90°} - A_{180°} + A_{270°} - B_{45°} - B_{135°} + B_{225°} - B_{315°}, \tag{46}$$

$$\cos \tau = (A_{0°} + A_{90°} + A_{180°} + A_{270°})\, I/U = (B_{15°} + B_{135°} + B_{225°} + B_{315°})\, I/Q. \tag{47}$$

The comparison of the phase difference determined from Eq. (47) with laboratory determination (see, e.g., Plumb, 1960) permits us to determine the effective wavelength of our polarimetric apparatus.

C. *Polarization Parameters Expressed in Magnitudes*

In many cases in astronomical photometry it is more convenient to use magnitudes instead of intensity differences. We shall denote by $m(\varphi)$ the magnitude of a star observed after its light passes through an ideal analyzer set at the position angle φ. We shall also denote by $m^*(\varphi)$ the magnitude of a star observed through a quarter-wave plate set at position angle $\psi = 0°$ and through an analyzer set at position angle φ. The quantities p_x, p_y, and p_v defined by equations

$$p_x = m(90°) - m(0°), \tag{48}$$

$$p_y = m(135°) - m(45°), \tag{49}$$

$$p_v = m^*(45°) - m^*(135°), \tag{50}$$

we propose to call the *Stokes parameters expressed in magnitudes*. The first two of these parameters were introduced for the first time by Behr (1956) and Davis (1955).

We shall express these parameters in terms of conventional Stokes parameters. From Eq. (48) and from the definition of stellar magnitude we have

$$p_x = -2.5 \log [I'(90°)/I'(0°)]. \tag{51}$$

Hence we have

$$\frac{I'(90°)}{I'(0°)} = \exp\left(\frac{\ln 10}{2.5} p_x\right). \tag{52}$$

Since $\tanh x = (e^{2x} - 1)/(e^{2x} + 1)$, we put

$$x = \frac{1}{2} \frac{\ln 10}{2.5} p_x \approx 0.4605\, p_x \tag{53}$$

and we obtain by means of Eq. (34)

$$\tanh (0.4605\, p_x) = \left[\frac{I'(0°)}{I'(90°)} - 1\right] \Big/ \left[\frac{I'(0°)}{I'(90°)} + 1\right] = \frac{I'(0°) - I'(90°)}{I'(0°) + I'(90°)} = \frac{Q}{I}. \tag{54}$$

Similar relationships may be obtained for p_u and p_v by means of Eqs. (35) and (46). Since the largest observed degree of polarization of stellar light is $P = 0.10$ we may take advantage of the fact that $\tanh x \approx x$ for $x \ll 1$ (e.g., for $x = 0.10$, $\tanh x = 0.997\, x$) and obtain

$$Q/I = 0.4605\, p_x, \tag{55}$$

$$U/I = 0.4605\, p_y, \tag{56}$$

$$V/I = 0.4605\, p_v. \tag{57}$$

The quantity p, defined by

$$p = (p_x^2 + p_y^2)^{1/2}, \tag{58}$$

will be called the *amount of polarization* (expressed in magnitudes). From Eqs. (7), (8), (10), (11), and (55) – (58) results

$$P = 0.4605\, p, \tag{59}$$

$$P_v = 0.4605\, |p_v|, \tag{60}$$

$$\tan 2\theta = p_y/p_x. \tag{61}$$

The Stokes parameters expressed in magnitudes are especially convenient in statistical investigations of stellar polarization and in describing the instrumental polarization. The only case when the conventional Stokes parameters Q, U, V must be used is in correcting the measurements of stellar polarization for the polarization of the sky background. This can be done most simply by subtracting the values of Q, U, V describing the polarization of sky background alone from those obtained from measurements of starlight combined with the light of sky background surrounding the star.

In stellar-astronomical applications it is most convenient to relate the Stokes parameters to the galactic coordinate system. Replacing the position angle θ in Eqs. (10) and (11) by $\theta_G - 90°$, where θ_G is position angle of the plane of vibrations in the galactic coordinate system, we obtain from Eqs. (55) – (59) the Stokes parameters expressed in magnitudes and galactic coordinates:

$$Q_G = p \cos 2(\theta_G - 90°), \tag{62}$$

$$U_G = p \sin 2(\theta_G - 90°). \tag{63}$$

Since the measurements of stellar magnitudes obey in most cases the Gaussian law of errors, the same is true for the Stokes parameters expressed in magnitudes. This results from the linearity of Eqs. (48) – (50). This property of parameters p_x, p_y, p_v, Q_G, and U_G is a very important argument for using them in all statistical considerations.

Since, however, in most of the papers on polarization of starlight the amount of polarization p and the position angle θ were used, their statistical properties are worth considering. Let us consider the amount of polarization p and position angle of the plane of vibrations θ as obtained from the measurements of a star for which the true (free from observational errors) values of these quantities are p_0 and θ_0. The mean errors of the Stokes parameters, p_x and p_y, obtained from the same measurements are assumed to be equal to one another and equal to ϵ. The probability densities of the random functions p and θ, resulting from the discussion of the properties of the two-dimensional random vector, are

$$f(p) = \frac{p}{\epsilon^2} \exp\left(-\frac{p^2 + p_0^2}{2\epsilon^2}\right) J_0\left(i\frac{pp_0}{\epsilon^2}\right), \tag{64}$$

$$g(\theta) = \pi^{-1/2}\left\{\pi^{-1/2} - \eta_0 \exp(\eta_0^2)\,[1 - \operatorname{erf}(\eta_0)]\right\} \exp(-p_0^2/2\epsilon^2), \tag{65}$$

where

$$\eta_0 = 2^{-1/2}(p_0/\epsilon) \cos 2(\theta - \theta_0), \tag{66}$$

$J_0(ix)$ is the zero-order Bessel function of the imaginary argument, and $\operatorname{erf}(x)$ is the Gaussian error function.

As results from Eq. (64) the most probable observed value, p, of the amount of polarization is always larger than the true value, p_0; in asymptotic cases these two values are connected by the relation

$$p = \begin{cases} (p_0^2 + \frac{1}{2}\pi\epsilon^2)^{1/2} & \text{for } p_0 \approx 0, \\ (p_0^2 + \epsilon^2)^{1/2} & \text{for } p_0 \gg \epsilon. \end{cases} \tag{67}$$

The general form of this relation may be found in the paper by Serkowski (1958b).

The mean error ϵ_p of the amount of polarization understood as the rms deviation of the observed value of p from the most probable value given by Eq. (67) is

$$\epsilon_p = \begin{cases} \epsilon(2 - \frac{1}{2}\pi)^{1/2} & \text{for } p_0 \approx 0, \\ \epsilon & \text{for } p_0 \gg \epsilon. \end{cases} \tag{68}$$

The rms deviation σ_p of the observed amount of polarization from the true value p_0 is, of course, larger and equals

$$\sigma_p = \begin{cases} 2^{1/2}\epsilon & \text{for } p_0 \approx 0, \\ \epsilon & \text{for } p_0 \gg \epsilon. \end{cases} \tag{69}$$

The mean error ϵ_θ of the position angle θ is

$$\epsilon_\theta = \begin{cases} 12^{1/2}\pi \text{ rad} = 51.96 & \text{for } p_0 \approx 0, \\ \frac{1}{2}\epsilon/p \text{ rad} = 28.65\,\epsilon/p & \text{for } p_0 \gg \epsilon. \end{cases} \tag{70}$$

The complicated statistical properties of p and θ make it clear that these parameters should be replaced in statistical discussions by the much more convenient Stokes parameters.

D. *Instrumental Polarization*

The objective or mirror of the telescope is likely to introduce both linear and circular instrumental polarization. In the case of mirrors both of these kinds of polarization may result from the defects of the aluminum layer. The objective of a refractor may introduce the circularly polarized component because of strains in the glass. This effect may be quite large even for the glass which is generally considered as being of highest quality (Serkowski, 1960a).

We shall assume that the objective introduces the small phase difference $\tau(\lesssim 90^\circ)$ between the components of the electric vector vibrating in planes, for which the position angles are ψ and $90^\circ + \psi$. Moreover, we shall assume

that the initially unpolarized light, after passing the objective, has the degree of polarization $P_0(\ll 1)$ and that the position angle of its plane of vibrations is φ. If slightly polarized stellar light passes through such an objective, the matrix describing the transformation of Stokes parameters is obtained by multiplying the square matrices on the right-hand sides of Eqs. (20) and (23). Performing this multiplication (in whatever order) and neglecting the squares and cross-products of small quantities we obtain the transformation equations:

$$Q'/I' = P_0 \cos 2\varphi + [1 - \sin^2 2\psi \sin \tau \tan(\tau/2)]Q/I + \\ + [\sin 2\psi \cos 2\psi \sin \tau \tan(\tau/2)]\, U/I - (\sin 2\psi \sin \tau)\, V/I, \quad (71)$$

$$U'/I' = P_0 \sin 2\varphi + [\sin 2\psi \cos 2\psi \sin \tau \tan(\tau/2)]\, Q/I + \\ + [1 - \cos^2 2\psi \sin \tau \tan(\tau/2)]\, U/I + (\cos 2\psi \sin \tau)\, V/I, \quad (72)$$

$$V'/I' = (\sin 2\psi \sin \tau)\, Q/I - (\cos 2\psi \sin \tau)\, U/I + V/I. \quad (73)$$

We shall express the constants P_0, φ, ψ, and τ, characterizing the polarizing properties of the objective, in terms of more convenient constants defined by the equations:

$$\Delta p_x = (P_0 \cos 2\varphi)/0.4605, \quad (74)$$

$$\Delta p_y = (P_0 \sin 2\varphi)/0.4605, \quad (75)$$

$$c_1 = \sin 2\psi \sin \tau \approx 2 \sin 2\psi \tan(\tau/2), \quad (76)$$

$$c_2 = -\cos 2\psi \sin \tau \approx -2 \cos 2\psi \tan(\tau/2). \quad (77)$$

Now replacing the ratios of Stokes parameters in Eqs. (71) - (73) by the Stokes parameters expressed in magnitudes and assuming $p_v = 0$, the aforementioned equations take the form

$$p'_x = p_x - \tfrac{1}{2} c_1 p'_v + \Delta p_x, \quad (78)$$

$$p'_y = p_y - \tfrac{1}{2} c_2 p'_v + \Delta p_y, \quad (79)$$

$$p'_v = c_1 p_x + c_2 p_y, \quad (80)$$

where the primed parameters characterize the light leaving the objective, and the unprimed characterize the incident stellar light. Equations (78) - (80) may be used for correcting the observations for the effects of instrumental polarization. If there is no linear instrumental polarization (i.e., if $\Delta p_x = \Delta p_y = 0$) it may be easily seen that the amount of polarization after passing the objective is

$$p' = [p^2 - (p'_v)^2]^{1/2}, \quad (81)$$

which means that the objective may depolarize the incident light, and the amount of depolarization depends on the position angle of its plane of vibration

E. *Photographic Polarization Measurements*

The photographic method of measuring plane polarization, although much less accurate than the photoelectric measurements, permits us to obtain data on the polarization of numbers of faint stars in a relatively short time. The best way in which most of the systematic errors may be avoided is to photograph the sky through two identical plane-parallel calcite plates placed near to the photographic plate. The calcite plates should be cut parallel to their natural cleavage planes. The principal sections of these two plates should be perpendicular to one another (cf. Bartl, 1959; Serkowski, 1958c, 1960b). Because of the birefringence of calcite two images of each star are formed on the photographic plate, both affected in the same way by astigmatism. According to Eqs. (48) and (49) the magnitude difference between these two images formed by properly oriented calcite plates gives the corresponding Stokes parameters expressed in magnitudes.

To eliminate the instrumental errors (cf. Hall and Serkowski, 1961) at least 8 exposures should be made, each on a different photographic plate, at position angles of the calcite plates differing by 45°. Thus, each Stokes parameter is determined from 4 exposures. The mean error of its determination will be $\pm 0^m.02$, assuming that the magnitude difference of two neighboring stars may be determined from one photographic plate with a mean error as small as $\pm 0^m.04$. Reliable results can be obtained only if stellar images on the photographic plate are not crowded. The number of pairs of images per square centimeter of the photographic plate should not exceed 15 if gross errors resulting from blending are to be avoided.

V

POLARIZATION OF LIGHT BY ALIGNED DUST GRAINS

A. *Changes of Stokes Parameters Along the Optical Path*

The transformation matrix for Stokes parameters, given by Eq. (16), can be used for describing the scattering of light. The case which is interesting in discussion of interstellar polarization is scattering in the forward direction, i.e., scattering without change of direction of light, at scattering angle equal to zero.

We shall assume that the scattering medium is optically anisotropic and the directions **l** and **r**, defined by Fig. 1, are parallel to the main axes of the tensor describing this anisotropy. The medium is not isotropic because the dust grains of which it is composed are aligned. The aligning mechanism has axis of symmetry parallel to direction **l**.

The passage of light of wavelength λ through the scattering layer of thickness s containing n_g scattering grains in unit volume is described by Eqs. (12) and (13) with coefficients

$$A_1 = 1 - q_0 S_1(0), \tag{82}$$

$$A_2 = 1 - q_0 S_2(0), \tag{83}$$

$$A_3 = A_4 = 0, \tag{84}$$

where

$$q_0 = n_g s \lambda^2 / 2\pi, \tag{85}$$

and $S_1(0)$, $S_2(0)$ are so called *amplitude functions* for forward scattering, depending on the properties of scattering grains (van de Hulst, 1957).

Extinction and polarization of light due to scattering can be formally described as passage of light through the refracting medium with complex *index of refraction:*

$$\begin{aligned} m_j &= 1 - i(2\pi)^{-2} n_g \lambda^3 S_j(0) \\ &= 1 + (2\pi)^{-2} n_g \lambda^3 \{\mathrm{Im}[S_j(0)] - i\,\mathrm{Re}[S_j(0)]\}; j = 1, 2; \end{aligned} \tag{86}$$

where $j = 1$ refers to the light with electric vector vibrating in the plane determined by direction $\mathbf{r}$, while $j = 2$ refers to that with electric vector vibrating in a perpendicular plane; symbols Re and Im denote the real and imaginary parts of the function considered.

Equation (86) tells us that the imaginary part of the refraction coefficient which describes absorption, or more generally, extinction (extinction = absorption + scattering) is proportional to $\mathrm{Re}[S_j(0)]$. The term $\mathrm{Im}[S_j(0)]$ describes the phase retardation; the phase difference between the light which traveled the path s in the scattering medium and that which traveled the same path in vacuum is

$$\epsilon_j = 2\pi\lambda^{-1} s[\mathrm{Re}(m_j) - 1] = q_0\,\mathrm{Im}[S_j(0)]; j = 1, 2; \tag{87}$$

which results from the known relation between the coefficient of refraction and the phase velocity of light. Hence the phase difference between the light bundles polarized in perpendicular planes is

$$\epsilon_1 - \epsilon_2 = q_0\{\mathrm{Im}[S_1(0)] - \mathrm{Im}[S_2(0)]\}.$$

The real parts of the amplitude functions fulfill the relations

$$\mathrm{Re}\,[S_1(0)] = \pi\lambda^{-1} S_r, \tag{88}$$

$$\mathrm{Re}\,[S_2(0)] = \pi\lambda^{-1} S_l, \tag{89}$$

where S_l and S_r are the *mean extinction cross sections* of a dust grain for light

with electric vector vibrating in a plane determined by the directions 1 and **r**, respectively. By analogy we can define quantities $S_r^* = 2\epsilon_1/n_g s$ and $S_l^* = 2\epsilon_2/n_g s$ fulfilling the relations

$$\mathrm{Im}\,[S_1(0)] = \pi\lambda^{-1} S_r^*, \tag{90}$$

$$\mathrm{Im}\,[S_2(0)] = \pi\lambda^{-1} S_l^*. \tag{91}$$

It follows from Eqs. (82), (83), and (88) – (91) that the coefficients in Eqs. (14) and (15) are

$$a_1 = 1 - q_0\,\mathrm{Re}\,[S_1(0)] = 1 - \tfrac{1}{2} S_r\, n_g\, s, \tag{92}$$

$$a_2 = 1 - q_0\,\mathrm{Re}\,[S_2(0)] = 1 - \tfrac{1}{2} S_l\, n_g\, s, \tag{93}$$

$$b_1 = -\tfrac{1}{2} S_r^*\, n_g\, s, \tag{94}$$

$$b_2 = -\tfrac{1}{2} S_l^*\, n_g\, s. \tag{95}$$

Now we shall compute the derivatives of the Stokes parameters over the path s. By substitution of Eqs. (92) – (95) we can obtain from Eq. (16) the Stokes parameters for the light which passed through a scattering layer of thickness ds. Putting in Eq. (16) $I = I(s), Q = Q(s), I' = I(s + ds), Q' = Q(s + ds)$ and neglecting $(ds)^2$ we have

$$I(s + ds) = I(s) - \tfrac{1}{2}(S_r + S_l) n_g\, I(s)ds + \tfrac{1}{2}(S_r - S_l) n_g\, Q(s)ds, \tag{96}$$

$$Q(s + ds) = Q(s) - \tfrac{1}{2}(S_r + S_l) n_g\, Q(s)ds + \tfrac{1}{2}(S_r - S_l) n_g\, I(s)ds, \tag{97}$$

and hence

$$dI(s)/ds = -\tfrac{1}{2} n_g[(S_r + S_l)\, I - (S_r - S_l)\, Q], \tag{98}$$

$$d[Q(s)/I(s)]/ds = \tfrac{1}{2} n_g (S_r - S_l)\,[1 - (Q/I)^2]. \tag{99}$$

The increment of extinction A, expressed in magnitudes over the path ds, is connected with the increment of intensity I over this path by the relation

$$dA = [5/(2 \ln 10)]\, dI/I \approx -1.086\, dI/I. \tag{100}$$

By substitution of Eqs. (55) and (100) we can now express the Eqs. (98) and (99) in magnitudes:

$$dA = \tfrac{1}{2} 1.086\, n_g[(S_r + S_l) - 0.4605(S_r - S_l)\, p_x]\, ds, \tag{101}$$

$$dp_x = 1.086\, n_g (S_r - S_l)\,[1 - (0.4605\, p_x)^2]\, ds. \tag{102}$$

Similarly, from Eq. (16) result the equations

$$dp_u = \tfrac{1}{2} n_g [(S_r^* - S_l^*) p_v - 0.4605(S_r - S_l) p_x p_u] ds, \tag{103}$$

$$dp_v = \tfrac{1}{2} n_g [(S_r^* - S_l^*) p_u + 0.4605(S_r - S_l) p_x p_v] ds. \tag{104}$$

The above equations are valid when the position angle θ, which defines the Stokes parameters by means of Eqs. (10) and (11), is measured from direction 1 which is assumed to be parallel to the axis of symmetry of the mechanism aligning the dust grains. Moreover, the angle θ should be measured in a plane perpendicular to the line of sight and intersecting the path element ds. For our further discussion it will be convenient to replace θ by $\theta + \Theta$ where Θ is the *position angle of the local axis of symmetry* of the aligning mechanism, measured in galactic coordinates at the intersection of the axis of symmetry with the path element ds. The Stokes parameters which will now be expressed in magnitudes in a galactic coordinate system will, in accordance with Eqs. (62) and (63), be denoted by Q_G, U_G, and V_G (where $V_G = p_l$). These Stokes parameters in new coordinate system are connected with old ones by Eq. (17) where $\varphi = -\Theta$. Equations (101) – (104) expressed in the new coordinate system are

$$dA = \tfrac{1}{2} 1.086\, n_g \{(S_r + S_l) - 0.4605(S_r - S_l)[Q_G \cos 2(\Theta - 90°) + U_G \sin 2(\Theta - 90°)]\} ds, \tag{105}$$

$$dQ_G = 1.086\, n_g \{(S_r - S_l)[1 - (0.4605\, Q_G)^2] \cos 2(\Theta - 90°) - 0.4605^2 (S_r - S_l) Q_G U_G \sin 2(\Theta - 90°) + 0.4605(S_r^* - S_l^*) V_G \sin 2(\Theta - 90°)\} ds, \tag{106}$$

$$dU_G = 1.086\, n_g \{(S_r - S_l)[1 - (0.4605\, U_G)^2] \sin 2(\Theta - 90°) - 0.4605^2 (S_r - S_l) Q_G U_G \cos 2(\Theta - 90°) + 0.4605(S_r^* - S_l^*) V_G \cos 2(\Theta - 90°)\} ds, \tag{107}$$

$$dV_G = 1.086\, n_g \{0.4605(S_r^* - S_l^*)[Q_G \sin 2(\Theta - 90°) - U_G \cos 2(\Theta - 90°)] - 0.4605^2 (S_r - S_l) V_G [Q_G \cos 2(\Theta - 90°) + U_G \sin 2(\Theta - 90°)]\} ds. \tag{108}$$

Let us suppose that Q_G, U_G, and V_G are small, so that their squares and cross-products can be neglected. Moreover, we shall assume that V_G is negligibly small

as compared to Q_G or U_G and that $(S_r - S_l) \ll (S_r + S_l)$. Now Eqs. (105) - (108) reduce to

$$dA = \tfrac{1}{2}1.086(S_r + S_l)\, n_g\, ds, \tag{109}$$

$$dQ_G = 1.086(S_r - S_l)\, n_g \cos 2(\Theta - 90°)\, ds, \tag{110}$$

$$dU_G = 1.086(S_r - S_l)\, n_g \sin 2(\Theta - 90°)\, ds, \tag{111}$$

$$dV_G = \tfrac{1}{2}(S_r^* - S_l^*)\, n_g[Q_G \sin 2(\Theta - 90°) - U_G \cos 2(\Theta - 90°)]\, ds$$
$$= 0.4605[(S_r^* - S_l^*)/(S_r - S_l)]\,(Q_G\, dU_G - U_G\, dQ_G). \tag{112}$$

Integrating these equations we can obtain the dependence of extinction and polarization on distance and on the direction of the axis of symmetry of the aligning mechanism if only the mean extinction cross sections of dust grains are known. These cross sections will be discussed in the next two subsections of this article.

B. *Extinction Cross Sections*

The extinction cross sections S_l and S_r are mean cross sections and depend on the degree of alignment of dust grains. If the grains are strongly elongated but their axes are distributed at random, we have $S_r = S_l$ and the dust does not polarize transmitted light.

We shall assume for simplicity that each dust grain has an axis of symmetry, which means that it is a solid of revolution. Extinction produced by such grain is described by three extinction cross sections σ_E, σ_H, and σ_S corresponding to the axis of symmetry of a grain parallel to the electric vector of the incident light, parallel to its magnetic vector, and parallel to the direction **S** of the incident light, respectively; for grains small compared to the wavelength we have $\sigma_H = \sigma_S$. The angle between the *direction of the axis of symmetry of the aligning mechanism*, **B**, and the axis of symmetry of the individual dust grain is (according to notations of Davis and Greenstein, 1951) denoted by α_Z.

The degree of alignment of dust grains is characterized by the *distribution parameter F*, defined by the equation

$$F = \tfrac{1}{3} - \langle \cos^2 \alpha_Z \rangle, \tag{113}$$

where angular brackets denote averaging over all dust grains. Parameter F is defined so that $F = 0$ for random distribution of the axes of symmetry. If all the axes of symmetry are parallel to **B** we have $F = -\frac{2}{3}$ and when all are perpendicular, $F = \frac{1}{3}$.

The problem of expressing the extinction cross sections of dust grains which are not small compared to the wavelength and have the axis of symmetry arbitrarily oriented with respect to the direction **S** of incident light, by the cross sections σ_E, σ_H, and σ_S, is still unsolved. We shall describe the approximate procedure which was developed by Davis (1959). The unit vector perpendicular to the direction **S** of incident light and situated in the plane defined by **S** and **B** is denoted by $\mathbf{e}_l$; $\mathbf{e}_r$ denotes a unit vector perpendicular to this plane. The angle between **B** and **S** is denoted by ν' (Fig. 2). The real

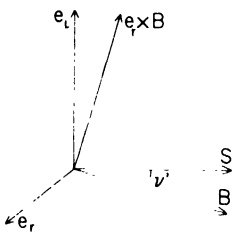


FIG. 2. Definition of angles and directions. All the vectors except e_r are situated in the same plane.

distribution of the axes of symmetry is replaced by the distribution in which the axes of symmetry are directed only toward **B** and toward two directions perpendicular to **B**, namely, $\mathbf{e}_l \times \mathbf{B}$ and $\mathbf{e}_r$. If the distribution parameter has to be equal to F, the relative frequencies of dust grains with axes of symmetry directed towards these three directions should be in the ratio

$$(\tfrac{1}{3} - F) : (\tfrac{1}{3} + \tfrac{1}{2}F) : (\tfrac{1}{3} + \tfrac{1}{2}F). \tag{114}$$

The polarizing properties of the medium will not change much if the grains directed along **B** and $\mathbf{e}_r \times \mathbf{B}$ are redistributed so that they are oriented along **S** and $\mathbf{e}_l$, taking $\cos^2 \nu'$ of the grains along **B** to **S**, and $\sin^2 \nu'$ ro $\mathbf{e}_l$. The fractions oriented along **S**, $\mathbf{e}_l$, and $\mathbf{e}_r$ are now in the ratio

$$\begin{aligned} f_s : f_l : f_r &= [(\tfrac{1}{3} - F)\cos^2 \nu' + (\tfrac{1}{3} + \tfrac{1}{2}F)\sin^2 \nu'] : [(\tfrac{1}{3} - F)\sin^2 \nu' + \\ &+ (\tfrac{1}{3} + \tfrac{1}{2}F)\cos^2 \nu'] : [\tfrac{1}{3} + \tfrac{1}{2}F] = \\ &= [\tfrac{1}{3} + (\tfrac{3}{2}\sin^2 \nu' - 1)F] : [\tfrac{1}{3} - (\tfrac{3}{2}\sin^2 \nu' - 1)F] : [\tfrac{1}{3} + \tfrac{1}{2}F]. \end{aligned} \tag{115}$$

Taking the relative frequencies f_s, f_l, and f_r as weights and assuming that cross sections σ_E, σ_H, and σ_S are identical for all grains, we obtain the mean extinction cross sections for the components of the electric vector vibrating parallel to $\mathbf{e}_r$ or $\mathbf{e}_l$, respectively (cf. Davis, 1959)

$$\begin{aligned} S_r &= f_s \sigma_S + f_l \sigma_H + f_r \sigma_E \\ &= \tfrac{1}{3}(\sigma_E + \sigma_H + \sigma_S) - [(\tfrac{3}{2}\sin^2 \nu' - 1)(\sigma_H - \sigma_S) - \tfrac{1}{2}(\sigma_E - \sigma_H)]F, \end{aligned} \tag{116}$$

$$S_l = f_s\sigma_S + f_l\sigma_E + f_r\sigma_H$$
$$= \tfrac{1}{3}(\sigma_E + \sigma_H + \sigma_S) - [(\tfrac{3}{2}\sin^2\nu' - 1)(\sigma_E - \sigma_S) + \tfrac{1}{2}(\sigma_E - \sigma_H)]F. \quad (117)$$

Hence

$$S_r + S_l = \tfrac{2}{3}(\sigma_E + \sigma_H + \sigma_S) - (\sigma_E + \sigma_H - 2\sigma_S)(\tfrac{3}{2}\sin^2\nu' - 1)F, \quad (118)$$

$$S_r - S_l = \tfrac{3}{2}(\sigma_E - \sigma_H)F\sin^2\nu'. \quad (119)$$

Inserting the terms (118) and (119) into Eqs. (109) – (111) and integrating over the path interval of length S we obtain the extinction and Stokes parameters for a star situated at distance S:

$$A = 1.086\,S\langle[\tfrac{1}{3}(\sigma_E + \sigma_H + \sigma_S) - \tfrac{1}{2}(\sigma_E + \sigma_H - 2\sigma_S)(\tfrac{3}{2}\sin^2\nu' - 1)F]n_g\rangle, \quad (120)$$

$$Q_G = 1.086\,\tfrac{3}{2}S\langle(\sigma_E - \sigma_H)F n_g \sin^2\nu' \cos 2(\Theta - 90^\circ)\rangle, \quad (121)$$

$$U_G = 1.086\,\tfrac{3}{2}S\langle(\sigma_E - \sigma_H)F n_g \sin^2\nu' \sin 2(\Theta - 90^\circ)\rangle, \quad (122)$$

where angular brackets denote the averaging over the space between us and the stars considered. The term proportional to F in Eq. (120) may cause the color-dependence of interstellar extinction to depend on the direction of the orientation of dust grains as was suggested also by Johnson and Morgan (1955), Hiltner and Johnson (1956), Greenberg (1960b, 1960c) and Wilson (1960).

In the case when the stars considered are situated on the galactic equator the trigonometric terms in Eqs. (121) and (122) can be expressed simply by the direction cosines of the axis of symmetry **B** of the aligning mechanism. If ξ, η, and ζ are the direction cosines of the axis of symmetry in the coordinate system in which OY is in the direction of the light ray and OZ is perpendicular to the galactic plane (cf. Davis, 1955) then

$$\sin^2\nu'\cos 2(\Theta - 90^\circ) = \xi^2 - \zeta^2, \quad (123)$$

$$\sin^2\nu'\sin 2(\Theta - 90^\circ) = 2\xi\zeta. \quad (124)$$

C. *Polarizing Properties of Interstellar Dust*

To estimate the polarizing properties of interstellar dust grains their shape can be approximated either by ellipsoids or by long cylinders. There exists no theory of light scattering by ellipsoids of arbitrary size. It was estimated by van de Hulst (1950) that polarization produced by prolate spheroids with an axial ratio of 1:2 is half that produced by long cylinders. The approximate calculations were also made by Stevenson (1953), Shatilov (1960), and Greenberg (1960a). The cross sections for ellipsoids have been obtained experimen-

tally by Greenberg (1960b) who observed the scattering of 3-cm microwaves on ellipsoidal lucite models of comparable dimensions. The theoretical cross sections for long cylinders were computed by van de Hulst (1950, 1957).

The observational data on the wavelength dependence of interstellar polarization are still insufficient. For several stars this wavelength dependence was observed by Hiltner (1950; his more recent observations are reported by van de Hulst, 1957) and Gehrels (1960); their results are presented in Fig. 3.

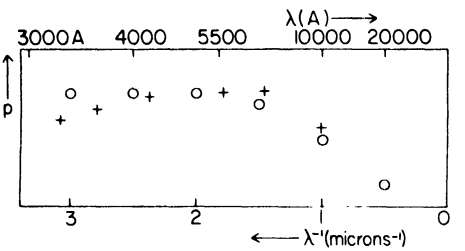


FIG. 3. The observed color dependence of interstellar polarization expressed on an arbitrary scale. The open circles are Hiltner's values; the crosses are those of Gehrels (1960).

Polarization of several other stars was measured in three colors by Behr (1959a) who found that polarization in the ultraviolet is slightly smaller than in the blue, while the polarization in the yellow is for some stars smaller than in the blue, for others larger.

The comparison of observed wavelength dependence of polarization and extinction with cross sections of dust grains obtained by Greenberg and van de Hulst was made by Hall and Serkowski (1961). The general conclusion is that the observed wavelength dependence of interstellar polarization and extinction and the observed values of the ratio of polarization to extinction can be explained on the assumption of dielectric, substantially elongated dust grains which have an index of refraction not smaller than 1.4 and diameters of the order of 0.3μ. As results from data published by Greenberg[4] (1960b) the extinction cross sections for prolate spheroids of equatorial diameter equal to a half wavelength, axial ratio 2:1, and index of refraction 1.6 are $\sigma_E \approx 0.8\lambda^2$, $\sigma_H \approx 0.6\lambda^2$, and $\sigma_S \approx 0.9\lambda^2$.

Interstellar polarization and extinction may be produced also by iron grains; this possibility has been discussed by Fick (1954, 1955), Güttler (1952), and Zimmermann (1957). For wavelengths shorter than 2000 A the iron grains, the

[4] Greenberg (1960b) denotes σ_E, σ_H, and σ_S by $\sigma_{E||}$, $\sigma_{E\perp}$ and $\sigma_{K||}$, respectively.

diameters of which are assumed to be around 0.06 μ, are polarizing light in a plane perpendicular to that for longer wavelengths.

The iron grains will also introduce appreciable circular polarization. As results from computations made by van de Hulst (1957) the ratio $(S_r^* - S_l^*)/(S_r - S_l)$ is near 3 for the iron grains 0.06 μ in diameter, for visual light. Inserting this value into Eq. (112) we see that circular polarization V_G amounting to several thousands of a magnitude can be expected for stars showing high linear polarization. The necessary condition is that the axis of symmetry of the aligning mechanism must vary strongly along the path which the light traverses as it comes from the star.

Cayrel and Schatzman (1954) assume that the interstellar polarization is caused by graphite flakes much smaller than visual wavelengths. The extinction cross section for light with the electric vector vibrating in the plane of flake is much larger than for the light polarized in the perpendicular plane. One graphite flake per 20 classical dust grains of spherical shape is sufficient to explain the observed polarization of stellar light.

According to Platt (1956, 1960) the observed interstellar polarization and extinction may be produced by paramagnetic unsaturated large molecules only about 10 A in diameter. Such molecules are expected to be of aspherical shape and highly paramagnetic. They are pure absorbers and the extinction should be almost independent of the orientation of the particles (Greenberg, 1960c). The total bulk of such particles, sufficient to explain the observed extinction, is only about 1/200th that of classical particles.

VI

DEPENDENCE OF INTERSTELLAR POLARIZATION ON GALACTIC COORDINATES

A. *Theoretical Mean Values of Stokes Parameters*

In the subsequent discussion it is assumed for simplicity that the terms $\sin^2 \nu' \cos 2(\Theta - 90°)$ and $\sin^2 \nu' \sin 2(\Theta - 90°)$ in Eqs. (121) and (122) are random functions independent of the random function $(\sigma_E - \sigma_H) F n_g$. Similarly it is assumed that $\sin^2 \nu'$ is independent of the term $(\sigma_E + \sigma_H - 2\sigma_S) F n_g$ in Eq. (120).

We define the angle α between the local direction $\mathbf{B}$ of the axis of symmetry of the aligning mechanism and the mean direction $\mathbf{B}_0$ of this axis averaged over the interval between us and the considered star. If, for example, the dust grains are oriented by a galactic magnetic field, $\mathbf{B}$ and $\mathbf{B}_0$ are the local and mean

directions of this field. Now we consider the plane *KLMN* (Fig. 4) tangent to the celestial sphere at the point B_0 of the intersection of this sphere with direction $\mathbf{B}_0$. The points of intersection of the directions **B** of the local axis of symmetry with plane *KLMN* are denoted by *B*. Our next assumption is that

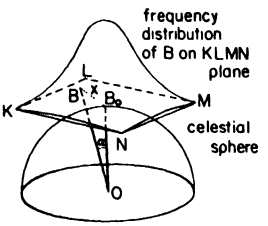


FIG. 4. The assumed distribution of the points *B* on the plane *KLMN* is assumed to be the bivariate normal distribution; *OB* is the direction of the local axis of symmetry of the aligning mechanism.

the distribution of points *B* on the plane *KLMN* is *bivariate normal distribution*, symmetrical with respect to point B_0.

The distance x between the points *B* and B_0 on the *KLMN* plane equals $\tan\alpha$. The density distribution of this distance is given on our assumptions by the well known formula

$$f(x) = \frac{2}{\alpha_1^2}\, x \exp\left(-\frac{x^2}{\alpha_1^2}\right), \tag{125}$$

where α_1 is the root-mean-square value of x, i.e. the *rms tangent of the angular deviation* of the local direction of the axis of symmetry of the aligning mechanism from its mean value.

The distribution on a celestial sphere of the directions **B** corresponding to the density distribution given by Eq. (125) is shown in Fig. 5 as a function of the angle α.

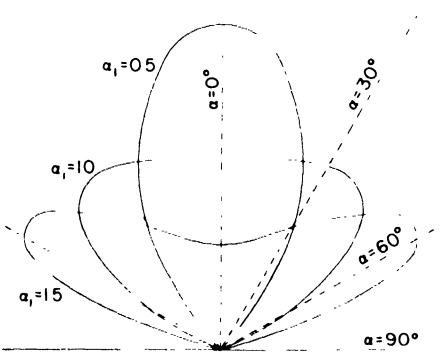


FIG. 5. The assumed distribution of the directions **B** of the local axis of symmetry of the aligning mechanism for three values of parameter α_1.

To express the aforementioned terms $\langle \sin^2 \nu' \cos 2(\Theta - 90^\circ) \rangle$ and $\langle \sin^2 \nu' \sin 2(\Theta - 90^\circ) \rangle$ in galactic coordinates we shall consider the spherical

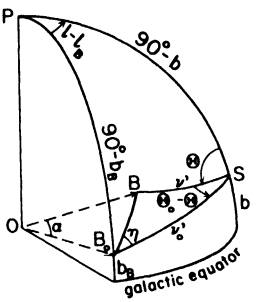


FIG. 6. Relation of angles ν' and Θ to the galactic coordinate system; OB and OB_0 are the local and mean axes of symmetry of the aligning mechanism.

triangles B_0PS and B_0BS (Fig. 6) where P is the northern galactic pole and S is the star considered. From the triangle B_0BS we find the relations:

$$\cos \nu' = \cos \nu'_0 \cos \alpha + \sin \nu'_0 \sin \alpha \cos \eta, \tag{126}$$

$$\cos(\Theta_0 - \Theta) = (\cos \alpha - \cos \nu'_0 \cos \nu')/\sin \nu'_0 \sin \nu', \tag{127}$$

$$\sin (\Theta_0 - \Theta) = \sin \alpha \sin \eta/\sin \nu', \tag{128}$$

where ν'_0 is the angle between $\mathbf{B}_0$ and direction $\mathbf{S}$ to the star, Θ_0 is the position angle of the mean axis of symmetry of the aligning mechanism, measured in the galactic coordinate system, and η is the angle between the plane defined by the local and mean axes of symmetry and the plane defined by the mean axis of symmetry and direction $\mathbf{S}$ from the observer, at O, to the star. From Eqs. (126) – (128) we get

$$\sin^2 \nu' \cos 2(\Theta_0 - \Theta) = 1 - (\cos \nu'_0 \cos \alpha + \sin \nu'_0 \sin \alpha \cos \eta)^2 - 2 \sin^2 \alpha \sin^2 \eta, \tag{129}$$

$$\sin^2 \nu' \sin 2(\Theta_0 - \Theta) = 2 \sin \alpha \sin \eta(\cos \alpha - \cos^2 \nu'_0 \cos \alpha - \tfrac{1}{2} \sin 2 \nu'_0 \sin \alpha \cos \eta)/\sin \nu'_0. \tag{130}$$

Since $\Theta = 90^\circ - (\Theta_0 - 90^\circ) = (\Theta_0 - \Theta)$ we have

$$\sin^2 \nu' \cos 2(\Theta - 90^\circ) = \cos 2(\Theta_0 - 90^\circ) [\sin^2 \nu' \cos 2(\Theta_0 - \Theta)] + \sin 2(\Theta_0 - 90^\circ) [\sin^2 \nu' \sin 2(\Theta_0 - \Theta)], \tag{131}$$

$$\sin^2 \nu' \sin 2(\Theta - 90^\circ) = \sin 2(\Theta_0 - 90^\circ) [\sin^2 \nu' \cos 2(\Theta_0 - \Theta)] - \cos 2(\Theta_0 - 90^\circ) [\sin^2 \nu' \sin 2(\Theta_0 - \Theta)], \tag{132}$$

where, from the spherical triangle B_0PS,

$$\sin^2 \nu_0' \cos 2(\Theta_0 - 90^\circ) = \sin^2(l - l_B) + \sin^2 b[\sin^2 b_B - \cos^2 b_B \cos^2(l - l_B)] - \sin^2 b_B[1 + \sin^2(l - l_B)] + \tfrac{1}{2}\sin 2b \sin 2b_B \cos(l - l_B), \tag{133}$$

$$\sin^2 \nu_0' \sin 2(\Theta_0 - 90^\circ) = \sin 2(l - l_B) \sin b \cos^2 b_B - \sin(l - l_B) \cos b \sin 2b_B; \tag{134}$$

where l and b are the galactic longitude and latitude of the star while l_B and b_B are the galactic coordinates of the mean axis of symmetry $\mathbf{B}_0$. In general the values l_B and b_B are different for each star.

Now, in order to express the right sides of Eqs. (131) and (132) in terms of galactic coordinates we need only to average the Eqs. (129) and (130) over the angles α and η. From our previous assumptions, the angle η is the random variable which is independent of α and assumes with equal probability all the values from 0 to 2π. This means that for natural number n

$$\langle \sin n\eta \rangle = \langle \cos n\eta \rangle = 0, \tag{135}$$

$$\langle \sin^2 \eta \rangle = \langle \cos^2 \eta \rangle = \tfrac{1}{2}, \text{ etc.}, \tag{136}$$

and the Eqs. (129) and (130) averaged over η are

$$\langle \sin^2 \nu' \cos 2(\Theta_0 - \Theta) \rangle_\eta = (1 - \tfrac{3}{2} \sin^2 \alpha) \sin^2 \nu_0', \tag{137}$$

$$\langle \sin^2 \nu' \sin 2(\Theta_0 - \Theta) \rangle_\eta = 0. \tag{138}$$

Expressing $\sin^2 \alpha$ in terms of $x = \tan \alpha$ and averaging it by making use of the probability density given by Eq. (125) we obtain

$$\langle \sin^2 \alpha \rangle = 1 + \alpha_1^{-2} \exp(\alpha_1^{-2})\, Ei(-\alpha_1^{-2}), \tag{139}$$

where $Ei(t)$ is the exponential integral; the graphs of $\langle \sin^2 \alpha \rangle$ and of the function $C_0(\alpha_1)$ defined by the equation

$$C_0(\alpha_1) = 1 - \tfrac{3}{2}\langle \sin^2 \alpha \rangle, \tag{140}$$

are given on Fig. 7.

By virtue of Eqs. (124), (135), and (136) we also have

$$\langle \sin^2 \nu' \rangle_{\eta,\alpha} = \sin^2 \nu_0' + (1 - \tfrac{3}{2} \sin^2 \nu_0') \langle \sin^2 \alpha \rangle. \tag{141}$$

Combining Eqs. (120) – (122), (131), (132), (137), (138), (140), and (141) we have finally the expressions for extinction and Stokes parameters for a star situated at distance S:

$$A = 1.086\, S\{\tfrac{1}{3}\langle(\sigma_E + \sigma_H + \sigma_S)\, n_g\rangle - \tfrac{1}{2}\langle(\sigma_E + \sigma_H - 2\sigma_S)\, F\, n_g\rangle\, C_0(\alpha_1)\,(\tfrac{3}{2}\sin^2\nu_0' - 1)\}, \quad (142)$$

$$Q_G = 1.086\, \tfrac{3}{2} S\langle(\sigma_E - \sigma_H)\, F\, n_g\rangle\, C_0(\alpha_1)\sin^2\nu_0' \cos 2(\Theta_0 - 90°), \quad (143)$$

$$U_G = 1.086\, \tfrac{3}{2} S\langle(\sigma_E - \sigma_H)\, F\, n_g\rangle\, C_0(\alpha_1)\sin^2\nu_0' \sin 2(\Theta_0 - 90°), \quad (144)$$

where averaging is over the path to the star and the coefficients $\sin^2\nu_0' \cos 2(\Theta_0 - 90°)$ and $\sin^2\nu_0' \sin 2(\Theta_0 - 90°)$ are given by Eqs. (133) and (134). These coefficients depend on the properties of the interstellar medium between us and the considered star and are not expected to depend smoothly on galactic coordinates.

We may however average the axis of symmetry of the aligning mechanism over a large part of the galaxy, replacing the galactic coordinates l_B and b_B in Eqs. (133) and (134) by the averaged values $\overline{l_B}$ and $\overline{b_B}$. In the simplest case, when $b = \overline{b_B} = 0$, Eqs. (142) – (144) take the form

$$\bar{A} = 1.086\, S\{\tfrac{1}{3}\langle(\sigma_E + \sigma_H + \sigma_S)\, n_g\rangle - \tfrac{1}{2}\langle(\sigma_E + \sigma_H - 2\sigma_S)\, F\, n_g\rangle\, C_0(\alpha_1)\,[\tfrac{3}{2}\sin^2(l - \overline{l_B}) - 1]\}, \quad (145)$$

$$\overline{Q_G} = 1.086\, \tfrac{3}{2} S\langle(\sigma_E - \sigma_H)\, F\, n_g\rangle\, C_0(\alpha_1)\sin^2(l - \overline{l_B}), \quad (146)$$

$$\overline{U_G} = 0, \quad (147)$$

where α_1 is now the rms tangent of the angular deviation of direction **B** from the mean direction specified by the galactic coordinates $\overline{l_B}$ and $\overline{b_B}$. It must be assumed, of course, that these tangents of angular deviations have the probability density of the form given by Eq. (125).

B. *Dispersion of Stokes Parameters*

As can be seen from Eqs. (143), (144), and (146) these equations cannot be used for determining the factor $C_0(\alpha_1)$ occurring in them. The knowledge of $C_0(\alpha_1)$, and hence the parameter α_1, is important for understanding the mechanism aligning the dust grains. For that reason it is worth while to compute the dispersion of Stokes parameters; this seems to be the only way of determining the value of parameter α_1.

We shall make the same assumptions as were made when computing the mean values of Stokes parameters in a former subsection. Taking into account

Eqs. (118) – (122) and neglecting the small term proportional to F in Eqs. (118) and (120) we may write Eqs. (109) – (111) in the form (cf. Serkowski, 1958b).

$$dA = (\bar{A}/S)\,[1 + \delta(\mathbf{s})]\,d\mathbf{s}, \tag{148}$$

$$dQ_G = (\bar{Q}_G/S)\,[1 + q(\mathbf{s})]\,d\mathbf{s}, \tag{149}$$

$$dU_G = (\bar{Q}_G/S)\left[\frac{\bar{U}_G}{\bar{Q}_G} + u(\mathbf{s})\right] d\mathbf{s}, \tag{150}$$

where $\mathbf{s}$ is the radius vector of a given point in space and random functions $\delta(\mathbf{s})$, $q(\mathbf{s})$, and $u(\mathbf{s})$ are defined by the equations:

$$\delta(\mathbf{s}) = \frac{(\sigma_E + \sigma_H + \sigma_S)\,n_g}{\langle(\sigma_E + \sigma_H + \sigma_S)\,n_g\rangle} - 1, \tag{151}$$

$$q(\mathbf{s}) = \frac{[1 + \delta_0(\mathbf{s})]\,\sin^2\nu' \cos 2(\Theta - 90^\circ)}{\langle \sin^2\nu' \cos 2(\Theta - 90^\circ)\rangle} - 1, \tag{152}$$

$$u(\mathbf{s}) = \frac{[1 + \delta_0(\mathbf{s})]\,\sin^2\nu' \sin 2(\Theta - 90^\circ)}{\langle \sin^2\nu' \cos 2(\Theta - 90^\circ)\rangle} - \frac{\langle \sin^2\nu' \sin 2(\Theta - 90^\circ)\rangle}{\langle \sin^2\nu' \cos 2(\Theta - 90^\circ)\rangle}, \tag{153}$$

and the random function $\delta_0(\mathbf{s})$ is defined by the equation

$$\delta_0(\mathbf{s}) = \frac{(\sigma_E - \sigma_H)\,F\,n_g}{\langle(\sigma_E - \sigma_H)\,F\,n_g\rangle} - 1. \tag{154}$$

We assume that $\delta(\mathbf{s})$, $\delta_0(\mathbf{s})$, $q(\mathbf{s})$, and $u(\mathbf{s})$ can be treated as homogeneous and isotropic stochastical processes characterized by the equations

$$\langle\delta(\mathbf{s})\rangle = \langle\delta_0(\mathbf{s})\rangle = \langle q(\mathbf{s})\rangle = \langle u(\mathbf{s})\rangle = 0, \tag{155}$$

$$\langle\delta^2(\mathbf{s})\rangle = \text{const.};\ \langle\delta(\mathbf{s}_1)\,\delta(\mathbf{s}_2)\rangle = \langle\delta^2(\mathbf{s})\rangle\,R_1(|\mathbf{s}_1 - \mathbf{s}_2|), \tag{156}$$

$$\langle\delta_0^2(\mathbf{s})\rangle = \text{const.};\ \langle\delta_0(\mathbf{s}_1)\,\delta_0(\mathbf{s}_2)\rangle = \langle\delta_0^2(\mathbf{s})\rangle\,R_2(|\mathbf{s}_1 - \mathbf{s}_2|), \tag{157}$$

$$\langle q^2(\mathbf{s})\rangle = \text{const.};\ \langle q(\mathbf{s}_1)\,q(\mathbf{s}_2)\rangle = \langle q^2(\mathbf{s})\rangle\,R_3(|\mathbf{s}_1 - \mathbf{s}_2|), \tag{158}$$

$$\langle u^2(\mathbf{s})\rangle = \text{const.};\ \langle u(\mathbf{s}_1)\,u(\mathbf{s}_2)\rangle = \langle u^2(\mathbf{s})\rangle\,R_4(|\mathbf{s}_1 - \mathbf{s}_2|), \tag{159}$$

where the angular brackets denote averaging over $\mathbf{s}$, the symbol $|\mathbf{s}_1 - \mathbf{s}_2|$ denotes the distance between the points with radius vectors $\mathbf{s}_1$ and $\mathbf{s}_2$, and the correlation functions $R_j(|\mathbf{s}_1 - \mathbf{s}_2|)$, following Chandrasekhar and Münch (1952), are specified as

$$R_j(|\mathbf{s}_1 - \mathbf{s}_2|) = \exp(-|\mathbf{s}_1 - \mathbf{s}_2|/s_{0j}); \qquad j = 1, 2, 3, 4. \tag{160}$$

The constants s_{0i} are called the *microscales* of the fluctuations in corresponding quantities.

Making use of Eqs. (148) and (156) we find that the variance of extinction may be written in the form

$$\sigma_A^2 = \langle A^2 \rangle - (\bar{A})^2 = \frac{(\bar{A})^2}{S^2} \left\langle \int_0^S \int_0^S \delta(\mathbf{s}_1)\, \delta(\mathbf{s}_2)\, d\mathbf{s}_1\, d\mathbf{s}_2 \right\rangle$$

$$= \frac{2(\bar{A})^2 \langle \delta^2 \rangle}{S^2} \int_0^S \int_0^{s_2} R_1(s_2 - s_1)\, ds_1\, ds_2, \tag{161}$$

where s_1 and s_2 are the lengths of vectors $\mathbf{s}_1$ and $\mathbf{s}_2$. Using Eq. (160) we find

$$\int_0^S \int_0^{s_2} R_1(s_2 - s_1)\, ds_1\, ds_2 = s_{01} \int_0^S \left[1 - \exp\left(-\frac{s_2}{s_{01}}\right)\right] ds_2$$

$$= s_{01} S - s_{01}^2 [1 - \exp(-S/s_{01})] \approx s_{01} S, \tag{162}$$

provided that $s_{01} \ll S$. Hence, by Eq. (161)

$$\sigma_A^2 = 2(\bar{A})^2 \langle \delta^2 \rangle s_{01} S. \tag{163}$$

Similar computations give the variances of the Stokes parameters Q_G and U_G on the assumption that $s_{0i} \ll S$:

$$\sigma_Q^2 = 2(\overline{Q_G})^2 \langle q^2 \rangle s_{02} S, \tag{164}$$

$$\sigma_U^2 = 2(\overline{Q_G})^2 \langle u^2 \rangle s_{01} S. \tag{165}$$

Now we shall express $(\overline{Q_G})^2 \langle q^2 \rangle$ and $(\overline{Q_G})^2 \langle u^2 \rangle$ in terms of galactic coordinates and the parameter α_1. Making use of Eqs. (142) – (144) and (151) – (159) we find

$$(\bar{A})^2 \langle \delta^2 \rangle = (1.086\, \tfrac{1}{3} S)^2 \langle [(\sigma_E + \sigma_H + \sigma_S)\, n_g - \langle (\sigma_E + \sigma_H + \sigma_S)\, n_g \rangle]^2 \rangle, \tag{166}$$

$$(\overline{Q_G})^2 \langle q^2 \rangle = (1.086\, \tfrac{3}{2} S)^2 \langle [(\sigma_E - \sigma_H) F n_g]^2 \rangle \langle [\sin^2 \nu' \cos 2(\Theta - 90^\circ)]^2 \rangle + (\overline{Q_G})^2, \tag{167}$$

$$(\overline{Q_G})^2 \langle u^2 \rangle = (1.086\, \tfrac{3}{2} S)^2 \langle [(\sigma_E - \sigma_H) F n_g]^2 \rangle \langle [\sin^2 \nu' \sin 2(\Theta - 90^\circ)]^2 \rangle + (\overline{U_G})^2. \tag{168}$$

For obtaining the dependence of variances of Stokes parameters on galactic coordinates we must compute the averages of the trigonometric terms in

Eqs. (167) and (168). By substitution of Eqs. (131) and (132) these terms take the form

$$[\sin^2\nu'\cos 2(\Theta-90°)]^2 = \cos^2 2(\Theta_0-90°)\,[\sin^2\nu'\cos 2(\Theta_0-\Theta)]^2 + \sin^2 2(\Theta_0-90°)\,[\sin^2\nu'\sin 2(\Theta_0-\Theta)]^2 + \tfrac{1}{2}\sin 4(\Theta_0-90°)\sin^4\nu'\sin 4(\Theta_0-\Theta), \quad (169)$$

$$[\sin^2\nu'\sin 2(\Theta-90°)]^2 = \sin^2 2(\Theta_0-90°)\,[\sin^2\nu'\cos 2(\Theta_0-\Theta)]^2 + \cos^2 2(\Theta_0-90°)\,[\sin^2\nu'\sin 2(\Theta_0-\Theta)]^2 - \tfrac{1}{2}\sin 4(\Theta_0-90°)\sin^4\nu'\sin 4(\Theta_0-\Theta). \quad (170)$$

After inserting here the values from Eqs. (129) and (130) and averaging over η, the last terms in Eqs. (169) and (170) vanish and the terms in square brackets are

$$\langle[\sin^2\nu'\cos 2(\Theta_0-\Theta)]^2\rangle_\eta = \tfrac{1}{2}\sin^4\alpha(\tfrac{11}{4}\sin^4\nu_0' - 3\sin^2\nu_0' + 5) + \sin^2\alpha\cos^2\alpha(-3\sin^4\nu_0' + \sin^2\nu_0' + 2) - 2\sin^2\alpha(\sin^4\nu_0' - \sin^2\nu_0' + 1), \quad (171)$$

$$\langle[\sin^2\nu'\sin 2(\Theta_0-\Theta)]^2\rangle_\eta = \tfrac{1}{2}\sin^4\alpha(1-5\sin^2\nu_0') + 2\sin^2\alpha\sin^2\nu_0'. \quad (172)$$

Averaging the terms $\sin^4\alpha$ and $\sin^2\alpha\cos^2\alpha$ by making use of the probability density given by Eq. (125) we obtain[5]

$$\langle\sin^4\alpha\rangle = (2+\alpha_1^{-2})\langle\sin^2\alpha\rangle - 1, \quad (173)$$

$$\langle\sin^2\alpha\cos^2\alpha\rangle = 1-(1+\alpha_1^{-2})\langle\sin^2\alpha\rangle, \quad (174)$$

where $\langle\sin^2\alpha\rangle$ is given by Eq. (139). Now, by Eqs. (166) – (174) the variances of Stokes parameters for a compact group of stars, given by Eqs. (164) and (165), can be written in the explicit form

$$\sigma_Q^2 = 2(s_{03}/S)\{[1.086\,\tfrac{3}{2}S\langle(\sigma_E-\sigma_H)F n_g\rangle]^2(\langle\delta_0^2\rangle+1)[C_1(\alpha_1)\cos^2 2(\Theta_0-90°)\sin^4\nu_0' + C_2(\alpha_1)\sin^2\nu_0' + C_3(\alpha_1)] - (\overline{Q_G})^2\}, \quad (175)$$

$$\sigma_U^2 = 2(s_{04}/S)\{[1.086\,\tfrac{3}{2}S\langle(\sigma_E-\sigma_H)F n_g\rangle]^2(\langle\delta_0^2\rangle+1)[C_1(\alpha_1)\sin^2 2(\Theta_0-90°)\sin^4\nu_0' + C_2(\alpha_1)\sin^2\nu_0' + C_3(\alpha_1)] - (\overline{U_G})^2\}, \quad (176)$$

[5] When computing the averages given by Eqs. (139), (173) and (174) the Eqs. (6), (9), and (11) of chapter 4.2 of Erdelyi *et al.* (1954) were used.

where the values of the trigonometric terms can be found from Eqs. (133) and (134) while the functions $C_1(\alpha_1)$, $C_2(\alpha_1)$, and $C_3(\alpha_1)$ are defined by the equations:

$$C_1(\alpha_1) = \tfrac{1}{8}[(30 + 35\alpha_1^{-2})\langle \sin^2 \alpha\rangle - 27], \tag{177}$$

$$C_2(\alpha_1) + C_3(\alpha_1) = 2\langle \sin^2 \alpha \cos^2 \alpha\rangle, \tag{178}$$

$$C_3(\alpha_1) = \tfrac{1}{2}\langle \sin^4 \alpha\rangle. \tag{179}$$

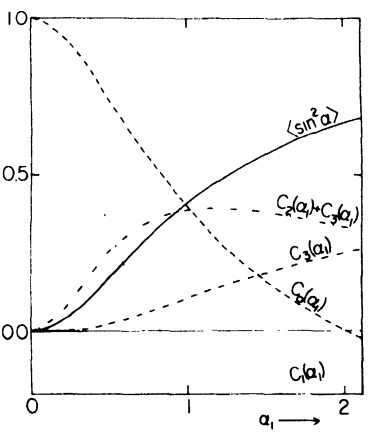


FIG. 7. Functions $\langle \sin^2 \alpha\rangle$, $C_0(\alpha_1)$, $C_1(\alpha_1)$, $C_2(\alpha_1) + C_3(\alpha_1)$, and $C_3(\alpha_1)$.

The graphs of these functions are given in Fig. 7. As results from Eqs. (154), (155), and (157) the coefficient $\langle \delta_0^2\rangle + 1$ in Eqs. (175) and (176) is given by

$$\langle \delta_0^2\rangle + 1 = \langle [(\sigma_E - \sigma_H) F n_g]^2\rangle / \langle (\sigma_E - \sigma_H) F n_g\rangle^2. \tag{180}$$

We may now discuss the large-scale behavior of variances of Stokes parameters on replacing l_B and b_B in Eqs. (133) and (134) by $\overline{l_B}$ and $\overline{b_B}$. Let us consider the case when the axis of symmetry of the aligning mechanism is directed towards the galactic equator (which means $\overline{b_B} = 0°$ and $\overline{\Theta_0} = 90°$) and the stars considered are also on the galactic equator. We shall denote by $\overline{Q_G}(90°)$ the value of $\overline{Q_G}$ for $|\, l - \overline{l_B}\,| = 90°$. If the direction to the stars is parallel to the mean axis of symmetry of the aligning mechanism, i.e., if $|\, l - \overline{l_B}\,| = 0°$, Eqs. (175) and (176) reduce to

$$\sigma_Q^2(0°) = 2(s_{03}/S)\,[\overline{Q_G}(90°)]^2\,(\langle \delta_0^2\rangle + 1)\, C_3(\alpha_1)/[C_0(\alpha_1)]^2, \tag{181}$$

$$\sigma_U^2(0°) = 2(s_{04}/S)\,[\overline{Q_G}(90°)]^2\,(\langle \delta_0^2\rangle + 1)\, C_3(\alpha_1)/[C_0(\alpha_1)]^2. \tag{182}$$

On the other hand, if $b = \overline{b_B} = 0°$ and the direction to the stars is perpendicular to the axis of symmetry (i.e., if $|l - \overline{l_B}| = 90°$) we have, by Eqs. (146) and (147),

$$\sigma_Q^2(90°) = 2(s_{03}/S)\,[\overline{Q_G}(90°)]^2\,\{(\langle\delta_0^2\rangle + 1)\,[C_1(\alpha_1) + C_2(\alpha_1) + C_3(\alpha_1)]/[C_0(\alpha_1)]^2\} - 2(s_{03}/S)\,[\overline{Q_G}(90°)]^2, \tag{183}$$

$$\sigma_U^2(90°) = 2(s_{01}/S)\,[\overline{Q_G}(90°)]^2\,(\langle\delta_0^2\rangle + 1)\,[C_2(\alpha_1) + C_3(\alpha_1)]/[C_0(\alpha_1)]^2. \tag{184}$$

Combining Eqs. (181) – (184) we have

$$\sigma_Q^2(0°)/\sigma_U^2(0°) = s_{03}/s_{01}, \tag{185}$$

$$\sigma_U^2(90°)/\sigma_U^2(0°) = [C_2(\alpha_1) + C_3(\alpha_1)]/C_3(\alpha_1), \tag{186}$$

$$\frac{\sigma_Q^2(90°) + 2(s_{03}/S)\,[\overline{Q_G}(90°)]^2}{\sigma_U^2(90°)} = 1 + \frac{C_1(\alpha_1)}{C_2(\alpha_1) + C_3(\alpha_1)}. \tag{187}$$

Having obtained sufficiently accurate values of the variances of the Stokes parameters, we may use the Eqs. (181) – (187) for estimating the parameters α_1, $\langle\delta_0^2\rangle$, s_{03}, and s_{01}. The independent method of estimating the microscales s_{0l} will be discussed in Section VIII, B.

C. *Observational Results*

The theoretical expressions for the mean values and variances of Stokes parameters Q_G and U_G will now be compared with values derived from observations. We shall limit our discussion to stars in low galactic latitudes as only here is sufficient observational material available.

For computing the mean values and standard deviations of Stokes parameters[6] we use all the stars in the Hall (1958) and Behr (1959b) catalogues, which are situated in the galactic equatorial belt and for which reliable values of the distance modulus and interstellar reddening are known. We also use the polarization measurements of stars with known interstellar λ4430 band intensities (Krzemiński, 1959) and of stars in open clusters M29 (Hiltner, 1954b), NGC 2244 (Hoag and van P. Smith, 1959) and those measured by Krzemiński (1961) in NGC 2169, 7243 and in J. Stock's cluster in Perseus. Our galactic coordinates and position angles θ_G used for computing the Stokes parameters refer to the new galactic pole (Blaauw *et al.*, 1959).

The dependence of Stokes parameter Q_G on distance shown in Fig. 8 is

[6] More details of these computations are given in another paper (Serkowski, 1961).

based on stars with galactic latitude $|b^{II}| \geq 3°0$ for distance moduli larger than 9^m0 (i.e., for distances larger than 630 pc) and with $|b^{II}| \geq 6°0$ for nearer stars. These stars are arranged in 30° longitude intervals. The data on Fig. 8 show that the distance dependence for stars with distance moduli larger than 9^m is only slight, so we are justified in considering all these stars together.

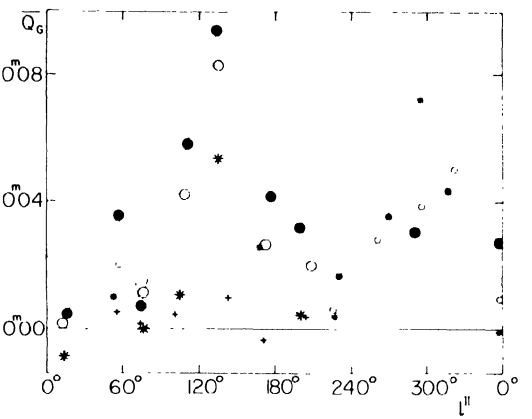


FIG. 8. Dependence of the mean values of the Stokes parameter Q_G on galactic longitude and distance. Full circles are the mean values for stars with distance moduli $m_0 - M \geq 11^m0$; open circles for $9^m0 \leq m_0 - M < 11^m0$; asterisks for $7^m0 \leq m_0 - M < 9^m0$; and crosses for $5^m0 \leq m_0 - M < 7^m0$. Larger symbols are based on 20 or more stars, while smaller symbols are based on 7 to 19 stars.

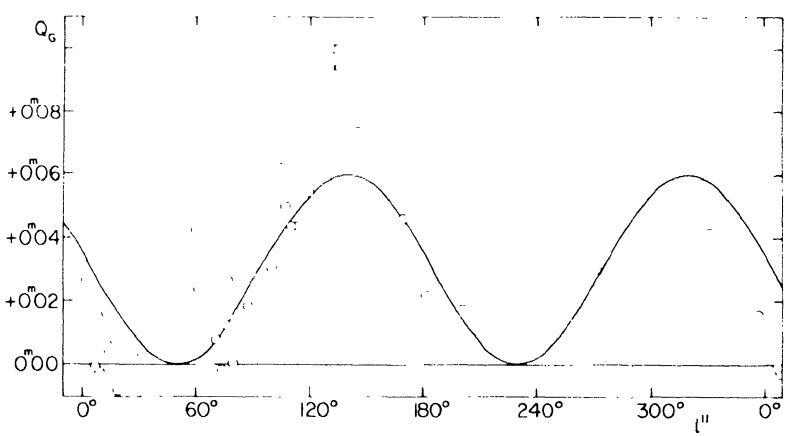


FIG. 9. The mean values of the Stokes parameter Q_G in intervals of galactic longitude, l^{II}, chosen so that the number of stars in the interval is between 20 and 30. Only stars with $|b^{II}| \geq 3°0$ and more than 630 pc distant were used. The double sine wave is arbitrarily drawn with minima at $l^{II} = 50°$ and 230°.

For a more detailed discussion of the longitude dependence of Stokes parameters and their standard deviations only the stars for which $|b^{II}| < 3°0$ and more than 630 pc distant were used. They were grouped into the intervals of galactic longitude of width such that not less than 20 and not more than 30 stars are contained in each interval. The mean values of Stokes parameters for these intervals are shown in Figs. 9 and 10 while the rms deviations of individual values from the mean values are given in Figs. 11 and 12.

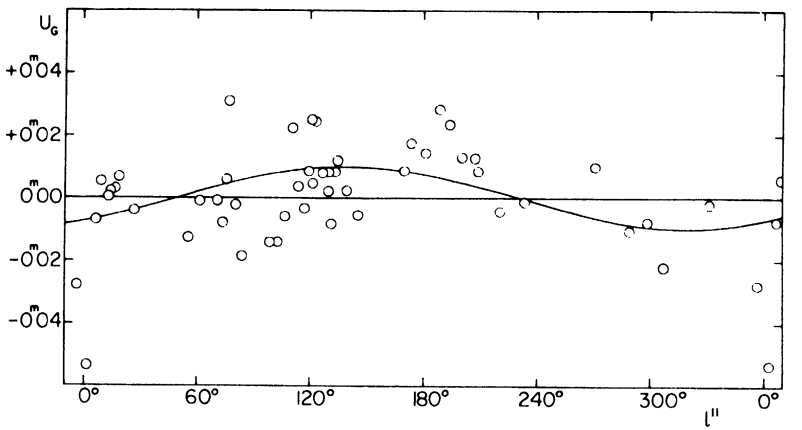


FIG. 10. The mean values of the Stokes parameter U_G for the same stars as those used in Fig. 9. The sine wave is arbitrarily drawn with minimum at $l^{II} = 320°$.

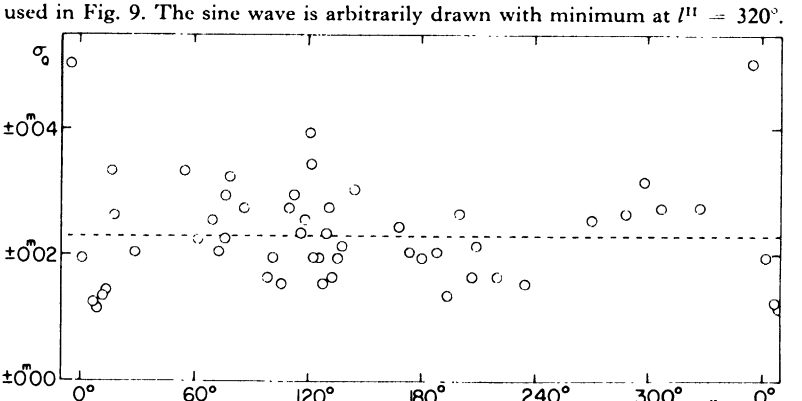


FIG. 11. The standard deviations σ_Q of the Stokes parameter Q_G from its mean values for the same stars as those used in Fig. 9.

Neglecting the unequal height of two maxima in Fig. 9, which remains unexplained, the values of $\overline{Q_G}$ shown in this figure may be represented by the double sine wave, in agreement with Eq. (146). The galactic longitudes

at which the minima of $\overline{Q_G}$ occur are the longitudes $\overline{l_G}$ towards which is directed the mean axis of symmetry of the mechanism aligning the interstellar dust grains. These longitudes are approximately $\overline{l_G}^{II} = 50°$ and 230° and coincide

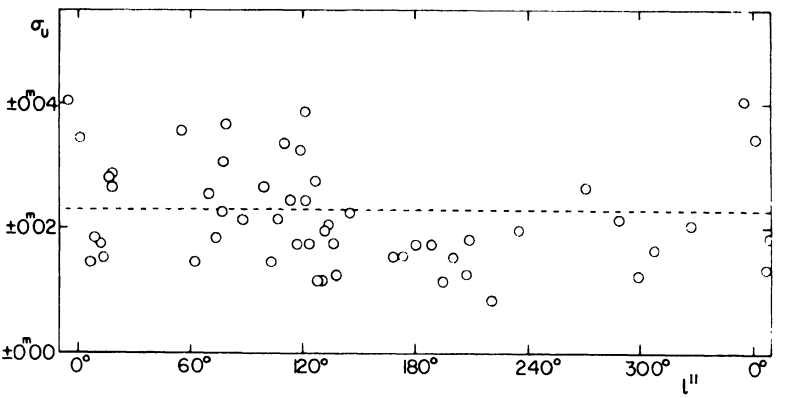


FIG. 12. The standard deviations σ_U of the Stokes parameter U_G from its mean values for the same stars as those used in Fig. 9.

quite closely with directions of galactic spiral arms as determined by Morgan *et al.* (1953) from the distribution of O-type associations. Assuming that the axis of symmetry of the aligning mechanism is directed parallel to the galactic spiral arms we should take into account the curvature of these arms, and diminish the first of the values of $\overline{l_G}^{II}$, quoted above, by some 12° and increase the second value by the same amount. We are not, however, introducing these corrections in the sine curve drawn in Fig. 9.

According to Eq. (147) the mean value of Stokes parameter U_G should be zero for all galactic longitudes if $b = \overline{b_G} = 0°$. However Fig. 10 shows some systematic trend of $\overline{U_G}$ in agreement with a similar longitude dependence of position angle θ_G pointed out by Shain (1957) and Schmidt (1958). The parameter $\overline{U_G}$ seems to assume its maximum value somewhere between the galactic longitudes 120° and 210° and a minimum value between 300° and 30°.

If the future observations confirm that $\overline{U_G}$ considered as a function of galactic longitude may be represented as a single sine wave with the maximum around the galactic longitude $l^{II} = 140°$, this effect can be explained by assuming that the axis of symmetry of the aligning mechanism is inclined at an angle $\overline{b_B}$ to the galactic plane. This can be seen from Eqs. (134) and (144); this last equation for stars on the galactic equator takes the form

$$\overline{U_G} = -\tfrac{1}{2}\overline{Q_G}(90°) \sin 4\,\overline{b_B} \sin (l - \overline{l_B}), \tag{188}$$

where $\overline{Q_G}(90°)$ is the mean value of Q_G for $|l - \overline{l_B}| = 90°$. Comparing the amplitudes of sine curves in Figs. 9 and 10 we can find the value of $\overline{b_B}$ from Eq. (188). Namely, we obtain the following galactic coordinates of the direction of the axis of symmetry of the mechanism aligning the interstellar dust grains

$$\overline{l_B}^{II} = 50°, \quad \overline{b_B}^{II} = -5° \quad \text{and} \quad \overline{l_B}^{II} = 230°, \quad \overline{b_B}^{II} = +5°. \tag{189}$$

The longitude dependence of $\overline{U_G}$ is equally well pronounced for the distant stars as for those nearer than 630 pc. For distant stars $\overline{U_G}$ shows strange behavior in the direction of the galactic center where it assumes large negative values.

The galactic longitude of the axis of symmetry of the aligning mechanism was determined also by Behr (1959b) who used only the stars nearer than 250 pc, both in low and high galactic latitudes, obtaining $\overline{l_B}^{II} = 62°$ and 242 with mean errors of $\pm 5°$.

Behr is using the system of coordinates, called by him "Lokale Spiralarm-system." The pole of these coordinates is in the direction of the axis of symmetry of the aligning mechanism. Computing the position angle θ'' of the plane of vibration in this system of coordinates Behr found that, for stars nearer than 250 pc situated near the equator of this system, the values of θ'' are systematically positive. He supposes that the directions of the axis of symmetry of the aligning mechanism are tangent to a helix with its axis along the spiral arm of the galaxy. The mean value of θ'' gives the helix angle.

The observations of more distant stars do not reveal the effect found by Behr. If such an effect is present for distant stars the mean values of the Stokes parameter U_G would be positive for all galactic longitudes for stars near to the galactic equator, which is not observed (cf. Fig. 10). The polarization measurements of nearby southern stars are necessary to confirm Behr's suggestion.

Figures 11 and 12 can be used for estimating the ratios of the variances for which the theoretical values are given by Eqs. (185) – (187). Because of the very large scatter only qualitative results can be drawn from these figures:

a. The values $\sigma_Q(0°)$ seem to be equal to $\sigma_U(0°)$, which means that the micro-scales s_{03} and s_{04} are equal one to another.

b. The values σ_U at those galactic longitudes where $\overline{Q_G} = 0$ are at best slightly smaller than those for galactic longitudes for which $\overline{Q_G}$ has a maximum. This means that $C_2(\alpha_1)/C_3(\alpha_1)$ is not a large quantity and α_1 must be near, or slightly larger than unity.

c. The values $\sigma_Q(90°)$ are nearly equal to $\sigma_U(90°)$ which supports the estimate of α_1 given in point b.

d. The mean value of the standard deviation of both Stokes parameters, being of the order of $\pm 0^{m}023$ suggests, according to Eqs. (181) – (184), that $(\langle\delta_0^2\rangle + 1)\, s_{0j}/S \approx 1/30$ for $j = 1, 2$.

The standard deviations plotted in Figs. 11 and 12 are affected by the dispersion in the distances of stars. The really trustworthy values of standard deviations can be obtained from data on stars within open clusters or associations which are all practically at the same distance. Some discussion of such data will be given in Section VIII, B.

D. *Polarization and Extinction*

The square root of the sum of the squares of the Stokes parameters Q_G and U_G for an individual star, given by Eqs. (143) and (144), equals its amount of polarization:

$$p = 1.086\, \tfrac{3}{2} S \,|\, (\sigma_E - \sigma_H) F n_g \, C_0(\alpha_1) \,|\, \sin^2 \nu_0'. \tag{190}$$

We shall evaluate $\sin^2 \nu_0'$ from this equation and substitute into Eq. (142), obtaining

$$A = 1.086\, S \{ \tfrac{1}{3} (\sigma_E + \sigma_H + \sigma_S) n_g + \tfrac{1}{2} (\sigma_E + \sigma_H - 2\sigma_S) F n_g \, C_0(\alpha_1) \} - A_p p, \tag{191}$$

where the coefficient A_p is approximately the same for all the stars.

This means that the total absorption should depend slightly on polarization. Writing Eq. (191) for different colors and taking the ratios, we find that the ratio E_{U-B}/E_{B-V} of the reddening determined from U and B colors to that determined from B and V colors should depend linearly on the ratio p/A. Greenberg and Meltzer (1960) found that this ratio of reddenings is larger for stars viewed along the galactic spiral arm (in Cygnus) as compared to those viewed across the arm (in Cassiopeia). Their results are, however, biased by the fact that the stars of spectral types characterized by high values of the ratio of reddenings are relatively more numerous in Cygnus than in Cassiopeia. The sample computations for stars of few selected spectral types, taken from Hiltner's (1956) catalogue show (Serkowski, 1961) that the dependence of the ratio of reddenings on polarization, if any, is at least five times smaller than suggested by Greenberg and Meltzer's data.

The above subtle effect has of course negligible influence on the general form of the dependence between the interstellar extinction and polarization. From Eqs. (145) and (146) it can be seen that both $\overline{A}$ and $\overline{Q_G}$ are proportional to the distance S, and for given galactic coordinates should increase with distance. This means that for a given small region of the sky the ratios $\overline{Q_G}/\overline{A}$ should be independent of distance if the polarizing efficiency of the interstellar medium is everywhere the same.

The observed dependence of the ratio $\overline{Q_G}/\overline{A_v}$ on galactic longitude and distance is shown in Fig. 13 where the same stars are used as in Fig. 8; here

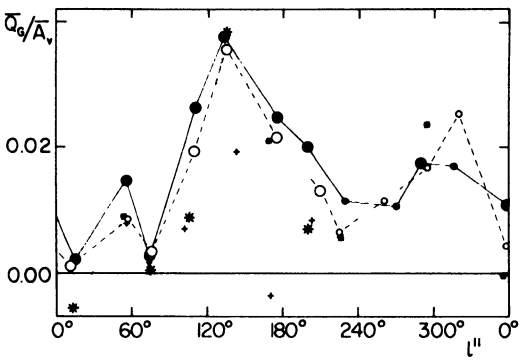


FIG. 13. Dependence of the ratio of Stokes parameter $\overline{Q_G}$ to visual extinction $\overline{A_v}$ on galactic longitude and distance for the same stars as those used in Fig. 8. Full circles are ratios for stars with distance moduli $m_0 - M \geqslant 11^m.0$; open circles for $9^m.0 \leqslant m_0 - M < 11^m.0$; asterisks for $7^m.0 \leqslant m_0 - M < 9^m.0$; and crosses for $5^m.0 \leqslant m_0 - M < 7^m.0$. Larger symbols are based on 20 or more stars, while smaller symbols are based on 7 to 19 stars.

A_v is defined as the reddening E_{B-V} multiplied by a factor 3. The dependence of the ratio $\overline{Q_G}/\overline{A_v}$ on distance, evident in Fig. 13, can be attributed to the effect of selection: among the distant, highly polarized stars only those were observed which are not too strongly dimmed by interstellar extinction. This explanation was questioned by Pacholczyk (1959a) who pointed out that the distance dependence of the ratio of polarization to extinction is even more pronounced for supergiants; these stars are practically free of this selection effect. Pacholczyk (1959b) also finds a similar distance dependence of the ratio of Q_G to the intensity of the interstellar $\lambda 4430$ absorption band. His conclusion that polarization is produced more effectively in rarefied H II regions between the spiral arms of the galaxy finds support in theoretical estimates of distribution parameter F in H I and H II regions made by Grzedzielski (1958).

Hiltner (1956) and Schmidt (1958) investigated the dependence of the ratio p/A_v on A_v in narrow intervals of galactic longitude and distance. They found that this ratio is a decreasing function of A_v. According to Schmidt we have

$$p/A_v = \alpha - \beta A_v, \tag{192}$$

where α and β are constant for each interval of galactic longitude. The constant β, called "depolarization parameter" by Schmidt, is always positive and proportional to the mean ratio p/A_v for a given longitude.

The fact that the ratio p/A_v decreases with increasing A_v can be explained by the properties of the quantity p, which is defined as always positive. If there is some scatter in the values of the Stokes parameters Q_G and U_G for individual stars and if $\overline{U_G} = 0$ the difference between the mean values of p and Q_G will be large if $\overline{Q_G}$ is small, and will be small if $\overline{Q_G}$ is large. Thus even if the ratio Q_G/A is independent of A the ratio p/A will be a decreasing function of A. In those galactic longitudes where $\overline{Q_G}$ vanishes, the parameter β will also vanish because $\overline{Q_G}$ will be equal to zero for all the intervals of A.

It may be deduced from Eqs. (142) and (143) that the ratio Q_G/A should be independent of A if the distribution parameter F is independent of n_g and if the small term proportional to F in Eq. (142) is neglected.

The diagrams of Q_G/A_v as a function of A_v were made by Serkowski (1961) for different intervals of galactic longitude; all the available stars with galactic latitude $| b^{II} | < 6°0$ without regard to distance were taken into account. These diagrams show no trace of the dependence of Q_G/A_v on A_v for all galactic longitudes except $125° < l^{II} < 155°$. The diagram for this last interval is shown in Fig. 14. More than two-thirds of the stars plotted in this diagram are at

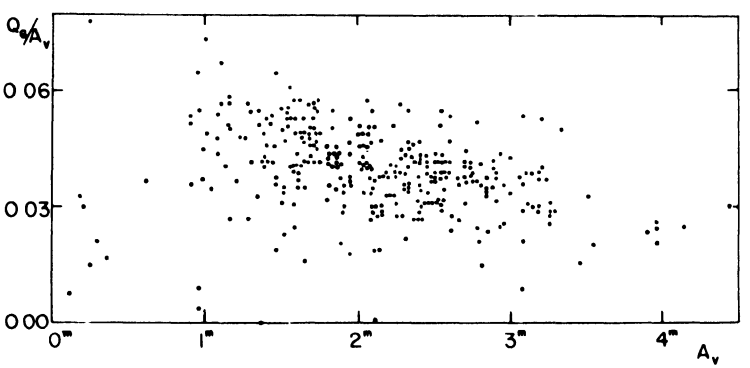


FIG. 14. Dependence of the ratio Q_G/A_v on A_v for individual stars in galactic longitudes $125° < l^{II} < 155°$ and galactic latitudes $| b^{II} | < 6°0$.

distances larger than 1600 pc which means that they belong the the Perseus arm. Nearly half of these distant stars are members of the association surrounding the Double Cluster in Perseus.

As will be more fully discussed in Section VIII, A, there is some evidence of a relationship between the distribution parameter F and the number of dust grains n_g per unit volume, along the path to the Double Cluster in Perseus and probably along the path to all the Perseus spiral arm. This relationship can explain the observed dependence of Q_G/A_v on A_v.

VII

ALIGNMENT MECHANISMS

A. *Collisions of Dust Grains*

In the last two sections we estimated the influence of the extinction cross sections and the orientation of the axis of symmetry on stellar polarization. The present section will be devoted to the estimates of the distribution parameter, which depends on the nature of the aligning mechanism.

Following the fundamental paper by Davis and Greenstein (1951) we shall express the distribution parameter in the form suitable for discussion of the alignment mechanism.

Let us introduce the system of coordinates in which one coordinate axis is in the direction **B** of the axis of symmetry of the aligning mechanism while the other axis is perpendicular to the plane determined by **B** and by the direction **S** of incident light (Fig. 15). We assume that the dust grain is rotating and its

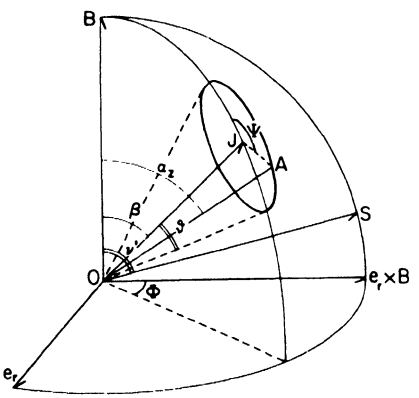


FIG. 15. Definition of angles describing the orientation of a single dust grain.

angular momentum **J** (which Davis and Greenstein denote by **H**) makes an angle β with the direction **B** of the axis of symmetry of the aligning mechanism, and an angle ϑ with the axis of symmetry OA of the dust grain. The axis of symmetry of a dust grain describes the cone when the grain is rotating. The angle between the axis of symmetry of the dust grain and that of the aligning mechanism will be denoted by α_Z.

Let

$$f(\beta, \vartheta, a)\, n_g\, d\beta\, d\vartheta \tag{193}$$

be the number of dust grains per cubic centimeter so oriented that β lies between β and $\beta + d\beta$ and ϑ lies in range from ϑ to $\vartheta + d\vartheta$; n_g is the total number of dust grains per cm^3 and a is the mean radius of the grain.

If there are no forces orienting the dust grains the function $f(\beta, \vartheta, a)$ assumes a certain form depending on the collisions of dust grains with atoms of gas and is independent of a. We shall denote this form, corresponding to the equipartition of energy, by $f_e(\beta, \vartheta)$. Assuming the Maxwell-Boltzmann distribution, Davis and Greenstein (1951, Appendix 2) found that

$$f_e(\beta, \vartheta) = \tfrac{1}{2}\gamma^{1/2} \sin\beta \sin\vartheta(\gamma \cos^2\vartheta + \sin^2\vartheta)^{-3/2}, \tag{194}$$

where γ is the ratio of the moment of inertia of a dust grain about its equatorial axis to that about its axis of symmetry. Here and in future we assume for simplicity that the dust grains are ellipsoids of revolution.

If a small torque is acting on a dust grain the function $f(\beta, \vartheta, a)$ may be written in the form

$$f(\beta, \vartheta, a) = f_e(\beta, \vartheta) + f_1(\beta, \vartheta, a), \tag{195}$$

where the disturbance $f_1(\beta, \vartheta, a)$ depends on the nature of the aligning mechanism.

We can easily find that the value of $\cos^2\alpha_Z$ averaged over all dust grains is

$$\langle\cos^2\alpha_Z\rangle = \int_0^{\pi/2}\int_0^{\pi} \langle\cos^2\alpha_Z\rangle_{\Psi,\Phi} f(\beta, \vartheta, a)\, d\beta\, d\vartheta, \tag{196}$$

where the index Ψ, Φ denotes averaging over these angles which are defined by Fig. 15; the angles β and ϑ should remain unchanged during this averaging. We have also

$$\int_0^{\pi/2}\int_0^{\pi} \langle\cos^2\alpha_Z\rangle_{\Psi,\Phi} f_e(\beta, \vartheta)\, d\beta\, d\vartheta = \frac{1}{3}. \tag{197}$$

By substitution of Eqs. (196) and (197) into Eq. (113) we can write the definition of the distribution parameter in the form

$$F = -\int_0^{\pi/2}\int_0^{\pi} \langle\cos^2\alpha_Z\rangle_{\Psi,\Phi} f_1(\beta, \vartheta, a)\, d\beta\, d\vartheta. \tag{198}$$

The dust grains are subject to the aligning torque while, on the other hand, the collisions of grains with gas atoms and ions are destroying this alignment. After attaining the equilibrium, the sum of changes of the distribution parameter due to these two causes becomes equal to zero, which we can write as

$$\left.\frac{dF}{dt}\right|_{\text{torque}} + \left.\frac{dF}{dt}\right|_{\text{coll}} = 0, \tag{199}$$

where the time derivative with the index "torque" is computed when the aligning torque only is acting, while that with the index "coll" is computed when only the collisions with gas are at work.

If the influence of collisions on the alignment of dust grains is negligibly small, the term $\langle \cos^2 \alpha_Z \rangle$ will be 0 or 1, depending on the character of the alignment. Hence F, as a result of Eq. (113), will be equal to 1/3 or $-$ 2/3. On the other hand, let us assume that collisions of dust grains with gas atoms or ions have so strong an influence on the alignment of dust grains that

$$f_1 \ll f_e. \tag{200}$$

Davis and Greenstein make this assumption and instead of strict computation of the derivative $dF/dt|_{\text{coll}}$ on the ground of statistical mechanics they make only the rough estimate of this derivative expressing it in terms of the conventionally defined relaxation time; as stressed by Davis (1958) this is the weakest point of their theory. They assume, namely, that

$$\left.\frac{dF}{dt}\right|_{\text{coll}} = -\frac{F_l}{\tau}, \tag{201}$$

where $F_l = F$ for $F_l \ll 1/3$, and the relaxation time τ is defined by the equation

$$\tau = (m_g/m_H)\, t_{H,g}; \tag{202}$$

$t_{H,g}$ here denotes the average time interval between the consecutive collisions of a dust grain with hydrogen atoms or ions, while m_g and m_H denote the mass of a dust grain and hydrogen atom, respectively. For the grain containing a sufficiently large number of molecules we have

$$t_{H,g} = 1/(\pi a^2 v_H n_H), \tag{203}$$

where πa^2 is the cross-sectional area of the dust grain, v_H is the rms velocity of gas atoms relative to the dust grain, and n_H is the number of gas atoms per unit volume. Neglecting the thermal motions of dust grains, being much smaller than those of the gas, we find v_H from the known formula

$$v_H = (3k\, T/m_H)^{1/2}, \tag{204}$$

where k is Boltzmann's constant and T is the temperature of the gas. By substitution of $m_g = \frac{4}{3}\pi \rho_g a^3$, where ρ_g is the internal density of the dust grain, we find the relaxation time

$$\tau = \frac{4}{3(3k\, m_H)^{1/2}} \cdot \frac{\rho_g\, a}{n_H\, T^{1/2}} = 5.05 \times 10^{19} \frac{\rho_g\, a}{n_H\, T^{1/2}}. \tag{205}$$

From Eqs. (199) and (201) we obtain

$$F_l = \tau \frac{dF}{dt}_{\text{torque}}; \tag{206}$$

the derivative on the right-hand side of this equation is equal to the time derivative of the expression on the right-hand side of Eq. (198). Since in Eq. (198) only $f_1(\beta, \vartheta, a)$ can depend on time, Eq. (206) takes the form

$$F_l = -\tau \int_0^{\pi/2} \int_0^{\pi} \langle \cos^2 \alpha_Z \rangle_{\psi,\Phi} \frac{\partial f_1}{\partial t} \, d\beta \, d\vartheta, \tag{207}$$

where, by spherical trigonometry (cf. Davis and Greenstein, 1951, Appendix 1),

$$\langle \cos^2 \alpha_Z \rangle_{\psi,\Phi} = \cos^2 \beta \cos^2 \vartheta + \tfrac{1}{2} \sin^2 \beta \sin^2 \vartheta. \tag{208}$$

To evaluate the term $\partial f_1 / \partial t$ in Eq. (207) let us regard each grain as characterized by a representative point in $\beta - \vartheta$ space. The density of the representative points will be $f(\beta, \vartheta, a)$, as defined by Eq. (195). These points move with the velocity

$$\mathbf{v} = \langle \dot{\beta} \rangle \mathbf{e}_\beta + \langle \dot{\vartheta} \rangle \mathbf{e}_\vartheta, \tag{209}$$

where angular brackets denote the averaging over one full rotation of the dust grain, dots denote the time derivatives, and $\mathbf{e}_\beta$, $\mathbf{e}_\vartheta$ are unit vectors along the coordinates axes. Since points corresponding to dust grains never vanish, the usual equation of continuity gives

$$\frac{\partial f}{\partial t} = -\operatorname{div}(\mathbf{v} f). \tag{210}$$

Since $\partial f_e / \partial t = 0$, by inequality (200) (which simply means that the time of relaxation is very short) and Eqs. (209) and (210) we have

$$\frac{\partial f_1}{\partial t} = -\frac{\partial}{\partial \beta} (\langle \dot{\beta} \rangle f_e) - \frac{\partial}{\partial \vartheta} (\langle \dot{\vartheta} \rangle f_e). \tag{211}$$

By substitution of Eqs. (208) and (211) Davis and Greenstein finally write Eq. (207) in the form

$$F_l = \tau \int_0^{\pi/2} \int_0^{\pi} (\cos^2 \beta \cos^2 \vartheta + \tfrac{1}{2} \sin^2 \beta \sin^2 \vartheta) \left[\frac{\partial}{\partial \beta} (\langle \dot{\beta} \rangle f_e) + \frac{\partial}{\partial \vartheta} (\langle \dot{\vartheta} \rangle f_e) \right] d\beta \, d\vartheta. \tag{212}$$

For evaluating the average derivatives $\langle \dot{\beta} \rangle$ and $\langle \dot{\vartheta} \rangle$ in this equation we have to make more detailed assumptions concerning the mechanism aligning the dust grains.

B. *Alignment Due to Paramagnetic Absorption*

Among the proposed alignment mechanisms the best explanation of the observations gives the alignment mechanism proposed by Davis and Greenstein (1951) which is based on the effect of paramagnetic absorption. Its principle can be explained in the following way (cf. van de Hulst, 1955).

Let us suppose that a paramagnetic or ferromagnetic dust grain is rotating around the axis parallel to the direction of an external magnetic field. The collisions of the grain with gas atoms with a velocity perpendicular to the direction of the magnetic field cause only a change in the angular velocity of the grain thus approaching the state of equipartition of energy. If, on the other hand, the velocity of the gas atom is not perpendicular to the direction of the magnetic field, collision causes the deviation of the axis of rotation of the grain from the direction of the magnetic field. This means that each volume element inside the grain will periodically change its magnetization due to the rotation of the grain. The movement of the grain is now affected by internal damping, called *paramagnetic absorption*, which is caused by the changes of magnetization. Davis and Greenstein have shown that the result of such damping is a decrease in the angle β between the axis of rotation of the grain and the direction of the magnetic field, and a decrease in the kinectic energy of rotation of the grain.

As results from the discussion of the Poinsot ellipsoid of inertia, the smallest value of the kinetic energy of rotation for a given value of angular momentum corresponds to the rotation of a body around the shortest axis of the ellipsoid of inertia. Hence, as a result of the effect of paramagnetic absorption the grains become aligned so that they rotate around their shortest axes directed parallel to the direction of the magnetic field. In order to explain the observed dependence of the Stokes parameter Q_G on galactic longitude we must assume that the galactic magnetic field is directed, on the average, parallel to the spiral arms of the galaxy.

The vector of angular velocity of a dust grain, $\boldsymbol{\omega}$, is obtained as the sum of the rotation of the grain around its axis of symmetry OA and the rotation around the direction of the angular momentum **J**. This last rotation, called the nutational motion by Davis and Greenstein, is the result of the rotation of the axis of symmetry OA around **J**. "*One nutation*" is called the single full rotation of the axis OA around **J**, as determined by a nonrotating observer. Due to nutation, the vector $\boldsymbol{\omega}$ quickly changes its direction in space and its direction relative to the dust grain.

If there are no external forces we have $\mathbf{J} = \text{const}$. If there are aligning forces with axis of symmetry in direction **B**, the vector of angular momentum **J** is rotating slowly around **B**; this motion is called *precession* by Davis and Greenstein.

As was shown by these authors, if there is no torque the equipartition of energy between dust and gas occurs. The kinetic energy of rotation of the dust grain, R_e, should in this case be equal to the mean kinetic energy of the gas atoms, i.e., we should have

$$R_e = \tfrac{3}{2}kT. \tag{213}$$

On the other hand we have

$$R_e = \tfrac{1}{2}\omega_e^2 \overline{I_g}, \tag{214}$$

where ω_e is the angular velocity of the dust grain, corresponding to the equipartition of energy and

$$\overline{I_g} \approx \frac{5}{3} a^5 \rho_g, \tag{215}$$

is the mean moment of inertia for the grain of average radius a and density ρ_g. Hence the rms angular velocity of dust grains, assumed to be equal to equipartition velocity, is

$$\omega_e \approx 1.57 \cdot 10^{-8} T^{1/2}/(a^{5/2} \rho_g^{1/2}) \text{ rad/sec}, \tag{216}$$

which for $a = 2 \times 10^{-5}$ cm, $\rho_g = 1$, and $T = 10^2$ in H I regions and 10^4 in H II regions gives the angular velocity of dust grains

$$\omega_e = \begin{cases} 10^5 \text{ rad/sec in H I regions,} \\ 10^6 \text{ rad/sec in H II regions.} \end{cases} \tag{217}$$

To consider in more detail the alignment mechanism based on paramagnetic absorption we shall recall the definitions of some parameters describing the properties of magnetic materials. The strength of a microscopic magnetic field **H** in magnetic material is connected in the cgs system of units with *magnetic flux density* **B** (called also magnetic induction and being the strength of a microscopic magnetic field), by the relation

$$\mathbf{H} = \mathbf{B} - 4\pi\mathbf{M}; \tag{218}$$

where **M** is *magnetization*, which is equal to the vector sum of the magnetic moments of all the molecules of magnetic material in unit volume. Hence the magnetic moment of a dust grain is $V_g\mathbf{M}$ where V_g is the volume of a dust grain.

In para- and diamagnetics, vectors **M** and **B** are proportional to **H** in a constant magnetic field; we have

$$\mathbf{M} = \chi\mathbf{H}, \tag{219}$$

$$\mathbf{B} = \mu\mathbf{H}, \tag{220}$$

where coefficients χ and μ are *magnetic susceptibility* and *permeability*, respectively. From Eqs. (218) – (220) we find

$$\chi = (\mu - 1)/4\pi. \tag{221}$$

For diamagnetics we have $\chi < 0$ and $\mu < 1$; for a vacuum $\chi = 0$ and $\mu = 1$; for paramagnetics $\chi > 0$ and $\mu > 1$. Since for para- and diamagnetics $\mu \approx 1$ we have approximately

$$\mathbf{M} \approx \chi \mathbf{B}. \tag{222}$$

Let us suppose that the magnetic material is in a magnetic field varying sinusoidally according to the equation $\mathbf{B} = \mathbf{e}\, B_0 \exp[i(\omega t + \epsilon_0)]$ where $\mathbf{e}$ is a unit vector and $B_0 = \text{const}$. In general, magnetic susceptibility is a complex quantity, $\chi = \chi' - i\chi''$, where the imaginary part χ'' depends on frequency. Hence we have by Eq. (222)

$$\mathbf{M} = \mathbf{e}\, \mathbf{B}_0(\chi' - i\chi'')\,[\cos(\omega t + \epsilon_0) + i \sin(\omega t + \epsilon_0)[. \tag{223}$$

The real part of this expression gives the magnetization

$$\mathbf{M} = \mathbf{e}\, \mathbf{B}_0[\chi' \cos(\omega t + \epsilon_0) + \chi'' \sin(\omega t + \epsilon_0)]. \tag{224}$$

For $\omega = 0$, i.e., for static magnetic field, we have $\chi'' = 0$ and $\chi' = \chi_0$, where χ_0 is static magnetic susceptibility. The imaginary part, χ'', of magnetic susceptibility determines the amount of heat generated by an alternating magnetic field, i.e., it determines the so called *magnetic absorption.*

To compute the torque on the dust grain, which equals the time derivative of its angular momentum $\mathbf{J}$, we shall consider, following Davis (1958), the constant magnetic field resolved into components along axes that rotate with the grain. Let these axes be the usual principal axes of an axially symmetric grain. They are localized in the usual way by means of Eulerian angles in a nonrotating system of coordinates whose polar axis lies along the angular momentum of the grain. Now the magnetic flux density represented as a function of time is

$$\mathbf{B}(t) = \sum_{i,k} \mathbf{e}_i\, B_{ik} \cos(\omega_{ik}\, t + \epsilon_{ik}), \tag{225}$$

where $\mathbf{e}_i$ $(i = 1, 2, 3)$ are unit vectors along the axes fixed with respect to grain while B_{ik}, ω_{ik}, and ϵ_{ik} are constants which can be expressed in terms of Eulerian angles.

Magnetization corresponding to each trigonometric term, such as, $\mathbf{e}_1 B_{11} \cos(\omega_{11} t + \epsilon_{11})$ is

$$\mathbf{e}_1 B_{11}[\chi' \cos(\omega_{11} t + \epsilon_{11}) + \chi''_{11} \sin(\omega_{11} t + \epsilon_{11})] = \mathbf{e}_1 \chi_t B_{11} \cos[(t - t_0)\omega_{11} + \epsilon_{11}], \tag{226}$$

provided that $\chi' = \chi_t \cos(\omega_{11} t_0)$ and $\chi''_{11} = \chi_t \sin(\omega_{11} t_0)$, where

$$t_0 = \frac{(\chi''/\omega)}{\chi'} \ll 1 \tag{227}$$

is a constant; according to former assumptions about χ' and χ'' the present conditions give approximately $\chi'' \approx \chi' \omega_{11} t_0$. Since χ'' depends on frequency it is different for each value of ω_{ik}.

We are dealing with linear theory and for that reason we can treat each of the terms which are summed in Eq. (225) in the same way and superpose them, obtaining the magnetization

$$\mathbf{M} = \sum_{i,k} \mathbf{e}_i B_{ik} \chi_t \cos[(t - t_0)\,\omega_{ik} + \epsilon_{ik}] \approx \chi' \mathbf{B}(t - t_0), \tag{228}$$

where $\mathbf{B}(t - t_0)$ is the magnetic flux density in the moment $t - t_0$. Hence, in a rotating system of coordinates, in the moment t magnetization has the same direction as $\mathbf{B}(t)$ had in the moment $t - t_0$; this is the effect of *paramagnetic relaxation.* Magnetization expressed in the inertial system is

$$\mathbf{M} \approx \chi' [\mathbf{B} + (\boldsymbol{\omega} t_0) \times \mathbf{B}], \tag{229}$$

where $\boldsymbol{\omega} t_0$ is the infinitesimal rotation by the angle $\omega t_0 = \chi''/\chi'$ radians.

The torque $d\mathbf{J}/dt$ acting on the dust grain in a magnetic field characterized by magnetic flux density $\mathbf{B}$ is

$$d\mathbf{J}/dt = V_g \mathbf{M} \times \mathbf{B}, \tag{230}$$

where $V_g \mathbf{M}$ is the magnetic moment of the dust grain. Hence, by Eqs. (227) and (229) we have

$$d\mathbf{J}/dt = V_g \chi'' \omega^{-1} (\boldsymbol{\omega} \times \mathbf{B}) \times \mathbf{B}. \tag{231}$$

Let $\mathbf{e}_\sigma$ be the unit vector perpendicular to $\mathbf{B}$ and directed in the plane defined by $\mathbf{B}$ and $\mathbf{J}$. Denoting by $\mathbf{J}_\pi$ and $\mathbf{J}_\sigma$ the components of $\mathbf{J}$ parallel to $\mathbf{B}$ and parallel to $\mathbf{e}_\sigma$, respectively, we have

$$J_\pi = J \cos\beta; \quad J_\sigma = J \sin\beta = J \tan\beta \cos\beta = J_\pi \tan\beta. \tag{232}$$

Hence, making use of the fact that, by Eq. (231), $d\mathbf{J}/dt$ is the vector product of some vector and vector $\mathbf{B}$, we have

$$\left\langle \frac{dJ_\pi}{dt} \right\rangle = \left\langle \frac{d\mathbf{J}}{dt} \cdot \mathbf{B} \right\rangle = 0, \tag{233}$$

$$\left\langle \frac{dJ_\sigma}{dt} \right\rangle = \left\langle \frac{d(J_\pi \tan\beta)}{dt} \right\rangle = \frac{J}{\cos\beta} \langle \dot{\beta} \rangle. \tag{234}$$

Taking into consideration Eqs. (231), (233), and (234) Davis and Greenstein represent the components of angular momentum **J** as products of corresponding components of angular velocity of the dust grain and the moments of inertia of the dust grain, obtaining, after somewhat lengthy calculations,

$$\langle \dot{\beta} \rangle = -\frac{\chi'' V_g B^2}{\omega I_g \gamma} \sin\beta \cos\beta(\gamma \cos^2\vartheta + \sin^2\vartheta), \tag{235}$$

where I_g and $I_g\gamma$ are the moments of inertia of the dust grain about its axis of symmetry and equatorial axis, respectively. As results from Eq. (235), if $\beta < 90°$ initially, we have $\dot{\beta} < 0$ which means that **J** becomes oriented parallel to **B**; if β; if $\beta > 90°$ initially, we have $\dot{\beta} > 0$ and **J** becomes antiparallel to **B**. Hence in each case the directions of vectors **J** and **B** become more accordant in the course of time.

Similarly, averaging over one nutation the time derivative of the kinetic energy of rotation of the dust grain, $\dot{R} = \omega\, d\mathbf{J}/dt$, Davis and Greenstein obtain

$$\langle \dot{\vartheta} \rangle = \frac{\chi''\, V_g\, B^2}{\omega I_g \gamma} (\gamma - 1) \sin\vartheta \cos\vartheta \,(1 - \tfrac{1}{2}\sin^2\beta). \tag{236}$$

Since $0° \leqslant \vartheta \leqslant 90°$ this equation shows that for $\gamma > 1$ (i.e., for prolate spheroidal grain) $\dot{\vartheta} > 0$ and ϑ is increasing; for $\gamma < 1$ (for oblate spheroid) $\dot{\vartheta} < 0$ and ϑ is decreasing. Thus in both cases the grain tends to orient its longest axis perpendicular to the direction of the magnetic field.

The asymptotic value F_l of the distribution parameter given by Eq. (212) is now, by Eqs. (235) and (236), after integrating over β and ϑ (Davis and Greenstein, 1951, Appendix 4),

$$F_l = \frac{\chi''}{\omega} \cdot \frac{V_g\, B^2\, \tau}{I_g}\, \Gamma(\gamma), \tag{237}$$

where $\Gamma(\gamma)$ is a constant depending on the ratio of the axes of the dust grain. Davis and Greenstein use the approximate expression

$$\frac{V_g}{I_g}\Gamma(\gamma) \approx \pm \frac{0.05}{a^2 \rho_g}; \text{ (sign plus for } \gamma > 1, \text{ minus for } \gamma < 1), \tag{238}$$

which gives values accurate within a factor of 2 if the ratio of the longest to shortest axis of the grain is larger than 1.3.

Using Eqs. (205), (237) and (238) we may write the distribution parameter for prolate spheroidal grains in the form

$$F = \begin{cases} \frac{1}{3} & \text{for } F_l \gg \frac{1}{3}, \\ F_l & \text{for } F_l \ll \frac{1}{3}, \end{cases} \tag{239}$$

where

$$F_l = 2.5 \times 10^{18} \frac{B^2}{a\, n_{\mathrm{H}}\, T^{1/2}} \cdot \frac{\chi''}{\omega}. \tag{240}$$

For oblate spheroidal grains F will be negative but $\sigma_E - \sigma_H$ in Eqs. (121) and (122) will also have a different sign from that for prolate spheroids and the resulting polarization will be in the same plane for both kinds of grains; in each case the long dimension of the grains is perpendicular to the magnetic field.

The Eq. (240) was used by Davis (1959) to explain why different stars may have a different wavelength dependence of polarization, as was found by Behr (1959a). This equation suggests that the stronger the magnetic field, the larger are the grains which may be aligned completely by this field. Hence in a strong magnetic field polarization is produced, on the average, by larger dust grains than in a field of lower intensity. The factor $\sigma_E - \sigma_H$ in Eqs. (143) and (144) depends on the size of dust grains expressed in terms of wavelength. Let us assume that this factor has a maximum as a function of wavelength. This maximum will be at longer wavelength in a strong magnetic field where the dust grains producing polarization are, on the average, larger than in the weak field.

Davis and Greenstein (1951), on the basis of theory and experiments described by Gorter (1947), assume that for the dust grains whose paramagnetic properties are due to the admixture of iron ions, the ratio χ''/ω encountered in Eq. (240) equals

$$\chi''/\omega \approx 2.5 \times 10^{-12}/T_{\mathrm{g}}, \tag{241}$$

where T_{g} is the internal temperature of the dust grains. This relation is valid only for dust grains not much smaller thaf 0.01 μ and containing not more than 30 percent of iron per weight.

Henry (1958) generalized the Davis-Greenstein theory for the case of ferromagnetic dust grains. Equations (237) - (240) remain valid in this case; only the ratio χ''/ω becomes dependent on the ratio of axes of spheroidal grains. Henry assumes the ratio of axes 2:1 and obtains for monocrystals of iron or nickel

$$\chi''/\omega \approx 3 \times 10^{-7}, \tag{242}$$

almost independently of temperature, while for ferrites such as, e.g., Fe_2O_3

$$\chi''/\omega \approx 2 \times 10^{-10}, \tag{243}$$

for temperatures near absolute zero. The advantage of the use of ferrite grains in explaining interstellar polarization is their high index of refraction, near 3 for Fe_2O_3. For so high an index of refraction the polarizing efficiency is supposed to be very high.

The Davis-Greenstein mechanism can also be applied to diamagnetic grains such as graphite flakes discussed by Cayrel and Schatzman (1954); the planes of the flakes will be aligned perpendicular to the magnetic field. From their data we find that for graphite

$$\chi''/\omega \approx 2 \times 10^{-12}/T_g^2. \tag{244}$$

If we insert the expressions (241) – (244) into Eq. (240) and assume $n_H T^{1/2} = 100$ (which is approximately valid both for H I regions and for H II regions between the gas clouds), $T_g = 10°K$, $a = 0.04\,\mu$ for iron grains and graphite flakes and $0.2\,\mu$ for other materials, we obtain that $|F_l| \gg 1/3$ and the alignment is practically complete for the following magnetic flux densities

$$B \gg \begin{cases} 5 \times 10^{-5} \text{ gauss for graphite flakes,} \\ 3 \times 10^{-5} \text{ gauss for paramagnetic grains,} \\ 1 \times 10^{-6} \text{ gauss for ferrites,} \\ 1 \times 10^{-8} \text{ gauss for iron grains.} \end{cases} \tag{245}$$

Since the estimates of galactic magnetic fields on other grounds show that they are of the order of 10^{-6} to 10^{-4} gauss, the alignment of dust grains can be explained satisfactorily by the Davis-Greenstein theory.

It may be supposed that the Platt particles are completely aligned even in a very weak field because they are highly paramagnetic and very small.

C. *Other Aligning Mechanisms*

The alignment of dust grains by interaction with gas flowing in a direction perpendicular to the galactic plane was suggested by Gold (1952). According to this author the long axes of the grains tend to be parallel to the relative velocity. Zirin (1952) suggests that such alignment would be with the long axis normal to the direction of relative motion. Both of these arguments were discussed thoroughly by Davis (1955) who showed that the alignment of dust grains by interaction with gas is much too small to explain the observed polarization.

The theory of alignment of ferromagnetic grains by a strong magnetic field, several orders of magnitude higher than that given for iron grains by Eq. (245), was discussed by Spitzer and Tukey (1951). In a strong field the torque on ferromagnetic grains will stop the spinning of the grains. In this case they will be aligned as compass needles with their long axes parallel to the magnetic field. For such grains the magnetic field must be perpendicular to the galactic plane and the observed longitude dependence of polarization cannot be explained.

An argument against the alignment of dust grains by gas flow or by a strong magnetic field are the results of the polarization measurements of stars behind the filamentary nebulae. The position angles of the plane of vibration for such stars are well correlated with position angles of the filaments. This was shown in the Pleiades by Hall (1955) and van den Bergh (1956) and in other regions by Shain (1955, 1956a, 1956b; cf. also Elvius, 1959). These results can be explained only on the assumption that the filaments are directed along the magnetic lines of force.

Davis and Greenstein (1951) discuss critically other possible methods of producing alignment: the Rowland effect which becomes important if the dust grains bear electrostatic charges and the eddy currents in a conductor. They show that these mechanisms cannot explain the observed interstellar polarization, but the eddy currents have significant influence on the behavior of dust grains if they are pure iron.

VIII

FLUCTUATIONS OF POLARIZATION IN SMALL AREAS OF THE SKY

A. *Correlation between Polarization and Extinction in Open Clusters*

For a sufficiently strong magnetic field the distribution parameter F, defined by Eq. (113), assumes a constant value. In this case high correlation between polarization and extinction would be expected. It may be seen from Eqs. (142)-(144) and (190) that the extinction, as well as the amount of polarization, and the Stokes parameters Q_G and U_G for a given star are now proportional to $\overline{n_g}S$ where $\overline{n_g}$ is the number of dust grains per cubic centimeter averaged over the path to the star and S is the distance to star.

Such good correlation is not expected for a weaker magnetic field which does not fulfill the inequality (245). According to Eqs. (239) and (240) the distribution parameter now becomes inversely proportional to n_H, the number of gas atoms or ions per cubic centimeter. It seems probable that the ratio of densities of interstellar gas and dust is fairly constant (for discussion of this problem see Bok, 1955). On this assumption the product n_gF becomes independent of n_g. This means that no correlation between polarization and extinction is expected other than the obvious correlation produced by the distance effect. For a group of stars which are all in the same distance no correlation at all is expected.

Little or no correlation between polarization and reddening has in fact been observed for the open clusters NGC 457 and 7380 (Hoag, 1953), NGC 2244

(Hoag and van P. Smith, 1959; Grigoryan and Smak, 1960), NGC 7243 (Krzemiński, 1961), IC 4725 (Serkowski, 1961), J. Stock's cluster in Perseus (Larsson-Leander and Serkowski, 1959; Serkowski, 1958b; Krzemiński, 1961), Double Cluster in Perseus (Hiltner, 1956; Serkowski, 1958a, 1958b) and the associations I Cep and II Per (Grigoryan, 1957), I Lac (Krzemiński and Oskanjan, 1961) and III Cep (Serkowski, 1960b). For ten of sixteen associations investigated by Semeniuk (1960) the coefficient of correlation between polarization and interstellar reddening is less than 0.3.

The dependence of the Stokes parameter Q_G and the ratio Q_G/A_V on A_V for the stars within the radius of 45 min of arc around the Double Cluster in Perseus is shown in Fig. 16. The left diagram of this figure shows the lack of correlation between Q_G and A_V. If Q_G and A_V are independent random variables the mean values of Q_G/A_V for narrow intervals of A_V should be equal to $\overline{Q_G}/A_V$, where $\overline{Q_G}$ is the value of Q_G averaged over all the stars under consideration. The function $\overline{Q_G}/A_V$ is represented by a solid line in the right diagram of Fig. 16. This diagram shows spurious "depolarization" caused simply by the

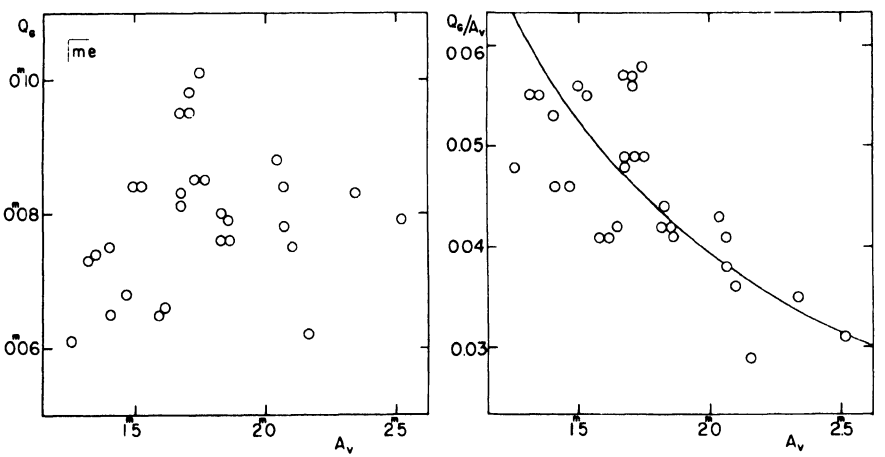


FIG. 16. Dependence of the Stokes parameter Q_G (left diagram) and the ratio Q_G/A_V (right diagram) on visual extinction A_V for the stars within the radius of 45 min of arc around the center of the Double Cluster in Perseus. The solid line in the right diagram is a hyperbole, the equation of which is $Q_G/A_V = \overline{Q_G}/A_V$. The lines marked *m.e.* in the upper left corner represent the mean errors of measurements.

lack of correlation between Q_G and A_v. In the same way one can probably explain the "depolarization" shown in Fig. 14 for stars which belong mostly to the Perseus spiral arm.

For some galactic clusters polarization and reddening are pretty well correlated. Such correlation was found for M 29 (Hiltner, 1954b), NGC 663 and 1502

(Hoag, 1953), NGC 2169 (Krzemiński, 1961), and for the association VI Cygni (Hiltner, 1954a, 1956). This correlation may be explained by assuming that either the magnetic field is strong and F is constant or that an appreciable part of both extinction and polarization is produced inside the cluster. In this last case the stars embedded more deeply into the nebula surrounding the cluster will be both more strongly reddened and more strongly polarized.

The correlation between polarization and equivalent width of λ 4430 interstellar absorption band was found by Pacholczyk (1959b) and Krzemiński (1959) to be smaller than the correlations between polarization and extinction and between the extinction and equivalent width of λ 4430 for the same stars. Pacholczyk concludes that the coefficient of partial correlation between the polarization and this equivalent width is negligibly small and that there is no direct connection between polarization and the intensity of interstellar absorption bands; the observed correlation being caused by the fact that both these quantities are correlated with interstellar extinction.

B. *Applications of Autocorrelation Analysis*

The analysis of the dependence of the polarization of a star on its position in an open cluster or association permits us to evaluate the microscales s_{03} and s_{04} of the polarizing properties of the interstellar medium. These microscales are defined by Eq. (160) and are the characteristic distances such that the coefficient of correlation between the values of quantities $q(\mathbf{s})$ or $u(\mathbf{s})$ in points separated by that distance falls to $1/e$ as compared to unity for zero distance.

To determine the microscales, the stars in an open cluster are connected in pairs in all possible combinations. The pairs are distributed in groups

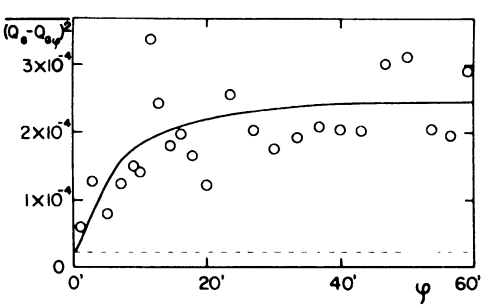


FIG. 17. The mean squares of differences in the Stokes parameter Q_G vs. angular distance φ of the stars in the Double Cluster in Perseus. The dashed line with ordinate $2\epsilon^2 = 0.22 \times 10^{-4}$ represents the errors of measurement; the solid line has been computed from Eqs. (246) and (249) for the microscale $s_{03} = 1.5$ pc.

according to the angular distance φ of the stars in a pair. For every pair the mean square of the difference in the corresponding Stokes parameter is computed. These values, averaged over the intervals of angular distance φ, are the values of *structural function* for the corresponding Stokes parameter. The structural function obtained in this way on the basis of the values of the Stokes parameter Q_G for stars in the Double Cluster in Perseus (Serkowski, 1958b) is shown in Fig. 17.

The expected, theoretical shape of the structural function represented by the full line in Fig. 17 may be obtained in the following way. The value of the structural function corresponding to angular distance φ is

$$\langle (Q_G - Q_{G\varphi})^2 \rangle = 2(\langle Q_G^2 \rangle - \langle Q_G Q_{G\varphi} \rangle) = 2\sigma_Q^2[1 - r(\psi)], \qquad (246)$$

where Q_G and $Q_{G\varphi}$ are the values of the Stokes parameter Q_G for two stars separated by angular distance φ, and $r(\psi)$ is the coefficient of correlation between Q_G and $Q_{G\varphi}$ equal to

$$r(\psi) = (\langle Q_G Q_{G\varphi} \rangle - \langle Q_G \rangle^2)/\sigma_Q^2. \qquad (247)$$

The coefficient $r(\psi)$ is a function of a dimensionless parameter

$$\psi = \varphi S/s_{03}. \qquad (248)$$

By Eqs. (149), (152), (158), and (164) we have

$$r(\psi) = \frac{1}{2\langle q^2 \rangle s_{03} S} \left\langle \int_0^S \int_0^S q(\mathbf{s}_1)\, q(\mathbf{s}_2)\, d\mathbf{s}_1\, d\mathbf{s}_2 \right\rangle, \qquad (249)$$

where the directions of the vectors $\mathbf{s}_1$ and $\mathbf{s}_2$ are inclined at an angle φ to each other. The average in Eq. (249) can be found by numerical integration. This integration was made by Kruszewski who tabulated the function $r(\psi)$ (for his results see Serkowski, 1958b).

The polarization measurements of the nearby stars which are in nearly the same direction as the Double Cluster in Perseus show that the polarisation of stars in this cluster is produced mainly in the regions which are relatively near to the sun. If this is so, Eq. (246), when compared with the structural function obtained from the observations, will give too large a value of the microscale. The microscale obtained in this way can be treated as the upper limit of the true microscale. Hence the structural function presented in Fig. 17, when compared with Eqs. (246) and (249), gives us the inequality

$$s_{03} \leqslant 1.5 \text{ pc}. \qquad (250)$$

Similar values of the upper limit can be obtained for s_{01} and s_{04} on the basis of the structural functions for the reddening and the Stokes parameter U_G for stars in the Double Cluster in Perseus (Serkowski, 1958b).

C. *Estimates of Magnetic Flux Density from Polarization Data*

The variations in the plane of polarization have been used by Davis (1951, 1955) and Chandrasekhar and Fermi (1953) for estimating the strength of the galactic magnetic field. They show that the inertia of interstellar motions of rms velocity v in a conducting medium of density ρ gives rise to Alfvén waves running along the mean direction of the magnetic field. The magnetic flux density is then given by an equation derived by Chandrasekhar and Fermi (1953) (cf. also Aller, 1956)

$$B = (4\pi\rho/3)^{1/2}\, v/\alpha, \tag{251}$$

α being the root-mean-square tangent of the deviation of the position angle of the magnetic lines of force from its mean value; this deviation we have denoted by $\Theta - \Theta_0$. If we are looking perpendicular to the mean direction **B** of the magnetic field we have $\nu_0' = 90°$ and, from Eqs. (127) and (128),

$$\alpha = 2^{-1/2}\, \alpha_1. \tag{252}$$

where α_1 is defined by Eq. (125).

As we have estimated in Section VI, C the parameter α_1 is equal to or slightly larger than unity. This estimate is confirmed by the analysis of polarization of the Double Cluster in Perseus. For this cluster, we have $\overline{Q_G} = 0^m.079$ and the ratio of variances of the Stokes parameters $\sigma_Q^2/\sigma_U^2 = 0.60 \pm 0.14$ (m.e.).The microscale s_{03} found for this cluster is given by Eq. (250). Inserting these values into Eq. (187) we find that $C_2(\alpha_1) + C_3(\alpha_1) \approx -2.7\, C_1(\alpha_1)$. Looking at Fig. 7 we see that this approximate relation is fulfilled only for $\alpha_1 \gtrsim 1$.

On the assumption that $\alpha_1 = 1$, $\rho = 2 \times 10^{-24}$ gm/cm^3, and $v = 12$ km/sec (Spitzer, 1956) the Eqs. (251) and (252) give the magnetic flux density

$$B = 5 \times 10^{-6} \text{ gauss}. \tag{253}$$

This estimate of the galactic magnetic field is in good agreement with estimates based on the condition that the gravitational pressure equals the sum of material and magnetic pressures (Chandrasekhar and Fermi, 1953; Spitzer, 1956).

List of symbols[7]

A	extinction expressed in magnitudes
A_V	visual extinction assumed to be equal to reddening E_{B-V} multiplied by 3
a	mean radius of dust grain
$\mathbf{B}$	magnetic flux density; in general, direction of the local axis of symmetry of mechanism aligning dust grains
$\mathbf{B}_0$	mean direction of the axis of symmetry of aligning mechanism, averaged over the interval between us and the considered star
b	galactic latitude of the star
b_B	angle between the galactic plane and the direction $\mathbf{B}_0$
$C_j(\alpha_1)$	functions defined by Eqs. (140) and (177)–(179); $j = 0, 1, 2, 3$
E_l, E_r	components of electric vector $\mathbf{E}$ of light wave
$\mathbf{e}$	unit vector
F	distribution parameter, defined by Eq. (113)
I_g	moment of inertia of dust grain along its axis of symmetry
I	intensity of light
$I'(\varphi)$	intensity of light after passing the polarizer set at position angle φ
$\mathbf{J}$	angular momentum of dust grain
$\mathbf{l}$	vector perpendicular to the ray of light, lying in the plane of meridian of equatorial coordinate system and directed towards the northern hemisphere
l	galactic longitude of the star
l_B	galactic longitude of the direction $\mathbf{B}_0$
$\mathbf{M}$	magnetization
$m(\varphi)$	magnitude of a star observed through an analyser set at position angle φ
m_g	mass of dust grain
m_H	mass of hydrogen atom
n_g	number of dust grains per cubic centimeter
n_H	number of hydrogen atoms or ions per cubic centimeter
P	degree of polarization, defined by Eq. (7)
P_0	degree of polarization of initially natural light which passed the imperfect polarizer
P_v	degree of ellipticity, defined by Eq. (8)
p	amount of polarization expressed in magnitudes, defined by Eq. (58)
p_x, p_y, p_v	Stokes parameters expressed in magnitudes and equatorial coordinates, defined by Eqs. (48)–(50)
Q	Stokes parameter, defined by Eq. (4)

[7] Only repeatedly used symbols are listed.

Q_G Stokes parameter expressed in magnitudes and galactic coordinates, defined by Eq. (62)

$\overline{Q_G}(90°)$ mean value of Q_G for $\nu_0' = 90°$

$\mathbf{r}$ vector perpendicular to vectors $\mathbf{l}$ and $\mathbf{S}$

$\mathbf{S}$ vector in the direction of propagation of light

S distance of star

S_l, S_r mean extinction cross sections of a dust grain for light with electric vector vibrating in a plane determined by the direction $\mathbf{l}$ and $\mathbf{r}$, respectively

$\mathbf{s}$ radius vector of point in space

s_{0j} microscales of fluctuations, defined by Eq. (160); $j = 1, 2, 3, 4$

T temperature of interstellar gas

T_g internal temperature of dust grain

T_l, T_r transmission of two parallelly or perpendicularly oriented polarizers

U Stokes parameter, defined by Eq. (5)

U_G Stokes parameter expressed in magnitudes and galactic coordinates, defined by Eq. (63)

V Stokes parameter, defined by Eq. (6)

V_g volume of dust grain

x tangent of angle α

α angle between the directions $\mathbf{B}$ and $\mathbf{B}_0$

α_Z angle between the axis of symmetry of the aligning mechanism and the axis of symmetry of individual dust grain

α_1 root-mean-square tangent of the angular deviation of the local direction of the axis of symmetry of aligning mechanism from its mean direction

β angle between the vectors $\mathbf{B}$ and $\mathbf{J}$; also the angle whose tangent is the ratio of the axes of the polarization ellipse (Fig. 1)

γ ratio of the moment of inertia of dust grain about its equatorial axis to that about its axis of symmetry

δ, δ_0 quantities defined by Eqs. (151) and (154)–(157)

η angle defined by Fig. 6

Θ position angle of direction $\mathbf{B}$ measured in galactic coordinates

Θ_0 position angle of direction $\mathbf{B}_0$ measured in galactic coordinates

ϑ angle between $\mathbf{J}$ and the axis of symmetry of dust grain

θ position angle of the plane of vibration of electric vector measured in equatorial coordinates

θ_G position angle of the plane of vibration of electric vector measured in galactic coordinates

λ wavelength

ν' angle between the direction to the star and direction $\mathbf{B}$

ν_0' angle between the direction to the star and direction $\mathbf{B}_0$

$\sigma_A, \sigma_Q, \sigma_U$ root-mean-square deviations of extinction A and Stokes parameters Q_G and U_G, expressed in magnitudes, from their mean values

$\sigma_E, \sigma_H, \sigma_S$ extinction cross sections of dust grain corresponding to the axis of symmetry of grain parallel to the electric vector of incident light, parallel to its magnetic vector and parallel to the direction of propagation of light, respectively

τ relaxation time, defined by Eq. (202); also the phase difference between the components E_l and E_r of the electric vector of light wave

φ position angle of the polarizer (analyzer); also the angular distance between the two stars

χ', χ'' real and imaginary parts of magnetic susceptibility, χ

ψ position angle of the retardation plate; also the parameter defined by Eq. (248)

ω angular velocity of dust grain

Acknowledgments

In conclusion, I wish to thank Dr. L. Davis and Dr. J. S. Hall for reading the manuscript and helpfull suggestions.

References

Aller, L. H., 1956. "Gaseous Nebulae," p. 289. Wiley, New York.
Bartl, E., 1959. *Mitt. Univ. Sternw. Jena* **39**.
Behr, A., 1956. *Nachr. Akad. Wiss. Göttingen.* p. 205; *Veröff. Univ. Sternw. Göttingen* **114**.
Behr, A., 1959a. *Z. Ap.* **47**, 54; *Veröff. Univ. Sternw. Göttingen* **124**.
Behr, A., 1959b. *Nachr. Akad. Wiss. Göttingen*, p. 185; *Veröff. Univ. Sternw. Göttingen* **126**.
Behr, A., 1960. *Lowell Obs. Bull.* **4**, 292.
Billings, B. H., 1951. *J. opt. Soc. Amer.* **41**, 957.
Blaauw, A., Gum, C. S,, Pawsey, J. L., and Westerhout, G., 1959. *Ap. J.* **130**, 702.
Bok, B. J., 1955. *I. A. U. Symp.* No. 2, p. 221.
Brandmüller, J., and Hoffmeister, C., 1953. *Optik* **11**, 1.
Cayrel, R., and Schatzman, E., 1954. *Ann. Ap.* **17**, 555.
Chandrasekhar, S., 1946. *Ap. J.* **103**, 351.
Chandrasekhar, S., 1950. "Radiative Transfer," p. 24ff. Oxford Univ. Press (Clarendon), London and New York.
Chandrasekhar, S., and Fermi, E., 1953. *Ap. J.* **118**, 113.
Chandrasekhar, S., and Münch, G., 1952. *Ap. J.* **115**, 103.
Davis, L., Jr., 1951. *Phys. Rev.* **81**, 890.
Davis, L., Jr., 1955. "Vistas in Astronomy," Vol. I, p. 336. Pergamon Press, New York.
Davis, L., Jr., 1958. *Ap. J.* **128**, 508.
Davis, L., Jr., 1959. *Z. Ap.* **47**, 59.

Davis, L., Jr., and Greenstein, J. L., 1951. *Ap. J.* **114**, 206; *Mt. Wilson and Palomar Reprint* **40**.
Dollfus, A., 1957. *Ann. Ap.* Suppl. No. 4.
Dombrovski , V. A., 1949. *Dokl. Akad. Nauk Armyansk. S. S. R.* **10**, 199.
Dombrovski , V. A., 1953. *A. Zh.* **30**, 603.
Elvius, A., 1959. *Arkiv Astr.* **2**, 309; *Uppsala Medd.* **121**.
Erdelyi, A., Magnus, W., Oberhettinger, F., and Tricomi, F, G., 1954. "Tables of Integral Transforms," Vol. I. McGraw-Hill, New York.
Fick, E., 1954. *Z. Physik* **138**, 183.
Fick, E., 1955. *Z. Physik* **140**, 308.
Gehrels, T., 1960. *A. J.* **65**, 466 and 470.
Gehrels, T., and Teska, T. M., 1960. *P.A.S.P.* **72**, 115.
Gold, T., 1952. *M.N.R.A.S.* **112**, 215.
Gorter, C. J., 1947. "Paramagnetic Relaxation." Elsevier, Houston, Texas.
Greenberg, J. M., 1960a. *J. appl. Phys.* **31**, 82.
Greenberg, J. M., 1960b. *Lowell Obs. Bull.* **4**, 281 and 285.
Greenberg, J. M., 1960c. *Ap. J.* **132**, 672.
Greenberg, J. M., and Meltzer, A. S. 1960. *Ap. J.* **132**, 667.
Grigoryan, K. A., 1957. *Soob. Byurakan. Obs.* **22**, 49.
Grigoryan, K. A., and Smak, J. M., 1960. *Soob. Byurakan. Obs.* **28**, 3.
Grzedzielski, S., 1958. *C. R.* **246**, 890; *Contr. Inst. Ap., Paris* **A235**.
Güttler, A., 1952. *Z. Ap.* **31**, 1.
Hall, J. S., 1948. *A. J.* **54**, 39.
Hall, J. S., 1949. *Science* **109**, 166.
Hall, J. S., 1952. *A. J.* **57**, 12.
Hall, J. S., 1955. *Mém. Soc. Sci. Liège* [4] **15**, 543.
Hall, J. S., 1958. *Publ. U. S. nav. Obs.* **17**/VI.
Hall, J. S., and Mikesell, A. H., 1949. *A. J.* **54**, 187.
Hall, J. S., and Mikesell, A. H., 1950. *Publ. U. S. naval Obs.* **17**/I.
Hall, J. S., and Serkowski, K., 1961. "Stars and Stellar Systems" (G. P. Kuiper, ed.), Vol. III. Univ. of Chicago Press, Chicago, Illinois, in press.
Henry, J., 1958. *Ap. J.* **128**, 497.
Hiltner, W. A., 1947. *Ap. J.* **106**, 231.
Hiltner, W. A., 1949a. *Science* **109**, 165.
Hiltner, W. A., 1949b. *Ap. J.* **109**, 471.
Hiltner, W. A., 1950. *Phys. Rev.* **78**, 170.
Hiltner, W. A., 1951a. *Ap. J.* **114**, 241; *Contr. McDonald Obs.* **201**.
Hiltner, W. A., 1951b. *Observatory* **71**, 234.
Hiltner, W. A., 1954a. *Ap. J.* **120**, 178; *Contr. McDonald Obs.* **238**.
Hiltner, W. A., 1954b. *Ap. J.* **120**, 367; *Contr. McDonald Obs.* **240**.
Hiltner, W. A., 1956. *Ap. J. Suppl. Ser.* **2**, 389; *Contr. McDonald Obs.* **269**.
Hiltner, W. A., 1959. *Ap. J.* **130**, 340; *Contr. McDonald Obs.* **309**.
Hiltner, W. A., and Johnson, H. L., 1956. *Ap. J.* **124**, 367; *Contr. McDonald Obs.* **266**.
Hoag, A. A., 1953. *A. J.* **58**, 42, and private communication.
Hoag, A. A., and van P. Smith, E., 1959. *P.A.S.P.* **71**, 32.
Janssen, E., 1946. *Ap. J.* **103**, 380.
Johnson, H. L., and Morgan, W.W., 1955. *Ap. J.* **122**, 142.
Krzemiński, W., 1959. *Acta astr. Cracoviae* **9**, 231; *Warsaw Reprint* **93**.

Krzemiński, W., 1961. *Acta astr. Cracoviae* **11**, 7; *Warsaw Reprint* **108**, and private communication.
Krzemiński, W., and Oskanjan, V., 1961. *Acta astr. Cracoviae* **11**, 1; *Warsaw Reprint* **107**.
Larsson-Leander, G., and Serkowski, K., 1959. *Arkiv Astr.* **2**, 295; *Stockh. Obs. Medd.* **113**.
Lyot, B., 1929. *Ann. Obs. Paris-Meudon* **8**, Pt. 1, 102.
Mikesell, A. H., Hoag, A. A., and Hall, J. S., 1951. *J. opt. Soc. Amer.* **41**, 689.
Morgan, W. W., Whitford, A. E., and Code, A. D., 1953. *Ap. J.* **118**, 318.
Pacholczyk, A. G., 1959a. *Acta astr., Cracoviae* **9**, 17; *Warsaw Reprint* **75**.
Pacholczyk, A. G., 1959b. *Acta astr. Cracoviae* **9**, 90; *Warsaw Reprint* **85**.
Platt, J. R., 1956. *Ap. J.* **123**, 486.
Platt, J. R., 1960. *Lowell Obs. Bull.* **4**, 268, 278, and 311.
Plumb, R. C., 1960. *J. opt. Soc. Amer.* **50**, 892.
Reimer, L., 1957. *Optik* **14**, 83.
Schmidt, T., 1958. *Z. Ap.* **46**, 145; *Veröff. Univ. Sternw. Göttingen* **123**.
Semeniuk, I., 1960. Private communication.
Serkowski, K., 1958a. *Rev. Mod. Phys.* **30**, 952; *Warsaw Reprint* **78**.
Serkowski, K., 1958b. *Acta astr. Cracoviae* **8**, 135; *Warsaw Reprint* **72**.
Serkowski, K., 1958c. *Postepy astr.* (*Cracow*) **6**, 160.
Serkowski, K., 1960a. *Lowell Obs. Bull.* **4**, 296.
Serkowski, K., 1960b. *Acta astr. Cracoviae* **10**, 227; *Warsaw Reprint* **105**.
Serkowski, K., 1961. *Lowell Obs. Bull.* **5**, and *Acta astr. Cracoviae* **11**, both in preparation.
Shain, G. A., 1955. *A. Zh.* **32**, 381 and 489.
Shain, G. A., 1956a. *Izv. Krim. Obs.* **16**, 181.
Shain, G. A., 1956b. *A. Zh.* **33**, 469.
Shain, G. A., 1957. *A. Zh.* **34**, 3.
Shatilov, A. V., 1960. *Optika i Spektroskopiya* **9**, 86 and 233.
Spitzer, L., Jr., 1956. *Ap. J.* **124**, 20.
Spitzer, L., Jr., and Tukey, J. W., 1951. *Ap. J.* **114**, 187.
Stevenson, A. F., 1953. *J. appl. Phys.* **24**, 1134 and 1143.
Thiessen, G., and Broglia, P., 1959. *Z. Ap.* **48**, 81.
van de Hulst, H. C., 1950. *Ap. J.* **112**, 1.
van de Hulst, H. C., 1955. *Mém. Soc. Sci. Liège* [4] **15**, 393 and 609.
van de Hulst, H. C., 1957. "Light Scattering by Small Particles." Wiley, New York.
van den Bergh, S., 1956. *Z. Ap.* **40**, 249; *Veröff. Univ. Sternw. Göttingen* **115**.
Wilson, R., 1960. *M.N.R.A.S.* **120**, 51.
Zimmermann, O., 1957. *Z. Naturf.* **12a**, 647.
Zirin, H., 1952. *Harv. Obs. Bull.* **921**, 26.

Author Index

Italic numbers indicate page on which complete reference may be found.

A

Alexander, J. B., 174, *284*
Allen, C. W., 115, *162*
Aller, L. H., 87, *103*, 183, 240, 282, *284*, *285*, 347, *350*
Ambartsumian, V. A., 48, 65, 75, *99*
Arakelyan, M. A., 58, *100*
Artiukhina, N. M., 89, *99*

B

Baade, W., 174, *284*
Babcock, H. W., 50, 86, *99*, *100*, 178, 179, 229, 282, *284*
Badalian, H. S., 72, *99*
Bartl, E., 307, *350*
Bateson, F. M., 58, *99*
Behr, A., 115, *162*, 293, 299, 300, 301, 303, 314, 324, 328, 341, *350*
Berman, L., 208, *284*
Billings, B. H., 297, 298, *350*
Blaauw, A., 176, *284*, *285*, 324, *350*
Blackwell, D. E., 115, *162*
Böhm, K.-H., 92, *99*
Bok, B. J., 343, *350*
Bonsack, W. K., 82, 83, 85, 86, *99*
Bottlinger, K. F., 208, *284*
Bowen, E. G., 136, *162*
Brandmüller, J., 296, *350*
Brandt, J. C., 242, 244, 281, 282, *284*
Broglia, P., 73, *99*, 301, *352*
Brown, R. H., 180, *285*
Brownlee, R. R., 66, 83, *99*, *100*
Brun, A., 55, 58, *99*
Bucerius, H., 232, 281, *284*
Buddhue, J. D., 118, *162*
Bullard, E. C., 108, *162*
Burbidge, E. M., 71, *99*, 181, 184, 222, 226, 228, 246, 247, *284*
Burbidge, G. R., 68, 71, *99*, *100*, 181, 184, 222, 226, 228, 246, 247, *284*
Burgers, J. M., 26, *44*

C

Cameron, A. G. W., 85, *100*
Camm, G. L., 212, 217, 238, 281, *284*
Carrus, P. A., 26, *44*
Castaing, R., 138, *162*
Cayrel, R., 315, 342, *350*
Chackett, K. J., 107, *162*
Chandrasekhar, S., 166, 169, 284, 290, 292, 295, 320, *350*
Chavira, E., 53, 58, 80, 81, *100*
Chisnell, R. F., 14, 16, *44*
Code, A. D., 327, *352*
Coffeen, M. F., 91, *103*
Contopoulos, G., 250, *284*
Coutrez, R., 218, 229, *284*
Cox, A. N., 66, 84, *99*, *100*
Craig, H., 83, *103*

D

Davis, D. N., 115, *163*
Davis, L., Jr., 303, 311, 312, 313, 332, 333, 334, 335, 338, 340, 341, 342, 343, 347, *350*, *351*

de Vaucouleurs, G., 181, 249, *284*, *285*
Dolidze, M. V., 52, 58, *100*
Dollfus, A., 301, *351*
Dombrovski, V. A., 93, 100, 290, 291, *351*
Duchesne, M., 179, 180, *285*
Dzigvashvili, R. M., 217, *285*

E

Ebert, R., 68, *100*
Eddington, A. S., 212, *285*
Eelsalu, H., 177, *285*
Eichhorn, H., 192, *285*
Elvey, C. T., 50, *100*
Elvius, A., 343, *351*
Elvius, T., 172, *285*
Erdelyi, A., 322, *351*

F

Fedorovich, V. P., 58, *100*
Fehrenbach, C., 282, *285*
Fermi, E., 347, *350*
Fick, E., 314, *351*
Field, G. B., 83, *102*
Fireman, E. L., 83, *100*
Flather, E. M., 91, *103*
Fowler, W. A., 85, *100*
Fox, P. A., 26, *44*
Frank-Kamentskii, D. A., 26, 27, 31, 43, *44*
Frederiksson, K., 138, *162*, *163*
Fredrick, L. W., 91, *100*
Freundlich, E. F., 226, *285*
Fricke, W., 217, 219, *285*

G

Gandel'man, G. M., 26, 27, 31, 43, *44*
Gaposchkin, S., 174, *285*
Gehrels, T., 300, 314, *351*
Gliese, W., 170, 217, 229, 281, *285*
Götz, W., 50, 58, *100*
Gold, T., 342, *351*
Golden, J., 107, *162*
Goldschmidt, V. M., 83, 85, *100*
Goldstine, H. H., 28, *44*
Gordon, I. M., 94, *100*
Gorter, C. J., 341, *351*
Greenberg, J. M., 313, 314, 315, 329, *351*
Greenstein, J. L., 47, 51, 52, 58, 82, 83, 85, *99*, *100*, 311, 332, 333, 335, 336, 340, 341, 343, *351*
Grigoryan, K. A., 344, *351*
Grotrian, W., 115, *162*
Grubissich, C., 54, 58, *102*
Grzedzielski, S., 330, *351*
Güttler, A., 314, *351*
Gum, C. S., 324, *350*
Gurevitch, L. E., 64, *100*

H

Haas, F., 26, *44*
Härm, R., 83, *102*
Hain, K., 43, *44*
Hall, J. S., 290, 300, 301, 307, 314, 324, 343, *351*, *352*
Hansa, M., 118, *162*
Haro, G., 51, 53, 58, 80, 81, 92, *100*
Hazard, C., 180, *285*
Hazlehurst, J., 41, *44*
Heckmann, O., 211, *285*
Henize, K. G., 58, *100*
Henry, J., 341, *351*
Henyey, L. G., 66, 77, 97, *100*
Herbig, G. H., 47, 49, 50, 51, 52, 54, 56, 57, 58, 59, 62, 63, 69, 71, 72, 76, 77, 78, 80, 81, 82, 87, 88, 91, 92, 95, 97, 98, *100*, *101*, *102*
Hill, E. R., 176, *285*
Hiltner, W. A., 94, *101*, 290, 299, 300, 313, 314, 324, 329, 330, 344, 345, *351*
Hins, C. H., *285*
Hoag, A. A., 93, *101*, 300, 324, 344, 345, *351*, *352*
Hoffleit, D., 58, *101*
Hoffmeister, C., 54, 58, 62, *101*, 296, 350
Horstman, E. L., 83, *101*
Howard, R., 83, *102*
Hoyle, F., 108, *162*
Hunger, K., 82, 94, *101*
Hunter, W., 119, 126, 138, 141, *162*, *163*

I

Idlis, G. M., 203, 213, 214, 281, *285*
Iriarte, B., 53, 58, 80, 81, 94, *100*, *101*

J

Janák, F., 231, 281, *285*
Janssen, E., 290, *351*
Jeans, J. H., *285*
Johnson, H. L., 60, 69, 71, 97, *101*, 313, *351*
Jones, A. F., 58, *99*
Jones, C. W., 26, 27, *44*
Joy, A. H., 47, 48, 49, 50, 51, 52, 58, 69, 80, *101*

K

Kahn, F. D., 68, *100*, 167, *285*
Kerr, F. J., 181, 249, *285*
Kholopov, P. N., 48, 52, 54, 55, 58, 69, *101*
Kiladze, R. J., 242, 281, *285*
Knox-Shaw, H., 58, *101*
Kopal, Z., 26, *44*
Kron, G. E., *101*
Krzemiński, W., 324, 344, 345, *351*, *352*
Kukarkin, B. V., 171, 174, *285*
Kurokin, N., 57, *101*
Kurth, R., 169, *285*
Kushwaha, R. S., 42, *44*
Kuzmin, G. G., 170, 212, 215, 241, 281,*285*
Kwee, K. K., 177, 242, 249, 252, 274, 276, *285*

L

Laevastu, T., 143, *162*
Lallemand, A., 179, 180, *285*
Langebartel, R. G., 250, *285*
Larsson-Leander, G., 344, *352*
Lebedinsky, A. I., *44*
Le Levier, R., 66, 77, 97, *100*
Lenouvel, F., 73, *99*, *101*
Lense, J., 256, *285*
Levee, R. D., 66, 77, 97, *100*, *102*
Limber, D. N., 70, *102*
Lindblad, B., 211, 250, *285*
Lindblad, P. O., 254, *285*
Liu, Y. H., 147, *163*
Lohmann, W., 208, 209, 210, 223, 281, 282, *285*
Lovell, A. C. B., 116, 130, 135, *162*
Loverring, J. F., 110, *163*
Luyten, W. J., 97, *102*
Lyot, B., 297, *352*

M

McCrea, W. H., 64, *102*
McLaughlin, D. B., 52, 58, *102*
Maffei, P., 54, 58, *102*
Magnus, W., 322, *351*
Makemson, M. W., 208, *285*
Mannino, G., 54, 58, *102*
Manova, G. A., 53, 58, *102*
Martynov, D., 58, *102*
Mason, B., 106, *162*
Mason, B. J., 109, *163*
Mayall, N. U., 178, 183, 209, 236, 282, *285*, *287*
Mayeda, T., 107, 108, 120, *163*
Mayer, P., 176, *286*
Mele, A., 108, *163*
Mellis, O., 143, *162*
Meltzer, A. S., 329, *351*
Menon, T. K., 91, *102*
Mercer, E. R., 107, *162*
Mestel, L., 68, 96, *102*
Mikesell, A. H., 290, 300, 301, *351*, *352*
Mikisha, A. M., 230, *285*
Millman, P. M., 150, *163*
Mills, B. Y., 169, *285*
Mirzoian, L. V., 93, *102*
Mitchell, R. I., 97, *101*
Mohr, J. M., 176, 222, *285*, *286*
Moreno, A., 53, 58, *100*
Morgan, H. R., 176, *286*
Morgan, W. W., 58, *100*, 313, 327, *351*, *352*
Münch, G., 91, *103*, 178, 179, 181, *286*, 320, *350*
Münch, L., 178, *286*
Muller, C. A., 177, 242, 249, 252, 274 276, *285*
Murray, J., 118, 138, *163*

N

Nininger, H. H., 106, *163*

O

Oberhettinger, F., 322, *351*
O'Connell, D. J. K., 168, *286*
Odgers, G. J., 42, *44*
Öpik, E. J., 115, 137, 143, 144, 148, 149, 151, *163*
Ogorodnikov, K. F., 210, *286*
Ono, Y., 15, *44*
Oort, J. H., 170, 172, 176, 177, 178, 184, 221, 228, 229, 230, 276, 279, 281, *286*
Oskanjan, V., 344, *352*
Osterbrock, D. E., 87, *102*
Owen, E. A., 147, *163*

P

Pacholczyk, A. G., 330, 345, *352*
Paneth, F. A., 107, *162*
Parenago, P. P., 48, 53, 54, 58, 69, *102*, 170, 171, 175, 176, 201, 217, 274, *286*
Parkin, D. W., 119, 126, 138, 141, *162*, *163*
Partridge, W. S., 112, *163*
Pavlovskaya, E. D., 174, *286*
Pawsey, J. L., 324, *350*
Payne-Gaposchkin, C., 2, *44*
Pearce, J. A., 281, *286*
Perek, L., 169, 173, 187, 223, 248, 249, 250, 258, 259, 261, 264, 266, 274, 281, *286*
Petit, M., 58, *102*
Petri, W., 255, *286*
Pettersson, H., 118, 137, *163*
Pettit, H. B., 115, *163*
Pilowski, K., 217, *286*
Plaskett, J. S., 281, *286*
Platt, J. R., 315, *352*
Plumb, R. C., 302, *352*
Ponomareva, G. A., 58, *102*
Poveda, A., 225, 282, *286*
Prendergast, K. H., 181, 184, 226, 246, 247, *284*

R

Raimond, E., 172, 178, 254, *287*
Reasbeck, P., 107, *162*
Reimer, L., 301, *352*
Renard, A. F., 118, *163*
Reynolds, J. H., 87, *102*
Richardson, R. S., 83, *100*
Richtmyer, R. D., 28, *44*
Rinehart, J. S., 112, *163*
Ringwood, A. E., 108, *163*
Roach, F. E., 115, *163*
Robbertse, W. P., 26, *44*
Rogers, M. H., 26, 44, *45*
Rosino, L., 54, 55, 58, *102*
Rotschi, H., 137, *163*
Routh, E. J., *286*
Routley, P. M., 83, *102*
Rudkjøbing, M., 47, 52, 58, 80, *103*
Rugoor, G. W., 178, *286*
Russell, H. N., 65, *102*

S

Safronov, V. S., 170, 230, 281, *286*
Sakashita, S., 15, *44*
Sakurai, A., 7, *45*
Salpeter, E. E., 66, 83, *102*
Sandage, A. R., 70, *102*
Sanford, R. F., 76, 82, *102*
Sayer, A. R., 2, *45*
Schatzman, E., 44, *45*, 315, 342, *350*
Schilt, J., 217, *286*
Schmidt, M., 166, 172, 251, 254, 256, 274, 275, 281, 282, *286*
Schmidt, T., 327, 330, *352*
Schürer, M., 169, *286*
Schwarzer, D., 83, *100*
Schwarzschild, K., 217, 282, *287*
Schwarzschild, M., 66, 84, *102*, 239, *287*
Semeniuk, I., 344, *352*
Serkowski, K., 290, 305, 307, 314, 320, 324, 329, 331, 344, 346, 347, *351*, *352*
Severnyi, A. B., 93, *102*
Shain, G. A., 327, 343, *352*
Shatilov, A. V., 313, *352*
Sher, D., 96, *103*
Shklovski, I. S., 168, *287*

Siedentopf, N., 115, *162*
Simon, R., 11, *45*
Singer, S. F., 151. *163*
Slettebak, A., 78, 79, *102*
Smak, J. M., 173, *287*, 344, *351*
Smith, E., 93, *101*
Spalding, J. F., 77, 78, *101*
Spitzer, L., Jr., 65, 68, 83, 96, *102*, 342, 347, *352*
Stacey, F. D., 110, *163*
Starikova, G. A., 54, *102*
Stevenson, A. F., 313, *352*
Štohl, J., 176, *286*
Strand, K. A., 58, 90, *102*
Strassl, H., 211, *285*
Struve, O., 47, 52, 58, 80, *100*, *102*, *103*
Suess, H. E., 83, *103*

T

Takase, B., 259, 260, 281, 282, *287*
Tandberg-Hanssen, E., 115, *163*
Taylor, G. I., 5, 6, 43, *45*
Temesváry, S., 68, *100*
ten Bruggencate, P., 229, 281, *287*
Terrazas, L. R., 58, *100*
Teska, T. M., 300, *351*
Thiessen, G., 301, *352*
Thomas, L. H., 66, *103*
Torgård, I., 238, 255, *287*
Tricomi, F. G., 322, *351*
Trumpler, R. J., 252, *287*
Tsitsin, F. A., 230, *285*
Tukey, J. W., 342, *352*

U

Underhill, A. B., 71, *103*
Uranova, T. A., 89, *103*
Urey, H. C., 83, *103*, 107, 108, 120, *163*

V

van Albada, G. B., 213, *287*
van Biesbroeck, G., 80, *101*
van de Hulst, H. C., 115, 163, 172, 178, 254, *287*, 291, 292, 294, 296, 308, 313, 314, 315, 336, *352*
van den Bergh, S., 96, *103*, 343, *352*
Vanfleet, H. B., 112, *163*
van Maanen, A., 91, *103*
van P. Smith, E., 324, 344, *351*
van Rhijn, P. J., 176, *287*
van Woerden, H., 172, 178, 254, *287*
Varsavsky, C. M., 58, 69, 71, 78, 87, *103*
Velghe, A. J., 58, *103*
Vetešník, M., 217, *287*
Volders, L., 172, 183, *287*
von Hoerner, S., 43, 44, 68, *100*, 223, *287*
von Neumann, J., 28, *44*
Vorontsov-Velyaminov, B. A., 41, *45*
Vyasovov, V. V., 58, *100*

W

Walker, M. F., 41, *45*, 58, 61, 69, 79, *103*, 179, 180, *285*
Watson, F. G., 106, 107, *163*
Wayman, P., 255, *287*
Weaver, H. F., 252, *287*
Wehner, G. K., 161, *163*
Wenzel, W., 50, 52, 54, 58, 81, 89, *103*
Westerhout, G., 172, 177, 242, 249, 252, 274, 276, *285*, *287*, 324, *350*
Weston, E. B., 58, 87, 93, *103*
Whipple, F. L., 2, *44*, 109, 137, 154, *163*
White, W. C., 112, *163*
Whitford, A. E., 327, *352*
Whitham, G. B., 8, 11, 15, 19, *45*
Wilson, O. C., 91, *103*
Wilson, R., 313, *352*
Winchell, A. N., 109, *163*
Woltjer, L., 167, *285*
Woolley, R. v. d. R., 170, *287*
Wyse, A. B., 236, 282, *287*

XYZ

Yamazaki, H., 15, *44*
Yasuda, H., 261, 281, *287*
Young, J., 110, *163*
Zacharov, I., 118, *162*
Zagar, F., 255, *287*
Zimmerman, O., 314, *352*
Zirin, H., 342, *352*

Subject Index

A

Absorption lines, displacement of, 41
  widths (for T Tauri Stars), 76
Accretion of matter by the stars, 47, 63
  rate of, 145, 150
Adiabatic atmosphere, 18, 28, 31
Adiabatic constant, 38
Adiabatic propagation of waves, 42
Achondrites, 106
Alfvén waves, 347
alignment mechanisms, 332
  by eddy currents, 343
  by gas flow, 342, 343
  by magnetic fields, 342, 343
  by paramagnetic absorption, 336
  by Rowland effect, 343
Amplitude function (for forward scattering), 308
Analyzer, definition of, 298
  desirable properties of, 299
  ideal, 245, 249, 301
  imperfect, 296, 299
Andromeda, nebula, 166, 260
  expansion of nucleus, 179
  mass of, 209, 282
  rotation of, 178, 200, 237
Anemometer, 120
Antarctic composite particles, 158
Antarctic dust, 156
Antarctic ice-cliff experiment, 145
Antarctic metallic flakes, 157, 159
Apocentric velocities, 251
Aqarids, δ-(meteor shower), 130
Aquila rift, 74
Arietids (meteor shower), 117, 161
Association, ϕ Persei —, 69, 91
Asteroids, 111, 112, 114
  belt of, 113
Atmosphere, adiabatic, 18, 28, 31
  expanded, 38, 41, 42
  isothermal, 38
  logarithmic, 138
  polytropic, 27
  radiative, 27, 28
  temperature of, 40
  total mass of, 41
Autocorrelation analysis, 345
Axis of symmetry, latitude of, 320, 323
  longitude, 327, 328

B

B-stars, 176
Babcock's curve, 237
Background variables, 62
Balmer decrement, 92
Bardsey Island, 119
Barringer Crater, 113, 114
Beryllium, abundance of, 86
Biela's comet, 135
Bielids (meteors), 135
Blast, degeneration of, 6
Blast wave, degenerate, 9
  initial, 40
Bode's missing planet, 108, 116
Bottlinger's force law, 207
  distribution of mass for, 243
Braking power, of dense clouds, 64
Bromoform, 148, 156
Brown recorder, 300
Bucerius's model, 232

C

Calcite crystal, 296
Calcite plate (plane-parallel), 293, 300, 387
Calcium (interstellar), 173

Canon Diablo meteorites, 113
Carbon-nitrogen cycle, 66
Carbonades, 108
Cepheid variables, 62, 176, 200, 231, 242
Chandrasekhar-Schoenberg model, 70
Chlorite, 107
Chondrites, 106, 110
  carbonaceous, 107, 108
  Lubbock, 108
  metamorphosed, 108
Chondritic meteorites, 110
Chondrules, 106, 109, 139
Chromosphere, 42
Circular birefringence, 294
Circular orbits, stability of, 271
Circular polarization of light, by dust grains, 290, 313
Circularly polarized component, measurement of, 290
Circularly polarized light, decomposition into, 293, 301
Clouds, of gas and dust, 108
Cluster, χ and h Persei, 96
Cohenite, 113
Collisions of dust grains, 332
Colour dependence on extinction, 313
  on polarization, 314, 324, 341
Colour-magnitude diagrams, of young clusters, 69
Cometary break-up, 117
Cometary residues, 149
Comets, spectra of, 109
Complex refraction index, 308
Contract discontinuity, interaction with shock wave, 14, 16
  path of, 15
Contact region, 15
Contact surface, 14, 15
  difference in pressure, 17
Continuity, equation of, 169, 194, 273
Contraction, of interstellar clouds, 65, 66, 68
  of T Tauri-stars, 48, 61
  time-scale of, 67, 68, 98
  tracks of, 66, 70, 77
Convective equilibrium, of the Sun, 84
Corona, inner, 115
  outer, 115
Cosmic dust, 107, 114
Cosmic spherules, deep-sea iron, 125
Craters, impact, 112
  laboratory experiments with, 112
  meteoritic, 113
Cross-section (mean), for extinction, 308, 311, 312
Curve of growth, analysis, 82, 87, 92

D

Deap-sea deposits, 118
Deep-sea sediments, 137
Deap-sea stony spherules, 148
Degeneracy (gas), 2
Degree of ellipticity of light polarization, 293
Depolarizer, Lyot's, 296, 299, 300
Depolarization, by objective, 306
  parameter, 330
  spurious, 344
Density, continuity of, 35
  discontinuous changes of, 14, 15
  distribution, integral equation for, 241
  laws, 167, 170, 191, 194, 245-264, 273
    exponential, 261
    Gaussian, 258
    parabolic, 247
    Schmidt's, 252
    Zagar's, 255
Deuterium burning, 68
Diamagnetic grains, 342
Diamonds, 108
Displacement, of absorption lines, 41
Double stars, T Tauri-type, 69, 76, 79, 84
  catalogue of, 80
Dust, interplanetary, 116, 120, 122, 130, 135, 155
Dust-ball model, 149
Dust, collector of, 121
Dust fragments, collected on polar snow, 118
  interplanetary, 114, 141
  iron contents of, 118, 136, 144
  nickel-to-iron ratios, 118
  velocity and direction of, 141
Dust grains, interstellar, 291
Dust particles, emission of radiation by, 116
  interplanetary, 115
  movement towards the sun, 116
  polarizing ability of, 115

E

Early-type stars, association with T Tauri stars, 63
Earth, magnetic field of, 151
Eclipses, of the Sun, 115
Eclipsing variables, 62, 290
Eddy currents (alignment mechanism), 343
Effective wavelength, of polarimetric apparatus, 302
Ejection of mass, energy of, 89
  from Novae, 13, 33
  speed of, 31
  from T Tauri-stars, 68, 87
Electric-vector direction for eclipsing variables, 290
Electron capture, 85
  photographs, 156
  probe X-ray analyzer, 125, 158, 159
  scattering, in stellar atmospheres, 28, 290
Ellipsoidal hypothesis, 195, 196, 212
Ellipsoidal velocity-distribution, 212
Elliptical polarization, of natural light, 292
  of simple wave, 292
Emergence of shock waves, at the surfaces of Novae, 28, 30, 31, 32
  gravitational, 40, 41
  kinetic, 32, 40
  potential, 37
  thermal, 32, 37, 38, 40, 41
Entropy, constancy of, 31
  function, 10
Equality of ages, of clusters and association stars, 95
Equi-density surfaces, of globular clusters, 275
  of Me dwarfs, 203, 217
  of RR Lyrae stars, 167
Equilibrium conditions, for contracting stars, 66
  for fluid spheres, 66
Equipartition of energy between gas and dust, 337
Escape velocity, from gas clouds, 91
  from Novae, 36
Escaping mass from Novae, 33, 34, 36, 37
Evolutionary interpretation of T Tauri stars, 63
Expanding atmospheres of Novae, 38, 41, 47
Explosion, energy of, 27, 36
Exponential density distribution, in galaxies, 261
Extinction cross-section, mean, 308, 311, 312
  relation to polarization, 329
  variance of, 321
Extra-terrestrial dust, 105

F

F-component, of the solar corona, 115
Ferrite dust grains, 341, 342
Ferromagnetic dust grains, 336, 341, 342
Flakes (iron or meteoritic), 126, 130, 148, 159
Flash variables, 55, 60
Flow field, expanding, 3, 32
  interaction with reflected wave, 30
Fluid core (of the Earth), 110
Focoidal shells, 193
Following waves, 16, 22
Forbidden lines, 87
Foreground emission objects, 63
Forsterite, 139, 141
Fragmentation, of dust particles, 99
Free-free emission, 92
Free iron, 107
Frequency function, of stellar velocities, 169, 195, 293

G

Galaxy, central density of, 202
  collisions of, 184
  composite model of, 273
  mass of, 207
  mass determination of, 281
Galactic gas, condensed from halo, 178
  orbits, law of, 250
  rotation, curves of, 176, 178
Gas behind the shock, velocity of, 36
Gas flow alignment, 342
Gas pressure, 41, 42
Gas sphere, self-gravitating, 8
Geminids (meteor showers), 128, 133, 136
Giacobinid meteor shower, 138
Giants, in young clusters, 71
Globular clusters, 166, 179

equi-density surfaces of, 275
kinetic energy of, 224
Globules, 74
Gould's belt, 57
Graphite flakes (dust), 342
Gravitational contraction, 48, 61, 65, 66
time-scale of, 67, 68, 98
tracks, 66, 70, 77
Gravitational energy, 40, 41
release of, 66
Gravity, influence of on high-speed particles, 32
material returning under, 32
Greenland, 126

H

H-R diagrams of young clusters, 66, 96
Hα, emission stars in H I regions, 62
H II regions, 61
Hx, objective-prism surveys, 57
Halley Bay, 145, 148
Halley's comet, 117
Helix angle, of spiral mechanism, 328
Harbig-Haro objects, 58
Heterogeneous spheroids, with confocal strata, 264
attraction and potential of, 267
density laws, 247
Homogeneous spheroids, 226, 273
Homologous contraction, 66, 78
Hyades, 97, 98
Hydrochloric acid, 128, 133, 146
Hydrogen, continua, 92
densities, 172, 173
ionized, 172
neutral, 166, 167, 177
distribution of, 274
radial velocities of, 176, 252
rotation curve of, 178, 274
Hydrogen lines, broadening of, 94

I

Ice nuclei, 136
Ices, 148
Idlis's model, of mass-distribution in the galaxy, 203
Ile d'Onessant, 126
Infalling material, 32, 63
Initial blast wave, 40
Instrumental polarization, 305
due to mirror, 305
due to objective, 305
Intersection of sound-wave with shock, 22
Interstellar absorption lines and bands, 291
Interstellar dust, as cause of polarization, 291
dielectric, 314
ferrites, 341, 342
graphite flakes, 315, 342
iron grains, 314, 341, 342
paramagnetic grains, 342
Interstellar dust clouds, 105
Iron, 107, 134
concentration of, 123, 128, 129, 130, 133, 135
core of the Earth, 110
dust, accretion rate of, 145
flakes of, 124, 126, 131, 132, 145, 152, 153, 156
Irreversible dissipation of energy, 38
Irreversible heating, 10, 38
Isothermal atmosphere, mass of, 40
temperature of, 40

J

Jeans' theorem, 195

K

K-giants, 176
Kamacite, 107, 110, 111, 147
Kelvin time-scale (contractional), 67, 69, 71, 89, 97
Keplerian orbits, 201, 222, 251
Kinematic properties of stars, 170
Kinetic energy, conversion of, 32
of material escaping from the Novae, 37, 40
Kramer's opacity, 66
Kuzmin's model of the mass distribution in the galaxy, 215

L

Lagrangian coordinates, 20, 21, 28, 30

Le Chatelier principle, 111
Light curves, classification of, 55
Linear approximation (to spherical gas flow), 8, 11, 13, 20
Lithium, abundance, 71, 81, 93
depletion by convection, 84
interstellar, 83, 85
isotope ratio, 86
lifetime in the Sun, 84
in meteorites, 83, 85
nucleosynthesis of, 85
in rocks, 83, 85
Local spiral system (Behr's), 328
Luminosity function of a cluster, 96, 166
Lyot's depolarizer, 296, 299, 300

M

Mach number (of supersonic flow), 16, 41, 44
Macro-turbulence (in T Tauri-stars), 86
Magellanic clouds, 166, 249
Magnesium, 107, 139
Magnetic absorption, 338
Magnetic alignment, 342
Magnetic fields, 42, 68, 122, 123, 291
Magnetic flux, density of, 337, 339, 342
Magnetic material, 122, 130, 134
Magnetic measurements (of rocks), 122
Magnetic particles, 120
Magnetic pressure, 42
Magnetic rocks, 134
Magnetic susceptibility, 338
Magnetite, 147, 150
Magnetization, 337, 339
Main Sequence, deviations from, 70
zero-age, 66, 67, 69, 70, 77
Mantle-core interface, in the Earth, 108
Mason's reaction, 107, 109
Mass, distribution in the Galaxy, 211, 212
ejection from Novae, 2, 33, 34, 36, 37, 40
ejection from T Tauri stars, 68, 87, 89
ejection from Me-dwarfs, 56, 95
of Novae, 2, 40
Mass-luminosity ratio, 225, 239
Metallic fragments (interplanetary dust), 109
Metallic iron dust, 118
in air, 127
rate of accretion, 119
Metallographic observations, 107
Metamorphosed chondrites, 108
Meteor showers, 106, 123, 144
Meteoric activity and accretion rate, 136
Meteoric dust, 117, 149
Meteorites, 106, 110, 112, 116, 143, 149
composition of, 106
disintegration of, 136
erosion of, 116
formation of, 112
metallic, 111
stony, 105, 136, 143
Micro-chondrules, 139
Micro-pores, on skin of artificial satellites, 154
Mezzin head, 126
Mica crystal, 296
Model atmospheres, 26
Modulation function, 24, 25
Moments of velocities, 175
Momentum, upward propagation of, 41
Monochromatic depolarizer, 298
Motion, outward of gases in Novae, 32, 33

N

Natural light, definition of, 292
Nebulae, polarization by, 343
Needles, dust, 126
Nickel, 120
Nickel and iron ratios, in dust, 118, 160
Nova (BW) Vulpeculae, 42
Nova Herculis 1934, 41
Novae, 2, 168
Nutation of dust grains, 336, 340

O

Objective-prism, Hα surveys by, 57
Oblate spheroïds (dust grains), 340, 341
Octahedrite, nickel, 110
Ogrodnikov's model, of mass-distribution in the galaxy, 210
Olivine, 106, 107, 147, 148, 149, 159, 161
Oort's constant, 228
parameters, 176, 177, 188, 201, 249, 277
rotation formula, 207
Opacity, due to electron scattering, 28

due to photoelectric absorption, 28
Kramer's, 66
Orion nebula, cluster of, 90, 96
gas motion of, 91
radio observations of, 91
stars in, 60, 61, 63, 69, 71, 74, 75, 76, 97
variables in 53, 54, 61
Orion population, 60, 96
Orion variables, 60, 76, 86
Orionids (α-), 11, 128

P

P Cygni-characteristics, 59, 88
Pallasite, 107, 108
Parabolic distribution law, 247
Parabolic galactic orbits, 250
Paramagnetic absorption, 336
Paramagnetic grains, 342
Paramagnetic relaxation, 339
Parenago's model, of mass-distribution in the galaxy, 200, 211, 215
Particles, magnetic, 120
Path of rarefaction wave, 14
of reflected wave, 16
of shock wave, equation of, 21, 23, 24, 25, 31
of sound waves, 20
Permeability, magnetic, 338
Perseids (ξ-), 117, 118, 120, 127, 161
dust contribution from, 135
Perseid meteor, 150
Perseus arm (of the galaxy), 331
Petrie dish, 120, 124, 125, 126, 134, 147
Phase-difference, due to objective, 303
due to polarizers, 296, 302
lack of correlation of, 292
Photoelectric absorption, 28
Photosphere (of Novae), rate of rise of, 41
Plane-polarized light, decomposition into, 293
Planet, embryonal, 108
interior of, 111
silicate mantle of, 108
Planetary breakup, 111
Planetary nebulae, 168
radial velocities of, 208
Pleiades, 47, 48
Plessite, 126
Poinsot ellipsoid of inertia, 336
Poisson's equation, 169, 199
applicability to the Galaxy, 211
Polarization, amount of, 303, 329
by aligned dust, 307
correlation with λ 4430 band, 345
correlation with extinction, 343
distance dependence of, 330
by dust particles, 115
extinction ratio with, 291
fluctuation of, 343
instrumental, 305
linear, 93, 94
measurement, 115, 290, 307
parameters, magnitudes of, 302
partial, 293, 295
variation of with galactic coordinates, 291
Polarizer, transformation properties of, 295, 296
Polarizing microscope, 158
Polarizing properties of ellipsoids, 313
of interstellar dust, 313
of long cylinders, 313
Polaroid sheets, 296, 299
Polytropic atmosphere, 27
Polytropic relation, 22, 28, 29, 36, 38
Polytropic stars, 27, 39
Populations, stellar, 168, 174, 200
of T Tauri stars, 75
Potential energy, 37
Potential of plane discs, 234
Potential spheroids, 189, 193
Poynting-Robertson effect, 116, 117, 135
Precession of dust grains, 336
Pre-maximum absorption spectrum (of Novae), 41
Principal absorption spectrum (of Novae), 41
Progressive wave, 9
Prolate spheroidal grains, 340, 341
Proton-proton reaction, 66
Pyroxene, 106, 107

Q

Quadrantids, 135, 136
Quarter-wave plate, 297
Quartz crystals, 296

R

Radial velocities, of T Tauri-stars, 84
Radiation damping, 94
Radiation pressure, 41, 115, 117
Radiative atmosphere, 27, 28
Radiative cooling, 41
Radiative energy release, 42
Radiative heat transfer, 41, 66
Radius, characteristic (of Novae), 2, 6, 37, 40
  of T Tauri stars, 78
Rankine-Hugoniot shock wave conditions, 5, 17, 28
Rarefaction wave, 10, 14, 18, 32, 33, 36
Reddening (interstellar), correction for, 77
Reflected wave, 16, 18, 30
Relaxation time, 334, 335
Retardation plate, 296, 297, 301
Roche model, 11
Rosette nebula, 74
Rotation, of the galaxy, 226, 227
  in T Tauri stars, 76, 77, 78, 79
RR Lyrae stars, 167, 168, 217, 264, 275
  distribution of, 173
  observed density of, 202
  periods of, 174
Rowland effect, 343

S

Saint Agnes (Scilly Islands), 119
Satellites, 118, 154
  recoverable, 137
Scale height, 39
Schreibersite, 113
Schwarzschild's model of mass distribution in the galaxy, 236
Scilly Don flakes, 159
Scintillation, effect on polarization of, 300, 301
Scorpio-Centaurus, H I clouds, 54, 62
Secondary bodies (Urey's), 109
Sediments, deep-sea, 137
Sedimentation, rate of, 137, 155
Separation of ejected material, 32
Shell, formation of after maximum of Novae, 42
  lines in T Tauri stars, 87
  velocity of, 42
Shell features (in Novae), 32
Shock front, 16
Shock path, equation of, 21, 23, 24, 25, 31
Shock speed, 21, 25, 26, 28, 30, 31
Silica gel, 134
Similarity law (for spherical gas flow), 5, 26, 27, 31, 32, 43
Small disturbances, propagation of, 22
Solar models, 84
Solar radiation, 109
Solar system, 149
Sound, velocity of, 20, 21, 36
Sound wave, equation of, 20
  propagation as, 38, 40, 42
South Sandwich Islands, 148
Spallation reactions (nuclear), 86
Spectral types, of T Tauri-stars, 56, 78
Spectrum-magnitude relation, 69
Spheroids, geometry of, 184
  potential of, 189
Spherules, air-borne, 119
  black magnetic, 118, 125, 137, 143, 149, 150, 155
  cosmic, 118, 137, 138, 139, 140, 141
  deep-sea iron, 125
  density of, 138, 142
  industrial, 119
  iron, 140, 143, 144, 151
  olivine, 161
  silicate, 138
  stony, 143, 144
Spiral arms, affecting polarization, 291, 327
Sputnik III, 162
Stability, of circular orbits, 271
  of fluid sphere, 4
Steady-state, hypothesis of, 169
Stochastic processes, 320
Stokes parameters, additivity of, 293
  definition of, 291, 292
  dispersion of, 319
  errors of, 304
  dependence on galactic coordinates, 302, 303, 304, 326, 342
  mean values of, 315
  for plane-polarized beams, 293
  properties of, 293, 304
Strength of shock wave, 16, 19, 21, 23, 25, 36

Striations, 125
Strong shock, 34
Subdwarfs, 168
Sub-system, of variable stars, 168, 171, 175, 194
Sun, primaeval, 84
Supergiants, 168
Supernovae, 7, 44
Supersonic flow, 3
Synchrotron radiation, 43
Systematic velocities, 196

T

T Tauri nebula, 87, 88
T Tauri-like stars, 58, 82
T Tauri-stars, 47, 48
  catalogue of, 49
  colours of, 78
  double, 69, 76, 79, 89
    catalogue of, 80
  evolutionary interpretation of, 63, 95
  macro-turbulence in, 84
  magnetic activity, lack of, 86
  mass of, 81
  photometric properties of, 48
  population in solar neighbourhood, 75
  proper motions of, 84, 89
  radial velocities of, 76, 77, 78, 79, 89
  shell lines of, 87
  space density, 63
  spectral classification of, 78
  spectrophotometric characteristics of, 56
  spectrum-magnitude relation, 69
  statistics of, 74
  variation in radius of, 78
  velocity dispersion of, 63, 90
  width of absorption lines, 63
Taenite, 107, 110, 147
Tars, 109
Taurids (β-), 161
Taurus-Auriga, HI-clouds, 54, 62, 63, 64, 69, 71, 75, 91, 98, 99
Taylor variables, 43
Temperature gradient, 32
Temperature of clouds forming the stars, 96
  of surfaces of Novae, 2
Thermal energy, 32, 33, 37, 38, 40, 41
Time-scale, Kelvin's (for gravitational contraction), 67, 69, 71, 89, 97
Torsion balance, 122, 123
Torsion wire, 134
Trapezium cluster, 98
Troilite, 113
Troposphere, 130
Turbulence in cloud-forming stars, 96
Turbulent broadening of Balmer lines, 93, 94

U

U Geminorum-stars, 62
Ultra-violet excess, 70, 91
Undisturbed fluid, sound waves in, 20, 21
Uniqueness of age, 72
Unpolarized light, decomposition into, 293
Upper atmosphere, turbulence in, 136
Ursids, dust contribution from, 135, 136

V

Vanguard III, 162
Variable stars: RW Aurigae, 54, 55, 62, 72, 73, 74, 87
  SU Aurigae, 72
  ξ Coronae Australis, 54
  CQ Cephei, 290
  UX Monocerotis, 92, 94
  T Orionis, 54
  UY Orionis, 92
  RY Persei, 240
  U Sagittae, 290, 291
  T Tauri, 72, 76, 82, 86, 87, 88, 93, 168
  RR Tauri, 54
  RY Tauri, 54, 55, 72, 76, 77, 78, 82, 93
  UX Tauri, 69, 72, 76
  XZ Tauri, 72
  EY Tauri, 55
Veiling of absorption lines, 73
Velocity, circular, 201, 219, 220
  ellipsoid, 169, 199
  of escape, 201, 232
  of gas behind the shock front, 36
  of material ejected from Novae, 2
  of sound at stellar centre, 36
Velocity dispersion, of stars, 175, 176
  of T Tauri stars, 63, 90

Velocity distribution of stars, 170, 194
Virial theorem, 223
Viscosity, artificial, 28
Volcanic ash, 148

W

Wake of shock, hydrodynamics of, 16, 19, 20, 23, 27, 28, 34, 35
Water bowl, 127
Wave, blast, 5
  element intersecting shock, 20
  plane, 26, 27
  progressive, 9
  spherical, 26, 27
Wavelength dependence of observed polarization, 314, 329, 341
Wavelength of disturbance, 13
Wavelet of shock, strength of, 23
Wax ball model, 149, 151
Weak shock, 34, 35
Widmanstätten figures, 110, 111, 112, 113
Width of absorption lines for T Tauri stars, 63
Wollaston prism, 300
Wyse and Mayall's model of galaxy, 236

X

X-ray analyser, 125
  powder photographs, 139, 147, 159, 162
Xenon in chondrites, 87

Y

Yasuda's model of the galaxy, 261

Z

Zagar's density law, 255
Zeeman components of absorption lines, 290
Zero-age Main Sequence, 66, 67, 69, 70, 77
Zodiacal cloud, 116, 117, 143, 154
Zodiacal gas, rotating cloud of, 151
Zodiacal light, 114, 115, 137, 155
  axis of symmetry, 115
  spectrum of, 115